KfK 3800
CSNI 95
Februar 1985

Proceedings of the CSNI Specialist Meeting on Nuclear Aerosols in Reactor Safety

4th - 6th September, 1984
Karlsruhe, Federal Republic of Germany

Edited by:
W. O. Schikarski, W. Schöck
Laboratorium für Aerosolphysik und Filtertechnik

Kernforschungszentrum Karlsruhe

KERNFORSCHUNGSZENTRUM KARLSRUHE
Laboratorium für Aerosolphysik und Filtertechnik

KfK 3800

CSNI 95

Proceedings of the CSNI Specialist Meeting on Nuclear Aerosols in Reactor Safety

4th - 6th September, 1984
Karlsruhe, Federal Republic of Germany

Sponsored by:
OECD Committee on the Safety
of Nuclear Installations (CSNI)

Co-sponsored by
German Nuclear Society (KTG) and
Association for Aerosol Research (GAeF)

Hosted by:
Kernforschungszentrum Karlsruhe (KfK)

Edited by:
W.O. Schikarski and W. Schöck

Kernforschungszentrum Karlsruhe GmbH, Karlsruhe

Kernforschungszentrum Karlsruhe GmbH
ISSN 0303-4003

FOREWORD

The prediction of the release and transport of nuclear aerosols associated with postulated accidents in nuclear power plants is necessary for the assessment of the radiological consequences of these accidents and hence is an important aspect of reactor safety evaluation. The nature and behavior of nuclear aerosols can potentially influence both the course and the consequences of reactor accidents. For example, nuclear aerosols can affect the performance of engineered safety systems (e.g. containment, air cleaning systems) as well as the magnitude, dispersion and effects of the radioactive source term leaked to the atmosphere. As a result of the extreme environment associated with nuclear aerosols, they exhibit very dynamic physical and chemical behavior and pose special analytical and experimantal problems different from those associated with aerosols found under industrial and ambient conditions.

The CSNI Specialist Meeting on Nuclear Aerosols in Reactor Safety held at Gatlinburg in 1980 was the first major internaional conference on nuclear aerosols in reactor safety. Since that time, considerable progress on research and development has been made.

The meeting of the CSNI Group of Experts on Nuclear Aerosols in Reactor Safety, held in March 1983, therefore recommended that another Specialist Meeting on this topic be held in mid to late 1984, by which time a supplementary State-of-the-Art Review was prepared by the Group.

The purpose of the Meeting was to discuss the conclusions of the Review in depth and provide a forum for the exchange of information between aerosol research specilists, reactor designers, and regulators regarding the realistic assessment of radiological consequences of reactor accidents in LWRs, LMFBRs, and GCRs. Emphasis was placed on the technical aspects of the subject and on new information beyond the Proceedings of the Gatlinburg Meeting (NUREG/CR-1724, ORNL/NUREG/TM-404, CSNI-45, October 1980) and the State-of-the-Art Review, particularly in the field of severe LWR accidents.

In the Opening Session welcome adresses were given by Dr. H.H. Hennies, Member of the Board of Kernforschungszentrum Karlsruhe and President of the German Nuclear Society, and by Dr. D.F. Torgerson, Chairman of CSNI Principal Working Group No. 4 (Source Term and Environmental Consequences). The keynote paper was presented by M. Silberberg of the US-Nuclear Regulatory Commission. Seven sessions were structured according to the main topics covered by the Meeting. A final plenary session took place at the end of the Meeting to summarize the state-of-the-art and to identify remaining problems.

A program committee served in program planning, paper review and organizing the meeting. The members of the program committee were

F. Abbey, UKAEA (UK) , Chairman
W.O. Schikarski, KfK (FRG) , Co-Chairman
W. Schöck, KfK (FRG) , Technical Secretary
W. Schütz, KfK (FRG) , Ass. Techn. Secretary
J. Royen, OECD
J. Fermandjian, CEA (F)
K.O. Johansson, Studsvik Energiteknik AB (S)
S. Kitani, JAERI (J)
T.S. Kress, ORNL (USA)
J.F. Van de Vate, ECN (NL)

The editors - also on behalf of the program committee - wish to express their thanks to the delegates and participants from the various countries for their contribution in making the meeting successful. Special thanks are offered to the sponsoring organization, the OECD Committee on the Safety of Nuclear Installations, to the co-sponsoring societies, the German Nuclear Society, and the Association for Aerosol Research, and to the host of the meeting, Kernforschungszentrum Karlsruhe, for their continuous support and cooperation.

W.O. Schikarski
W. Schöck

Contents

Page

Opening Session

SOURCE TERM REASSESSMENT: ISSUES AND PERSPECTIVES

M. Silberberg
W. Pasedag

U.S. NUCLEAR REGULATORY COMMISSION
WASHINGTON, D.C. 20555

ABSTRACT

The status of the NRC source term reassessment effort is briefly presented in terms of NRC contractor effort, documentation and schedule. The technical progress being made towards incorporating phenomena in source term modeling that were not included in WASH-1400 is presented. Some of the key technical issues that have been identified in current source term estimation are discussed. Finally, some perspectives gained from the on-going source term analyses and peer review are presented.

Introduction

The purpose of this paper is to: highlight the status of the NRC source term reassessment effort of the NRC contractors; present observations on overall technical progress and the key technical issues emerging from these studies; and briefly discuss important perspectives that might be gained from a broad view of source term analyses. Definitive positions on quantitative source term estimates and the related methodology have not yet been developed by the NRC staff, and hence, are beyond the scope of this paper.

A summary of the current accident source term position in the United States (primarily based upon the views of the NRC staff) was prepared for the CSNI Principal Working Group No. 4.[1] The status of accident source terms was related to the regulatory and licensing process in the United States. It noted current and projected regulatory policy development activities in the U.S. that were closely tied to source term considerations, including Severe Accident Policy, Safety Goal Policy and Revised Siting Rulemaking. In 1983 the Commission decided to better characterize accident source terms before proceeding with new siting regulations and changes to existing and proposed regulations and policies (e.g., emergency preparedness).[2] Regulatory change will be considered if the reassessment of the accident source terms so warrants.

Status of NRC Source Term Reassessment

In 1983 an interim Accident Source Term Office (ASTPO) was created to focus the NRC staff reassessment efforts. The program elements of the source term reassessment were described previously [3]. The purpose of ASTPO is to coordinate the work of NRC contractors and to assure through peer review of improved methodologies (primarily models and codes) that can be used for estimating accident source terms. The principal NRC contractor effort is the source term estimates provided by Battelle Columbus Laboratories (BCL) for a number of plants representing the types of light-water reactor designs licensed in the U.S. These estimates have been published in a multiple volume set of final draft reports, BMI-2104. Previous drafts were available last year as part of the specialist peer review process.

Although the BCL estimates have not been weighted to account for sequence occurrence probability, nor for probable containment performance, the calculations indicate that significant source term reductions appear likely for many severe accident sequences. It should be emphasized that the staff has taken no position on the Battelle studies pending completion of the peer review process. We believe a thorough peer review of the scientific basis for source term estimation is an essential part of the reassessment of accident source terms. Hence, in addition to a specialist review, a broad-based, independent review of source term science is now in progress by a special study group of the Americal Physical Society (APS), at the request of the NRC.

Additional contractor effort in support of the source term reassessment includes reports reviewing the following: the technical basis of the methodology used for the BCL source term estimates, to be published by Oak Ridge National Laboratory as ORNL-TM 8842 in September 1984; a scoping study on the quantitative estimation of uncertainties involved in the BMI-2104 source term estimates, to be published by the Sandia National Laboratory by early Fall 1984 (SAND 84-0410).

The NRC source term report summarizing the staff's evaluation and conclusions reached from the NRC contractor analyses will be released in draft form for public comment in early 1985 as NUREG-0956, after the completion of the APS peer review. This report will briefly describe the methodology developed by NRC contractors, discuss the status of its validation (including ongoing research programs), and describe its applicability. Specific sample applications of the methodology to BWR and PWR plants with different types of containment will be given. Although the subject of the report is accident source terms, it will also include estimates of the probabilities associated with the several accident sequences analyzed for each plant type to give a risk perspective of the revised source term estimates. The conclusions about the validity and applicability of the revised source term methodology will include the perspective gained from the thorough peer review of this topic.

In support of NUREG-0956, the staff, supported by contractors, is developing two NUREG reports to reassess containment behavior during accidents because of the importance of containment performance on accident consequences. Two groups are involved; the Containment Loads Working Group (CLWG) and the Containment Performance Working Group (CPWG). The reports of these groups are expected to be available by early Fall 1984 as NUREG-1079 for the CLWG report and NUREG-1037 for the CPWG report.

Technical Progress in Source Term Modeling

Over the past several years, a general consensus that has developed concerning Reactor Safety Study (RSS) [3] source term estimates is that they are conservative (pessimistic) with respect to the quantity and timing of radionuclide releases to the atmosphere.[4] This acknowledged pessimism in the RSS methodology arises from several phenomena, considered too difficult to quantify, that were neglected; these include engineered safety feature effectiveness and simplified models used to analyze fission product transport. Qualitative reviews [5] listed the most significant of these shortcomings of the RSS approach as: the assumption that the dominant form of iodine is elemental (I_2) rather than CsI; neglect of fission product retention in the reactor coolant system (RCS); neglect of the steam-condensing environment in the containment (or other structures); omission of water pool scrubbing in saturated BWR suppression pools; and lack of detailed modeling of aerosol behavior in the containment, other structures, and in the fission product release pathway and in the containment.

Significant progress has been made in the development of fission product release and transport models intended to replace omissive or conservative simplified analyses. Models exist today to quantitatively address each of the issues listed above. For example, models for fission product retention in the RCS have been developed [6] which account for condensation on wall surfaces and particles, sorption on RCS steel surfaces, particle deposition resulting from settling, diffusion, impaction, thermophoresis, and agglomeration of particles resulting from brownian motion, gravitation,and turbulence. Not surprisingly, a mechanistic treatment of these phenomena requires detailed knowledge of the thermal hydraulic conditions in the RCS during the accident.

Competing phenomena which limit the source term reduction anticipated from the mechanisms enumerated above are also needed. Volatile fission products can condense on surfaces where they are retained or on aerosols which could carry the condensing radionuclide to the containment. Also, modeling of RCS deposition of the relatively volative fission products Cs, I, and Te cannot be considered complete without considering the potential for later emissions from the primary systems as a result of re-vaporization of deposited materials, resuspension of settled aerosols, and vessel de-pressurization in high pressure core melt scenarios. Similarly, the limitations of the assumption of cesium iodide as the dominant form of iodine are being established by continuing investigations of iodine chemistry under primary coolant conditions. While thermodynamic equilibrium and kinetic calculations confirm that CsI is the dominant chemical form in high radiation fields [7], potential complications from reactions with control materials (silver or boron carbide) and other core constitutents need to be investigated and resolved. None of these effects are expected to attenuate the role of CsI as the dominant form of iodine.

The modeling of aerosol behavior in the containment has made rapid progress by building on the extensive methodology developed for LMFBRs. Improved models available today address not only aerosol agglomeration and settling phenomena, but also include the effects of a condensing atmosphere (steam condensation, diffusiophoresis).[8] As is the case in the RCS, the limiting effect appears to be our ability to provide the detailed thermal hydraulic input required for these models. Steam condensation effects appear to be extremely sensitive to small changes in supersaturated conditions. Small variations in the accident sequence, or plant parameters, can change the humidity of an atmosphere and alter the predicted aerosol behavior.

Analyses of engineered safety features (e.g., containment sprays, suppression pools) show that these systems are highly effective even though the accident may have progressed in severity beyond their design basis. Passive systems, such as the BWR suppression pool, provide an effective means of scrubbing aerosols from a steam air atmosphere, even if the pool water is near saturation. Detailed investigation by several organizations [9], [10] of the phenomena involved indicate a very strong dependence of suppression pool decontamination factors on aerosol particle size between 0.3 and 3 um. Another sensitive parameter is the ratio of condensible vs. non-condensible gases.

The most important engineered safety feature is the containment system. Those accident sequences for which the containment integrity is maintained result in relatively minor releases, even if leakage exceeding the design basis by as much as an order of magnitude or eventual failure of the containment after many hours of containment integrity are considered. Conversely, the largest source terms are those resulting from an early failure or by-pass of the containment. As noted before, because of the importance of the containment, NRC's source term reassessment effort includes two specialists working groups to investigate containment loads and containment leakage behavior.

Although a quantitative application of the models of these phenomena is premature pending the APS review, it is apparent, without quantification, that the combined effect of all of the retention mechanisms will reduce the source terms. Accident sequences found to be risk-dominant in previous analyses, however, generally include a postulated failure of ESFs requiring electric power or backup water sources, or involve leakage paths which by-pass ESFs. The source terms for such sequences, therefore, would depend primarily on natural attenuation processes. The overall effectiveness of natural fission product attenuation processes depends strongly on the specific accident sequence postulated for a specific plant design, as noted above. It is apparent, therefore, that the final outcome of the application of mechanistic fission product attenuation models will be strongly dependent on the specific accident sequence and the plant parameters.

Key Technical Issues for Source Term Estimation

During the course of the source term reassessment, the analyses and the reviews have given insight into a number of important technical issues about fission product release and transport phenomena. The issues presented here are not an exhaustive list; they represent those areas that are believed to have the greatest impact on source term estimates. The key issue about the containment failure mode including by-pass is not shown in the list.

1. Natural Circulation in Reactor Vessel

   In the state-of-the-art methods, it is assumed that the flow of gases and aerosols in the upper plenum is one-dimensional. More realistic behavior, supported by advanced thermal-hydraulic analysis, indicates that recirculation would occur in the upper plenum because of large temperature gradients. Including natural circulation would act to enhance considerably the retention of fission products and aerosols in the RCS. Natural circulation can also increase heat losses from the core, influence the core melt progression, and influence the RCS boundary integrity for high pressure sequences.

2. Core Melt Progression

   Large uncertainties exist in the modeling of core melting, slumping, and vessel melt-through because of the absence of data. Uncertainties in these phenomena give rise to uncertainties in hydrogen generation, and the quantity, temperature and composition of molten material. These phenomena have an important impact on containment loads, ex-vessel releases, thermal-hydraulics, fission product chemistry, and deposition in the RCS.

3. Control Rod Vaporization

   The mode and timing of control rod vaporization is very important during core degradation (prior to slumping) because silver aerosols can condense, interact, and coagglomerate with fission products. If they are present at the time of substantial fission product release, they can influence deposition. In NRC contractor analyses, considerable silver aerosol generation is assumed; IDCOR's contractors neglect silver.

4. Fission Product Retention and Revaporization in the RCS

The deposition of fission products in the RCS piping and upper plenum surfaces predicted by codes such as TRAPMELT can be substantial, but with large uncertainty because potentially important phenomena are omitted. Once deposited on RCS surfaces, the fission products can be revaporized by local heating from decay heat and be transported out of the RCS to the containment. This process would be especially important if the timing of revaporization occurs during the period when containment failure might be predicted to fail.

5. Tellurium Retention

Experiments indicate that Te is retained on unoxidized Zr. Hence, while released Cs and I have an opportunity for retention in the RCS, Te can be carried with the molten core material as the RPV is breached and into the reactor cavity where it can be released directly to the containment via core-concrete interaction. The IDCOR contractor analyses do not model Te behavior as described, hence, it should not be too surprising to observe that for a given accident sequence, assuming all other things equal, higher Te releases to the environment are obtained in the BCL estimates when compared with the IDCOR contractor estimates. These differences are significant and in most cases have an important impact on accident consequences.

Perspectives Gained to Date

Over the past 18 months the ASTPO staff has had the opportunity to reflect on the work of our contractors, the work of others in the U.S. and abroad, as well as the comment and discussion of the peer review process. Some of the more important perspectives that appear to be emerging are presented. These technical perspectives are not staff positions.

1. Source Term Methodology

Improvement over WASH-1400 now being obtained in source term estimation is a result of the availability of a larger data base and advancements in the methodology. But the methodology is much more complex than WASH-1400 and depends heavily on codes. The methodology incorporates additional phenomena which require more detailed knowledge of a plant design and accident sequences conditions. As a result source terms cannot be generalized to other plant designs. The concept of "across-the-board" source terms contradicts the most recent research findings.

The methodology is still being improved and validated. As noted in the previous section, there are a number of key unresolved technical issues which require additional data and improved models. Further progress in the methodology does not appear possible without incorporating mechanistic treatment of phenomena such as the thermal-hydraulics of the RCS during the core melt and vessel melt-through phases.

2. Balance of Emphasis and Practical Limitations

Considerable attention in the area of source term estimation is now being given to certain parts of the methodology such as containment aerosol behavior, RCS aerosol behavior or in characterization of the chemistry of a specific fission products, e.g., radioiodine. There is no doubt that our understanding of these areas has improved as a result of the considerable work that has been done. Further progress, however, now requires further emphasis on the less advanced areas, e.g., core melt progression, in order to resolve the remaining source term issues and reduce the high level of uncertainties associated with current estimates.

There is of course a practical limitation to the level of reduction of uncertainties. We expect that residual uncertainties will remain in spite of the significant progress expected in the data base and improved methodology the next two years. This results from the complexity in some of the phenomena that are being modeled and the limitation in the difficult experimental technology available for assessing the interactive effects of multiple phenomena over the full range of accident conditions. The practical limit to our experimental verification capabilities also comes into play when analyses are attempted with the goal of showing further reductions in release fractions which already represent several orders of magnitude reduction from previous (e.g., WASH-1400) estimates. The practical value of such efforts is questionable, because the residual uncertainties in such areas as chemistry and thermal-hydraulics present throughout the accident sequence challenge the confidence in the results of such analyses.

3. Uncertainty Analysis

Treatment of the uncertainties in severe accident phenomena and their propagation through the analysis of source term estimates needs more detailed consideration than it has received to date. Such effort is difficult because of the many, complex phenomena involved and their feed back on source term estimates. Improved uncertainty analysis, however, will make an important contribution to the framework needed for resolution and closure of the issues and the related identification of research priorities, criteria for validation of the methodology, and future regulatory applications.

REFERENCES

1. R. W. Houston, "Current National Source Term Position and Practices for the United States," SINDOC(84)67, Part V, July 5, 1984

2. "U.S. Nuclear Regulatory Commission Policy and Planning Guidance 1984," NUREG-0885, Issue 3, January 1984

3. M. Silberberg, et al., "An Overview of the Status of NRC Reassessment of Technical Bases for Severe Reactor Accident Source Terms," Int'l. Mtg. on LWR Severe Accident Evaluation, Cambridge, Massachusetts, 1983

4. Reactor Safety Study, An Assessment of Accident Risks in U.S. Commercial Nuclear Power Plants, WASH-1400 (NUREG-75/014), U.S. Atomic Energy Commission, October 1975

5. M. Levenson and F. Rahn, "Realistic Estimates of the Consequences of Nuclear Accidents," Nuclear Technology, Vol. 53, No. 2, 1981

6. J. A. Gieseke, et al., Radionuclide Releases Under Specific LWR Accident Conditions, draft BMI-2104, Battelle Collumbus Laboratories, July 1983

7. E.C. Beahm and W. E. Schockley, "Iodine Volatility," Paper submitted for the ANS Topical Meeting on Fission Product and Source Term Research, July 1984

8. H. Bunz, M. Kayro, and W. Schöck, "NAUA-Mod4, A Code for Calculating Aerosol Behavior in LWR Core Melt Accidents, Code Description and User's Manual," preliminary paper presented at a workshop held at Electric Power Research Institute, Palo Alto, CA. (March 1982) to be revised and published as KfK-3554 by Kernforschungszentrum Karlsruhe.

9. W. J. Marble, et al., "Retention of Fission Products by BWR Suppression Pools During Severe Reactor Accidents," paper presented at International Thermal Reactor Safety Meeting, Chicago, August 1982

10. P. C. Owczarski, et al., "Technical Bases and User's Manual for SPARC," Appendix B of BMI-2104, Vol. 2 op. cit.

Session I: Aerosol Formation

Chair: K.K. Murata (SNL, USA)
W. Schütz (KfK, FRG)

REMARKS ON METHODS OF EVALUATION OF AEROSOL SOURCES RELATED TO PWR CORE MELTDOWN ACCIDENTS

J. Peter Hosemann
Karlsruhe Nuclear Research Center, P.O. Box 3640, D-7500 Karlsruhe

ABSTRACT

This paper gives the perspective on fission product behavior and source term research of the Project Nuclear Safety (PNS) at the Karlsruhe Nuclear Research Center (KfK). It tries to demonstrate the conceptional background of the KfK core melting program, which has been started in 1973, and which is scheduled to be terminated by 1986. The paper also summarizes the main findings of the SASCHA program, with the aid of which the enveloping fission product release from the primary system into the containment during a PWR core melt accident has been investigated. Within more than 10 years of PWR core meltdown research in depth we developed an understanding of the most relevant phenomena which forces us at the time being to describing the complex physical relationships as easy and as plausible as possible, based on uncontested laws of nature, rather than to running the program more and more into refined specifications. Especially with respect to aerosol generation, transportation, removal, resuspension, and release into the environment, this attempt led to the following conclusions:

- According to the present state of knowledge the tools are not at hand for calculating core degradation in a detailed manner and, starting from that basis, for calculating the element specific activity release from the primary circuit as a function of the time in a manner which would be reliable from the scientific point of view. However, the calculation can be replaced by a plausible and, at the same time, physically justifiable estimate of the upper limit.

- The fractions of release from the fuel determined in the experiment are undoubtedly in the range of 70% to 100% for the radiologically most important elements I, Cs, Te. The reduction in release from the primary circuit due to deposition is 50% at the maximum. A considerable portion resuspended must be deducted from that value. The retention of iodine and aerosol particles in the safety containment amounts to several orders of magnitude (up to 5). Likewise, the decrease in the population dose by spread and dilution in the environment and due to other parameters attains several orders of magnitude (up to 7). Consequently, particle retention by a factor of 2 or 3 in the primary circuit is negligible.

- Our present knowledge is completely satisfactory for analyzing the so-called source term in core melt accidents. The wish to develop more detailed codes related to core degradation and to activity release from the primary circuit has many understandable causes. However, there is no single technical reason in favor of spending much money in order to materialize this wish.

BACKGROUND

As early as in 1973 first studies were started in the Federal Republic of Germany on hypothetical core meltdown accidents in light water reactors. It has been an established fact from the outset that hypothetical accidents, i.e., accidents going beyond the design basis accidents, should not be the subject of any licensing issues whatsoever. The rationale underlying research activities related to hypothetical events has been - at any rate for the Project Nuclear Safety implemented at the Karlsruhe Nuclear Research Center- the following plain finding:

- The core meltdown accident constitutes the inevitable consequence of a permanent positive difference between generated and removed thermal power. This is the reason why, eventually, all emergency cooling measures will serve the primary purpose of avoiding a core meltdown accident!

Although more than 90 % of LWR safety research in the Federal Republic of Germany had been pursued with the objective to prove that design basis accidents can be safely controlled, it was still legitimate to ask what will actually happen in case that the emergency cooling measures will not perform as scheduled, if necessity arises.
Outside the Federal Republic of Germany this question gained importance in the context of probabilistic risk assessments only. To be able to assess the safety of light water reactors in a responsible manner we had to solve three essential questions when we started our studies ten years ago:

- Which are the initiating events and which time dependent failure of emergency cooling systems will lead to core meltdown accidents not capable of being controlled?

- How do uncontrolled core meltdown accidents proceed in terms of physics, chemistry and mechanics and which passive barriers already provided in the reactor building will prevent such accidents from propagating?

- Which are the realistic impacts on the environment to be expected from core meltdown accidents?

Much attention has been paid to the first question in Germany during the last decade. It resulted in the requirement to carry out a careful technical systems analysis and to solve the thermohydraulics problems associated with it. Today we are in a position to give a satisfactory answer to the decisive specific questions using the methods elaborated. However, this does not imply the absence of wishes concerning the "tools" which have to be improved in order to solve thermohydraulics problems.

For German pressurized water reactors extensive studies were conducted on the question which failures of emergency cooling systems are permitted to occur in addition and which cooling channel blockages are tolerable in case of the design basis accident (Guillotine break of a main coolant pipe) without causing uncontrolled melting of the core (FEBA results: 90%). The phenomenological range of indeterminacy between the manageable loss-of-coolant accident and the core meltdown accident propagating in an uncontrol-

led way is probably so narrow that work on this subject should not be continued. Especially the question whether the core is bound "to melt down or not to melt down" in a design basis accident can be answered solely on the basis of the thermohydraulic analysis of a strict sequence of the system.

The situation is not as transparent for a core meltdown beginning at high pressure in the primary loop, i.e. if the leaks are small. To initiate uncontrolled core meltdown one has to postulate in this case the failure of a much greater number of emergency measures over a much longer period of time. Logically, this implies that also the "range of indeterminacy regarding core meltdowns taking place or not taking place" will become much wider. One can especially think of the onset of accidents in which the operators undertake a variety of manual countermeasures which might be successful or not successful. These accidents do no longer strictly follow a defined technical sequence of the system and hence their development cannot be adequately conceived before occurrence.
Completely independent of the events preceding a core meltdown accident on the "high pressure path", the water level in the reactor pressure vessel will attain the upper edge of the core at some time after occurrence of the accident (e.g. after 3 or 4 hours). Generally, the following courses of events are possible.

- Either no water is available for emergency cooling: in this case the water level will continue to decrease practically independent of the leak size at an integrally averaged velocity of 4 m/h (slower at the beginning and faster later on);

- or water is available for emergency cooling but the amount is insufficient; in this case the water level will decrease at an accordingly slower rate;

- or the core can be reflooded in time; in this case we can stop bothering about it.

The second case is of no importance for risk assessments because "a bit water available for emergency cooling" defies definition (despite the fact that we bear in mind TMI-2).

Still - as in the first case - the water level meaningfully defined in one way or the other, would continue to decrease. There is no doubt that also on the high pressure path a core condition will be attained quite soon which will propagate by slumping and, eventually, adopt a configuration no longer amenable to cooling. Restoring of emergency cooling from this moment on will no longer be a suitable means of preventing the core from melting down. This moment should be attained as soon as the water level has been laid bare e.g. half of the core height. Less than 30 minutes will pass from the time preceding the onset of core dryout - with e.g. half of the core degraded - until uncontrolled core meltdown.

This makes obvious that expensive research work is not reasonable for practical reactor safety if it is intended to produce the evidence that a partially degraded core within the small "time window" of 15 - 30 minutes is just amenable to recooling although no coolant water had been available within the 3-4 h preceding this time interval.

It must be left open whether from the point of view of basic research it would be interesting to be able to describe any possible condition of the reactor core as a system of time dependent separate effects. At any rate, the widened knowledge so derived would not modify one of the few rules in reactor safety which does not admit of an exception and which says

"Keep the core under water and the containment tight!"

It is hardly conceivable that operators could face a situation in which they would have to decide whether or not to reflood an uncooled core.

What was said above is the philosophy behind the KfK/PNS decision to restricting the SASCHA fission product release program on uncontrolled in-vessel core meltdown situations only. Thus, our element specific data are enveloping data, which correspond to the releases from a liquid melt.

The second general question formulated above concerns the sequence of core meltdown accidents. As it was already briefly mentioned we are proposing to care only about two situations in the Federal Republic of Germany which envelop all extreme in-vessel situations, namely:

- the low pressure path and
- the high pressure path, each of them resulting in an uncontrolled core meltdown.

From the out-of-pile investigations of the melting behavior of fuel rods performed by the Project Nuclear Safety we have derived adequate information about the general phenomenology of slumping. We recognized the complexity of core degradation and realized at an early stage of our studies that detailed knowledge of the stochastic process of core degradation is not necessary. Simple energy balances, similar to those established in WASH 1400, are fully adequate because the time interval of core degradation is short as compared with other relevant sequences following core degradation. We have accumulated sufficient knowledge of the RPV failure both for the low pressure case and the high pressure case. We cannot make out an aerosol generation mechanism spraying at elevated pressure tons of molten material from the reactor pressure vessel into the containment. We know that the interaction of melt and concrete basemat determines the time of containment overpressure failure by sump water ingression and subsequent evaporation. Regarding the problem of H_2 explosions we expect enlightenment from the studies supported by the USNRC and EPRI. As to German pressurized water reactors we are meanwhile in a position to rule out that steam explosions will lead to a precocious failure of the reactor pressure vessel or, which would be even worse, a failure of the containment. We are performing the BETA project in Karlsruhe in order to demonstrate that the codes describing the melt/concrete interaction (CORCON in the USA, WECHSL together with KAVERN in Germany) represent adequately the sequence of core meltdown in this respect.

Finally, we have placed the emphasis of all our studies of the "source terms" on the time dependent interplay of radioactivity release from the primary circuit and driving thermodynamic forces as a function of the postulated leak cross sections and release paths from the containment. Although this seems trivial, it is not taken into account in a consequent manner in many cases and thus leads to incomplete information which is likely to be

erroneously evaluated.

A number of analyses performed in Germany and in the USA supported the finding that the type and date of failure and the resulting driving forces are outwardly dominating regarding the respective "source terms".

This leads to a simple statement addressed to aerosol researchers which says:

> Particle removal is fastest at high number concentrations but at the same time possible leakages are worst.

Some years ago we already made it plausible for pressurized water reactors of German design that retention of radioactivity in the primary circuit plays indeed a secondary role compared with retention mechanisms in the containment, in the sump and in adjacent spaces, especially if strong, not yet investigated resuspension mechanisms must be expected to occur in the primary loops. Therefore, we did not initiate codes resembling the Trap-Melt code but we are obviously following with interest these code developments as well as the experiments performed at Hanford, Oak Ridge and Marviken. The more details we got to know, the more we found our opinion confirmed.

According to the present state of knowledge we must expect only late overpressure failure of the containment in much more than 90 % of all conceivable core meltdown accidents. This justifies our development of the NAUA code which describes the removal behavior of aerosol systems in the containment and in other spaces in the presence of steam. By the German/Swiss DEMONA program we wish to demonstrate the adequate accuracy of the NAUA code in combination with the thermodynamic containment codes. We think a factor 3 - 5 will be sufficient to demonstrate the accuracy.

We performed the SASCHA program which is presently verified at ORNL. We believe that it gave us a sufficiently good estimate of the upper limit of aerosol release into the containment. We are able to show with the help of NAUA that even a reduction in the release of non-radioactive aerosols by 400 % will not have any noticeable effects on the source terms. We have developed an iodine release model by which for the first time, the attempt was made to link in a synopsis sequences which seem to be relevant. A consensus of prominent scientists in this field has been reached regarding many partial aspects. An extremely helpful seminar was devoted to this subject at ORNL. Where it had not been possible to accumulate complex knowledge for the time being, we were able to make accepted plausibility considerations. But validation by experiments of separate effects is still to be obtained which can be treated in a meaningful manner by use of the model.

An agreed but pessimistic assumption is that 99% of the iodine inventory will be released in the form of cesiumiodide, whereas a best estimate value is 99.9%. The analyses of some core meltdown scenarios made evident that more or less the small fraction of 1% or 0.1% of gaseous iodine dominates the environmental hazard because of the effectiveness of the aerosol removal processes.

At any rate, we are today in a position to consider more realistically than before the release of the most important nuclide (I-131) for the consequence of an accident.

We performed studies which made it clearly evident that it is just wrong to suppose a PWR containment to burst under the impact of overpressure. It is more rightly assumed that a leak of limited size will occur which needs to be quantified in future work. We are conducting special studies on this problem. But already now we are capable of controlling the situation by defintion of a best estimate case and a worst case. Even the worst case leads to a drastical reduction of the source term.

Some remarks about the third general question will be added, which relates to the consequence of core meltdown accidents:

It continues to be true that "source term" research and development of accident consequence models with special regard to atmospheric diffusion are far from being satisfactorily coordinated. Both in the Federal Republic of Germany and elsewhere it seems to turn up that pressurized water reactors - in a realistic consideration - will not cause early fatalities. The number of "late fatalities from cancer" is determined by application of so many linearly smoothing constants that the dependence on location and time of environmental impacts is practically no longer relevant.

In other words: The determination of accident consequences is based more or less on the multiplicative evaluation of the "source terms".

It can be stated that the methods of "source term" quantification have meanwhile been developed to a satisfactory state. Even if at present an error in the results up to one order of magnitude must be expected the problems at hand can be considered as settled. Consequently, no claims in excess should be made concerning the accuracy of the methods of determination of the accident consequences. In many cases this means that the accident consequence models have to be drastically simplified. Above all, the assumption underlying them must be made much more transparent. In other words: It is logical that the accuracy of determination of effects must be geared to the accuracy of determination of causes.

Not only in the determination of effects but also, generally speaking, in the field of hypothetical accidents it is decisively important that plausible considerations are given priority over comprehensive computer codes which are not capable of providing a clear relationship of causes and effects and whose accuracy cannot be indicated. Generally, the requirement must be made that application of sophisticated codes must not be a substitute for the deeper understanding of relevant relationships or, formulated very globally:

"More transparent individual analyses and less Super Codes!"

Before it can now be explained how we at KfK evaluate the aerosol sources (release from the primary loops into the containment) the main findings of our SASCHA program have to be reported.

SASCHA RESULTS AND THEIR APPLICATION

With the aid of the SASCHA facility, out-of-pile experiments were carried out to study the relevant parameters influencing the fission product release and aerosol formation under LWR core melting conditions. The investigations include:

- size distribution and chemical composition of aerosol particles,
- influence of steam supply and degree of Zircaloy oxidation on the release behavior,
- determination of fractional release rate coefficients,
- fission product release during melt/concrete interaction, and
- estimates of integral values for the release of radioacitvity and aerosol mass from the primary system.

It was found that even from these small scale experiments the integral activity release can be determined with an accuracy better than +/- 15% for specific assumptions on the primary system temperatures.

The SASCHA facility was constructed for melting tests using slightly radioactive samples. The samples were composed of short fuel rods with a simulated burnup and representative amounts of structural material. Above the crucible, a heated aerosol transport line was installed which consists of a 4000 cm^3 glass vessel, an automatic filter changer, a cascade impactor, and a specific iodine filter. By comparing the initial nuclide activities of the sample with those collected on the components of the transport line, the fractional release has been determined as a function of temperature and time.

The most relevant parameters to characterizing the aerosol system (particle size distribution, particle number concentration, mass concentration, and chemical composition of the aerosol particles) have been analyzed by using a 8 stage cascade impactor. The median values for the size distributions of 9 experiments were found to be 0.1 micrometers, and the corresponding geometric standard deviation was 2.13. The particle number concentration was determined to be 10^7 - 10^8 particles/cm^3. As both results did not depend strongly on the variation of the experimental parameters, such as fuel temperature and steam flow rate, they are assumed to be realistic within one order of magnitude. It should be pointed out, however, that the results relate to a very early appearence of the aerosol because its age is equivalent to the short transportation time of the aerosol particles from the melt material to the cascade impactor.

The chemical composition of the aerosol particles was analyzed by use of a X-ray photoelectron spectroscopy. The samples for these analyses were small pieces of 8 different glassfiber filters which had been used for aerosol collection in a release experiment with steam atmosphere and with a maximum fuel temperature of 1900°C. It was found that the aerosol precipitates were composed mainly of the elements Ag, In, Cd, Cs, I, Te, and O. The predominant chemical form of iodine was CsI; in addition, some AgI was identified along with larger amounts of metallic silver. As the cesium concentration in the fuel was ten times higher than that of iodine, the main chemical form of cesium was CsOH. Tellurium and indium were identified as oxides while cadmium was found to occur as hydroxide. Because the aerosol particles are built up by condensation and coagulation, the reported chemical forms can be present together within single aerosol particles. This is expected to occur also in the reactor core where the inhomogeneous temperature distribution will lead to a simultaneous evaporation of elements with even larger differences in the vapor pressure than in the SASCHA crucible. In addition, the aerosol particles emerging from different zones of the core will be mixed up homogeneously by thermohydraulic effects, so that there is no chance to trace the transport of individual elements through the primary system or

even through the containment building.
Therefore, an attempt at precisely calculating the release of individual fission products or structural materials as a function of core temperature and core geometry is assumed to be not trustworthy as it will be explained below.

Two experiments were carried out to investigate the release during melt/concrete interaction with respect to the following questions:

- Do we have to expect the complete release of those highly volatile fission products which may have been retained in the melt until RPV failure?

- Is it possible that some of the low volatile fission products are converted into chemical forms with increased volatility due to oxidation by the steam emerging from the concrete?

It was found that up to 20 % of the iodine had been retained in the fuel during the fast heatup phase. This fraction was nearly completely released within the first 3 minutes of the interaction. A similar behavior is expected for the residual amounts of Kr, Xe, Br, Rb, Cs, and Cd in the core melt after the RPV failure.

The two elements Te and Ag were released by 40 and 60 %, respectively. These numbers are especially significant if the release of these elements inside the pressure vessel is overestimated.

The release of Mo and Ru was found to be very low although both elements can form oxides with increased volatility (MoO_2, RuO_2). To a small degree this effect may have occured for Ru because its release was higher by about a factor of 20 in comparison to release tests in steam without concrete. Nevertheless, as the integral release of Ru and Mo was less than 0.01 % and 0.1 %, respectively, it is concluded that neither element will contribute significant amounts to the total activity release.

Because it is asumed that during a core melt accident major parts of the core will attain a temperature of 2400°C, this temperature was regarded to be most relevant for the determination of a complete set of release rate coefficients. The data set includes the main fission and activation products as well as the most important elements of the structural materials. Because the elements I, Cs, and Cd were almost completely released at temperatures around 2000°C, it was impossible to determine precise release rates at 2400°C. Therefore the value k.GT.0.5 in the Table should be taken as a rough estimate only.
The elements Te, Sb, and Ag were found to have a relatively high volatility in the temperature range between 1900°C to 2200°C. In these cases it was also possible to investigate the temperature dependence of the release rates. The SASCHA data for Te and Sb are lower by a factor of 2 - 3 than the corresponding data of NUREG-0772. Even larger discrepancies were found for the fission products Ba, Zr, and Ru. The value of 10^{-4} min^{-1} for Ba corresponds to release conditions leading to a high oxidation of the Zircaloy cladding. As discussed above, the Ba release rate can be higher by two orders of magnitude if the oxidation is assumed to be low. However, this case is quite unlikely. The low release rates of Ru and Zr resulting from our experiments appear to be much more likely than the values of the

NUREG- 0772 report because of the low vapor pressures of metallic Ru as well as of ZrO_2. Also the formation of highly volatile RuO_2 can be excluded in a steam atmosphere for temperatures higher than 1800°C.

Fractional Release Rate Coefficients at 2400°C in Steam

$$A(T,t)/A_o = \exp(-k(T)\cdot(t/min))$$

Element	k (min^{-1})		Element	k (min^{-1})
I, Cs, Cd	.GT.0.5	a)	Zr	10^{-5}
In	0.2	b)	U	$2\cdot10^{-4}$
Ag	0.14	c)	Np	10^{-5}
Te	0.071	c)	Fe	10^{-3}
Sb	0.043	c)	Cr	10^{-3}
Ba	10^{-4}	c)	Co	10^{-3}
Mo	10^{-4}		Mn	0.01
Ru	10^{-6}		Sn	0.014
Ce, Nd	10^{-5}			

a) estimated value
b) extrapolated from 2200°C
c) k depends on the degree of Zircaloy oxidation
(values in the Table correspond to complete oxidation)

For the low pressure path the integral release of aerosol particles into the containment can be calculated by using the experimentally determined release rate coefficients. This evaluation uses the mean temperature of the dry part of the core as function of time, which is expected due to BOIL calculations.(But it should be mentioned, that this is not very significant for the application of our method). The temperature curve reaches a first maximum of 2200°C while the water level drops down to the lower core support plate. The onset of melting occurs at temperatures between 1900 °C and 2200°C. The melted $(ZrU)O_x$ phases move downwards in terms of a stop-and-go-process: they refreeze in lower and cooler zones which are just above or below the water level and due to an increase of the melting temperature by ongoing oxidation, and they melt again as the core proceeds to dry out. When the core support plate fails, core material slumps down piecemeal and will be quenched by the residual water in the lower part of the pressure vessel. While this water is evaporated the core material melts again. Finally the pressure vessel fails at a melt temperature of about 2400°C. For the calculation of the integral release until RPV failure, the two release phases are substituted by two time intervals of 15 minutes each at 2200°C and 2400°C. Both of these temperatures are significant with respect to the physical core degradation process: 2200°C has been found experimentally in the NIELS facility to be the temperature where the melt inside the partially oxidized claddings breaks through and is poured into the cooling channels. 2400°C is the maximum temperature of the metallic/oxidic two-phase-melt at RPV meltthrough, calculated with the THEKAR code. It is apparent that the total release will be overestimated rather than underestimated by this method. This is even more so because both time intervals are attributed to the whole core mass, ignoring the fact, that substantial parts are cooled by water and steam.

This leads to an integral activity release from the fuel by 16+/-2 % of the radioactive core inventory. About 16 % of this amount (which is more than a 0.99 fraction) is due to the release of the 9 elements Kr, Xe, Br, I, Rb, Cs, Se, Te, and Sb.

The small relative uncertainty was estimated by means of some rather simple arguments which - among other aspects - consider also the surface to volume ratio of the small scale SASCHA experiments and the use of fuel with simulated burnup. The highly volatile fission products are mainly released during or prior to the first time interval of 15 min duration at 2200°C. The fuel rods are mostly unmolten under these conditions. But when the fuel melts the former physical structure of the fissium pellets has no longer any influence on the release rates. Hence an overestimation of the release comes into question only if large fractions of the core do not participate in the melting process. This case is excluded, however, since it is intended to determine enveloping release data which are valid for a broad spectrum of core melt accidents. On the other hand, there is no danger of underestimation, because an almost complete release of the highly volatile fission products was assumed (100 % for Kr, Xe, Br, I, Rb, Cs; 80 % for Se, Te, and 53 % for Sb).

The less volatile elements, e.g. Ba, Ru, Ce, are essentially released at the highest temperatures, i.e. from the liquid melt. Because of the high surface to volume ratio of the melt in the SASCHA tests, the measured release is rather too high than too low. Finally, it should be mentioned that also the assumption of a 15 minutes temperature plateau at 2400°C for the whole core mass is highly conservative.

The integral mass of the released aerosol particles from the primary circuit was calculated in a similar way. By using a minimum/maximum approach for the calculation it was found that the aerosol mass emerging from the primary system will be in the range of 700 kg - 3500 kg. As the additional amount of aerosol generated by the melt/concrete interaction is not sufficiently known at present, and as an uncertainty factor of 4 in the aerosol mass is not extremely relevant as mentioned above, it is recommended to use an integral mass of 3500 kg for the calculation of the aerosol behavior in the containment building for the low pressure path of a German type 1300 MW_{el} PWR. Removal inside the primary system is ignored because of the lack of knowledge about resuspension mechanisms during steam explosions and subsequent water hammers.

Quite different with many respects is our method to evaluate the particle mass release into the containment during the high pressure path scenario (e.g. complete station power blackout). In this case the flow rates through the pressure relief valve behind the pressurizer (which shuts and opens alternating until it sticks open when the pressure is stabilized at about 170 bar) are much less than that during the low pressure path. Assuming the same particle generation rate from the melting fuel, this would lead to a significant higher particle mass concentration inside the primary system. It is experimentally evident, that particle mass concentrations higher than 150 g/m^3 are physically not possible. To assuming a constant mass concentration of 200 g/m^3 is therefore rather conservative. Using the SASCHA data as described above to obtain the relative element specific composition of the aerosol particles and combining this with the "leak rate" into the

containment gives us the upper limit of the integral aerosol release into the containment until RPV failure. By this trick we are not obliged to take care either of particle plate out effects on the primary circuit walls or of possible resuspension effects during the virulent depressurization after RPV failure and the subsequent accumulator flooding. In addition the biological shield will fail, causing in turn the ejected fuel debris to be flooded by the sump water. The question whether the flooded core debris can be cooled or can not be cooled remains still open. Nevertheless, we assume the underwater release of the remainder of the highly volatile elements I and Cs up to a 100 %. I and Cs will dissolve in the sump water. The iodine model is then applied to the I_2 release from the liquid suspension.

Based on this technical background one can summarize the philosophy at KfK/PNS behind the evaluation of aerosol sources related to PWR core meltdown accidents.

PHILOSOPHY AND CONCLUSION

Not only the release of radioactivity from the primary circuit is of interest with a view to the source term but likewise the release of non-radioactive masses as gas and particles. Besides a number of parameters concerning geometry, thermodynamics and e.g. leakages, the removal behavior of an aerosol system in the safety containment is influenced essentially by the number concentration of the airborne particles, the statistical probability density function of their diameters, the particle density, the particle shape, the solubility in water of the particles, and by a number of other aerosolphysical variables. The radioactivity of the particles plays a minor role in this context; this applies also to the internal heat sources generated by postdecay processes. Given the high particle number concentration - as typical of core melt accidents - the rate of coagulation is so high that particle composition soon undergoes macroscopic homogenization. As a matter of fact, local differences in the compartments of the safety containment regarding aerosol concentration, velocity and direction of flow, thermodynamic state etc. can neither be taken into account in aerosol codes. It is rather necessary to assume homogeneous conditions at least for each reference volume. Compared to the quick processes of homogenization, the residence time of particles in the reference volume considered is always very long. The foregoing arguments lead us to the fomulation of

> Principle 1:
> In all phases of aerosol transport the elements must be assumed to be homogeneously distributed both on the aerosol particles and within individual reference volumes. The major fraction of aerosol mass is not made up of the radiologically important fission product nuclides but of the long-lived and stable isotopes of the fission products (Cs-133, Cs-135, I-129), of the fuel (U-238), and of the structural materials (above all those of Sn, Mn, Fe, Cd, In and Ag).

Core degration follows the steadily falling water level. Aside from the fact that core components may fall into the residual water both as solids and as liquids where release through evaporation is spontaneously stopped, higher temperatures than in the zone immediately above the water level will occur in the upper dry core region (inasmuch as it still exists). Besides on the stochastic slumping processes, the precise temperature distribution depends

on the decay heat produced by the single rod and, obviously, also on the geometry dependent Zr/H_2O-reaction. The axial temperature distributions differ radially in the core zone. It results from this fact that in the whole dry core zone always simultaneous evaporation takes place of highly volatile elements in various forms of oxidation (bottom and external parts) and of little volatile elements (top and internal parts). The little volatile elements form condensation aerosol particles after short transport paths already (order of magnitude: cm). The highly volatile elements on their way first pass rising temperature fields which means that they condense later. Particles already present serve as heterogeneous condensation nuclei. On account of the high particle density a violent process of agglomeration takes place in addition. This leads us to the formulation of

Principle 2:
In the course of core degradation heterogeneous condensation and coagulation in the dry core zone are so violent that possible knowledge of particle release from the core zone which is specific to an element or even isotope and dependent on location and time is an information, which is not necessary. As a matter of fact, the uncertainties in the determination of temperature distribution and the stochastic nature of core slumping are precluding anyway prediction of a location and temperature dependent rate of evaporation according to the present state of knowledge.

A noticeable release of activity takes place at the earliest when the water level attains the upper core edge. It depends on the events preceding the accident which system pressure prevails at that point in time in the reactor pressure vessel (RPV) and which decay heat power is still available in the core. For PWR equipped plants of the 1000 MWe class complete evaporation of the RPV beginning at the point in time indicated always occurs within about one hour, independent of the history. This means that gas and aerosol particle release from the primary circuit is strictly limited in time compared with the duration of the time sequence after release into the safety containment. This leads us to the formulation of

Principle 3:
Modeling of the time function for the release of mass from the primary circuit is of secondary importance as compared with the integral mass release into the safety containment.

The following considerations will show that, considering the present state of knowledge, it is an unreasonable endeavor to calculate aerosol depositions in the primary circuit with the help of computer codes. But there are still other arguments opposing it: The surface of all airborne particles in the RPV (residual water level e.g. in the center of the core) is higher by one or more powers of ten than the surface of the structures and walls. Consequently, the interactions of particles greatly outbalance those of particles and walls. In addition, depositions on solid walls are much slower processes than interactions of particles with number concentrations of more than $10^6 cm^{-3}$. Obviously, potential interactions also depend decisively on the chance the particles have to get into the immediate neighborhood (diffusion zone) of walls. If the steam evaporation rate is relatively high (double ended break) the particle residence time in the primary circuit is very short so that noticeable depositions on the walls can be excluded. More time will be available on the high pressure path. To be able to model realistic-

ally the depositions on internal structures (especially in the upper RPV plenum) one would have to calculate the actual path of particles or particle clouds with vortexes, dead water zones, flow reversals, etc. This in turn would call for a fine nodal network for thermohydraulics calculations of the RPV. The present state of the art in thermohydraulic codes may permit much, but it does not permit that! One of the reasons is that because of lacking knowledge of slumping exact time functions cannot be determined for residual water evaporation rates and still less for local flow distributions of steam and H_2. But even if one succeeded in calculating depositions on walls and structures of the primary circuit, they could not be used until it would be possible to calculate potential resuspensions as well. But no approach whatsoever is presently recognizable in aerosol physics to do this calculation. The situation is likewise unclear for the high pressure path of a core melt accident in which, until depressurization of the primary system, several 100 kg of particle material are initially deposited on the walls. It is also a question still to be answered which fraction of it is entrained or detached when the accumulators are evacuated shortly after RPV failure. For the low pressure path, even on optimistic assumptions, a retention of not more than 50% is considered possible today. This factor 2 disappears completely in the uncertainty range of knowledge of events taking place in the RPV. This eventually leads us to the fomulation of

Principle 4:
On account of the complexity of events taking place in the RPV it seems impossible, considering the present state of knowledge, to model particle depositions in the primary circuit in a realistic way. Therefore, physically justifiable, plausible assumptions should be preferred to any such attempt.

In the majority of release categories the fission product elements iodine, cesium and tellurium are predominantnly responsible for the radiological consequences; tellurium, inter alia, because a decay product of one of its isotopes is a highly radiotoxic iodine nuclide (I-132). Iodine and cesium are released by 100% from the fuel and tellurium by 50 to 80%. Release of these elements into the environment is determined to a much greater extent by their physical and chemical behavior in the safety containment, in the annulus, and in the adjacent compartments than by their behavior in the primary circuit. An important role play aerosol removal, washing water-soluble precipitates off the walls, chemical reactions in the sump water and in the gas phase, and the vapor pressure of the resulting iodine compounds. The (very optimistic) retention factor 2_6 indicated before for the primary system is contrasted e.g. by a factor 10^6 for the safety containment in release category FK6. This leads us to the formulation of

Principle 5:
The radiologically important elements iodine and cesium are released by 100% from the fuel.
Retention in the safety containment and in other compartments of the plant is higher by several orders of magnitude compared with the primary circuit. Therefore, the physical and chemical behavior of these elements, after they have left the primary system, plays the decisive role for their release into the atmosphere. The situation is similar for tellurium which is released by 50-80% from the fuel.

A completely different argument should be mentioned in this context: In the

so-called "worst case" of the new release category 6 (300 cm^2 leak in the safety containment after attainment of 9 bar, direct release from the annulus in the absence of filters) less than 10^{-4} of the iodine inventory is released.

This corresponds to a release of 0.08 g I-131 and an activity of about 10^4 Ci, respectively. The following ingestion dose factor can be assumed for I-131 taken in with the food: $g_i = 1.55 \times 10^7$ rem/Ci. Consequently, a fictitious cumulative dose for the ingestion case of 1.55×10^{11} rem can be calculated from 10^4 Ci (undistributed). In conformity with ICAP 26 a number of 1.25×10^{-4} fatalities per rem was assumed in Phase A of the Risk Study. So, if one suitably distributed 0.08 g I-131 with the food among a sufficiently great number of the population, the result would be 19.4 million late fictitious cancer fatalities. But actually the parameters included in the Accident Consequence Model (not to be treated here) imply that the real number of late fatalities from cancer caused by the ingestion of iodine is lower by up to 10^7 times. Similar considerations can be made for other fission and decay products. Consequently, the following statement can be formulated as

Principle 6:
The retention of activity (except for gases) in the safety containment and in adjacent compartments attains several orders of magnitude (10^4 to 10^5 for FK 6). The funcitons describing the distribution towards the outside as well as emergency protective measures and other elements allowing to evaluate the consequences of accidents produce a "dilution effect" which, related to the population dose, likewise adopts many orders of magnitude (e.g. 10^7). The wish to develop computer codes necessitating much work in terms of modeling theory and high costs with which retentions in the primary circuit by the factor 2 to 3 could be calculated seems negligible with this background! This is true for related large scale experiments too.

ADDITIONAL LITERATURE

W. Braun, K. Hassmann, H.H. Hennies and J.P. Hosemann "The Reactor Containment of German Pressurized Water Reactors of Standard Design", Proceedings of the International Conference on Containment Design, June 17-20, 1984, Toronto, Ontario

H. Albrecht, H. Wild "Review of the Main Results of the SASCHA Program on Fission Product Release under Core Melting Conditions" ANS Meeting 'Fission Product Behavior and Source Term Research', Snowbird, July 15-19, 1984

J.P. Hosemann "The KfK/PNS Perspective on Fission Product Behavior and Source Term Research" ANS Meeting 'Fission Product Behavior and Source Term Research", Snowbird, July 15-19, 1984

J.P. Hosemann, D. Haschke "DEMONA: Aerosol Removal Experiments", EIR-Bericht Nr. 505, November 1983

K. Hassmann and J.P. Hosemann "Consequences of Degraded Core Accidents", Nuclear Engineering and Design 80 (1984) P. 285 - 99

THE CHARACTERISATION OF AG-IN-CD CONTROL ROD AEROSOLS GENERATED AT TEMPERATURES BELOW 1900K

J P Mitchell, A L Nichols, J A H Simpson

Technology Division, AEE Winfrith, Dorchester, Dorset, UK

ABSTRACT

Any substantial quantities of aerosol generated during the relatively early stages of a severe accident in a light water reactor will originate from the volatile components of the reactor core. These aerosols will be formed by vapour condensation in superheated steam. In a series of experiments at AEE Winfrith emphasis has been placed on the formation of such aerosols from the control rod alloy (80Ag-15In-5Cd). The cadmium component is particularly volatile, and studies have been made of the release of this material. In some of the experiments 4 cm lengths of the control rod alloy have been sealed in 304 stainless steel tubes and heated until they burst. Temperatures up to 1900K were achieved by means of an induction furnace. Aerosols were formed immediately after the failure of the stainless steel tube. These aerosols were sampled on to Nuclepore filters and their aerodynamic size distribution was measured by inertial spectrometers. Deposition foils were used to collect debris for microscopic examination and elemental analysis. An assessment was made of the elemental distribution following this release, and these data were compared to the deposition behaviour of cadmium and control rod alloy vaporised from an open system.

INTRODUCTION

Many light water reactors operate with control rods made of 80Ag-15In-5Cd alloy clad in 304 stainless steel. There is approximately 2800 kg of control rod alloy distributed through the reactor core and it would constitute a major source of volatile material in a severe reactor accident. The stainless steel will fail at a relatively low temperature, and the resultant release of the control rod materials could affect fission product transport in the primary circuit and the containment [1]. Unoxidised Zircaloy guide tubes will form low-melting eutectics with indium and silver (1520K [2]), and relatively high concentrations of aerosol containing cadmium, indium and silver may be generated.

The Ag-In-Cd alloy melts at 1100K and will not damage the core so long as this molten material remains within its cladding. However, at approximately 1700K the cladding will fail, and the subsequent behaviour of the alloy will depend upon the accident sequence. If the circuit has become depressurised, the high vapour pressure of cadmium at these temperatures (approximately 10^7 Pa) will result in a relatively violent expulsion of cadmium vapour and molten silver-indium when the cladding fails. Most of the liquid alloy will flow down the space between the cladding and Zircaloy guide tubes to cooler regions of the core. The possibility of any aerosol formation will depend on temperature, pressure and the highly localised concentrations of cadmium vapour. Any resultant mixture of vapour-aerosol could react with fission product vapours, along with tin, manganese and boric oxide generated at higher temperatures from the Zircaloy cladding, stainless steel and boric acid. Published data characterising this type of behaviour are very sparse. The recent experiments of Parker et al [3] support earlier evidence for eutectic formation between silver and Zircaloy. They have also reported cadmium aerosol data in a hydrogen-argon atmosphere [4], formed by the condensation of cadmium vapour generated by a plasma torch.

Significant fission product attenuation by high density aerosols has been proposed [5], but this is difficult to quantify. A programme of work is currently underway at AEE Winfrith to generate these aerosols and assess their effects. The initial studies have concentrated on behaviour of the control rod elements in an argon atmosphere.

EXPERIMENTAL PROCEDURE

A 40 kW, 25 kHz induction furnace with a tantalum susceptor has been used to heat cadmium powder, and clad and unclad control rod alloy up to approximately 1900K (Figure 1). The sample was contained in a silica glass vessel (volume of 4.5×10^{-3} m^3) containing zirconia insulation, but with a relatively open geometry. Two distinctly different sampling systems were used, depending upon the proposed analysis:

(i) Zircaloy foils were located immediately above the heated sample and within the tantalum susceptor, and a Zircaloy-lined thermal gradient tube (450 mm long and 25 mm diameter) was attached to the exit port of the glass containment;

(ii) a dilution chamber (volume of 0.053 m^3) was attached to the exit port for rapid sampling to achieve some degree of aerosol stabilisation prior to analysis.

High purity argon (< 5 ppm oxygen) was introduced at the base of the silica glass vessel, and a flow rate of 0.002 m^3 min^{-1} was maintained for 1 h before and during each experiment. The flow rate of the carrier gas through the apparatus was measured by a mass flow meter calibrated to an accuracy of 5%.

The unclad samples of cadmium powder and control rod alloy were heated in open alumina crucibles that were held in position on a zirconia platform. The clad control rod alloy (40 mm long and 8.75 mm diameter) was held in the vertical position with a zirconia insert (Figure 1). In order to minimise any extraneous aerosol, the apparatus was heated up to the planned maximum temperature without the sample. The system was then allowed to cool before being dismantled, cleaned and reassembled with the sample. Thermocouples were used to monitor the sample temperature, the gas temperature immediately above the sample, the gas and foil temperatures in the thermal gradient tube, and the gas temperature in the dilution chamber.

Experiments were carried out in an argon atmosphere and are listed in Table 1. In experiments 1 to 6 emphasis was placed on obtaining representative micrographs of the deposits collected on the various Nuclepore filters and in the thermal gradient tube. This was done by means of an SEM/EDAX system (scanning electron microscopy/energy dispersive analysis of x-rays), which was also used to determine the elemental composition of the deposits for comparison with the corresponding data from standard analytical techniques. The resulting micrographs were used to measure the primary particle size distribution of any aerosol using a Zeiss TGZ 3 particle counter. On average 150 particles were sized from each micrograph. In experiments 7 to 10 the dilution chamber was used to stabilise any aerosol agglomerates that were formed. The aerosol was collected in the chamber over a 45 sec period before the chamber was isolated for aerosol analysis. The aerodynamic particle size distribution of the resulting agglomerates was measured by means of an inertial spectrometer [6] and a Stöber spiral duct centrifuge [7, 8], and additional samples were collected on Nuclepore filters for microscopic studies. Any other debris such as ruptured cladding and severely damaged Zircaloy were examined, and the glass vessel and zirconia insulation were washed with 20% HNO_3 to give additional mass balance data.

RESULTS

Experiments 1 and 2 with the cadmium powder were carried out at relatively low temperatures (1080K) and produced deposits in the thermal gradient tube that had a crystalline structure, with no evidence of aerosol formation, agglomeration and deposition (Figure 2). No interaction was observed between the cadmium vapour and the various deposition foils.

Table 1: Experimental Arrangement and Particle Size Analysis

Experiment	Sample	Maximum Temperature K	Geometry	Aerosol Particle Size Analysis	
				Primary	Agglomerates
1	Cd powder (121 mg)	1080	A	NA	NA
2	Cd powder (38 mg)	1080	A	NA	NA
3	unclad alloy (24 g)	1700	A	NA	NA
4	unclad alloy (24 g)	1870	A	NA	NA
5	clad alloy (24 g)	1750	A	✓	✓
6	clad alloy (24 g)	1690	A	ND	ND
7	clad alloy (24 g)	1760	B	✓	ND
8	clad alloy (24 g)	(∿ 1720)	B	✓	✓
9	clad alloy (24 g)	1750	B	✓	✓
10	clad alloy (24 g)	1550	B	ND	✓

A, thermal gradient tube
B, aerosol dilution chamber

NA, not applicable
ND, not determined

Experiments 3 and 4 with unclad alloy generated a mixed deposit of crystals and spherical particles along the thermal gradient tube. When the sample was heated to 1700K this mixed deposit consisted almost entirely of cadmium with very little trace of indium (< 1% by weight) and silver (< 0.2% by weight). However, mass balance data indicated that 90% of the cadmium and approximately 10% of the indium and silver had evaporated from the crucible, and it is believed that the indium and

silver plated out on the zirconia insulation. This effect was even more pronounced for the sample heated to 1870K, when 99.99% of the cadmium, 25% of the indium and 10% of the silver evaporated from the crucible, although the resultant deposit in the thermal gradient tube was predominantly cadmium with only traces of indium and silver.

When the control rod alloy was sealed in 304 stainless steel, the cladding burst between 1550 and 1760K with a significant release of material. The Zircaloy cylinder close to the sample (Figure 1) was damaged extensively during all of these experiments. A high concentration of vapour was ejected from the break and condensed rapidly to form an aerosol. In experiments 5, 6 and 7 the cladding failure occurred in the sidewall, and EDAX indicated that the resulting aerosol was composed almost entirely of cadmium. Efforts were made to achieve a mass balance, and the data for experiment 5 are given in Table 2. Approximately 95% Ag, 99% In and 75% Cd fell into the catchpot, and the airborne debris consisted almost entirely of Cd. The imbalance in the data for silver was attributed to the absorption of this element into the zirconia insulation. The aerosol that was generated in these experiments consisted of spherical particles (Figure 3) that differed from the more irregular crystalline debris produced by the unclad alloy. These small primary particles had a visual mean diameter of 0.32 μm with a geometric standard deviation of 1.6.

Table 2: Mass Balance following Cladding Burst (Experiment 5): Control Rod Elements

	Ag	In	Cd
Initial weight of specimen (g)	19.1	3.6	1.2
Debris in catchpot (g)*	18.1	3.5	0.9
Vapour deposit-aerosol (g)	0	0	0.26

*also significant quantities of zirconium

The cladding failure occurred at the top endcap in experiments 8 and 9, and significant quantities of silver were found in the resulting aerosol (as much as 20% in some samples analysed by EDAX). The primary particles of the mixed cadmium-silver aerosol exhibited similar physical characteristics to the cadmium aerosols observed in experiments 5, 6 and 7. These submicron particles agglomerated in the dilution chamber to produce long and complex chain-like structures containing from 50 to 300 primary particles per agglomerate (Figure 4). The agglomerates had a log normal particle size distribution with an aerodynamic mass median diameter (AMMD) of 3.2 μm and a geometric standard deviation of 1.6 as measured with the Stober spiral duct centrifuge. A lower AMMD of 1.2 μm was measured using

the inertial spectrometer, and further efforts are required to improve the sampling procedures for both instruments in a closed argon atmosphere. In experiment 10 failure occurred at the bottom endcap. All of the indium and silver were deposited in the catchpot and only a small amount of cadmium vapour-aerosol was transported to the dilution chamber.

In the clad experiments the extent of aerosol formation and the resulting elemental composition were dependent on the location of clad failure. A break in the sidewall directed the vapour-liquid jet towards the Zircaloy cylinder and this resulted in the liquid phase flowing down into the catchpot (experiments 5, 6 and 7); failure at the top of the sample forced the jet away from the surrounding structures, and significant quantities of the silver were transported into the thermal gradient tube with the cadmium (experiments 8 and 9). Although these experiments show that the aerosol source term depends on the failure mechanism, the resulting data can be used to calculate a maximum vapour-aerosol concentration for the apparatus of approximately 100 g m^{-3} if the initial burst release is confined to the silica vessel (volume of 4.5 x 10^{-3} m^3).

DISCUSSION

The experiments were carried out in a reaction vessel containing argon at atmospheric pressure. This environment does not represent conditions in the reactor core during a severe accident, and future work will include the addition of hydrogen and steam. In some accidents the primary circuit pressure will remain at a relatively high value as the fuel degrades, whilst in other circumstances the pressure will drop to below 10^6 Pa. Other complications involve the steam oxidation of Zircaloy which affects the silver release from the core.

Unclad Cadmium Powder

The crystalline appearance of the cadmium debris in the thermal gradient tube (Figure 2) supports a vapour deposition process rather than aerosol formation. The cadmium vapour begins to condense when its vapour pressure in the inert carrier gas exceeds the saturated vapour pressure corresponding to the temperature of the metal surface in the thermal gradient tube. Under these conditions an equation can be derived [9] that relates the mass deposited M_a (gmol m^{-2}) to the temperature T (K):

$$M_a = -\frac{\alpha}{T^2} \cdot \exp(-\Delta H/RT)$$

where ΔH is the latent heat of vaporisation of cadmium (J $gmol^{-1}$) and R is the universal gas constant (J K^{-1} $gmol^{-1}$). The factor α is dependent on the experimental conditions. The data for experiment 1 are plotted in Figure 5 and show reasonable agreement with this theoretical prediction for a simple vapour condensation process.

Unclad Control Rod Alloy

Figure 6 shows the vapour pressures of cadmium, indium and silver as functions of temperature in accordance with Raoult's law of partial pressures. These calculations give a fractional release per min of 100% Cd, 3% In and 0.2% Ag inventories at 1700K, and 100% Cd, 15% In and 1% Ag inventories at 1870K. These data have been compared with the experimental observations. There was some enhancement of the silver and indium release fractions in the laboratory studies at these temperatures, and examination of the subsequent debris in the thermal gradient tube indicated a vapour transport and deposition process. These experiments support the assessment by Wichner and Spence [10] in terms of solution formation and Raoult's law for a system in equilibrium.

Clad Control Rod Alloy

Apart from one experiment the 304 stainless steel failed between 1690 and 1760K, when the cadmium vapour pressure inside this container was approximately 10^7 Pa (Figure 6). This is much higher than the vapour pressures of indium and silver (approximately 10^3 Pa for both elements). These data have been used to calculate the fractional inventory released as a function of temperature (Figure 7). The elements will only be released after the rod has ruptured and on this basis most of the cadmium should be emitted as the cladding bursts, together with 3% per min of the indium and 0.25% per min of the silver inventories. Any subsequent interaction with the Zircaloy will change the elemental composition of the airborne material that leaves the silica vessel. Despite this effect, the vapour pressure calculations show that the vapour-aerosol release per min at 1720K would consist of 88% Cd, 8% In and 4% Ag. This interpretation of the data is acceptable for such a short length of control rod alloy heated isothermally, but a direct extrapolation in terms of this release mechanism would not be appropriate for a full length control rod.

A plasma torch has been used by Parker et al [4] to generate cadmium metal aerosols that have an average primary particle diameter of 0.27 μm, 200 primary particles per agglomerate and an agglomerate AMMD of 8.6 μm as measured with a LASL spiral duct centrifuge. The aerosols formed in the majority of the clad control rod experiments consisted mainly of cadmium, and the primary particle size distribution was in good agreement with the data of Parker et al. However, the agglomerates formed during a 45 sec period after the cladding failed had a lower AMMD of 3.2 μm as measured by the Stöber spiral duct centrifuge and 1.2 μm as measured by the inertial spectrometer. The AMMD ranges of the Stöber spiral duct centrifuge and inertial spectrometer are 0.08 to 5 μm and 1 to 10μm respectively. Larger particles will not enter these analysers, and further efforts are required to measure the AMMD unambiguously. Steam condensation effects also need to be examined, and experiments have been proposed to determine if the large chain agglomerates lose this fine structure in a similar manner to UO_2 and metal oxide aerosols in steam [11, 12].

CONCLUSIONS

Ag-In-Cd control rods will be a major source of vapour release from the core at approximately 1720K, the temperature at which 304 stainless steel cladding fails. The temperature profile of the core will induce sidewall failure of the cladding: liquid indium and silver will flow to cooler regions of the core and cadmium will be the dominant vapour-aerosol release.

The precise form of any release (vapour/aerosol) will depend on many factors including the primary circuit pressure.

(i) When the 304 stainless steel clad melts at high circuit pressures, the vapour species from the control rod alloy will be transported at a relatively slow and uniform rate. The unclad alloy experiments suggest a simple vapour transport and surface condensation mechanism, although the mass balance data for indium and silver indicate some deviation from Raoult's law of partial pressures.

(ii) At low circuit pressures high concentrations of cadmium vapour will be rapidly released when the 304 stainless steel clad ruptures at 1720K. This supersaturated vapour produces an aerosol composed of spherical submicron particles (visual mean diameter of 0.32 μm) which agglomerate rapidly in argon to form complex chain-like structures (aerodynamic mass median diameter of approximately 3.2 μm). The formation of such extensive agglomerates is questionable in a steam environment, and further studies are desirable in an atmosphere containing superheated steam.

ACKNOWLEDGEMENTS

The authors wish to thank B R Bowsher, G R Brown, A F Kingsbury, N A Rowe and A R Taig for assistance and helpful discussions during this work.

REFERENCES

1. Gittus, J. H., PWR Degraded Core Analysis, ND-R-610(S), 203, 1982.

2. Hagen, S., Experimental Investigations of the Meltdown Phase of UO_2-Zircaloy Fuel Rods under Conditions of Failure of Emergency Core Cooling, PNS Progress Report 1978(2), KfK 2750, 90, 1979.

3. Parker, G. W., Creek, G. E., Sutton, A. L., in ORNL LMFBR Aerosol Release and Transport Program Quarterly Progress Report for July-September 1981, Editors: T S Kress, M L Tobias, NUREG/CR-2299 Vol 3, 18, 1982.

4. Parker, G. W., Creek, G. E., Sutton, A. L., in ORNL Aerosol Release and Transport Program Quarterly Progess Report for October-December 1981, Editors: R E Adams, M L Tobias, NUREG/CR-2299 Vol 4, 12, 1982.

5. Levenson, M., Rahn, F., Realistic Estimates of the Consequences of Nuclear Accidents, Nucl. Tech. 53, 99, 1981.

6. Prodi, V., Melandri, C., Tarroni, G., de Zaiacomo, T., Formignani, M., Hochrainer, D., An Inertial Spectrometer for Aerosol Particles, J. Aerosol Sci, 101, 411, 1979.

7. Stöber, W., Flachsbart, H., Size-separating Precipitation of Aerosols in a Spinning Spiral Duct, Environ. Sci. Technol., 3, 1280, 1969.

8. Smith, A. D., An Assessment of a Spiral Duct Centrifuge Using Standard and High Concentration Aerosols, AEEW - M 2077, 1982.

9. Bowsher, B. R., Dickinson, S., Nichols, A. L., High Temperature Studies of Simulant Fission Products: Part I, Vapour Deposition and Interaction of Caesium Iodide, Caesium Hydroxide and Tellurium with Stainless Steel, AEEW - R 1697, 1983.

10. Wichner, R. P., Spence, R. D., Quantity and Nature of LWR Aerosols Produced in the Pressure Vessel During Core Heatup Accidents - A Chemical Equilibrium Estimate, NUREG/CR-3181, 1984.

11. Bunz, H., Schöck, W., Measurements of the Condensation of Steam on Different Aerosols under LWR Core Meltdown Conditions, Proceedings of the CSNI Specialists Meeting on Nuclear Aerosols in Reactor Safety, Gatlinburg, Tennessee, NUREG/CR-1724, 171, 1980.

12. Schöck, W., Mercier, O., Fromentin, A., Friedrich, G., Generation and Properties of Highly Concentrated Metal Oxide Aerosols in a Steam Atmosphere, J. Aerosol Sci., 15, 341, 1984.

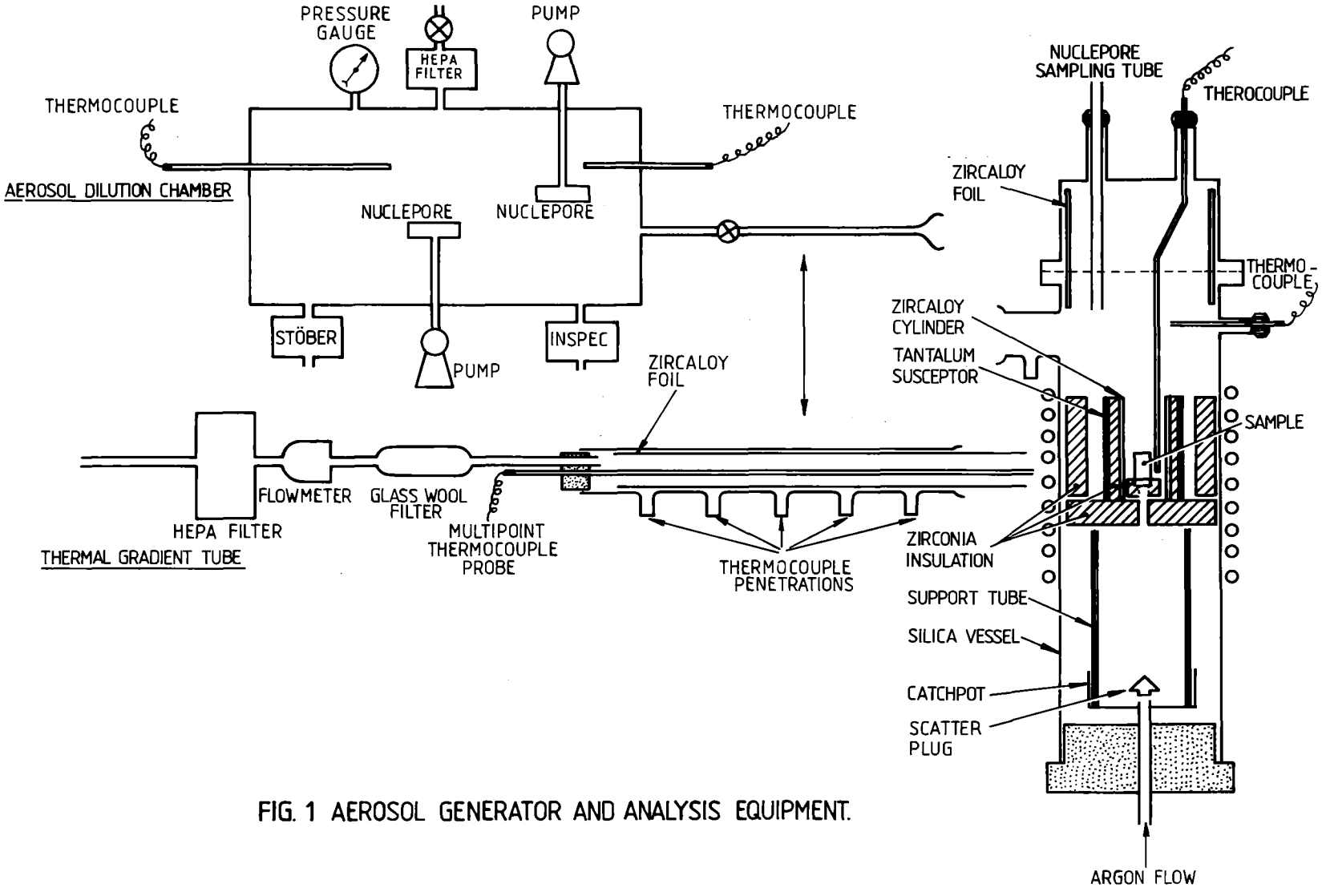

FIG. 1 AEROSOL GENERATOR AND ANALYSIS EQUIPMENT.

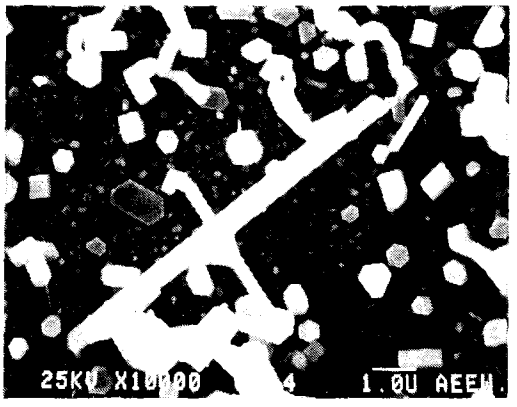

WALL TEMPERATURE 413K

WALL TEMPERATURE 373K

FIG. 2. EVAPORATION OF CADMIUM FROM AN OPEN CRUCIBLE: DEPOSIT ALONG THERMAL GRADIENT TUBE

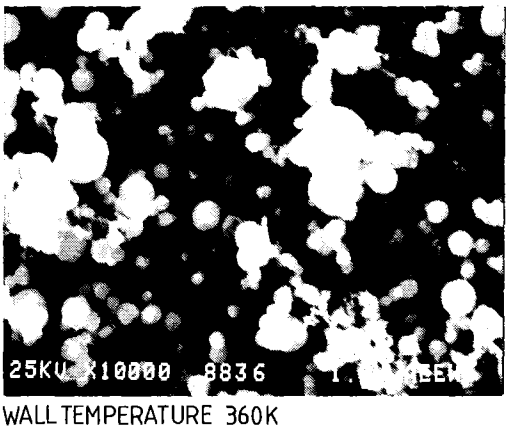

WALL TEMPERATURE 360K

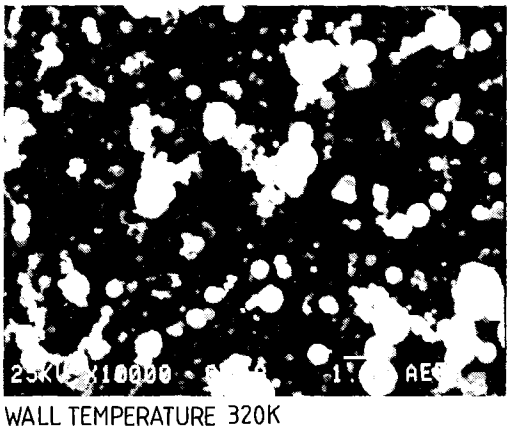

WALL TEMPERATURE 320K

FIG. 3. CADMIUM CONTROL ROD AEROSOL FROM BURST CLADDING: DEPOSIT ALONG THERMAL GRADIENT TUBE

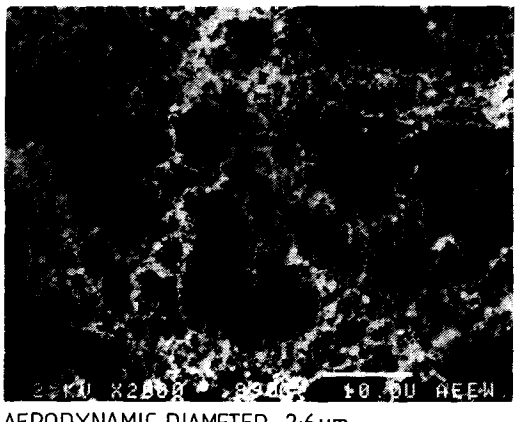

AERODYNAMIC DIAMETER 2·6μm

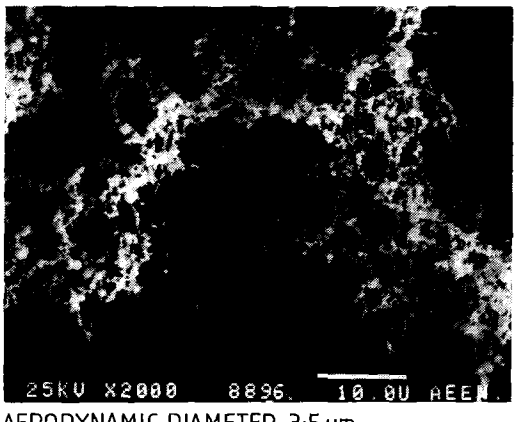

AERODYNAMIC DIAMETER 3·5μm

FIG. 4. CADMIUM-SILVER CONTROL ROD AEROSOL FROM BURST CLADDING: DEPOSIT ON NUCLEPORE FILTER OF THE INERTIAL SPECTROMETER

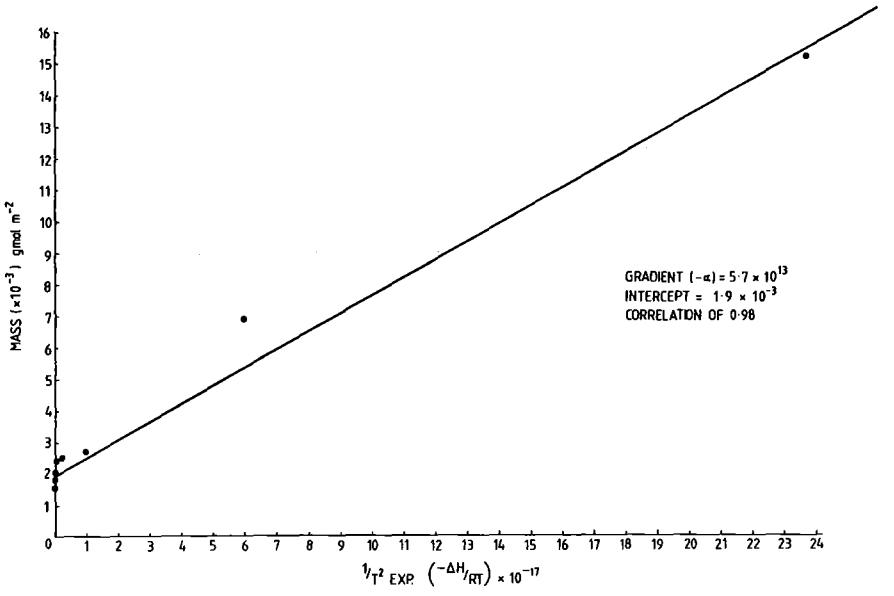

FIG.5 CADMIUM MASS DEPOSITED AS A FUNCTION OF $^{1}/_{T^2}$ EXP $\left(^{-\Delta H}/_{RT}\right)$

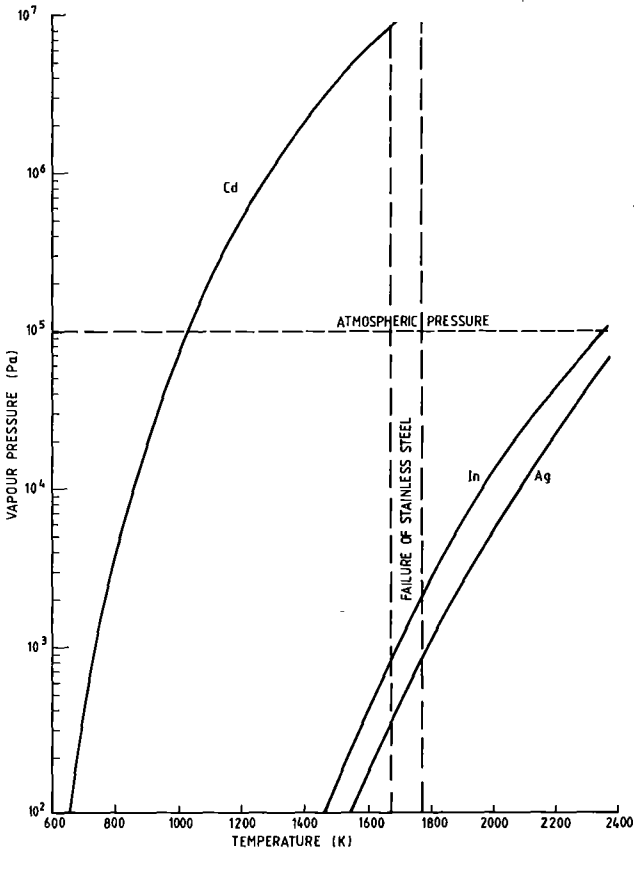

FIG.6 VAPOUR PRESSURE OF CONTROL ROD ELEMENTS AS A FUNCTION OF TEMPERATURE.

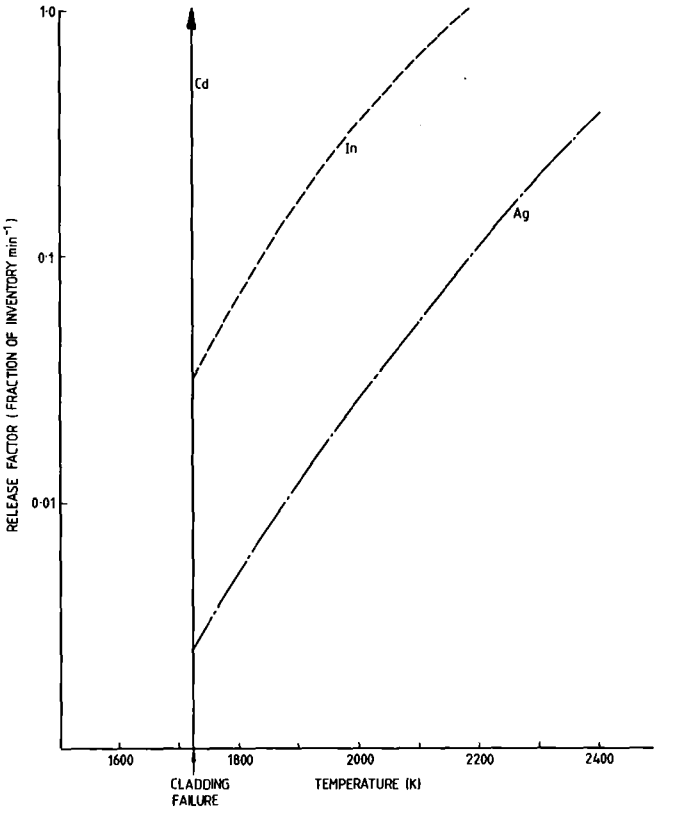

FIG.7 RELEASE FACTOR (FRACTION OF INVENTORY) OF CONTROL ROD ALLOY CONSTITUENTS (24g) FOR A SEALED SYSTEM AS A FUNCTION OF TEMPERATURE

Winfrith

CHEMICAL STATE EVALUATION OF THE CONSTITUENTS OF AEROSOL PARTICLES FORMED IN LWR CORE MELTING EXPERIMENTS

H. Moers, H. Klewe-Nebenius, G. Kirch
G. Pfennig, and H. J. Ache
Kernforschungszentrum Karlsruhe, Institut für Radiochemie
Postfach 3640, 7500 Karlsruhe, FRG

ABSTRACT

The investigation of aerosol samples collected during the laboratory scale simulation of a pressurized water reactor core meltdown by use of X-ray photoelectron spectroscopy (XPS) permitted the chemical speciation of the detected aerosol constituents silver, cadmium, indium, tellurium, iodine, and cesium. The aerosols were released in a steam atmosphere over a temperature range of 1200 - 1900 °C of the melting charge, which corresponds to the heat-up phase of a core meltdown accident.

A comparison of the elemental analysis results obtained from XPS with those achieved from electron probe X-ray micro analysis (EPXMA) revealed differences between the composition of the aerosol surface and the bulk composition of those aerosols, which were collected at higher melting charge temperatures. This is explained by differences in volatility of the aerosol constituents. The transition between surface and bulk composition could be confirmed using XPS in combination with argon ion bombardment.

INTRODUCTION

A severe nuclear light water reactor (LWR) accident can result in the meltdown of the reactor core. This is assumed to occur after a loss-of-coolant accident with subsequent failure of the emergency core cooling system (1). The core meltdown will be accompanied by the release of various core constituents, i. e. fission and activation products and inactive structural materials. This release will take place in either gaseous form (e. g. noble gases) or as aerosol particles which result from vaporization and recondensation of part of the core constituents (2).

Knowledge about the composition of the aerosols and especially the chemical speciation of their constituents is important in order to estimate the hazard potential caused by a hypothetical LWR core meltdown. Aerosols provide a relatively large surface compared to their volume, which increases the importance of surface effects.

X-ray photoelectron spectroscopy (XPS) is an analytical technique, which allows elemental analysis and also chemical speciation, the latter being a consequence of varying chemical shifts of the photoelectron and Auger electron kinetic energies of different compounds of the same element (3). Furthermore, the information depth of XPS is only a few nanometers, making it sensitive to the outermost sample surface layer. Electron probe X-ray micro analysis (EPXMA), in contrast, collects information from a region of about one micrometer thickness (4) and can therefore be used to perform an elemental bulk analysis of the aerosol samples. The use of a combination of XPS and argon ion bombardment permits a stepwise progressing from the surface into the bulk and thus the evalution of a depth profile.

EXPERIMENTAL

Details of equipment and experimental procedure for the simulation of a LWR core meltdown have already been described elsewhere (5, 6). The aerosol samples investigated in this work were generated in an experimental facility designed for the simulation of LWR core meltdown accidents in a laboratory scale. They were produced in a special run using inactive materials to avoid radioactive contamination of the XPS and EPXMA spectrometers. The starting material, which simulated the composition of a pressurized water reactor core, consisted of 90 g uranium dioxide, 51 g zircaloy, 100 g steel, and 4.4 g neutron absorber (80 wt % Ag, 15 wt % In, 5 wt % Cd). To the uranium dioxide inactive isotopes of fission products were added in amounts corresponding to a burn-up of 44,000 MWd/t uranium. This mixture was heated to temperatures ranging from 1200 °C to 1900 °C, and steam of 130 °C was passed over the melting charge. Aerosols were collected on eight glass fiber filters for 150 seconds each during the temperature range indicated above.

XPS spectra were recorded in a Vacuum Generators ESCALAB 5 electron spectrometer at a base pressure of 10^{-9} mbar. Electrons were excited using unmonochromatized magnesium and aluminium Kα radiation, and electron kinetic energies were measured with a hemispherical analyzer operated in the constant analyzer energy (CAE) mode. Binding energies and kinetic energies are

given relative to the silver $3d_{5/2}$ photopeak of the silver component in the samples. Photopeak intensities were corrected for photoionization cross sections (7).

Argon ion bombardment of the samples was performed using 5 keV Ar^+ ions, and XPS spectra were recorded after various sputtering times. The sputtering conditions were characterized by sputtering an anodically oxidized tantalum foil, where the same current density as applied to the aerosol samples yielded a sputtering rate of about 0.4 nm per minute. EPXMA was performed in an International Scientific Instruments SMSM 1 scanning electron microscope. X-rays were excited on a filter area of about 3 mm^2 using 25 keV electrons, and X-ray energies were determined over an energy range of 1 to 10 keV using an energy dispersive spectrometer (Kevex μx 7000 Si(Li) detector) which was attached to the scanning electron microscope. Peak areas were determined for the main X-ray transition of each element observable in the given energy range ($K\alpha_{1,2}$ and $L\alpha_{1,2}$, respectively). $L\alpha_{1,2}$ peak intensities were corrected for different primary ionization rates using relative correction factors, which were calculated for pure elements according to (4 a) from the following equation:

$$I_q = k\, A_q^{-1}\, \omega_q\, (E_o\, E_{c,q}^{-1} - 1)^{1.67} \qquad (1)$$

In this formula I_q is the primary X-ray intensity of element q, A is the atomic weight, ω is the fluorescence yield, E_o is the primary energy of the ionizing electrons, and $E_{c,q}$ is the minimum "critical" energy of an electron necessary to perform ionization in the given shell. The proportionality constant k is assumed to depend on the respective shell but not on atomic number.

Table 1 lists the values used for the calculation, the calculated relative intensities of the $L\alpha_{1,2}$ transitions ($I_{Ag,rel} = 1$), and the resulting correction factors, by which the experimental $L\alpha_{1,2}$ peak intensities were multiplied.

Table 1: Values used for calculation in equation 1, calculated relative intensities $I_{q,rel}$ of $L\alpha_{1,2}$ transitions and correction factors $(I_{q,rel})^{-1}$

q	A_q	ω_q (Ref.4b)	$E_{c,q}$ (keV) (Ref.4c)	$I_{q,rel}$	$I_{q,rel}^{-1}$
Ag	107.9	0.047	3.350	1.00	1.00
Cd	112.4	0.050	3.537	0.92	1.09
In	114.8	0.054	3.730	0.88	1.14
Te	127.6	0.068	4.341	0.73	1.37
I	126.9	0.073	4.558	0.72	1.39
Cs	132.9	0.084	5.011	0.65	1.54

E_o = 25 keV; $I_{q,rel} = I_q \cdot I_{Ag}^{-1}$

RESULTS AND DISCUSSION

Elemental surface and bulk analysis: Fig. 1 shows an XPS spectrum measured for the aerosol sample collected at 1630 °C. In contrast to EPXMA, the determination of elemental composition and signal intensities in XPS is straightforward due to the lack of peak interferences. Besides those photoelectron signals, which belong to elements from the sample, one also observes the C 1s photopeak resulting from surface contamination with carbon containing adsorbates.

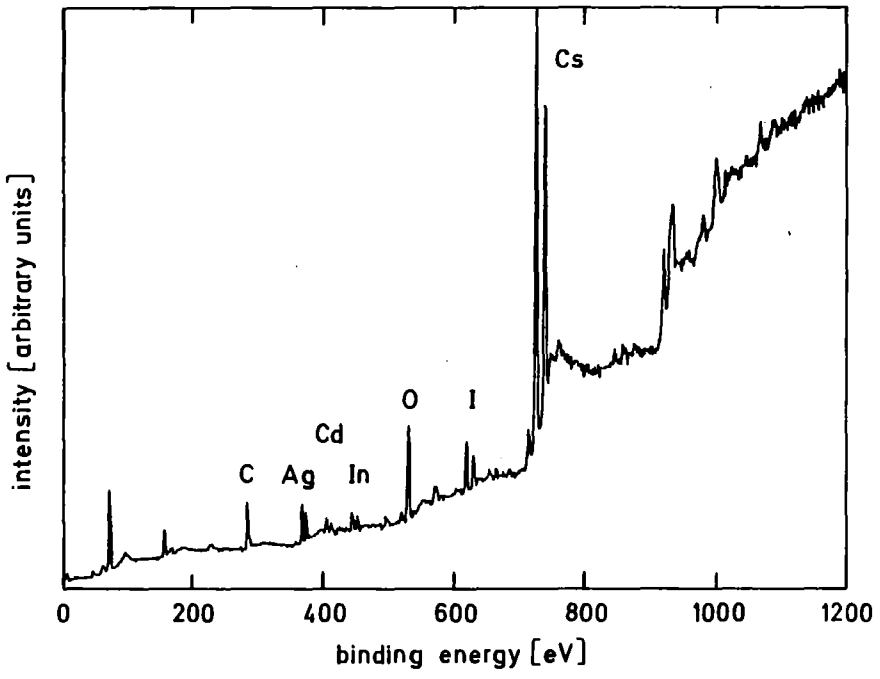

Fig. 1: XPS spectrum of the aerosol sample collected at 1630 °C.

The spectra are more complex in EPXMA. In some of the samples X-ray peaks from the glass fiber filter support are detected in addition, which is due to the much larger information depth of this technique, and which results in interferences with aerosol sample signals. Fig. 2 a shows an EPXMA spectrum of the same aerosol sample as used for the spectrum in Fig. 1. Fig. 2 b shows for comparison the spectrum, which is measured for a clean glass fiber filter (showing elements Al, Si, K, Ca, Ba, Zn). The peaks of glass fiber filter material are scaled to approximately the same height in both spectra. Besides the effect of overlapping signals from the glass fiber filters, the determination of elemental signal intensities of aerosol components was complicated by the fact that each element provides several X-ray lines (K series and L series, respectively), which may overlap with those from other elements. The signal intensities, therefore, had to be evaluated after subtraction of the glass fiber

filter signals by performing a multiplet analysis based on the shapes of spectra of pure elements. The accuracy of this procedure is certainly low, especially for elements with small concentrations, and will introduce larger errors into the calculated atomic fractions. Therefore, no correction besides the one for different primary ionization rates was applied (e. g. corrections for fluorescence and absorption).

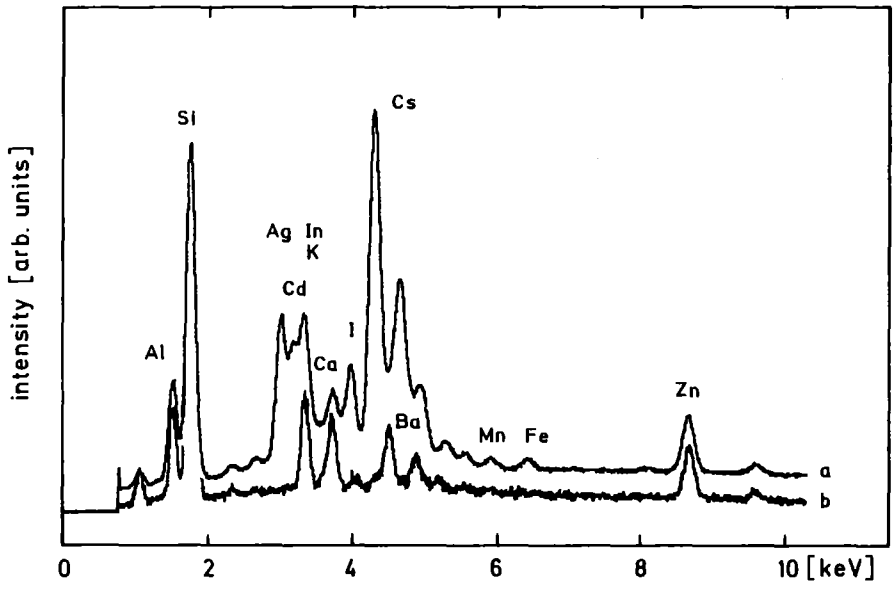

Fig. 2: EPXMA spectrum of the aerosol sample collected at 1630 °C (a), and of an uncharged glass fiber filter (b).

In addition to those elements, which were already detected by XPS (silver, cadmium, indium, tellurium, iodine, cesium), and to those elements, which were attributed to components of the glass fiber filter, EPXMA showed the presence of small amounts of chromium, iron, and manganese in samples collected at temperatures above 1400 °C.

When comparing the results of XPS and EPXMA, one has to take into account that for the latter as an energy dispersive spectrometer a Si(Li) detector was used, which is shielded by a beryllium foil of several micrometers thickness. Consequently, elements with an atomic number of about 10 or less (e. g. O and C) cannot be determined. A comparison of the results achieved by XPS and EPXMA, respectively, is therefore restricted to elements detectable with both techniques.

Fig. 3 shows the composition of each aerosol fraction as it was determined (8) by XPS (upper diagram) and EPXMA (lower diagram). Iron, chromium, and manganese are omitted from the lower diagram because of their low signal intensities, which contribute only up to a few atomic percent. As can be seen from Fig. 3, the sample collected at 1720 °C shows an unsystematical behavior. This sample had been inadvertently charged too low during the meltdown experiment.

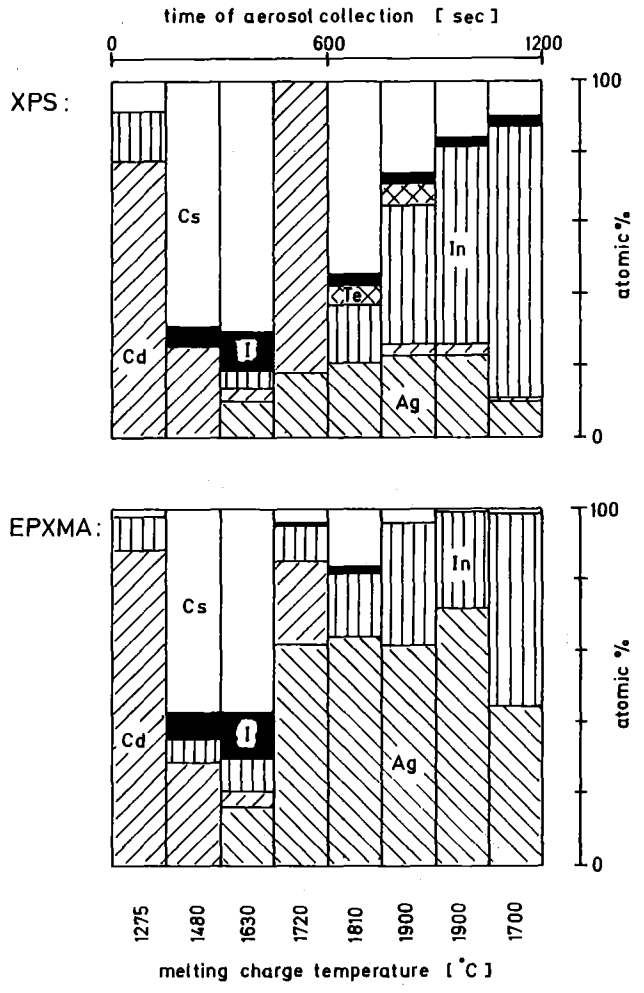

Fig. 3: Comparison of surface composition (XPS) and bulk composition (EPXMA) of the aerosol fractions.

It can be seen from both diagrams that the composition of the aerosols as a function of melting charge temperature is governed by the volatilities of the elements, which are present in the melting charge. Easily volatile elements (cadmium from the neutron absorber, cesium and iodine as fission products) appear at lower temperatures, while less volatile elements (silver and indium from the neutron absorber) require higher temperatures for the release. The general release behavior is similar in both diagrams. Differences arise for tellurium, which was not detected by EPXMA and concerning the absolute atomic fractions. At lower temperatures the composition of aerosol surface (as probed by XPS) and aerosol bulk (as probed by EPXMA) are fairly identical.

At higher melting charge temperatures EPXMA shows a significant enrichment of silver in the aerosol bulk, while the surface is significantly different showing a larger concentration of indium and cesium and the presence of iodine. These

observations correspond to the enrichment of more volatile species on the aerosol surface. The differences between bulk and surface composition can also be established using XPS, if the surface of the aerosols is stepwise argon ion etched and the resulting "new" surface subsequently measured by XPS. The results of this procedure applied to the aerosol sample collected at 1900 °C are shown in Fig. 4. The left part of the figure represents the surface composition of this aerosol fraction after various sputtering times. For comparison, the bulk composition as evaluated by EPXMA is given in addition. It can be seen that with increasing sputtering time XPS reveals an aerosol composition below the primary surface, which is fairly similar to the bulk composition.

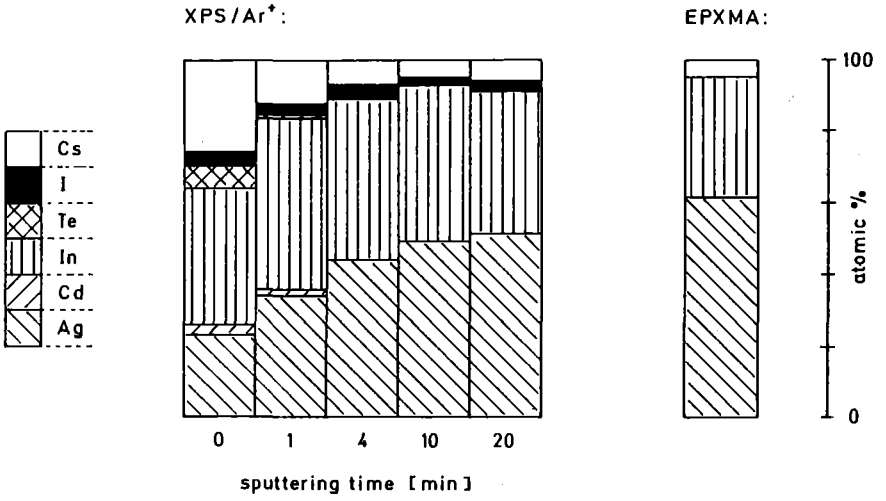

Fig. 4: Comparison of the surface composition after various sputtering times and bulk composition of an aerosol sample collected at 1900 °C.

Chemical speciation: XPS permits in addition the chemical speciation of the elements forming the samples. Speciation of an element is based on the determination of the binding energy of the main photopeak, of the kinetic energy of a selected Auger transition, and of the modified Auger parameter (9). The evaluation of these data resulted in the detection of silver metal, silver iodide, cesium hydroxide, cesium iodide, cadmium hydroxide, indium oxide, and tellurium dioxide (8). However, it was stated that these assignments were only valid for the main amount of each element, and therefore some elements may have contributions of different chemical states, which we want to show here for the example of tellurium.

Fig. 5 a shows the XPS spectrum of the energetic region, where tellurium 3d photoelectrons appear. The spectrum is composed of four resolved components. The leftmost peak belongs to silver (Ag $3p_{3/2}$). The other two main peaks clearly belong to tellurium in tellurium dioxide, which can be proved by determining the accurate binding energies, the peak intensity ratio, and the spin-orbit coupling constant. The small peak between those two of tellurium dioxide,

on the other hand, could in principle result from a photoelectron transition in either tellurium metal or chromium metal, especially since EPXMA shows a small amount of chromium, too. A clear distinction cannot be performed, because the second peak of the tellurium 3d doublet or the chromium 2p doublet, respectively, is hidden under the silver $3p_{3/2}$ photopeak.

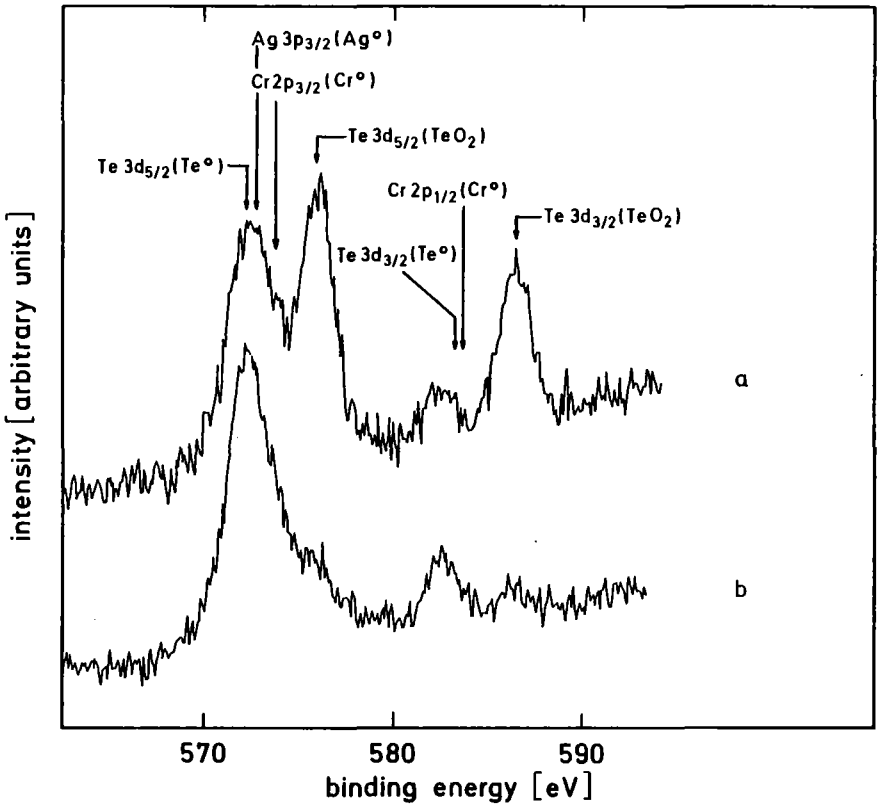

Fig. 5: XPS spectrum of an aerosol sample collected at 1900 °C showing the energy range of tellurium 3d photopeaks. (a) spectrum without sputtering, (b) spectrum after one minute sputtering.

Nevertheless, the peak position is closer to the value expected for tellurium $3d_{3/2}$ in tellurium metal than to the one for chromium $2p_{1/2}$ in chromium metal. In addition, we do not have any indication for the presence of oxidized chromium, and the detection of chromium metal without that of chromium oxide does not seem very likely remembering the experimental conditions during the formation of the aerosols. We, therefore, favor the presence of tellurium metal.

Fig. 5 b shows the XPS spectrum of the same sample after one minute argon ion etching. The peaks attributed to tellurium dioxide have almost disappeared (compare Fig. 4), while the resolved one of tellurium metal is still

present. Since tellurium dioxide is not decomposed to the metal under argon ion bombardment (10), the observed behavior indicated that tellurium dioxide is only a surface component of the aerosols, while tellurium metal is a bulk component, which is confirmed by further sputtering.

Further investigations of the chemical states of aerosol constituents, especially of iodine, will be published elsewhere (8).

Acknowledgment: The authors thank Dr. H. Albrecht and Mr. H. Wild for the preparation of the aerosol samples and for valuable discussions.

REFERENCES

1. A. Bayer and F. W. Heuser, Nucl. Saf. 22, 695 (1981).

2. D. O. Campbell, A. P. Malinauskas, and W. R. Stratton, Nucl. Technol. 53, 111 (1981).

3. D. Briggs and J. C. Riviere in "Practical Surface Analysis by Auger and X-ray Photoelectron Spectroscopy" (Eds. D. Briggs and M. P. Seah), pp. 87, Wiley, Chichester (1983).

4. S. J. B. Reed, "Electron Microprobe Analysis", Cambridge University Press, Cambridge (1975).
a) Chap. 15, p. 275; b) Chap. 15,p. 277; c) Appendix, p. 379.

5. H. Albrecht, V. Matschoss, and H. Wild, Nucl. Technol. 40, 278 (1978).

6. H. Albrecht and H. Wild, "Behavior of I, Cs, Te, Ba, Ag, In, and Cd during Release from Overheated PWR Cores", International Meeting on Light Water Reactor Severe Accident Evaluation, August 28 - September 1, 1983, Cambridge, Mass.

7. J. H. Scofield, J. Electron Spectrosc. Relat. Phenom. 8, 129 (1976).

8. H. Moers, J. G. Dillard, G. Kirch, H. Klewe-Nebenius, G. Pfennig, and H. J. Ache, to be published in Surf. Interface Anal.

9. C. D. Wagner, L. H. Gale, and R. H. Raymond, Anal. Chem. 51, 466 (1979).

10. H. M. Naguib and R. Kelly, Rad. Effects 25, 79 (1975).

Importance of Aerosol Sources and Aerosol Retention Capability of Containment Systems in LMFBR-Safety

G. Heusener, W. Marth
Kernforschungszentrum Karlsruhe

Abstract

The design of containment systems of prototype fast breeder reactors were strongly influenced by the request to overcome consequences of Core Disruptive Accidents (CDA). For this reason, a number of engineered safeguards like double containment, core catcher etc. are often installed.

In the case of commercial size fast breeder reactors which are presently in the planning stage it is planned to put more emphasis on preventive measures. The CDA shall not be made a basis of the design. Consequently no engineered safeguards are provided for.

The CDA, however, will be investigated in the frame of risk analyses to show that the risk of large breeder reactors is acceptably low.

This requires that aerosol formation processes as well as inherent retention capabilities are to be described as realistically as possible.

In the present paper the main aerosol generating processes which occur in the course of a CDA as well as the main retention capabilities are discussed. Areas are determined where further R+D would be worthwhile.

I. Introduction

As this is a specialists' meeting on Aerosols and not a specialists' meeting on Fast Reactor Systems, it might be useful to start a talk on the importance of Aerosols in LMFBR Safety with a brief survey of the status of LMFBR development.

I.1 Plants in Operation

The 250 MW LMFBR power station Phenix (France) has had a very good operating record since its start-up in 1973/74. The capacity factor averaged over ten years is about 60%.

The 250 MWe Prototype Fast Reactor (Great Britain), like Phenix, has its fuel reprocessed on a semi-industrial scale and recycled with remarkable success.

A special feature of the BN 350 power station (USSR) is its use of part of its thermal energy for producing 80 000 t/d of fresh water through distillation from the salt water of the Caspian Sea.

The BN 600 power station (USSR) is the largest LMFBR plant at the present time. Since its commissioning phase 1980-82, it has had a very smooth operating record.

The 400 MWth Fast Flux Test Facility (USA) is now in its fifth 100-day power cycle. Its fourth cycle (December 1983 through April 1984) was characterized by continuous operation and a peak burnup of 103 000 MWd/t.

Various experimental LMFBR plants, such as the EBR-II (USA), BR 10 and BOR-60 (USSR), KNK II (Germany) and Joyo (Japan) are delivering valuable information, especially on fuels and materials behaviour under fast neutron irradiation. For instance, an experimental fuel element of KNK II has attained 130 000 MWd/t peak burnup.

The LMFBR operating experience gained up to now shows that during normal operation and maintenance the radiological exposure for personnel can be kept very low.

I.2 Plants under Construction

The 1200 MWe power station Super Phenix 1 (France) has been under construction since 1977 and is to go into operation in 1985/86.

The 300 MWe power station SNR 300 has been under construction since 1973 and will start up late in 1986. It is a joint venture of West Germany, Belgium and the Netherlands. Utilities from these states and of Italy are also share-holders of Super-Phenix 1.

Site preparations are going on for the 280 MWe power station Monju (Japan). Many of its components have been ordered. Construction of the plant itself is to begin in fall 1985, start-up after 1990.

The 15 MWe Fast Breeder Test Reactor (India) has been under construction since 1972. Start-up is scheduled for 1985.

The 130 MWth PEC (Italy), a fast neutron test reactor, has been under construction since 1974. It is planned to go into operation in 1990.

Construction of the BN-800 (USSR) has started in 1984.

I.3 Projects in the Planning Stage

A detailed design including a safety concept in agreement with the French licensing authorities has been elaborated for a 1500 MWe power station Super-Phénix 2 (SPX 2), to be constructed after 1986.

Preliminary design studies have been made for a 1400 MWe power station SNR 2 (Germany). France and Italy are also to be share-holders of this plant. Great Britain has prepared a design for a 1300 MWe Commercial Demonstration Fast Reactor (CDFR).

Beside the studies for SPX 2, SNR 2 and CDFR there are additional studies underway in the US as well as in Japan. However, at present the European projects - especially SPX 2 and SNR 2 - probably have the greatest chance of realisation. This is why some special features of these projects will be discussed in this paper.

I.4 European Cooperation

In 1977 several agreements between France and Germany were concluded with the objective to cooperate in LMFBR development. This Franco-German co-operation was enlarged in January 1984, when a Memorandum of Understanding was signed by the governments of the Federal Republic of Germany, France, Britain, Italy and Belgium in preparation for an extended breeder cooperation in Western Europe. The aim of this cooperation includes construction of the above mentioned reactors SPX 2, SNR 2 and CDFR.

For this purpose, industrial companies and research organisations of Germany, Great Britain, France, Italy and Belgium have pooled their individual activities concerning the development and construction of fast breeder reactors. Such a collaboration aims at a concerted construction program of fast breeder reactors, based on a full exchange of breeder know-how.

This cooperation will comprise: a mutual harmonization of R+D-projects, the joint planning, construction and introduction of fast breeder plants into the market. It includes a close industrial cooperation also in the manufacture of components, as well as concerted action by the partners vis-à-vis third parties.

I.5 Status of LMFBR Development - Summary

It can be stated that the development of Fast Breeder Reactors has left its early stages of beginning and now is entering into a phase of deployment. Industrial aspects, international cooperation in all areas and economical problems become more important than in the past.

This causes manufacturers to reconsider designs and safety concepts with the consequence that there is a feedback on R+D programs.

In this talk I would like to show that because of certain design modifications aerosol production and retention processes in the future will be even more important than in the past.

For LMFBRs in-plant radionuclide retention of fission products is one of the most dominant mechanisms in limiting the risks to the public. Retention of aerosols which might have been generated during a serious accident plays a major role. The effectiveness of the retention is primarily influenced by the design of the containment system as well as by inherent safety features specific to LMFBRs.

In-plant retention of fission products can be achieved by two principal methods, either by filtering the containment atmosphere before its release to the environment, or by assuring containment integrity over an extended time interval in the post accident phase. Either method alone can provide a significant safety margin in limiting the risk, whereas both methods in combination practically assure a minimization of risk.

The following discussion will contrast the different approaches taken with respect to prototype reactors in the 300 MWel class on one side, and commercial size reactors such as SNR 2 or SPX 2 on the other side.

We will show, that whereas in the case of prototype reactors retention was guaranteed by a number of engineered safeguards in the case of commercial size reactors much more importance must be placed on inherent safety features.

The main point of discussion will be aerosols generated in a hypothetical Core Disruptive Accident (CDA), because it is this accident which governs the risk of LMFBRs to the public and its political acceptance.

The main aerosol generating processes which occur in the course of such an accident will be discussed as well as the main retention possibilities. Areas will be determined where further R+D would be worthwhile.

II. Safety Criteria for Breeder Reactors

II.1 Safety Philosophy for Prototype Reactors in the 300 MWe Class

II.1.1 Role of CDA

Prototype Reactors in the 300 MWe Class were designed late in the sixties and the licensing process started early in the seventies. At that time only limited experience for construction and operation of LMFBRs was available. The only experience originated from construction and operation of smaller reactors like EBR II, DFR etc.

It was mainly the gap of experience which caused people to be conservative and therefore in nearly all projects the request was formulated that appropriate measures be foreseen to withstand the consequences of a CDA.

It can be stated that probably the CRBR and SNR 300 suffered most from this request and that's why the situation for SNR 300 shall be briefly explained.

II.1.2 Measures for SNR 300

In the following the most important requirements as well as the respective measures will be explained. This will be done without trying to be complete. The consequences of a CDA which were to be considered in SNR 300 were

- mechanical consequences
- thermal consequences
- radiological consequences.

II.1.2.1 Mechanical Consequences

With respect to mechanical consequences it is well known that SNR 300 was designed in such a way, that 370 MW (expansion of the fuel to the available cover-gas volume) can be contained in the primary system. This value roughly corresponds to the 1200 MWs (expansion to 1 atmosphere) which was requested by the US-NRC for CRBR. In order to fulfill this requirement the reactor vessel as well as the piping systems had to be constructed in an appropriate way. In addition, special devices inside the vessel were foreseen, like a dip plate, a shield tank and others. Special attention was given to the vessel head, which was clamped.

II.1.2.2 Thermal Consequences

To overcome thermal consequences mainly means, that the core debris can be safely cooled for a long period of time. This goal first was reached by installing an external cooling device (core catcher) into the reactor cavity. Later it was shown that with a high degree of confidence the fuel will be retained inside the vessel. Because of this the core catcher system can be considered as a back-up.

II.1.2.3 Radiological Consequences

The measures mentioned above ensure that no major release of radionuclides to the containment building will occur. Nevertheless, additional measures are foreseen to further mitigate the transfer of radioactivity to the containment building.

The primary system is completely enclosed by a nitrogen-filled containment region, which is called the "inner containment". Steel liners and special engineered systems ensure that only limited damage to the concrete will occur.

Aerosols and radionuclides, which escape the inner containment reach the outer containment. Appropriate measures are foreseen which prevent that machinery and electrical equipment will be damaged by the aerosols. Aerosols, which escape from the outer containment reach the so-called "reventing gap". This gap is kept at under-pressure.

Leakages coming from the environment as well as those coming from the containment building are revented into the containment. In such a way a zero-release is ensured for a couple of days. When reventing is no longer possible, a controlled release via filters is foreseen.

II.1.2.4 Containment System of SNR 300

The short description of the SNR 300 containment system given above cannot be complete, but we hope it demonstrates the numerous different measures foreseen in SNR 300. Fig. 1 summarizes the systems. The main barriers and systems which are justified only by the CDA are

- a primary system, able to withstand 370 MWs mechanical energy
- the possibility to cool the core debris inside the vessel or
  - as a backup - outside the vessel by a core catcher
- an inerted inner containment
- the outer containment surrounded by the reventing gap
- the filter system which is foreseen for a final controlled release.

It might be worthwhile to point out that, because of the rather large numbers of different barriers and the long time interval before containment venting through a filter system is initiated, the calculated consequences in terms of risk were not very sensitive to the assumptions about the radiological source term associated with a CDA. In other words: one could afford to be quite pessimistic, when defining the radiological source term of the primary system.

II.1.3 Risk Studies for SNR 300

The effectiveness of the above mentioned measures became evident when risk studies were performed for SNR 300. Two studies have been performed, one by GRS /1/ at the request of the so-called "Enquete Commission" of the German Bundestag; the other nearly at the same time in a cooperation effort by KfK/ Interatom/SAI /2/.

Results of these studies are published elsewhere. They cannot and will not be repeated here.

However, one item should be mentioned: as long as mechanical energy releases from a CDA are lower than 370 MWs, there will in no circumstance be a significant release of radioactivity to the environment ("significant" at this point means releases causing early fatalities or a considerable number of late fatalities). The only possibility to calculate such releases is to assume more or less artificially, that the mechanical energy release is so high, that the primary system fails catastrophically and as a consequence the whole containment system will be breached within a few minutes.

The probability of occurrence of such an event is believed to be extremely small. It has been estimated that only about 10^{-3} of all CDA's would lead to energy releases exceeding the design value of SNR 300.

This situation automatically brings us to the question whether it is justified to spend such a significant effort to control the consequences of an extremely improbable event.

II.1.4 Situation at other Prototype Reactors

The short description of the SNR 300 situation does not mean that the CDA was considered only in the case of this reactor. For Monju this problem is still under discussion during the planning, licensing and construction phase, as was the case for all prototype reactors with the exception of the plants in the USSR.

Measures foreseen differed, but in all cases CDA's strongly influenced the design.

II.2 Safety Criteria for Commercial LMFBR's

The fact that in the case of prototype reactors the CDA plays such an overwhelming role and had such a strong influence on the whole plant design, was never considered to be precedent for future commercial size reactors. A couple of positive developments could be observed in the Seventies.

- A great deal of experience has been gained during construction and operation of fast breeder reactors
- The components of the nuclear system - especially shutdown rods - turned out to be extremely reliable
- The phenomena occurring in the course of a CDA are now much better understood. Analyses show that even if a CDA is postulated, the mechanical load to the system most probably will be benign.

Thus the question arose on how to formulate safety criteria for large breeder reactors. While this is, of course, a very broad area including a large number of important items, the problem of how to handle the CDA in the future has always been the most sensitive point of discussion.

Two international workshops were held to discuss Safety Criteria and Design Options of Large Breeder Reactors. One Symposium was held at Naperville, Tennessee, in November 1982, the other at Paris in May 1983.

In the following we would like to describe the criteria which - with respect to the CDA - are applied or proposed for SPX 2 and SNR 2.

We have chosen these two reactors because the discussion on the safety criteria in both cases is well advanced (in the case of SPX 2 the discussion is basically finished).

Both SPX 2 and SNR 2 are large pool type reactors. In the frame of the Franco-German Cooperation the design has been harmonized to a large extent, though there are still some differences resulting from special national circumstances and requirements.

II.2.1 Criteria for SPX 2

We have mentioned that the discussion on the safety concept for SPX 2 is finished. A document has been released on the safety criteria to be applied. The main content of this document has been published in Paris at the above mentioned workshop /4/.

With respect to the CDA problem it is clearly stated that the CDA shall not be made a basis of the design but will be considered as a"residual risk".

Neither the manufacturer, i.e. Novatome, nor the CEA-DRNR intend to analyse this type of accident. Furthermore it is not to be expected that the licensing authorities will ask for such an analysis during the licensing process. But as a matter of a general improvement of the safety properties of the plant, some special measures are foreseen:

- The roof of the vessel will be optimized in such a way that it can withstand the same static pressure as the vessel itself. Furthermore, it shall be optimized also with respect to dynamic load
- There will be a SPX 1 type core catcher device inside the vessel.

However, no special scenarios are defined and will be discussed with respect to these special measures.

II.2.2 Criteria for SNR 2

In the case of SNR 2 the situation is not so advanced as compared to SPX 2. A first version of a safety concept has been drafted by Interatom, the vendor, together with ESK, the operator of the plant. This safety concept is presently under discussion. The Federal Minister of Internal Affairs has installed an ad-hoc Advisory Group which is supposed to give comments in autumn 1984.

This safety concept also has been presented at Paris by Interatom/ESK /5/. In addition KfK has presented a paper describing its own point of view /6/.

In the following we will try to give a very short description of the point of view of Interatom/ESK on one side and KfK on the other side.

Interatom/ESK claim that by additional improvements of the preventive measures a core destruction not only can be made extremely improbable but can be excluded altogether. Improvements of preventive measures include e.g. decay heat removal by natural convection only, special design of the primary pumps, special core design etc.

Therefore in the present design of SNR 2 no special measures are foreseen to mitigate or even withstand CDA consequences.

The point of view of KfK did not necessarily contradict this concept. Also in the opinion of KfK the preventive measures can and should be made so reliable that the CDA should not have a direct bearing on the design. However, KfK pointed out that from the past we learned that also political acceptance of this technology must be assured. The political acceptance will require some evidence that the risk of LMFBR's will not be greater than the accepted risk of LWR's.

Therefore we expect that probabilistic risk analyses for LMFBR's will be performed in the future as it is the case for LWR's. These studies will include also the extremely unlikely event of core destruction (again as it is the case for LWR's).

It will depend on the result of these risk assessments whether or not additional measures are to be foreseen. We at KfK expect that a plant though built without considering CDA's nevertheless has significant capabilities to reduce consequences of a core meltdown. Only if these inherent capabilities should not be sufficient to reduce the risk to an acceptable level, the need for special measures might arise.

We have mentioned that the SNR 2 concept is presently under discussion. However, the most probable elements of the final decision can be summarized as follows:

- it is not necessary to consider CDA in the design
- risk studies which include CDA considerations shall compare the risk coming from different reactor concepts. In the framework of these studies CDA's will be investigated and the consequences will be determined.

II.3 Containment System of SNR-2

It has been mentioned earlier that the present design of SNR 2 does not take into account any aspect of CDA's. In this respect this design goes even beyond the French SPX 2 design, where CDA's are not considered, but some global measures are foreseen.

Fig. 2 shows a schematic view of the SNR 2 reactor building. The comparison with the SNR 300 shows the following main differences:

- there is no double containment system in case of SNR 2
- there is no reventing possibility
- the vessel head is not clamped but is connected to the primary system only by its weight
- there are no special devices like core catcher etc.

The outer containment has to withstand aircraft crash, according to the German rules. This requires a rather thick concrete structure. The design limit for the overpressure of this building is about 200 mbar.

The containment system of SNR 2 may be considered as the end point of a steady development of LMFBR containment systems. This can be demonstrated by looking at Fig. 3 and Table 1 which show the design principles of SNR 300, SPX 1, SPX 2 and SNR 2.

II.4 Safety Design Features in Comparison

We have discussed the case of SNR 300. The CDA was considered in much detail and it was necessary to show in a consistent way that the consequences of CDA's could be kept under control. The plant is equipped with a sophisticated double containment system as well as with an external core catcher.

The situation is similar in the case of SPX 1. Also this plant has to withstand the consequences of CDA. There is an internal core catcher and the primary system can withstand mechanical energy releases. A double containment system is established by the so-called dome.

In the case of SPX 2 there is no double containment and no consideration of CDA in the design. However some global measures are foreseen. The roof is to be optimized with respect to dynamic load and the primary system is clamped. The plant is equipped with an internal core catcher.

Finally in the case of SNR 2 there again is only a single containment, no measures are foreseen to contain CDA consequences. The roof is not clamped and there is no core catcher at all.

It should be strongly emphasised here that this development should not be understood as a reduction of safety. On the one hand manufacturers claim that the preventive measures - which are not discussed in this paper - are increased significantly. On the other hand there are inherent safety features which in the future must be exploited.

In the case of SNR 2 the licensing discussions and procedures have just been started. The years to come will show whether the inherent safety potential of the design will be sufficiently high to reduce the risk to an acceptable level. This will require additional R+D as well as risk studies which will be performed in parallel to the detailed design.

This brings us back to the Aerosol item because the realistic (not necessarily pessimistic) description of aerosol formation processes and retention possibilities will be one of the essential parts which are needed to demonstrate this goal.

III. Aerosol Source Terms and Retention Capabilities

III.1 General Remarks

Numerous comprehensive review papers have been presented in the past on various occasions /7/, /8/. The last comprehensive review of the different aerosol sources which occur during a core meltdown in LMFBR's has been presented at the first specialists' meeting of this series by R. Reynolds and T. Kress /9/. We will not repeat this detailed review, nor will we try to be complete, but rather point out some processes which in the light of the above design changes are considered to be specially important.

III.2 Courses of the Accident

The relevant paths of the accident with respect to aerosol problems are shown in fig. 4 which is similar to the respective figure taken from Reynolds' publication /9/. Two main paths have to be distinguished: the core disruptive accident may either lead to energy releases or to a non-energetic core meltdown.

As the safety philosophy of SNR 2 as well as SPX 2 emphasizes accident prevention in preference to mitigation of accident consequences, their primary systems are not designed to stand major energy releases. This is an important difference as compared to prototype reactors where the primary system usually was able to withstand significant energy releases.

The consequence is that for SNR 2 and SPX 2 - once the occurrence of a CDA has been postulated - the probability of an immediate breach of the primary system is much higher than for prototype reactors. As a consequence of the breach of the primary system, radionuclides as well as significant amounts of sodium might be expelled into the air-filled reactor containment leading to an immediate, possibly extended, sodium spray fire. The resulting pressure build-up challenges the containment structures.

In the case of non-energetic behaviour there will be no mechanical load of the primary vessel but rather thermal load. The question arises whether the core debris can be cooled inside the vessel. If this is not the case, sooner or later the fuel together with the sodium will flow into the reactor cavity. Fuel and fission products will be released from the sodium pool. Later on sodium/concrete/fuel or stainless-steel/concrete reactions will occur and will add to the aerosol generation.

If the vessel integrity can be maintained, aerosols inside the vessel will be generated over a long period of time and may be released to the outer containment via leakages in the primary system.

Consequently we distinguish between the instantaneous source term S_o generated during a power burst and accompanied by release of mechanical energy, and a delayed source term S_D representing a later stage of the accident with a generation of aerosols during a long period of time.

III.3 The Instantaneous Source Term S_o

In the case of an energetic power excursion which might be caused either by sodium voiding, fuel movement etc. or by secondary criticalities after an originally non-energetic accident, a high pressure bubble consisting of a multiphase mixture of vaporized, liquid and debrised fuel will be formed. Beside the fuel vaporized fission products, noble gases, other core materials and sodium are contained in this bubble.

The escape of radionuclides from the primary system, i.e. through the head of the vessel, depends on the dynamic behaviour of this bubble as well as on the damage to the vessel head which might be caused by the mechanical energy.

While there is clarity concerning the mechanical load to the primary system, the dynamics of the vapour bubble, the vaporization, fragmentation and condensation processes are not yet sufficiently well understood in spite of quite a number of experiments. Therefore significant uncertainties had to be taken into account. This is normally done by making pessimistic assumptions.

In the following we will identify some typical processes, point at the pessimistic assumptions used in the past and explain why a large potential exists to reduce aerosol formation.

III.3.1 Vaporization of Fuel and Non-volatile Fission Products

It is a common assumption that fuel and non-volatile fission products stay together and that for both components the same fraction of the inventory of the core will be vaporized.

Vaporization occurs during the disassembly - though, because of the normally small void fraction, only limited quantities will vaporize. Larger quantities will vaporize during the following expansion phase. The final fraction of vaporized fuel depends on the fuel temperatures which have been obtained during the power excursion. Previous calculations for the fraction of vaporized fuel during disassembly and expansion were based on isentropic expansion assumptions. These calculations lead to some 10% of vaporized fuel, e.g.in the case of SNR 300 such a calculation for a power excursion leading to an energy release which is close to the design limit would result in 12% vaporized fuel /1/. Similar figures have been published for CRBR /9/.

Of course it has been known for a long time that the assumption of isentropic expansion is far too pessimistic. Therefore in a global way a reduction has been introduced. In the case of SNR 300 only 3% were used in the further analysis instead of the above mentioned 12% /1/. However, even this lower value probably is far too pessimistic. SIMMER calculations have been performed for a similar case. These calculations take into account self mixing processes of the fuel as well as heat transfer to the structures and the surrounding sodium.

The calculations showed that at a certain point in time the fraction of vaporized fuel never exceeded a few thousandths /10/. Of course, this does not mean that only these small quantities have been vaporized; because vaporization and condensation are taking place at the same time. Nevertheless, it can be expected that the fraction of fuel and non-volatile fission products significantly can be decreased if the internal and external heat losses are taken into account in a realistic way. A close cooperation should be established with those groups who do SIMMER analyses for the expansion phase. Up till now mainly the mechanical aspects have been considered in the SIMMER analyses. The influence of aerosol production, however, is certainly of equal importance.

III.3.2 Bubble Expansion

Another significant retention capability is given by the sodium covering the core. The above mentioned bubble has to expand and to penetrate a thick layer of sodium. During the time needed for the expansion the aerosol mass concentration inside the bubble may change drastically by a number of different processes.

Aerosols will be generated by fuel vapor condensation. On the other side, washing-out due to settling of entrained sodium droplets and inertial impaction during bubble oscillations may be very efficient removal processes. In addition, we have aerosol sedimentation, diffusion, coagulation etc.

Quite a number of experimental programs deal with bubble formation, bubble behaviour and related aspects, e.g. aerosol transport. There will be a paper on the experimental KfK-program FAUST later on in this session. At the last specialists' meeting results of the American FAST-program have been reported /11/.

Furthermore, in France the Excobulle- and Caravelle- programs deal with this subject. Experiments and code development on bubble behaviour are also being performed in Japan.

So far, the results of these experimental programs are extremely encouraging. Very large retention factors for aerosols have been observed, for instance in the FAUST-program, retention factors lager than 10^4 were observed. Similar results have been reported from the FAST-tests /11/. However, in all the theoretical studies up till now only factors were assumed which are lower by orders of magnitude. For instance, in the risk study for SNR 300, a factor of onyl about 6 was used /1/. Additional experiments are planned for the future which will cover parameters which are not sufficiently well investigated up till now. They hopefully will confirm the very large retention capability of the sodium pool.

For further discussion of this item reference is made to the following paper on the FAUST Program.

II.3.3. Transport through the Vessel Head

The escape of aerosols to the outer containment is strongly influenced by the response of the head of the vessel to the mechanical energy release. If the roof basically can withstand the mechanical energy an escape can only occur through leakages. There is probably no immediate challenge to the integrity of the outer containment. Normal aerosol processes, like coagulation and sedimentation, will take place and they will lead to a significant reduction of the aerosol density because sufficient time will be available till a final release to the environment occurs. In this connection it is important to consider the influence of aerosols on the equipment which is inside the outer containment. This situation is the normal outcome of all studies performed for prototype reactors. If, however, the roof fails (this might be the most probable outcome for commercial-size reactors) the situation becomes rather uncertain. It may be postulated that large quantities of sodium will be expelled into the outer containment which - in the case of SNR 2 and SPX 2 - is air-filled. The resulting spray fire may lead to a pressure buildup whose rate will mainly depend on the quantities of sodium and other parameters assumed in the calculation of the sodium spray fire.

As the containment buildings are not designed to withstand high pressures, an overpressure of a couple of hundreds of millibars is sufficient to breach the containment. Again, because of lack of information in this area extremely pessimistic assumptions have been used which in the case of SNR 300 lead to the failure of the outer containment by overpressure within a few minutes /1/, /2/. There is some experimental evidence in the FAUST program showing that the mass of liquid expelled through open holes might be not very large /12/. However, much more information is needed in this area in order to come to firm conclusions. This is true for the mass of sodium expelled (which is, of course, a function of the amount of mechanical energy) as well as for the parameters determining the resultant spray fire.

III.4 The Delayed Source Term S_D

Both in the case of an energetic excursion and in the case of an energetically benign course of the accident; we have to deal with the delayed source term.

In the worst case the core debris cannot be cooled inside the vessel, with the consequence of a thermal failure of the reactor vessel. In the case of SNR 2, fuel and liquid sodium will then fall onto bar concrete where the fuel/sodium/concrete interaction immediately leads to a challenge of the containment system. The fuel will remain, nevertheless, covered by sodium preventing any significant quantity of fuel and non-volatile fission products to become airborne.

Results of the NALA experiments which have been presented at the last meeting and will be presented later on in this session show that the sodium has a significant retention capability, especially for the fuel. Retention factors larger than 10^3 can be expected /13, 14, 15/ for hot, but non-boiling pools.

Retention factors for boiling pools which are significant lower than for non-boiling pools have been reported by Berlin /18/.

In general it can be stated that the delayed source term does not significantly influence the risk, because of the long time intervals up to release to the environment.

This is however true, only if there is no immediate breach of the containment building caused, for instance, by sodium/concrete or fuel/concrete interaction. A better understanding of the sodium/concrete interaction therefore seems necessary. We are therefore at KfK planning to start a program to investigate the sodium/concrete interaction in large scale experiments.

III.5 Retention Capability of the Containment

It is well known that the most important retention capability is given when the leak tightness of the containment system is guaranteed for a long period of time thus forcing the aerosols finally to sediment inside the building. However, even if there would be cracks and openings in the concrete, there are probably still retention possibilities. Studies performed by Morrewitz showed that aerosol leakages through a multiple bend leak path caused rapid plugging /16/. In addition the aerosols escaping through the leak path were observed to have very much larger diameters than the original aerosols. Van de Vate has investigated gas and aerosol leak rates through artificial cracks in basaltic concrete /17/. The test showed decreasing flow rates indicating plugging. Leak paths to the concrete walls of the containment building are very long and have rough surfaces. Aerosols attempting to escape through these cracks most likely block the path and limit the released aerosol to a small fraction of the mass that entered into the crack.

IV. Conclusion

We have restricted ourselves in this paper to aerosol problems connected to a core disruptive accident, because it is this accident which in our opinion governs the risk to the public, though it is extremely improbable.

The above discussion which was not intended to give a comprehensive review was to show that risk investigations for future commercial size LMFBR's have to rely much more on a realistic description of aerosol formation and retention processes than the assessments which were performed for the prototype reactors.
Additional efforts certainly are needed in the areas I have mentioned and others which are not discussed in this paper.

The future research in aerosol physics as well as in other safety areas must take into account the implications given by the planned modifications of the containment systems. The goal is to use realistic and proven data and models to show that the inherent capabilities are sufficient to reduce the risk to an acceptable level.

Finally it should be mentioned that there are other incidents and accidents which are not discussed in this paper, but which also produce large quantities of aerosols. For instance, large sodium fires are certainly extremely important and must be investigated also in the future.

Though the occurrence of these incidents might endanger the reactor itself, they do not form an immediate and major contribution to the risk to the public, as long as a safe state of the core itself can be ensured.

/1/ Risiko-orientierte Analyse zum SNR 300
Bericht GRS-51, 1982

Risk-oriented Analysis of the SNR 300 (Summary)
Bericht GRS-56

/2/ M. Schikorr, E. Rumble et al.
Conditional Risk Assessment of SNR-300
KfK Report, to be published

/3/ D. Struwe, P. Royl, R. Fröhlich
Vessel failure event tree analysis of SNR-300 for a hypothetical unprotected loss-of-flow accident
LMFBR Safety Topical Meeting, Paris, July 19-23, 1982, p.II-625

/4/ French Presentation on Safety Criteria of SPX-2 at the Workshop on Safety Criteria and Options in Fast Breeder Reactors Design
Paris, May 1983

/5/ H. Hübel et al.
Presentation on Safety Criteria at SNR-2
Ibid.

/6/ D. Smidt, G. Heusener, D. Struwe
Safety Design of Large Fast Breeder Reactors
Ibid.

/7/ W.O. Schikarski
On the State of the Art in Aerosol Modelling for LMFBR Safety Analysis, Proceedings Int. Mtg. on Fast Reactor Safety and Related Physics, Vol. IV, pp. 1907-1914, Chicago (1976)

/8/ M. Silberberg, Chairman, "Nuclear Aerosols in Reactor Safety",
A State-of-the-Art Report by a Group of Experts of the OECD-NEA Committee on the Safety of Nuclear Installations (June 1979)

/9/ A.B. Reynolds, T.S. Kress
Aerosol Source Considerations for LMFBR Core Disruptive Accidents
Proc. of the CSNI Specialists' Meeting on Nuclear Aerosols in Reactor Safety, Gatlinburg, Tenn., 1980 ORNL/NUREG/TM-404 (1080) p.1

/10/ P. Schmuck
Private Communication

/11/ A.L. Wright, T.S. Kress, A.M. Smith
ORNL Experiments to Characterize Fuel Release from the Reactor Primary Containment in Serve LMFBR Accidents
Proc. of the CSNI Specialists' Meeting on Nuclear Aerosols in Reactor Safety, Gatlinburg/Tennessee 1980
ORNL/NUREG/TM-404 (1980), page 57

/12/ W. Schütz, J. Minges, W. Haenscheid
Investigations on Bubble Behavior and Aerosol Retention in Case of a LMFBR Core Disruptive Accident.
The KfK-FAUST Tests
Paper No. 3 of this Meeting

/13/ H. Sauter, W. Schütz
Aerosol Release from a Hot Sodium Pool and Behavior in Sodium Vapor Atmosphere
Proc. of the CSNI Specialists' Meeting on Nuclear Aerosols in Reactor Safety, Gatlinburg/Tennessee, 1980
ORNL/NUREG/TM-404 (1980), page 84

/14/ H. Sauter and W. Schütz
Fuel and Fission Product Release from a Hot Sodium Pool; Removal of Methyl Iodide in Sodium Aerosol Atmosphere
KfK
Paper No. 4 of this Meeting

/15/ H. Sauter, W. Schütz
Aerosol- und Aktivitätsfreisetzung aus kontaminierten Natriumlachen in Inertgasatmosphäre
KfK 3504, Juli 1983

/16/ H.A. Morewitz, et al.
Attenuation of Airborne Debris from Liquid-Metal Fast Breeder Reactor Accidents,
Nuclear Technology, Vol. 46, December 1979, p. 332.

/17/ J.F. Van de Vate, et al.
Aerodynamic Properties of Aerosols and their Leakage through Concrete Containment Structures
Fast Reactor Safety Meeting, Seattle, Aug. 19-25, 1979, p. 804

/18/ M. Berlin, et al.
Evaluation of the Sodium Retention Factors for Fission Products and Fuel,
Proc. of the LMFBR Safety Topical Meeting, Lyon, 1982,
Vol. III, p. III-369.

	SNR 300	SPX 1	SPX 2	SNR 2
Mechanical energy which can be contained by the primary system	HIGH	HIGH	LOW	VERY LOW
Core catcher	External potential for internal retention exists	Internal	Internal	No
Double containment	YES	YES	NO	NO

Table 1: Containment Principles

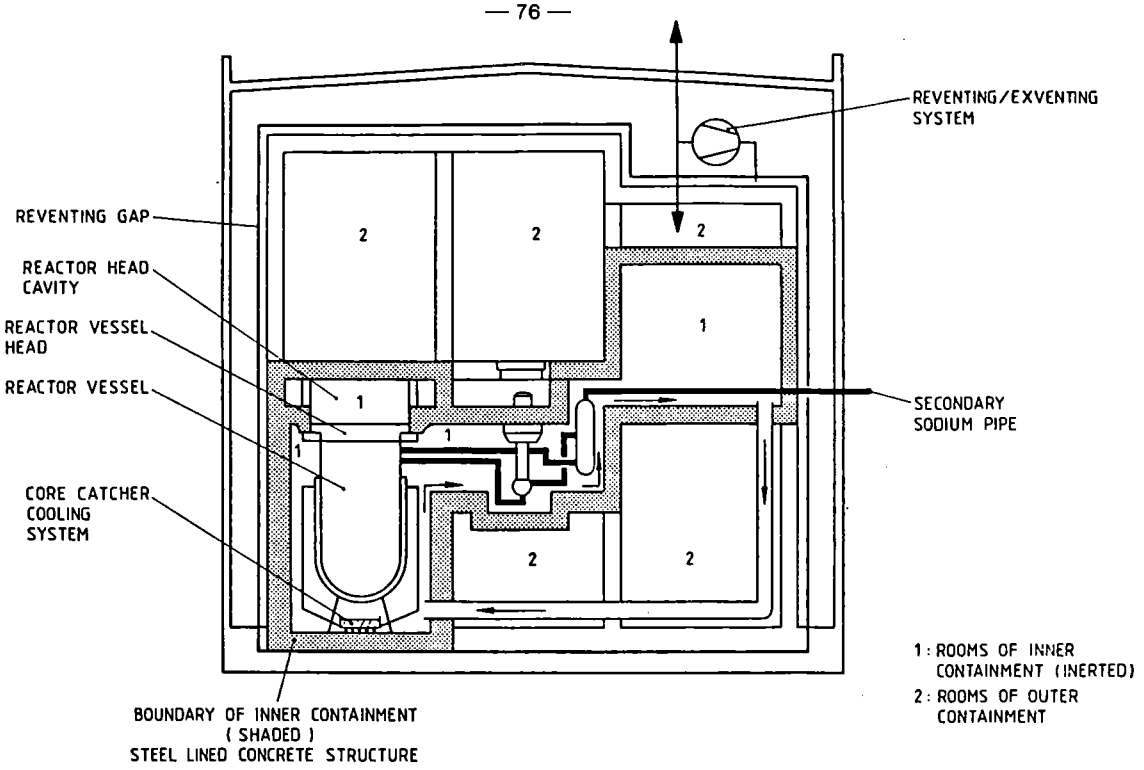

Fig. 1

SCHEMATIC CROSS-SECTION OF SNR 300 REACTOR BUILDING

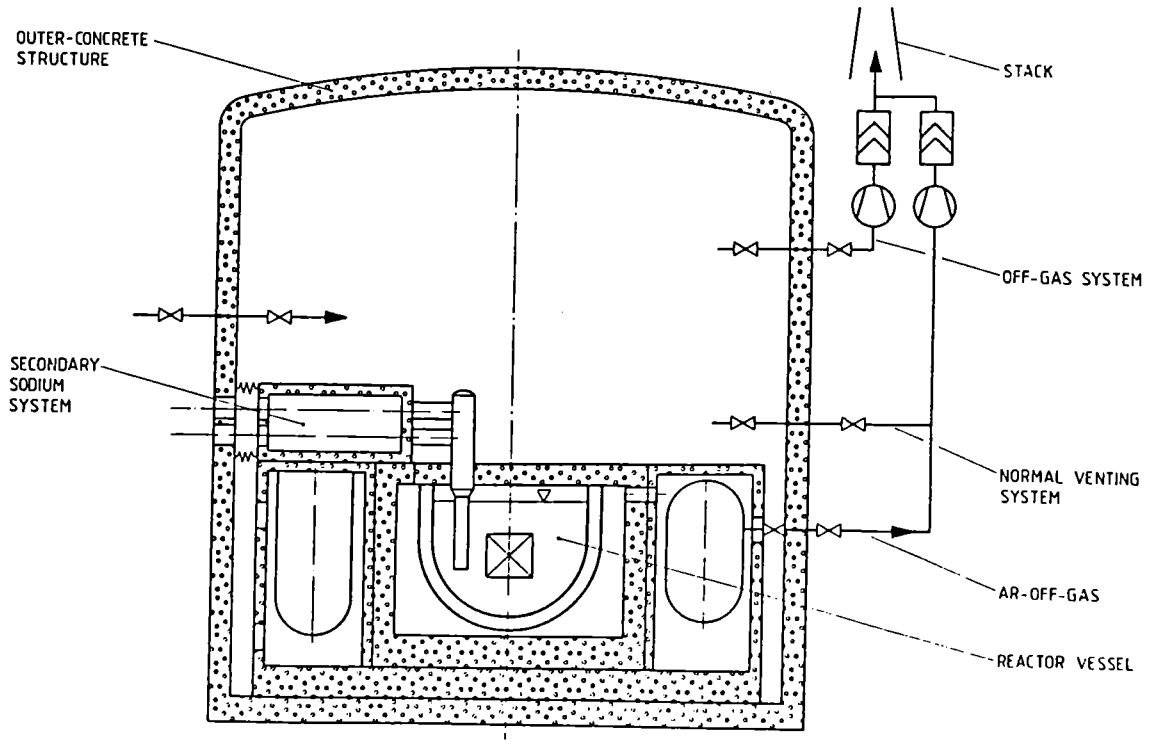

Fig. 2

SCHEMATIC CROSS SECTION OF SNR 2 BUILDING

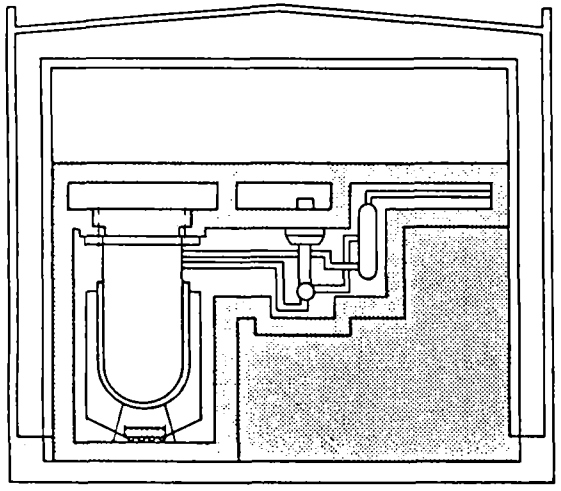

SNR 300

SPX 2

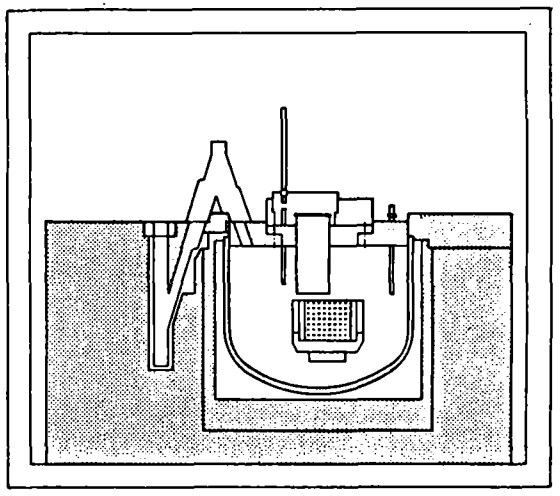

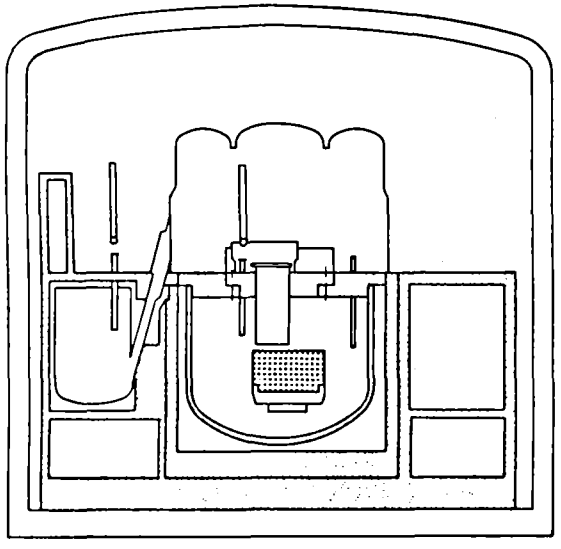

SPX 1

SNR 2

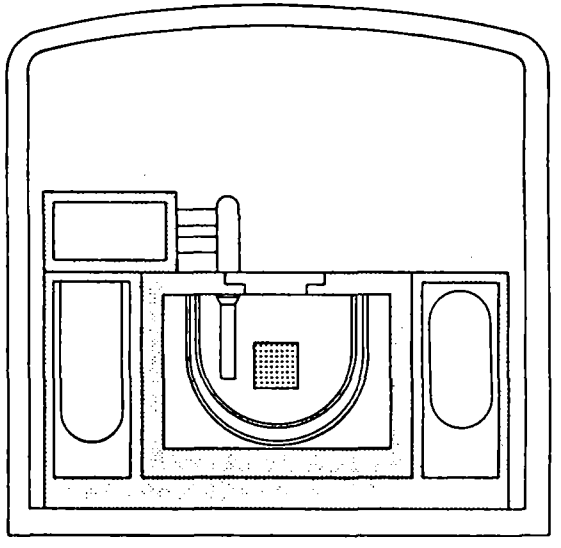

KfK

Fig. 3

Containement Systeme

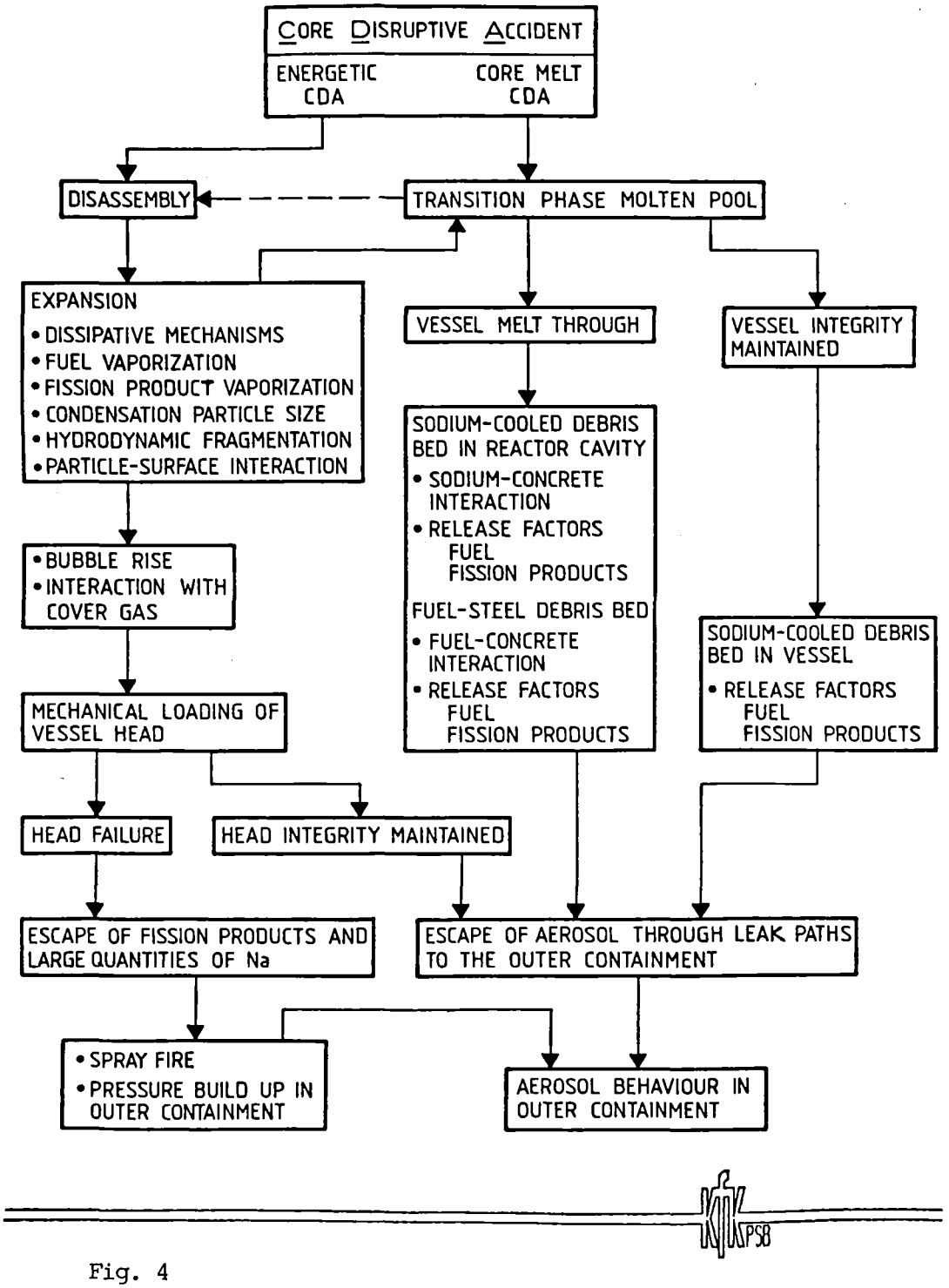

Fig. 4

LMFBR CORE DISRUPTIVE ACCIDENT FLOW CHARTS

Investigations on Bubble Behaviour and Aerosol Retention in Case of a LMFBR Core Disruptive Accident: The KfK-FAUST Tests

W. Schütz, J. Minges, W. Haenscheid

Kernforschungszentrum Karlsruhe GmbH
Laboratorium für Aerosolphysik und Filtertechnik I
Postfach 36 40, 7500 Karlsruhe, W-Germany

ABSTRACT

FAUST is a KfK program to give contributions to the assessment of the primary source term. Correlations between bubble and aerosol behaviour, especially the aerosol transport into the cover gas, are investigated by simulation tests. In the first phase, experiments with rupture disk discharge of gas-particle-mixtures into a water pool at two geometries are performed. In the second phase, the water pool is replaced by a sodium pool.

Important quantities to be measured are: 1) the period of the pressure pulses in bubble and cover gas, 2) the retention factor RF, defined as the ratio of the amount of particles discharged and trapped in the cover gas 3) the entrained coolant liquid in bubble and cover gas, and 4) the coolant and particle mass escaping through defined openings in the cover plate.

In the paper, experimental details, parameters, and results are presented, as well as theoretical onsets to understand bubble and cover gas behaviour and particle removal. The bubble oscillation period is usually small compared to the bubble rise time. The retention factors are $> 10^4$ in most cases, indicating the existence of very efficient particle removal processes. The overall process may, in first order, be described by the assumption of a coolant piston performing linear and adiabatic oscillations between two gas volumes. Important particle removal mechanisms are impaction during the heavy bubble oscillation and wash-out by sedimentation of the entrained coolant.

1. INTRODUCTION

1.1 HCDA, Aerosols, Source Terms

The fuel of liquid metal cooled fast breeder reactors has the potential - although at an extremely low probability - to reach highly energetic states (temperatures of the order of 6000 K) during a transient power excursion caused by loss of coolant flow /1/. The excursion may occur on the time scale of milliseconds. The high fuel vapor pressure (of the order of 7 MPa) will initiate core disruption. It is assumed that a fuel/sodium vapor bubble will be produced which rapidly expands into the sodium pool ($\approx$800 K) in the upper plenum, imparting kinetic energy to the coolant and to internal structures. The sodium slug may impact the reactor vessel head, causing damage and leaks and thus provide a pathway for the escape of radioactive material (mostly aerosols which are transported in the rising bubble) from the cover gas into the containment. Thus, aerosol transport and retention in the expanding, oscillating and rising bubble is an important issue.

Safety and risk analysis must provide estimates of the radiological consequences (or the radiological source terms) of hypothetical core disruptive accidents (HCDA). We define the 'primary or instantaneous source term' as the amount of radioactive material which is released from the reactor vessel head into the (inner) containment due to partial vaporization of the core material, formation and rapid expansion of a fuel/sodium vapor bubble, aerosol and fission gas transport in the rising bubble, release into the cover gas, and finally escape into the containment through leaks caused by slug impact. A variety of aerosol formation processes and related particle sizes is expected: Very small particles from fuel vapor condensation ($\leq$ 0.1 µm), larger particles from fragmentation processes ($\geq$ 10 µm), small coolant droplets from vapor condensation ($\approx$ 2 µm), and large coolant droplets from entrainment processes ($\geq$ 100 µm). For a more detailed summary, see, e.g., ref. /2/.

1.2 Aerosol Absorption in a Stable, Rising Bubble

The absorption of aerosols in a rising stable bubble (i.e. no change of bubble radius, no entrainment processes) is mainly due to inertial deposition, sedimentation and diffusion. Approximative expressions for the corresponding absorption coefficients, valid for spherical bubbles, are given by Fuchs /3/. In table 1, results from calculations based on these coefficients are given for the example of iron dust particles in a rising spherical bubble. In most cases, the absorption coefficients are relatively low, especially if the bubble is large, and particles have a good chance to be transported inside the bubble and released into the cover gas. If we define a retention factor RF as the ratio of aerosol mass initially inside the bubble and aerosol mass released into the cover gas, we calculate values of the order of 1 in case of large stable spherical bubbles. It should be mentioned, however, that the assumption of sphericity is a strong simplifiction: Large bubbles become cap-shaped, which makes the treatment of the aerosol behaviour more complex.

1.3 Absorption During Bubble Expansion and Oscillations

However, before dealing with aerosol behaviour in a rising bubble, it is necessary to investigate processes which affect the aerosol system during bubble formation. Bubble formation in the HCDA case is characterized by an initial high pressure discharge and subsequent rapid oscillations (due to cover gas compression and re-expansion) until eventually a stable rising bubble will be formed. Usually, frequency and overall duration of the oscillations occur on a much shorter time scale ($\approx$ 100 msec) than the subsequent buoyant bubble rise (seconds). So, as a first approximation, expansion/oscillation and rise a well as the related aerosol processes may be treated separately. Two important aerosol removal mechanisms related to the expansion/oscillation phase are: 1) Aerosols dispersed in a rapidly oscillating volume may impact the interphase since their inertia causes a 'phase shift' . Preliminary calculations (see chapter 4 and fig. 3) have shown that this process is very efficient. 2) A gas-liquid interface may become instable when it is subject to acceleration. When the acceleration is perpendicular to the interface, Rayleigh-Taylor instabilities will cause entrainment of liquid droplets into the gas volume /4/, sometimes in fairly large amounts. These droplets will mix with the aerosols and possibly cause a rapid settling.

Both processes, impaction and entrainment settling, may be very efficient to remove aerosols from the bubble volume, and lead to significantly larger RF values.

1.4 The KfK-FAUST Tests

FAUST (Freisetzung von Aerosol unter Störfallbedingungen) is an experimental KfK program to investigate the behaviour of rapidly expanding, oscillating and rising bubbles in water and sodium, and the corresponding formation, transportation and removal of particles. The goal is to give a contribution to a realistic assessment of the LMFBR-HCDA primary source term. In the first phase (FAUST-1), experiments with rupture disk discharge of gas-particle mixtures into a water pool at room temperature are performed. In the second phase (FAUST-2), the water pool is replaced by a sodium pool. There is no strong scaling to a reactor; geometrical parameters are subject of variation. Important quantities to be measured are the retention factors, the period of pressure pulses in bubble and cover gas, the amount of entrained coolant liquid in bubble and cover gas, and the coolant and particle mass escaping through defined openings in the cover plate. In the paper, experimental details, parameters, and results of the tests up to the present stage are presented. Theoretical onsets to understand bubble and cover gas behaviour and particle removal will be described, too.

2. DESCRIPTION OF THE TEST FACILITIES

The basic arrangement is a high pressure volume (simulating a reactor core) which is separated by a rupture disk from a cylinder containing a liquid pool and a compressible cover gas zone. The high pressure volume is located underneath the liquid pool; it is usually filled with simulation material to be discharged, e. g. iron or nickel powder.

FAUST-1A is a test facility with a 1.45 liter cylindrical high pressure volume (max. design pressure 10 MPa) and rupture disks of 5 cm diameter. The pool container is a lucite cylinder of 0.3 m diameter and 1 m height, surrounded by a water-filled rectangular cylinder to avoid optical distortion. The container is closed by a plate which has magnets for iron or nickel powder trapping. In addition, a movable magnetic 'star' is installed to trap airborne magnetic material in the cover gas after the discharge. The discharge is triggered by a plunger which destabilizes the rupture disk. The time from zero to a full opening of the discharge cross section is about 3 msec. Two high speed movie cameras are installed, normally running at 2000 frames/sec, for observation of the discharge zone and the gover gas zone. Pressure pulses are measured by transducers located at the bottom of the high pressure volume and at bottom and top of the pool cylinder, and recorded by transient recorders. Parameters of variation are discharge pressure (0.3 - 2.0 MPa), pool height (0 - 0.9 m) and particle size (1 - 100 µm Fe/Ni). All tests were done at room temperature.

FAUST- 1B (see fig. 1) has the same high pressure volume, but a different pool geometry: 0.6 m in diameter, and 0.6 m height. This geometry is closer to reactor conditions, whereas, in the previous case, a tall cylinder was chosen to allow for a wider range of pool height (and bubble rise time) variation. The cover plate has two valve-operated openings to

simulate leaks. Particles which are transported into the cover gas are trapped either inside on magnets or, if passing the leaks, outside on filters. Parameters of variation are discharge pressure (0.4 - 3.0 MPa), pool height (0 - 0.5 m), particle size (1 - 100 µm), and opening status of the leaks.

FAUST- 2B is a small-scale setup for rupture disk discharge into sodium. Mainly designed for under-sodium component testing, it will also deliver first results on bubble behaviour and particle retention in liquid sodium. The most important components are a 4 liter/10 cm diameter high pressure volume (max. 4 MPa), inconel rupture disks (up to 1.200 °C), a pool cylinder of 0.1 m diameter and 0.8 m height, a cover plate with a pneumatically driven valve to simulate leaks, and an external volume for trapping of material which passed the openings. The setup is equipped with an ultrasonic detection system and pressure transducers designed for high temperatures and sodium environment. At the present stage, typical experimental parameters are: Discharge of 1 MPa argon into 2.5 liters of sodium at temperatures (isothermal) up to 500 °C.

FAUST-2B will have a larger sodium pool (up to 300 liters) in a 0.6 m diameter/1 m height stainless steel vessel.

3. EXPERIMENTAL RESULTS

Until now, 31 tests of the 1A series, 19 tests of the 1 B series and 2 under-sodium tests of the 2 A series have been performed. A selection of experimental parameters and results is summarized in tab. 2.

Concerning the 1A tests, the following statements can be made: Bubble expansion changes from an initially hemispherical shape to a planar shape, causing a piston-type upward acceleration of the water pool with subsequent oscillations and correlated pressure pulses due to cover gas compression and re-expansion. The maximum cover gas pressure is significantly lower than the discharge pressure. At large pool height (0.9 m) numerous pressure pulses are registrated (ten or more), at medium height (0.6 m) typically five, whereas at low height (< 0.3 m) a straight penetration is possible (however, with strong water mixing). The oscillation period is between 40 and 80 msec, depending somewhat on pool height, but practically not on discharge pressure. Strong entrainment processes are observed in bubble and cover gas. Due to this, the water piston may, after a few oscillations, disassemble completely into a gas-water-mixture at low and medium pool height. At larger pool height, a stable center part remains, and a buoyantly rising bubble with the typical cap-shape is observed. The absorption of particles is found to be very efficient, especially during the expansion and oscillation phase. Airborne metal powder particles in the covergas after the discharge have never been observed. If the total discharge mass of metal powder is 10 g, and if the detection limit for covergas particles of 1 mg is considered, we find retention factors $RF > 10^4$. Nevertheless, particles were captured by the magnets in some cases, especially at lower pool height. It can clearly be stated from high speed film evaluation that these particles were "fished" out of the water by the magnets and had never been airborne in the cover gas.

In case of the 1B tests where the discharge opening is relatively small compared to the pool diameter, a jet-like expansion is usually

observed rather than a hemispherical one. However, during re-compression, we observe the transition into a piston-type configuration similar to the 1A tests.

The oscillation period is shorter compared to the 1A tests, again somewhat depending on pool height, but not significantly depending on discharge pressure. Entrainment processes in bubble and cover gas appear to be of similar magnitude and efficiency. Airborne particles have not been observed in the cover gas, even at low pool height (although there was material penetration), since there is a strong wash-out by entrainment. So, we may state again that RF 10^4. We have not observed significant differences between tests with normal water and with degassed water (e.g. 3 days at 0.03 MPa). The amount of water passing through the openings in the cover plate was found to be rather small (typically several milli-liters) and no particles have been found on the outside filters so far.

Presently, the 2A tests are under way, but still at a stage of component testing. Rupture disk discharge tests of argon at 1.5 MPa into a 500 °C sodium pool were performed. First results indicate that the amount of sodium released through leaks exceeds somewhat the released amount of water.

4. THEORETICAL ONSETS TO UNDERSTAND PARTICLE RETENTION AND BUBBLE BEHAVIOUR

Theoretical considerations related to the FAUST tests are presently under way in three areas:

A) Particle retention in a rising bubble
B) Particle retention during bubble expansion
C) Bubble and cover gas behaviour

A) Results of calculations with simplified assumptions (rising spherical bubble, absorption coefficients as given by Fuchs) have already been described and discussed in chapter 1.2 and tab. 1. Absorption of aerosols in a large rising bubble is relatively low.

B) Absorption of particles enclosed in an oscillating bubble is subject of the PAROGA calculations. We assume particle motion according to Stoke's law, and piston-type adiabatic oscillations of the water pool between bubble and cover gas. Entrainment is not considered. Particles may be absorbed by impaction on the water surface since their motion is characterized by a phase shift due to their inertia. A typical example (FAUST-1A geometry, 20 µm particles) is shown in fig. 3 . The particles are already getting absorbed during the first oscillation.

C) The time behaviour of bubble and cover gas volume, pressure, temperature etc. including entrainment is subject of the MOFA calculations. Two different approaches to describe the expansion phase were included: The hemispherical type using Rayleigh's equation, and the planar (piston) type. Best agreement with experimental results (especially the bubble period) was found when using the piston type. Concerning the entrainment rates, first calculations show agreement with Corradini's model in case of the cover gas, whereas the assumption of additional entrainment mechanisms seems to be necessary for the bubble volume.

5. CONCLUSIONS

Phenomena related to aerosol transport and bubble behaviour in case of an HCDA were investigated by discharging a high pressure gas-particle mixture into a water pool. As a next step, similar tests with hot sodium are under way. Calculations show that particles in a stable, rising bubble have a good chance to be transported into the cover gas. However, heavy bubble oscillations and strong entrainment in the beginning phase cause inertial impaction and wash-out and, thus, a very efficient particle removal. Since airborne particles in the cover gas were never observed, we conclude RF > 10^4 as retention factor for our conditions.

It needs to be pointed out, however, that fuel vapor condensation causing aerosol formation during (and not before) bubble expansion, oscillations and rise hast not been included in our considerations yet and needs further attention.

With respect to aerosol retention, our results may be compared to the ORNL-FAST tests /5/. Even with significantly smaller particles than in our case ($\leq$ 0.1 µm, produced by capacitor discharge vaporization of UO_2 under water), no airborne particles were found in the cover gas.

References

/1/ P. Royl et al., Untersuchungen zu Kühlmitteldurchsatzstörfällen im abgebrannten Mark-1A-Kern des Kernkraftwerks Kalkar, KfK 2845 (Dezember 1979)

/2/ W. Schikarski, W. Schütz, Nuclear Aerosols and LMFBR Source Term Analysis, Proc. of the LMFBR Safety Topical Meeting, Lyon/France 1982, III-347

/3/ N.A. Fuchs, The Mechanis of Aerosols, Pergamon Press, New York (1964)

/4/ M. L. Corradini, Heat Transfer and Fluid-Flow Aspects of Fuel-Coolant Interactions, MIT Report No. COO-2781-12TR (1978)

/5/ A. L. Wright, T. S. Kress, A. M. Smith, ORNL Experiments to Characterize Fuel Release from The Reactor Primary Containment in Severe LMFBR Accidents, Proc. of the CSNI Specialists Meeting on Nuclear Aerosols in Reactor Safety, Gatlinburg 1980, ORNL/NUREG/TM-404 (1980)

particle radius [µm]	bubble radius [cm]	absorption coefficients α_i [m^{-1}]	α_s [m^{-1}]	α_d [m^{-1}]	fraction absorbed [m^{-1}]	retention factor RF
0.1	0.5	0.037	0.0066	0.1195	0.151	1.18
1.0	0.5	3.747	0.660	0.0378	0.989	90.91
0.1	5.0	0.0012	0.00021	0.0021	0.004	1.004
1.0	5.0	0.119	0.021	0.00067	0.131	1.15

Tab. 1: Absorption of iron dust particles in a stable, spherical, rising bubble, calculated with the equation

$$dc/dx = - (\alpha_i + \alpha_s + \alpha_d) \cdot c,$$

for 1 m bubble rise path, with c = particle concentration in the bubble α_i, α_s, α_d = absorption coefficients for inertial deposition, sedimentation, and diffusion, as given by Fuchs /3/.

exp.	discharge overpressure (MPa)	pool height (cm)	particles Ni/Fe: total mass discharged (g)	particles Ni/Fe: diam. (μm)	particles Ni/Fe: trapped on magnets (mg)	RF_W	RF_A	bubble period (msec)	first overpressure peak in cover gas (MPa)
6	0.98	60	10.0	< 44	< 1	$> 10^4$	$> 10^4$	82	0.16
9	1.50	30	25.2	< 44	20	$1.24 \cdot 10^3$	$> 3 \cdot 10^4$	69	0.17
12	0.3	30	34.6	< 44	< 1	$> 3 \cdot 10^4$	$> 3 \cdot 10^4$	60	0.02
15	1.50	60	28.3	1	< 1	$> 3 \cdot 10^4$	$> 3 \cdot 10^4$	77	0.32
16	1.50	60	36.0	100	< 1	$> 3 \cdot 10^4$	$> 3 \cdot 10^4$	76	0.33
17	1.0	90	30.0	100	85	$0.4 \cdot 10^3$	$> 3 \cdot 10^4$	42	0.63
18	0.98	90	31.3	1	< 1	$> 3 \cdot 10^4$	$> 3 \cdot 10^4$	42	0.57
19	0.98	30	30.1	1	< 1	$> 3 \cdot 10^4$	$> 3 \cdot 10^4$	57	0.08
20	1.0	15	30.0	1	1435	21	$> 3 \cdot 10^4$	(50)	0.06
22	0.39	90	30.0	100	< 1	$> 3 \cdot 10^4$	$> 3 \cdot 10^4$	59	0.16
23	0.40	15	29.9	1	1643	18	$> 3 \cdot 10^4$	(80)	
24	1.0	90	20.0	100	3.4	$5.9 \cdot 10^3$	$> 2 \cdot 10^4$	44	0.63
25	1.0	30	20.0	100	5.0	$4 \cdot 10^3$	$> 2 \cdot 10^4$	66	0.11
26	2.0	30	20.0	100	35	$0.6 \cdot 10^3$	$> 2 \cdot 10^4$	(60)	0.36
27	1.99	60	30.0	1	< 1	$> 3 \cdot 10^4$	$> 3 \cdot 10^4$	74	0.6
29	1.0	60	30.0	< 44	< 1	$> 3 \cdot 10^4$	$> 3 \cdot 10^4$	81	0.19

Tab. 2: Selection of FAUST-1A tests (pool diameter .3 m, vessel height 1 m, closed system, particles trapped by magnets)

RF_W = "retention factor water", defined as ratio of total mass discharged and total mass trapped on magnets. The trapped particles were "fished" out of the water and were not airborne in the cover gas

RF_A = "rention factor airborne", defined as ratio of total mass discharged and airborne mass in cover gas after discharge.

Exp. No.	discharge overpressure (MPa)	pool height (cm)	particles: total mass (g)	particles: diameter (µm)	RF_W	RF_A	bubble period (msec)	leak status	water outside leak (ml)	particles on filter
102	1.99	40	32.2	< 44	> $3 \cdot 10^4$	> $3 \cdot 10^4$	48	1		
103	1.98	40	29.8	1	> $3 \cdot 10^4$	"	47	1		
104	1.0	20	30.0	1	20	"	37	1		
106	0.4	40	30.0	< 44	> $3 \cdot 10^4$	"	41	1		
107	1.01	50	30.0	< 44	> $3 \cdot 10^4$	"	41	1		
108	1.51	10	31.0	1	15	"	-	1		
109	1.01	40	31.0	< 44	> $3 \cdot 10^4$	"	52	2	~ 5	
110	1.51	40	30.0	< 44	> $3 \cdot 10^4$	"	56	2	~ 5	
111	1.99	40	30.0	1	> $3 \cdot 10^4$	"	47	1		
112	2.0	40	30.0	1	> $3 \cdot 10^4$	"	47	1		
115	0.33	40	30.0	1	> $3 \cdot 10^4$	"	46	3	0	0
116	1.03	50	30.0	1	> $3 \cdot 10^4$	"	48	3	~ 1	0
118	3.01	40	30.0	1	> $3 \cdot 10^4$	"	46	3	86	0
119	2.94	50	29.8	100	> $3 \cdot 10^4$	"	37	3	375	< 1

Tab. 3: Selection of FAUST-1B tests (pool diameter 0.6 m, vessel height 0.6 m, system closed or with openings, particles trapped by magnets or on filter)

RF_W, RF_A: see tab. 2; leak status 1: closed; leak status 2: Two openings Ø 4 cm each, with plastic bag; leak status 3: One opening Ø 4 cm , with filter, as shown in fig. 1

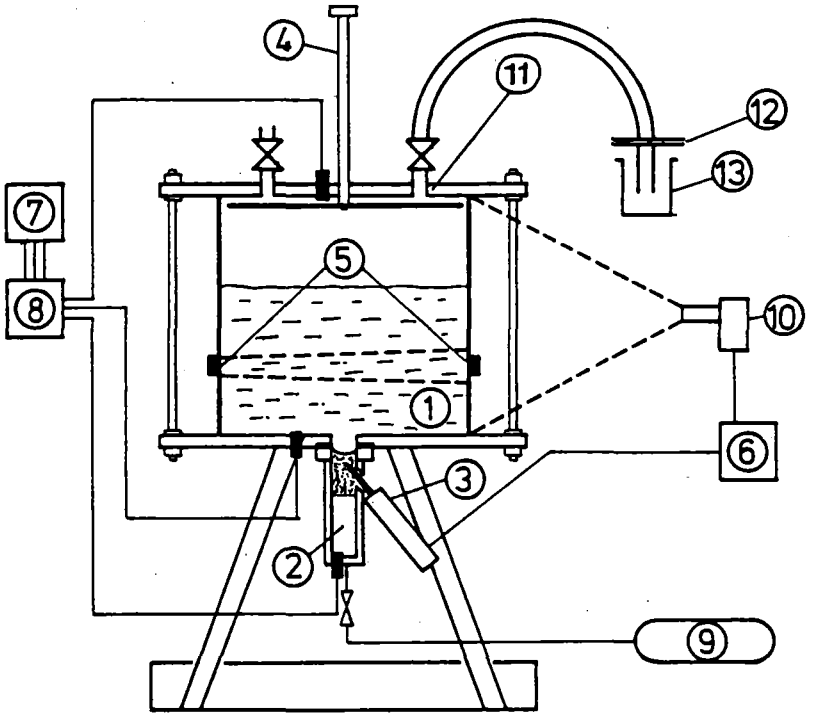

Fig. 1: FAUST-1B facility for discharge of a high pressure gas/particle-mixture into a water pool at room temperature

1 Lucite cylinder, 60 cm Ø, 60 cm height, water
2 High pressure volume 1450 cm³ with rupture disk Ø 5 cm and particles (Fe or Ni)
3 Plunger, pneumatically driven
4 Magnetic "star" (movable) to collect particles in cover gas
5 Ultrasonic system (preparing sodium tests)
6 Timing electronics
7 Transient recorder, multiprogrammer, computer
8 Pressure measurement
9 Nitrogen supply
10 High speed movie camera
11 Cover plate with openings Ø 4 cm
12 Filter for sampling of released material
13 Sampling of released water

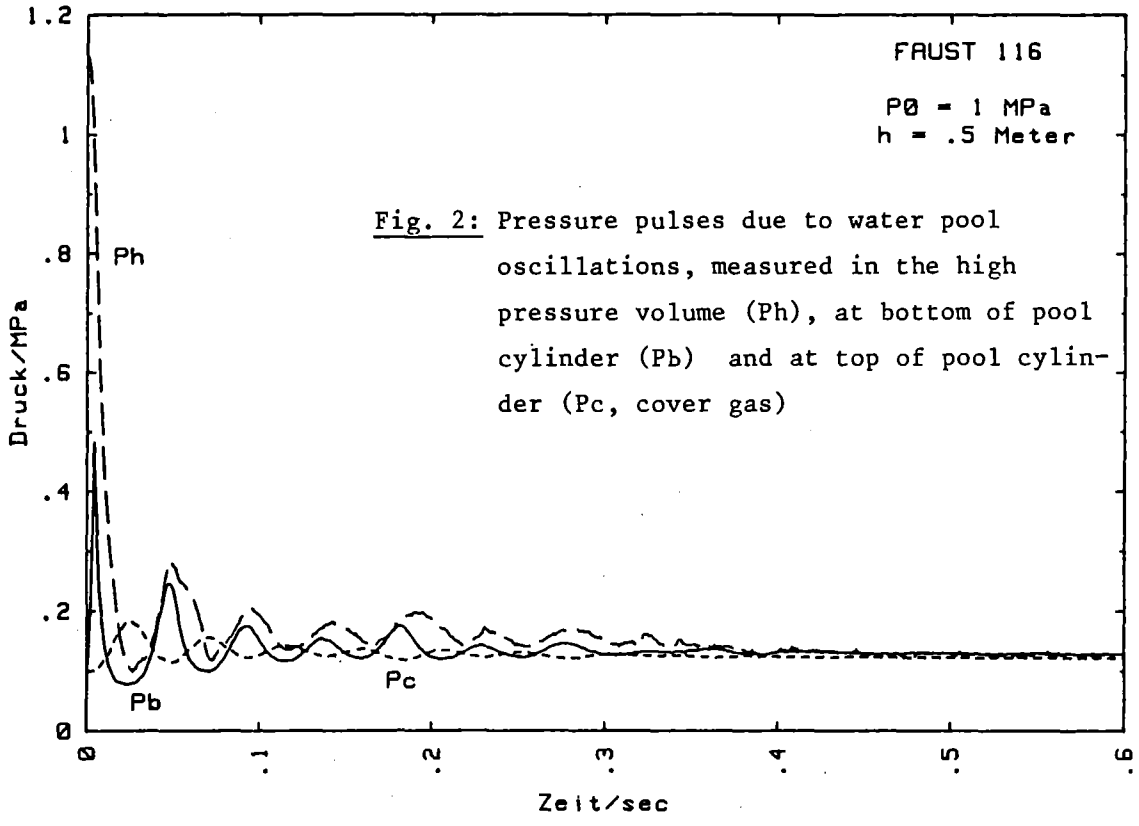

Fig. 2: Pressure pulses due to water pool oscillations, measured in the high pressure volume (Ph), at bottom of pool cylinder (Pb) and at top of pool cylinder (Pc, cover gas)

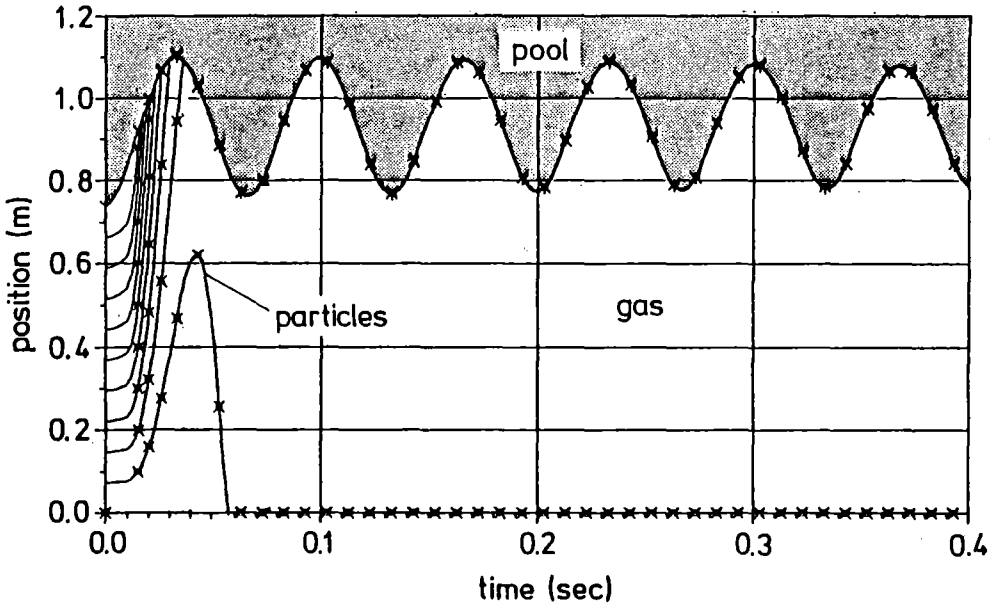

Fig. 3: PAROGA calculation: 1.1 MPa discharge of 20 µm iron particles at FAUST-1A geometry

Fuel and Fission Product Release from a Hot Sodium Pool; Removal of Methyl Iodide in Sodium Aerosol Atmosphere

by

H. Sauter and W. Schütz

Kernforschungszentrum Karlsruhe GmbH
Laboratorium für Aerosolphysik und Filtertechnik I
D-7500 Karlsruhe, W.-Germany

ABSTRACT

The release of fuel and fission products from hot sodium into an inert-gas atmosphere, the vaporization rate of sodium, and the behaviour of the sodium aerosol in a closed vessel are being studied in the NALA program at the Karlsruhe Nuclear Research Center. Pilot-scale trials (1 kg Na; 531 cm^2 pool area; 481-632 °C; 0.2 to 20 g of UO_2, NaI and SrO added; 2.2 m^3 tank heated to about 130 °C) and laboratory-scale glove-box tests (100 g Na; 38.5 cm^2 pool area; 550 °C; 0.2-5 g of UO_2 and SrO; release material collected in cold traps and filters) were performed. The main purpose of the experiments was to determine retention factors RF for U, I and Sr, including the behaviour of RF as a function of time and space. The retention for U and Sr in the sodium pool is very high; in the initial phase (about 10 % pool vaporization) it is in the range of RF = 10^3-10^4 for U and 500 for Sr, and it tends to increase with time. In contrast, RF values between 1 and 11 were found for iodine. The release of iodine can be attributed to vaporization processes; several models have been devised to account for it in this way. A number of indicators point to mechanical release (in particle form) for UO_2 and SrO.

As far as the theoretical part of the program is concerned, a fitting formula for the specific vaporization rate of sodium has been achieved on the basis of the vaporization rate proportional to the vapor pressure. The sodium aerosol system was studied through the mass concentration, the particle size distribution and the deposition behaviour. Model calculations were also performed with the PARDISEKO code. Agreement with experiment could not be achieved unless a modulus was introduced to allow for turbulent deposition. In the 2.2 m^2 tank, additional tests were performed on the decay speed of methyl iodide (20 ppm) under the presence of metallic sodium aerosols in argon or nitrogen atmosphere as well as under the influence of burning sodium or sodium fire aerosols in synthetic air.

1. Introduction

In a severe LMFBR accident with an extremely low probability of occurence (HCDA), large quantities of fuel, fission products and sodium may escape into the containment as a result of tank failure. So that the containment load and any possible release of the core inventory and sodium into the environment can be estimated, it is important to study the radiological source terms by experimental and model-theoretical means. The instantaneous or primary source term is due to the energetic expansion of the fuel into the coolant, which causes the formation of a bubble and the release of material from openings in the tank cover. In addition to the primary source term, a delayed or secondary source term, essentially

associated with core-melt CDA's and sodium vaporization, must be considered. The sodium is heated by decay heat and vaporizes into the inner containment to form an aerosol. Fuel and fission products may be entrained with it by various release mechanisms. Of interest in the derivation of the secondary source term are the activity released from the sodium pool, the amount of sodium vaporized, and the behaviour of the aerosol in the (inner) containment.

The NALA program at the Karlsruhe Nuclear Research Center (KfK) is contributing, mainly through experiments, to studies on this topic. Experimental parameters were mainly related to SNR 300 - conditions, especially the core catcher problem. In the NALA I phase /1/, laboratory tests were performed with on the order of 100 g of sodium and on the order of 1 g of UO_2 or fission products (Cs, NaI, SrO). The purposes of the NALA II phase /2/ included the following: to demonstrate that the NALA I results can be scaled up; to perform tests at pool and gas temperatures typical of an accident and with natural convection; to investigate the sodium aerosol system; to gain supplementary information about the retention factor, chiefly about its time dependence, and about release mechanisms; to determine the vaporization rates of sodium under reactor-specific temperature conditions; and to perform auxiliary modeltheoretic calculations for the aerosol system, using the PARDISEKO code.

In the paper, we will focus on NALA II, reporting experimental and theoretical results. Parameters and first results from a new program (METANA) on the decay of organic iodine compounds in sodium aerosol atmosphere will briefly be described, too.

2. Experimental Setups

Two different experimental setups were used in NALA II. Pilot-scale trials (T1 - T8; about 1 kg Na with UO_2, NaI and SrO; pool area 531 cm^2) were performed in a heated 2.2 m^3 tank (Fig. 1). These experiments served mainly to determine the retention factors RF of U, I and Sr in the initial phase of pool vaporization, to determine the sodium vaporization rates under accident-typical temperature conditions, and to investigate the behaviour of sodium aerosols (mass concentration, particle size, deposition). Laboratory-scale trials (G1 - G4; about 100 g of Na with admixtures of UO_2 and SrO; pool area 38.5 cm^2) were carried out in a glove box (Fig. 2); the quantities released were withdrawn and collected in cold traps and on filters. These experiments had the principal aim of determining the time dependence of RF for U and Sr and the spatial distribution of the concentration in the released sodium.

All the trials were conducted in an inert-gas atmosphere (Ar or N_2). Except for the UO_2, only nonradioactive material was used. Because of the accuracy of detection, it was necessary to work with higher fission-product concentrations than would occur under accident conditions.

3. Results and Interpretation

3.1 Iodine

For iodine release, RF values between 1 and 11 were found, with some proportionality between RF and the initial pool concentration. Calculation

with the Rayleigh equation for the distillation of a two-component mixture, with activity coefficients from Castleman and Tang, yielded RF values of about 3 which were largely independent of temperature and concentration. This conclusion agrees with the NALA I experimental findings. The concentration dependence in NALA II may be attributable to the fact that the concentration distribution in the pool was not homogeneous. Layer-by-layer analysis after a run (in the resolidified sodium) reveals iodine enrichment at the surface, then a depleted middle zone and finally a high enrichment near the bottom of the crucible. A model formulation based on iodine release from the surface layer also leads to results that are correct as to order of magnitude; for practical purposes, however, this model cannot be used, since it requires additional information from the experiment (surface enrichment). When all the results are assembled (NALA I, NALA II, French experiment /3/, Rayleigh equation), it may be concluded that risk analyses with RF = 3 give a realistic estimate of the iodine release.

3.2 Uranium and Strontium

The sodium pool has a very high retention capacity for uranium and strontium. Nonetheless, in uranium trials with 20 µm particles, traces were found in the released sodium significantly above the limit of detection; the RF(U) values obtained were between 10^3 and 10^4, in good agreement with NALA I. No significant relation can therefore be seen between RF and the pool size. In the case of strontium, the inductively coupled plasma method was used to determine the RF reliably; the values were in the range of RF(Sr) = 500 (Tab. 1).

The time dependence of U and Sr release was also seen to be pronounced. The release rates decline (i.e., RF increases) with time. This is the opposite of the situation in distillation theory, where the release rate must increase as the pool concentration rises. On the other hand, there are many indications that release takes place in particle form; for example, the position dependence of deposition in the 2.2 m^3 tank was very inhomogeneous (the highest concentrations generally occurred on the top cover) and displayed a characteristic pattern in the glove-box trials (highest concentration on the sampling hood, decreasing with distance from the source, as would correspond to the sedimentation behaviour of particles). Tests with dyes in water, considered as an analogous system, confirm this finding. If release is in particle form, the surface enrichment, which was also seen in most of the U and Sr trials, would play a crucial role. But no analytic expression could be found for this in the present work. The uranate reaction might affect the particle properties in the pool (size reduction), but there is no evidence that it is directly involved in the release mechanism (e.g., by raising the vapor pressure). The supposition made in NALA I, that higher RF values are found under natural convection than under forced convection, was confirmed. Particularly in the case of Sr release (NALA I, forced convection: RF = 20), this difference is very striking. The dependence of RF on the UO_2 particle size in the pool was investigated with 10 µm and 200 µm particles. A clear relationship could be seen; in the latter case, the limit of detection was reached at RF = 1.9×10^4 (Tab. 2a, b).

If experimental information on uranium release is assembled (NALA I, NALA II, the French PAVE experiments /3/, it can be concluded that RF = 10^3 gives a conservative estimate of the fuel release from nonboiling sodium

pools. In realistic evaluations, RF should be taken as increasing with time. The situation is similar for Sr, with RF = 500.

3.3 Sodium vaporization, sodium aerosols

For the sodium vaporization rate under the conditions prevailing in the 2.2 m³ tank (130 °C gas temperature, natural convection), the best fit is given by $\log \dot{m} = 8.062 - 5426/T - 0.5 \log T$, where m is in kg Na/m² - hr and T is in kelvins. The approximate proportionality to the vapor pressure is given by the very convenient relation $\dot{m} = 0.1\ p$, where $\dot{m}$ is in the same units as above and p is in torrs. Sodium aerosol mass concentrations of up to 20 g Na/m³ were measured in the tank. After the source is turned off, the decline in concentration can be approximately described by two exponential functions with a characteristic knee. The sodium aerosol diameters (50 % values of mass distribution), measured with an impactor, lay between 0.6 (less than 1 sec after production) and 2.5 µm at the maximum concentration. The deposition behaviour was characterized by very small quantities (< 1 %) on the top cover and large quantities (> 80 %) on the bottom cover. Deposits in the tank wall region were mostly found on horizontal projections. In modeltheoretic studies with the PARDISEKO code, calculations were performed of the mass concentration, particle diameter and deposition behaviour /4/. Agreement with the experimental values could not be achieved until a modulus was introduced to allow for turbulent deposition (Fig. 3a, b).

4. Decay of Methyl Iodide in Sodium Aerosol Atmosphere

Organic iodine compounds may be formed by reaction of fission iodide with organic material (dyes, insulation, carbon in sodium etc). The most likely candidate is methyl iodide CH_3I (abbrev. MeI). Since it is in the gas phase, it will - unlike NaI - penetrate the aerosol filters and contribute significantly to the radiological source term. It is very difficult to study MeI formation under accident conditions; however, the study of the decay (i.e. its medium life time) when exposed to sodium aerosols is of similar importance. In the METANA program, experiments on the decay of MeI in metallic sodium aerosol and sodium fire aerosol atmosphere are performed, using the 2.2 m³ NALA tank, equipped with an infrared spectrometer. In the trials investigating the decay of MeI in an inert gas atmosphere under the influence of sodium aerosols, lifetimes of 20 ppm MeI were found varying between 35 min at 0.04 g/m³ aerosol mass concentration down to less than 2.5 min (detection velocity limit) at 1.0 g/m³, respectively. However, lifetime values measured were found to be strongly dependent on natural convection within the vessel, and thus on pool heating necessary to generate the above mass concentrations.

Therefore additional trials with forced convection will give apparatus independent values. Iodine was quantitatively detected as sodium iodide after a number of runs, whereas the methyl radical was found to form methane to about one third of the initial available mass. The rest is assumed to form metallo-organic compounds with the sodium. Trials on decay in sodium fires and in synthetic air under the influence of fire aerosols are in progress. Both cases yield decay rates; but volatile organic compounds sometimes generated when starting a sodium fire interfered with methyl iodide infrared absorption measurement at our first trials. By doing some diagnostic and cleanup work, the problem is under control now.

Literature

/1/ W. Schütz, UO_2 and Fission Product Release from Sodium Pools (in German), KfK 3010 (1980)

/2/ H. Sauter and W. Schütz, Aerosol and Activity Releases from a Contaminated Sodium Pool (in German), KfK 3504 (1983)

/3/ M. Berlin, E. de Montaignac, J. Dufresne and G. Geisse, Evaluation of the Sodium Retention Factors for Fission Products and Fuel, Int. Meeting LMFBR Safety, Lyon, France, July 1982

/4/ H. Bunz and H. Sauter, Aerosol Behaviour in a Closed Vessel under the Regime of Natural Turbulent Convection, 11th GAeF Conference, München 1983

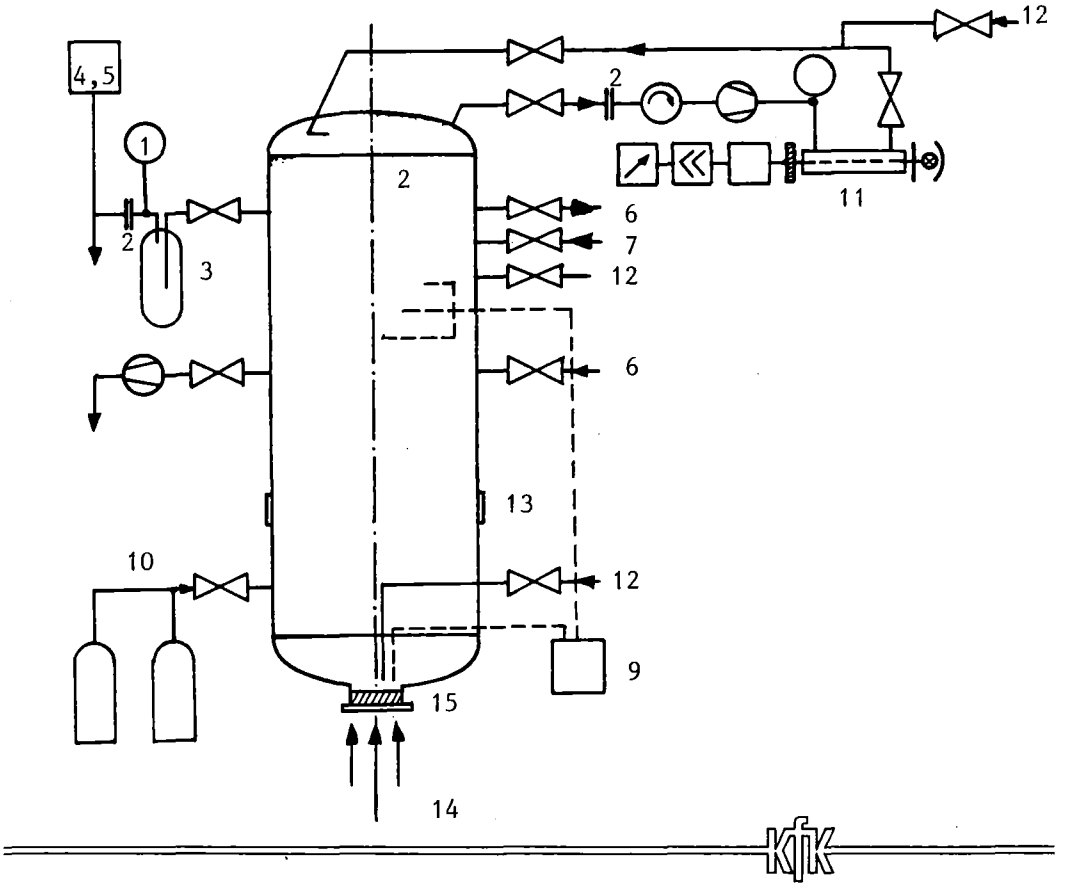

Fig. 1:

Measurement and monitoring devices for trials in the 2.2 m³ tank.
(1) Pressure measurement; (2) filter; (3) cold trap; (4) oxygen measuring instrument; (5) hydrogen measuring instrument; (6) wash-bottle set; (7) instrument for continuous determination of sodium aerosol concentration; (8) eight-stage Andersen impactor; (9) temperature measurement (2 thermocouples in sodium pool, 6 thermocouples in gas space, 2 thermocouples on top cover); (10) controlled supply of gas; (11) IR-spectrum analyzer; (12) MeJ-injection ports; (13) window; (14) heating of sodium pool; (15) sodium

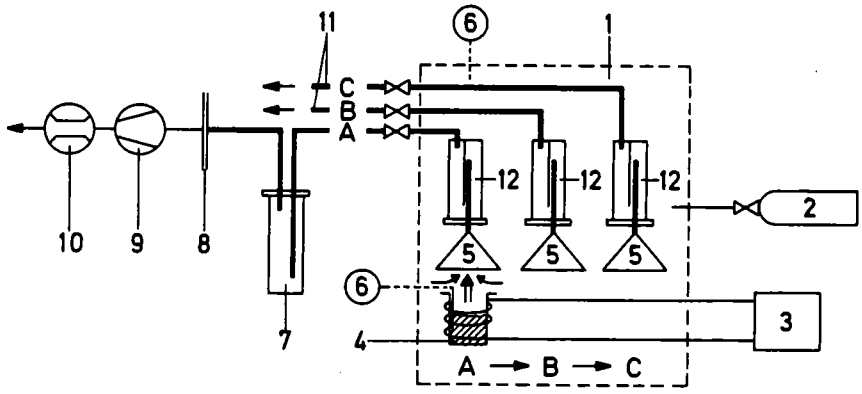

Fig. 2:

Laboratory-scale setups with half-open crucible in a glove box

(1) Glove box, inert (N_2) atmosphere, continuous O_2 monitoring

(2) Nitrogen supply

(3) Power supply for electrical heating of crucible

(4) Stainless-steel crucible, diameter 7 cm, height 10 cm, heated, containing about 100 g of Na and admixtures

(5) Hood at beginning of sampling system

(6) Temperature measurement

(7) Cold trap

(8) Filter (pore size 0.2 μm)

(9) Pump

(10) Measurement of volumetric gas flow rate

(11) Sampling system (7, 8, 9, 10) repeated

(12) Collector immediately downstream of hood

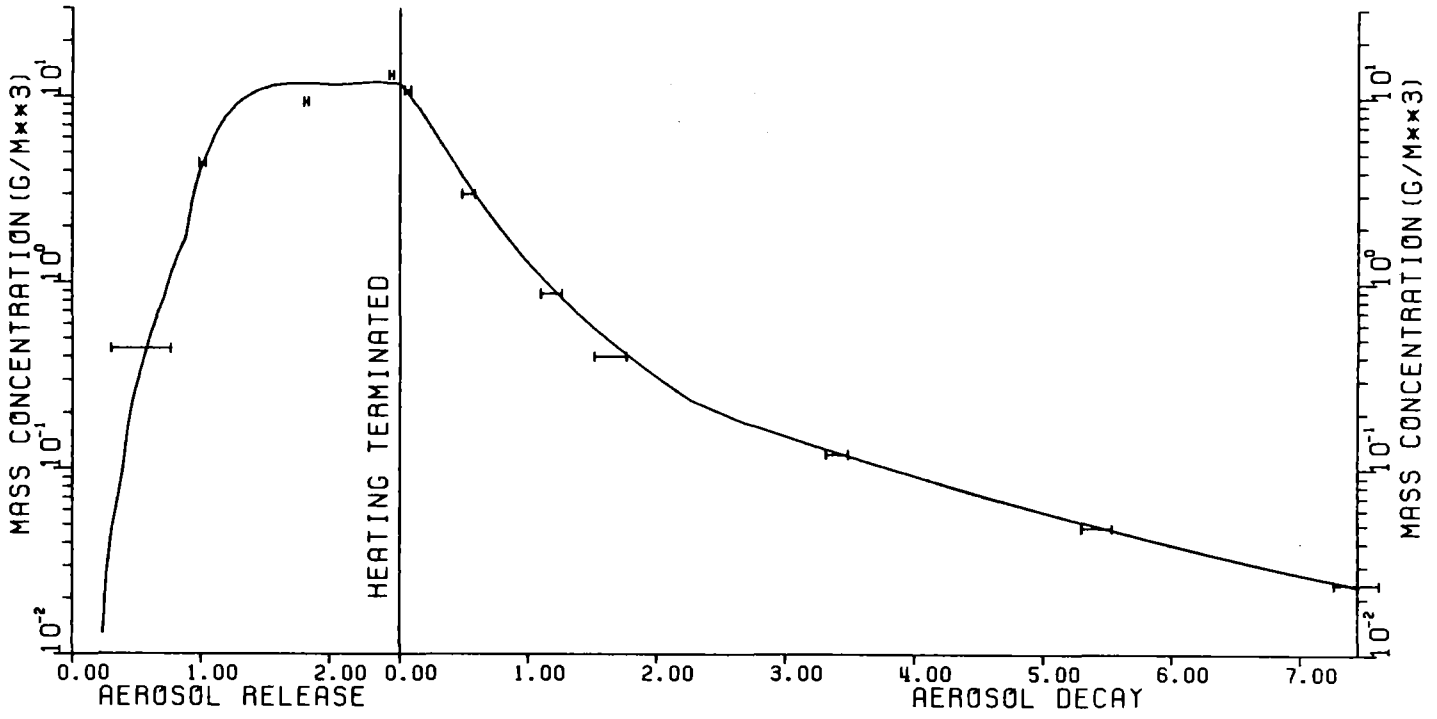

Fig. 3a:

PARDISEKO sample calculation: mass concentration versus time (trial T7). The bars represent the time interval for each wash-bottle sample. The time scale starts over after the pool heating is cut off.

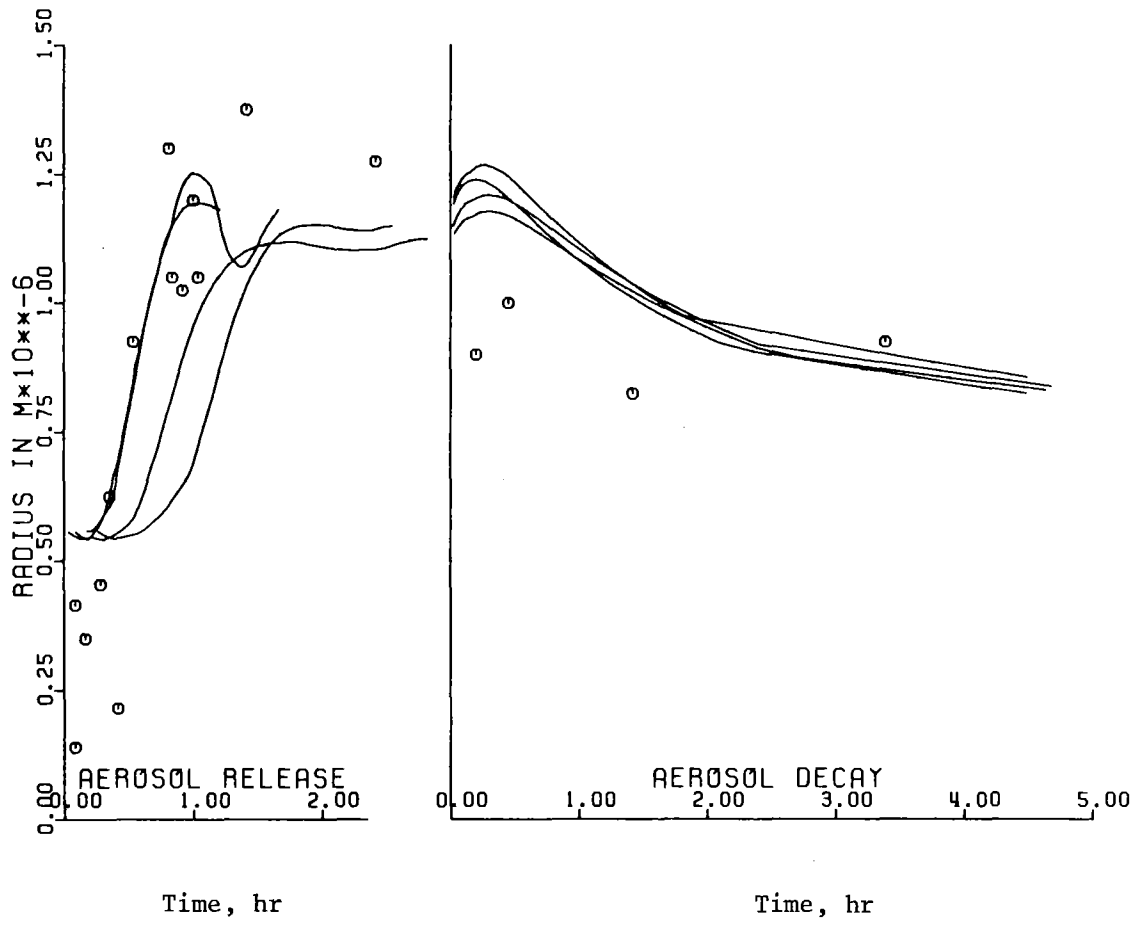

Fig. 3b:

PARDISEKO sample calculation: mean particle diameter versus time (trials T5-T8). The points are impactor measurements in trials T3-T5, plotted separately for heating and reheating phases.

1	2			3	4
Trial No.	Normalized Sr concentration in interval			Retention factor over whole run (6 hr)	Remarks
	I	II	III		
G 2	1	0,65	0,52	502	
G 3	1	0,72	0,61	580	(Note 1)
G 4	1	0,96	0,74	688	(Notes 1) 2)

Table 1: Strontium release, glove-box trials; time dependence of Sr concentration in released sodium and retention factor (RF).

$$RF = \frac{(Sr/Na)_{pool,\ initial\ value}}{(Sr/Na)_{released}}$$

Remarks: (1) Some samples were oxidized CO_2-free. (2) Samples were prepared glass-free.

Trial No.	Particle size, /¯µm¯/	Retention factor	RF limit of detection
T 5	200	$19{,}0 \cdot 10^3$	$20 \cdot 10^3$
T 6	20	$1{,}5 \cdot 10^3$	$20 \cdot 10^3$
T 7	20	$8{,}2 \cdot 10^3$	$40 \cdot 10^3$

Tab. 2a: Uranium release, trials in 2.2 m³ tank: retention factors

Trial No.	Retention factor RF					Normalized uranium concentration in released sodium in interval			Remarks
	in interval			averaged	overall				
	I	II	III	(I+II+III)	(Note 1)	I	II	III	
G 1				2)	$2{,}7 \cdot 10^5$				(Note 3)
G 3	$2{,}0 \cdot 10^4$	$3{,}7 \cdot 10^4$	$4{,}0 \cdot 10^4$	$4{,}0 \cdot 10^4$	$3{,}0 \cdot 10^4$	1	0,55	0,15	
G 4	$0{,}6 \cdot 10^4$	$1{,}1 \cdot 10^4$	$3{,}0 \cdot 10^4$	$1{,}2 \cdot 10^4$	$2{,}0 \cdot 10^4$	1	0,62	0,19	(Note 4)

Tab. 2b: Uranium release, glove-box trials: retention factors and normalized uranium concentration
Length of interval: about 2 hr.

Notes:
1) Includes all sodium and uranium for which time dependence could not be found (e.g., on outside of crucible, on thermocouple, etc.)
2) If all U is assumed released in 6 hr, RF = $6.7 \cdot 10^4$
3) Complete vaporization of sodium; time 27.5 hrs. 4) 10 µm UO_2 particles; G1 and G2: 20 µm UO_2 particles

Aerosols Released from Solvent Fire Accidents in Reprocessing Plants

S. Jordan and W. Lindner

Kernforschungszentrum Karlsruhe GmbH
Laboratorium für Aerosolphysik und Filtertchnik I
Postfach 3640, D-7500 Karlsruhe, W.-Germany

1. Introduction

Kerosene mixed with Tributylphosphate is used as solvent in nuclear reprocessing plants. Despite several precautions an incident might be that solvent leaking out from a reprocessing column spreads over the ground and starts burning. Solvent fires in nuclear processing plants are a burden on structures and components by pressure and heat development. There is also a potential risk from the release of fuel and fission product particles during the fire. The radioactive particles are attached to solvent fire soot aerosols.

For the calculation of the thermodynamic and radiological consequences of solvent fire accidents in reprocessing plants it is necessary to investigate the burning rates, particles release, particle characteristics and the activity release.

2. Thermodynamics of solvent fires

To estimate the consequences of burning solvents and to develop safety measures, pool fires were investigated by TBP-Kerosene mixtures as well as by organic aqueous mixtures. Kerosene- and Kerosene-TBP fires were performed in circular pans up to 2 m^2 surface area in the free atmosphere as well as in closed containments of sizes up to 220 m^3 /1/.

The specific burning rates were found to increase with increasing burning area: In the free atmosphere the burning rate increased from 80 $kg/m^2 \cdot h$ for a 0,1 m^2 to 120 $kg/m^2 \cdot h$ for a 2 m^2 area. In closed containments the rates were 40 - 50% lower than for fires in open air (Fig. 1).

The burning rate is determined by the vapor pressure of the solvent and the diffusion of oxygen to the evaporating solvent. The increasing burning rate with increasing area might be explained by a stronger oxygen transport to the burning area due to turbulent convection in large fires. This was confirmed by Kerosene fires with forced convection simulating a ventilation system in a reprocessing cell.

The oxygen concentration at which the fire extinguishes in closed containmenmts, depends on the containment volume, the burning area and the TBP-concentration increasing in the solvent during the fire. Fig. 2 shows the development of TBP-concentration during a pool fire. Usually the fire extinguishes at oxygen concentrations between 17.5 and 11%.

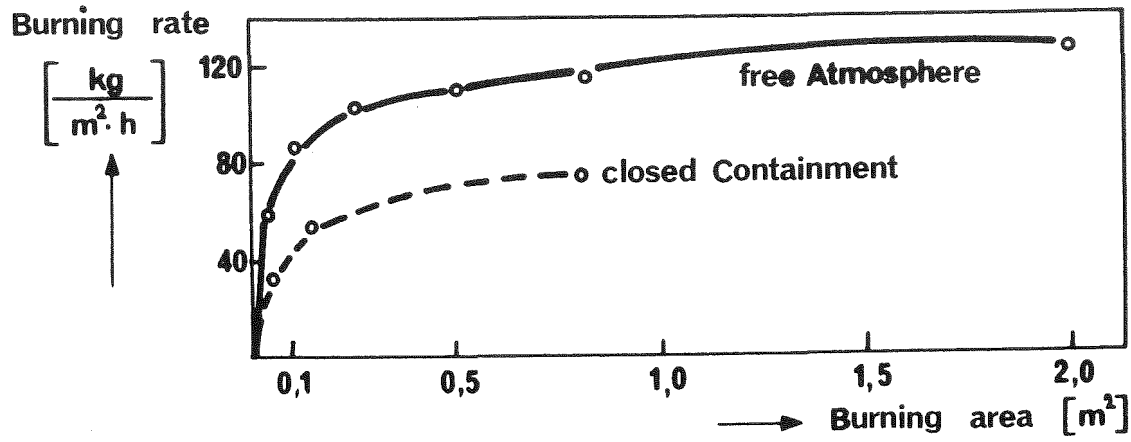

Fig. 1: Burning rate of pool fires

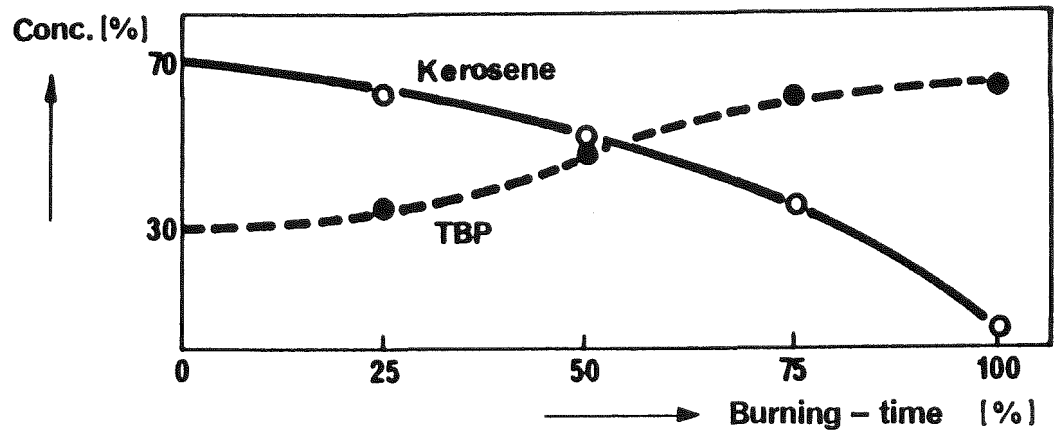

Fig. 2: Solvent concentration during pool fires

Fires of organic-inorganic mixtures without any extraction were performed in a first step only with Kerosene as the organic liquid.The duration and the burning rate of the fire depend on the ratio of the organic-aqueous phase, the pool depth and burning area. The course of the mixture fire is shown schematically in Fig. 3. During the first phase of the fire only Kerosene is burning in the upper layer of the pool, without any influence of the lower inorganic phase. As soon as the lower layer of the pool reaches a temperature above 100 °C, intensive boiling is observed which is accompanied by a release of HNO_3 decomposition products. In this phase the temperature in the pool is always close to 100 °C. As soon as the aqueous phase is evaporated, Kerosene burns at the same rate as in the first phase. This behaviour is observed for all Kerosene-HNO_3 ratios above 2 and pool depths below 3.5 cm.At lower Kerosene-HNO_3 volume ratios not all HNO_3 is evaporated; here phase 2 lasted until the extinguishment of the fire; a phase 3 was not observed.

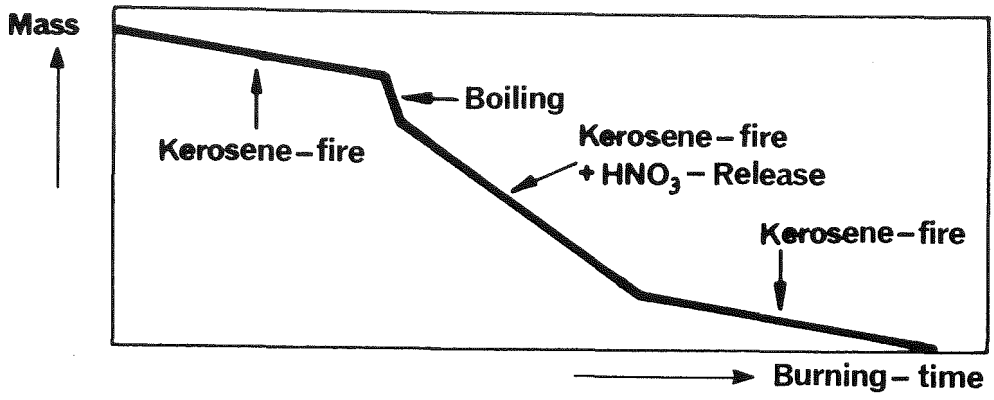

Fig. 3: Course of HNO_3-Kerosene pool fire

In a second step fires with HNO_3-extracted Kerosene/TBP mixtures were investigated. By extraction of HNO_3 with Kerosene/TBP mixtures, HNO_3-concentrations in the organic phase up to 4 mol/l were attained. The course of the fire follows the scheme of Fig. 3: At a temperature of 130 135 °C the TBP-HNO_3-complexe decomposes and the burning rate increases substantially. The intensity of the decomposition increases with increasing HNO_3-concentration. Compared with the burning rate of the unloaded solvent the overall burning rate increases by max. 25%. During the decomposition of the HNO_3-TBP complex the temperature in the solvent increases to 200 °C. During this process the solvent has a red colour; brown-yellow smoke is released. At the end of the fire decomposition products of TBP (Butene) are burning.

A quite similar behaviour of the burning development was observed for mixtures of Kerosene and TBP loaded whith extracted Uranylnitrate. Here the intensity of burning during the decomposition of the Nitrate-TBP-complex is smaller than for the HNO_3-TBP/Kerosene mixtures.

3. Solvent Fire Aerosols

The formation of aerosols during Kerosene fires is due to incomplete burning. The aerosols are composed mainly of soot but contain HDBP and phosphoric acid in Kerosene/TBP mixture fires.

In contrast to the burning rate the aerosol formation rate is not constant during the whole period of burning. Kerosene-TBP mixtures have a substantially higher aerosol formation rate in fires than pure Kerosene. The integral aerosol formation is for Kerosene fires about 2% of the burned solvent, for Kerosene-TBP mixtures 70/30) about 14% with maximum values of 25% shortly before the extinguishment of the fire. Fig. 4 demonstrates the portion of solvent formed as aerosols during the fire. Increasing the TBP-concentration during the fire - as shown in Fig. 2 - increases the aerosol formation. TBP was identified as the aerosol forming substance. The development of aerosol production is the same for fires in the free atmosphere and in vented containments.

In closed containments the aerosol release shows the same tendency: increasing rate with burning time and a peak shortly before extinguishment.

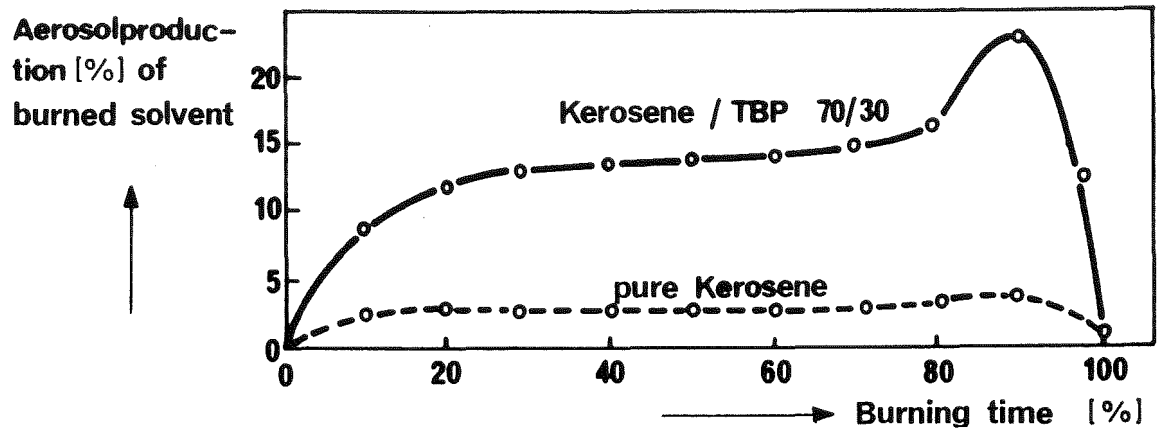

Fig. 4: Aerosol formation rates during pool fires

Soot aerosols are composed of chain-like agglomerated small primary particles. The evaluation of electron microscopic photographs yields a geometric diameter of primary particles of d = 0.05 µm. These particles agglomerate already in the flame; single particles have not been identified.

The size and shape of these agglomerates depend on solvent composition, type of burning (pool fire, spray fire) and composition of the atmosphere (relative humidity). Particles released from fires involving Kerosene-TBP mixture have a chain structure at the beginning of the fire; at the end of the fire (high TBP concentration) particles resemble more to droplets /2/. A chemical analysis has shown that these particles absorb large quantities of phosphoric acid and oil derivatives. These liquid substances produce clotted soot agglomerates. A similar effect was observed in Kerosene spray fires because of incomplete burning of spray droplets. Droplets-like particles were also observed during fires in closed containments; they probably resulted from the absorption of water produced in large quantities in the course of burning.

The particles sizes measured under different conditions are combined in table 1. The smallest aerodynamic mass equivalent mean diameter was found for pool fires in the free atmosphere: d = 0.22 µm. Particles in closed containments and spray fire aerosols were slightly larger, attaining up to d = 0.45 µm.

Experimental conditions	Mass median aerodynamic diameter	Standard deviation	Median geometric number rel. diameter	Standard deviation
Primary particles	-	-	0.05	1.5
Free atmos. outside the flame (pool fire)	0.22	2.0	0.3	1.6
Closed vented containment	0.34	1.8		
r.h. 90% (pool fire)	0.35	2.0	0.3	1.8
Free atmos- (spray fire)	0.45	1.8	-	-

Tab. 1: Diameters of solvent fire aerosols

4. Fuel Particle Release

A special facility was designed to investigate the release of fuel from burning solvent. A schematic diagram is shown in Fig. 5. 50 ml of solvent was burned in a 6.5 cm diameter crucible. The whole quantity of airborne reaction products and released particles were sucked into a pipe system. All particles in the gas stream were deposited on a membran filter, type SM 65 (1.2 µm pore size), followed by a second membran filter (SM 30, 0.45 µm pore size), to assure 100% deposition. Several safety measures had to be considered to avoid any release of Uranium particles into the environment.

The solvent was loaded with different concentrations of Uraniumnitrate 1.0 - 10.5 - 50.2 - 69.5 - 84.4 g Uran/liter. These are typical concentrations in the reprocessing process.

The whole quantity of Uranium released during one experiment was determined integral by X-ray spectrometry. That included particles deposited on the walls of the pipe as well as the particles deposited on the first analytic filter. No Uranium could be indicated on the second membran filter.

In preparation for the spectrometric measurements the released soot and the filter material were solved in mixtures of HNO_3 and H_2SO_4. The spectrometer was calibrated with solutions of Cobalt. Each determined Uranium concentration has an error of $\pm$ 5%. The release rate of Uranium from burning solvent was found to be proportional to the Uranium concentration in the solvent: The release rate for a concentration of 1 g U/l is 0.7%, while the rate increases to 1.4% at 84 g U/l. The actual measured dependence is shown in Fig. 6.

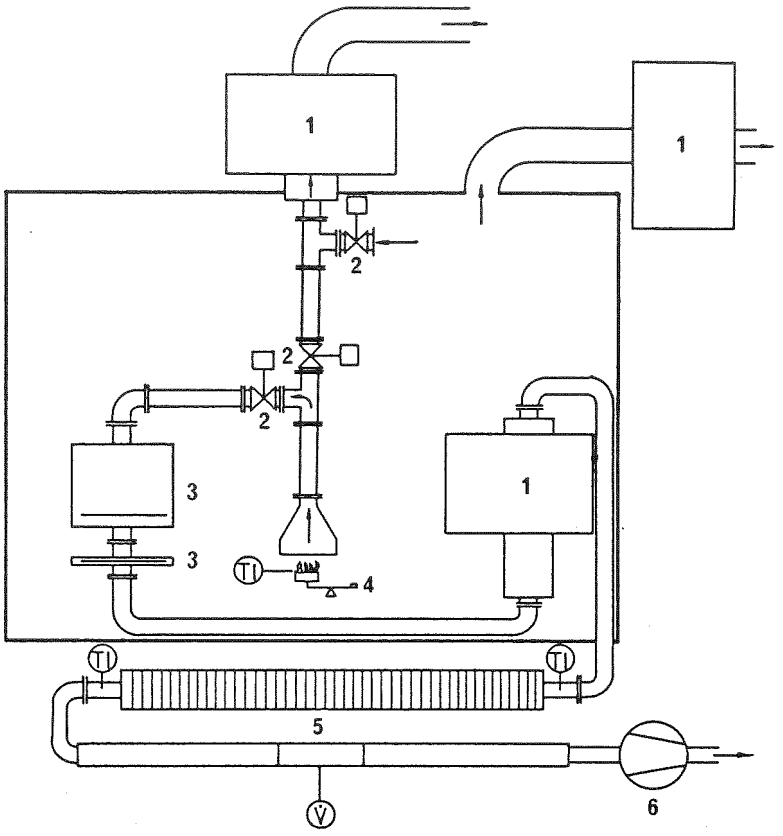

1 HEPA filter
2 Valves
3 Analytic filter
4 Balance with burning pool
5 Air cooler
6 Vacuum pump

Fig. 5: Facility for the investigation of Uranium release during solvent fires

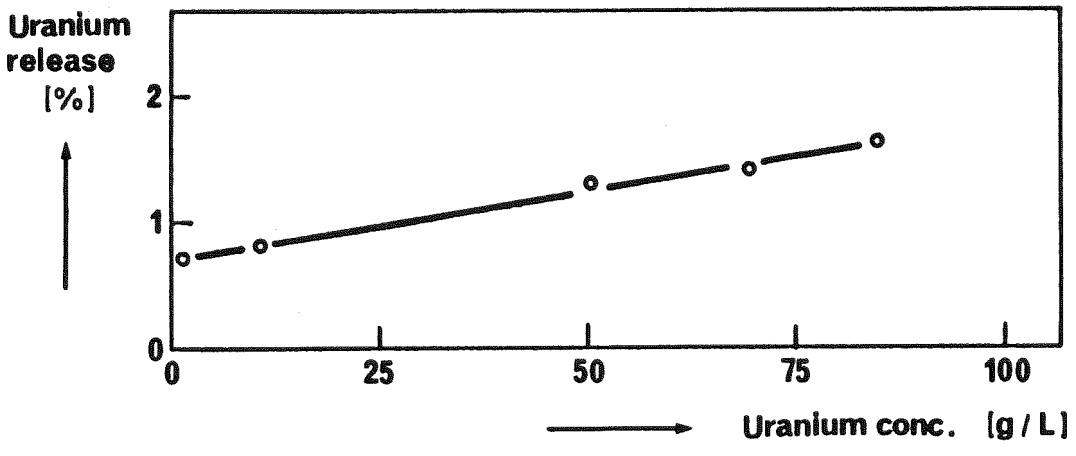

Fig. 6: Uranium release during solvent fires

One reason for the dependence of the relative Uranium release rate from the Uranium concentration in the pool might be the measured dependence of the burning rate from the Nitrate concentration as reported in the last chapter. High concentrations of Nitrate in the organic phase cause high turbulences and strong bubbling in the burning solvent which favours the release of Uranium particles. The integral burning rates for the experiments which were the basis for the values in Fig. 6 are shown in Fig. 7

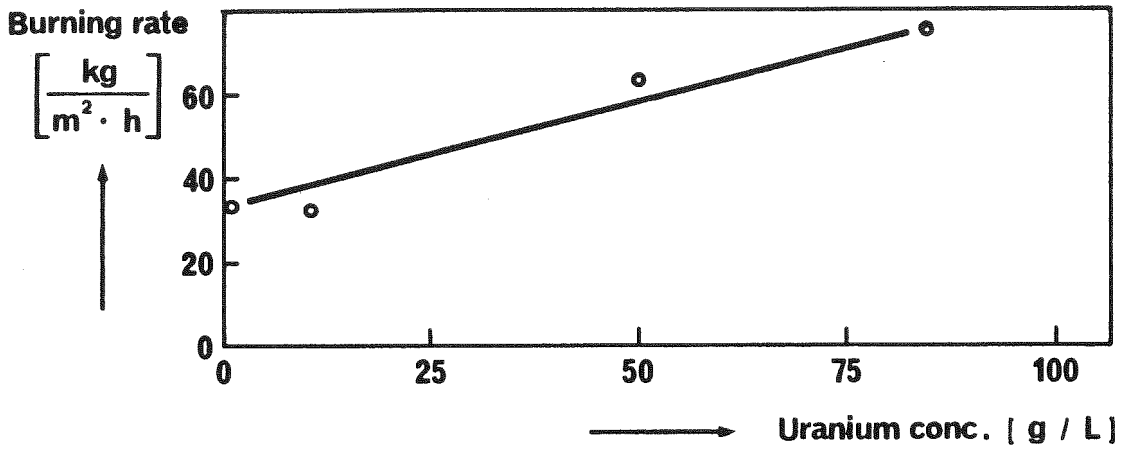

Fig. 7: Burning rate of solvent with different Uranium concentration

5. Conclusions

Thermodynamic, aerosol characterizing and radiological data of solvent fires in reprocessing plants have been established in experiments. These are the main results:

- Depending on the ventilation in the containment, Kerosene-TBP mixtures burn at a rate up to 120 kg/m² h.

- The aqueous phase of inorganic-organic mixtures might be released during the fire. The gaseous reaction products contain unburnable acidic compounds.

- Solvents with TBP-Nitrate complex shows higher (up to 25%) burning rates than pure solvents (Kerosene-TBP). The Nitrate complex decomposes violently at about 130 °C with a release of acid and unburnable gases.

- Up to 20% of the burned Kerosene-TBP solvents are released during the fire in the form of soot particles, phosphoric acid and TBP decomposition products. The particles have an aerodynamic mass median diameter of about 0.5 µm.

- Up to 1.5% of the Uranium fixed in the TBP-Nitrate complex is released during solvent fires.

Literature:

/1/ S. Jordan and W. Lindner: The Behaviour of Burning Kerosene, Aerosol Formation and Consequences
CSNI Specialists Meeting, April 26-28, 1983, Los Alamos/U.S.A.

/2/ S. Jordan and W. Lindner: Aerosolentstehung bei Kerosinbränden
9th Conference 'Aerosols in Science, Medicine and Technology'
23-25 September 1981, Duisburg/F.R.G.

RELEASE AND DISPERSION OF OVERHEATED LIQUIDS FROM PLUTONIUM-NITRATE TRANSFER CONTAINERS

H.D. Seehars, D. Hochrainer, M. Spiekermann

Fraunhofer-Institut
für Toxikologie und Aerosolforschung
Grafschaft/Sauerland
Germany

ABSTRACT

Potential traffic accidents of 18B-transfer containers with liquid Pu-nitrate during road transportation may induce an exposure of the Titanium vessel itself to a fire due to the ignition of the leaking fuel up to a critical level, causing the burst of the vessel and the more or less complete release of the contents in form of liquid aerosol particles.

Here it is reported on experiments with the original Titanium vessels and a quadrivalent Cerium-nitrate solution used as a substitute with similar physico-chemical properties as the Pu-nitrate solution.

Total release of mass as well as of the respirable particle mass fraction is strongly dependent on the orientation of the vessel. Maximum release, connected with a high bursting pressure and the total destruction of the vessel, is observed in case of the vertical orientation of the vessel.

According to the weak temporal variability of the low wind speed (between 3 and 4.5 m/s) and direction parallel to the centre of the measuring area strong horizontal variations of the inhalation hazard occured in the range less than 50 m from the origin, while spatially homogenous inhalation hazards were observed in the range of more than 50 m up to 200 m, almost independent on the orientation of the vessel. The extremely high total particle mass fractions between 1.6 and 8.6 mg at distances up to 50 m are noticeable.

Scanning electron microscope analysis and electron probe microanalysis of Cerium particles deposited up to distances of 100 m from the origin, indicated their deposition in the liquid state.

INTRODUCTION

Within the scope of the fuel cycle, in the Federal Republic of Germany the 18B-container is used to transport a nitric solution of Pu(IV)-nitrate from the fuel reprocessing plant to the fuel element fabrication plant. This container exists of a cladding material, a phenolic resin foam material and a resistant inner vessel of metallic Titanium with a volume of 11.5 l (Schulz-Vorberg, B. et al., 1979).

Potential traffic accidents during transportation may induce a destruction of the cladding to such a degree that the Titanium vessel itself may be exposed to a fire due to the ignition of the leaking gasoline. The heat energy transfer causes an increasing temperature and overpressure in the vessel up to a critical value, resulting in the burst of the vessel and the more or less complete release of the liquid contents in form of liquid or solid aerosol particles with a wide variety of particle sizes.

On account of safety requirements it is impossible to handle Pu-compounds during outdoor experiments. Hence, it seems to be reasonable to use a nitric solution of Ce(IV)-nitrate as a substitute of Pu(IV)-nitrate according to the following arguments:

1. The Lanthanides and Actinides are characterized by a similar electronic configuration.
2. The Lanthanides and Actinides are characterized to a certain extent by a chemical similarity.
3. Cerium is tri- and quadrivalent, Plutonium additionally penta- and hexavalent.
4. The quadrivalent Pu- and Ce-nitrate compounds are soluble to a high degree in nitric acid in a wide variety of concentrations.
5. The quadrivalent Pu- and Ce-nitrates are decomposed at temperatures between 200 and 220 degrees centigrade into the quadrivalent oxides.
6. Comparing acid solutions with high elemental concentrations of Pu and Ce (e.g. 250 g/l), the mass differences due to the conversion of a droplet into a solid salt particle are not very evident.

EXPERIMENTS

During the experiments three original Titanium vessels, filled with a Cerium nitrate solution of 250 g Ce/l in 5 molar nitric acid, were exposed to a fire at three different spatial orientations. Characteristic temperature and pressure behaviour within the vessel was studied up to the moment of the burst. An array of 7 dust sampling devices along a sector of a circle with a centre angle of 40 degrees and distances

between 20 and 200 m from the origin was used to learn something about the release and dispersion of a droplet cloud with very high initial droplet velocities of some 500 m/s. Membrane filters were used to collect as well the total as the respirable particle fraction, the latter derived from separation techniques with a horizontal elutriator. The neutron activation comparator technique was applied to determine the collected mass on the filters. Additionally, the total particle mass fraction was collected on Nuclepore filters at distances between 50 and 200 m from the origin to identify single particles containing Cerium, by electron probe microanalysis and to investigate their surface properties by scanning microscope analysis.

The two-dimensional expansion of the cloud of Cerium nitrate as a function of time was determined by a camera of type Canon equipped with a winder.

The volume of the liquid in the vessel was 8 l, corresponding to 75 % of the volume of the vessel.

RESULTS

The vessels were horizontally, nearly horizontally and vertically exposed to the fire. The experiments demonstrated that the degree of destruction of the vessel was strongly dependent on its spatial orientation (table 1).

table 1: Bursting pressure, temperature and time as a function of the orientation of the vessel

Exp. No.	Orientation of the vessel	p_B (MPa)	T_B (^oC)	t_B (min)
1	0^o(h)	1.85	18.5	2.40
2	5^o(n.h.)	4.25	92.0	3.13
3	90^o(v)	6.95	244.0	8.70

h: horizontal; n.h.: nearly horizontal; v: vertical

Total destruction of the vessel with fragments being found in a distance of 40 m from the origin was observed along with the vertical orientation of the vessel, whilst the experiment with the horizontal orientations only resulted in a partial destruction in form of a crack of a length between 15 and 25 cm parallel to the logitudinal axis of the vessel.

The physical process is the increase of pressure in a closed system caused by the external energy intake. The increasing temperature of the solution in the system produces

an increase of vapour pressure above the liquid surface. Nevertheless, the medium retains its state of aggregation, until the proportionality limit of the Titanium metal is attained. In this moment the wall of the vessel at one point in the range of the gas/vapour phase begins to flow and bursts in a split of a second. Instantly after the explosion, the partial or total release of the liquid contents occurs along with the simultaneous formation of droplets or solid particles. The generated particle size spectrum is particularly dependent on the initial droplet velocity, the initial droplet diameter, the surface tension and the viscosity of the solution due to the effect of aerodynamic breakup processes on the fragmentation events of droplets.

The evaluation of the inhalation risk implies the determination of the totally released respirable particle fraction which is not amenable to direct measurements. However, this parameter may be derived from the assumption that the concentration of the pollutant at one measuring point near the ground in the range of 20 m from the origin and the spatial dimensions of the moving cloud of pollutant above this point are known (table 2).

table 2: release of total mass and the respirable particle mass fraction as a function of the orientation of the vessel.

Exp. No.	I (deg.)	$1-\frac{M^{V}_{tot}}{M_{tot}}$ (%)	$M^{RPF,Ce}_{20}$ (µg)	$M^{RPF,Ce}_{tot}$ (g)	$M^{RPF,Ce}_{tot}/M_{tot}\cdot 100$ (%)
1	0	60	n	n	n
2	5	91	11	3.2	0.16
3	90	100	54	64.0	3.20

I : orientation of the vessel.

M^{V}_{tot} : remaining mass of elemental Cerium in the vessel.

M_{tot} : total mass of Cerium in the solution.

$M^{RPF,Ce}_{20}$: mass of elemental Cerium, belonging to the respirable particle fraction, determined on the backup filter of the elutriator, in a distance of 20 m from the origin, by neutron activation analysis.

$M^{RPF,Ce}_{tot}$: totally released respirable mass fraction of particles.

n : no data.

Maximum release rates of respirable particle fraction were observed during the experiment with the vertical orientation of

the vessel corresponding to the high bursting pressure of 7 MPa and the complete release of total mass of the contents. Because of the unexpected results of the first experiment with a low bursting pressure of only 1.9 MPa and extremely low temperature of the liquid, release rates of the respirable particle fraction could not be determined. However, according to the low level of total release of mass, the release rate of the respirable particle fraction is expected to be essentially lower than 0.16 %.

Dispersion experiments were used to estimate the inhalation hazard and the total mass concentration of the pollutant in different distances up to 200 m from the point of explosion. Fig. 1 shows the horizontal variations of these parameters for the nearly horizontal orientation of the vessel.

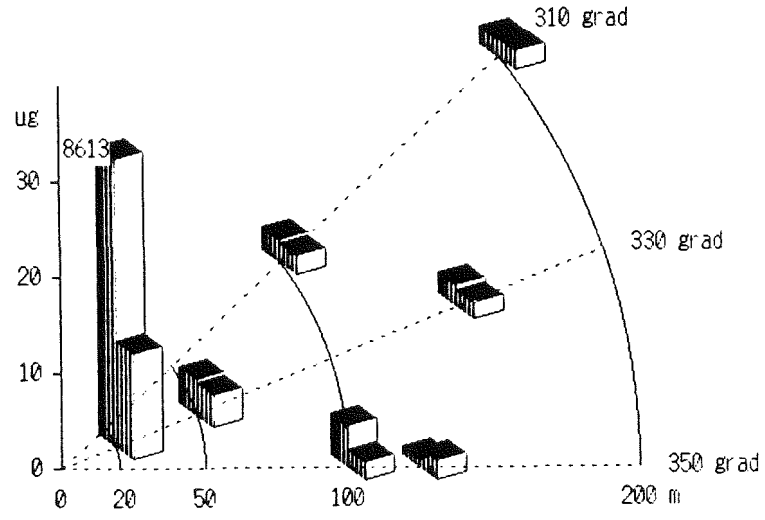

Fig. 1: Inhalation hazard and total particle mass vs distance from the point of explosion (Exp. 2).
Orientation of the vessel: nearly horizontal.

Levels of total or respirable mass fraction exceeding a mass of 30 µg, are noted on the top of each column. According to the meteorological conditions during the experiment with a windspeed of 3 m/s, a weak variability of windspeed and -direction during the movement of the droplet cloud across the measuring area and decreasing turbulence in the afternoon along with the decreasing solar radiation, spatially homogenous and relatively high level inhalation hazards were observed in the range between 50 and 200 m from the point of explosion. Note the extremely high level of 8.6 mg of total particle mass fraction at a distance of 20 m. Presumably, very large droplets were catapulted during the more or less directed spontaneous release against the filter.

Apart from a somewhat higher windspeed of 4.5 m/s and an obviously stronger turbulence in the surface layer because of the intensive solar radiation towards noon, the

meteorological conditions during the experiment with the vertical orientation of the vessel did agree very well with those of the preceeding experiment. Taking account however of the "isotropic" release of droplets because of the total destruction of the vessel and the high bursting pressure the strong horizontal variations of the total particle mass fraction and inhalation hazard along the central ray of the measuring area are explainable to a high degree (Fig. 2).

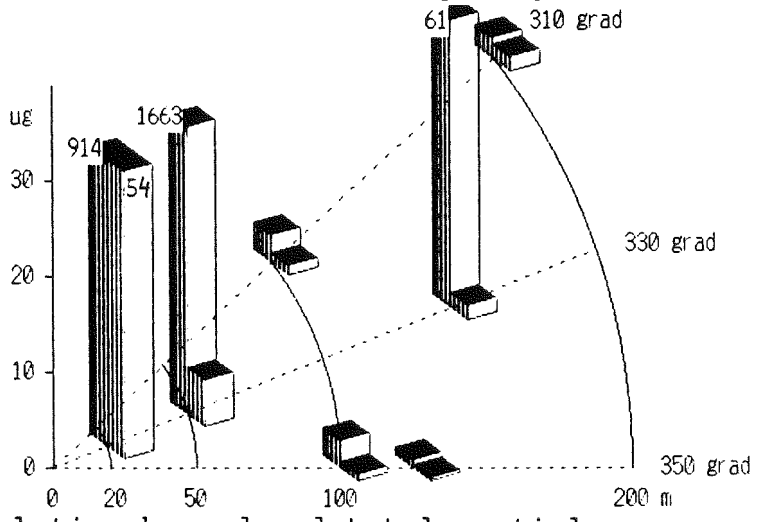

Fig. 2: Inhalation hazard and total particle mass vs distance from the point of explosion (Exp. 3). Orientation of the vessel: vertical.

Considering the low levels of inhalation hazard at distances of more than 50 m we have taken account of the dilution effects of turbulence in the surface layer.

Remembering the different clearance of inhaled particle mass in the lung with regard to Pu(IV)-oxide and Pu(IV)-nitrate it is important to know whether the particles inhaled in the range of the scene of accident have a liquid or solid state. Scanning electron microscope analysis and electron probe microanalysis of Cerium particles deposited on the filters up to distances of 100 m from the point of explosion demonstrate that the particles were in the liquid state, as can be realized from Fig. 3. Obviously both particles are not far away from having a sherical shape. The upper particle has a projected diameter of approximately 17 µm and is characterized by two almost linear cracks running from the particle centre to its periphery. The white shade at the top of the particle is an iron particle which has deposited on the drop afterwards and has somewhat mixed with the liquid. The cracks arose during the phase of drying of the droplet from developing strain forces inside the drop. The lower fotograph shows a particle with a projected diameter of 11 µm and a zone of fracture located at the lateral part of the particle.

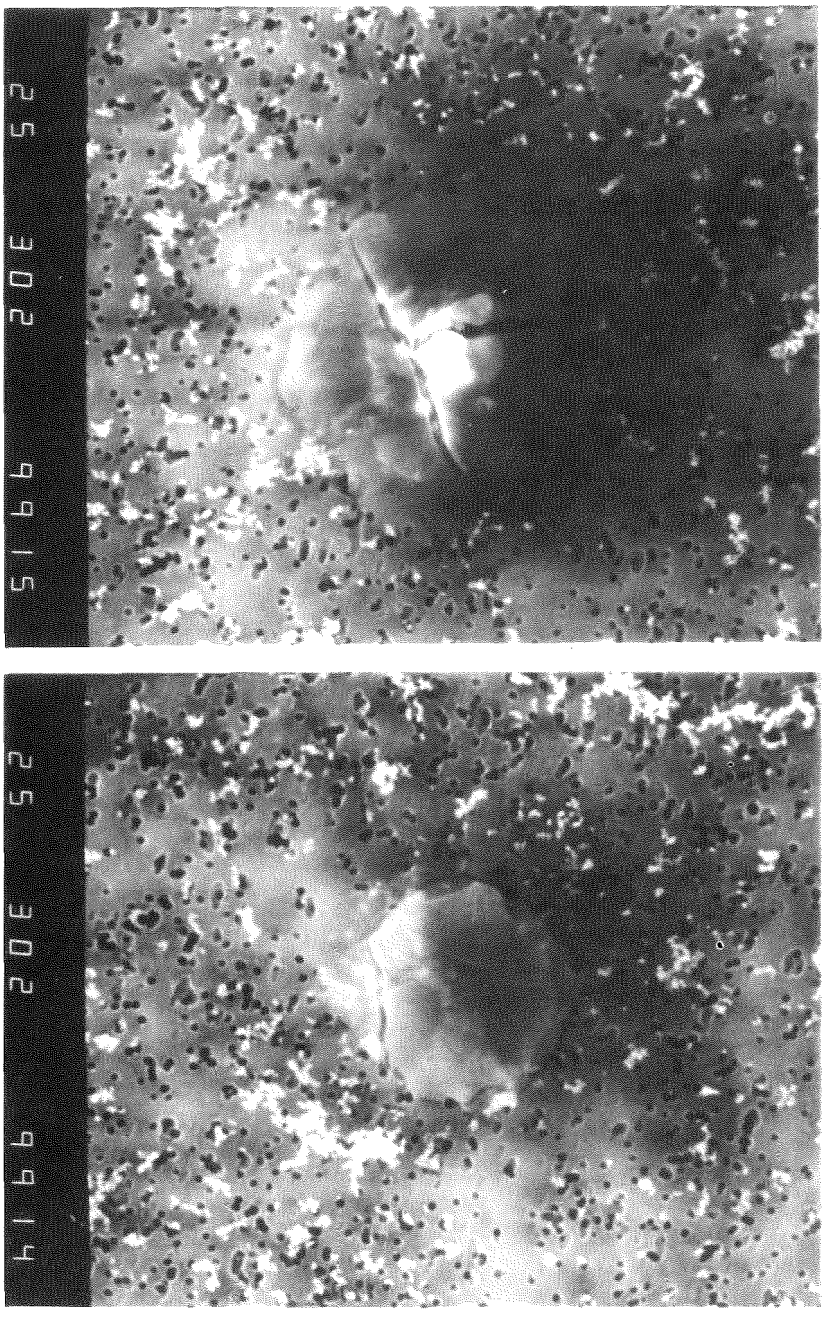

Fig. 3: Two particles containing Cerium, deposited at 100 m distance from the point of explosion.
magnification: 3000 x

REFERENCES

1. Schulz-Vorberg, B. et al., "Klassifizierung und Sicherheitsreserven von Transportbehältern für radioaktive Stoffe".
Abschlußbericht Bundesanstalt für Materialforschung
BMI SR 35

FISSION PRODUCT RETENTION IN DESIGN BASIS FAULTS

C. Smedley
National Nuclear Corporation Limited
Whetstone, Leicester, England.

ABSTRACT

The paper addresses primary coolant behaviour and fission product retention in design basis faults taking place in the auxiliary building of a PWR. The purpose is to enable a realistic estimate to be made of the radiological consequences of these faults and also to enable fission product removal to be claimed in the filtration plant of the emergency exhaust system.

Design basis faults of interest include pump seal leaks and pipe ruptures in the Residual Heat Removal System and in the Chemical and Volume Control System. These are associated with the discharge of superheated or subcooled primary coolant into a compartment of the building. The coolant flashes (if superheated) and fragments to drops which are then available for transport through the compartments and ventilation system. For the purposes of this paper, fission products (iodine and caesium) are assumed to remain associated with the water phase during flashing and transportation (i.e. large partition coefficients are assumed). The analysis is therefore restricted to the hydrodynamic behaviour of primary coolant.

The aim of the analysis is to predict the release of primary coolant in the form of water and steam to the filtration system. The following topics are considered:

1. Flashing and atomisation of the primary discharge to arrive at steam release rates and an estimate of drop sizes.
2. Response of the building (i.e. pressurisation transient).
3. Retention of primary liquid in the compartment in which the fault occurs. This is treated very simply because of the difficulty in defining flow paths and velocity profiles, but is expected to be highly significant.
4. Retention of primary liquid in the ducting of the ventilation system. Drop removal is estimated by applying available deposition theories and by allowing for evaporation.
5. Removal in the filtration plant. This requires an assessment of the form in which fission products reach the filters (i.e. as particulate, vapour or in aqueous solution) as well as the expected loading imposed (i.e. mass flux, concentration and humidity).

Results are presented to show the effect on the amount of coolant retention of the three major parameters (i.e. drop sizes, flow velocity and duct diameter). The analysis is also applied to a simple representation of the building ventilation ducting which shows that, depending on drop sizes, the fraction of liquid discharged from the rupture which reaches the filtration plant may be as small as 1%.

Several problems and uncertainties are identified including drop sizes, retention in a compartment (which is particularly important to demonstrate for non-flashing discharges) and the definition of a nett deposition velocity to account for the interaction between the various deposition processes.

1. INTRODUCTION

The radiological consequences of design basis faults for the Sizewell 'B' PWR are based on conservative assumptions with respect to fission product retention within the plant. For faults taking place in the auxiliary building, to which this paper is restricted, the assumption is made that all fission products contained in the discharged primary coolant are released to the atmosphere. In many cases, however, this assumption is considered to be unnecessarily conservative and means of estimating more realistic consequences are described in this paper.

2. DESCRIPTION OF FAULTS

Design basis faults taking place in the auxiliary building are associated with leakage of primary coolant from the Residual Heat Removal System (RHRS) and the Chemical and Volume Control System (CVCS) as a result of postulated failures such as pipe cracks, guillotine breaks or pump seal leaks. These systems may be functioning either in normal operation or in a post fault condition. The faults are divided into two categories depending on whether the temperature of the coolant is above or below 100°C. The significance of this distinction is that, when the temperature is above 100°C, flashing of the discharge will take place together with some degree of pressurisation of the building and it is necessary to establish the extent and consequences of such pressurisation. Faults of interest are listed in Table 1 which also defines the relevant thermodynamic condition.

For the purposes of analysis, the assumption is made that all water remaining after flashing is fully fragmented to drops by the flashing process itself and/or by atomisation. Complete fragmentation is also assumed in faults for which the temperature of the coolant is below 100°C, although it is expected that only a small proportion will remain airborne.

3. AUXILIARY BUILDING RESPONSE

The auxiliary building consists of a large number of separate compartments occupying four levels. Compartments in which are housed hardware containing primary coolant (e.g. pipes, pumps, heat exchangers, chemical treatment plant) are provided with inlet and extract ventilation ducts as well as a drain system to collect any leaked coolant. Some compartments are connected by fire/smoke vent panels.

Under normal conditions the building atmosphere is serviced by a ventilation system. On detection of a primary coolant leak in the building (or following a LOCA in the containment), the air intake system is isolated and an emergency exhaust system is actuated. This utilises the same ductwork as the normal system but separate fans are used to draw air/steam through emergency exhaust filters. For the Sizewell 'B' station, it has been estimated that the exhaust system is capable of preventing pressur-

isation for all leak rates associated with the faults of Table 1, except for faults 1(a) and 3(a). Where flashing takes place, some degree of local pressurisation will result with venting to adjoining compartments, but overall, the steam release and associated radio-activity will be withdrawn by the exhaust system. For larger leak rates with flashing, although the exhaust system will accommodate a fraction of the discharge, some steam and activity will reach exterior walls and may leak directly to the atmosphere. Retention is only addressed therefore for faults in which there is no significant pressure transient. For this reason, faults 1(a) and 3(a) are excluded from further analysis, although it should be noted that the radiological consequences of these faults are sufficiently low even with the assumption of zero retention.

TABLE 1 DESIGN BASIS FAULTS

	Pressure (bar)	Temperature (°C)
1. RHR pipe crack		
(a) Normal operation	30	177
(b) Normal operation	30	<100
(c) Post-LOCA operation	20	<100
2. RHR pump seal failure		
(a) Normal operation	30	177
(b) Normal operation	30	<100
(c) Post-LOCA operation	20	132
(d) Post-LOCA operation	20	<100
3. CVCS faults		
(a) Pipe break	41	146
(b) Pipe break	41	<100

4. CHEMISTRY CONSIDERATIONS

It is assumed that the important fission products (caesium and iodine) are sufficiently non-volatile during flashing and during transport through the building, to remain associated with the water phase. Retention of fission products can then be quantified in terms of the retention of primary liquid. This assumption may not however always be justified. In some cases, where evaporation of drops proceeds to near dryness, there is evidence to indicate that iodine is sufficiently volatile to partition into the vapour phase. The resulting small particulate would then contain only the non-volatile species (caesium). In these circumstances retention can only be claimed by virtue of the performance of the filtration plant of the emergency exhaust system (see section 7.3).

5. RETENTION PROCESSES

Processes considered in estimating retention are (i) deposition of drops on surfaces by turbulence, (ii) gravity settling, (iii) thermophoresis and (iv) evaporation. A brief description is given below together with relations for the deposition velocity for each process. The theoretical expressions are taken from the review in [1].

5.1 Deposition by turbulence

Deposition by turbulence is strongly dependent on drop sizes. For sub-micron sized drops, turbulent diffusion is dominant. In the size range 1-100 μm, deposition takes place as a result of the momentum acquired by the drops from the turbulent velocity component of the gas stream normal to the surface (eddy diffusion-impaction regime). As drop sizes increase, particle inertia becomes more important. Surface roughness also has a pronounced effect and it is assumed in this analysis that all surfaces are smooth resulting in conservatively low deposition velocities.

The turbulent deposition velocity (V_t) is expressed in dimensionless form (V^+) as $V^+ = V_t/U_*$ where U* is the friction velocity.

In the turbulent diffusion regime, V^+ is given by

$V^+ = 0.057 \ (D_p/\nu)^{2/3}$

where D_p = drop diffusivity

ν = kinematic viscosity of the carrier gas.

For drops greater than 0.1 μm in diameter, the deposition velocity is related to a dimensionless relaxation time (σ) defined as

$\sigma = U_*^2 \ t_r/\nu$

where t_r = relaxation time = $4 \ d\rho_l/3C_D \ \rho_g \ U_t$

here d = drop diameter

C_D = drag coefficient (function of drop Reynolds number)

U_t = terminal velocity of drop

ρ_l, ρ_g = density of liquid and gas phases.

Approximate relations, adequate for the present purposes, are presented in [1] for calculating the deposition velocity in the eddy diffusion-impaction regime ($\sigma<17$) and in the inertial regime ($\sigma\geq17$):

For $\sigma<17$; $V^+ = 0.057 \ (D_p/\nu)^{2/3} + 4.5\times10^{-4}\sigma^2$

where it is assumed that turbulent diffusion and eddy diffusion act independently so that the overall deposition velocity is given by the sum of the two components.

For $17<\sigma<200$; $V^+ = 0.13$

and for $\sigma>200$; $V^+ = \frac{2.6}{\sqrt{\sigma}} \left[1 - \frac{50}{\sigma}\right]$

5.2 Gravity settling

The gravitational deposition velocity (V_g) is given by the relation $V_g = gt_r/2$, where g is the acceleration due to gravity and the factor of $\frac{1}{2}$ is included to account for the interaction of turbulence on the settling velocity. The variation of this parameter (retardation factor) with flow properties and turbulence is considered in [2] and it is considered that the value of $\frac{1}{2}$ is reasonable.

5.3 Thermophoresis

The thermophoretic force experienced by drops in the temperature gradient between the carrier gas and walls is a function of the Knudsen number of the drop, λ/d, where λ is the mean free path of the gas molecules ($\sim 0.1\mu m$). For drop sizes greater than $1\mu m$, the thermophoretic velocity V_e can be expressed as

$$V_e = 0.0858\ k_B\ \theta d\ (Kn)^{3/2}/d_m^2\ \mu$$

where k_B = Boltzmann's constant, d_m = gas mean molecular diameter, θ = temperature gradient, d = drop diameter, Kn = Knudsen number and μ = dynamic viscosity of gas phase.

The temperature gradient is determined over the thickness of the laminar sublayer and may be expressed as

$$\theta = U_*^2\ \frac{(Tgas - Twall)}{(U-5u^*)},$$ where U is the velocity of the gas phase.

5.4 Evaporation

Evaporation of drops is considered either in steam or air depending on the temperature of the discharging coolant. For faults in which flashing takes place with the formation of saturated steam, evaporation results from the enhancement of vapour pressure by curvature effects and is prominent for small drops of a few microns in size. The change in diameter of a drop with time can be described by the following relation [3]:

$$d_t^3 = d_o^3 - 48\ k\alpha T_s\ t/\rho_\ell^2\ L^2$$

where d_t = diameter at time t, d_o = initial diameter, k = thermal conductivity of steam, α = surface tension, T_s = saturation temperature and L = latent heat.

For faults in which the discharge temperature is below 100°C, drop evaporation in air takes place by mass transfer, the rate of which is given by the usual relation as follows:

$$\text{mass transfer rate, } N = \frac{KA}{R}\left[\frac{p_\ell}{T_\ell} - \frac{p_a}{T_a}\right]$$

where A = surface area of drop
R = gas constant
p_ℓ = vapour pressure of water at temperature T_ℓ
p_a = vapour pressure of water in air at T_a
K = mass transfer coefficient obtained from the empirical relation of [4] i.e. $Sh = 2.0 + 0.6\ Re^{1/2}\ Sc^{1/3}$.

In the treatment of evaporation, the reduction in vapour pressure as a result of dissolved solids is neglected, but may be sufficient to prevent complete evaporation to dryness.

A further removal process is provided by condensation of steam on cool walls which sets up a nett mass flux to the wall in which drops are entrained. The resultant deposition velocity is dependent on the steam concentration which is unknown (except at locations local to the break) and the process is therefore neglected. It is likely to be important for removal of small drops.

6. ESTIMATION OF DROP SIZES

Data on drop sizes under representative conditions (Table 1) are not available in the literature for either flashing or non-flashing jets. It has therefore been necessary to apply a theoretical method together with a sensitivity study. For all faults considered, drop sizes are calculated via a critical Weber number (We_c) to arrive at a maximum stable size, d_{max}.

i.e. $d_{max} = We_c \, \alpha / \rho_g \, U^2$

Here ρg is the density of steam atmosphere and U is the relative velocity between liquid and vapour. The distribution of sizes below this maximum is assumed to be given by an upper limit log-normal function as found in many spray applications (although this may not be valid for flashing jets).

The value of the critical Weber number applied is 13 as recommended in [5] for sudden exposure of drops to a gas stream. Inherent in this treatment is the assumption that fragmentation by hydrodynamic processes dominates over thermal fragmentation by flashing (where appropriate).

In considering RHRS faults, the relative velocity (U) in the above equation is taken to be the velocity of the discharging jet which, for conservatism, is calculated by neglecting frictional losses through the break. In the case of pump seal failures, considerable friction loss is expected to occur through the degraded seal and other components of the pump. A more realistic assessment is not available at the present time but is the subject of further investigation. The jet velocity is therefore given by the following relation:

$$U = (2 \Delta P / \rho_\ell)^{1/2}$$

For flashing jets, ΔP is the difference between the liquid supply pressure and the saturation pressure at the relevant temperature.

For the CVCS fault considered (fault 3(b) of Table 1), the relative velocity is simply the superficial liquid velocity at the outlet of the pipe.

Drop sizes calculated by this method are independent of geometry of the break and, therefore, for faults in the RHRS, no distinction is made between pump seal failures or pipe cracks. Maximum drop sizes and discharge velocities are given in Table 2 together with the mass median diameter ($d_{v\mu}$) and the 1% limit on the distribution (i.e. 1% of the liquid mass below this size). For faults in which the RCS temperature is above 100°C the fraction of the discharge which flashes to steam is also given in Table 2.

It is recognised that a large amount of uncertainty is associated with these drop sizes and experimental data is required. A break-up process which is not accounted for is that caused by impaction of the discharging jet on nearby obstacles. Some idea of the importance of this can be inferred from the correlation for drop sizes produced by two impinging non-flashing jets as given in [7]. Extrapolating this correlation to RHRS conditions results in smaller drop sizes by a factor of between 2 and 3. It is considered that the greatest uncertainty in drop sizes is associated with flashing jets and the data of [6] suggest that a sensitivity analysis with a reduction factor of 10 may be suitable.

TABLE 2 DROP SIZE ESTIMATES

	Temperature (°C)	d_{max} (μm)	$dv\mu$ (μm)	$d_{1\%}$ (μm)	U (m/s)	Steam fraction
RHR pipe crack						
Normal operation	177	270	93	14	68	0.15
Normal operation	< 100	212	73	11	78	-
Post-LOCA operation	132	350	120	18	60	0.06
Post-LOCA operation	< 100	323	110	16	63	-
CVCS pipe breaks	< 100	large			2	-

7. CALCULATION OF RETENTION

The fractional retention of primary liquid is estimated by considering firstly, removal in the compartment, secondly, removal in the ventilation ducts and, thirdly, removal in the filtration system.

7.1 Retention in the compartment

A large proportion of the discharge from the rupture, remaining as water, can be expected to be retained in the compartment in which the fault occurs by, for example, gravity settling and wetting of walls and surfaces. This liquid would then enter the radioactive drain system. The quantity involved cannot be estimated precisely; much will depend on the flow pattern set up by entrainment of air into the jet, the performance of the ventilation system and the orientation of the break. A highly simplified estimate may be made by assuming a uniform velocity profile vertically upwards through the compartment determined by the ventilation withdrawal rate (see section 7.2) and the cross-sectional area of the compartment. By applying Stokes' law, a cut size can be arrived at above which drops settle out under gravity. The cut size so obtained is approximately 10μm which is equivalent to almost complete liquid removal in the compartment. In reality, however, jetting effects and the existence of a non-uniform velocity profile will dominate and may result in a larger cut size. The rough calculation does indicate, however, the degree of conservatism in the case which follows.

7.2 Retention in the ventilation ducting

Because of the uncertainty in claiming retention in the compartment, the conservative assumption is made that all of the atomised liquid enters the ventilation system. Retention is then estimated by applying the deposition theories of Section 5. The following points are relevant to the analysis:

(i) The flow velocity in all ducts is assumed to be equal to the design figure of 10m/s. A sensitivity calculation is included in which the velocity is reduced to 5 m/s.

(ii) The deposition theories applied are only applicable to straight ducts where the flow is fully developed. Removal has therefore been estimated in straight runs of ducting in excess of ten equivalent diameters in length which are free from bends and junctions. Figure 1 indicates the layout, which has been simplified to three runs of ducting representing the sections A-B, D-F and F-J in the basement of the building.

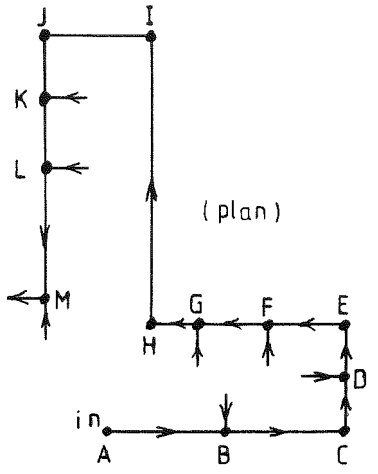

duct	dimensions (mm)	length (m)	effective L/D
A-B	100 x 100	2.7	27
B-C	100 x 150	2.3	-
C-D	100 x 150	1.0	-
D-E	150 x 200	6.5	60
E-F	150 x 200	7.0	
F-G	150 x 250	9.0	162
G-H	150 x 260	3.3	
H-I	150 x 260	11.9	
I-J	150 x 260	12.7	
J-K	150 x 260	1.2	-
K-L	250 x 350	2.2	-
L-M	250 x 450	1.7	-

Figure 1 Ducting Layout in Basement of Auxiliary Building

(iii) Deposition velocities and removal rates are calculated using a computer programme incorporating the removal processes considered. The drop size distribution is discretised into a number of intervals (10 has been used throughout). For each size interval, a deposition velocity is calculated for each process considered based on the average drop size in that interval. The duct length is divided into a number of intervals (10) and quantities of liquid removed and evaporated are calculated in each interval for each size interval.

The ducts under consideration are of rectangular section and the nett deposition velocity depends on the orientation of the surface. For upward facing surfaces, all deposition processes are assumed to act independently so the overall deposition velocity (V_U) is the sum of the individual components:

i.e. $V_u = V_t + V_g + V_e$

For downward facing surfaces, gravity will interfere with other processes and the overall deposition velocity (V_d) is then given by the following:

$V_d = V_t - V_g + V_e$ ($= 0$ if $V_g \geq V_t + V_e$)

The deposition velocity on vertical surfaces (V_v) is given by the sum of the individual components, excluding gravity:

i.e. $V_v = V_t + V_e$

The fractional removal (R) over length z of a rectangular duct of height h and width w can be shown to be given by the following relations:

for upward facing surfaces, $R_u = 1 - \exp(- V_u z/Uh)$

for downward facing surfaces, $R_d = 1 - \exp(- V_d z/Uh)$

for vertical facing surfaces, $R_v = 2(1 - \exp(- V_v z/Uw))$

so that the total fractional removal is given by the sum of the above three components.

Component deposition velocities are shown in Figure 2 for flow velocities of 10 m/s and 5 m/s. It is evident that the major removal processes in the size range of interest (see Table 2) are gravity separation and turbulence. For significantly smaller drops (e.g. few tens of microns), all three deposition processes considered are important. Deposition velocities also vary with duct diameter (decreasing with increasing diameter) but to a negligible extent compared with the variation with the drop size.

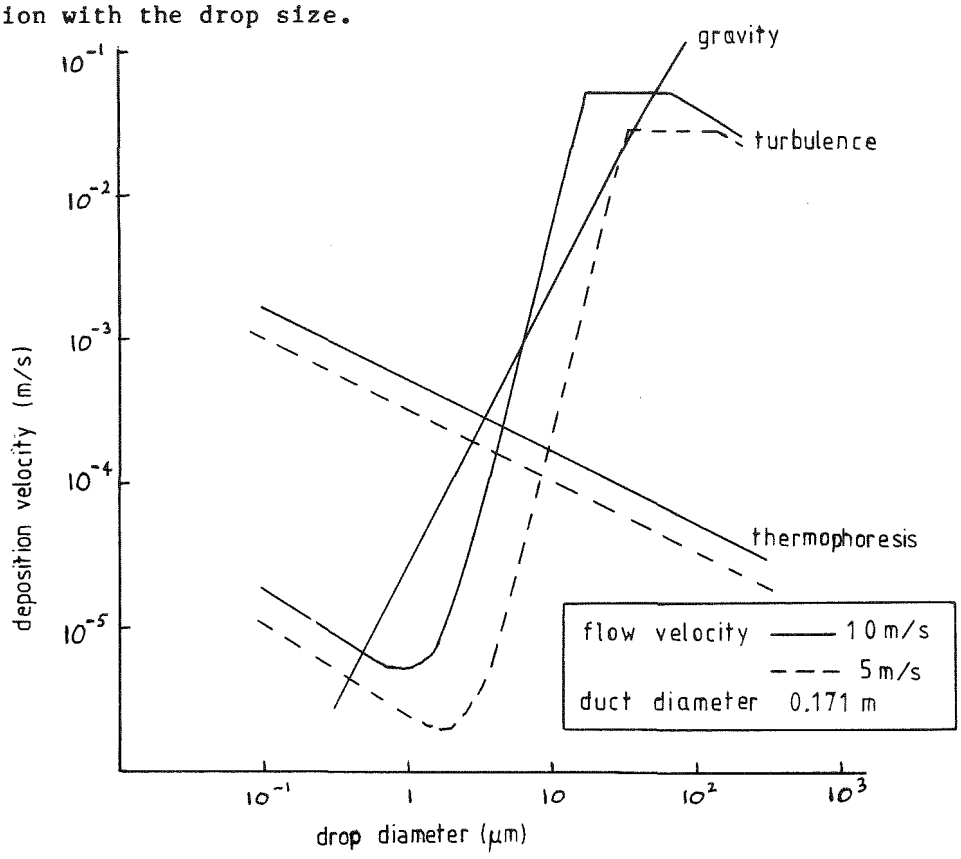

Figure 2 Component Deposition Velocities

The percentages of liquid released from the ducts after deposition and evaporation for the three duct sections considered are given in Table 3. These results are applicable to fault 2(a) in Table 1 in which flashing takes place. Slightly smaller releases are obtained for fault 2(c) because of the larger estimated drop sizes. The results show that the majority of the liquid is retained in the basement ducting with little variation with flow velocity (i.e. 99% for 10 m/s and 97% for 5 m/s). Drops remaining airborne have a maximum size of approximately 20μm and these are assumed to be released to the filtration plant.

Reducing drop sizes by a factor of 10 reduces the amount of deposition such that approximately 50% of the original liquid is released from the basement ducts. In addition, the smaller drops in this range are evaporated to dryness (assumed to occur when the drop size falls below 0.1 μm) leaving a solid particle containing fission products. These particles represent approximately 2% of the original liquid mass and are assumed to reach the filters. Further evaporation of drops will take place during transport from the basement to the filtration system and so the final mass evaporated will be somewhat larger.

TABLE 3 LIQUID RELEASED FROM DUCTS (%)

Maximum drop diameter (μm)	Flow velocity (m/s)	Duct section A-B	D-F	F-J
270	10	43	9	1
270	5	31	7	3
27	10	85	72	50
27	5	91	81	58

For non-flashing discharges (faults 1(b), 1(c), 2(b), 2(d)) evaporation rates are sufficiently high such that all liquid is evaporated before significant deposition takes place. In this case, therefore, chemistry considerations become important (as discussed in Section 4) as well as the performance of HEPA filters (Section 7.3).

In the case of fault 3(b) of Table 1 (i.e. CVCS pipe break) because drop sizes are very large it is considered unreasonable to assume that complete removal does not take place in the compartment.

7.3 Retention in the filtration system

The filtration plant of the emergency exhaust system will contain HEPA filters to remove fine particulates and charcoal filters to remove radioactive species in the vapour phase (iodine). In order to ensure that these items perform efficiently, it is necessary to ensure that airborne water drops are removed. Demisters are to be installed for this purpose.

From the results of Section 7.2, the requirements of the demisters are to remove water drops with size below 20μm at mass loadings corresponding to between 1% and 50% of the leak rates associated with faults 2(a) and 2(c) (i.e. flashing discharges). In addition, evaporated drops approximately 0.01μm in size, must be removed in the HEPA filters. Demister performance has been quoted as 99% efficiency for drop sizes greater than 3μm based on which adequate removal will take place. Regarding HEPA filter performance, the particulate size of interest (0.01μm)approaches the lower limit of these devices (BS3298 sodium flame test) and so the removal efficiency cannot be quantified at the present time. This is particularly relevant to faults in which flashing does not take place.

8. UNCERTAINTIES

The major uncertainties in the analysis are as follows:

(i) Drop sizes - removal rates are highly dependent on drop sizes and data is required. Experimental work is proceeding within the UK nuclear industry to measure drop sizes and distributions from representative breaks under flashing and non-flashing conditions.

(ii) Retention in the compartment - this is expected to be very significant but is difficult to justify at the present time. It is particularly important for faults in which the RCS temperature is below 100°C since, if it is assumed that liquid reaches the ventilation ducts, then rapid evaporation results in the formation of small particulates which may penetrate HEPA filters. Experimental proposals are to be made to address retention mechanisms in a compartment.

(iii) Overall deposition velocity - it is assumed that all deposition processes considered act independently so that the overall deposition velocity is given by the sum of the components. The validity of this assumption is not known.

(iv) Filtration system performance - assuming that the performance of the demisters can be verified, fission product retention may be limited by the efficiency of HEPA filters in removing fine particulates (0.01μm in size) produced by drop evaporation.

(v) Chemistry uncertainties arising from the possibility of iodine volatilisation.

9. CONCLUSIONS

An assessment of the retention of primary liquid and fission products in design basis faults taking place in the auxiliary building of the Sizewell 'B' PWR results in the following conclusions:

(i) A large amount of retention can be expected in the compartment in which the fault occurs (as much as 99%).

(ii) For faults in which flashing takes place, if it is assumed that all liquid enters the ventilation system, then removal by deposition in the ducts is dependent on drop sizes. The extent of removal will be between 50% and 99%. Drops which are not deposited will be removed by demisters.

(iii) For faults in which flashing does not take place, drops which enter the ventilation system will evaporate to dryness and the final retention depends on the performance of the HEPA filters.

REFERENCES

1. Wood, N.B., "The Mass Transfer of Particles and Acid Vapour to Cooled Surfaces", J. Institute of Energy, Vol. 54, 76-93, June 1981.

2. Kubie J., "Settling Velocity of Droplets in Turbulent Flows", Chem. Eng. Science, Vol. 35, 1787-1793, 1980.

3. Gardner, G.C., "Evaporation of Small Water Drops Containing Salt in a High Pressure Steam Environment", J. Fluids Eng., Vol. 103, 113-118, 1981.

4. Ranz, W.E., Marshall, W.R., "Evaporation from Drops", Chem. Eng. Progress, Vol. 48, No. 3, 141-146, 1952.

5. Hinze, J.O., "Fundamentals of the Hydrodynamic Mechanism of Splitting in Dispersion Processes, " A.I. Ch. Eng. J., Vol. 1, No. 3, 289-295, 1955.

6. Brown, R., York, J.L., "Sprays Formed by Flashing Liquid Jets", A.I. Ch. Eng. J., Vol. 8, No. 2, 149-153, 1962.

7. Tanasawa, Y., et al, Technology Reports of the Tohoku University, (22,72), 1957.

Session II: Aerosol Processes

Chair: J.A. Gieseke (BCL, USA)
H. Bunz (KfK, FRG)

Recent Developments in Research on Nuclear Aerosol Processes

W. Schöck

Kernforschungszentrum Karlsruhe GmbH
Laboratorium für Aerosolphysik und Filtertechnik I
Postfach 36 40, D-7500 Karlsruhe 1, FRG

Introduction

The modelling of aerosol processes for nuclear aerosols and reactor safety has been discussed comprehensively for the first time in an Expert Group's report /1/ and during the Specialists Meeting on Nuclear Aerosols in Reactor Safety /2/ in 1980. At that time the interest was focussed mainly on fast breeder reactor related problems. Little work was reported on LWR aerosol behaviour which also reflected the state of knowledge. E. g. among the existing computer codes there was only one which had ab initio been developed for applications in LWR risk analysis. Likewise the modelling of steam and water related aerosol processes was not fully developed.

Due to different stimulating experiences the activities in LWR aerosol research have considerably increased and the state of knowledge was much advanced. This is clearly represented in the program of the present Specialists Meeting which almost exclusively deals with LWR related phenomena. Much work was done to investigate aerosol processes and essential progress was made.

An appendix to /1/ was written /3/ with emphasis on LWR related problems. Much of the following discussion is based on this work with additions of some recent developments that were known to the author.

In this paper the progress made will be reported first. Then a discussion of the relative importance of the processes for different applications is given. This will be restricted to scenarios in LWR core melt accidents. Finally an attempt is made to judge the today's state of the art in the

light of the requirements of LWR risk assessment.

Progress in Aerosol Processes Research

As usual the discussion of aerosol processes will be structured in two groups: interaction processes and depletion processes. Further processes which are not aerosol processes per se but are influencing the aerosol will be reported too. E. g. leakage is not an aerosol process but a phenomenon of the enclosure, but since leakage depletes particles from the airborne aerosol system it will be treated as a depletion process.

Interaction processes

By definition aerosol interaction processes are processes wich may change any of the aerosol properties but do not remove particles from the airborne state. In the highly concentrated aerosol system of an LWR during a core melt accident these processes are very important. The relevant processes are agglomeration and condensation/evaporation.

Agglomeration

The basic equations for Brownian, gravitational and turbulent agglomeration of aerosol particles remains unchanged. The work to be mentioned here concerns the values of the coagulation shape factor and the formulation of the collision efficiency for gravitational agglomeration.

Until recently the coagulation shape factor has always been estimated by parametric fitting of measured mass concentration changes to code calculations which was very unsatisfactory because more than one parameter had to be tuned. The first direct measurement of this shape factor was reported in 1983 /4/. By proper choice of the experimental conditions the brownian coagulation could be isolated from other aerosol processes, the shape factor was evaluated from measured changes in the particle size distribution. Dry aerosols of platinum oxide and unranium oxide were used and values of the coagulation shape factor of 1.8 for platinum oxide and 3.2 for uranium dioxide aerosol were measured.
It is interesting to note that these values are approximately equal to the

dynamic shape factor of the aerosol used in the experiments. Evaluating the shape factor also indicated that the Fuchs correction to the coagulation frequency had to be used. Such corrections, however, are important only for a very short initial phase with nuclear aerosols /5/ until the particle sizes have grown to values which do not require such corrections.

The correct formulation of the collision efficiency of gravitational agglomeration has recently been discussed again. In most of the codes the gravitational agglomeration kernel is formulated following Fuchs

$$K_g(r_1, r_2) = \pi \cdot \varepsilon \cdot f^2 \cdot (r_1 + r_2)^2 \cdot |v_s(r_1) - v_s(r_2)|$$

$$\varepsilon = 3/2 \cdot \left(\frac{r_1}{r_1 + r_2}\right)^2 \quad ; \quad r_1 << r_2$$

in two of the codes this has been replaced by the formulation of Pruppacher and Klett

$$K_g(r_1, r_2) = \pi \cdot \varepsilon \cdot f \cdot (r_1 + r_2)^2 \cdot |v_s(r_1) - v_s(r_2)|$$

$$\varepsilon = 1/2 \cdot \left(\frac{r_1}{r_1 + r_2}\right)^2 \quad ; \quad r_1 << r_2$$

The rationale is discussed in detail in /6/. The probable consensus might be that the factor 1/2 in the Pruppacher Klett formulation represents the physical situation better than the factor 3/2, and that the use of f or f^2 is a matter of definition. The present situation, however, is that codes differ by a factor of 3f in the gravitational collision kernel. This in fact leads to large discrepancies among code predictions when gravitational agglomeration is important /7/. The need is clearly obvious for an experimental investigation of this effect which has often been demanded but is still missing.

Condensation

The process of growth of particles by condensation of steam and the inverse process of evaporation of droplets can be modelled with sufficent accuracy by use of the Mason formula /8/. The rate of change of the thermodynamic parameters governing this process is slow enough to justify the assumptions made in deriving the equation. The condensation rate depends on the particle size, the saturation ratio and the temperature, in that order, the temperature governing the material properties of steam and water. The saturation ratio in turn is changed by the process. Therefore, the numerical

efforts in computing condensation and evaporation are great, all conceivable simplifications can be valid only for limited ranges of parameters and have to be used very cautiously.

Given a general consensus on using the Mason formula, the problem arises in providing the saturation ratio with the necessary precision.
Supersaturation in a core melt aerosol system will always be very low, less than 1 % typically.

This small quantity has to be calculated from the results provided by containment thermodynamics codes, a method which is often impracticable. It still works in a situation where steam is added to a saturated atmosphere. Then the excess steam can be translated into a supersaturation within one computational time step, and when the time step is short enough this method will give reliable results.

The problem becomes more complicated, however, when supersaturated conditions are created not by addition of steam but through cooling processes. This situation has only recently been analyzed /9/. If the cooling of the aerosol system occurs by heat transfer to a wall (or structural surface) only a very small fraction of the steam condenses on particles, most of it condenses directly onto the wall. The aerosol fraction decreases with decreasing temperature difference between bulk system and wall, moreover, it becomes negative when the temperature difference is only a few degrees. The latter situation is encounterd in the containment at later stages of the accident, which means that, in the absence of a steam source, existing droplets will evaporate during the cooling process.

Concerning the cooling by a spray, analogous results were found since a spray acts thermodynamically similar as a cold wall. Steam was seen to condense mainly onto the spray droplets, only when the spray is very cold a considerable fraction of the steam condensed on aerosol particles.

These results for steam condensation in cooling environments have been obtained only thermodynamically. The data have not been used in aerosol behavior computations for which, up to now, condensation on particles was only taken into account when steam sources were in action.

Condensation of steam onto soluble particles is an important phenomenon for LWR nuclear aerosol behavior because a fraction of the released aerosol consists of soluble material. Condensation on, or rather dissolution of, such particles occurs at saturation ratios well below 100 %. All aerosol codes described in /1/, however, ignore the existence of this process.

Depletion processes

Depletion processes deplete particles from the aerosol system. They either remove them from the airborne state permanently by deposition on a wall or floor or deplete them from the system under consideration by transport through a leak or intercompartmental flows.

Gravitational sedimentation

Sedimentation undoubtedly is the most efficient removal mechanism for nuclear aerosols. Moreover, it is the best understood and modelled aerosol effect. The only uncertainty is in the values of the dynamic shape factor and/or effective density of the particles which are needed as input data for the calculation.

In connection to the measurement of coagulation shape factors mentioned above /4/ also the dynamic shape factor was measured in a dry environment. Size dependent values of $1.1 < \chi < 3.6$ for platinum oxide aerosol and $2.6 < \chi < 3.3$ for uranium dioxide aerosol were measured in a size range well below 1 µm. The UO_2-aerosol also contained a coarse fraction with $\chi = 1.2$, further the size dependence of χ was completely different for the two materials.

In condensing atmospheres the shape factor problem is less severe because particles are spherified and compacted. A shape factor of unity can be used when, for sedimentation, an effective density of the particles is assumed which is roughly 50 % of the material density. Evidence supporting this concept has been obtained frequently.

Diffusiophoresis and Thermophoresis

A temperature gradient in the boundary layer at a wall causes diffusiophoretic and/or thermophoretic deposition of aerosol particles depending on the atmospheric conditions. Thermophoresis may occur alone when no condensation of steam on the wall takes place. Diffusiophoresis occurs when steam condenses on the wall and is then coupled to simultaneous thermophoresis. The problem in the analytical treatment of these effects is that the boundary layer thickness is a critical parameter but is very badly known under accident conditions.

The temperature gradient that is the cause of particle movement primarily induces a sensible heat flux in the case of thermophoresis and a latent heat flux, i.e. a mass flux of condensing steam, in the case of diffusiophoresis. Therefore, under given thermodynamic conditions the diffusiophoretic deposition rate is proportional to the mass flux of condensing steam and the thermophoretic deposition rate is proportional to the sensible heat flux. These fluxes can be obtained with much better quality from thermodynamic calculations than the boundary layer thicknesses. For diffusiophoretic deposition, in a further step, the mass flux can be substituted by the overall condensation rate. This has been reported recently together with direct measurements of diffusiophoretic deposition /10/. The agreement of the measured diffusiophoretic deposits with those calculated from total condensed steam confirmed the applicability of the formulation.

A similar analytical treatment of photophoretic deposition was given in /11/, but its effect estimated to be of low importance.

Diffusional deposition

A general consensus exists that Brownian diffusion as a deposition mechanisms is of very low importance in reactor accidents. Nevertheless, it is still being computed in most codes giving deposits which are orders of magnitude lower than those from other deposition effects.

Inertial deposition

Inertial deposition of particles from turbulent flows applied to reactor accidents is an upliving field of interest. Formerly inertial deposition was restricted to analytical work or at best to make up for differences in comparing calculations to measurements. Today the situation has improved in so far as a code calculating convective flows in simple geometries is available /12/ and has been used to provide input data for aerosol behaviour calculations. The calculated results were compared with measurements and a good agreement was observed /13/.

Leakage

A volumetric leak rate from an enclosure establishes an identically large depletion rate for the enclosed aerosol. So far the situation is quite clear. The more safety relevant question, how much of this aerosol escapes from the other side of the leak, is still not answered. So all codes assume no retention in the leak path which is certainly over-conservative.

It has been reported that the aerosol mass required to plug the leak channel is proportional to the cube of the channel diameter and an empirical proportionality factor was determined /14/. Further, the retention prior to plugging is proportional to the fourth power of the particle size /15/. However, all attempts to incorporate these results into an aerosol code have to fail because it is simply impossible to define the geometry of leak paths for a real containment with only a minimum of confidence.

Resuspension

In all codes the assumption is made that a particle that hits a surface disappears from the scene forever. The phenomena of re-release, which exist but are very weak, are completely neglected. So it is only a question of relative importance whether one should consider re-release phenomena or not. At the very moment when codes calculate e.g. airborne concentrations decreasing down to milligrams per cubic meter also very weak sources will become noticeable. The possible mechanisms for re-release are dry re-entrainment from a thick deposit, revolatilization of volatile fission

products by decay heat, entrainment of dissolved and resuspension of particulate material from a hot or boiling pool of water.

The first two mechanisms may occur only in the PCS when large deposits have accumulated. The resuspension from the sump in the containment could be a weak long term source of aerosols. A few activities have been initiated to investigate the rates of re-release and the properties of the particles that are released. Aerosol behaviour codes are ready to take into account the effects once they will have been quantified.

Relative importance of aerosol processes in different environments

Not all of the aerosol processes are of equal importance at the same time. The properties of the aerosol itself and the boundary conditions are responsible for different mechanisms to dominate. So the accuracy with which a process should be modeled depends strongly on the time and environment of interest. As was seen in the previous section also the state of model development is unequal for different processes. Therefore, the modeling is best when processes dominate which are well understood.

The relative importance of an aerosol process is the combined result of the particle properties and the external influence that acts on the particle, most generally the particle mobility and the external force. Both may of course change with time and space (It is interesting to realize that in the aerosol behaviour codes some sensitive particle properties as well as most of the external influences are largely treated as input data.)

The basic aerosol properties to be considered here are concentration, particle shape, particle density and particle size distribution. The main external influences are gravity, Brownian motion, convective and turbulent flows, thermal and concentration gradients. The effects of electrostatic and electromagnetic fields has been ruled out as unimportant. These few influence parameters allow a judgement of the ranking of individual aerosol processes in different environments.

the containment. Surface to volume ratios, temperatures and aerosol concentrations are higher; residence times, on the other hand, are much shorter. Flow velocities and steam saturation vary over a wide range of values. Therefore in addition to the processes dominating in the containment some others will be important, too.

Gravitational agglomeration may become noticeable when the aerosol concentration is very high (> 100 g/m³). Turbulent agglomeration and deposition may occur in pipes and at obstacles when the flow velocities are high. Thermophoresis in the reactor pressure vessel is a dominating effect shortly before melt through.

Still diffusional and photophoretic plateout are unimportant. Resuspension of deposited particles becomes the more likely the higher the retention in the primary circuit has been. Resuspension and revolatilization increase with the thickness of the deposited layer.

Pool scrubbing

In boiling water reactors the retention of particles when the aerosol bubbles through the pressure suppression pool is a favorable effect. A similar situation exists in all types of LWR when the leak in the PCS is via the steam generator or the pressurizer or when the molten core is submerged in the sump water.

The modelling of this situation has only recently been undertaken /16/. The models calculate in a first step the properties of the rising bubbles in the pool, then the aerosol removal in the bubble is calculated using the usual set of aerosol processes. Limited sensitivity studies have shown that the more important effects are inertial impaction, sedimentation, diffusional and diffusiophoretic deposition. Presently the experience with these models is limited, further investigations are to be recommended.

Current Status of Aerosol Modelling

From the previous sections it is apparent that the greater part of the work was done to improve already existing formulations and data bases. The

question immediately arises how long to continue this work, not from a scientific point of view but with respect to the application of the knowledge in risk assessment studies.

In the chain of calculations that have to be made in evaluating the risk of nuclear reactor accidents aerosol behaviour is only one part, as important as all the others but only one. The quality of the overall results depends not only on one step but on all of them. Therfore, it is of little value to improve one discipline much over the others because the final joint result will not reflect that.

The models that describe the aerosol behaviour in the containment are already more precise than some of the input data that they require. There is also little hope that this situation may be reversed in the future, not because the efforts are too low but because some phenomena during a core melt accident are simply unpredictable.

As an example: The total leaked aerosol mass from the contaiment depends slightly under-proportional to the total mass release into the containment. An increase of the aerosol source by a factor of two increases the total leaked mass by (almost) a factor of two. The scatter in values of leaked mass calculated by different codes using identical input is within the range of a factor of two or better /1/, on the other hand the data bases for aerosol release from the melting core scatter over almost one order of magnitude. Similar considerations can be made for the thermodynamic input for aerosol codes.

Slightly overstated the situation can be summarized as follows: The mechanistic behaviour of a given aerosol system in a given geometric, thermodynamic and thermalhydraulic environment is well understood and modelled, the remaining uncertainties can be attributed to poor knowledge of the required input information.

This statement is confirmed by experiences from many large scale experiments (e. g. /17/) where pre test preditions usually disagree with the measurement, but post test calculations taking into account the actual aerosol source parameters and the actual boundary conditions show very

good agreement with the measured aerosol behaviour.

The modelling of aerosol behaviour is one of the best developped disciplines in the field of nuclear accident risk assessment. Therefore, the todays need is not to refine and improve the modelling of single aerosol processes - with the few exceptions indicated above - but to improve the coupling to those models which provide the data that aerosol codes need.

References

/1/ Nuclear Energy Agency OECD (Ed.),greater Nuclear Aerosols in Reactor Safety,
CSNI NEA, SOAR No. 1, Paris (1979)

/2/ CSNI Specialist Meeting on Nuclear Aerosols in Reactor Safety, NUREG/CR-1724, ORNL/NUREG/TM-404, CSNI-45

/3/ Nuclear Aerosols in Reactor Safety, supplementary report to /1/, OECD/NEA Ed., in preparation

/4/ W. Zeller: Direkte Messung von Aerosolformfaktoren, KfK 3560 (1983)

/5/ G. Metzig: On the Theory of Brownian Coagulation of Aerosols for Knudsen Numbers Greater than 1, this conference

/6/ I.H. Dunbar, S.A. Ramsdale: Improvements in the Modelling of Sedimentation and Gravitational Agglomeration, this conference

/7/ I.H. Dunbar, J. Fermandjian et al: Comparison of Sodium Aerosol Codes, CEC publication EUR 9172 EN (1984)

/8/ W. Schöck, H. Bunz, M. Koyro: Messungen der Wasserdampfkondensation an Aerosolen unter LWR-unfalltypischen Bedingungen, KfK-3153 (1981)

/9/ C.F. Clement: Aerosol Growth in Vapour-Gas Mixtures Cooled through Surfaces, TP 897, AERE Harwell (1982)

/10/ H. Bunz, W. Schöck: Direct Measurements of Diffusiophoretic Deposition of Particles at Elevated Temperatures, 1st Int. Aerosol Conf., Minneapolis, Minn., September 17-21 (1984)

/11/ J.F. van de Vate: Investigations into the Dynamics of Aerosols in Closed Containers, ECN-report No. 86, Petten, NL (1980)

/12/ W. Cherdron: Berechnung der Konvektionsströmung bei Natrium-Flächenbränden in geschlossenen Behältern, Jahrestagung Kerntechnik, Frankfurt, 22.-24.5. (1984), Report ISSN 0720-9207

/13/ W. Cherdron, H. Bunz, S. Jordan: Properties of Sodium Fire Aerosols and Recalculations of their Behavior in Closed Containments, this conference

/14/ H.A. Morewitz: Leakage of Aerosols from Containment Buildings, Health Physics 42, 195 (1982)

/15/ J.F. van de Vate et al: Aerosol Leakage through Containment Walls, ENS-ANS Meeting on LMFBR Safety and Related Design and Operational Aspects, July 19-23, (1982) Lyon, France

/16/ W.J. Marble, T.L. Wong, F.J. Moody, D.A. Hankins: Retention of Fission Products by BWR Suppression Pools During Severe Reactor Accidents, Proceedings of ANS/ENS International Meeting on Thermal Reactor Safety, Chicago, Illinois, August 29- September 2 (1982)

/17/ W. Schöck et al: The DEMONA Project - Objectives, Results and Significance to LWR Safety, 5th Int. Meeting on Thermal Nuclear Reactor Safety, Karlsruhe, September 9-13 (1984)

Vapour Condensation on Particles: AEROSIM Modelling

I H Dunbar

UKAEA Safety and Reliability Directorate, Culcheth, UK

ABSTRACT

Condensation of steam in the bulk of the containment atmosphere enhances the growth of aerosol particles and hence increases their gravitational sedimentation rate. Containment thermal-hydraulic codes calculate a condensation rate based on the assumption that the atmosphere cannot go super-saturated. The AEROSIM code has been extended to take the condensation rate and calculate the consequences for aerosol behaviour. The results for a test case used in an earlier work examining diffusiophoretic removal are presented. In this case, with a high bulk condensation rate over a short period, aerosol fall-out is predicted to be very rapid.

1. INTRODUCTION

In severe LWR accidents a considerable fraction of the activity released from the core is likely to end up in the form of an aerosol in the containment building atmosphere. A crucial factor determining the eventual radiological source term to the environment is the rate at which the aerosol particles sediment out under gravity, thereby becoming less available for leakage to the atmosphere. This rate is very sensitive to particle size. In a typical containment a 1 μm radius particle has a lifetime of the order of a day, whereas a 10 μm radius particle settles out on average within 15 minutes. In some LWR accidents there may be phases when steam condenses in the bulk of the containment atmosphere. Because this steam condenses preferentially on the particles, condensation is an additional mechanism for particle growth, and hence for the enhancement of sedimentation.

This paper describes how particle growth due to condensation is being included in the aerosol behaviour code, AEROSIM. Section 2 describes the physical basis of the modelling, while section 3 describes how the model is treated in the AEROSIM approximation scheme. Some preliminary results are presented in section 4. It is important to stress that the AEROSIM code does not predict whether condensation will occur, or, when it does, how much steam will condense. This job is left to the containment thermal hydraulic codes. The task of AEROSIM is, for a given pattern of condensation, to predict the consequences of this in terms of aerosol growth and removal.

2. CONDENSATION MODELLING

In the absence of condensation, aerosol growth and removal are modelled using the familiar equation

$$\dot{C}(m,t) = \tfrac{1}{2} \int_0^m d\mu\ \phi(\mu, m-\mu)\ C(\mu,t)\ C(m-\mu,t) - C(m,t) \int_0^\infty d\mu\ \phi(m,\mu)\ C(\mu,t) - R(m)\ C(m,t) + S(m,t) \qquad (1)$$

Here C is the number concentration distribution; $\dot{C}$ is its partial time derivative, m refers to the mass of a single particle, S is a source term and R and ϕ are the removal and agglomeration rates respectively. If steam condenses on the particles such that the mass rate for a single particle of mass m is $\xi(m)$, then an extra term has to be added to (1):

$$\dot{C}(m,t)\big|_{cond} = -\frac{\partial}{\partial m} [\xi(m,t)\ C(m,t)] \qquad (2)$$

For a given partial pressure of steam, the condensation rate on a particle is given approximately by Mason's equation [1]. Following Clement [2], we used a dimensionless "condensation number":

$$Cn = K/(L\ D\ \rho'_{sE}\ (T)) \qquad (3)$$

where K = gas thermal conductivity
L = latent heat of evaporation of water
D = diffusivity of steam in air
ρ_{sE} (T) = equilibrium density of steam

ρ'_{sE} (T) = temperature derivative of ρ_{sE}

For a particle of radius r the mass rate of condensation is

$$\xi(r) = 4\pi r\, D \left[\frac{Cn}{Cn+S_o(r)}\right] \rho_{sE}\ (T)\ [S-S_o(r)] \qquad (4)$$

The supersaturation S is the ratio ρ_s/ρ_{sE} (T), where ρ_s is the density of steam in the bulk atmosphere, $S_o(r)$ is the ratio ρ_{sp}/ρ_{sE} (T_p), where T_p is the drop temperature and ρ_{sp} is the steam density at the drop surface. For pure water, $S_o(r) \to 1$ as $r \to \infty$. Equation (4) is derived in the appendix.

For (4) to be used in an aerosol code using a value of S taken from a thermal hydraulic calculation decoupled from aerosol behaviour, condensation on the aerosol would have to have only a small effect on the value of S. To examine this question let us consider a monodisperse aerosol with number concentration C_T. The change in supersaturation due to condensation has the form:

$$\dot{S} = -\lambda_C(r)\ [S - S_o(r)] \qquad (5)$$

where, from (4), the rate constant is

$$\lambda_C = 4\pi r\, D\, C_T \left[\frac{Cn}{Cn+S_o(r)}\right] \qquad (6)$$

As an example consider 1 μm radius water droplets with mass concentration 1g m^{-3}. Then using D = 1.93 $m^2\ s^{-1}$ and Cn = 0.041 (Clement [2]) we get

$$\lambda_C = 2.3 \times 10^5\ s^{-1}$$

This is many orders of magnitude greater than other aerosol process rates. To an excellent approximation, $S = S_o$ at all times. The thermal hydraulic codes (for example MACE [3]) assume that S = 1 at all times; steam is predicted to condense at such a rate as is required to maintain this equilibrium condition. (In principle, S_o should be used, depending on details of aerosol size and solute concentration, thereby introducing a dependence of the thermal hydraulics on the aerosol behaviour.)

The condensation version of AEROSIM is designed to take from thermal hydraulic codes a condensation rate, however calculated. What remains to be done is to distribute this total amount of water over the particle sizes. The size dependence of ξ has to be factored out:

$$\xi(m,t) = \xi_o(t)\ f(r) \qquad (7)$$

(Note that in all aerosol modelling it is assumed that a relationship between m and r is available.) In the case of equation (4) with $S_o = 1$ we have simply

$$f(r) = r \qquad (8)$$

The value of $\xi_o(t)$ is not needed because we assume knowledge of the total condensation rate.

So far the discussion has been in terms of condensation, but the formalism also holds for evaporation, when $S < S_o(r)$. However when modelling this it is necessary to ensure that of the total aerosol mass, only that which is water is allowed to evaporate. The airborne water has to be followed as a separate component; the version of AEROSIM discussed here does not do this, so its use is restricted to cases where evaporation does not occur or where the aerosol is pure water.

3. DISCRETISATION OF THE CONDENSATION MODEL

The discretisation procedure in AEROSIM starts with the choice of minimum and maximum masses, m_o and m_N. This range is then partitioned into N intervals

$$A_i = [m_{i-1}, m_i) \quad \text{for } i = 1, .., N$$

For each interval we define a midpoint and a width:

$$M_i = \tfrac{1}{2}(m_i+m_{i-1}) \quad , \; h_i = (m_i-m_{i-1}).$$

The quantities modelled by AEROSIM are the mass-weighted integrals

$$C_i(t) = \frac{1}{M_i} \int_{A_i} dm \; m \; C(m,t) \tag{9}$$

The total condensation rate, $Y(t)$, is related to the change in $C(m,t)$ by

$$Y(t) = V \int_o^\infty dm \; m \; \dot{C}(m,t)\big|_{cond} \tag{10}$$

where V is the containment volume. Using equation (2) and integrating by parts gives

$$Y(t) = V \int_o^\infty dm \; \xi(m,t) \; C(m,t) \tag{11}$$

Similarly the total mass condensed in interval A_i is

$$Y_i(t) = V \; \xi_o(t) \int_o^\infty dm \; f(m) \; C(m,t) \tag{12}$$

where we have also made use of equation (7). Now we approximate $f(m)$ by $f(m_i)$ and $C(m,t)$ by $C_i(t)/h_i$ in the interval A_i and get

$$Y_i(t) \approx V \; \xi_o(t) \; f(m_i) \; C_i(t) \tag{13}$$

Using the fact that all of these must add up to $Y(t)$ we arrive at the AEROSIM approximation

$$Y_i(t) = Y(t) \; [f(m_i) \; C_i(t) / \sum_{j=1}^{N} f(m_j) \; C_j(t)] \tag{14}$$

The change in C_i due to this condensation is given by (2) and (9):

$$\dot{C}_i(t)\big|_{cond} = \frac{1}{M_i} [\int_{A_i} dm \; \xi(m,t) \; C(m,t) - m_i \; \xi(m_i,t) \; C(m_i,t) + m_{i-1} \; \xi(m_{i-1},t) \; C(m_{i-1},t)] \tag{15}$$

We can approximate the first term, ie the integral, by $Y_i(t)/V$. The second and third terms are due to particle growth across the boundaries of the intervals. In the AEROSIM approximation these are based on the interval from which the particles are coming. For condensation therefore

$$\xi(m_i,t)\ C(m_i,t) \approx Y_i(t)/(V\ h_i) \tag{16}$$

while for evaporation

$$\xi(m_i,t)\ C(m_i,t) \approx Y_{i+1}(t)/(V\ h_{i+1}) \tag{17}$$

(Only (16) is at present included in AEROSIM.) This distinction is needed to present particles being transferred out of empty intervals. The AEROSIM approximation to (15) is therefore (condensation case):

$$\dot{C}_i(t)\big|_{cond} \approx \frac{1}{M_i\ V}\{Y_i(t)\ [1-m_i/h_i] + m_{i-1}\ Y_{i-1}(t)/h_{i-1}\} \tag{18}$$

In AEROSIM the interval edges are related by $m_{i+1} = m_i\ R$, where R is a fixed ratio. With this simplification (18) becomes

$$\dot{C}_i(t)\big|_{cond} \approx \frac{1}{M_i\ V}\{-\frac{1}{R-1}\ Y_i(t) + \frac{R}{R-1}\ Y_{i-1}(t)\} \tag{19}$$

4. PRELIMINARY RESULTS

The test case reported here is a simplified version of the case used by the present author [4] to study the effects of condensation on the walls. An instantaneous release (at t=0), of 648 kg of aerosol, supposed to represent the melt release in an S_2D accident, is followed, with the time-varying atmosphere conditions given on table 1. These are taken from the same MARCH run as was used in reference [4]. λ_d is the diffusiophoretic removal rate, and t_i is the initial time of the phase during which the quoted values hold. T is the temperature, p is the pressure and X_S is the mole fraction of steam. The most striking effect, as in the earlier study, is the steam spike, starting at 500 s. Caused by the core falling into water in the cavity after RPV melt-through, it leads to a transient increase in the rates of both bulk and wall condensation.

To discuss the results let us define masses m_{FA}, m_{FS}, m_{WA} and m_{WS}. F stands for fission product and core material and W stands for water. A stands for airborne mass, while S stands for sedimented mass. What we want to know is how m_{FA} as a function of time is affected by the condensation process. Unfortunately F and W masses are not followed separately in the present version of the code. All we know are the four sums:

$$m_W = m_{WA} + m_{WS} \quad , \quad m_F = m_{FA} + m_{FS}$$

$$m_A = m_{WA} + m_{FA} \quad , \quad m_S = m_{WS} + m_{FS}$$

For this study we approximate m_{FA} by

$$\tilde{m}_{FA} = m_A \times (m_F/(m_F+m_W)) \tag{20}$$

t_i/s	λ_d/s^{-1}	Y/kg s^{-1}	T/K	p/(10^5 Pa)	X_s
0	1.0 x 10^{-4}	0	372	2.10	0.46
500	4.5 x 10^{-4}	70	406	4.35	0.65
900	1.25 x 10^{-4}	35	398	3.67	0.65
1800	0.20 x 10^{-4}	4	391	3.21	0.60
12700	0	0	406	4.56	0.60

Table 1. Containment Atmosphere Conditions in Test Case.

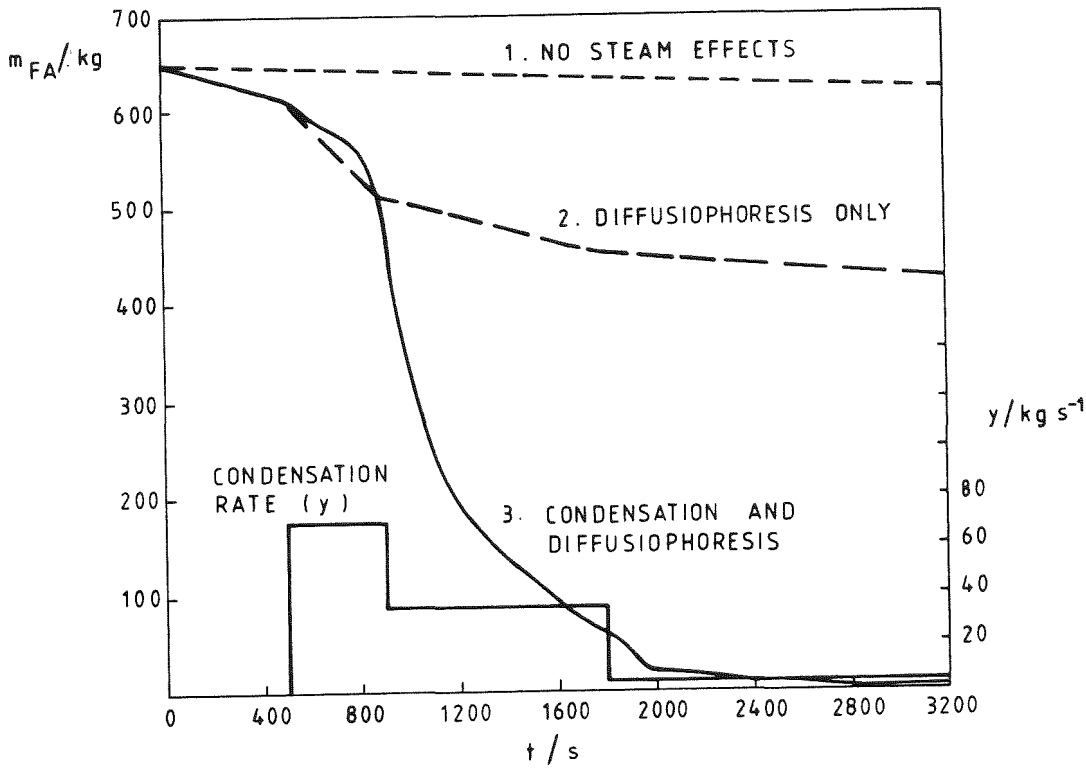

FIGURE 1 MASS OF CORE - DERIVED AEROSOL AIRBORNE, AND CONDENSATION RATE AS A FUNCTIONS OF TIME

The results are shown on Figure 1. All of the interesting phenomena occur within the first 3200 seconds. The histogram shows the condensation rate Y, and the three curves are of m_{FA} ($\tilde{m}_{FA}$ in the case with condensation). The upper curve (case 1) shows what is predicted with neither diffusiophoresis nor bulk condensation. The mass airborne falls linearly from 648kg to 620kg. This is typical of what is found when agglomeration-enhanced sedimentation is the main means of removal: an initial time interval of the order of an hour is needed before there is significant fall-out. In fact it is 4.4 hours before half of the aerosol is removed. The next curve down (case 2) shows the effect of including diffusiophoresis. The result is basically the same as presented in the Cambridge meeting paper [4]. The curve is approximately piecewise linear, corresponding to the step changes in λ_d. When most of the diffusiophoresis is over, at 1800 seconds, 30% of the mass has been removed compared with only 2% of the mass in the case without diffusiophoresis. This "lead" of almost 200kg caused by diffusiophoresis is eventually made up by gravitational settling, but the lead is not reduced to 50kg until 5.5 hours.

The lower curve (case 3) shows the dramatic effects of bulk condensation, as predicted by MACE. When condensation starts at 500 seconds the curve actually strays above that of case 2. This suggests that $\tilde{m}_{FA}$ has counted in some water mass. However, by 900 seconds $\tilde{m}_{FA}$ is dropping very rapidly and by 1600 seconds it is below 100kg. As the particles grow the water is forced to condense on larger and larger particles, so the water falls out even more rapidly. At 3200 seconds the code predicts a zero mass airborne. As the code is written, it can no longer allow bulk condensation, but this does not matter in the present case because the initial fission product aerosol has been removed.

It should be stressed again that all AEROSIM does is explore the consequences of a MACE prediction. In this accident, where the core falls into a wet reactor cavity MACE predicts 28 tonnes of water to condense in bulk between 500 and 900 seconds, and another 31.5 tonnes to condense between 900 and 1800 seconds. This water is applied directly to the particles, needing therefore no agglomeration time to take effect, and it overwhelms the 0.65 tonnes of core-derived aerosol present initially.

An effect which will tend to suppress bulk condensation is the heating of the containment atmosphere due to the decay of airborne fission products. MACE has a model for this source of heat. It predicts a mean decay power in the atmosphere of about 22MW during the first 600 seconds of the run, and of about 7MW during the second 600 seconds. The predicted condensation is occurring even in the presence of this decay heating. If the predictions of AEROSIM are correct this power will in fact be decreasing more rapidly as the fission products present as aerosols are washed out, so the tendency to suppress bulk condensation will be reduced.

5. CONCLUSIONS

Given a total rate of steam condensation in the bulk predicted by containment thermal hydraulic codes such as MACE, the AEROSIM code is now able to calculate the consequences for aerosol behaviour. Since condensation is very much faster than other aerosol processes, the modelling is based on the assumption that as much steam as needs to condense to maintain equilibrium does so instantaneously. The details of how this model is incorporated into AEROSIM have been given in Section 3.

The new modelling has been tried out on the S-LOCA case, as modelled by MACE, which was used in an earlier paper [4] to look at the effects of diffusiophoresis. For this accident sequence the core falls into a water-filled cavity, and, following the resultant steam spike, MACE predicts the condensation of a mass of steam approximately one hundred times greater than the initial aerosol mass. This mass is added directly to the aerosol particles, and the initial core-derived aerosol is predicted to be washed out in less than an hour.

This dramatic result should be seen more as a prediction of MACE than of AEROSIM, for it is in the thermal-hydraulics code that the crucial physical modelling is carried out. The result is not a statement of what is believed will happen in the accident sequence in question, but is intended to demonstrate the new capability of the AEROSIM code. It also indicates that condensation could be a major mechanism for aerosol retention if large quantities of water (such as a significant fraction of the water in a flooded reactor cavity) can be induced to condense over a short period of time.

REFERENCES

1. Mason, B J, The Physics of Clouds (OUP, 1971).

2. Clement, C F, Aerosol Growth in Vapour-Gas Mixtures Cooled Through Surfaces, Harwell Report TP.897 (1982).

3. Wooton, R O, Avci H I, MARCH Code Description and Users' Manual (BMI-2061, 1980).

4. Dunbar I H, The Role of Diffusiophoresis in LWR Accidents, Proceedings of the International Meeting on LWR Severe Accident Evaluation (Cambridge, Mass, 1983).

APPENDIX: DERIVATION OF MASON'S EQUATION

The aim of this appendix is to give a brief derivation of Mason's equation in the form it appears in this paper (equation (4)). The symbols are as defined in the body of the text. The derivation starts from steady state equations for mass and heat transfer:

$$\xi(r) = 4\pi r\, D\, (\rho_s - \rho_{sp}) \qquad (A1)$$

$$L\xi(r) = 4\pi r\, K\, (T_p - T) \qquad (A2)$$

The two equations are used to eliminate reference to the drop temperature. To do this we make the linear approximation:

$$\rho_{sE}\,(T_p) - \rho_{sE}\,(T) = \rho'_{sE}\,(T)\,[T_p - T] \qquad (A3)$$

It is assumed that $T_p - T$ is small enough for higher order terms to be negligible. The two equations can then be written as

$$\frac{1}{4\pi rD}\,\xi(r) = [\rho_s - S_o(r)\ \rho_{sE}\ (T_p)] \tag{A4}$$

$$\frac{L\rho'_{sE}(T)}{4\pi rK}\,\xi(r) = [\rho_{sE}\ (T_p) - \rho_{sE}\ (T)] \tag{A5}$$

(A5) is multiplied by $S_o(r)$ and the two equations are added

$$\frac{1}{4\pi rD}\,\xi(r)\ [1 + S_o(r)\ Cn^{-1}] = \rho_s - S_o(r)\ \rho_{sE}(T) \tag{A6}$$

Rearranging this gives the final result

$$\xi(r) = 4\pi rD\ \left[\frac{Cn}{Cn + S_o(r)}\right]\ \rho_{sE}(T)\ [S - S_o(r)] \tag{A7}$$

Calculation of the Diffusion Slip Velocity for Nuclear Aerosols*

by

S.K. Loyalka and C.C. Yuan
Nuclear Engineering Program
University of Missouri-Columbia
Columbia, Missouri 65211

ABSTRACT

Severe core damage accidents in nuclear reactors can release aerosols, fission gases, and water vapor into the primary coolant system and the reactor containment. Since gradients of vapor and gas concentrations are established, the aerosol particles can experience forces caused by the diffusion of the gases. These diffusiophoretic forces contribute to the movement and deposition of the aerosols. Reliable results for these forces for all particle sizes are still not available, but in the large particle limit the forces can be expressed in terms of the diffusion slip velocity for which results have been obtained by several authors in the past. We report in this paper the computed results for the diffusion slip velocity for some conditions pertinent to postulated light water reactor (LWR) accidents and to recent National Safety Pilot Plant (NSPP) containment experiments. We used an updated version of the computer program (DIFSLIP) developed previously and we find that the results are model dependent.

*This work was supported by the U.S. Nuclear Regulatory Commission.

INTRODUCTION

Severe core damage accidents in a light water nuclear reactor can release aerosols, water vapor and fission gases into the primary coolant system and the reactor containment. Since gradients of vapor and gas concentrations are established, the aerosols can experience forces caused by the diffusion of gases. Such forces are known as diffusiophoretic forces and they contribute to the movement and deposition of aerosols.

A complete description of these forces is complicated, but in the large particle limit it is known that the force can be expressed in terms of the diffusion slip velocity.

The diffusion slip velocity has been discussed by Kramers and Kistemaker (Ref. 1). These authors described experimental measurements and gave rudimentary theoretical explanations of their measurements.

More recently, Loyalka (Ref. 2) obtained an expression for the slip based on a solution of the Boltzmann equation and general boundary conditions. Lang and Loyalka (Ref. 3) compared the theoretical results and experimental data. They showed that the expression in Ref. 2 together with the assumptions of the Lennard-Jones potential and diffusive reflection coefficients can provide satisfactory agreement with the available experimental data if suitable choices for the accommodation coefficients are made.

The purpose of the present work is to compute values of the diffusion slip for environments relevant to reactor accidents. We first summarize the results of various models (Ref. 1-10) for calculating diffusion slip, and then use a program developed by Loyalka to obtain results for conditions related to postulated reactor accidents.

The diffusion slip velocity can be used directly to obtain the contribution of diffusiophoresis to aerosol deposition. For example, the aerosol behavior equation can be expressed as:

$$\frac{\partial n(v,t)}{\partial t} = L(n,n) + \frac{\partial}{\partial x}\left(\psi(x)\, n(v,t)\right) + S(v,t) - \frac{A_c}{V_c}(v_d + v_g + v_t + \ldots)$$

where $n(v,t)$ is the particle size distribution ($n(v,t)dv$:#/cm^3). L is the collision operator, $S(v,t)$ is the source term, A_c is the containment area (cm^{2}P, V_c is the containment volume cm^3), and V(cm/sec) is the aerosol velocity. For good estimations of $n(v,t)$, it is important to have verified expressions for the various functions in the above expression, and it is our purpose to explore the results for V_d, the diffusion slip.

THEORETICAL MODELS

The aerosol particle velocity in a binary gas mixture in which two gases diffuse into each other can be expressed as:

$$v_d = -\sigma_{12} D_{12} \frac{dx_1}{dz}$$

where σ_{12} is called the diffusion slip factor, D_{12} is the binary

diffusion coefficient, and x_i is the mole fraction. A positive σ_{12} here implies that the particle moves in the direction of diffusion of the heavier species (Ref. 1). We will discuss expressions for σ_{12}, based on the assumption that the gaseous average molecular velocity is zero. Effects of the Stefan flow can, however, be directly built into equation (2) or (1).

The earliest result on σ_{12} is due to Kramers and Kistemaker. These authors used momentum balance at the surface but employed a simple ansatz for molecular distribution incident on the surface. The expression applied only to Maxwellian molecules, but even here it can lead to results that may be in error qualitatively.

The work of Brock extends the results of Kramers and Kistemaker to arbitrary molecular interaction laws--but the basic approximation regarding distribution of incident molecules is retained. Zhdanov uses basically similar arguments.

Lang, Breton, and Shendelman used kinetic models, moments, and other methods to improve the previous results. They removed one of the basic weaknesses of the earlier works as regards approximations to the distribution incident on the surface. The results, however, still are limited because of a lack of good kinetic models for gas mixtures.

A general expression, based on the use of Boltzmann and arbitrary gas surface interaction laws and the use of a variational technique was reported by Loyalka (1971). The accuracy of the expression was verified by comparisons with some exact results for model equations, and it is believed that the expression is, in general, accurate to within 1%, provided the intermolecular and gas-surface interaction laws are known.

The above results are summarized in a paper by Lang and Loyalka (Ref. 4), where comparisons with available experimental data are also given.

For the purposes of the present work, we used, with slight modifications, a computer program DIFSLIP that had been developed in conjunction with the work described in Ref. 3,4. The program provides results for the various models, once the molecular parameters and the mixture conditions are specified. As presently structured, the program is quite simple and straightforward. Some modifications of the program, however, might be in order. In particular, it should be quite straightforward to incorporate MATPRO routines for calculation of molecular parameters.

RESULTS

For specific calculations, we considered conditions relevant to the NSPP experiments. We considered nearly saturated water vapor in air, at atmospheric pressure and temperature. Our results for two situations are reported in Table I (except for the variational expression, other results were calculated for unit accommodation coefficients ($\alpha_1 = \alpha_2 = 1$), only). We find that there is a wide disparity in the results obtained by the use of the various models. Also the results are quite sensitive to the choice of α_1 and α_2 . We have found, however, at least for the water vapor-air mixture σ_{12} is only slightly sensitive to temperature and pressure, and the thermal diffusion effects.

It appears to us that to resolve the discrepancies between models, clean experimental measurements are needed. In view of the apprarent insensitivity of to temperature and pressure, these measurements perhaps need to be carried out only for a few

selected, well-defined conditions and for different aerosol materials.

REFERENCES

1. Loyalka, S.K.., "Mechanics of Aerosols in Nuclear Reactor Safety: A Review", Progress in Nuclear Energy, 12, 18(1983).

2. Kramers, H.A. and Kistemaker, J., "On the Slip of a Diffusing Gas Mixture Along a Wall", Physica, 10, 699(1943).

3. Loyalka, S.K., "Velocity Slip Coefficient and the Diffusion Slip Velocity for a Multicomponent Gas Mixture", Physics of Fluids, 14, 2599(1971).

4. Lang, H. and Loyalka, S.K., "Diffusion Slip Velocity: Theory and Experiment", Zeitschrift Fur Naturforschung, 27A, 1307(1972).

5. Brock, J.R., "Forces on Aerosols in Gas Mixtures", Journal of Colloid Science, 18, 489-501(1963).

6. Zhdanov, V.M., "Theory of Slip at the Boundary of a Gaseous Mixture", Soviet Physics-Technical Physics, 12, 134(1967).

7. Shendalman, L.H., "Low-Speed Transport of Gas Mixtures in Long Cylindrical Tubes According to the BGK Model", Journal of Chemical Physics, 51, 2483(1969).

8. Breton, J.P., "Interdiffusion of Gases Through Porous Media: Effect of Molecular Interactions", Physics of Fluids, 12, 2019(1969).

9. Breton, J.P., "The Diffusion Equation in Discontinuous Systems", Physica, 50, 365(1970).

10. Chapman, S. and Cowling, T.G., Mathematical Theory of Non-Uniform Gases, Cambridge University Press, London, 1970, Third Edition.

TABLE I. Diffusion Slip Coefficient for Different Humidities (Air and Water Vapor Gas Mixture) at 1 atm. and 300°K

Mole-Fractions		Accommodation Coefficients		Diffusion Slip Coefficients							
x_1 (Air)	x_2 (Water)	α_1	α_2	Loyalka 1+	Loyalka 2*	Kramers & Kistemaker	Waldmann	Breton	Shendalman	Lang	Zhdanov
0.9645	0.0355	0.5	0.5	0.2299	0.2276	0.2138	0.0211	0.0435	-0.3262	0.3348	0.2157
		0.5	1.0	-0.5316	-0.5372						
		1.0	0.5	0.6341	0.6335						
		1.0	1.0	0.2442	0.2415						
0.9612	0.0388	0.5	0.5	0.2302	0.2278	0.2139	0.0211	0.0435	-0.3244	0.3341	0.2159
		0.5	1.0	-0.5305	-0.5361						
		1.0	0.5	0.6355	0.6348						
		1.0	1.0	0.2445	0.2418						

+Loyalka 1: with thermal diffusion coefficient term.

*Loyalka 2: without thermal diffusion coefficient term.

The diffusion slip coefficient σ_{12} is related to the diffusion slip velocity (v_d, cm/sec) by:

$$v_d = -\sigma_{12} D_{12} \frac{\partial x_1}{\partial z}$$

where D_{12} is the diffusion coefficient of species 1 (heavier molecules-air) in the mixture, and $\partial x_1/\partial z$ is the concentration gradient. Here, a positive sign for σ_{12} would indicate that the diffusiophoretic force drives the aerosols away from the containment walls.

On the Theory of Brownian Coagulation of Aerosols for Knudsen Numbers Greater than 1

G. Metzig

Kernforschungszentrum Karlsruhe GmbH
Laboratorium für Aerosolphysik und Filtertechnik I
Postfach 36 40, 7500 Karlsruhe, W-Germany

Abstract

Smoluchowski's theory of Brownian coagulation of aerosols in air as well as the corrections from Fuchs and Davies are discussed with respect to Knudsen numbers greater than 1. Own considerations to the coagulation theory are also presented, leading to a correction of Smoluchowski's theory which pays more attention to the experimental results. PARDISEKO IV calculations were made to demonstrate the consequences when using the different corrections.

Nomenclature

k	: Boltzman constant
l	: mean free path
m	: mass of one unit; in air of one so-called "air-molecule"
r	: radius
v	: mean velocity
C	: Knudsen-Weber-(Cunningham) slip correction
D	: diffusion coefficient
K	: coagulation constant
Kn	: Knudsen number
Pe	: Peclet number
T	: temperature in Kelvin
η	: viscosity
ρ	: density
ϕ	: gas kinetic constant equal 0.491

Subscripts

g	: gas
p	: particle
SM	: Smoluchowski
F	: Fuchs
D	: Davies
M	: Metzig
GK	: gas kinetic conditions

Introduction

The scientific discussions about the Brownian coagulation constant of spherical monodisperse as well as polydisperse aerosols in air are still going on. Two adapted theories are available to evaluate the Brownian coagulation constant, namely Smoluchowski's (1916) and the free molecule theory. Each is valid for a limited range of the Knudsen-numbers only. Which theory is usable depends on the size of the aerosol particles and/or on the mean free path of the carrier gas molecules. Difficulties occur between the two theories in the so-called transition regime. Many investigators (Fuchs, 1964; Hidy and Brock, 1970; Friedländer, 1977; Davies, 1979 etc) tried to find a formula describing the Brownian coagulation constant as a unique function in the whole Knudsen number range. The formulae from Fuchs and Davies are coupled to Smoluchowski's coagulation constant K_o but are corrected with a correction factor. This one from Fuchs is explainable by his concentration jump theory, while Davies interpolates for Knudsen numbers greater than 15 between the values of K_o and those under gas kinetic conditions. He introduced a function of the Peclet number associating convective and diffusive motion.

In this paper, a new interpolation between Smoluchowski's theory and the gas kinetic conditions is presented. The new correction factor is not based on an own theory. The factor is based on Fuchs' concentration jump theory and under special considerations of the experimental results from Shon (1979) and Fuchs and Sutugin (1965).

On the other side, evaluating the coagulation constant in the transition regime from experiments run into difficulties too, due to problems in measuring ultrafine particles. The dilemma is to exclude other removal processes. In Mercer's (1978) review the errors which occured in experiments are specified.

The exact knowledge of the coagulation constant over the whole range of Knudsen numbers is for example of importance for simulations of aerosols in closed containments. Especially when ultrafine particles are present, i.e. early state situations, the effect in changing the removal rate is the greatest. The longer the experiment or the simulation runs, the smaller is the influence of the coagulation constant in the transition regime. It is well known that longtime experiments produce always the same distribution independent of the initial distribution.

The coagulation constant

Under the well-known assumptions, the rate of coagulation is controlled by the Smoluchowski coefficient of coagulation

$$K_{sm} = \frac{4 \cdot k \cdot T}{3 \cdot \eta} \qquad (1)$$

which is dependent on the properties of the carrier medium but independent of the size and density of the particles. Adapting this expression to gases, the Knudsen-Weber-(Cunningham) slip correction has to be included. The necessary coefficients are taken from Metzig (1983). The resulting

$$K_o = K_{sm} \cdot C = \frac{4 \cdot k \cdot T}{3 \cdot \eta_g} \cdot \left\{1 + 1.2\,Kn + .432\,Kn \cdot e^{-1.039/Kn}\right\} \qquad (2)$$

equation is valid only for small Knudsen numbers ($Kn = l_g / r_p$) and for big particles, respectively. Equation (2) has been confirmed by many experiments. However, this is not so in the case of large Knudsen numbers or small particles. The coagulation is now controlled by the gas kinetic theory. The idea is that very small particles have the same behaviour like the gas molecules. According to Jeans' gas kinetic theory (1925), the coagulation constant is

(3)

but independent on the Knudsen-number and independent on the condition of the carrier gas. Involving this, equation (3) becomes

$$K_{GK} = \frac{4 \cdot \eta_g}{\sqrt{2} \cdot Kn \cdot \phi \cdot \rho_g \cdot \sqrt{\frac{3 \cdot k \cdot T}{m_g}}} \cdot \sqrt{\frac{6 \cdot k \cdot T \cdot Kn \cdot \phi \cdot \rho_g \cdot \sqrt{\frac{3 \cdot k \cdot T}{m_g}}}{\eta_g \cdot \rho_p}} \qquad (4)$$

Now the physical and thermodynamical properties of the particles and the carrier gas, respectively, jointly control the coagulation constant under gas kinetic conditions.

It is evident that the coagulation constant increases for small Knudsen numbers (following Smoluchwoski's theory) up to a maximum and decreases when changing to gas kinetic conditions.

If equation (2) and (4) are combined the resulting coagulation constant curve will have a sharp bend. That is in contradiction to processes which happen in nature.

Fuchs' correction

Fuchs tried to find a smooth curve transferring Smoluchowski's theory into the gas kinetic conditions. He explained the correction with his concentration jump theory. In his opinion the coagulation constant is described by the following equation:

$$K_F = K_{sm} \cdot C \cdot \left(\frac{1}{1 + G_o}\right) \qquad (5)$$

with

$$G_o = \frac{4 \cdot D}{r_p} \cdot \sqrt{\frac{\pi \cdot m_p}{8 \cdot k \cdot T}} \qquad (6)$$

Davies (1979) disagrees with this correction theory. He refuses

to believe the analogy between the coagulation of particles and evaporation and condensation of gas molecules. He refers to an underestimation of the rate of coagulation as Kn rises from 0.5 to 15 (see fig. 1). Indeed, in this Knudsen number range no experiment yields such low coagulation constants as predicted by Fuchs' theory.

Davies' coagulation

Davies agrees that the coagulation constant must change to gas kinetic conditions for Knusden numbers above 15. In his correction the decrease of the coagulation constant is affected by the Peclet-number which is invariable in problems associating convective and diffusive motion.

$$Pe = \frac{2 \cdot v_p \cdot r_p}{D} \tag{7}$$

This can be explained as follows (Davies, 1979): The mean velocity at which a particle passes another particle, with which the possibility of collision exists, is proportional to v_p; during the time of passing, the velocity of approach of the particles, due to Brownian motion, is proportional to $D/2\ r_p$. Equation (7) is the ratio of the distance travelled at the velocity of translation to the distance diffused on account of Brownian motion, during the same short time interval.

It is necessary to find a function of Pe which will interpolate between the values of K_o and K_{GK}. According to Davies the interpolation is restricted to Knudsen numbers greater than 15. The coagulation constant due to Davies is now:

$$K_D = K_{sm} \cdot C \cdot \left\{ 1 + \frac{8 \cdot e^{[-9.03 \cdot Pe]}}{2 \cdot Pe} \right\}^{-1} \tag{8}$$

In my opinion the value of 15 is choosen to high. As will be shown later, there is no difference when using K_o or K_D in PARDISEKO IV calculations. This is also in contrast to a number of experiments. The coagulation constant curve should mark the lower boundary of all coagulation constant values found in experiments. Zeller (1983) who performed direct measurements of aerosol shape factors had to reduce the coagulation constant K_o to get agreement between measured and calculated size distributions. His maximum in Knudsen number was 13.2.

According to all statements mentioned above, own considerations were carried out.

Own consideration

No independent theory exists in the transition regime. An interpolation between gas kinetic and hydrodynamic conditions can be made only. Fuchs and Davies presented different physical conceptions of the coagulation process in the transition-regime leading to different descriptions of the coagulation constant. Meanwhile, more experiments are available and can be used to find a good approximation to the "true" coagulation constant curve.

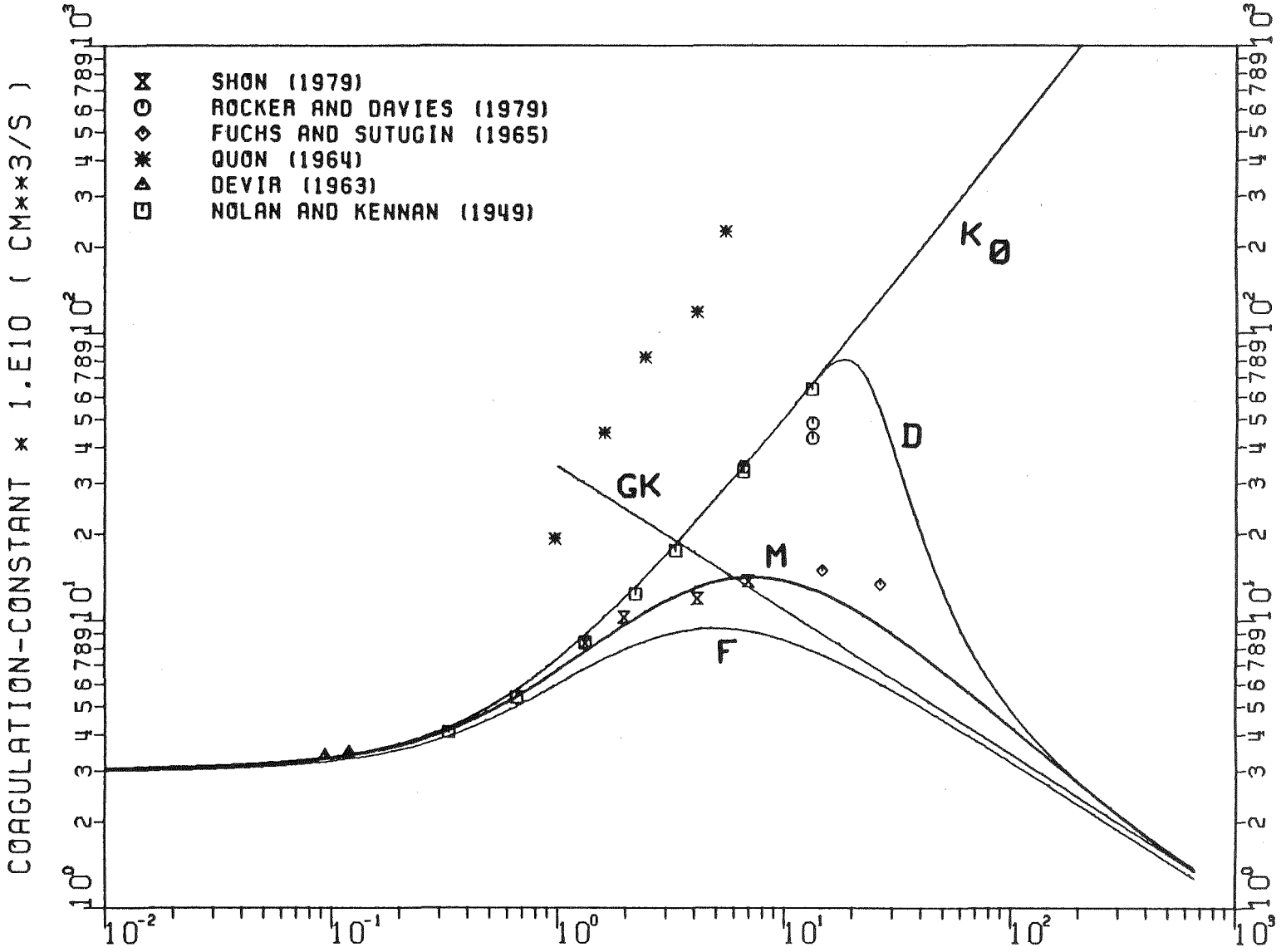

Fig. 1:

(Air, 293 Kelvin, spherical particles of unit density)

The following conditions must be fulfilled:

- For Knudsen numbers smaller than 0.1, the coagulation constant is K_o
- The theoretical coagulation constant curve represents a lower boundary
- The curve is of smooth character
- For very large Knudsen numbers, the coagulation constant must approach the gas kinetic value.

The latter requirement is well accepted. Furthermore Davies (1979) demonstrated that before this situation is reached the coagulation constant is greater than the corresponding gas kinetic value. This is because the effective collision radius of the particles becomes greater than the particle radius due to Brownian motion of the particles in a plane perpendicular to the direction of their relative velocity when approaching each other.

In consideration of the above statements, of Fuchs' concentration jump theory, and of experimental results the following expression is worked out:

$$K_M = K_{sm} \cdot C \cdot \left(\frac{1}{.985 + M_o} \right) \tag{9}$$

with

$$M_o = G_o \cdot \left\{ \frac{2 + Kn/25}{1 + Kn/100} \right\} \tag{10}$$

The coagulation constant curves for each theory mentioned above are plotted in figure 1. For better orientation, some experimental results are added. All calculations are done for air, 293 Kelvin, and spherical particles of unit density. The consequences when using the different corrections in computer programs for the calculation of the aerosol behaviour are discussed in the next section.

PARDISEKO IV calculations

Adapting the coagulation constant to computer programs, like PARDISEKO IV (Bunz, 1983), the coagulation of particles with different radii has to be taken into account. For that, in all equations the physical properties of one particle must be replaced by an average value of these properties of the two different particles.

For all PARDISEKO IV calculations, the thermodynamic conditions are chosen like those shown in figure 1. Only the Brownian coagulation process is considered, other removal effects are excluded. The mass (figure 2) and the number concentration (figure 3) are plotted versus the mass equivalent radius at three different times (0, 1.2, 30 seconds after start). The initial distribution is selected for Knudsen numbers between 25 and 230. Within one second, Davies' and Smoluchowski's coagulation constant, respectively, produce exactly the same number concentration as well as mass distribution. Using Fuchs', correction the particle growth due to Brownian

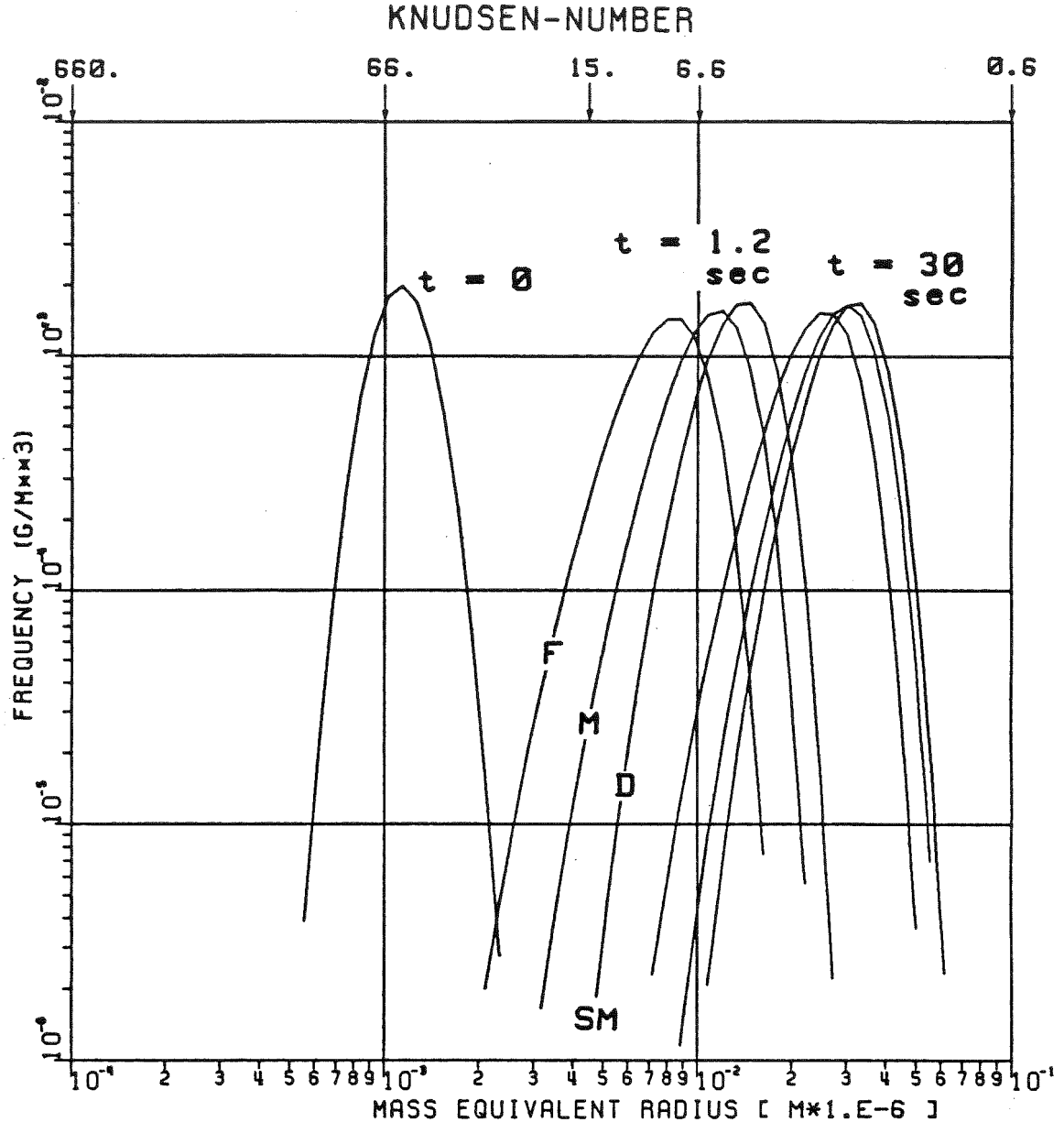

Fig. 2: PARDISEKO 4 calculations

(Air, 293 Kelvin, spherical particles of unit density)

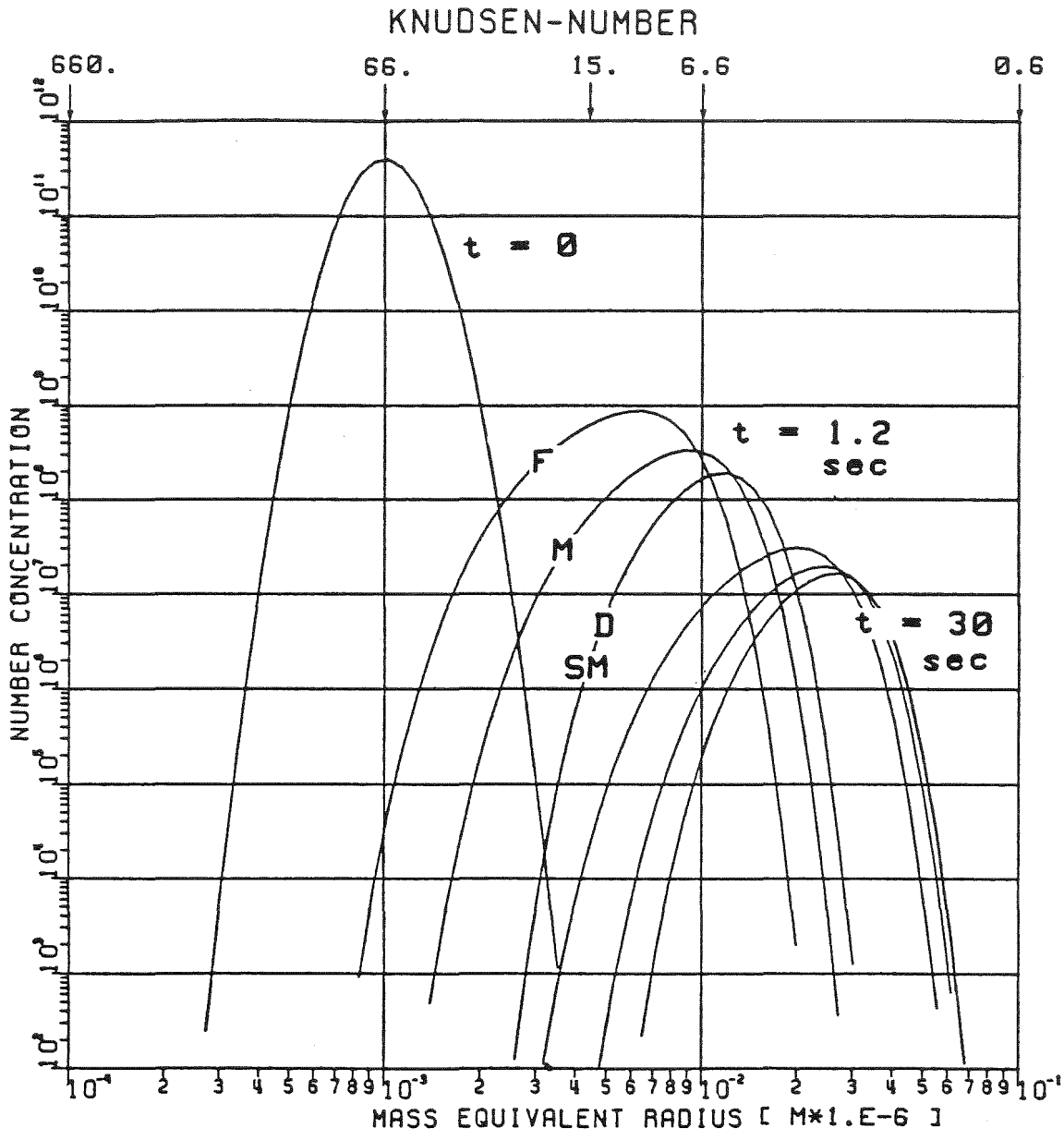

Fig. 3: PARDISEKO 4 calculations

(Air, 293 Kelvin, spherical particles of unit density)

coagulation is not as fast as observed in experiments. With Metzig's correction, the results are in between. Whether this correction describes the true conditions or not can be checked with experiments only. The observation period in such an experiment must be within a few seconds having an initial distribution like above. During longer observation times, after 10 minutes at the latest, all corrections produce the same distribution. Therefore in this case, Smoluchowski's coagulation constant is sufficient. The correction is necessary for short-term calculations and of importance for source term evaluations and for nucleation processes.

References:

Bunz, H., 1983: PARDISEKO IV: Ein Computerprogramm zur Berechnung des Aerosolverhaltens in geschlossenen Behältern, KfK-Bericht 3545, Kernforschungszentrum Karlsruhe

Davies, C.N., 1979: Coagulation of Aerosols by Brownian Motion, J. Aerosol Sci., 10, pp 151-161

Devir, S.E., 1963: On the Coagulation of Aerosols (part I). Journal of Colloid Science, 18, pp 744-756

Friedländer, S.K. 1977: Smoke, Dust and Haze. In: Atmospheric Aerosols. Ed. by S. Twomey, Elsevier, Amsterdam

Fuchs, N.A., 1964: The Mechanics of Aeosols. Pergamon Press, Oxford

Fuchs, N.A. and A. G. Sutugin, 1965: Coagulation Rate of Highly Dispersed Aerosols. Journal of Colloid Science, 20, pp 492-500

Hidy, G.M. and J.R. Brock, 1970: The Dynamics of Aerocolloidal Systems. Pergamon Press, Oxford

Jeans, J.H., 1925: The Dynamical Theory of Gases. Dover Publications, New York

Mercer, T.T., 1978: Fundamentals of Aerosol Science, edited by D.T. Shaw, Chapt. 2, Wiley, New York

Nolan, P.J. and E.L. Kennan, 1949: Condensation Nuclei from Hot Platinum: Size, Coagulation Coefficient and Charge-distribution. Proc. Royal Irish Academy, 52, (1948-1950); pp 171-190

Quon, J.E., 1964: Experimental Determination of the Coagulation Rate Constant for Nuclei. Int. J. Air Wat. Poll., Pergamon Press, 8,pp 355-368

Rooker, S.J. and C.N. Davies, 1979: Measurements of the Coagulation Rate of a High Knudsen-number Aerosol with Allowance for Wall Losses. J. of Aerosol. Sci., 10, pp 139-150

Shon, S.-N., 1979: An Experimental Study of the Coagulation of Aerosols by Brownian Motion. Thesis of PH.D. State University of New York at Buffalo

v. Smoluchowski, M., 1916: Drei Vorträge über Diffusion, Brown'sche Molekularbewegung und Koagulation von Kolloidteilchen. Physik. Zeitschr., XVII, pp 557-599

Zeller, W., 1983: Direkte Messung von Aerosolformfaktoren. KfK-Bericht 3560, Kernforschungszentrum Karlsuhe

MODELS OF DEPOSITION OF AEROSOLS FROM TURBULENT FLOWS

A. Willers
Queen Mary College
Mile End Road
London E1

ABSTRACT

Aerosols in enclosed systems can be deposited on surfaces by the combined effects of Brownian motion and turbulent transport. These processes are modelled both in circuit and containment codes (e.g. TRAP-MELT, COPDIRC).

The work reported here falls into two parts:-

(i) deposition due to Brownian diffusion

(ii) deposition due to turbulent impaction

In the case of Brownian diffusion the work of Fuchs was used as a starting point to the formulation of a number of simple models of deposition. The results obtained were compared to the predictions of the Davies model in TRAP-MELT. Agreement was adequate - approximately ± 20% over the range of particle sizes for which Brownian diffusion is the dominant deposition mechanism.

In the case of deposition due to turbulent impaction, the particle frequency response method as proposed by Lee and Durst was investigated. By considering the experimental results of a number of workers, a quantitative model was arrived at which predicted the deposition velocity over the range of particle sizes of interest to within a factor of six or better.

INTRODUCTION

In calculating the release of radioactive material to the environment during a core meltdown sequence, the retention of fission products in the RPV and primary circuit is of major importance. It is now generally accepted that a significant proportion will be in aerosol form. Models predicting the behaviour of this aerosol over the release path are therefore of benefit.

The work reported here is concerned with the modelling of aerosol deposition in two regimes of removal: that dominated by Brownian diffusion and that dominated by turbulent impaction. In the case of Brownian diffusion controlled deposition a number of simple models for calculating the deposition velocity will be presented. The modelling of turbulent impaction deposition will be investigated by developing the idea of particle frequency response to the eddies of the turbulent fluid.

MODELLING OF DIFFUSIONAL DEPOSITION

The early work on deposition of aerosols as exemplified by Fuchs [1], made use of the idea of a boundary layer. Turbulent eddies were considered to bring the particles up to a point in the flow, the boundary layer, deposition thereafter being caused by Brownian diffusion. Fuchs took the boundary layer to extend to the point at which the turbulent core fluid velocity equalled the near wall viscosity controlled fluid velocity.

The turbulent velocity was considered to be given by Prandtl's formula [2].

$$\frac{u}{u^*} = 2.5 \ln\left(\frac{zu^*}{\upsilon}\right) + 5.5 \qquad z > \frac{20\upsilon}{u^*} \qquad (1)$$

The viscosity controlled velocity was considered to be given by

$$\frac{u}{u^*} = \frac{zu^*}{\upsilon} \qquad z < \frac{5\upsilon}{u^*} \qquad (2)$$

The difference in regions of applicability was overcome by extrapolating (1) and (2) to the point z at which the predicted velocities were equal,

$$z = 11.635 \frac{\upsilon}{u^*} = \delta_L$$

where δ_L was defined as the velocity boundary layer.

Fuchs then made use of the idea put forward by Boussinesq [3] that the turbulent eddy diffusivity can be represented by a scalar. Prandtl's argument that momentum and mass transfer by turbulence use the same physical mechanisms could then be used to equate the two diffusivities

$$\upsilon_t = \varepsilon_t$$

However, work by Prandtl [4] gave

$$1.4 < \varepsilon_t / \upsilon_t < 2.0$$

while work by Sherwood and Woertz [5] gave

$$\varepsilon_t / \upsilon_t = 1.6$$

Taking the value given by Sherwood and Woertz and combining it with the model of turbulent diffusivity put forward by Landau and Levich [6], Fuchs obtained, for turbulent diffusivity within the velocity boundary layer

$$\varepsilon_t = 0.64\ u^* \frac{z^4}{\delta_L{}^3} \qquad z < \delta_L \qquad (3)$$

He then defined a diffusional boundary layer thickness, δ_D, as the point at which

$$D_B = \varepsilon_t\ (\delta_D)$$

where D_B is the coefficient of Brownian diffusion.

Using the concepts of δ_D and δ_L put forward by Fuchs, it is possible to formulate a number of models of deposition. The four cases considered are detailed below.

Case 1

Particles diffuse to within a distance δ_D of the wall. Thereafter deposition is controlled solely by Brownian diffusion. Using Fick's equation

$$j = D_B \frac{dC}{dz}$$

with a constant coefficient of Brownian diffusion, the deposition velocity is calculated as

$$V_1 = \frac{D_B}{\delta_D}$$

Case 2

Diffusion of particles between δ_D and δ_L is controlled solely by turbulent diffusion, while between the wall and δ_D, Brownian diffusion is the only transport mechanism. Assuming an averaged value of turbulent diffusivity, the deposition value is given by

$$V_2 = \left(\frac{\delta_D}{B} + \frac{\delta_L - \delta_D}{\bar{\varepsilon}_t} \right)^{-1}$$

where $\bar{\varepsilon}_t$ is the averaged turbulent diffusivity.

Case 3

As Case 2 but ε_t is given, not by a constant, but by (3). This gives

$$V_3 = \frac{D_B}{\delta_D} \left(\frac{3}{4 - \left(\frac{\delta_D}{\delta_L} \right)^3} \right)$$

Case 4

The above cases have been artificial in that they have considered turbulent diffusion to be negligible in comparison to Brownian diffusion inside the diffusional boundary layer. Case 4 considers both Brownian and turbulent diffusion to be operative over the whole region of the velocity boundary layer. The deposition velocity is then given by

$$V_4 = \left[\frac{K}{2D_B} \cdot \ln\left(\frac{\delta_L^2 + 2K\delta_L + 2K^2}{\delta_L^2 - 2K\delta_L + 2K^2}\right) + \tan^{-1}\left(\frac{2K\ L}{2K^2 - \delta_L^2}\right)\right]^{-1}$$

where $$K = 4\sqrt{\frac{D_B\ \delta_L^3}{2.56\ u^*}}$$

COMPARISON OF MODELS

In order to check the results of these four cases, it was decided to compare them to those of an accepted model. The model of Davies [7] as used in the TRAP-MELT code [8] was chosen.

The physical parameters chosen as a test case were those of Liu and Agarwal [9]. The results are plotted in Fig. 1.

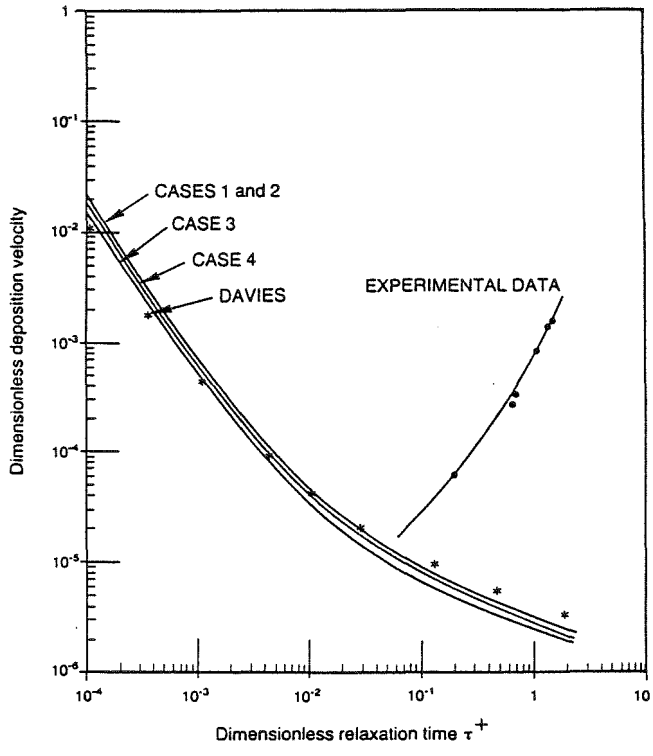

Fig. 1. Comparison of models with that of Davies

The results show close agreement over a large range of particle sizes. A cut-off to the applicability of the results is given by the experimental results for increasing particle size.

MODELLING OF TURBULENT DEPOSITION

In considering the turbulent deposition of aerosols, the modelling of Hjelmfelt and Mokros [10] as adopted by Lee and Durst [11] was examined. The model considers the idea of a particle's frequency response to the turbulent fluctuations in the fluid, starting with the Lagrangian governing equation of motion of a spherical particle in a moving turbulent fluid [12]. This equation was first derived by Tchen [13].

By expressing the fluid and particle velocities by their Fourier integrals,

$$V_f = \int_0^\infty (\xi \cos wt + \lambda \sin wt)\, dw$$

$$V_p = \int_0^\infty \eta\, (\xi \cos (wt + \beta) + \lambda \sin (wt + \beta))\, dw$$

it can be shown that η obeys the qualitative frequency relationship as shown in Fig. 2.

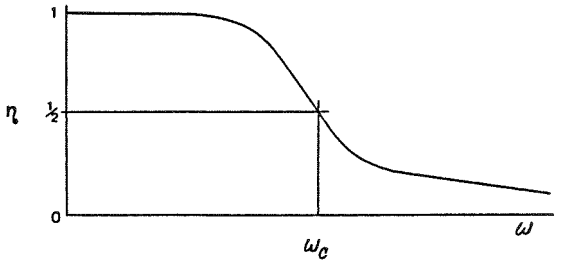

Fig. 2. Variation of η with frequency

It can further be shown that η is directly connected to the diffusional characteristics of the particles [12] through the following expression

$$\frac{\varepsilon_p}{\varepsilon_f} = \frac{\int_0^\infty \eta^2 E_f(n)\, dn}{\int_0^\infty E_f(n)\, dn}$$

where ε_p and ε_f are the turbulent eddy diffusivities of the particles and the fluid respectively, and $E_f(n)$ is the Lagrangian energy spectrum as a function of wave number, n. Thus η gives a measure of the effectiveness of the initiation of particle eddy diffusion caused by the fluid

eddy diffusion which is present in the flow. In particular when $\eta = 1$ and thus $\varepsilon_p = \varepsilon_f$, the particle's motion is completely controlled by the diffusional motion of turbulent eddies in the surrounding fluid. On the other hand, when $\eta = 0$, and thus $\varepsilon_p = 0$, the particle's motion is completely independent of the diffusional motion of turbulent eddies in the surrounding fluid and is therefore governed by the quasi-laminar viscous interaction of the mean motion of the surrounding fluid flow field.

In an effort to overcome the difficulties presented by the fact that the changeover from $\eta = 1$ to $\eta = 0$ is not discrete but continuous, Lee and Durst defined a cut-off frequency w_c, such that $\eta = \frac{1}{2}$ when $w = w_c$. For $w > w_c$ the particle motion was assumed dependent on the turbulence, for $w < w_c$ independent.

Knowing the physical parameters of the fluid and the particle it is thus possible to calculate a frequency of eddy motion such that above this frequency the particle motion is independent of the turbulence. As the eddy frequency of the turbulence increases on approaching boundaries, the particle can expect to see a cut-off point in the flow. This is called the cut-off radius. Lee and Durst used experimental frequency data to predict this cut-off radius.

In presenting their results, Lee and Durst utilised the parameter dp_c, defined as

$$dp_c = dp\ (Ns)_c \cdot \left(\frac{2\pi u^*}{\upsilon R}\right)^{\frac{1}{2}}$$

where $(Ns)_c = \left[\frac{\upsilon_f}{w_c dp^2}\right]^{\frac{1}{2}}$ is the critical Stokes' number w_c being the cut-off frequency

dp_c is a non-dimensional particle size based on the fluid frequency. The cut-off radius, r_c, as a function of dp_c was given by Fig. 3.

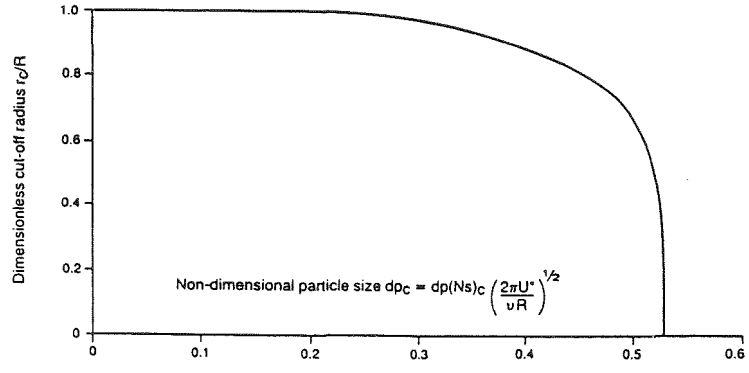

Fig. 3. Variation of Cut-off Radius as a Function of dp_c

While useful in qualitative work it does not provide sufficient information to predict the cut-off radius with any accuracy - especially for $dp_c < 0.3$ where the non-dimensional cut-off radius is almost indistinguishable from unity. It was therefore decided to use the experimental particle deposition data from a number of sources [9, 14-16] to produce

a quantitative relationship between the non-dimensional cut-off radius and the non-dimensional particle size for $dp_c < 0.3$. Figure 4 shows the results.

In calculating the dimensionless cut-off distances from the wall, the eddy diffusivities presented by Owen [17] were used. The concentration gradients at cut-off were assumed equal to the velocity gradients as calculated from von Karman [18].

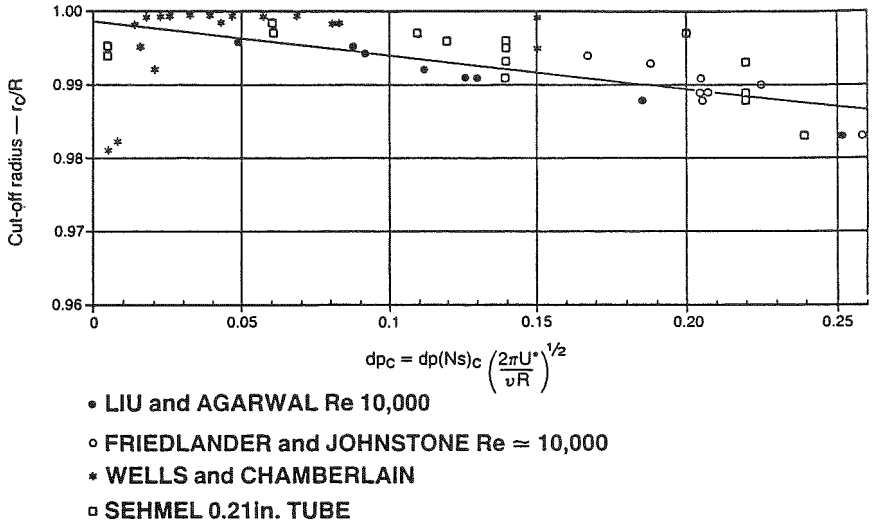

Fig. 4. Experimental Variation of Cut-off Radius with dp_c

The graph is not as one would immediately expect. As dp_c decreases it would be expected that the normalised cut-off radius, r_c/R, would increase, approaching unity. This is the case until $dp_c < 0.03$, when the cut-off radius begins to decrease. As the theory of turbulent deposition does not predict this, one of two conclusions are arrived at. Firstly, the turbulence modelling is inaccurate. Alternatively the assumption that turbulence is the only deposition mechanism is incorrect. The latter conclusion seems the most likely in view of the fact that deposition due to Brownian diffusion is known to dominate deposition for very small particles. If the data for $dp_c < 0.03$ is disregarded as being influenced by Brownian diffusion, it is possible to fit a curve linking r_c/R to dp_c. This was done using a least squares routine. A low order polynomial was chosen in order to keep the curve simple. It was found that the equation

$$1 - \frac{r_c}{R} = 0.6012.\ 10^{-3} + 0.5181.\ 10^{-1}\ dp_c$$

fitted the results adequately. This curve had the fault that for a zero value of dp_c, r_c/R was not unity. This condition was forced onto the curve by dropping the constant term. It was not considered that accuracy was seriously affected. This led to the adoption of the equation

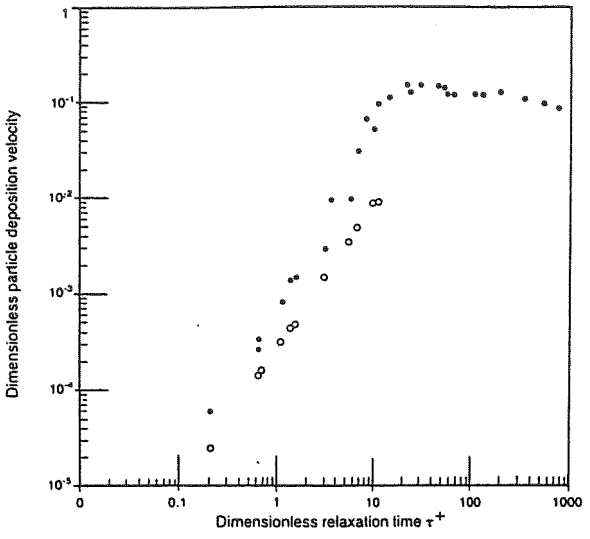

Fig.5. Data of Liu and Agarwal

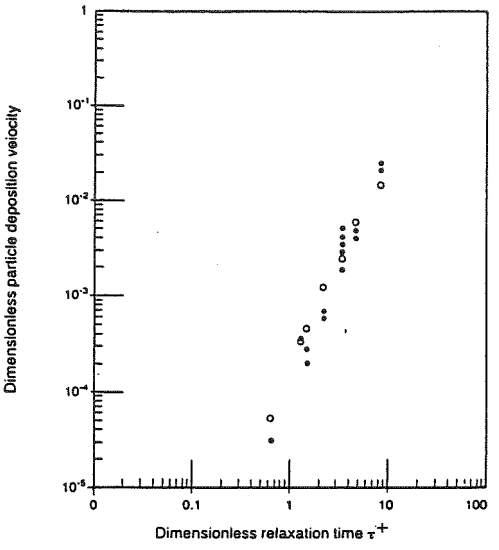

Fig.6 Data of Friedlander and Johnstone

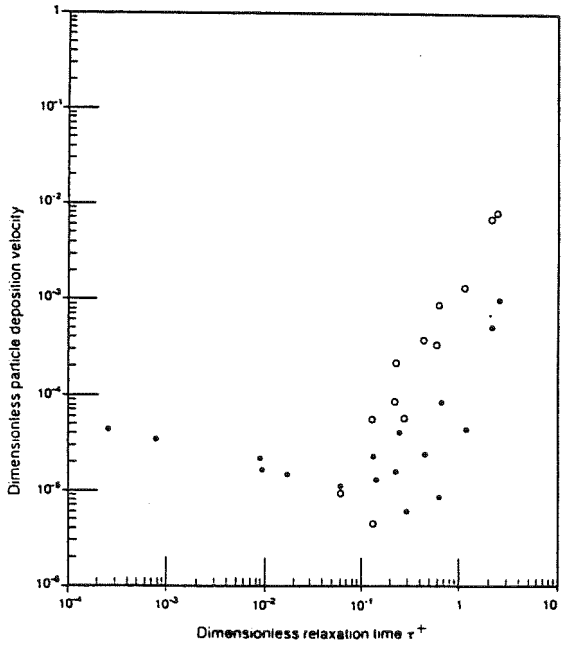

Fig.7. Data of Wells and Chamberlain

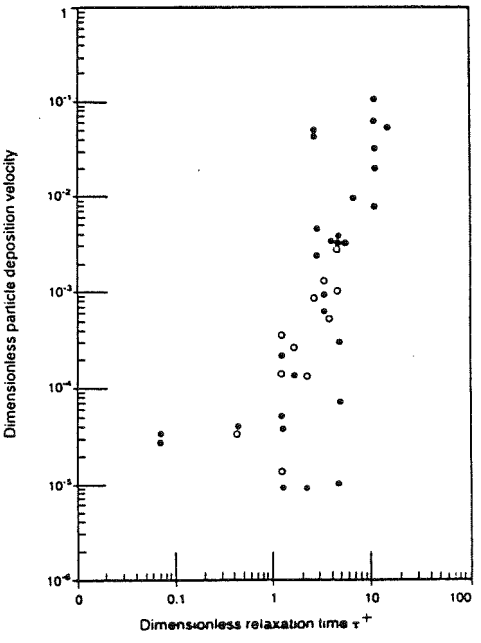

Fig.8. Data of Sehmel

Key - •EXPERIMENTAL ○THEORETICAL

$$1 - \frac{r_c}{R} = 0.05181\ dp_c \qquad (4)$$

$$0.03 < dp_c < 0.25$$

as describing the turbulent deposition for the range of particle sizes $0.03 < dp_c < 0.25$. Figures 5 to 8 show the reworked experimental data using (4). The results would appear to be reasonable.

CONCLUSIONS

Two regimes of particle deposition have been investigated. Brownian diffusion dominated and turbulent diffusion dominated. In considering Brownian diffusion a number of simple models have been postulated. The results obtained using these models have been compared. Agreement was usually better than 30%.

The modelling of Lee and Durst has been extended to provide a working model for the prediction of the turbulent deposition of particles. The results show agreement to within a factor of 6 or better.

REFERENCES

[1] Fuchs
"The Mechanics of Aerosols"
Pergamon Press.

[2] L. Prandtl
"Uber Die Ausgebildete Turbulenz"
ZAMM 5 1925 pp 136]139
and Proc. 2nd Intern. Congr. Appl. Mech.
Zurich 1926 pp 62]75.

[3] J. Boussinesq
Mem. pres. par div. savant a l'acad. sci. Paris
Vol 23 pp 46 1877,

[4] L. Prandtl
Fuhrer durch Stromungslehre
Braunschweig, Kap 3 No. 4 1949.

[5] T. Sherwood, B. Woertz
Ind. Eng. Chem. Vol 31 pp 1034 1939.

[6] V. Levich
"Physico Chemical Hydrodynamics"
Acad. Sci USSR Moscow Chap 3 1952.

[7] C. N. Davies
"Deposition from Moving Aerosols"
"Aerosol Science" C. N. Davies Ed.
Academic Press.

[8] TRAP-MELT Users Manual. NUREG/CR - 0632, BMI-2017.

[9] B Y H Liu and J K Agarwal
"Experimental Observation of Aerosol
Deposition in Turbulent Flow"
J Aerosol Sci 1974 Vol 5 No 2 pp 145-55

[10] A T Hjelmfelt Jr and L F Mokros
"Motion of Discrete Particles in a Turbulent Fluid"
Appl. Scientific Res 1966 Vol 16 pp 149-161.

[11] S L Lee and F Durst
"On the Motion of Particles in Turbulent Duct Flows"
Int J of Multiphase Flow. 1982 Vol 8 No 2 pp 125-146.

[12] O Hinze
"Turbulence"
McGraw Hill

[13] C M Tchen
"Mean Value and Correlation Problems Connected with the Motion of Small Particles in a Turbulent Fluid"
PhD Thesis 1947, Delft.

[14] S K Friedlander and H F Johnstone
"Deposition of Suspended Particles from Turbulent Gas Streams"
Ind Engrg Chem 1957 Vol 49 pp 1151-56.

[15] A C Wells and A C Chamberlain
"Transport of Small Particles to Vertical Surfaces"
Br. J. Appl. Phys. 1967 Vol 18 pp 1793-99.

[16] G A Sehmel
"Aerosol Deposition from Turbulent Airstreams in Vertical Conduits"
BNWL - 578.

[17] P R Owen
"Aerodynamic Capture of Particles"
E G Richardson Ed.
Pergamon Press.

[18] T von Karman
Proc. 3rd Int. Congr. Appl. Mech.
Stockholm Pt 1 p 85.

Improvements in the Modelling of Sedimentation and Gravitational Agglomeration

I H Dunbar and S A Ramsdale
UKAEA Safety and Reliability Directorate, Culcheth, UK

ABSTRACT

In nuclear safety applications the most important processes affecting aerosol removal in containments are gravitational sedimentation and gravitational agglomeration. The existing models in the AEROSIM code for these processes were not strictly accurate for larger particles. As the particle radius grows above 30μm the terminal velocity becomes less than that predicted by Stokes law. For particles greater than 10μm in radius the collision efficiency may become greater than that used for smaller particles. In the modelling of sodium fires it was noted that an appreciable mass is predicted to accumulate in particles with radius greater than 100μm. Steam condensation on particles in PWR containments is another potential mechanism for rapid particle growth. Models were therefore included in AEROSIM for the terminal velocity and collision efficiency of the larger particles. In a test case, a hypothetical sodium fire, it was found that the new terminal velocity made a negligibly small difference in all the results. The enhanced collision efficiency caused more mass to accumulate above the cutoff radius of 100μm, but the sum of this mass and the settled mass, which can reasonably be expected to represent the real settled mass, was little changed.

1. Motivation for the Extended Modelling

Gravitational sedimentation is the most important aerosol removal mechanism under the majority of accident conditions. It is especially effective in removing larger particulate material, which is relatively stable against diffusional deposition. The relative motion of particles as they fall at different speeds depending on their sizes also gives rise to so-called "gravitational agglomeration". This process is itself the most important agglomeration mechanism for particles in the size range of greatest interest (radii between 0.5 and 5μm). It was this interplay between sedimentation and gravitational agglomeration, together with the importance of these mechanisms to aerosol behaviour, which motivated the modelling extensions described below.

The extensions made concern the calculation of the terminal velocity of aerosol particles and the collision efficiency ε as a function of particle size. Most containment aerosol codes use Stokes' law to determine the fall speed of the particles. However this breaks down at higher Reynolds numbers, when it over-predicts the terminal velocity. In AEROSIM, an empirical correlation has been fitted piecewise, using data relating the drag coefficient to the Reynolds number. It is then possible to use an iterative scheme to deduce the terminal velocity.

The modelling of the collision efficiency has also been extended to cover larger particle sizes. The theoretical work of Klett and Davis[1] predicts that the collision efficiency increases significantly as the larger particle radius goes above 10μm. Previous models due to Fuchs[2] and Pruppacher and Klett[3] give rise to a collision efficiency which is a function of the ratio of particle radii r/R only. A simple analytic form has been fitted to the numerical results of Klett and Davis to account for the additional dependence on R.

The two modelling extensions affect only larger particles (radii greater than 10μm) and are therefore necessary only in cases where agglomeration is rapid enough to convert a substantial proportion of the available aerosol mass into such particles. The work was motivated by the observation that in the modelling of short, intense sodium fires, substantial amounts of aerosol mass accumulated above the upper cutoff particle radius even when this radius was set as high as 100μm, and also by the expectation that in the future AEROSIM will be used to model situations where aerosol particles grow rapidly due to steam condensation. In this work the effects of the model changes are investigated in a hypothetical sodium fire case. Because the effects of the two changes are in opposite directions (larger particles are more readily formed, but they then settle out less quickly), the changes are considered first separately and then together.

2. Terminal Velocity Calculation

The terminal velocity of a falling particle is usually calculated in terms of the drag coefficient, C_D, and the Reynolds number, Re, which for a spherical particle are defined by:-

$$Re = \frac{2\rho_2 \, ur}{\eta}, \tag{1}$$

$$C_D = \frac{F_D}{\frac{1}{2}\rho_2 \, u^2 \times \pi r^2} \tag{2}$$

where

r = particle radius
u = terminal velocity
ρ_1 = particle density
ρ_2 = atmospheric density
η = dynamic viscosity
F_D = drag force

At the terminal velocity, the drag force F_D balances the gravitational force, and neglecting the buoyancy force (since $\rho_2 << \rho_1$), we have that

$$F_D = \frac{4}{3} \pi \rho_1 r^3 g. \tag{3}$$

Substituting (3) into (2), we may now write the terminal velocity u in terms of the drag coefficient C_D as

$$u = \left[\frac{8g}{3} \frac{\rho_1}{\rho_2} \frac{r}{C_D}\right]^{\frac{1}{2}} . \tag{4}$$

Equation (4) as it stands does not determine u explicitly, since C_D is itself a function of u. However when Re is small enough (in practice, less than 0.3) the inertia term in the Navier-Stokes equation can be neglected. An exact solution can then be obtained (Batchelor[4]). The resulting drag force is (Stokes law)

$$F_D = 6\pi r \eta u ,$$

$$\text{ie} \quad u = \frac{2g\rho_1}{9\eta} r^2 , \quad C_D = \frac{24}{Re} \tag{5}$$

For typical nuclear aerosols with $\rho_1 \approx 10^3 \text{kg m}^{-3}$, these results are accurate up to a radius of around 30μm. Above this radius, (5) begins progressively to overestimate u. Empirical correlations between C_D and Re are available for these larger Reynolds numbers. One such (used in the US code, HAA-4A) is that due to Klyachko (Fuchs[2]):

$$C_D = \frac{24}{Re} + \frac{4}{Re^{1/3}}$$

This formula is a good approximation up to Reynolds numbers of 1000, but has the disadvantage that it is difficult to invert and implement in a computer code.

Instead it was decided to use a simpler empirical formula, namely

$$C_D = a\ Re^{-b} \tag{7}$$

and fit this to the available experimental data on a piecewise basis. The advantage of this is that (7) can be inverted directly to give

$$u(r) = \left[\frac{8}{3}\frac{\rho_1}{\rho_2}\ gr\ \frac{1}{a}\ \left(\frac{2\rho_2 r}{\eta}\right)^b\right]^{\frac{1}{2-b}} \tag{8}$$

The values of a and b were found for different ranges of Re by fitting the experimental results of le Clair et al[5,6], reported by Pruppacher and Klett[3]. The ranges and values are:

Re	a	b
0 - 0.3	24	1
0.3 - 3	26.75	0.91
3 - 30	20.77	0.68
30 - 300	11.85	0.515
300 - 3000	2.33	0.23
> 3000	0.37	0

Equation (8) is not fully explicit in that the choice of a and b depends on Re and hence on the velocity. AEROSIM uses an iterative technique. Given a value of Re and hence of a and b, u(r) is calculated. If the corresponding new Re is outside the assumed range, then the calculation is repeated with the new a and b. Starting from the Stokes law Reynolds number, this procedure converges rapidly; in general only two or three iterations are needed. However, the terminal velocity, u(r), is required as part of the integrand for the calculation of the removal rates and agglomeration rates. For this reason, it was decided to optimize computing time further by using the iterative scheme only for the particle sizes corresponding to the edges of each mass interval. Thereafter a quadratic fit is used for the integration procedures. The loss of accuracy in doing this was found to be very small, whilst computing times were reduced to within 1% of those previously encountered when using the standard Stokes formula for all particle sizes.

The remaining problem in implementing the new terminal velocity calculation in AEROSIM was to decide how to incorporate the mobility shape factor, χ. Up to now it has been assumed that the particles are rigid spheres. At present, deviations from spherical shape are accounted for in the particle mobility function:-

$$B(r) = \frac{1}{6\pi\eta\chi r}\ c \tag{9}$$

where c is the Cunningham correction factor. Stokes' terminal velocity is then written in the form

$$u_s(r) = \frac{4\pi}{3}\rho_1\ g\ r^3\ B(r) \tag{10}$$

In view of the way χ occurs in the Stokes velocity, it seems reasonable to remove a factor of r^3 from the righthand side of (8), and then in the remaining r - dependence to replace r by χr. Equation (8) then becomes:

$$u(r) = \chi^{-(\frac{5-4b}{2-b})} [\frac{8}{3} \frac{\rho_1}{\rho_2} gr \frac{1}{a} (\frac{2\rho_2 r}{\eta})^b]^{\frac{1}{2-b}} . \quad (11)$$

3. Collision Efficiency Modelling

The gravitational agglomeration rate for a larger particle of radius R and a smaller of radius r, falling with terminal velocities U and u respec tively is

$$\phi_G(r,R) = \pi (r+R)^2 (U-u) \varepsilon (r,R) \quad (12)$$

The collision efficiency, ε, measures the deviation from the situation where the larger particle simply collects all the smaller particles lying in its path. The most commonly used collision efficiency model in containment aerosol codes is that due to Fuchs:-

$$\varepsilon_F(r,R) = \frac{3}{2} (\frac{\kappa}{1+\kappa})^2, \quad (13)$$

where $\kappa = r/R$. However this was developed for a stationary spherical collector, and it has recently been argued [7] that a formula due to Pruppacher and Klett[3] is more appropriate:-

$$\varepsilon_{PK}(r,R) = \frac{1}{2} (\frac{\kappa}{1+\kappa})^2 . \quad (14)$$

Numerical calculations carried out by Klett and Davis[1] indicate that (14) is indeed more accurate, provided that $\kappa << 1$. As the particles become comparable in size, the smaller particle begins to perturb the flow around the larger, and a better fit to numerical solutions is obtained if one uses (14) up to $\kappa = 0.5$ and then give ε the constant value, $\varepsilon = 0.05$ above this. This option, referred to below as "truncated Pruppacher - Klett" (TPK) is available in AEROSIM for use when $R < 10\mu m$.

Klett and Davis predict that for a given κ the value of ε will increase as R increases above $10\mu m$. They solve numerically the equations of motions of two interacting spheres using the Carrier-modified Oseen solution for flow around a sphere[3]. Compared with previous work using the Stokes solution[8] greater approximations have to be made in the boundary conditions, but there is evidence that inertia corrections are much more important in the two-sphere case than in the one-sphere case.

Klett and Davis calculate for water droplets falling under atmospheric condition, and present their results in terms of R. In order to generalize the results it was assumed that the collision efficiency would scale like a dimensionless measure of R. This was chosen to be the Reynolds number corresponding to the Stokes terminal velocity (ν is kinetic viscosity):

$$\xi = \frac{4g}{9\nu^2} \frac{\rho_1}{\rho_2} R^3 \quad (15)$$

(Besides κ and ξ there is one more independent dimensionless parameter relevant to the collision efficiency. However here it is assumed that ε

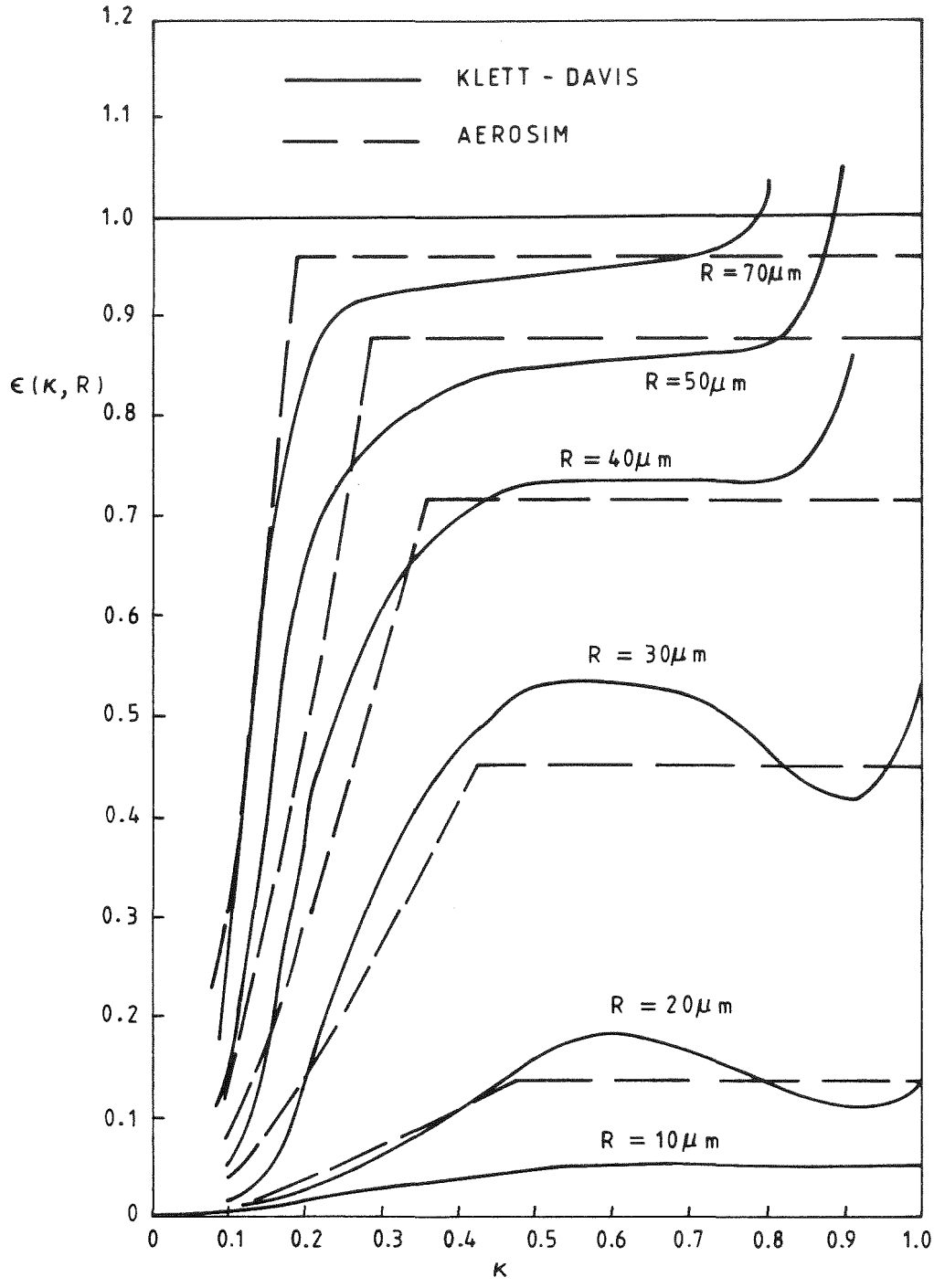

FIGURE 1 KLETT - DAVIS COLLISION EFFICIENCIES AND THE AEROSIM APPROXIMATION

depends only on these two parameters.) The analytic approximation chosen for implementation in AEROSIM is a generalization of the TPK formula, to which it reduces for $\xi < 0.11$:

$$\varepsilon_{KD}(\kappa,\xi) = \begin{cases} N(\xi)\ (\frac{\kappa}{1+\kappa})^2 & \kappa<\kappa_o(\xi) \\ N(\xi)\ (\frac{\kappa_o(\xi)}{1+\kappa_o(\xi)})^2 & \kappa>\kappa_o(\xi) \end{cases} \qquad (16)$$

where

$$N(\xi) = \begin{cases} 0.47 & \xi<0.11 \\ 0.47 + 9\ (\xi-0.11)^{3/4} & \xi>0.11 \end{cases} \qquad (17)$$

and

$$\kappa_o(\xi) = \frac{0.5 + 0.03\xi}{1 + 0.4\xi} \qquad (18)$$

Figure 1 shows the comparison between the Klett-Davis results and this formula. The aim was to approximate the general rise in ε. In doing this much of the detailed κ dependence has been averaged out.

4. Results

To investigate the effects of the modifications, we set up a sample test run. A sodium oxide aerosol (effective density 1.2×10^3 kg m^{-3}) with an initial airborne mass of 1693 kg, distributed lognormally with $r_g = 0.21\mu m$ and $\sigma_g = 1.93$, is modelled in a containment volume of 3.1×10^4 m^3. This aerosol is supposed to be the end result of burning 1 tonne of sodium in 10 minutes. The results of the four runs are shown below on table 1 for the final time, 1.64×10^4 s.

Masses (in kg) at 16 400 s	Stokes Velocity		Corrected Velocity	
	TPK (00)	KD (01)	TPK (10)	KD (11)
M (airborne)	70	71	70	71 (57)
M (wall)	2.9	2.8	2.9	2.8 (2.9)
M (floor)	1577	712	1580	715 (930)
M (leak)	0.071	0.065	0.072	0.065 (0.068)
M (over)	43	907	40	904 (703)

Table 1. Mass Balance for Model Variations, Cut-off radius = 100μm except for 11(numbers in brackets), where it is 200μm.

The masses on the table are respectively the mass still airborne, that diffused to the wall, that removed by sedimentation, that leaked to the environment (assuming a leak rate of 0.1%/day), and finally that which is predicted to agglomerate to particles with radius greater than 100μm, at which point it disappears from the calculation. The most obvious result is that correcting the terminal velocity makes very little difference to the results. This result is still valid if the mass median radius of the initial distribution is increased to 10μm. In equation (8), only particles with radii above 30μm are affected at all by the decrease in terminal velocity. In the highest radius range considered in this calculation, from 76.2μm to 100μm the reduction in sedimentation rate is on average a factor 0.55. However the maximum masses in this radius range

(attained in all four cases at t= 1400 s) range between 0.14% (case 00) and 0.55% (case 11) and these peak values last only for of the order of 1000 s. Therefore only a small fraction of the airborne mass is ever affected by the reduction in fall-out rates.

Changing from the TPK to the KD collision efficiency produces a bigger shift, namely 864 kg, from m (floor) into m (over), as agglomeration is enhanced at the expense of sedimentation. However if one takes the view that particles larger than 100μm will sediment out rapidly ($\lambda_G \approx 10^{-2}\ s^{-1}$), and that therefore m (over) should be added to m (floor) to give a total sedimentation mass, then the change of collision efficiency causes no difference in the final predictions of the whereabouts of the mass. The situation is looked at in more detail on figure 2, which shows m (over) and m (over) + m (floor) for cases 10 and 11 as a function of time. Around 2000 s on this scale (1400 s after the start of the calculation) there is a surge of agglomeration. Most of m (over) is accumulated around this time. As is to be expected this surge is stronger in case 11 than in case 10. However on a longer time-scale this difference is compensated for by increased sedimentation in 10, and the two m (over) + m (floor) curves come together again.

Table 1 also includes the results of another 11 calculation, this time with the cut-off set at 200μm. As expected the main effect is to shift mass (201 kg) from m (over) to m (floor). However even at this radius there is still a substantial accumulation of material above it. The other change is a transfer of 14 kg from the airborne to the sedimented mass. This is presumably because the particles between 100μm and 200μm are now still available for agglomeration with the smaller particles. Whether such large particles will in reality be available, well-mixed throughout the whole volume, is however open to question.

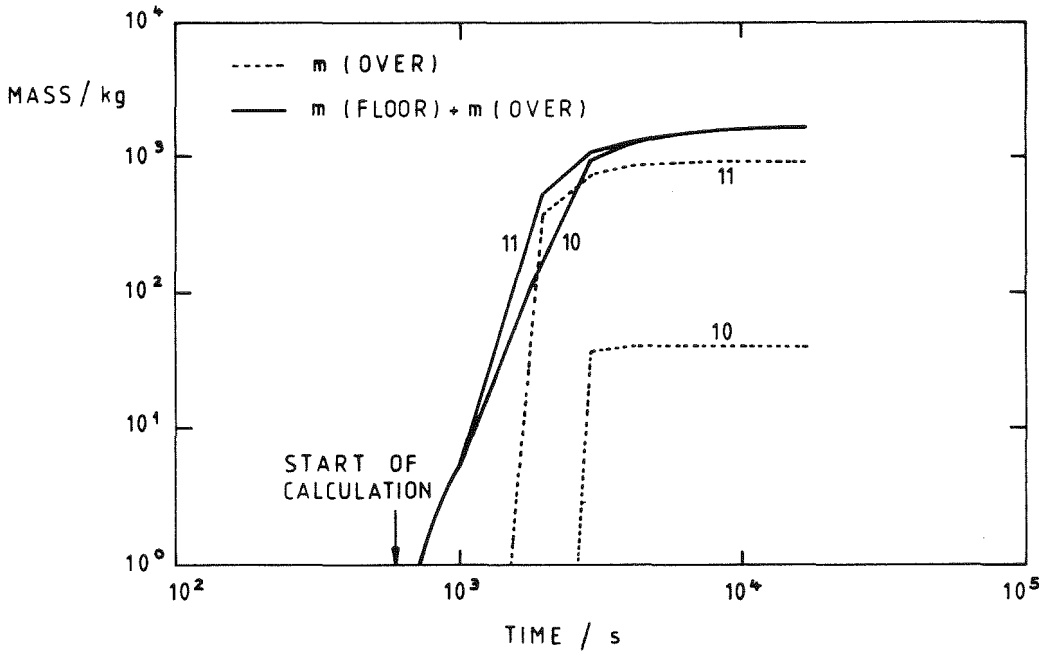

FIGURE 2 COMPARISON OF COLLISION EFFICIENCY MODELS

The inclusion of terminal velocities and collision efficiencies appropriate to the larger particles does not mean that the modelling of these particles is complete. As sizes increase, the well-mixed assumption will progressively break down. Even if a code which could model stratification due to settling were written, the input regarding flow velocities within the containment would probably not be available.

5. CONCLUSIONS

Extended models for the terminal velocity and collision efficiency of large particles are now available as options in AEROSIM, although they may be less important than originally thought. The velocity calculation should be of use when spray modelling is included in the code. The Klett-Davis collision efficiency results do not go up to the radii of spray droplets, so further extensions are needed here.

In the hypothetical sodium fire case investigated here, in spite of the large masses accumulated above the cut-off radius, there is little net effect of extending the terminal velocity and collision efficiency models. It appears that at any one time only a small fraction of the airborne mass exists as the large particles, and that since these particles are destined to sediment out rapidly, the details of their behaviour are less important. This is particularly true of the velocity correction. The collision efficiency change does alter substantially the size to which particles grow, but if one assumes m (over) can be added to the mass sedimented then there is no significant effect on the final result. The model changes have yet to be tested in cases where there is rapid growth due to steam condensation.

REFERENCES

1. J D Klett and M H Davis "Theoretical collision efficiencies of cloud droplets at small Reynolds numbers" J Atmos Sci 30 (1972), 107-117.

2. N A Fuchs "The Mechanics of Aerosols" Pergamon (1964).

3. H R Pruppacher and J D Klett "Microphysics of Clouds and Precipitation" D Reidel Pub Co (1978).

4. G K Batchelor "An Introduction to Fluid Mechanics" CUP (1970) pp229-244.

5. B P Le Clair, A E Hamielec and H R Pruppacher "A numerical study of the drag on a sphere at low and intermediate Reynolds numbers" J Atmos Sci 27 (1970) 308-15.

6. B P Le Clair, A E Hamielec, H R Pruppacher and W D Hall "A Theoretical and Experimental Study of the Internal Circulation in Water Drops Falling at Terminal Velocity in Air" J Atmos Sci 29 (1972) 728 - 740.

7. I H Dunbar and J Fermandjian "Comparison of Sodium Aerosol Codes" (to be published).

8. L M Hocking and P R Jonas "The collision efficiency of small drops" Quart J Roy Meteor Soc 96 (1970), 722-729.

Turbulent-Gravitational Collision Efficiency of Nuclear Aerosols*

by

T. Enomoto and S. K. Loyalka

Nuclear Engineering Program

University of Missouri-Columbia

Columbia, MO 65211

ABSTRACT

Estimations of fission-product release from postulated severe nuclear reactor accidents are sensitive to models used for collision cross-sections in aerosol behavior codes. Models of gravitational collisional cross-sections based on mechanistic considerations have been constructed in the recent past. The present paper investigates the role of turbulence in influencing collision cross-sections in synergism with gravitation.

A computer program that solves the dynamical equations of motion is described briefly, and some representative results for Na_2O particles are reported. For this case, the collision cross-sections are found to be about an order of magnitude higher than those obtained from models presently in use in the nuclear aerosol behavior codes.

*Work carried out under the sponsorship of the U.S. Nuclear Regulatory Commission.

INTRODUCTION

Estimations of fission-product release from postulated severe nuclear reactor accidents are sensitive to models used for collision efficiency in aerosol behavior analysis codes [1]. Pertmer and Loyalka [2] and Tuttle and Loyalka [3] have used mechanistic approaches to construct computer programs that provide results for gravitational collision efficiency. These results show that the expressions used in nuclear aerosol codes such as HAARM-3, NAUA, etc., can be in substantial error, both qualitatively and quantitatively.

In the aforementioned work of Pertmer and Loyalka and Tuttle and Loyalka, only the gravitational motion was considered, and turbulence was ignored. We have now constructed a computer program based on a mechanistic approach that provides results for collision efficiency under simultaneous presence of motion induced by turbulence and by gravitation.

EQUATIONS OF MOTION

If $\underline{U}(U_x,U_y)$ is the velocity of the particle m(= 1,2) and $\underline{V}(V_x,V_y)$ is the velocity of fluid, then the non-dimensional momentum equations for a turbulent field with Carrier-modified Oseen drag force approximation can be written as:

$$\frac{d\,U_{mx}}{dT} = 1.5A_f \frac{d\,V_{mx}}{dT} + \frac{H^4}{K}\left(1 - \frac{(\Lambda_m(U_{mx}-V_{mx})-\Gamma_m'(U_{my}-V_{my}))}{H_m^2}\right) \qquad (1)$$

$$\frac{d\,U_{my}}{dT} = 1.5A_f \frac{d\,V_{my}}{dT} + \frac{H^4}{K}\left(\frac{\Gamma_m(U_{my}-V_{my})-\Lambda_m'(U_{mx}-V_{mx})}{H_m^2}\right) \qquad (2)$$

$$\frac{d X_m}{dT} = U_{mx} - V_{mx}, \quad \frac{d Y_m}{dT} = U_{my} - V_{my} \qquad (3),(4)$$

where the velocity scale is the particle-1 terminal velocity, U_o, and the time scale is the particle-1 radius, a_1, over the particle-1 terminal velocity, a_1/U_o, so that $t = T\, a_1/U_o$, and $U = u/U_o$, where t is in seconds and U is in cm/sec. Also,

$$U_o = \frac{2a_1^2 g}{9\,\nu} \left(\frac{\rho_s}{\rho_f} - 1\right) \qquad (5)$$

$$H = a_2/a_1 \qquad (6)$$

$$H_m = \begin{cases} 1, & m = 1 \\ H, & m = 2 \end{cases} \qquad (7)$$

$$A_f = \frac{\rho_f}{\rho_s + 0.5\,\rho_f} \qquad (8)$$

$$K = \frac{2\rho_s H^4}{9\,\rho_f} \frac{U_o\, a_1}{\nu} \qquad (9)$$

ρ_s, ρ_f: Aerosols and fluid densities, respectively

g : Gravitational acceleration

ν : Kinematic viscosity.

Explicit expressions for these forces have been reported by Klett and Davis (1973) and are described in ref. 2.

The turbulent velocity $V_m(\underline{r}(t))$ and "turbulent acceleration" dV_m/dT are expressed as

$$\frac{d\,V_x}{dT} = \frac{d\,v_x(\underline{r})}{dt}\,\frac{a_1}{U_o^{\,2}} = v_x\,\frac{d\,v_x}{dx}\,\frac{a_1}{U_o^{\,2}} \tag{10}$$

$$\frac{d\,V_y}{dT} = \frac{d\,v_y(\underline{r})}{dt}\,\frac{a_1}{U_o^{\,2}} = v_y\,\frac{d\,v_y}{dy}\,\frac{a_1}{U_o^{\,2}} \tag{11}$$

and are constructed by assuming turbulence to be homogeneous and isotropic. In particular, we obtain the fluctuating velocities by using the expressions:

$$\overline{(V_r(\underline{x}+\underline{r}) - V_r(\underline{x}))^2} = D_{rr}(\underline{r}) = c(er)^{2/3} \tag{12}$$

and

$$\overline{(V_n(\underline{x}+\underline{r}) - V_n(\underline{x}))^2} = D_{nn}(\underline{r}) = \frac{4}{3}\,c(er)^{2/3} \tag{13}$$

where c, e, and r are respectively the structural function constant (=1), turbulent energy dissipation ratio (cm^2/sec^3) and distance.

Note that in the present case the collisional kernel is defined as:

$$\beta_{tg} = \varepsilon(a_1, a_2)\,\pi(a_1+a_2)^2\,|U_s(a_1) - U_s(a_2)| \tag{14}$$

where

$$\varepsilon(a_1,a_2) = \frac{2\int_o^\infty y\,P(y)\,dy}{(a_1+a_2)^2} \tag{15}$$

where a_1 and a_2 are the particle radii, y is the initial horizontal separation, and P(y) is the probability of collision. P(y) must be obtained by a solution of the dynamical equation for fluctuating turbulent field. $U_s(a_i)$ is the settling speed of particle i.

THE COMPUTER PROGRAM

A system flow chart of the computer program is given in Fig. 1. The program has three parts:

1) Specification of input data: environmental and aerosol conditions.
2) Generation of turbulent flow field by specification of appropriate correlations, transform matrices and random number generators.
3) Solutions of the dynamical equations of motion, collection of collision probability data, and computation of collision efficiency.

The program was tested by closed examination of each part, and comparison with the results of ref. 2 for no turbulence.

RESULTS

We have obtained results representative for Na_2O, UO_2 particles in air, and water droplets in air. We have found that even slight turbulence (e_t, the turbulence energy dissipation ratio 1 to 10 cm^2/sec^2), can have substantial influence on the computed values. For the same conditions, our results for the collision kernel (efficiency) are an order of magnitude higher than those obtained from the HAARM-3 expression for the collision kernel:

Figure 1

System Flow Chart (turbulence)

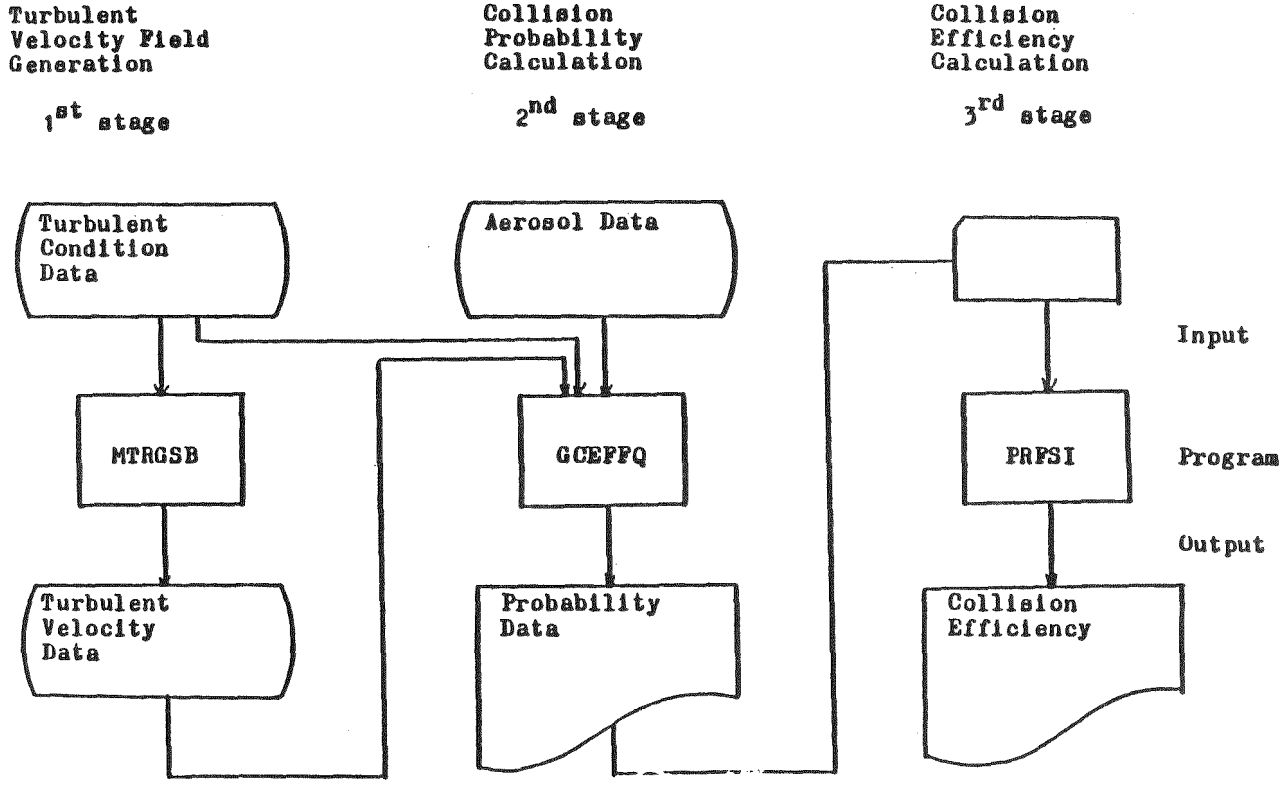

$$\beta_{tg} = \beta_t + \beta_g \tag{16}$$

where

$$\beta_g = \frac{2\pi g(\rho-\rho_g)}{9\mu} |a_1-a_2| (a_1+a_2)^3 \cdot \varepsilon \tag{17}$$

$$\beta_t = (\frac{8\pi\rho_g}{15\mu})^{\frac{1}{2}}(a_1+a_2)^3 e_t^{\frac{1}{2}} \varepsilon \tag{18}$$

$$+ (8\pi)^{\frac{1}{2}} \frac{2(\rho-\rho_g)}{9\mu} (1.3)(\frac{\rho_g}{\mu})^{\frac{1}{2}} (a_1+a_2)^3 |a_1-a_2| e_t^{3/4} \varepsilon$$

$$\varepsilon = \frac{3}{2} [\eta(a_1-a_2) \cdot \frac{a_2^2}{(a_1+a_2)^2} + \eta(a_2-a_1) \cdot \frac{a_1^2}{(a_1+a_2)^2}] \tag{19}$$

Here $\eta(x) = 1$, $x>0$, $\eta(x) = 0$, $x<0$; $\eta(x) = 1/2$, $x=0$. Note that we have written ε in a form that is symmetric to avoid slightly confusing representations of the past.

Our results for Na_2O particles are reported in table 1 and fig. 2-5, and show the substantial effect of turbulence. It would be of interest to study the impact of the present results on aerosol behavior prediction.

Table 1. Collision Kernels, $\beta(cm^3/sec)$

(Na_2O Particles)

$r_1(\mu m)$	a	0.2	0.4	0.6	0.8
20	HAARM-3 case				
	$\beta_{g'}$	7.154×10^{-6}	2.504×10^{-5}	4.292×10^{-5}	4.293×10^{-5}
	$\beta_{t'}$	1.250×10^{-7}	4.446×10^{-7}	7.861×10^{-7}	8.581×10^{-7}
	$\beta_{tg'}$	7.279×10^{-6}	2.548×10^{-5}	4.370×10^{-5}	4.379×10^{-5}
	Present work				
	β_g	2.958×10^{-5}	1.070×10^{-4}	1.240×10^{-4}	7.711×10^{-5}
	β_t	-	4.791×10^{-5}	$3\ 399 \times 10^{-5}$	6.347×10^{-6}
	β_{tg}	-	1.548×10^{-4}	1.580×10^{-4}	8.346×10^{-5}
30	HAARM-3 case				
	$\beta_{g'}$	3.623×10^{-5}	1.267×10^{-4}	2.172×10^{-4}	2.173×10^{-4}
	$\beta_{t'}$	2.596×10^{-8}	2.699×10^{-7}	8.140×10^{-7}	1.215×10^{-6}
	β_{tg}	3.625×10^{-5}	1.270×10^{-4}	2.181×10^{-4}	2.186×10^{-4}
	Present work				
	β_g	4.766×10^{-4}	8.275×10^{-4}	8.758×10^{-4}	5.967×10^{-4}
	β_t	5.300×10^{-5}	8.492×10^{-4}	4.138×10^{-5}	1.970×10^{-4}
	β_{tg}	5.296×10^{-4}	9.124×10^{-4}	9.172×10^{-4}	6.164×10^{-4}

Where the subscript "t" denotes turbulent case (for this case, turbulent energy dissipation ratio e = 10 cm^2/sec^3) and the subscript "g" denotes gravitational case (e = 0 cm^2/sec^3).

Parameters for Figures 2-5:

Identification Number	Symbol	Particle-1 radius $a_1(\mu_m)$	Range a	e
TG20	β_{tg}	20	0.4-0.8	10
G20	β_g	20	0.2-0.8	0
T20	β_t	20	0.4-0.8	10
TG20HAARM-3	β_{tg}'	20	0.2-0.8	10
G20HAARM-3	β_g'	20	0.2-0.8	0
T20HAARM-3	β_t'	20	0.2-0.8	10
TG30	β_{tg}	30	0.2-0 8	10
G30	β_g'	30	0.2-0.8	0
T30	β_t	30	0.2-0.8	10
TG30HAARM-3	β_{tg}'	30	0.2-0.8	10
G30HAARM-3	β_g	30	0.2-0.8	0
T30HAARM-3	β_t'	30	0.2-0.8	10

Where "e" stands for turbulent energy dissipation ratio in cm^2/sec^3.

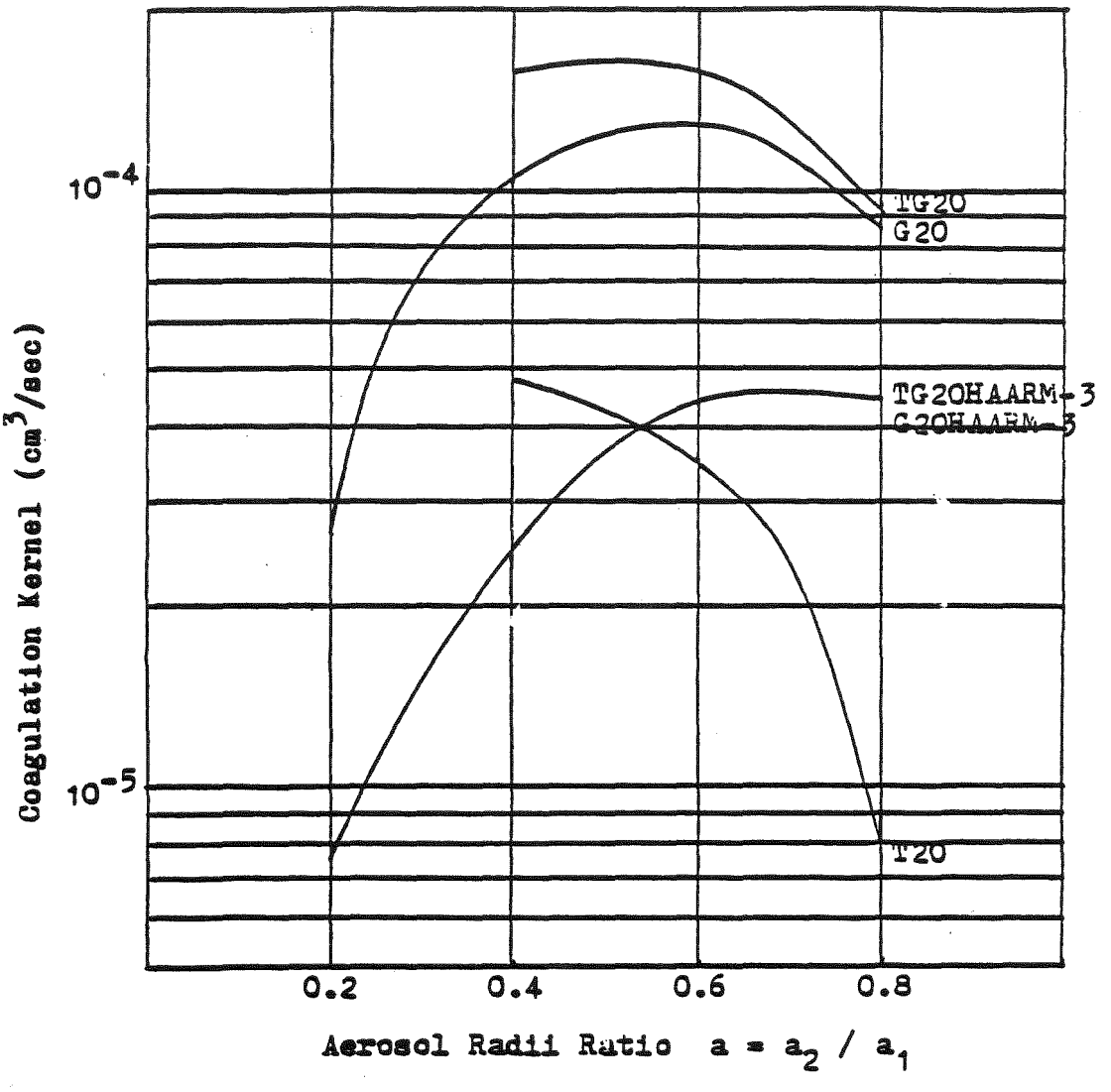

Figure 2 Coagulation Kernel (A)

Particle-1 Radius $a_1 = 20\mu m$

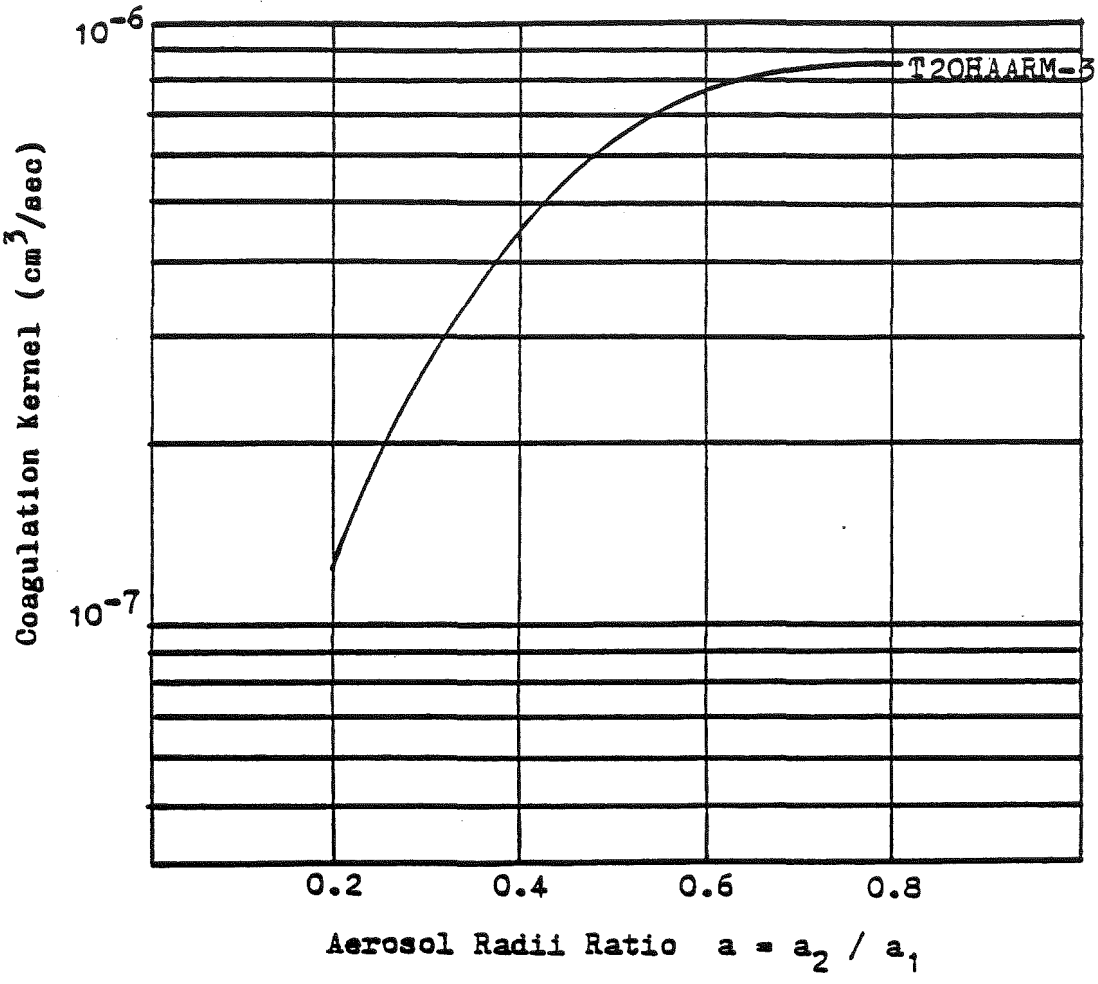

Figure 3 Coagulation Kernel (B)

Particle-1 Radius $a_1 = 20\mu$ m

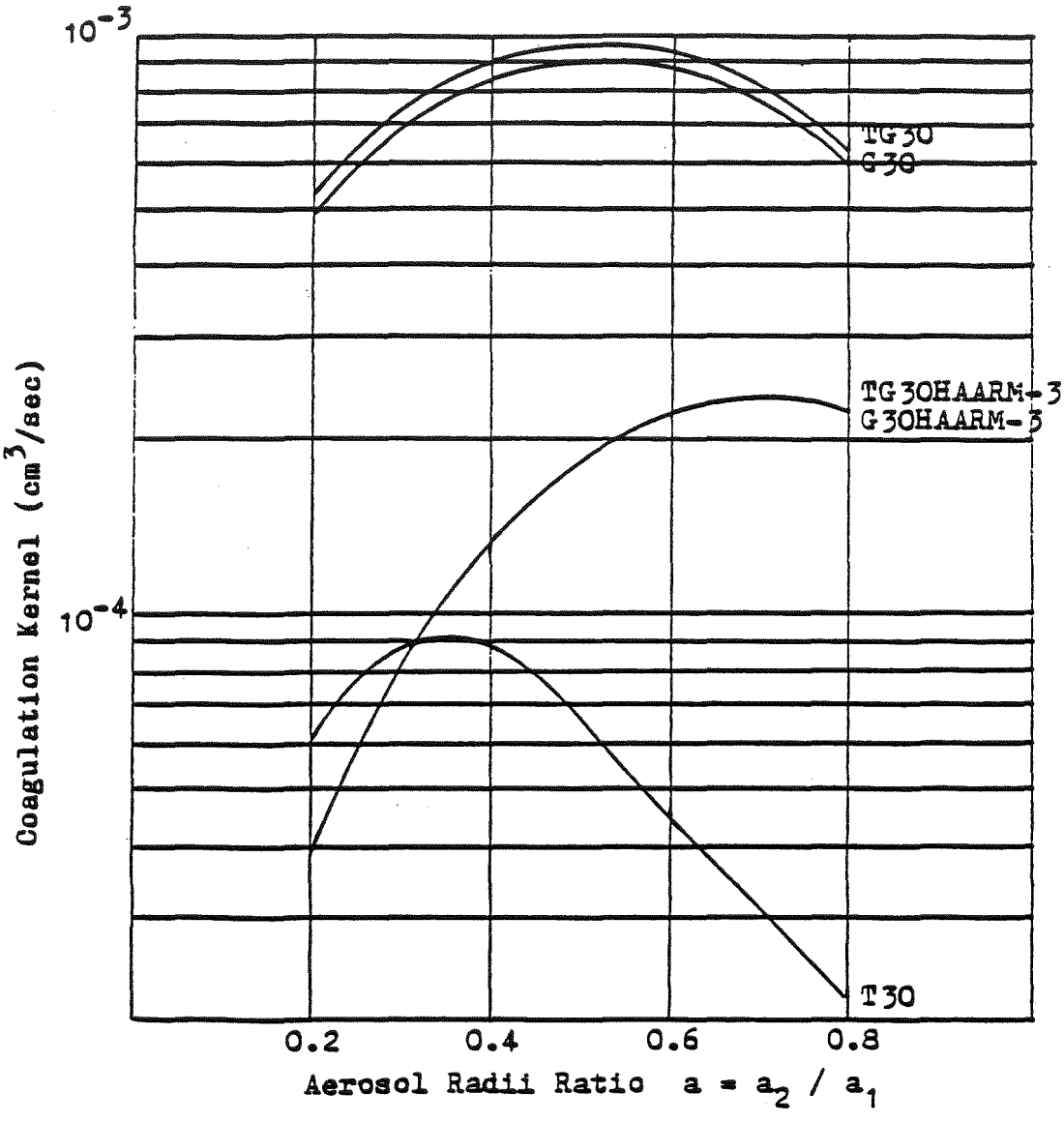

Figure 4 Coagulation Kernel (A)

Particle-1 Radius a_1 = 30 μm

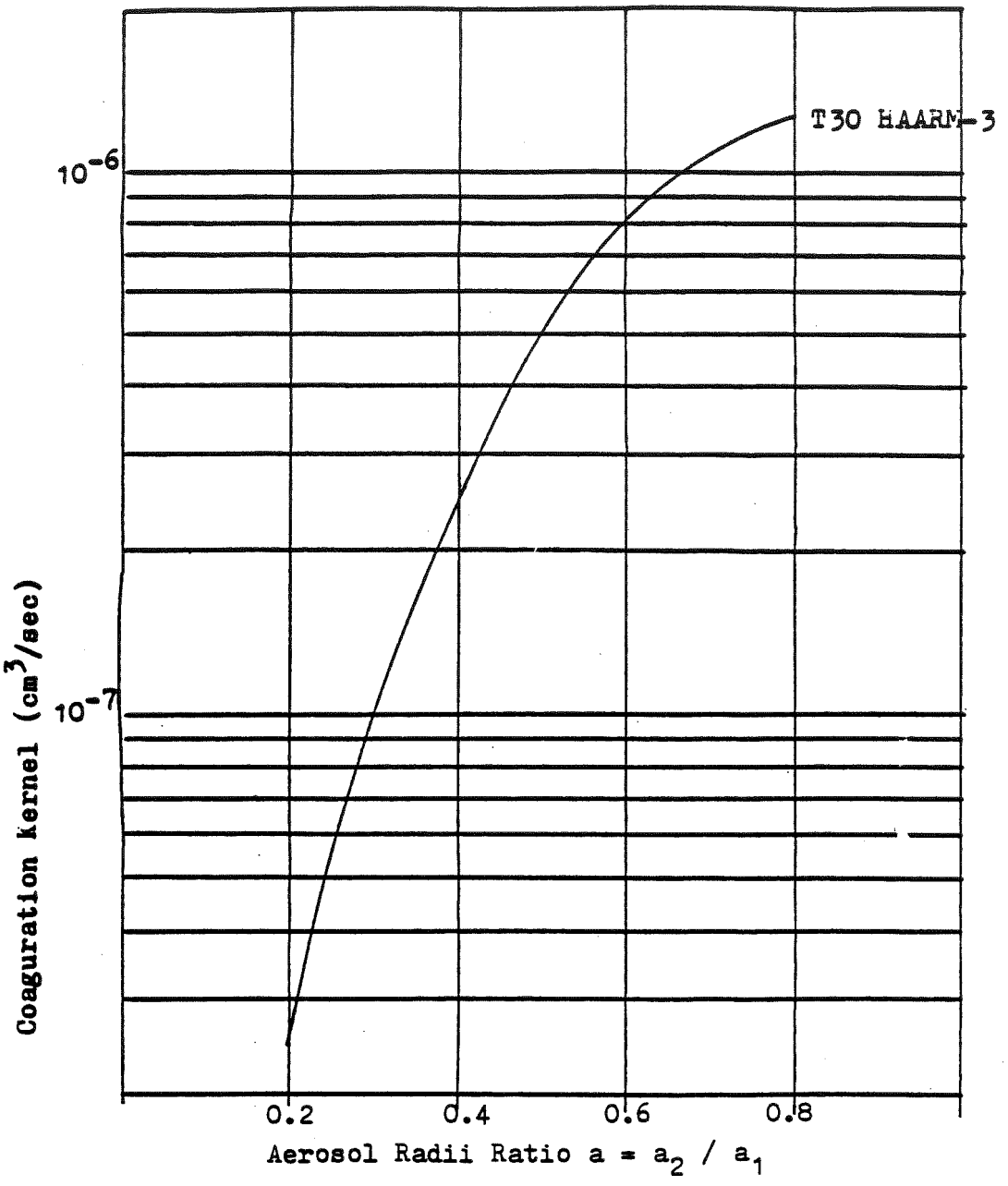

Figure 5 Coagulation Kernel (B)

Particle-1 Radius a_1 = 30 μm

REFERENCES

1. S. K. Loyalka, "Mechanics of Aerosols in Nuclear Reactor Safety: A Review", Progress in Nuclear Energy, 12, 1-56(1983).
2. G. A. Pertmer and S. K. Loyalka, Nuclear Technology, 47, 70(1980).
3. R. F. Tuttle and S. K. Loyalka, Nuclear Technology. (Papers I, II, III, submitted 1984).

MODELING OF MULTIPLE COMPONENT AEROSOLS -- SENSITIVITIES TO ASSUMPTIONS

H. Jordan, P. M. Schumacher, and V. Kogan

BATTELLE
Columbus Laboratories
505 King Avenue
Columbus, Ohio 43201

To be Presented at

THE CSNI SPECIALIST MEETING ON NUCLEAR AEROSOLS IN REACTOR SAFETY

September 4-6, 1984
Karlsruhe, Federal Republic of Germany

MODELING OF MULTIPLE COMPONENT AEROSOLS -- SENSITIVITIES TO ASSUMPTIONS

H. Jordan, P. M. Schumacher, and V. Kogan

BATTELLE
Columbus Laboratories
505 King Avenue
Columbus, Ohio 43201

ABSTRACT

Past experience in modeling single component aerosol behavior has revealed the fortuitous circumstance that excellent agreement between experiment and theoretical prediction can be achieved using size independent shape factors and a simple approximation (Fuchs) to the gravitational collision efficiency. In addition, for high concentrations, knowledge of the source particle size proved uncritical.

In this paper we examine the behavior of a two component (U_3O_8 and NaO_x) aerosol system with the aid of the MSPEC model that accounts for the dynamic evolution of particle composition as a function of size. We show that source particle size and shape factor size dependence play a significant role in this case. In addition, choice of a proper collision efficiency model is important. The predictions of the MSPEC model do not agree with those of a single component model that assumes instantaneous mixing of components across the full size spectrum.

INTRODUCTION

With the realization that high concentration aerosols are not stable --the dispersed phase coagulates and consequently settles, attempts at modeling aerosol behavior in reactor containments for severe accident conditions were initiated at several research institutions more than 15 years ago. Natural decay of the airborne activity in containment by aerosol mechanical means could be expected to dramatically reduce the radioactive source term to the environment resulting from leaks or breaches in that containment.

Until recently, all the computer codes that had evolved from these efforts at aerosol behavior modeling considered only single component aerosols. That is, particles of the aerosol were assumed of uniform chemical composition. For such a model, one must assume either internal mixing of the source particles or, if several sources of distinct components are considered, intimate, instantaneous mixing of a source component with the existing components of the dispersed phase, again leading to an apparently internally mixed aerosol. By contrast, the term "external mixing" implies the possible existence of particles of differing composition. The computer code MSPEC[1] was developed some time ago at BCL to model such a system. At about the same time, an equivalent code, MAEROS[2], was developed at Sandia.

It seems intuitive, nevertheless, that multiple component high concentration aerosols should coagglomerate quickly and that therefore a single component model should be adequate for their description. This may well be true for a large class of systems. There are, however, aerosol systems for which this intuition breaks down, largely because the agglomeration process mixes components only in one direction, that of increasing particle size. Multiple component models therefore appear necessary for accurate assessments of particle behavior under some conditions.

In some sense, the modeling success for single component aerosols has been remarkable. Excellent agreement between observed and predicted aerosol mass concentrations can be achieved despite the use of spherical particle models to describe the dynamics of aerosol particles with often very complex morphology. For the large aerosol particles that derive from the high agglomeration rates of high concentration aerosols, gravitational agglomeration is known to be important. Even here, a simple collision model (Fuchs) based on inertialess, spherical particles has proven sufficient. For systems with moderate particle concentrations as are often predicted for LWR containments under accident conditions, models which impose log normality on the particle size distribution for all times are successful. Finally, shape factors, which might be expected to be (multi-valued) functions of particle size perform well when taken as constants.

We suspect that much of this success is attributable to the inherent stability of the agglomeration equations. This stability results from the integral, in those equations, over the particle size distribution. Thus, the rate of change of particle mass in any size class is dependent not on the details of the size distribution as a whole, but only on its average properties. Predicting the rate of growth of just the mode of the particle size distribution is probably sufficient to predict aerosol mass concentration behavior.

There are some hints that in fact the tails of the particle size distribution may not be well modeled. Thus the long term (relative to cessation of the source) concentrations of sodium fire aerosols are consistently overpredicted by MSPEC relative to measured values. The long term population of aerosols derives, however, from the small particle tail of the early particle size distribution, not its mode. Then, the geometric standard deviation of the measured size distribution of sodium fire aerosols for long times is consistently much larger than the predicted value, again suggesting that the tails of the particle size distribution may not be well modeled, despite correct predictions of the aerosol mass concentration or third moment of the distribution.

If a multiple component aerosol does not immediately homogenize then the composition of the aerosol in effect traces details of the particle size distribution and one might indeed see a reflection of the adequacy of the particle behavior model in the concentration behavior with time of the individual components. In this paper we illustrate by calculational examples that this indeed appears to be the case. We find that predictions with MSPEC for a two component aerosol show sensitivities to parameters and models to which a single component aerosol behavior prediction is quite insensitive. Specifically, for the multiple component system, source particle size is important. Shape factors, which for a single component aerosol could be taken as constants, now may need to be size dependent. While a single component aerosol behavior prediction shows little sensitivity to whether the simple (Fuchs)[3] or a more mechanistic (Loyalka)[4] collision efficiency model is used, this is not the case for multiple component aerosols.

BRIEF DESCRIPTION OF THE MSPEC CODE

The MSPEC model for multiple component aerosols was evolved from the QUICK[5] model for a single component aerosol. In that model, the classical continuum particle size distribution approach is abandoned in favor of a direct analysis of the dynamics of the particle size histogram. Rate coefficients for particle removal at containment surfaces (assumed first order) and for particle-particle interactions (assumed second order) are taken from the continuum theory by ascribing a characteristic particle size to each size interval of the histogram and evaluating the coefficients of the continuum theory for this characteristic size. It is found in practice that model predictions of aerosol behavior are insensitive to choice of the characteristic size anywhere in the relevant size interval of the histogram provided at least some 20 size intervals are used to define it.

For a single component aerosol the dynamic equations therefore have the form:

$$\frac{dN_i}{dt} = \sum_k \sum_l K_{ikl} N_k N_l - R_i N_i - S_i \qquad (1)$$

where

N_i = Number of particles in interval i

R_i = Removal coefficient for interval i

K_{ikl} = Collision coefficient for collisions of particles in interval k and interval l leading to particles in interval i

S_i = Source rate for particles in interval i.

K_{ikl} is defined as the product of the continuum collision frequency coefficient evaluated at the characteristic sizes for intervals i and j and a distribution factor that assures conservation of particle mass and number. For logarithmic spacing of the size intervals, this factor is unique.

For a multiple component aerosol an analogous dynamic equation can be derived by considering the transfer of volume by component (rather than number) in a collision. Then, if X_{im} is defined as the volume fraction of component m in size interval i, $v_i X_{im} N_i$ is the total volume of component m in interval i and, with $N_{im} \equiv X_{im} N_i$,

$$\frac{d}{dt} N_{im} = \sum_{kl} K_{ikl} N_l N_k Z_{klm} - R_i N_{im} - S_{im}. \qquad (2)$$

Where v_i is the characteristic volume of interval i and

$$Z_{klm} \equiv \frac{X_{km} v_k + X_{lm} v_l}{v_l + v_m} \qquad (3)$$

is the volume fraction of component m in the collision product of particles from intervals k and l. Implicit and fundamental in this formulation is the assumption that particles of a given interval of the size histogram can be characterized by their average composition. This can strictly only be true if the dynamics of a particle are independent of its composition. To test the adequacy of this assumption by calculation would require a third index on N in Equation (2) and would probably be outside the bounds of present computer capabilities. Experimental verification is therefore necessary. Unfortunately, no unequivocal experimental results are available at present.

RESULTS CALCULATIONS WITH MSPEC ON TWO COMPONENT SYSTEMS

Gravitational agglomeration is known to play an important role in the growth of particles in dense aerosol systems. A full treatment of this process requires a description of the fluid dynamic interaction of two particles of arbitrary size and in arbitrary relationship to one another while under the influence of gravity. Numerous attempts at such an analysis have been made, the most recent and perhaps complete being that of Pertmer, et al[6]. This treatment is necessarily restricted to spherical particles, but accounts for particle inertia. It requires an iterative numerical solution that yields tabulated data for incorporation in aerosol behavior codes.

A simpler approach is to consider only collisions of inertialess particles that are very unequal in size. In this case the widely used Fuchs[7] expression for the collision efficiency results:

$$\varepsilon = \frac{3}{2}\left(\frac{r}{r+R}\right)^2 \qquad (4)$$

where r is the radius of the smaller particle and R is that of the larger. is the ratio of the actual collision cross-section to the geometric cross-section, $(r + R)^2$. Excellent agreement between predicted and measured aerosol behavior has been consistently achievable when using this expression on single component aerosol systems. A comparison of the Pertmer/Loyalka model (identified as GEPS) for particles of density 2.27 g/cm^3 with the Fuchs model is shown in Figure 1. Note the log scales on the ordinate and the R axis. Clearly the two models give widely differing results. In view of this difference, it is striking that the simple Fuchs model should prove adequate for the description of single component aerosol behavior. Even more striking was our discovery that application of GEPS in MSPEC for such systems gives results that differ little from those using the Fuchs model. An example of such a comparison is shown in Figure 2. This figure depicts the predicted behavior of a sodium oxide aerosol generated in a full sized containment by a sodium fire that consumes all available oxygen in one hour --surely an extreme case and one that should accent gravitational agglomeration. Both the mass concentration and the mass mean aerodynamic diameter are shown, with results using the Fuchs model drawn out in solid lines, those using GEPS for three different particle densities indicated by discrete points as deciphered in the key.

An explanation for this apparent insensitivity to widely differing values of the collision efficiency, ε, may lie in the fact that ε enters the dynamics equations only as an average over the size distribution. Figure 1 clearly shows regions where GEPS < Fuchs as well as regions where GEPS > Fuchs. On the average, both models may yield similar values. If this is so, then a multiple component system, for which composition tags individual sections of the distribution, may be expected to resolve differences between the two models.

To test this hypothesis, we reexamined data from a series of two component experiments[8] performed at ORNL some years ago. We chose NSPP-306 as most representative of likely accident conditions. For this experiment, aerosol source quantities, as determined from post test surface washes, do not yield believable results and values approximately one-half the measured values were used. We believe this procedure to be justified on the strength of past experience in comparison calculations for single component aerosol experiments for which the source terms were well defined. Thus, we assumed that 1650 kg of NaO_X were generated over a period of 0-25.3 minutes and that 151 g of U_3O_8 were generated between 43.9 and 56.9 minutes into the experiment.

The necessary shape factors[9] were taken from previous code fits to experimental data on the behavior of the individual components by themselves. U_3O_8 [χ = 3, γ = 15], NaO_X [χ = 1.3, γ = 2.5]. Agglomerates, which generally consist of both components, require a shape factor model that accounts for composition. No empirical data exist to determine such a model and indeed,

previous sensitivity studies by us have shown order-of-magnitude sensitivity of predicted aerosol mass concentrations on the choice of such a model. For the present calculations, we chose the following:

$$\chi = \Sigma_m \chi^3_m X_m$$
$$\gamma = \Sigma_m \gamma^3_m X_m \qquad (5)$$

This model makes some sense for the collision shape factor if one interprets that factor as the ratio between a geometric and volume equivalent diameter. Then Equation (5) is a statement of volume additivity, at least in the case of γ. More realistically, Equation (5) should be taken as an arbitrary example for the sake of illustration. Clearly, many other possibilities exist.

Figure 3 shows a comparison of MSPEC predicted aerosol mass concentrations with measured values. The solid lines depict predicted U_3O_8 and NaO_x concentrations using the Fuchs collision efficiency, the dashed lines those using GEPS (ρ = 2.27 g/cm^3) = the Loyalka efficiency. The result confirms our suspicions. A multiple component system does resolve the differences between the two models. Note that the NaO_x component is predicted to be higher by about a factor of 4 for the Loyalka model during the component interaction period. Note also that the Loyalka and Fuchs models predict virtually identical U_3O_8 behavior. This confirms previous single component aerosol behavior observations since U_3O_8 represents the bulk of the mass and therefore essentially traces the total mass of the aerosol. Figure 3 also exhibits predictions of mass concentration for the MSPEC code run in a single component mode. These curves are marked with an (s), while all curves derived from calculations using the multiple component mode are marked with an (m). The (s) mode assumes instantaneous homogenization across the total size histogram and can thus account for dilution but not dynamic effects on particle composition. Only results for the Fuchs collision efficiency model are shown. Those for the Loyalka model closely match these.

It is apparent that none of the predictions trace the total measured aerosol picture very well. Clearly, the single component model does not even reproduce the most obvious qualitative feature of the data: the split in mass concentration of the two species and must therefore be judged inadequate. The large quantitative difference between the (s) and (m) mode predictions forcibly illustrates the strong influence of the detailed treatment of compositional dynamics of the MSPEC model. While the long term measured behavior of the NaO_x component concentration is poorly reproduced, the remainder of the picture is predicted quite well, particularly with the Loyalka efficiency model.

Figure 4 illustrates the same conclusions for a system in which the roles of the two components are reversed. For this NSPP-305 case, 165.3 g of U_3O_8 aerosol were introduced first for a period of 5.75 minutes, followed by 1281 g of NaO_x aerosol from 6.7 to 23.7 minutes. Again the Loyalka model gives the best fit of the behavior of the initially introduced component. The single

species approximation now looks better but note it once again overpredicts the initially introduced component at early times, a characteristic of this approach.

The poor fit of experimental data exhibited in Figure 3 for NSPP-306 prompted trial calculations with change in source particle size and with shape factors that depend on particle size. Again, it is known from single component aerosol behavior calculations that relatively large changes in source particle size produce little change in mass concentration for these systems, provided significant agglomeration occurs, i.e., the concentrations are high. Also, shape factor models based on Kops'[10] observations (linear dependence of χ on volume equivalent particle diameter of iron oxide agglomerates up to some truncation size above which χ is a constant) do not, in our experience, produce a better fit of experimental data than shape factors that are assumed independent of particle size.

Figure 5 shows the effect of introducing a particle size dependent model for the shape factors of the pure components. The earlier shape factor mixing model is retained. The values of both χ and γ are assumed to vary linearly with volume equivalent diameter from a value of 1 for a primary particle to the previously used constant values when the primary particle count for the given component of the agglomerate reaches 5000, in agreement with Kops observations. Beyond this region, both χ and γ are assumed constant at their previous values. Two observations can be made. One, before the introduction of U_3O_8 aerosol, the fit of the NaO_x concentration data is now slightly worse and two, the fit of the NaO_x data after this point in time is slightly better. The fit of the dominant mass component (U_3O_8) remains essentially unchanged, as expected from our single component aerosol behavior experience. Overall, however, there is little to choose between the two shape factor models.

Again, from single component aerosol modeling experience, it is known that changes in source particle size for the NaO_x component of the NSPP-306 system will have little effect on predictions. The increase of source particle size for the U_3O_8 component may however influence the results. A reduction in the interaction rate between the two components and therefore a reduction in the growth and removal rate of the sodium fraction might be expected. To test this hypothesis, calculations were performed again with variable χ and γ but with the source geometric mean particle diameter raised from the 0.02 μm of the previous figures to 0.08 μm. The results, using the Fuchs collision efficiency model, are shown in Figure 6 and those for the Loyalka efficiency model are shown in Figure 7. In both figures the solid lines retrace the earlier results for 0.02 μm diameter source particles of the U_3O_8 component for comparison. There is not much to choose between the Fuchs and Loyalka models in this case, probably because with increase of source particle size, the population density of U_3O_8 has been reduced to the degree that interactions play a lesser role. However, it is clear that much better agreement is now achieved between the theoretically predicted NaO_x concentration and the measured data. In fact, the overall agreement between prediction and experiment, especially in Figure 6, is quite good, except for one datum, the NaO_x concentration at approximately 3000 minutes.

Finally, Figure 8 exhibits the performance of a single component mode calculation as a function of U_3O_8 source particle size variation. The

difference here is not pronounced and the fit of the data remains poor for this model.

SUMMARY AND CONCLUSIONS

The MSPEC code, a multiple component aerosol behavior model that considers the dynamic evolution of particle composition as a function of size, was applied to a system of U_3O_8 and NaO_x aerosol particles that was investigated experimentally in the ORNL NSPP-300 series. The initial calculation used the Fuchs collision efficiency model as well as source particle sizes and shape factors that had been determined to work well for each component aerosol in comparisons of code predictions with single component experiments. An intuitive shape factor mixing model was use to account for shape factor dependence on composition. The results of this calculation showed order of magnitude disagreement between the predicted and measured mass concentrations of the secondarily introduced component.

Much better agreement between experiment and theory was achieved by (1) increasing the source particle size of the U_3O_8 component, (2) allowing the shape factors of both components to vary with particle size, and (3) invoking a more mechanistic collision efficiency model than that of Fuchs.

These calculations are illustrative of sensitivities to parameter values and models that are absent in single component models and indeed single component aerosol systems. In particular:

(1) The behavior of at least one component is strongly dependent on the assumed (measured) source particle size of at least one component (not necessarily the same one).

(2) The use of shape factors that depend on particle size leads to results that are significantly different from those for constant shape factors.

(3) Significantly different mass concentrations are predicted for at least one component when a mechanistic collision efficiency model is substituted for the commonly used Fuchs approximation.

(4) Predictions of a multiple component model such as MPSEC and those of a single component model that accounts for multiple components by instantaneous mixing of composition across the particle size distribution, do not agree.

Clearly these observations present new challenges to the experimenter.

REFERENCES

1. Jordan, H., et al, "MSPEC User's Manual", NUREG/CR-2923, BMI-2100 (1982).

2. Gelbard, F., "MAEROS User's Manual", NUREG/CR-1391, SAND80-0822 (1982).

3. Fuchs, N. A., "The Mechanics of Aerosols", Pergamon Press (1964).

4. Pertmer, G. A. and Loyalka, S. K., "Gravitational Collision Efficiency of Post Hypothetical Core Disruptive Accident Liquid-Metal Fast Breeder Reactor Aerosols: Spherical Particles", Nuclear Technology, 47, 70 (1980).

5. Jordan, H., et al, "QUICK User's Manual", NUREG/CR-2105, BMI-2082 (1981).

6. Op cit.

7. Op cit.

8. Adams, R. E., et al, "Uranium Oxide and Sodium Oxide Aerosol Experiments: NSPP Mixed Oxide Tests 303-307, Data Record Report", NUREG/CR-2697, ORNL/TM 8325 (1982).

9. Jordan, H., et al, "Nukleare Aerosole im Geschlossenen System", KFK 1989 (1974).

10. J.A.M.M. Kops, et al, "The Aerodynamic Diameter of Branched Chain-Like Aggregates", RCN-74-064 (1974).

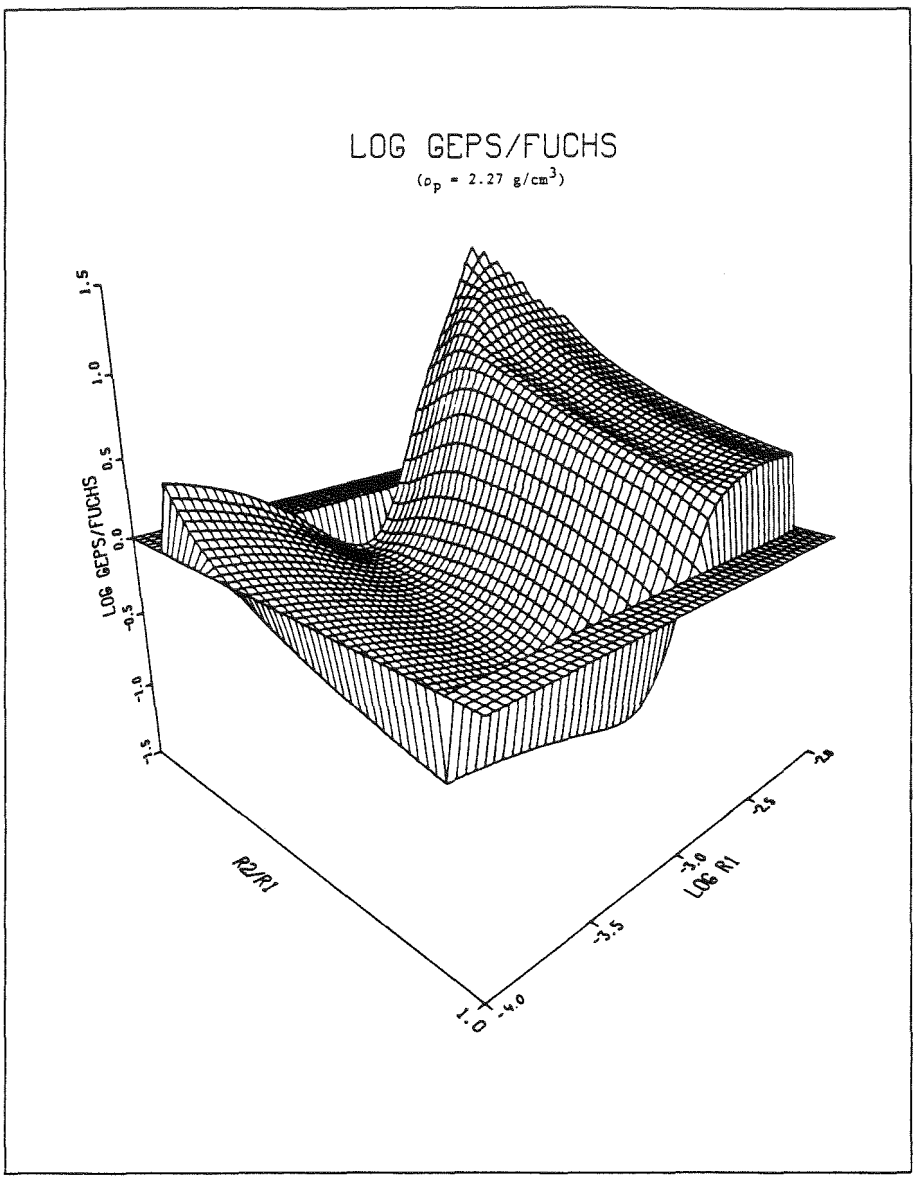

Figure 1. Comparison of Loyalka (GEPS) and Fuchs Gravitational Collision Efficiency Models.

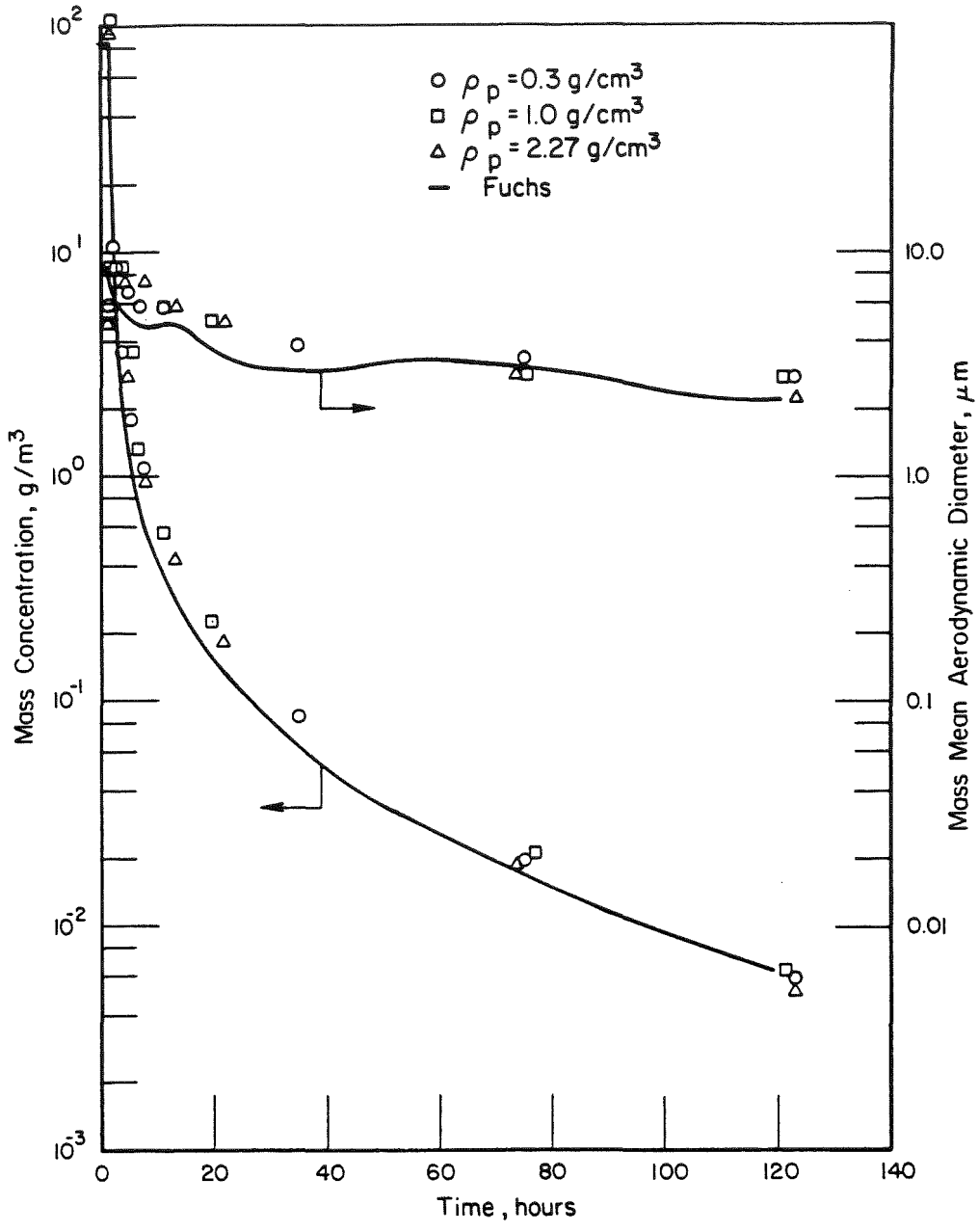

Figure 2. Prediction of Aerosol Behavior for a Severe, One-Hour Sodium Fire in Containment. Comparison of Loyalka and Fuchs Collision Efficiency Models.

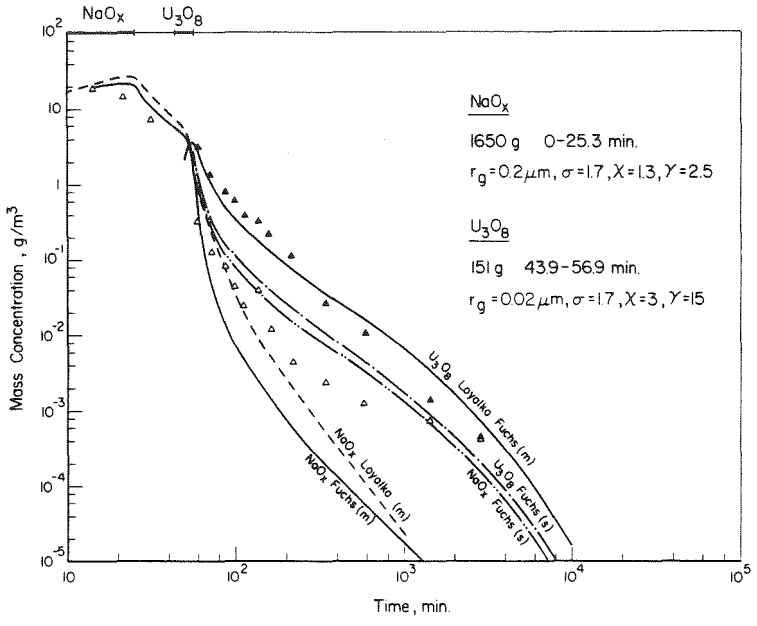

Figure 3. NSPP-306: Comparison of Calculated with Measured Mass Concentrations. The Influence of the Gravitational Collision Models Fuchs/Loyalka.

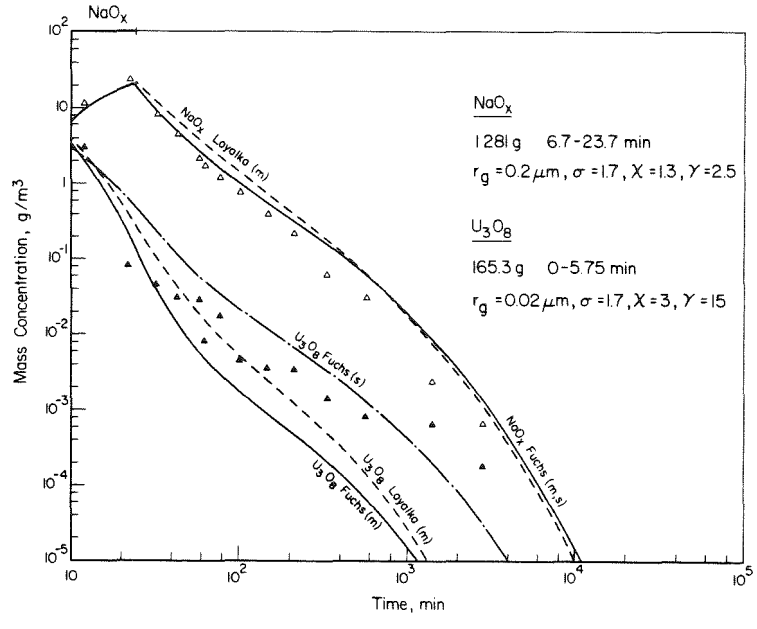

Figure 4. NSPP-305: Comparison of Calculated with Measured Mass Concentrations. The Influence of the Gravitational Collision Models Fuchs/Loyalka.

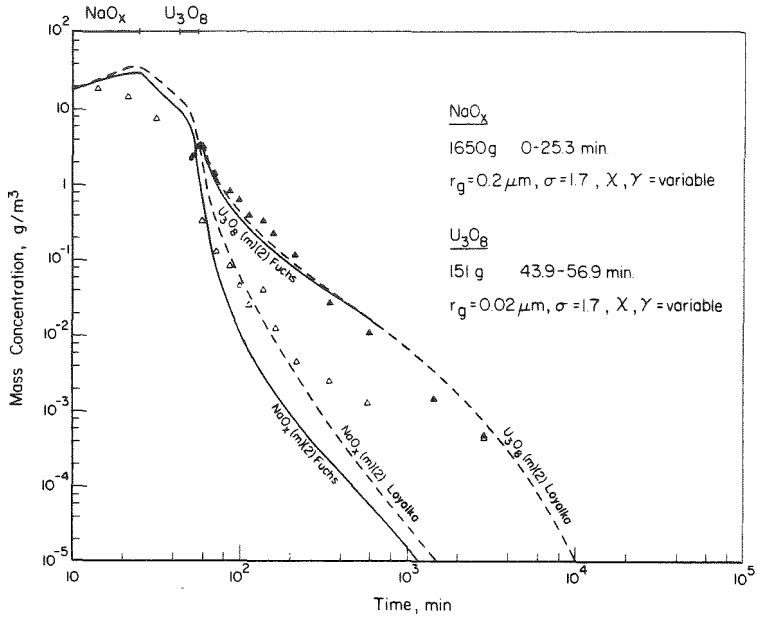

Figure 5. NSPP-305: Comparison of Calculated with Measured Mass Concentrations. The Effect of Size Dependent Shape Factors.

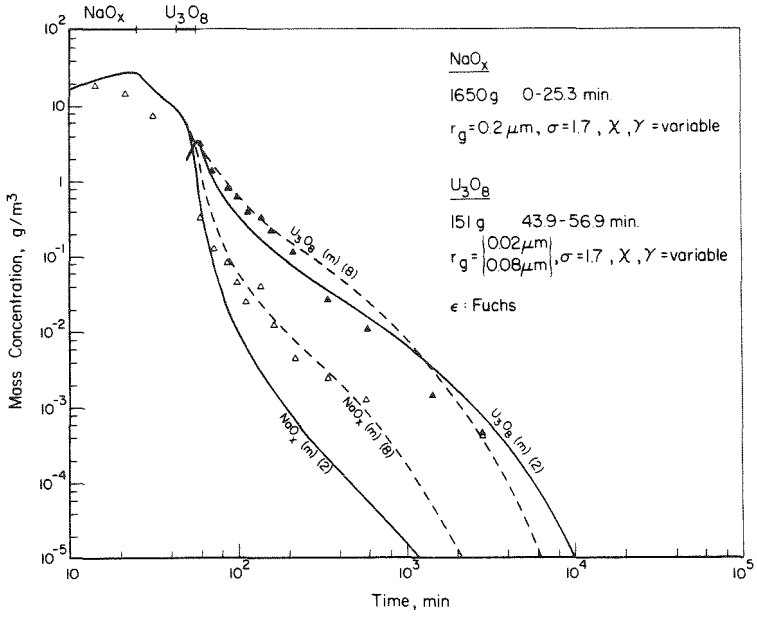

Figure 6. NSPP-306: Comparison of Calculated with Measured Mass Concentrations. The Effect of Source Particle Size. Fuchs Collision Efficiency Model.

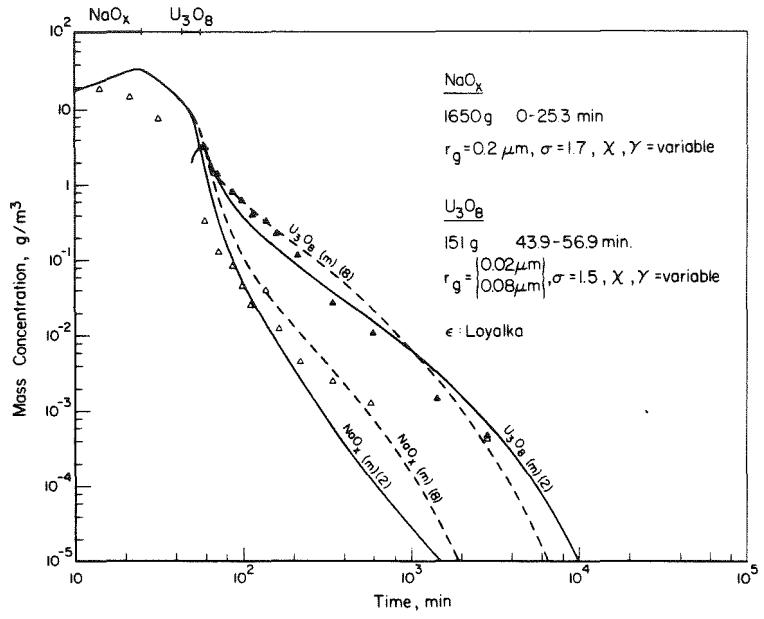

Figure 7. NSPP-306: Comparison of Calculated with Measured Mass Concentrations. The Effect of Source Particle Size. Loyalka Collision Efficiency Model.

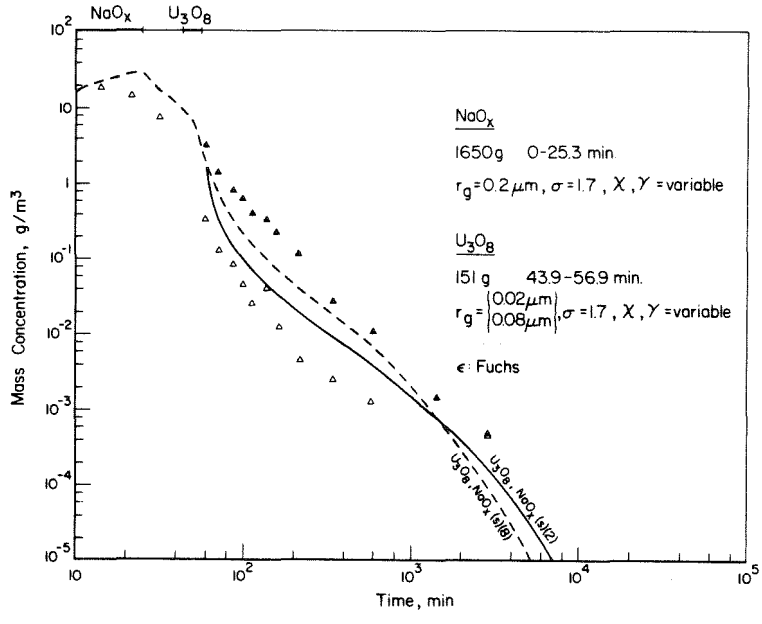

Figure 8. NSPP-306: Comparison of Calculated with Measured Mass Concentrations. The Effect of Source Particle Size on Single Component Code Predictions.

COAGULATION AND DEPOSITION OF TWO-COMPONENT AEROSOLS

J.D.R. Stock* S. Simons and M.M.R. Williams

Queen Mary College, University of London

Mile End Road, London, U.K.

ABSTRACT

It is normally assumed in calculations of the coagulation and deposition of a radioactive aerosol that the total airborne radioactivity at any time is proportional to the total airborne particulate mass. This, however, will not in general be true. In an LMFBR accident, the radioactive particles may initially be smaller than the non-radioactive particles by more than an order of magnitude. It follows that the airborne radioactivity will be underestimated at later times if it is assumed to be proportional to airborne mass. On the other hand, in a PWR accident the situation is the reverse, so that the above assumption would then yield an overestimate for the airborne radioactivity.

In order to deal with these difficulties, we have formulated the equation which governs the function P(m), where P(m)dm is the total airborne radioactivity per unit volume in particles with masses lying between m and m + dm. The formulation is exact if the coagulation kernel and deposition rate depend only on the total mass of the particles involved, being independent of their detailed composition. The equation for P can be discretised in such a form that in the absence of source and removal terms, radioactivity is exactly conserved in analogy with the mass-conserving discretisation of the equation for N. The resulting set of equations for both P and N has been solved numerically by the code AERORAD based upon the earlier code AEROSIM which calculates N alone. Preliminary results indicate that significant deviations can occur from the results obtained assuming airborne radioactivity to be proportional to airborne mass.

* Supported by Extra-Mural Research Contract No 4R 544 90B with the Safety and Reliability Directorate of the UKAEA.

INTRODUCTION

Prediction of the evolution of a radioactive aerosol through the processes of coagulation and deposition is an important aspect of research into the safety of nuclear reactors. Calculations have generally assumed that the total airborne radioactivity at any time is proportional to the total airborne particulate mass. This, however, is true only if the radioactivity per particle is initially proportional to the particle mass, and if the same relation holds in the case of any source term. Under general accident conditions, this will not be so, and a more accurate estimate of the quantity of radioactivity airborne is therefore warranted.

QUALITATIVE DISCUSSION

In a typical LMFBR accident, the mean particle size of the sodium oxide aerosol produced from the coolant may be much larger than that of the radioactive fuel aerosol. Consider the development of this combined aerosol, where for simplicity we first neglect coagulation. Since the dominant deposition mechanism is gravitational sedimentation which deposits the larger particles faster than the smaller ones, the non-radioactive particles will be preferentially removed. This means that the total airborne mass will decrease relatively more rapidly than the total airborne radioactivity. Thus, in this instance, airborne radioactivity will be underestimated if it is assumed to be proportional to airborne mass.

In a hypothetical severe PWR accident there may also be two distinct types of aerosol: that produced by the melting core inside the reactor pressure vessel, and that produced later by the core-concrete interaction. The former, carrying the bulk of the volatile fission products, will have had time to grow by agglomeration when the latter is produced.

Of course in practice, this picture is complicated by the process of coagulation, which will tend to mix the radioactive and non-radioactive materials together by forming composite particles. In the case of the sodium oxide/fuel aerosol for example, Brownian coagulation may deposit the small radioactive particles onto the larger neutral particles. This will give rise to a radioactivity per composite particle proportional to the particle radius (Twomey, 1977), resulting in the smaller particles having a greater radioactivity per unit mass than the larger ones. The previous qualitative argument for a discrepancy between proportional losses of radioactivity and mass is therefore essentially unchanged by this Brownian coagulation.

By considering a two-component rather than a one-component aerosol, it is possible to develop a more accurate formulation of the problem that follows the total airborne radioactivity in addition to the airborne mass, and thus to quantify the above statements.

THE MASS AND RADIOACTIVITY DISTRIBUTIONS

The relevant mathematics for the case of a two-component aerosol has been given by Simons (1981). Let n(m,s,t) be the number of particles at time t with masses in the range m to m + dm and radioactivities in the range s to s + ds per unit volume of space. Then the equation governing n takes the form

$$\frac{\partial n(m,s,t)}{\partial t} = \frac{1}{2}\int_0^m \int_0^s \phi(\ell, m-\ell)\, n(\ell,r,t)\, n(m-\ell, s-r, t)\, d\ell\, dr$$

$$- n(m,s,t) \int_0^\infty \int_0^\infty \phi(\ell,m)\, n(\ell,r,t)\, d\ell\, dr \; - R(m)\, n(m,s,t) + Q(m,s,t)\,, \qquad (1)$$

where $\phi(m,\ell)$ is the agglomeration kernel, R(m) is the removal rate and Q(m,s,t) is the source term. Taking the zeroth moment of (1) with respect to s, we recover the usual equation for the mass distribution of aerosol particles

$$\frac{\partial N(m,t)}{\partial t} = \frac{1}{2}\int_0^m \phi(\ell, m-\ell)\, N(\ell,t)\, N(m-\ell,t)\, d\ell$$

$$- N(m,t)\int_0^\infty \phi(\ell,m)\, N(\ell,t)\, d\ell - R(m)\, N(m,t) + S(m,t)\,, \quad (2)$$

where

$$N(m,t)\, dm = \int_0^\infty n(m,s,t)\, ds\, dm$$

is the total number of particles with masses in the range m to m + dm per unit volume of space, and

$$S(m,t) = \int_0^\infty Q(m,s,t)\, ds$$

is the source rate.

If we now take the first moment of equation (1) with respect to s, it may be shown that the result is

$$\frac{\partial P(m,t)}{\partial t} = \int_0^m \phi(\ell, m-\ell)\, N(m-\ell,t)\, P(\ell,t)\, d\ell$$

$$- P(m,t)\int_0^\infty \phi(\ell,m)\, N(\ell,t)\, d\ell - R(m)\, P(m,t) + S'(m,t), \quad (3)$$

where

$$P(m,t)\, dm = \int_0^\infty s\, n(m,s,t)\, ds\, dm$$

is the total radioactivity per unit volume of space contained in particles in the mass range m to m + dm, and the radioactivity source rate satisfies

$$S'(m,t) = \int_0^\infty s\, Q(m,s,t)\, ds$$

Given the solution of (2), N(m,t), equation (3) now determines the radioactivity distribution P(m,t). The total mass airborne per unit volume is given by

$$m(t) = \int_0^\infty m\, N(m,t)\, dm$$

while the total radioactivity airborne per unit volume is

$$J(t) = \int_0^\infty P(m,t)\, dm .$$

By splitting the mass axis into a set of intervals $[\alpha_i, \beta_i)$, $i = 0, 1, 2, \ldots$ with $\beta_i = \alpha_{i+1}$, equation (2) can be discretised to yield a set of simultaneous differential equations

$$\frac{dN_i}{dt} = \sum_{j=0}^{i} \sum_{k=0}^{j} \left(1 - \tfrac{1}{2}\delta_{jk}\right) \gamma_{ijk}\, \bar{\phi}_{jk}\, N_j N_k$$

$$- N_i \sum_{j=0}^{\infty} \bar{\phi}_{ij}\, N_j - R_i N_i + S_i \qquad (i = 0, 1, 2, \ldots), \qquad (4)$$

where the discretised quantities are defined by

$$m_i N_i = \int_{\alpha_i}^{\beta_i} m\, N(m)\, dm$$

$$m_i S_i = \int_{\alpha_i}^{\beta_i} m\, S(m)\, dm$$

$$h_i m_i R_i = \int_{\alpha_i}^{\beta_i} m\, R(m)\, dm$$

and

$$h_i h_j \bar{\phi}_{ij} = \int_{\alpha_i}^{\beta_i} \int_{\alpha_j}^{\beta_j} \phi(m,\ell)\, dm\, d\ell$$

with

$$h_i = \beta_i - \alpha_i \quad , \quad m_i = \tfrac{1}{2}(\alpha_i + \beta_i) .$$

Also,

$$\gamma_{ijk} = \frac{1}{m_i h_j h_k} \int_{\alpha_j}^{\beta_j} \int_{\alpha_k}^{\beta_k} (m+\ell)\, \theta_i(m+\ell)\, dm\, d\ell$$

where

$$\theta_i(x) = \begin{cases} 1 & \alpha_i \le x < \beta_i \\ 0 & \text{otherwise} \end{cases}$$

(Walker et al, 1978). It can be shown that in the case where the removal and source rates are zero, the equations (4) conserve mass exactly. This follows from the fact that the γ quantities satisfy the relation

$$\sum_{i=0}^{\infty} m_i \gamma_{ijk} = m_j + m_k$$

The discretisation of (3) can be carried out in a similar manner to that for equation (2). With the additional definitions

$$P_i = \int_{\alpha_i}^{\beta_i} P(m)\, dm$$

$$S_i' = \int_{\alpha_i}^{\beta_i} S'(m)\, dm$$

and

$$h_i \tilde{R}_i = \int_{\alpha_i}^{\beta_i} R(m)\, dm \ ,$$

the result is the set of equations

$$\frac{dP_i}{dt} = \sum_{j=0}^{i} \sum_{k=0}^{j} \left(1 - \tfrac{1}{2}\delta_{jk}\right) \gamma'_{ijk}\, \Phi_{jk} \left(N_j P_k + N_k P_j\right)$$

$$- P_i \sum_{j=0}^{\infty} \Phi_{ij} N_j - \tilde{R}_i P_i + S_i' \qquad (i = 0, 1, 2, \ldots) \ , \tag{5}$$

where the γ' quantities are defined by

$$\gamma'_{ijk} = \frac{1}{h_j h_k} \int_{\alpha_j}^{\beta_j} \int_{\alpha_k}^{\beta_k} \theta_i (m + \ell)\, dm\, d\ell \ .$$

It can be shown that in the absence of removal or source terms, radioactivity is conserved exactly, since the γ' satisfy the relation

$$\sum_{i=0}^{\infty} \gamma'_{ijk} = 1 \ .$$

In discrete form, the total mass and total radioactivity airborne per unit volume are $\sum m_i N_i$ and $\sum P_i$, respectively.

The program AEROSIM solves the equations (4) using the Gears method employed by the package FACSIMILE. A new code AERORAD, based upon AEROSIM, now solves the sets of equations (4) and (5) simultaneously, thereby enabling the mass and radioactivity distributions to be monitored separately.

It should be noted at this point that the validity of equations (1), (2) and (3) depends upon the assumption that the coagulation kernel ϕ and deposition rate R depend only on particle mass and not the detailed composition of the particle. Although a means of removing this assumption has been suggested by Simons (1982), it involves the coefficients Φ_{ij} and R_i becoming implicitly time-dependent, which is precluded by current methods of solution due to limitation of computing time.

Two cases are considered here for the initial aerosol:-

(a) Bimodal distribution: radioactive and non-radioactive materials both lognormally distributed but with different values of mean radius and standard deviation,

(b) Unimodal distribution: non-radioactive material lognormally distributed, with superimposed radioactivity proportional to an arbitrary power, β, of the particle radius.

A general approach to the sodium oxide/fuel problem will utilise case (a), while the assumption that radioactivity quickly becomes proportional to radius corresponds to case (b) with $\beta = 1$. An AERORAD run for the latter case with a representative set of parameters describing conditions in the reactor containment yielded a value for

$$\frac{J(t)/J(o)}{M(t)/M(o)}$$

of about 2, where J(t) and M(t) are respectively the airborne radioactivity and mass per unit volume after time t.

Another situation of interest is where an initial radioactive aerosol becomes mixed at later times with non-radioactive source material. Since the radioactivity is initially distributed uniformly throughout the particulate material, this can be modelled using case (b) with $\beta = 3$, together with a non-radioactive source term.

Work is currently in progress on both of the problems discussed here. It is intended to test the sensitivity of the results to various input parameters, particularly the thickness of the boundary layer for diffusional deposition, and also to run AERORAD with the number of mass bins, N, equal to 20, 40 and 60 in order to verify the convergence of the results with increasing N.

REFERENCES

1. Simons, S. (1981), Coagulation and deposition of radioactive aerosols, Ann. Nucl. Energy, 8, 287.

2. Simons, S. (1982), Condensation, coagulation and deposition of a multicomponent radioactive aerosol, Ann. Nucl. Energy, 9, 473.

3. Twomey, S. (1977), Atmospheric Aerosols, p.69, Elsevier, Amsterdam.

4. Walker, B.C., Kirby C.R. and Williams R.J. (1978), Discretisation and integration of the equation governing aerosol behaviour, SRD R98.

Session III: Interrelation of Thermal Hydraulics and Aerosol Behavior

Chair: P.N. Clough (SRD Culcheth, UK)
M.R. Kuhlman (BCL, USA)

REVIEW OF AREAS THAT MAY REQUIRE SIMULTANEOUS COUPLED SOLUTION OF THE THERMAL HYDRAULIC AND FISSION PRODUCT/AEROSOL BEHAVIOR EQUATIONS FOR SOURCE TERM DETERMINATION

T. S. Kress
Oak Ridge National Laboratory
Oak Ridge, Tennessee

ABSTRACT

In the determination of the behavior of nuclear aerosols in the reactor coolant system and in the containment for the development of severe accident source terms, present practice generally is to first perform thermal hydraulic calculations for specific plant types and sequences and then to utilize the results as input for separate fission product/aerosol dynamic transport calculations. It is recognized that there are several areas in which the thermal-hydraulics and the fission product/aerosol behavior may be significantly coupled and that it is then basically incorrect to do the analyses in a separated manner. This review paper produces a speculative list of these potentially coupled areas and attempts to assess the importance of the coupling for as many of the specific items that time has allowed before this conference.

INTRODUCTION

The determination of severe accident source terms must, by necessity it seems, rely on the use of complex computer codes that involve the solution of thermal-hydraulic models (generally heat transfer and fluid mechanics) to determine system temperatures, pressures, and flows and fission product/aerosol transport models to determine their movement and disposition. For example, the U.S. Nuclear Regulatory Commission has recently conducted a study (BMI-2104) with Battelle Columbus Laboratories using this type of procedure in reassessing the severe accident source terms for LWRs. In the BMI-2104 study, the MARCH-2.0 computer code was used to determine the core heat-up and melting behavior, the resultant steam and hydrogen production rates and core exit temperatures, the reactor coolant system (RCS) pressure, and the containment thermal hydraulic response including effects of ejection of steam from the RCS; core melt/concrete interaction to produce thermal and mass loading in the containment, combustible gas (H_2 and CO) burning, and natural convection and condensation heat transfer to surfaces.

The core fuel temperatures were input into CORSOR, a simple correlation model, to determine the release rates of fission products and aerosols into the core exit region.

The RCS pressure and the core exit steam and hydrogen flows and temperatures were input into MERGE which calculates flows, gas temperature, and surface temperature in several control volumes that represent the RCS. These, along with the fission product/aerosol release rates from CORSOR are input into TRAP-MELT which calculates the transport and deposition of the fission products and aerosols within the same control volume representation of the RCS. After MARCH calculates RCS vessel melt-through failure, the residual fission products not released into the RCS (along with other core materials) are assumed dropped into the reactor cavity. Here MARCH calculates additional steam/H_2 production from the debris thermal interactions with any water in the cavity.

Although MARCH also calculates the thermal and gas loadings in the containment due to the interactions of this debris (or melt) with the basemat concrete, a separate pair of codes, CORCON and VANESA, were used for the purpose of calculating fission product and aerosol release. CORCON calculates the thermal history of the melt, the concrete penetration, and the production of gases from concrete ablation and their subsequent chemical reactions with the melt. VANESA uses the output of CORCON for the thermal history of the melt and the gas production rate from the concrete to calculate the rate of release into containment of fission product vapors/aerosols, and their chemical composition. The containment thermal hydraulic response and steam sources calculated by MARCH, the fission product aerosols escaping the RCS into containment calculated by TRAP-MELT, and the fission product/aerosol sources from core-melt/concrete interactions calculated by VANESA are input into the NAUA code to calculate the transport and deposition of the aerosols within the containment volumes.

Because these codes were generally developed independently of each other and only "forward" coupling is accomplished, the above procedure leads to inconsistencies and to potentially incorrect results when there is significant two-way coupling between the thermal hydraulic and the material transport behavior. An integrated system that removes the inconsistences and provide simultaneous coupling is necessary to produce defendable source term estimates.

The above approach to source term development is illustrated schematically in Fig. 1 in terms of phenomenological areas rather than specific codes. The nature and direction of the present coupling is indicated by solid arrows whereas areas where simultaneous coupling is believed to be important are indicated by the dashed arrows.* The identification and nature of these areas suggested for coupling are discussed below.

SPECULATIVE LIST OF COUPLED ITEMS

The use of the term "coupled" in this paper implies that the mathematical model for the thermal hydraulics phenomena contains elements that include the fission product/aerosol transport phenomena and vice versa and that a simultaneous solution of these would result in a significant difference in either the thermal hydraulic behavior or the fission product/aerosol behavior compared to the separate solution with only input from the thermal hydraulics to the aerosol/FP transport. Items that should be coupled in this way have been pointed out by several people in different countries so the list below is not particularly original nor is it believed to be exhaustive. The order in which items are presented is more-or-less chronological as one would move from the core outward to the containment (so much as that is possible).

ITEMS AND NATURE OF COUPLING

(1) Fuel heat-up and melting — fission product release:

The release of fission products is driven by the fuel temperature and exposure time before slumping. As fission products escape from the fuel, they carry a portion of the decay energy, thus removing part of the internal heat for the fuel.

*It can be noted here that there appears to be only minor back coupling from the containment to the RCS up to the time of RCS failure so that separate sets of integrated systems are possible — one for the RCS and one for containment. The CONTAIN/MAEROS system at Sandia, for example, represents an integrated system for containment analyses that should be appropriate for the bottom part of Fig. 1.

(2) RCS thermal-hydraulics — nucleation/condensation of fission product vapors:

The rate of nucleation/condensation of fission product vapors into aerosols is determined by the rate of cooling of the carrier fluid as it passes through the RCS. However, on condensation the vapors give up their latent heat of vaporization to become a source of heat to affect the thermal hydraulics.

(3) RCS thermal hydraulics — released fission products as contributors to carrier fluid properties.

The RCS thermal hydraulics (flow rates, gas and surface temperature, heat transfer coefficients, etc.) influence the behavior of the aerosol/fission products. However, there may be sufficient quantities of fission products compared to the H_2/H_2O that they should be considered as part of the carrier fluid.

(4) RCS thermal hydraulics — released fission products as decay heat sources within the carrier stream.

The quantity of decay heat represented by the transported fission products could represent a significant internal heat source into the gas stream.

(5) RCS thermal hydraulics — deposited aerosols/fission products as decay heat sources on surfaces (revaporization).

(a) The deposited fission products/aerosols could provide a sufficiently strong local heat source to alter the system thermal hydraulics (surface temperatures) and perhaps revaporize volatiles.

(b) The relocation of the heat source distribution could alter the strength of natural circulation.

(6) Core/concrete thermal hydraulics — aerosol production:

The presence of a dense cloud of aerosols above the core/concrete interaction zone could shield thermal radiation thus increasing the melt temperature and enhancing aerosol production.

(7) Containment thermal hydraulics — water vapor condensation onto aerosols.

(a) The presence of aerosols in the containment provides a potential repository for water that could influence the containment thermal hydraulics with respect to the relative humidity.

(b) The presence of significant quantities of liquid water on aerosol particles could influence the severity of effects of hydrogen burns.

(8) Containment steam condensation — diffusiophoretic plate out of aerosols.

The deposition of aerosols on surfaces by diffusiophoresis could alter the steam condensation rates by their presence as local heat sources or as insulation.

(9) Containment natural convective mixing — aerosols.

The presence of aerosols as mass loadings and heat sources could alter the strength of natural circulation (affecting turbulence levels) and creating stratification of aerosols.

(10) Thermal hydraulic — fission product/aerosol removal in:

- Ice condenser
- Suppression pools
- Coolers
- Filter systems

SIGNIFICANCE OF VARIOUS COUPLED ELEMENTS EVALUATED TO DATE

We will now examine as many of the above items that there is time for before "press-time" to attempt to make some quantitative judgments as to their significance. The most direct approach for such evaluations would be to develop the coupled mathematical models, develop solutions, and compare results of calculations over appropriate ranges both with and without the coupling being operative. Unfortunately neither the time nor the resources were available for such a comprehensive approach. Some attempts were made along those lines with much simplified versions of coupled models that could be amendable to "hand" calculation. In general, however, no systematic approach was utilized.

Item (1): Core thermal hydraulics/fission produce release:

This is an area in which coupling appears fairly obvious and is, in fact, done to some extent in MARCH where the fission product inventory as a heat source in the fuel is altered as fuel melts by using the WASH-1400 release model. However since most of the "volatile" fission products can be released prior to fuel melting, this approach may or may not be adequate.

A very simplified approach is used for this assessment.

A calculation was made for a unit volume of fuel heating adiabatically (without heat losses to the steam or surroundings and without steam/Zr reaction energy). This could be viewed as a whole core heating up uniformly. On reaching a "melt" temperature of 2400°C, the temperature was held constant until full melting of the unit volume — at which time the calculation was discontinued. The calculation was made both

with and without fission product losses to give some insight as to the possible extent of influence. A CORSOR like release model was used. To produce the coupled solution, an iterative procedure was followed as outlined below:

Needed parameters for the calculation were assumed to have values as follows:

Operating reactor power = 2441 Mwt
Fuel melt temperature = 2400°C
Cp = 0.12 Btu/°F•lb
Ts (at time of start of calculation) = 1000°C
ΔH for melting = (0.12) (1029) Btu/lb
Total core fuel mass = 1.027×10^5 kg

Total decay heat power versus time after scram was determined from Ref. [2] to be:

Time (s)	0	1.5	10	30	110	1000	8547	1 day
Decay heat (percent of core operating power)	~7	6	5	4	3	2	1	~0.5

The relative contribution to the above decay power due to various fission product groups was estimated from an ORIGEN 2 run to be as follows.

Time	0	15 m	30 m	60 m	90 m	1 d
Group 1 [volatiles] (Xe, Kr, I, Br, Cs, Sb, Te)	0.39	0.37	0.35	0.34	0.33	0.28
Group 2 (Ba, Sr)	0.09	0.087	0.082	0.080	0.080	0.065
Group 3 (Ru, Tc, Rb, Sn)	0.13	0.074	0.059	0.046	0.042	0.036
Group 4 (Rare earths and others)	0.49	0.47	0.46	0.45	0.45	0.52

An examination of the accident sequences in Ref. [1] indicates that, for many of these, the core melts over a period of time for which a representative choice for the power level is about 1% (or according to the table above at ~142 minutes at which time the contribution to the power from the volatile group is about 0.30. Therefore the following assumptions are also made.

Decay power level = 1%
Group 1 fraction = 0.30
Group 2 fraction = 0.08
Group 3 fraction = 0.036
Group 4 fraction = 0.5

An initial adiabatic heat-up was calculated from

$$MC_p \frac{dT}{d\tau} = Q$$

up to the fuel melt temperature, after which the temperature was held constant for a time increment given by

$$\Delta t = M \Delta H_m / Q$$

This gave a linear change in temperature,

$$T = T_0 + (Q/MC_p)t \equiv a + bt,$$

up to fuel melt and constant thereafter.

The result of this initial calculation at 1% power level is indicated on Fig. 2 — which represent the thermal hydraulic situation for no coupling.

The fission product releases as a result of this thermal history were calculated using a CORSOR type release model as recommended in Ref. [3]:

$$\frac{dM_i}{dt} = -K_i M_i$$

where the release coefficients, Ki, are given by

$$K_i = Ae^{BT}/C_i$$

where, for the various nuclide groups,

Group 1, $C_1 = 1$
Group 2, $C_2 = 300$
Group 3, $C_3 = 10{,}000$
Group 4, $C_4 = 30{,}000$

and A and B are selected for three temperature range:

T (°C)	A	B
<1600	6.5×10^{-10}	1.061×10^{-2}
1600-2000	3.616×10^{-6}	5.22×10^{-3}
>2000	2.41×10^{-4}	3.12×10^{-3}

For a linear temperature transient, T = a + bt, solution of the above release model gives,

$$\ln\left(\frac{M_i}{M_{i0}}\right) = \left(\frac{A}{C_i}e^{Ba}\right)\left(\frac{1}{Bb}\right)\left[1 - e^{Bbt}\right]$$

The result of the application of this equation over the three temperature ranges using the original adiabatic heat-up temperature transient, $T = a + bt = 1000°C + (28.47)t$, is shown as the first iteration curve on Fig. 3 in terms of the fraction of decay heat remaining in the fuel as the fission products are lost. This represents the uncoupled fission-product transport result. It can be seen that essentially all of Group I is lost over the time period from about 25 min to ~50 min and very little of the other Groups are lost.

This fission-product loss curve was represented by a linear curve, $Q/Q_o = 1 - (\frac{0.3}{20})t$ starting at t = 25 min as shown on Fig. 3 and the temperature transient was recalculated from a solution of

$$MC_p \frac{dT}{dt} = Q$$

for:

Q = constant up to t = 25 min = Q_o

$Q = Q_o [1 - \frac{0.3}{20}]t$ for $25 < t < 45$ min

$Q = Q_o (0.7)$ thereafter

The result of this is shown as the "coupled solution" on Fig. 2. Linearizing this new temperature transient over two time periods and iterating on the fission product loss calculation gave the "2nd iteration curve on Fig. 3. Since this 2nd iteration curve is not significantly different from the 1st iteration, additional calculations were unnecessary.

The fission product losses by groups were calculated to be as shown in the table below in terms of the fraction remaining in the fuel:

Time min	0	10	~21	30	~36	40	50	60	70
Group 1	(1.0)[a]	(0.999)	(0.971)	(0.755)	(0.462)	(0.22)	(0.014)	~0	~0
	1.0	0.999	0.971	0.755	0.462	0.225	0.023	~0	~0
Group 2	(1.0)	(1.0)	(1.0)	(0.999)	(0.998)	(0.996)	(0.986)	(0.972)	(0.959)
	1.0	1.0	1.0	0.999	0.998	0.996	0.988	0.976	0.962
Group 3	(1.0)	(1.0)	(1.0)	(1.0)	(1.0)	(1.0)	(1.0)	(0.996)	(0.991)
	1.0	1.0	1.0	1.0	1.0	1.0	1.0	0.998	0.994
Group 4	(1.0)	(1.0)	(1.0)	(1.0)	(1.0)	(1.0)	(1.0)	(1.0)	(1.0)
	1.0	1.0	1.0	1.0	1.0	1.0	1.0	1.0	1.0

[a]Uncoupled solution ( ).

Interpretation of Figs. 2 and 3 suggest the following conclusions.

1. A coupled solution in this area would not much affect the fission product releases.
2. The timing of core melt and slump is slightly extended.

Coupling in this area appears to be only marginally important. However, it could become more important if temperatures exceed the "melt" temperature, when better models are available for core slumping behavior, or when there are improved fission product release models and data.

Item (2), (3), and (4). RCS thermal hydraulics/nucleation-condensation of fission product vapors; volatiles as decay heat sources; fission products as part of the carrier streams:

For aid in assessment of these items, a very simplified "control volume" analysis of an upper plenum was developed as follows:

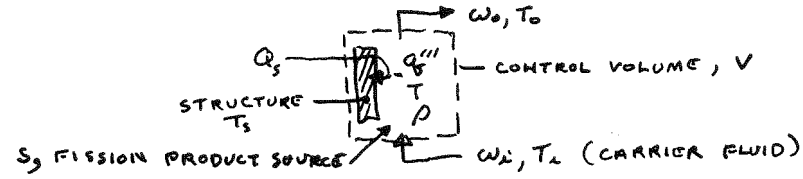

A simple energy balance gives:

$$\rho V C_{p_g} \frac{dT}{d\tau} = \omega_i C_{p_g} T_i - \omega_o C_{p_o} T - hA_s(T - T_s) + q''' V + \sum_i \omega_{cond_i} \Delta H_{fg_i}$$

where ω_{cond} is the rate of condensation of volatile fission products in the control volume, ΔH_{fg_i} is their latent heats of condensation, and q''' is the volumetric internal heat generation rate due to decay of fission products.

Auxiliary equations are:

- For the structure temperature: $M_s C_p \frac{dT_s}{dT} = hA_s(T - T_s)$

- For the concentration of fission products within the control volume: $\frac{VdC}{dt} = S - \frac{\omega_o}{\rho} C$.

Assume quasi-steady conditions for the fission product concentration so that

$$\frac{dC}{d\tau} \cong 0 \quad \text{or} \quad C = (S\rho/\omega_o) ,$$

and let the internal decay heat be C × P where P is the power per unit mass associated with the volatile fission products.

In addition, make the gross approximation that $\frac{dT_s}{dt} \simeq \frac{dT}{dt}$

(substantiated to some extent by detailed code calculations of upper plenum thermal hydraulics — see, for example, Ref. 1), so that

$$M c_{p_s} \frac{dT}{dt} = hA_s(T - T_s) .$$

With the above assumptions, the energy balance equation reduces to:

$$(\rho V c_{p_g} + M_s c_{p_s}) \frac{dT}{dt} = \boxed{\omega_i c_{p_g} T_i} - \omega_o c_{p_g} T + \boxed{s\rho PV/\omega_o} + \boxed{\bar{\omega}_c \Delta H_{sg}} .$$

The terms in the "boxes" can now be compared to evaluate their relative potential effects on the thermal transient. Some other assumptions on needed parameters are given below:

Because expressions for the equilibrium vapor pressures for CsI, CsOH, and Te were available from the TRAP-MELT code, use was made of the Clausius-Clapeyron relation to estimate values for ΔH_{fg} as follows:

Clausius- Clapeyron:

$$\frac{d(\ln P)}{dT} = \frac{\Delta H_{sg}}{RT^2}$$

or, alternatively

$$\frac{d(\ln P)}{d(\frac{1}{T})} = -\frac{\Delta H_{sg}}{R} ;$$

$$R = 1.987 \quad (cal/g\text{-}mole \cdot {}^\circ K)$$

From TRAP-MELT:

CsI: $\log_{10} P \sim -9678/T$

$\therefore \Delta H_{sg} = (9678)(1.987)(\ln 10) = 44.3$ kcal/mole

CsOH: $\log_{10} P \sim -6700/T$

$\therefore \Delta H_{sg} = (6700)(1.987)(\ln 10) = 30.6$ kcal/mole

Te: $\log_{10} P \sim -7980/T$

$\therefore \Delta H_{sg} = (7980)(1.987)(\ln 10) = 36.5$ kcal/mole

Therefore, assume a representative value of 30 kcal/mole for ΔH_{fg} for the volatile condensable fission product vapors. A volume, V, for the control volume must be selected for the decay heat term. Reference [1] utilizes a control volume for the grid plate above the core of 1.5 m^3 and a second control volume of 13 m^3 for the upper plenum region above the grid plate. Both of these values will be used for comparison. In addition, the values for the source rates of H2 and H2O along with CsI, CsOH, and Te and the inlet temperature, T_i can be extracted from Ref. [1] with a great deal of difficulty. These values, along with the calculated values for $\omega_i Cp_i T_i$; $S\rho PV/\omega_o$; and $\omega_c \Delta H_{fg}$ are presented in the tables below for a TMLB' and an AB sequence. The values for P include all of Group 1 at an assumed total decay power level of 1% for a 2441 Mwt core. The carrier stream flow rates, ω_i and ω_o, are the sum of the H2 and H2O rates extracted from Ref. 1. The values of Cp used were:

for H_2: C_p = 3.5 BTU/lb·°F (cal/g·°K)

for H_2O: C_p = 0.5 BTU/lb·°F (cal/g·°K)

Comparison of inlet enthalpy, decay heat, and heat of vaporization:

TMLB' sequence:

Time (s)	0	720	1440	1680	2700
Ti (°C)	900	1530	1860	1920	2050
ω_{H_2} (g/s)	0	89	108	70	4
ω_{H_2O} (g/s)	1813	169	18.8	1.28	0.011
ω_I (g/s)	0.17	5.70	7.67	3.43	1.56
ω_{cs} (g/s)	2.73	60.8	78.9	35.6	16.2
ω_{Te} (g/s)	0.001	7.42	10.32	7.67	4.1
$\Sigma\omega_{in} C_p T_{in}$ (kcal/s)	1.06×10^3	7.14×10^2	8.26×10^2	5.39×10^2	325
$\Sigma\omega_c \Delta H_{fg}$ (kcal/s)	0.64	16	22	10	5
$[\frac{S\rho PV}{\omega}]$: V = 1.5 m^3	7.08×10^{-3}	1.53	12.3	85.9	4.39×10^3
$[\frac{S\rho PV}{\omega}]$: V = 13 m^3 ($\frac{kcal}{s}$)	6.1×10^{-2}	13.3	107	744.3	3.81×10^4

AB sequence

Time (s)	0	240	660	1260	1500	1620
T_i (°C)	315	1200	1790	2030	2060	2060
ω_{H_2} (g/s)	91	96	113		1153	
ω_{H_2O} (g/s)	1891	398	178		163	
ω_I (g/s)	1.93	5.44	7.55	5.13	3.17	2.61
ω_{cs} (g/s)	25.1	58.6	79.7	52.1	31.4	13.5
ω_{Te} (g/s)	0.83	5.79	11.70	13.67	11.67	10.0
$\Sigma\omega_i Cp_i T_i$ $(\frac{kcal}{s})$	743	788	1.0×10^3		1.15×10^4	
$\Sigma\omega_c \Delta H$ $(\frac{kcal}{s})$	6	16	22	5.8		
$\frac{S\rho PV}{\omega}\|V = 1.5$ $(\frac{kcal}{s})$	43	88.8	162		36	
$\frac{S\rho PV}{\omega}\|V = 13$ $(\frac{kcal}{s})$	373	769	1.41×10^3		312	

Inspection of these tables reveals the following about these three areas of suspected coupling:

1. The latent heat of condensation for the condensable fissions product vapor species does not appear to be important.

2. The decay heat load of the volatiles as released in the upper plenum regions is generally important and can sometimes be dominant.

3. The quantities of fission product gases (Xe, Kr)) and condensable fission product species along with the quantities of aerosols can equal to and often exceed the combined H2 and H2O flows. Hence, the thermal hydraulic analyses should consider including these as prominent members of the carrier fluid in terms of flows, heat capacities, thermophysical properties, etc.

Item (5) RCS thermal hydraulics/deposited aerosols as decay heat sources on surfaces.

(a)Revaporization potential

For assessing the potential significance of this item, we are fortunate to have available an analyses by Ref. [4], which made use of the same codes used in the BMI-2104 Ref. [1], study: MARCH 2.0, MERGE, CORSOR, and TRAP-MELT. However, MERGE, CORSOR, and TRAP-MELT were completely integrated into a single package that could perform simultaneous coupled analyses of the RCS thermal hydraulics and fission product/aerosol transport. Some results of these coupled analyses have been obtained from the study and are presented here in Figures 4-7. These show clearly the effects of the deposited fission products as heat sources in driving up the RCS structure temperatures (to failure conditions) and subsequently revaporizing and driving off volatile species late in time.

It appears that this may be the most significant area for the RCS that needs a completely coupled treatment.

Item (5) b: Effect on natural circulation:

[analysis not completed at this time]

Item (6): Core/concrete thermal hydraulics/aerosol production and shielding of thermal radiation

Here again, we have some outside help. Reference [5] reports on a sensitivity study of the CORCON Code in which the effective core melt surface emissivity was varied over the values of 1.0 (base case), 0.05, and 0.001 to simulate the effects of an overlying cloud of aerosols in blocking the radiation heat transfer. The results of this study for the maximum temperature reached by the melt and the total evolved gases are given below:

Case	T_{max} (°K)	Total Gas (kg)
Base (ϵ = 1.0)	2310	9,900
ϵ = 0.05	2320	10,550
ϵ = 0.001	2450	12,250

The influence of these parameters on aerosol production are exponential for T and linear for the gas flow. Reference [5] estimated that the case for ϵ = .001 would have increased the aerosol generation rate by a factor of 10 compared to that of the base case. It is clear that this could be a significant area of coupling depending on the actual value of

effective emissivity that would represent the effect of the aerosols. Analyses have not been completed for this but preliminary estimates indicate values of the order of 0.01. Hence, the actual inclusion of this effect within the calculations that influence both gas and aerosol production is believed to be important.

Item (7): Containment thermal hydraulics/aerosol-water vapor interactions:

(a) Effects on relative humidity:

The concern here is the effect that water, airborne as condensed liquid on aerosol particles, might have on controlling the containment relative humidity which is calculated, in MARCH, without benefit of a coupled aerosol behavior analysis.

The Mason equation is used in NAUA to model the condensation/evaporation interactions of airborne water vapor and aerosol particles,

$$r\frac{dr}{dt} = \frac{S - \exp\left[2\sigma M/(\rho_\ell R T r)\right]}{\frac{\Delta H_{sg}}{RT}\left(\frac{\Delta H_{sg} M}{RT} - 1\right) + \frac{\rho_\ell RT}{M \Theta P_s}} \quad .$$

The mass of water exchange per unit containment volume associated with the change in size of N particles of size r is

$$M_w = -(4\pi r^2 \rho_\ell N_v)\frac{dr}{dt}$$

Hence, multiplying the Mason equation by

$$-4\pi r \rho_\ell N_v$$

will provide an expression for the rate of water vapor exchange with the containment atmosphere due to condensation/evaporation onto aerosols. Therefore a full mass balance, including sources of steam, S'/V, and condensation on the containment structures is given by

$$\frac{d\rho}{dt} = -4\pi r \rho_\ell N_v \left[\frac{\rho/\rho_\ell - \exp\left[2\sigma M/(\rho_\ell R T r)\right]}{\frac{\Delta H_{sg}\rho_\ell}{KT}\left(\frac{\Delta H_{sg} M}{RT} - 1\right) + \frac{\rho_\ell RT}{M\Theta P_s}}\right] - k\frac{A}{V}(\rho - \rho_a) + S'/V \quad .$$

This can be expressed as

$$\frac{d\rho}{dt} = -\lambda_{PART}\rho - \lambda_{COND.}\rho + K_1(t) + K_2$$

in which the "time constant" λ's are

$$\left|\lambda_{PART}\right| = (4\pi r \rho_\ell N_v) \Big/ \frac{P_s M}{RT_s}\left[\frac{\Delta H_{sg}\rho_s}{KT}\left(\frac{\Delta H_{sg} M}{RT} - 1\right) + \frac{\rho_\ell RT}{M\Theta P_s}\right], \quad (sec^{-1})$$

and $|\lambda_{cond}| = \left|\frac{kA}{V}\right| \ sec^{-1}$.

These time constants can be evaluated to estimate the potential relative influence on affecting containment airborne water vapor content:

For quantifying λ_{part}, the following parameter values were used:

ρ_ℓ = 1 g/cm^3 = 62.4 lb$_m$/ft^3
T = 250°F = 120°C = 393°K = 710°R
P_s = 29.8 psia
ΔH_{fg} = 945.5 Btu/lb$_m$
M = 18 lbs/lb-mole
R = 82.047 atm - cm^3/g-mole °K = 1206 psia - cm^3/g-mole °K
K = 0.015 Btu/hr - ft - °F
D = 0.25 cm^2/sec
R = 85.78 (ft-lb$_f$/lb$_m$ - °R)

It is seen that λ_{part} depends on the concentration of particles, C, through

$$N = 3C/4\pi r^3$$

and on the radius of the particles. Using the above values, λ_{part} can be expressed as $|\lambda| = 0.333\ C/r^2\ sec^{-1}$ if C is the concentration in g/m^3 and r is the particle radius in μm.

Parametric variation of these gives the various values for λ_{part} as shown below:

C \ r	0.1	1.0	5.0	10.0	100.0
.1	3.33	0.0333	.0013	.0003	3×10^{-6}
1.0	33.3	.333	.013	.003	3×10^{-5}
10.0	333	3.33	.13	.033	3×10^{-4}

It now remains to quantify λ_{cond}:

The relation used in MARCH-2.0 to calculate the heat transfer associated with steam condensation onto containment structures is

$$Q/A = h_c[T - T_w] \ ; \quad h_c \cong 10\ (BTU/hr\text{-}ft^2\text{-}°F) \ .$$

The rate of steam condensation that this would predict is given by;

$$Q/V\Delta H_{sg} = (h_c A/\Delta H_{sg} V)[T - T_w]$$

$$= (h_c A/\Delta H_{sg} V)T - \text{A CONSTANT TERM}$$

$$\text{or } (Q/V\Delta H_{sg}) \sim (h_c A/\Delta H_{sg} V)\frac{RT^2}{P}(\rho)$$

$\therefore$ k, in the expression

$$|\lambda_{cond}| \equiv \left|\frac{kA}{V}\right|$$

can be estimated as

$$k \sim h_c RT^2/\Delta H_{sg} P$$

or

$$\left|\frac{kA}{V}\right| \sim (h_c RT^2/\Delta H_{sg} P)(A/V)$$

Values used for the various parameters are:

h_c = 10 Btu/hr-ft^2-R
R^c = 85.78 ft-lb$_f$/lb$_m$-°R
T = 710 °R
ΔH_{fg} = 945.5 Btu/lb$_m$
P = 29.8 lb$_f$/in^2 144 in^2/ft^2
A/V = 1.292 10^5/1.8 10^6 ft^{-1} = .072 ft^{-1}

$$\therefore \lambda_{cond} = \frac{(10)(85.78)(710)^2(0.072)}{(945.5)(29.8)(144)} = 7.7 \text{ sec}^{-1}$$

Since 7.7 is generally $>\lambda_p$ [especially for 1 μm and bigger particle (droplet) sizes] the presence of condensed water vapor on aerosol particles would be assessed to not have much effect on containment humidity compared to condensation onto wall surfaces.

Item (7b): Effects of airborne liquid water on H_2 burns in containment

During some accident sequences, as much as 50 to 100 grams of water vapor per m^3 of containment volume have been calculated to be airborne as condensed onto particles. It is of interest to compare the heat absorbing capacity of this water on vaporization, $M_w \Delta H_{fg}$, compared to the potential heat addition to containments by H_2 burning. Estimates for H_2 mass addition to containment generally range from 100 to 600 kg. Assuming the heat of combustion for H_2 to be

$$\Delta H\,(\text{COMBUSTION}) \cong 61{,}000 \quad (\text{BTU/LB})$$

and ΔH_{fg} for vaporization of water = 948.5 Btu/lbm the relative energy release and absorbing capacities can be compared as shown below.

ΔH_{TOTAL} for 100 g/M^3 of water = 208 Btu/m^3

ΔH_{TOTAL} for 10 g/M^3 of water = 20.8 Btu/m^3

ΔH due to burning of 100 kg of H_2 = 263 Btu/m^3

ΔH due to burning of 600 kg of H_2 = 1578 Btu/m^3

It appears from the above that there could be circumstances (heavy water loadings and limited amounts of H_2) in which it would be important to consider this in the thermal hydraulics calculations.

Items (8), (9), and (10):

[Quantitative evaluation of these items has not been completed at this date]

REFERENCES

1. Gieseke, J. A., et al., "Radionuclide Release Under Specific LWR Accident Conditions," BMI-2104, Vols. 1-6, Battelle Columbus Laboratories, to be issued.

2. Winterton, R. H. S., Thermal Design of Nuclear Reactors, Pergamon Press, Oxford, 1981.

3. Kress, T. S., "Review of the Status of Validation of the Computer Codes Used in the NRC Accident Source Term Reassessment Study (BMI-2104)," Chapter VII (R. A. Lorenz), ORNL/TM-8842, Oak Ridge National Laboratory, to be issued.

4. "Source Term Safety Assessment of Radionuclide Releases Under Severe Accident Conditions at Indian Point 3 Nuclear Power Plant," study prepared for New York Power Authority by Risk Management Associates and New York Power Authority, provided by R. E. Deem, July 10, 1984.

5. Lipinski, R. J., et al., "Uncertainty in Radionuclide Release Under Specific LWR Accident Conditions," SAND84-0410/2, Sandia National Laboratory, to be issued.

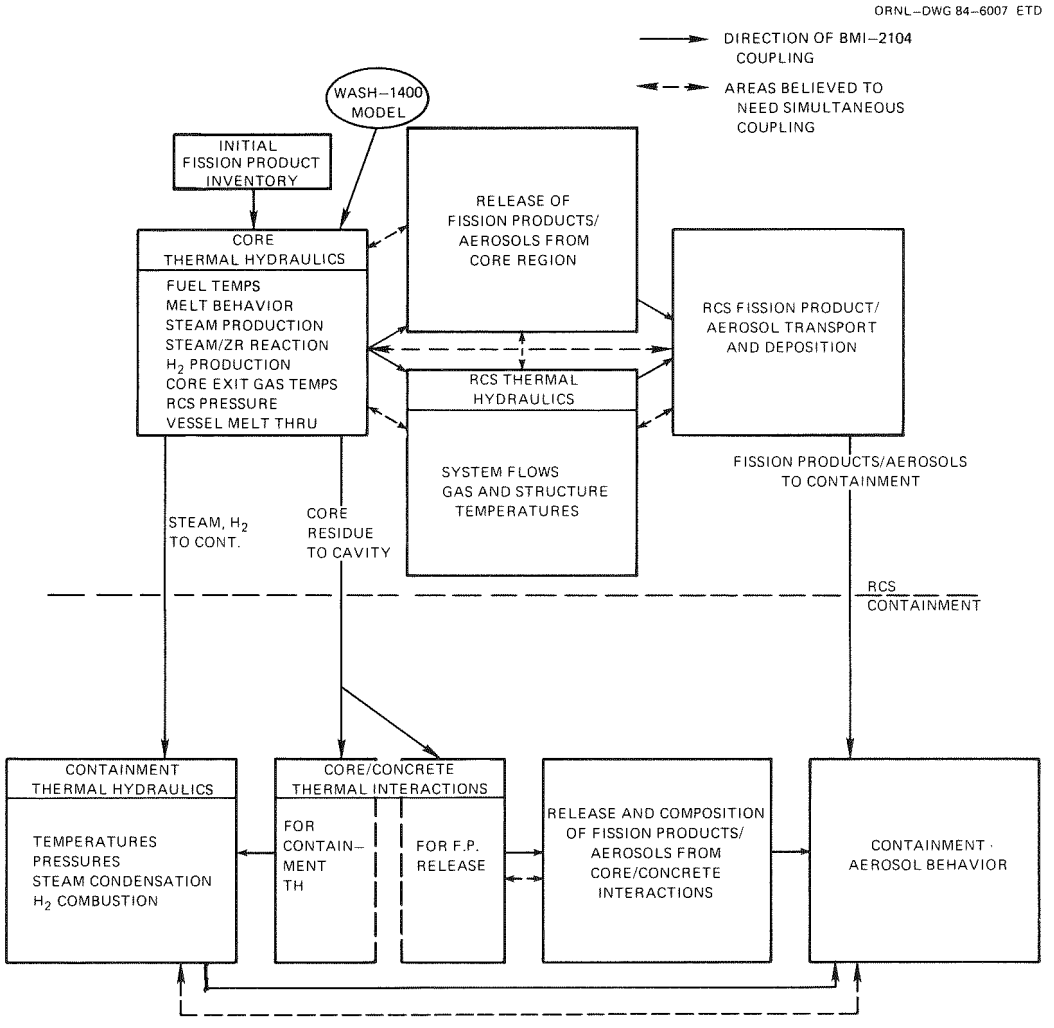

Fig. 1. Coupling among thermal hydraulic and aerosol transport phenomenology in source term determination

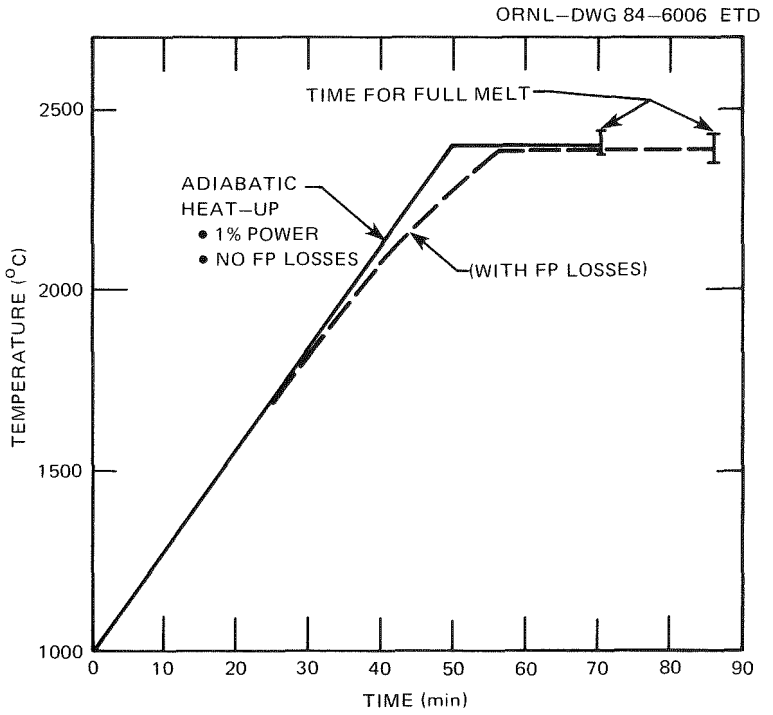

Fig. 2. Adiabatic heatup of a unit mass of fuel with/without fission product losses

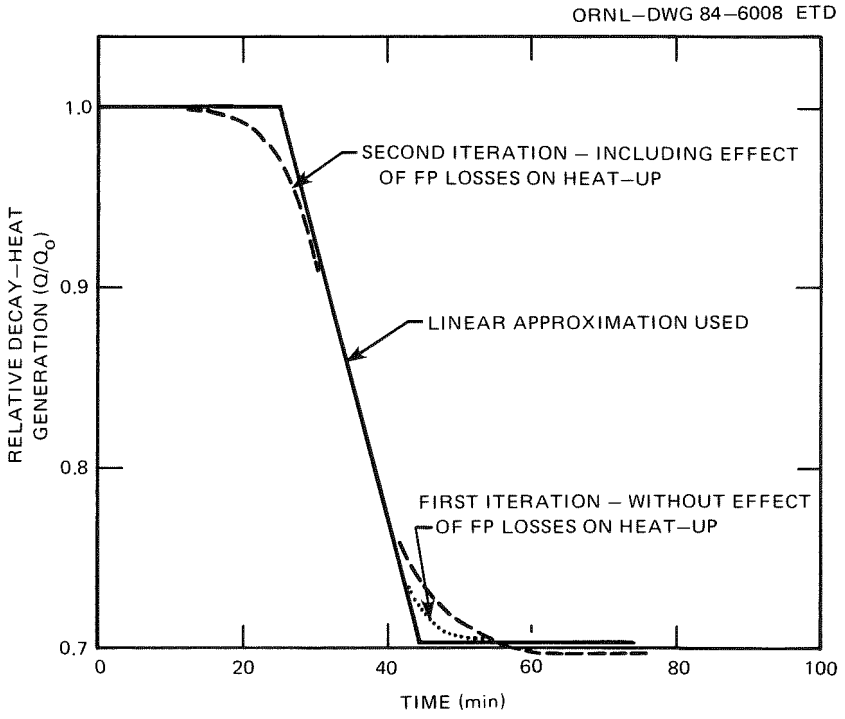

Fig. 3. Relative change in decay heat from unit mass of fuel as fission products are released during adiabatic heatup

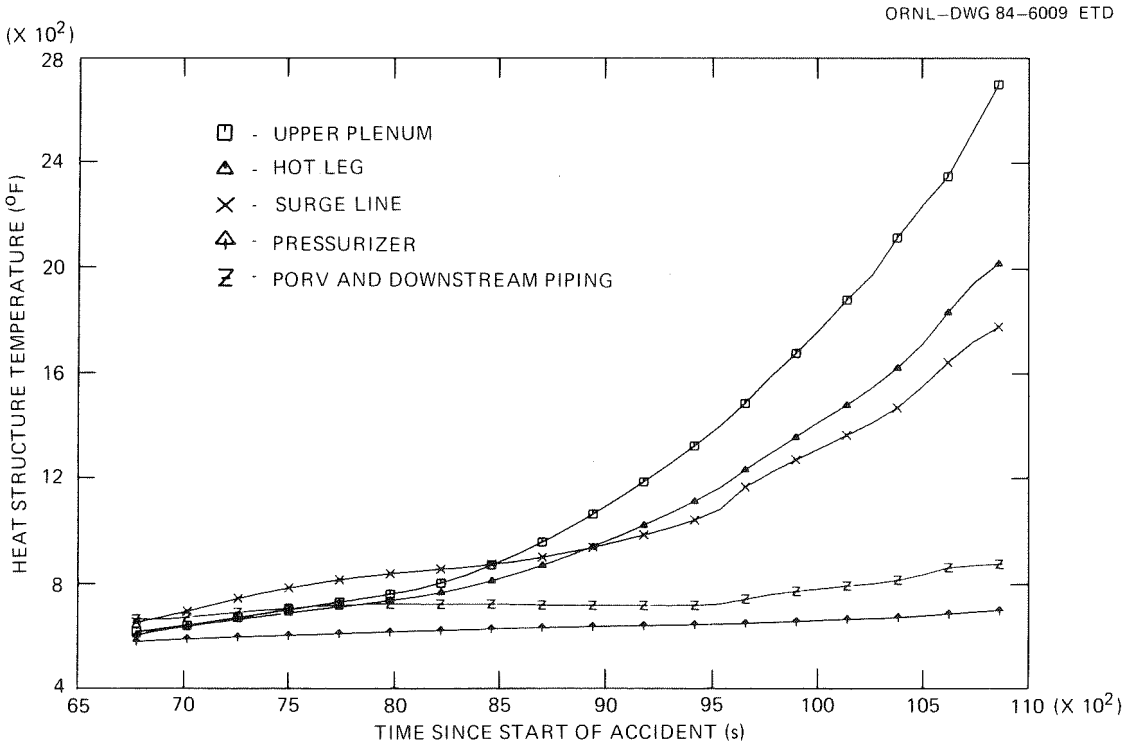

Fig. 4. Results for the RCS structure temperatures for a TMLB′ with integrated, coupled thermal hydraulics and fission product transport, Ref. [4]

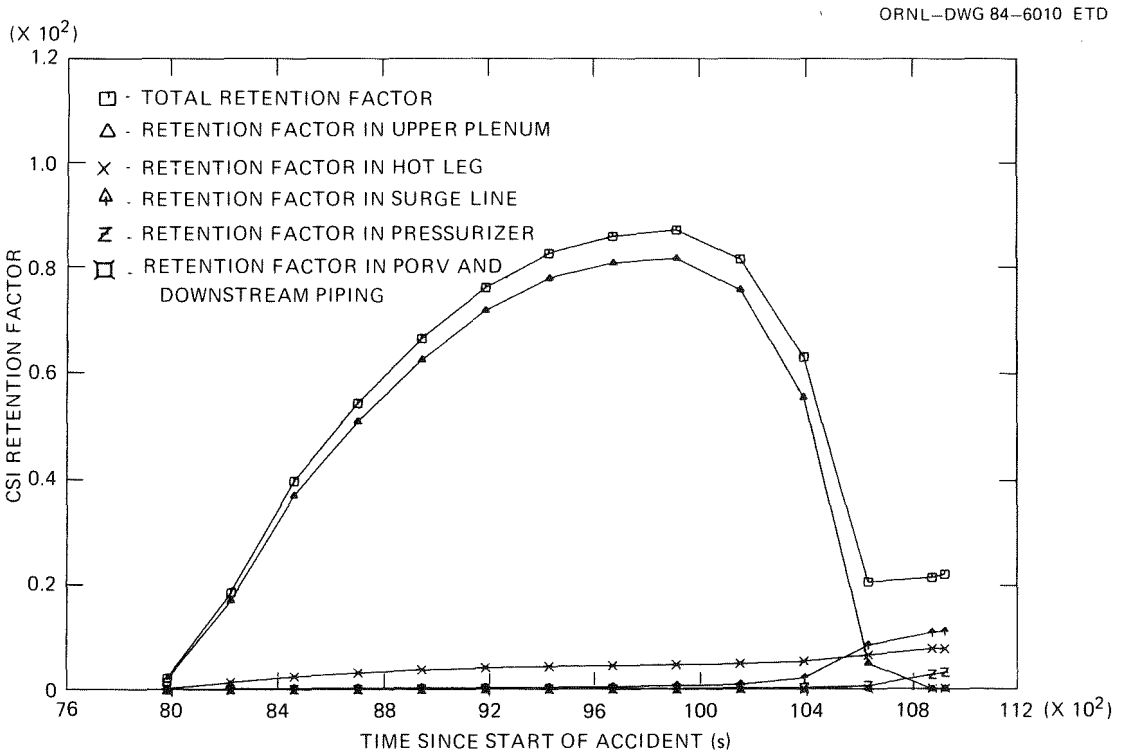

Fig. 5. Results for the fraction of core inventory of CsI retained on RCS surfaces for a TMLB′ with integrated, coupled thermal hydraulics and fission product transport, Ref. [4]

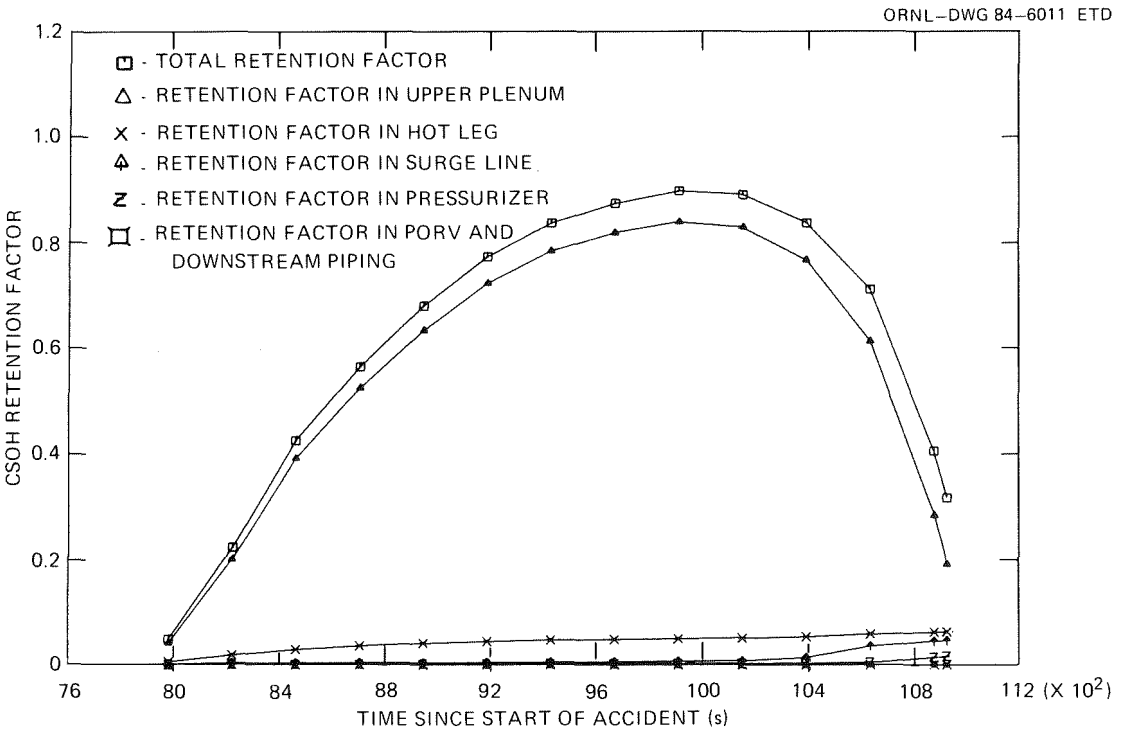

Fig. 6. Results for the fraction of core inventory of CsOH retained on RCS surfaces for a TMLB′ with integrated, coupled thermal hydraulics and fission product transport, Ref. [4]

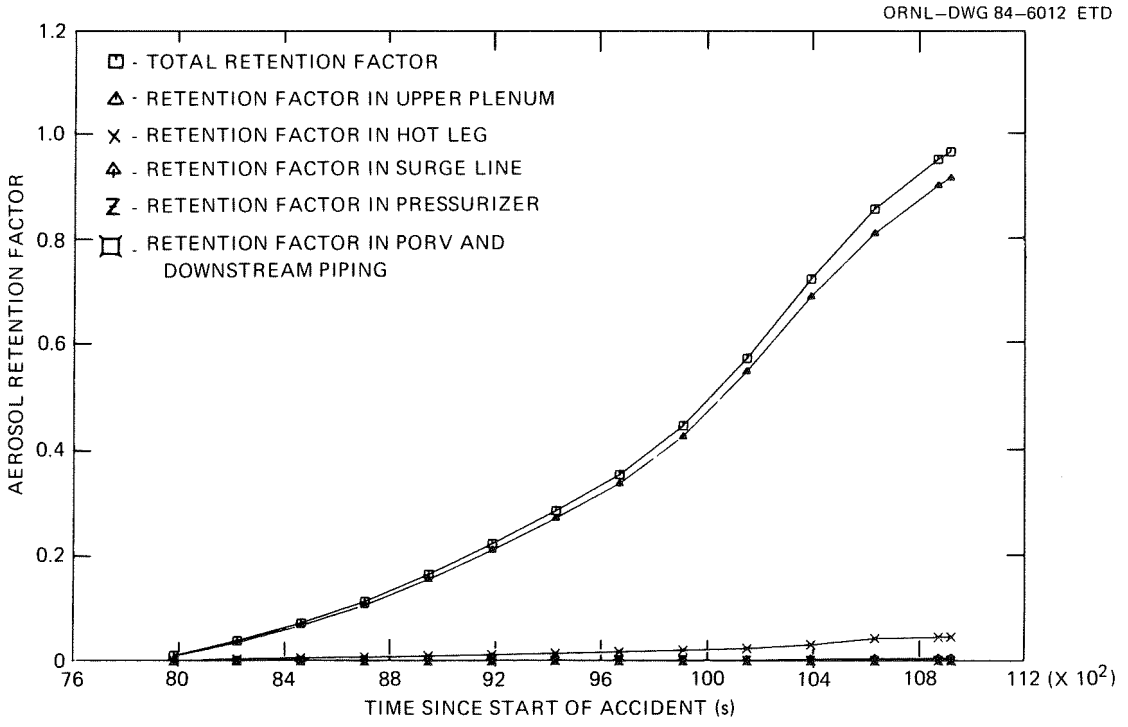

Fig. 7. Results for the fraction of aerosols (other than CsI, CsOH and Te) released from the core that are retained in the RCS for a TMLB´ with integrated, coupled thermal hydraulics and fission product transport, Ref. [4]

AEROSOL NUCLEATION AND GROWTH AND THEIR COUPLING TO THERMAL HYDRAULICS

C.F. Clement
Theoretical Physics Division, 424.4, AERE Harwell,
Didcot, Oxon OX11 ORA UK.

ABSTRACT

We examine the physical processes leading to vapour condensation as an aerosol in the formation and cooling of vapour-gas mixtures. Requirements for mathematical, computer and experimental modelling are discussed in relation to nuclear aerosols.

In the absence of sudden pressure drops we give a complete schematic set of equations which govern the motion of aerosol, vapour, gas and heat including radiation. The coupling to the aerosol equation is mainly through the droplet growth rate, $\dot{R}$, and a nucleation term whose possible forms are described. Rapid equilibration between vapour and aerosol means that the likely heterogeneous nucleation term must be treated separately.

General forms are given for the coupling terms in the equations for vapour concentration and temperature in terms of the local mass transfer rate to the aerosol. The properties of this quantity are shown clearly by an expression for it obtained in terms of Lewis and condensation numbers and the quantity, ξ, whose derivative gives the local total heat transfer rate. Sizes of these numbers are given for some relevant vapour-gas mixtures.

Throughout the paper we give the physical requirements necessary to make the transitions to the more calculable cases of uniform or well-mixed aerosols, and finally we discuss the case of initially unsaturated vapour-gas mixtures.

The interaction between aerosols and the thermal hydraulics of their containing gas is of interest in fields as diverse as reactor safety[1] and the physics of clouds in the atmosphere[2]. Many problems remain in the subject, but we report here mainly on recent advances in the understanding of aerosol formation and growth from vapour-gas mixtures. First, however, we consider the general problems of the subject in the modelling of nuclear aerosols. The main conclusions of this work are emphasized in the text.

Because of the difficulty in reproducing possible though unlikely, events, such as the emission of vapours from an overheated reactor core, we have to have recourse to mathematical, computer and experimental modelling of the subsequent processes which include aerosol formation and decay. This means acquiring a good enough understanding of the basic physical and chemical processes involved. Otherwise we may be forced into making unduly conservative assumptions such as assuming that all the vapour condenses into a persistant aerosol. This is a low density (< 0.1 kg m^{-3}) suspension of micron-sized droplets or particles with a long lifetime against removal processes: gravitational removal by fallout is fast for higher densities and larger particles[3]. We may look on heating a core as a giant distillation experiment and need to understand why it might be different from normal distillation processes in which no aerosols are usually formed at all. This applies particularly to experimental modelling where, unless the coupling between heat and mass transfer processes is taken into account, inappropriate

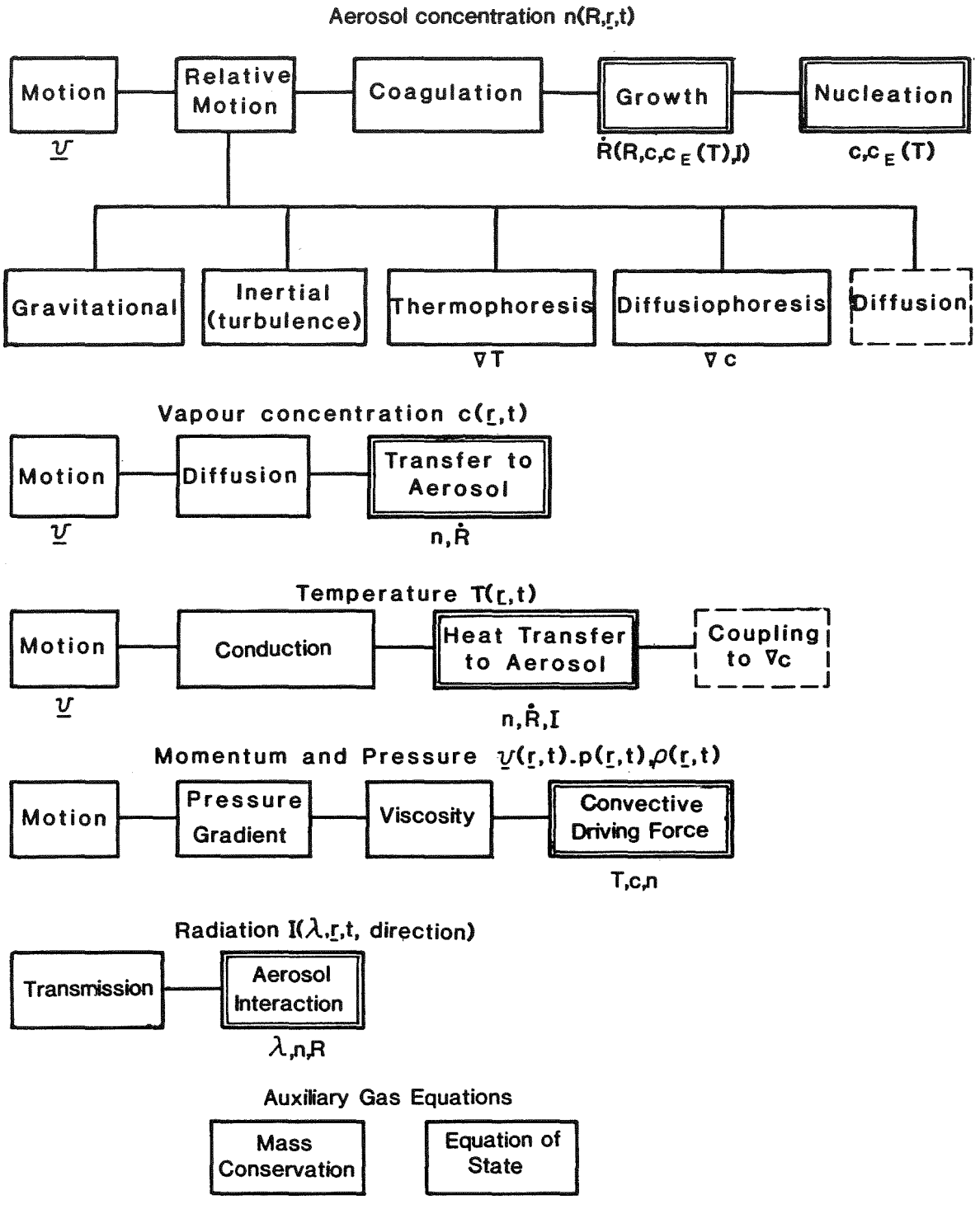

FIG.1.SCHEMATIC SET OF EQUATIONS FOR THE COUPLING BETWEEN THE AEROSOL AND THERMAL HYDRAULICS. VARIABLES ON WHICH THE STRONG COUPLING TERMS (RINGED) DEPEND ARE INDICATED.

results may be obtained. As opposed to aerosol decay processes which have a long lifetime, the formation processes are usually very fast which partially accounts for the present inadequate experimental work in the area.

Theoretical guidance is clearly needed in deciding which experiments to perform, and this raises the question as to whether there is an adequate mathematical framework at present in which the interaction between aerosols and thermal hydraulics may be examined. In figure 1 we give in a schematic form a minimum set of equations which are required to describe the three fluid system consisting of aerosol, vapour and gas. In order to discuss condensation it is necessary to include both the usual heat or temperature equation and an equation for the radiation intensity, $I(\lambda)$, which may be strongly coupled to the aerosol. Symbols used in figure 1 are defined in the nomenclature and we define here only the vapour concentration

$$c(\underline{r},t) = \rho_v(\underline{\rho},t)/\rho(\underline{r},t) \quad , \tag{1}$$

whose equilibrium values, $c_E(p,T(\underline{r},t))$, can be expressed in terms of the total pressure and the equilibrium vapour pressure, $p_{VE}(T)$.

In principle, the forms of most of the terms in these equations are known or can be derived, but problems still remain. One problem of particular interest concerns the convective driving force in the overall momentum equation whose normal form involves the coefficient of expansion, $\beta = -(1/\rho)(\partial\rho/\partial T)_p = 1/T$ for a simple gas. It was pointed out some time ago[4,5] that this term can change sign and convection be suppressed in a heavy vapour-light gas mixture, and recently that it can lead to 'upside-down' convection[6]. However, these treatments did not properly take into account the aerosol density. We hope to return to this subject elsewhere, but it is clearly of considerable potential importance because most nuclear vapours are heavy, i.e. have a greater molecular weight than the surrounding gas.

We assume that only one parameter, the radius R, is needed to characterise the aerosol size distribution, although this may not be sufficient for solid particles. Then the equation for the aerosol concentration, $n(R,\underline{r},t)$, takes the general form:

$$\frac{\partial n}{\partial t} + \underline{v}.\nabla n + \nabla.(n\underline{v}_d) + \nabla.(-D_p(R)\ \nabla n) + \frac{\partial}{\partial R}(n\dot{R}) = [K\ n^2] + S_N(R,\underline{r},t) \quad , \tag{2}$$

where $[Kn^2]$ represents the coagulation terms in whose detailed form we are not interested here.

The directional velocities relative to the fluid are contained in $\underline{v}_d$, which includes the gravitational velocity as well as those from thermophoresis and diffusiophoresis, proportional to ∇T and ∇c, respectively. Most current computer programs solve a spatially uniform version of eq. (2) with no growth term, no source term, S_N which arises from nucleation, and surface removal rates which arise from the $\nabla.$ terms. Because of the nonlinear nature of the coagulation terms even this simplified calculation is non-trivial. Even without coupling to the radiation field, whose transmission alone is a complex problem[7], it is obviously extremely difficult to include spatial dependence for the aerosol concentration as well as the coupling to c, T and $\underline{v}$ in a general computer program. Thus we have:

Conclusion 1 Considerable simplifications are required in the equations coupling the aerosol to thermal hydraulics before numerical solutions can be obtained.

Hitherto, we have neglected to explain that the dashes around the boxes in figure 1 denote that the terms in the equations are usually small. For the aerosol the diffusion term in eq. (2) is negligible for micron sized particles because the diffusivity, $D_p(R)$, is extremely small ($\lesssim 10^{-10}$ $m^2 s^{-1}$). Mathematically the neglect of this term implies that there are no second order spatial derivatives of $n(\underline{r})$ in eq. (2). Spatial discontinuities in $n(\underline{r})$ can then occur and, in fact, are commonly observed with aerosols:

Conclusion 2 Aerosols have sharp edges in space.

The movement of such boundaries is a difficult problem in general. They do not necessarily move with velocity $\underline{v}$ because, as we shall see, nucleation and growth are so rapid that the coupling terms can easily move the boundaries relative to the gas flow. Again this is observed with clouds.

For aerosols the only effective mixing mechanism is turbulent flow so that we have:

Conclusion 3 Criteria for the validity of the approximation of a spatially uniform aerosol are:

A. The whole spatial region is encompassed by turbulent flows.

B. Aerosol coagulation and removal times >> Turbulent mixing time.

The criterion A will be violated for an enclosed volume if convection does not exist or is suppressed in part of the volume. If convection does exist the aerosol number or mass density must be high to violate criterion B since turbulent mixing times are fast (typically seconds even for cavities of tens of metres in size).

In our remaining discussion a crucial role is played by the microscopic droplet growth rate, $\dot{R}$, whose form has been derived by a number of authors[8,9,10]. Heat transfer occurs between a droplet at temperature, T_d, and the surrounding gas at temperature T and, by radiation, with more distant aerosol and walls. The radiative heat loss from a droplet of radius R may be written as

$$\dot{q}_{rad} = 4\pi R^2 [A + B\ (T_d - T)/T] \quad . \tag{3}$$

where A and B are independent of T_d.

The effect of radiation to nearby gas (the term B) turns out to be negligible for micron-sized droplets, in which case we have

$$\dot{R} = \frac{1}{\rho_L} \left[\frac{S - 1 + \lceil RAD \rceil}{\lceil HEAT \rceil + \lceil MASS \rceil}\right] \quad , \tag{4}$$

which is valid for the supersaturation, $S = p_V(T)/p_{VE}(T)$, not too far from unity.

$$[\text{HEAT}] = \frac{\mu}{R_G\, T^2\, k_H} \equiv \frac{\mu_v}{R_G\, T^2} \left(\frac{1}{H} + \frac{R}{k'}\right) \quad , \tag{5}$$

$$[\text{MASS}] = \frac{R_G\, T}{\mu_v\, p_{VE}(T)} \left(\frac{1}{k_c} + \frac{R}{D'}\right) \quad , \tag{6}$$

where H and k_c are surface transfer coefficients and k' and D' are slightly modified[10] forms of the thermal conductivity and diffusivity which reduce to their normal values for large R and small p_v/p.

The radiative term is

$$[\text{RAD}] = L\, \mu_v A/(R_G\, T^2\, k_H) \quad . \tag{7}$$

An examination of these results leads to the following conclusions:

Conclusions 4 For small R, $\dot{R}$ is independent of R but $\dot{R} \sim 1/R$ for large R.

For water droplets, if we assume $S_A = 0.5$ for the sticking probability for water molecules which enters into the coefficient k_c, the critical transition radii are in the range 0.3 - 0.4μm. However, there is considerable uncertainty in S_A[10].

Conclusion 5 Even in the absence of supersaturations it is possible for radiation to promote condensation onto, or evaporation from, an aerosol.

Familiar examples of these processes occur in the atmosphere. In the reactor case the interaction with radiation would almost certainly be important in the region above the core.

Actual supersaturations may be calculated by solving the equation for vapour concentrations, $c(\underline{r},t)$, and using the relation[11],

$$S - 1 = \frac{[\mu_g p + (\mu_v - \mu_g)\, p_{VE}(T)]\, [c - c_E(T)]}{p_{VE}(T)\, [\mu_v - (\mu_v - \mu_g)c]} \quad . \tag{8}$$

In conjunction with eqs. (4)-(7) this relation completely specifies the growth term in the aerosol equation (2) in terms of the other variables, T, c, $c_E(T)$, R and I. Actually eq. (4) requires modification for tiny droplets and the factor S-1 should be replaced by $S - \exp[\alpha(T)/R]$, where α is given in terms of the surface tension, γ, and specific volume, v_L, of the condensate by

$$\alpha(T) = 2\gamma v_L/(k_B T) \quad . \tag{9}$$

Since α is of the order of nm the expression (4) is adequate outside the nucleation regime. Heterogeneous nucleation occurs for a given size, R_N, of impurity nucleus when S reaches the value given by

$$\ln S = \alpha(T)/R_N \quad . \tag{10}$$

In the reactor environment this type of nucleation is expected to predominate over homogeneous nucleation because of the likely presence of small impurity nuclei as well as ionizing radiation, although an exception could be in the small boundaries around spray droplets[12]. In principle, we could then use the modified eq. (4) with a knowledge of a density of impurity nuclei to calculate n in eq. (2) without the use of a specific source term S_N . However, this is not likely to be a useful approach for the following reasons. We have shown elsewhere[11] that equilibration between an aerosol and its vapour is a rapid process and that supersaturations cannot become large over large volumes. In the nucleation regime equilibration through the growth term and Smoluchowski diffusive coagulation term in the aerosol equation is likely to be even faster. The growth equilibration time is[13]

$$t_E = R_E \rho_L / 3 k_c \rho_a \quad , \tag{11}$$

where R_E is the final equilibrium droplet size and ρ_a the final aerosol density.

For $\rho_L/\rho_a \sim 10^5$ ($\sim 10^{-2}$ kg m^{-3} aerosol), $k_c \sim 10^2$ ms^{-1} and $R_E \sim 10^{-2}\mu$m, we would have $t_E < 10^{-5}$s. The corresponding number density would then be about 2.10^{18} m^{-3} which would given an initial timescale for coagulation of about 10^{-2}s.

Conclusion 6 Nucleation will be highly localised in space and very fast in time.

Because the timescale is much faster than that of the aerosol decay processes (e.g. gravitational fallout) described by eq. (2), a separate source term, $S_N(R,\underline{r},t)$, is appropriate. This term could be specified by:

(a) requiring that S exceeds a critical supersaturation, S , in a given spatial region, and

(b) converting the excess vapour into aerosol so that the region comes into thermal and vapour-aerosol equilibrium.

As long as R is not chosen to be too large, the size chosen for the aerosol in the nucleation term will not be critical: subsequent coagulation will rapidly remove any differences from different choices of starting conditions.

The local mass transfer rate to the aerosol is, per unit volume,

$$\dot{m}_v = 4\pi\rho_L \int R^2 \dot{R}\, n(R,\underline{r},t)\, dR \quad . \tag{12}$$

The source terms for the equations for c and T shown in figure 1 are, respectively, $-(1-c)\dot{m}_v/\rho$[11] and

$$\left[L\dot{m}_v - \int \dot{q}_{rad}\, n(R,\underline{r},t) dR\right]/\rho\bar{c}_p \quad . \tag{13}$$

The radiation term, whose specification will depend on the geometry and other radiative properties of the medium and enclosure, was omitted previously[11]. In this approximation we have completed an extended investigation of the physical factors which control aerosol growth[11] and have performed calculations for steam condensation[12]. We now summarise and slightly extend some of our results, bearing in mind that the possible effects of radiation are not included.

Using the coupling terms given here and knowing $\underline{v}$, we can, in principle, solve the equations for n, c and T. However, because of the rapid equilibration requirement[11], we know that, in the presence of an aerosol, $S \sim 1$ and $c \approx c_E(T)$, except possibly in small spatial regions. In this approximation, the equations for c and T can be solved first and the solutions used to obtain $\dot{m}_v$ and $\dot{R}$. If the dependence of $\dot{R}$ on R is known it is easy to invert eq. (12). For example, if $\dot{R} \sim 1/R$ we have

$$\dot{R} = \dot{m}_v/(4\pi\rho_L N\bar{R}R) \quad , \tag{14}$$

where

$$N\bar{R} = \int Rn(R,\underline{r},t)\, dR \quad . \tag{15}$$

In conjunction with eq. (4) this result can be used to determine S, and so check on the self-consistency of the approximation that $S \approx 1$[11]. The physics appears in terms of the dimensionless Lewis and condensation numbers:

$$Le = k/(D\rho\bar{c}_p) \quad , \tag{16}$$

$$Cn(T) = k/(LD\rho c'_E(T)) \quad . \tag{17}$$

Le describes the relative rates of heat and mass transfer, and Cn the ratio of the rate of latent heat removal by conduction to the rate of mass transport. In fact Cn is essentially the same as the ratio [MASS]/[HEAT], as given by eqs. (5) and (6) in the diffusive and conductive limit which has the same physical interpretation. Rather than in terms of T or c[11], we here express $\dot{m}_v$ in terms of the quantity

$$\xi = T + Lc_E/\bar{c}_p \quad . \tag{18}$$

For $Cn \gg 1$, and in general for Le close to 1, the <u>total</u> heat transfer rate including that at walls is given by $-k\nabla\xi$. Then, if we neglect the expected small dependences of $\bar{c}_p$, Le, and L on T, we obtain

$$\dot{m}_v = \frac{1}{L}\,\nabla.(k\nabla\xi)\,\frac{Cn}{(Le + Cn(1-c_E))(Cn + Le)}$$

$$\left\{1-Le + \frac{k(\nabla\xi)^2}{\nabla.(k\nabla\xi)}\,\frac{Cn}{Cn+Le}\left[\frac{Cn+Le^2}{Cn+Le}\,\frac{c''_E}{c'_E} - \frac{c_{pv} - c_{pg}}{\bar{c}_p}\,c'_E\right]\right\} \quad . \tag{19}$$

An examination of this expression gives all our previous general results[11] which we summarise here as conclusions:

Conclusion 7 Aerosol growth depends on diffusive and conductive currents. It is therefore mainly localised to boundary layers.

Conclusion 8 For Le≠1 and small enough $\Delta\xi$ (or ΔT), the sign of $\dot{m}_v$ depends on the sign of $\nabla.(k\nabla\xi)$ which is different depending on whether the mixture is being heated or cooled. In one of these cases the aerosol will evaporate.

Conclusion 9 For a fixed total heat transfer rate, $\dot{m}_v$ has a fairly sharp maximum in the temperature region where Cn ≈ 1.

The size of $\dot{m}_v$ in a boundary layer depends on the quantity $\Delta\xi\ c''_E/c'_E$, where $\Delta\xi$ is the change across the layer. This quantity also mainly determines the supersaturation possible in the layer.

To calculate heat and mass transfer rates in practice it may be possible to use the following procedure[14,5]:

Knowing v and a Reynolds number, or alternatively a Grashof number in a convective case, the heat transfer to a wall in a pure gas case may be determined by an experimental correlation. Provided, in the convective case, that convection is not affected by the condensation (at least true for Cn >> 1[11]), the same correlation in ξ gives the total heat transfer. From this we would get $\Delta\xi$ across the boundary layer and the missing element in calculating the ratio of aerosol to wall condensation in the well-mixed model[15,11,12].

We have proved that the well-mixed model with S = 1 in the boundary layers gives a maximum to this ratio[11], but have shown, both analytically and by explicit calculations[12], that allowing even only small supersaturations leads to a sharp decrease in the proportion of vapour condensing on the aerosol. Another effect which has emerged, and whose implications need further study, is that aerosol growth may not have the same sign throughout a boundary layer[10].

For large enough values of ΔT or $\Delta\xi$ the well-mixed model predicts dominant aerosol condensation for Cn >> 1 and dominant wall condensation for Cn << 1. Values of Le and Cn obtained so far for some nuclear aerosols are shown in Table 1. The values of Cn are given for p = 1 Atm. and those for other pressures may be obtained using the proportionaity of Cn to p.

Gas	Vapour	T°C	Le	Cn
Air	Water	0	0.85	1.3
		4	0.85	1
		50	0.85	0.1
		100	0.54	0.01
Argon	Sodium	200	$\gtrsim 1$	10^4
		520	1	1
		700	$\lesssim 1$	0.1
H_2O	CsI	1200	?	≈0.2
		980	?	≈ 1
		780	?	≈ 10

Table 1 Lewis and Condensation Numbers for some Vapour-Gas Mixtures Relevant to Reactors

The physical consequences for high temperature water vapour-air mixtures of having Le < 1 and Cn << 1 have been thoroughly explored elsewhere[11,12]. Without having a value of Le for CsI in steam, we cannot guess what sort of temperatures differences, ΔT, in boundary layers are necessary to produce an aerosol. At higher temperatures (> 1000°C), however, values of c_E''/c_E' for CsI indicate that values of ΔT needed are probably 4-6 times larger than those needed in water vapour-air mixtures.

Conclusion 10 Basic transport data are needed for possible nuclear vapour-gas mixtures, e.g. CsI and CsOH in steam.

Finally, we discuss what happens to initially unsaturated vapour-gas mixtures, as this may correspond more closely with some possible nuclear cases and certainly occurs in many distillation processes. The equations for vapour concentration, c, and temperature are mainly uncoupled. Mixing and diffusion will make c practically uniform. With cooling through walls the temperatures are lowest there, and this is where initial condensation takes place. The possibility of forming an aerosol depends on subsequently removing enough heat at walls, but not so much mass, so that the bulk of the mixture becomes supersaturated. In practice there are many examples where this does not happen e.g. water condensation on interior cold windows of a house. The process needs to be thoroughly characterised for possible nuclear aerosols.

We have not touched on some other well known processes, such as Ostwald ripening, which is probably important for high temperature water aerosols, and the influence of dissolved species. These can be included in a straightforward way, but the interaction between radiation and aerosol in turbulent convective flows is more difficult, and we are presently in the process of describing possible physical effects. In principle, these effects and the effects of radioactive heat sources are the major sources of uncertainty in the theory outlined here for dealing with nuclear aerosols. Within the present theory the main uncertainty lies in specifying supersaturations at which nucleation takes place, but at least we do have means of calculating the maximum possible fraction of vapour which condenses as an aerosol.

REFERENCES

1. "Nuclear Aerosols in Reactor Safety," CSNI Report to the OECD (June 1979), Supplementary State-of-the-Art Report (1983).

2. Manton, M. J., Rep.Progr. in Physics 46, 1393-1444 (1983).

3. Morewitz, H. A., Nucl.Tech. 53, 120 (1981).

4. Van de Vate, J. F. and Plomp, A. Nucl.Sci. and Eng. 56, 196-200 (1975).

5. Clement, C. F. and Hawtin, P. Proc.Int.Conf. on Liquid Metal Technology in Energy Production, Ed. M. H. Cooper, Seven Springs, Pennsylvania, p.603-9 (1976).

6. Clement, C. F. "The Behaviour of Heavy Vapour-Light Gas Mixtures" AERE-TP.897 (1982).

7. Siegel, R. and Howell, J. R. "Thermal Radiation Heat Transfer", McGraw Hill (New York 1972).

8. Wright, P. G., Proc.Roy.Soc.Edin. 66A, 65 (1962).

9. Fukuta, N. and Walter, L. A., J.Atmos.Sci. 27, 1160 (1970).

10. Barrett, J. C. and Clement, C. F. Report to be unpublished (1984).

11. Clement, C. F. "Aerosol Formation from Heat and Mass Transfer in Vapour-Gas Mixtures" AERE-TP.1003 (1984).

12. Clement, C. F. and Taylor, A. J. "Aerosol Growth by Steam Condensation in a PWR Containment", AERE-TP.1048 (1984).

13. Clement, C. F. "Models for the Growth and Dissolution of Small Particles in Liquids", AERE-TP.605 (1974).

14. Hills, A. W. D. and Szekely, J., J.Chem.Eng.Sci. 19, 79-81 (1964).

15. Clement, C. F. "Aerosol Growth in Vapour-Gas Mixtures Cooled Through Surfaces", AERE-TP.897 (1982).

NOMENCLATURE

A,B constants in eq. (3)
c vapour concentration
c_E' derivative of c_E with respect to T
c_p specific heat
$\bar{c}_p$ $(\rho_g c_{pg} + \rho_v c_{ov})/\rho$
Cn condensation number
D' modified vapour-gas diffusivity
D_p aerosol diffusivity
H surface heat transfer coefficient
I radiation intensity
k' modified therml conductivity
k_c surface mass transfer rate
k_H total heat transfer coefficient
K coagulation kernal
L latent heat of vaporisation
Le Lewis number
$\dot{m}_v$ mass transfer rate to aerosol per unit volume
n aerosol number density
N total aerosol number density
p total pressure
$\dot{q}_{rad}$ radiation heat loss from droplet
$\underline{r}$ position vector
R droplet or particle radius
$\bar{R}$ mean droplet radius
R_G gas constant
$\dot{R}$ radius growth rate
S supersaturation
S_A molecular sticking factor
S_N source term in aerosol equation
t time
T temperature
T_d droplet temperature
$\underline{v}$ velocity
$\underline{v}_d$ droplet velocity relative to fluid
v_L specific volume of condensate

Greek symbols

α length parameter (eq. (9))
β coefficient of expansion
γ surface tension
λ wavelength
μ molecular weight
ξ heat transfer quantity (eq. (18))
ρ total density
ρ_a density of aerosol
ρ_L density of condensate

Subscripts

E pertaining to equilibrium
g pertaining to gas
N pertaining to nucleation
v pertaining to vapour

THERMAL-HYDRAULIC BEHAVIOUR OF A CONTAINMENT ATMOSPHERE MEASURED IN THE DEMONA AEROSOL EXPERIMENTS

T.F. Kanzleiter
Battelle-Institut e.V.
Frankfurt am Main, FRG

ABSTRACT

The DEMONA experiments which are being conducted in the Battelle Frankfurt model containment (640 m^3 capacity) investigate the aerosol behaviour in a steam/air containment atmosphere under relevant core meltdown accident conditions (late containment failure caused by overpressure). Emphasis is also being laid on investigating the containment atmosphere's thermal hydraulics as these play an important role in aerosol behaviour.

The DEMONA experiments performed so far yielded the following thermal-hydraulic results:

Temperature distribution and steam/air composition of the containment atmosphere may be inhomogeneous. This is in contradiction to the well-mixed-volume assumption which is generally used as a basis for aerosol model computations. Two effects in the experiments were identified to produce an atmosphere stratification which may be very stable over an extended period of time:

- Injection of a medium of lower or higher density into an existing homogeneous containment atmosphere (e.g. steam into an air atmosphere or gas into a steam atmosphere) leads to "filling up" of the containment volume downward from the top or upward from the bottom.

- Diffusiophoretic processes continuing over extended periods of time may also lead to a stratified, inhomogeneous atmosphere or further intensify an existing stratification.

The experiments showed that mixing mechanisms which are due to natural convection often are not strong enough to overcome the stratification effects.

Thermal-hydraulic codes considering inhomogeneity effects are available; verification work is still in progress. The results are used as input for aerosol codes, single-node aerosol codes needing suitable averaged thermal hydraulic data. The further DEMONA evaluation will show what degree of accuracy can be reached in this way and which of the simplifications made appear permissible.

INTRODUCTION, OBJECTIVES

In the assessment of the risks resulting from nuclear power plants, the prediction of aerosol behaviour in the containment during a core meltdown accident plays a central role. The computer codes by which these predictions are being made are mainly based on separate-effect and integral tests on a small scale and under very idealised conditions. To broaden the verification basis of these codes, the DEMONA experiments in the Battelle Frankfurt model containment facility were started. These DEMONA experiments investigate the behaviour of metal oxide aerosols in a steam/air containment atmosphere under relevant core meltdown conditions (late overpressure containment failure) in a subdivided scale-model containment geometry of 640 m^3 volume. Emphasis is also being laid on investigating the containment atmosphere's thermal hydraulics, as these play an important role in aerosol behaviour and its modelling. The present paper describes thermal-hydraulic results of the first DEMONA experiments.

DEMONA TEST FACILITY

The main components of the DEMONA test facility and its main data are depicted in Fig. 1. It should be mentioned that the model containment is built from conventional reinforced concrete (not prestressed) without steel liner. The model containment thus has a certain leak rate, which was measured to be 70 % per day under DEMONA operation conditions.

Although the model containment is a scale model of a real PWR containment (volume scale 1:100), it has almost the same surface-area-to-volume ratio as a full-size plant. This is due to the fact that the model containment is almost "empty" in its interior, while a real PWR is equipped with a lot of steel components. But the major part of the surface area of the model containment is formed by concrete structures which are heated up much slower under accident conditions than the steel structures of the original. To compensate the influence of this effect on the aerosol behaviour, all internal structures of the model containment are preheated prior to the start of each DEMONA aerosol experiment.

TEST CONDITIONS

The DEMONA test programme consists of ten main experiments and additional pretests. This paper deals with the results of

- Pretest V 3 (performed on 14th July, 1983) and
- Main Test A 1 (performed 27th to 30th September, 1983).

Both of these tests were thermodynamics tests without aerosol injection that were aimed at checking the function of test facility and instrumentation under the same thermal-hydraulic conditions as specified for the later DEMONA aerosol experiments. In addition, the Main Test A 1 had the objective to yield experimental data for comparison with the results of thermal-hydraulic model calculations.

Pretest V 3 was the first long-term steam experiment that was performed in the DEMONA facility, starting with steam injection into the cold air-filled (1 bar) model containment. This pretest yielded some interesting thermal-hydraulic findings (see below), but it also suggested a change in the experimental procedure to reach the specified experimental conditions in the existing test facility.

As a result of the findings of Pretest V 3, Main Test A 1 was performed in a sequence of four phases:

1. Expelling of the air initially included in the model containment by steam injection at a pressure level of approximately 1 bar.

2. Heating up of the model containment structures by an atmosphere of pure steam of 1.7 bar pressure (115 °C saturation temperature). At the end of this phase, after approximately two days, all internal concrete structures haved reached a uniform temperature of 115 °C, the outer containment shell and the base mat showing an approximate steady-state temperature gradient from 115 °C at the inner surface to about 60 °C at the outer surface, the steam injection rate reaching a minimum necessary to cover steady-state heat losses and leakage.

3. Injection of a defined portion of air to reach the specified experimental conditions:

Total pressure	3 bar (= 0.3 MPa)
Partial pressure of steam	1.7 bar (saturation temperature 115 °C)
Partial pressure of air	1.3 bar (corresponding to 1.0 bar at 20 °C)

   In later DEMONA experiments, aerosol will be injected together with the air during this operational phase.

4. Steady-state operation under the specified experimental conditions. During this period, aerosol depletion will be measured in later experiments over a period of one or two days.

With minor modifications, this procedure was accepted to be used for the later aerosol experiments. The resulting thermal-hydraulic conditions are considered to be representative of core melt-down accidents.

RESULTS OF PRETEST V 3

Pretest V 3 covered the following steps:

- Steam injection into the model containment initially filled with air at 1 bar
- Discontinuation of the test because of a defect at the model containment by pressure relief and temporary opening of the manhole
- Repated injection of steam until a total pressure of 3 bar was reached
- Constant continuation of the pretest at 3 bar by feeding in additional steam to compensate condensation and leakage
- Tentative additional injection of air shortly before the end of the test.

Fig. 2 shows the measured time histories of the total pressure of the containment and of local partial steam pressures, the partial steam pressures being determined from temperature measurements on the assumption of a state of saturation.

During the first steam injection phase already, a pronounced vertical temperature and steam-content gradient in the model containment appeared, with high steam content in the upper zones and low steam content in the lower zones.

This steam-content gradient persisted throughout the pretest. By the temporary pressure relief and opening of the manhole, a major proportion of the air initially contained in the containment was lost. The amount of air enclosed was further reduced be leakage, so that - after about 6 hours' duration of the prestest - the air was almost completely removed from the upper containment zones. As a result, these zones contained an almost pure steam atmosphere at a temperature which was about 20 K above the desired mean containment temperature and resulted in inadmissibly high loads on the containment concrete structures and their plastics coating. Steam content and saturation temperature in the lowest zone of the containment, on the other hand, were still comparatively low at that time.

Shortly before the end of Prestest V 3, cold air was tentatively injected into the containment through the steam injection pipe instead of steam, the total pressure remaining constant at 3 bar. This did not result in a variation of steam content and temperature in the upper containment zones; in the middle and lower zones, however, these quantities showed a gradual decrease, as can be seen from Fig. 2. This is due to the fact that, due to gravity, the injected air gathered preferably in the lower zones of the containment volume and thus increased the steam-content and temperature gradient between the upper and lower zones.

The findings from Pretest V 3 may be summarised as follows:

- In a plant of technical size, a homogeneous steam/air atmosphere cannot be readily achieved; in general, a vertical temperature and steam-content gradient results. In the present pretest, the temperature in the upper containment zones was about 20 K above the desired mean value, and in the lower zones it was correpondingly lower.

- Injection of a medium of lower or higher density into an existing homogeneous containment atmosphere (e.g. steam into an air atmosphere or air into a steam atmosphere) results in a stratified, inhomogeneous atmosphere.

- The nonuniform temperature and steam-content distribution in the atmosphere leads to nonuniform heating of the concrete structures. This is a very unfavourable starting position for a possible later equalisation of temperature and concentration in the containment atmosphere.

RESULTS OF MAIN TEST A 1

Aerosol codes are normally based on the assumption of homogeneous atmosphere - homogeneous in terms of the thermal-hydraulic state and of the aerosol distribution - in the containment. To approach this ideal at least in the first main aerosol experiments, the mode of operation of the model containment facility was changed in comparison with that in Pretest V 3, and the above-described four-phase procedure was tried in the Main Test A 1.

The time histories of the total containment pressure and of some local partial steam pressures measured in the Main Test A 1 are presented in Fig. 3. During Phase 1 (expelling of air), steam was injected in the middle of the containment. The air originally contained in the model containment was then expelled by the resultant low overpressure through the opened bottom valves. Temperature measurements showed that the steam injected into the containment immediately moves upward and fills up the volume from above. As a result, a sharp front formed between the steam and the air below, which gradually moved downward with time. When a temperature measuring point location was reached, this resulted in a steep rise of the measured signal (see Fig. 3).

As soon as the descending steam front reached the bottom valves, these were closed. In the subsequent Phase 2, the containment pressure was raised to 1.3 bar and kept constant at this value for more than 40 hours by controling the injected steam flow. This phase was characterised by an approximately pure steam atmosphere in the model containment. All the temperature measuring points uniformly indicated saturation temperature, and the containment structures were uniformly heated by the condensing steam.

When stationary structure temperatures were reached in the internal and external walls of the model containment, the steam injection rate required for keeping the containment pressure constant had decreased to a low value (about 10 % of the initial value). This steam injection rate, which served for covering the stationary heat losses, was continued to be used in the further course of the experiment. In Phase 3, a specific volume of air was additionally injected through th same pipe as the steam, and thus the containment pressure was raised to the desired value of 3 bar. It was found that in the first instance the temperatures in the upper containment zones rise - according to the saturation condition - together with the pressure; this means that the upper zones continue to contain pure steam, as can be seen from Fig. 3. The injected steam/air mixture thus first enters the lower zones and later - with increasing reduction of the air-free steam zone by condensation - also the middle zones and finally also the upper containment zones (see Fig. 3). This is the opposite to Phase 1: Injection of an air/steam mixture of higher density into a homogeneous steam atmosphere leads to "filling up" of the containment volume from below. After removal of the original steam atmosphere by condensation, an almost uniform atmosphere finally results, which corresponds approximately to the injected air/steam mixture.

In Phase 4 of the experiment, the containment pressure was kept constant at a value of 3 bar by readjusting the steam injection rate. It was found

that the temperatures and the steam content in the upper and lower zones of the model containment diverge as a function of time. This is due to diffusiophoretic processes: Because of the heat losses, steam is continuously being condensed at the external walls and on the surfaces of the containment sumps from the existing air/steam mixture, whose air content thus increases locally. This, in turn, results in an increase in density, and the mixture which is richer in air descends into the lower containment zones, where the air content further increases by further condensation. As the result of the displacement of an increasing amount of air downward, the steam content and the temperature in th upper containment zones increases continually. This leads to the permanent increase in the steam-content gradient from top to bottom, i.e. to an increasing inhomogeneity of the containment atmosphere.

To facilitate the evaluation of the first DEMONA aerosol experiments (Nos. A 3 and A 4), it is planned to provide the steam injection point in the model containment at a lower level, i.e. in the zones which were enriched with air in Test A 1, in order thus to force homogenisation of the model containment atmosphere. For the future DEMONA aerosol experiments (Nos. A 5 to A 10) with more realistic conditions, on the other hand, the steam injection point will be provided again at the original position.

CONCLUSIONS

- As had been expected, only a pure steam atmosphere shows a uniform temperature distribution.

- In the case of an air/steam atmosphere, diffusiophoretic processes (continuous local steam condensation leading to air enrichment at structures with steady-state heat losses) may result in an increasing vertical gradient of temperature and steam content (stratification) in the containment atmosphere. The existence of effective counteracting mixing mechanisms cannot be assumed to be a matter of course.

- If a medium of higher or lower density is injectd into an existing containment atmosphere, the containment is "filled up" from the bottom or from the top in strata.

- Density stratifications with upward decreasing density formed in the containment atmosphere may be very stable.

- Thermal-hydraulic model calculations assuming a homogeneous containment atmosphere in general do not correspond to reality. If they are used only for the approximative calculation of mean values, e.g. for generating input data for aerosol codes, the limitations resulting from the incorrect calculation of local thermal-hydraulic and aerosol processes have to be carefully observed. Examples:

  — Condensation heat transfer at structures and sump water, affecting both the containment pressure history and aerosol processes.
  — Possible aerosol transport and removal by the diffusiophoretic air/steam separation processes observed.

— Saturation and local oversaturation of the atmosphere affecting the shape and behaviour of the aerosol particles and the generation of droplets.
— Effects of local differences in aerosol concentration on the aerosol removal processes (agglomeration and sedimentation) and the aerosol leak rate.

- Thermal-hydraulic codes considering inhomogenity effects are available, but have not yet been sufficiently verified by experiments. Aerosol codes are still predominantly based on the homogeneous approach using mean values. The evaluation of the future DEMONA experiments will show what degree of accuracy can be reached in this way and which of the simplifications made are permissible or should be modified.

REFERENCES

- W. Schikarski et al., DEMONA-Forschungsprogramm zur Untersuchung nuklearen Aerosolverhaltens, KfK 3636 (1983)

- T. Kanzleiter, DEMONA-Versuche, Kalibrierversuch A 1, Battelle Frankfurt, BIeV-R65.523-30-1 (1984)

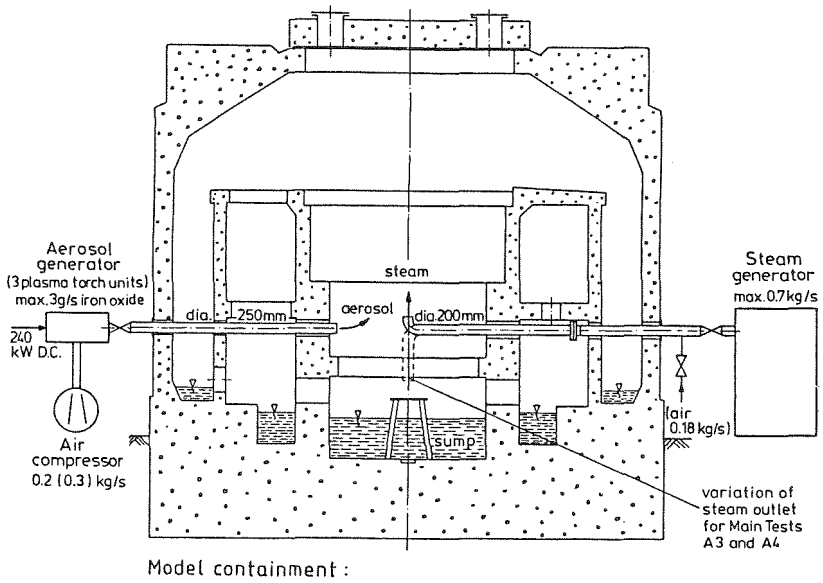

Model containment :

outer diameter		12.1 m
total volume		640 m³
pool surface areas	28 m²	
other horiz. ground surface areas	145 m²	total
ceiling surface areas	165 m²	1056 m²
vertical wall surface areas	718 m	
operational abs. pressure		3 bar
average temperature of cont. atm.		115 °C
maximum aerosol concentration		12 g/m³

Fig.1: DEMONA Test Facility

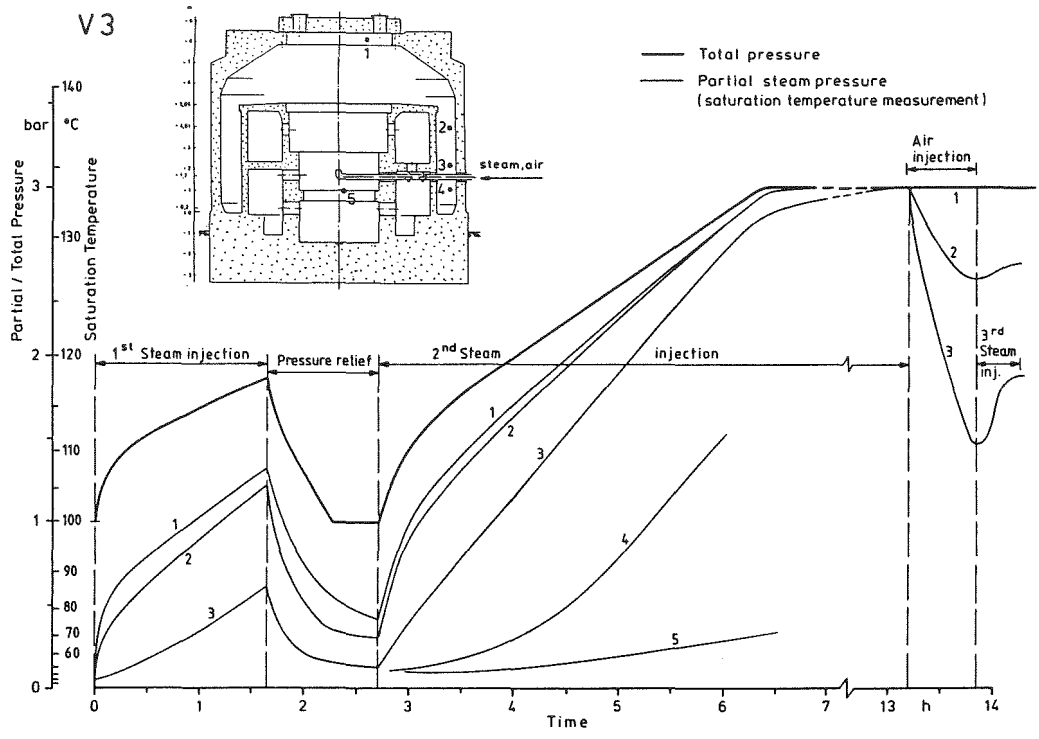

Fig. 2: Pre-Test V3: Steam Distribution in the Containment Atmosphere

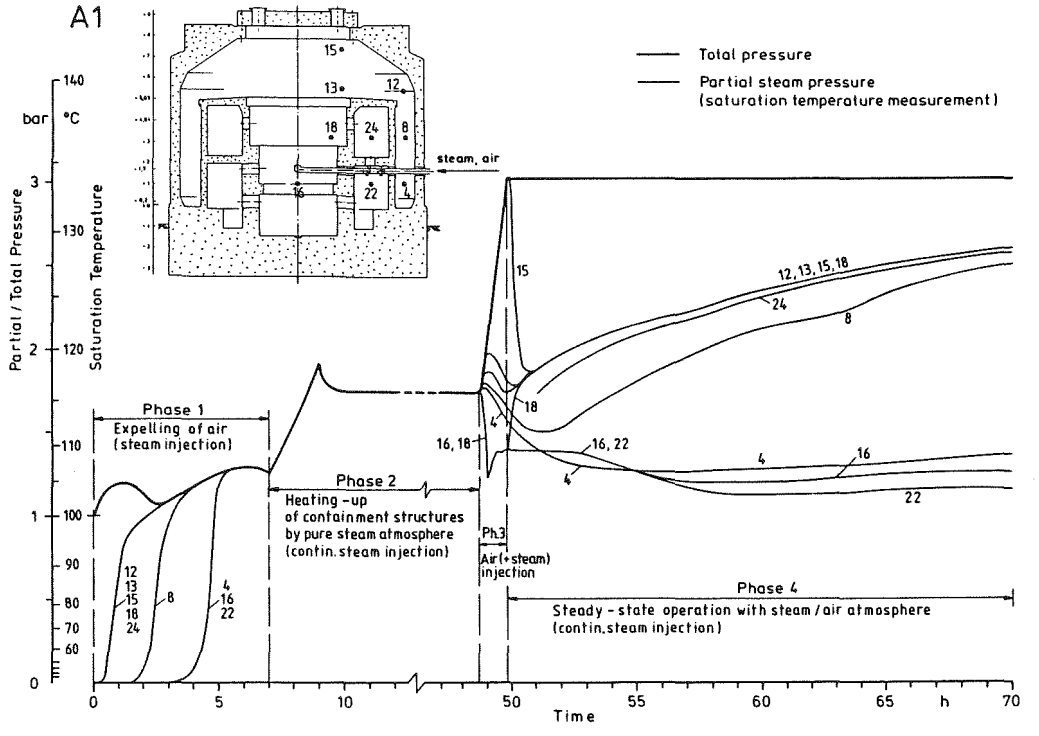

Fig. 3: Main-Test A1: Steam Distribution in the Containment Atmosphere

Predetermination of the Thermodynamical State in the DEMONA-Facility during Aerosol Injection with the Improved Containment Code COCMEL

by

J. Eyink and M. Fischer
Kraftwerk Union AG
8520 Erlangen
Federal Republic of Germany

Specialist Meeting on Nuclear
Aerosols in Reactor Safety,
Karlsruhe, 4. - 6. September 84

ABSTRACT

To calculate aerosol depletion in a wet post accident atmospere, computer codes like NAUA need detailed thermohydraulic data. To meet these requirements the thermohydraulic COCMEL-code, which is a one volume code being widely used for predicting pressure time histories after severe accidents, has been improved by adding new models. This paper describes the models and shows its suitability by some postcalculations of the first DEMONA leakage test (A1). Furthermore, a prediction of the thermodynamical state within the model-containment after injection of aerosols is given. This is important, because aerosols are injected together with a carry gas (air or steam) that has to remove part of the aerosol generators waste heat. Therefore, the injection may change pressure and temperature within the model containment close to design pressure or to values where the instrumentation would no longer work before a sufficient concentration of aerosols might be obtained. It is shown, however, that these problems could be solved by the use of an air-fog resp. steam-fog mixture as a carry gas for the aerosols.

INTRODUCTION

The overall behavior and suitability of the NAUA-code, which has been developed by KfK/LAF 1 during the last years, is going to be demonstrated by the DEMONA experiments at Battelle Frankfurt. NAUA needs, like any aerosol code, thermodynamical data of the atmosphere in which the aerosol-physical processes are taking place. This applies especially to condensation phenomena in the wet post accident atmosphere. However, computer codes developed so far to describe containment behavior after severe accidents, which chiefly means the pressure time history, are not modelled in such detail as to account for a sufficient precise description of condensation phenomena.

The KWU developed computer code COCMEL, a one volume code which is now widely used to predict pressure time histories in a PWR-containment after severe hypothetical accidents,has been improved to satisfy the requirements of the NAUA code. This has been done by adding a heat transfer model developed by IVA-Hannover. With the application of this new model, heat and mass transfer to the walls can be calculated separately. With the additional use of energy balances for the atmosphere, the condensation rate in the volume can be determined. It may than serve as a basis for the prediction of the condensation on aerosols.

In this paper a short description of the heat transfer model is given. Furthermore, a post calculation of one of the first starting experiments of DEMONA (A1) is presented for verification of the code. After that a predetermination of the atmospheric conditions within the Battelle-containment for several different modes of aerosol injection is given

THE CONDENSATION MODEL

In the previous COCMEL code the heat flow to the structures has been calculated by the equation

$$\dot{q} = \alpha \cdot A \cdot (T_a - T_w) \qquad (1)$$

where α accounts for both, the contribution of convection and condensation to the heat transfer. It may be derived for instance from the empirical Tagami-Uchida relation. T_a and T_w are the temperatures of the atmosphere and the wall surfaces resp. and A means the wall area. The mass of the condensed water was being calculated from the energy balance. Thus, one could not distinguish between condensation on the walls and within the volume.

Now, both effects have been separated. The convective heat transfer is still calculated according to equation 1 but with a modified heat transfer coefficient, whereas mass transfer is evaluated using the mass transfer coefficient ß:

$$\dot{m} = A \cdot \frac{ß}{R_s \cdot T_a} (P_s - P_{ssw}) \qquad (2)$$

with

$\dot{m}$	condensation rate (kg/s)
A	surface area of the walls (m^2)
R_s	specific gas constant for steam, based on the actual steam conditions (J/kg K)
T_a	temperature of the atmosphere (K)
P_s^a	partial pressure of the steam in the atmosphere (N/m^2)
P_{ssw}	saturation pressure of the steam for wall temperature (N/m^2)

α and ß are calculated from Nusselt and Sherwood numbers:

$$Nu = \frac{\alpha \cdot L}{\lambda_g} = 0.23 \, (Gr \cdot Pr)^{0.28} \qquad (3)$$

$$Sh = \frac{ß \cdot L}{D_g} = 0.25 \, (Gr \cdot Sc)^{0.28} \cdot 0.76^{P_{H_2}/P_{air}} \qquad (4)$$

with:

L	thickness of the boundary layer (m)
λ_g	heat conductivity of the atmosphere (W/m°K)
D_g	diffusion constant (m^2/s)
P_{H_2}/P_{air}	partial pressure of hydrogen and air, resp.
Gr, Pr, Sc	Grashof, Prandl and Schmidt number, resp.

the condensed water is added to the sump water with a temperature according to the surface of the walls.

POSTCALCULATION OF THE A1 LEAKAGE TEST

To check the overall behavior of the improved COCMEL version, post calculations have been performed for the leakage test experiment A1. The course of the experiment can be devided into several phases (see figure 1 for the time scale):

A: blow-out of the air by steam injection
B: steam injection at a constant pressure of 1.7 bar to reach a steady-state temperature distribution inside the walls
C: injection of hot air in order to raise the pressure up to 3 bar
D: continuous steam injection to compensate for leakage and condensation.

Fig. 1 compares the measured and the calculated feed rate of steam. The latter one was self-controlled by the code to hold the given constant pressure value.

Fig. 1

Comparison of Measured and Calculated Feed Rate for Leakage Test A1

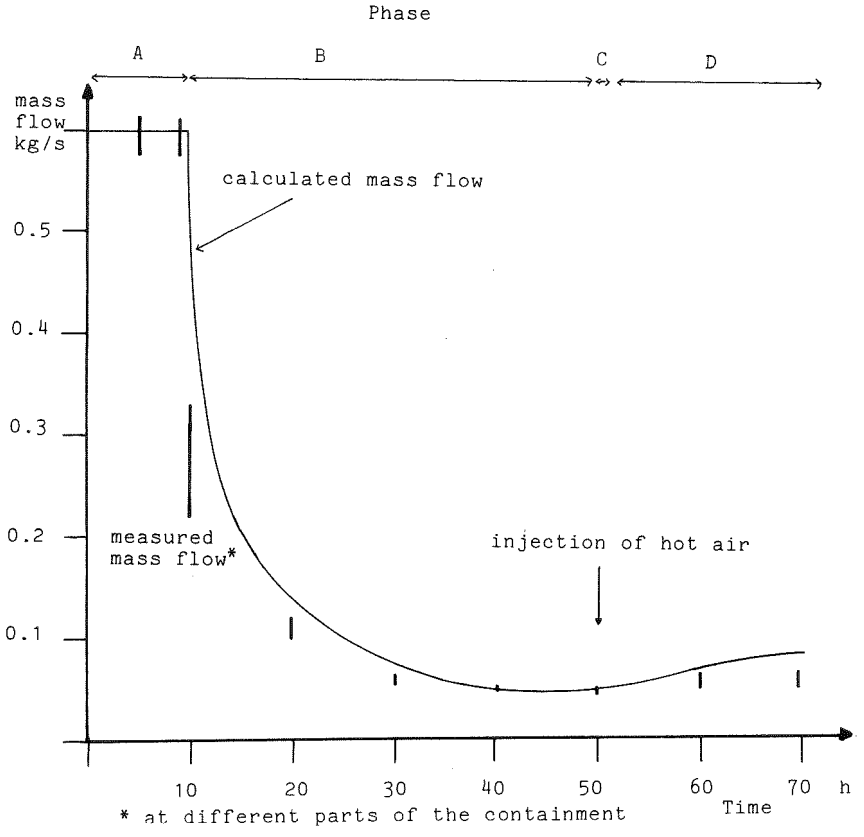

A general agreement can be taken from this figure which means that the condensation model is satisfying. However, the condensation rate on the aerosols has not been measured independently. Thus, condensation phenomena could only be validated on an integral basis. Fig. 2 compares the measured and calculated temperature of the atmosphere.

Fig. 2

Measured and Calculated Temperature of the Containment Atmosphere

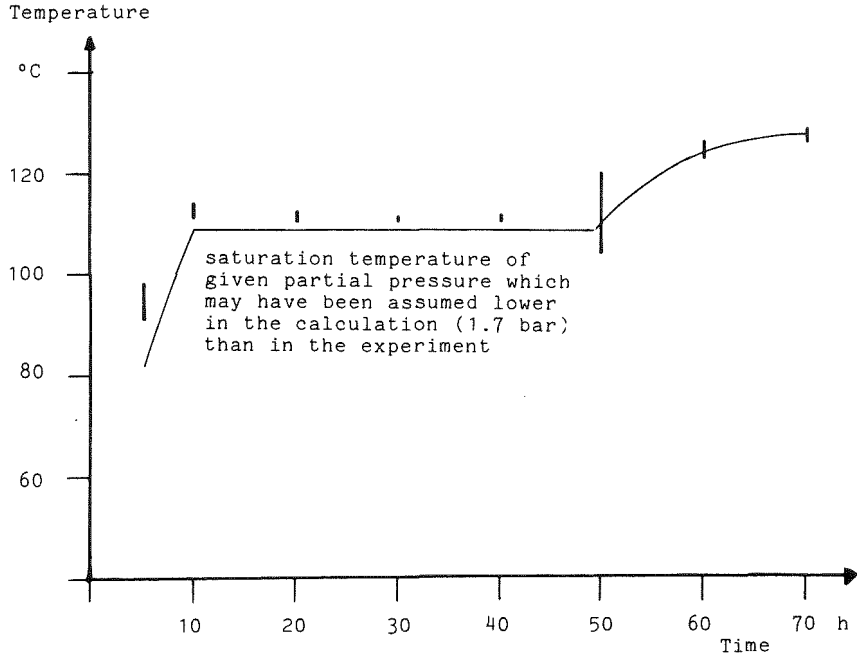

Because of the saturation conditions this temperatures also specify the partial pressure of the steam. So, the agreement of both curves is another indication of the validity of the condensation model.

PREDETERMINATION OF THE THERMODYNAMICAL STATE WITH RESPECT TO AEROSOL INJECTION

For the DEMONA experiment aerosols are produced by vaporizing powdered metal in a plasma torch. They are transported into the containment with air or steam as carry gas. There are several limitations to this gas flow: conditions within the containment atmosphere should not exceed design values for pressure (3 bar) and temperature (135 °C). To obtain

the desired concentration aerosol injection must be maintained over more than one hour and significant depletion within the feed line should be avoided. Therefore the gas-flow must be greater than about 0.1 m^3/s.

The most severe challenge,however, is to cool down the hot plasma gas removing a power of about 120 kW. To check, how these requirements can be satisfied, a set of parametric calculationshas been performed with the COCMEL code to predict the atmospheric state within the DEMONA facility after the aerosol injection. Table 1 shows the most import parameters for a selection of these calculations.

Table 1

Selection of Parametric Calculations to Predict the Thermodynamical State of the DEMONA-Atmosphere after Aerosol Injection

calc. number	carry gas	feed rate / kg/s /
1	air	1
2	air	0.2
3	steam	0.2
4	air/fog	0.15/0.05
5	steam/fog	0.15/0.05

Initial pressure within the containment: 1.7 bar
Thermal heat of the generators to be removed by the carry gas: 120 kW.

A low feed rate (around 0.2 kg/s) of both air or steam will result in an increase of atmospheric temperature well beyond the limitation values tolerated by the instrumentation. On the other hand, a sufficient large increase of the flow rate to about 1 kg/s would cause a fast pressure rise above the design pressure of the DEMONA-building. That means the aerosol concentration would be much to low compared with the concentration that is expected to occur in core melt-down scenarios. To reach such a concentration one expects to need about one hour (gas flow 0.2 kg/s). Table 2 (calc. number 1 and 2) summarizes the results of these calculations.

Table 2

Restriction for Feeding with Air or Steam

pressure: 3 bar, temperature: 135 °C

Calc number	Injection time to reach design pressure / s /	temperature of the containment after injection / °C /
1	700	114
2	3310	154
3	6140	162
4	4740	126
5	9740	132

Thus feeding with pure steam or gas is impossible because the above mentioned limitations will be reached before the aerosol concentration would be high enough. This applies to both, air and steam flow. A possible solution of this problem is the use of a fog-gas-mixture to cool the plasma torch. In this case most of the waste heat of the plasma generator will be consumed to evaporate the water droplets. The aerosols will therefore be transported into the containment by a steam-air-mixture. Table 2 also shows that by taking an air-fog-mixture as carry gas the temperature of the atmosphere will stay low and a sufficient amount of aerosols will be injected as well (calc. no. 4).

Fig. 3 shows the feedrates into the containment for this operation mode.

Nearly 30 % of the initital fog will be evaporated in this particular case. This means that even an increase of plasma generators power will not result in a higher temperature of the feed gas. Starting of aerosol injection Fig. 4 shows the temperature of both, the injection gas and the atmosphere as a function of time.

Fig. 3

Feed Rate into the Containment, Calc. No. 4

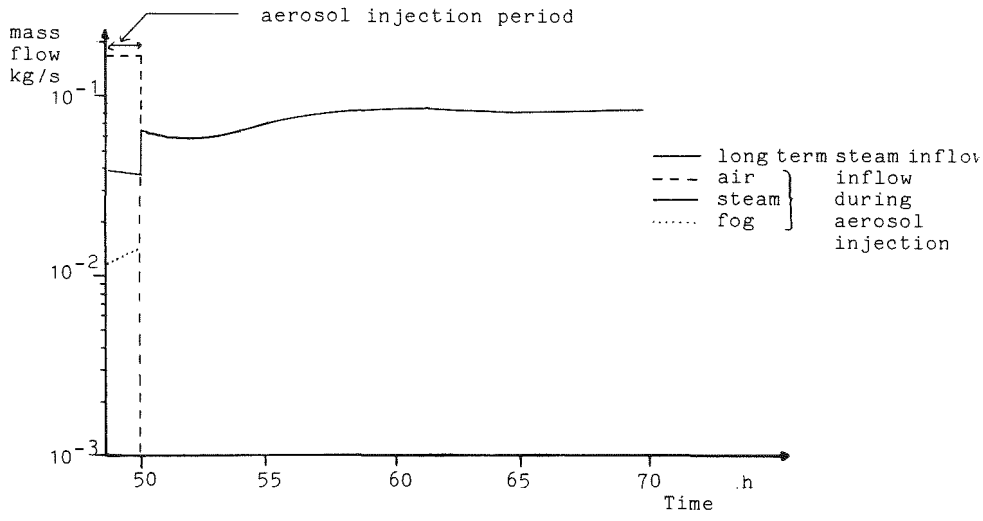

Fig. 4

Temperature of the Injection Gas and Atmosphere

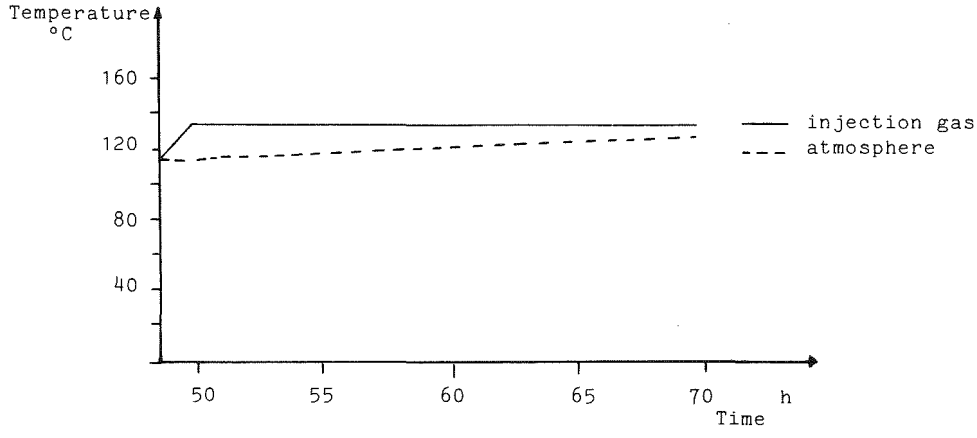

The inlet temperature will never increase the saturation value (133 °C) corresponding to the total pressure (of 3 bar). Therefore a sufficient low temperature throughout the containment is guaranteed. Furthermore, the practicable time period for aerosol injection of more than one hour (see table 2) will fullfill the requirements and may even be increased by passing over to a steam-fog-mixture as carry gas (calc. no. 5). There one has the advantage, that most of the injected steam may partly condensate onto the walls, a process which is highly favored by the reduced amount of inert gas.

Fig. 5 shows the condensation rate on the walls and within the atmosphere.

Fig. 5

Condensation Rate on the Walls and within the Volume

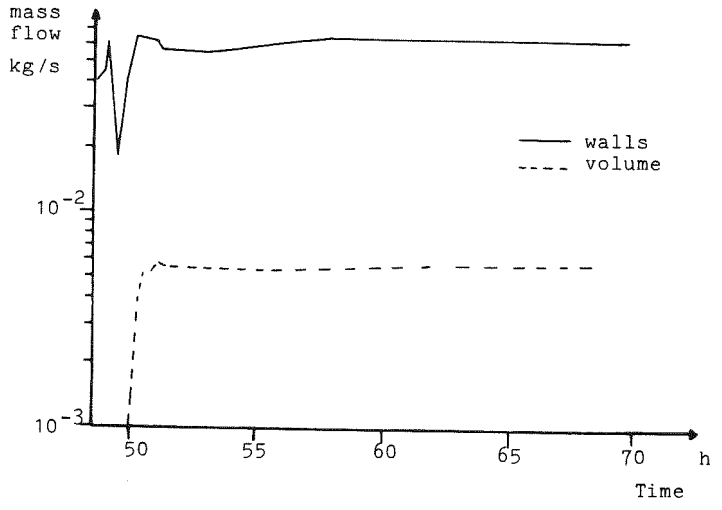

During the injection period the atmosphere becomes superheated and no volume condensation occures. Later with the increase of the noncondensable gas fractions the heat transfer rate at the walls also drops down. Both condensation rates will get back to their steady state values after the end of the aerosol injection.

CONCLUSION

The use of either pure air or pure steam as a carry gas for aerosol injection in connection with the DEMONA experiments is not possible because of the limitation to temperature and pressure within the model containment. However, using an air-fog or a steam-fog mixture to cool the plasma keeps atmospherical state tolerable with the advantage of a low aerosol temperature. Local temperature peaks can thus be avoided. By this method there will be no problem to reach a sufficient high concentration of aerosols within the test facility.

INTEGRATED AEROSOL AND THERMOHYDRAULIC ANALYSIS USING THE CONTAIN CODE*

K. K. Murata** J. L. Tills+, D. C. Williams**,

**Sandia National Laboratories
Albuquerque, NM 87185

+Jack Tills and Associates
Albuquerque, NM

ABSTRACT

CONTAIN is a code designed for integrated analysis of the containment response during severe reactor accident sequences. Features of the code with respect to aerosol and fission product behavior are briefly reviewed. Calculations using the code have been reviewed with respect to the need for integrated analysis in the areas of transport of fission product decay heat, fission product decay chains, and condensation on aerosols. Illustrative examples are presented for fission product decay heat and fission product decay chains. Results from a multi-cell calculation are presented which show substantial local variations in the aerosol concentration. This local variation may be highly significant in the assessment of integrated analysis effects. It is also shown that multi-cell analysis is very important for source term calculations.

*This work was supported by the U.S. Nuclear Regulatory Commission and performed at Sandia National Laboratories which is operated for the U.S. Department of Energy under Contract Number DE-AC04-76DP00789.

INTRODUCTION

The CONTAIN computer code is intended to be the U. S. Nuclear Regulatory Commission's best-estimate tool for the analysis of the thermohydraulic and radiological conditions within the containment building during a severe accident. The code has been under development for a number of years for both LWR and LMFBR applications, and the first version to be made available to the general reactor safety community has been released. This version is designated CONTAIN 1.0 (1).

The CONTAIN code has been developed from the start as a multi-cell code with an integrated treatment of thermohydraulic, aerosol, and fission product behavior. It treats a number of phenomenological areas which historically have been treated separately. Its scope, however, is limited by the fact that it does not treat processes within the primary system or outside of the containment building. The sources to the containment building from the primary system need to be supplied as input to the code. These are typically obtained from various primary system codes. Because of the specification of primary system sources on input, the effects of feedback from containment processes on the primary system cannot be addressed conveniently. However, the effects of feedback from aerosol and fission product processes on thermohydraulic processes within containment can be readily addressed.

The primary purpose of this paper is to present CONTAIN calculations which have implications for integrated analysis. Results for the three areas of integrated analysis which are potentially the most important and for which there are models in CONTAIN are presented. These are transport of fission product decay heat, fission product decay chains, and condensation on aerosols. Finally, to illustrate the importance of multi-cell analysis with respect to the assessment of integrated analysis effects and to the source term, results from a five-cell calculation will be presented. A number of results presented here are taken from the QUEST study (2), which used CONTAIN both for parametric studies and for calculating the final upper and lower bounding cases for the source term.

The aerosol module in CONTAIN is based on the MAEROS code (3) and has been extensively validated (4). The module uses a discrete representation of the particle size distribution and has standard models for aerosol processes, including diffusiophoresis and condensation and evaporation of water on aerosols. Between ten and twenty size classes, or sections, have been found more than adequate for a variety of containment analysis problems. Up to eight aerosol species or components can be independently specified. The particle composition in terms of the components is calculated separately for each size class. Thus, CONTAIN is a multi-component and multi-sectional code.

After thermohydraulics and aerosol behavior, fission product behavior is the third major area of integration in the code. CONTAIN uses a very flexible representation for the fission product inventory. The user may specify the inventory in terms of a combination of individual radionuclides or release groups. The fission products are considered to reside on a number of hosts within each cell. For example each aerosol component is a potential host as are the atmosphere gas, the structure surfaces, and the layers which define the lower cell, or pool, configuration. Radionuclide decay, decay heating, and transport with the atmosphere gases between cells are modeled. Both natural deposition and engineered systems removal of aerosols and the associated fission products from the atmosphere are modeled. The present operational engineered systems are containment sprays, ice condensers, and fan coolers.

A number of potentially significant effects which require integrated analysis are not modeled in CONTAIN. These include the effects of aerosols on radiative heat transport, the insulating effect of aerosol deposits on surfaces, the degradation of engineered systems, and the plugging of leak paths due to deposited aerosol materials. While these effects are currently not modeled, CONTAIN can play a key role in assessing the importance of these effects in the event that the local aerosol and fission product concentrations need to be obtained from a multi-cell analysis.

For a more complete synopsis of the code features, the reader should consult Ref. 5. For details on the models he should consult Ref. 1.

EFFECT OF TRANSPORT OF FISSION PRODUCT DECAY HEAT

After the beginning of core degradation in a severe accident a reasonable fraction of the decay heat may be associated with gaseous and aerosolized fission products released to the atmosphere. In a non-integrated analysis, the transport of these fission products within containment is not known at the time the thermohydraulics calculation is done, and the effects of the transport of the decay heat cannot be incorporated. In CONTAIN, the transport of aerosols and the atmosphere gases automatically results in the transport of the associated fission products and decay heat. For example, the settling of aerosols onto the floor results in the transfer of decay heat from the atmosphere to the floor.

The differences in the temperature and pressure in containment between a non-integrated analysis and an integrated analysis which includes the transport of decay heat can be significant. The comparison below which illustrates this fact is based on a MARCH calculation of a TMLB' sequence for the Bellefonte plant.

Fig. 1 gives the containment pressures for the MARCH calculation and for a number of CONTAIN calculations for Bellefonte TMLB'. MARCH simulates the release of fission products by calculating a fraction of the total decay heat which is assumed to heat the atmosphere directly. This decay heat is left in the atmosphere indefinitely. The CONTAIN calculations used the atmosphere decay power and the thermohydraulic sources calculated by MARCH. By comparing the CONTAIN calculation (CONTAIN-GAS) which assumed that the decay power heats the atmosphere and the one (CONTAIN-NONE) which assumed that no atmosphere decay heating is present, one can see that most of the pressure rise in containment is removed when the atmosphere decay heating is removed. The third CONTAIN calculation (CONTAIN-AEROSOL) shows the effects of assuming that the decay heat is associated with the aerosols. Because of aerosol deposition on structures and the subsequent reduction of heating of the atmosphere, the pressure is substantially reduced at late time. The effects of transport of decay heat are quite significant in this example.

The distribution of decay heat on the structures as a function of time is shown in Fig. 2. The relatively large amount of deposition on the walls is due to the large amount of steam introduced within containment following vessel failure in the TMLB' sequence. Condensation of the steam results in considerable diffusiophoresis to walls.

This calculation should be taken to be illustrative of the effects of transport and not best estimate, since MARCH does not consider the holdup of released fission products in the primary system. The lack of significant holdup which is assumed in the calculations is probably more representative of an AB sequence rather than of TMLB'. Also, both MARCH and CONTAIN consider the fission product heating to be local, whereas the portion due to gamma radiation is long range. The long range heating effects should reduce the effects described above.

EFFECT OF FISSION PRODUCT DECAY CHAINS

Previous fission product transport codes have generally neglected effects of the transformation in the chemical and physical properties of the fission product due to radioactive decay. The effect of such transformations after shutdown is to change slightly the abundance of elements in the total fission product inventory. However, natural deposition and engineered systems removal of fission products from the atmosphere are often quite effective in decontaminating the atmosphere. After a significant amount of decontamination has occurred, the effect of decay transformations may be quite significant in determining the fission product inventory remaining in the atmosphere.

One decay process which may be quite significant is the decay of 78 hour Te-132 into 2.3 hour I-132. The effect of this decay on the suspended radioactivity on containment was evaluated in the QUEST study (2) for the TMLB' base case for the Surry plant.

In the base case almost all of the existing inventory of iodine is released from the fuel prior to vessel failure or shortly thereafter. About 54 per cent of the iodine inventory is released to containment as CsI at vessel failure. Natural deposition processes in containment are quite effective in removing this early iodine. Tellurium, on the other hand, is only partly released in vessel and a substantial amount remains in the melt at the start of the core-concrete interaction. According to the VANESA code (6) the tellurium remaining in the melt during the core-concrete interaction is released slowly over many hours and incompletely, while iodine is released much more rapidly.

The CONTAIN code not only includes explicit representation of decay chains, but also permits reasonably realistic, though non-mechanistic, simulation of the release of tellurium and iodine from the melt. Calculations were performed for the QUEST base case with both the Te-131 and the Te-132 decay chains explicitly included.

When the decay processes are not modeled, the CONTAIN calculations show that very little radioiodine is airborne in the containment at late times. When decay processes are modeled, the decay of Te-132 in the melt to I-132, followed by rapid release of the iodine, can provide a significant amount of I-132 to the atmosphere. The iodine may persist for many hours or even days after the calculations neglecting decay predict the containment atmosphere to be almost entirely depleted of radioiodine.

Results are shown in Fig. 2. Between 7 and 10 hours following reactor shutdown, the I-132 airborne activity is seen to be about 20 MCi, which is roughly equal to the total curies suspended for all other species combined. For other conditions the I-132 effect could be as much as doubled. The figure also compares 8-day I-131 produced by decay of 30-hr Te-131 in the melt with I-131 released from the primary system (which is accounted for in the conventional calculations). These results show that modeling the Te-131 decay is relatively insignificant except at late times.

EFFECTS OF CONDENSATION ON AEROSOLS

In severe accident thermohydraulic codes other than CONTAIN, an ad hoc model is used to describe the removal of any liquid water condensed in the atmosphere. For example, the CONTEMPT code (7) assumes that any liquid formed settles with a fixed time

constant. In the MARCH code (8) the user may specify the fraction of liquid which is removed instantly to the sump; the rest settles with a fixed time constant.

In CONTAIN the user may treat the settling of the liquid water mechanistically within the aerosol module by specifying the liquid water in the atmosphere to be one of the aerosol component materials. Both condensation on and evaporation from aerosol particles are modeled. The rate of condensation and the distribution of the water vapor to particles of different sizes is controlled by the rate of diffusion of the water vapor to the particle. The rate depends on the degree of supersaturation or subsaturation present in the atmosphere.

In this section we give general arguments for the importance of an integrated approach in which the thermohydraulic calculation is done simultaneously with the aerosol calculation and the behavior of the liquid condensed on aerosols is calculated according to aerosol dynamics. We also discuss the fact that CONTAIN calculations indicate that condensation on aerosols is not prevalent after the initial blowdown.

We restrict the present discussion to periods after the blowdown, when the amount of suspended liquid is typically considerably smaller than the amounts encountered during the blowdown. The amount may be on the order of several tens of grams per cubic meter as opposed to 1000 g/m^3. However, such small amounts are significant in terms of aerosol inventory and in determining thermohydraulic conditions if the liquid is evaporating. Under evaporating conditions the role played by the heat of vaporization means that the liquid is much more important than the amount of mass present would indicate.

By not allowing the correct amount of suspended liquid to evaporate under superheating conditions, a non-integrated analysis will in general predict the wrong amount of superheat. The amount of superheat is important in two respects:

1) The shape factors of aerosols is sensitive to the amount of superheat. A small amount of superheat (say 25 K) may reduce the relative humidity to the point where the sphericalization of aerosols observed at high relative humidities (9) no longer occurs. Under nominal conditions, a superheat of 25 K can be removed by the evaporation of 20 g/m^3 of liquid.

2) If condensing conditions follow the period of superheated conditions, the difference in the superheat will affect the amount of water condensed. Consider, for example, the effect of the assumption commonly made in non-integrated analysis that any liquid is removed from the atmosphere as soon as it forms. In this case, if the atmosphere is rapidly superheated and then saturated, one can expect the amount

condensed to be too small by the actual amount of liquid present at the start of evaporation. Therefore, the ability of the non-integrated analysis to predict the correct amount of condensation on aerosols may be lost after a period of superheat.

Fig. 4 is shown to illustrate the differences in the relative humidity which can arise in integrated versus non-integrated analysis. The results in Fig. 4 are from CONTAIN calculations of the AB-d sequence for the Surry plant. The sources to containment are as specified in the Battelle source term study (10) for this sequence. (The substantial differences between the CONTAIN recalculation of this sequence and the MARCH results reported in Ref. 10 are discussed in Ref. 11.) In order to obtain the result labeled "non-integrated" in Fig. 4, the CONTAIN code was run with evaporation from aerosols turned off. With respect to the heat of vaporization, this procedure simulates a non-integrated analysis which assumes that liquid is removed as soon as it forms in the atmosphere.

The water aerosol concentrations in this sequence are rapidly reduced from the maximum of 2640 g/m^3 which occurred during the blowdown to the 34 g/m^3 which is present at the beginning of evaporation in the atmosphere at 15 minutes. Nevertheless, the "non-integrated" result considerably underpredicts the relative humidity as shown in the figure. The difference in relative humidity between the integrated and non-integrated results is 32 % at the start of evolution of the in-vessel aerosols at 27 minutes.

The differences in relative humidity in this example are probably too small to be significant with respect to shape factors. However, because of the rapid settling of the suspended water, the timing of the evolution of the in-vessel aerosols is critical to the magnitude of the differences between the integrated and non-integrated results. The relative significance of the water also depends on the amount of superheat introduced by the hot gases from the core. In other scenarios, the differences in the relative humidity may be significant with respect to shape factors.

With respect to the broader issue of whether condensation on aerosols is important in general, CONTAIN calculations seem to indicate that condensation is not prevalent at times after the initial blowdown when fission products are suspended. The review of a large number of CONTAIN calculations indicates that the conditions in containment are substantially different from those indicated by MARCH (8), which predicts that significant amounts of time can be spent either saturated or close to the saturation point. Most of the CONTAIN calculations involve accident sequences for large, dry PWR's in which the reactor cavity does not reflood and engineered systems are not available. They

indicate that despite allowing for evaporation from aerosols the containment atmosphere is significantly superheated during these periods. Therefore, the potential for condensation and significant effects from non-integrated analysis of condensation on aerosols appears to be small. These effects may occur immediately after the blowdown and during and after special events, such as compartment depressurization and steam explosions.

One conclusion from the QUEST study for Surry TMLB' (2) is that the superheat during the period of suspension of fission products may be large enough to prevent the sphericalization of aerosols which occurs at high relative humidity (9). Fig. 5 shows the relative humidity for the QUEST base case and the changes in the relative humidity due to both a dry heat source and a steam source at rates characteristic of the uncertainties in these types of sources. The relative humidity is in all cases lower at times than the value estimated in the QUEST study (2) for sphericalization.

For the sequences considered, the presence of an unexpected amount of superheat reduces condensation on aerosols from a prevalent decontamination mechanism to one which depends on special events which can be highly scenario dependent. The importance of an integrated approach to condensation on aerosols is obscured by the difficulty in characterizing these events.

EFFECTS OF MULTI-CELL ANALYSIS

The accurate assessment of the effects of aerosols on thermohydraulics may require knowing the local concentrations of aerosols within a specific part of containment. For example, the decrease in radiative transfer due to suspended aerosols is of interest with regard to the heating of overhead structures in a PWR reactor cavity during the core-concrete interaction. On the other hand, the plugging of leak paths by aerosols is of interest primarily in the upper containment. As shown by the multi-cell calculation discussed below, during a period when significant aerosols are being generated by the core-concrete interaction, the aerosol concentrations in both the cavity and the upper containment can be significantly different from what is expected from a single cell model of containment. The calculation also shows that significant local variations in the fission product inventory can be present and that multi-cell effects can either significantly increase or decrease the source term.

The following five cell calculation of a Surry TMLB' sequence was conducted for the QUEST (2). Fig. 6 shows the multi-cell configuration of the Surry plant, including flow paths, used for this problem. Cell 1, with a volume of 1200 m^3, is the cavity compartment and is the point of entry of all radionuclide and aerosol sources. Cell 2 is the basement, and

Cells 4 and 5 are steam generator compartments. Cell 3, with a volume of 33000 m^3, is the upper containment; it includes about two-thirds of the total containment volume and it is from this cell that releases to the environment would most likely occur due to containment leakage and/or failure.

Fig. 7 shows the aerosol mass concentrations in the reactor cavity (Cell 1) and upper containment (Cell 3). The aerosols prior to vessel failure at 157 minutes are composed entirely of water. The sharp reduction in mass concentration at vessel failure is due to the fact that the hot steam and gases released at vessel failure vaporizes these aerosols. They are, however, almost immediately replaced by in-vessel aerosols released to containment at vessel failure. Recondensation of water on aerosols does not occur except in the basement cells. This water is evaporated away relatively quickly and plays a minor role in aerosol processes. The core-concrete interaction which commences in the cavity following vessel failure generates copious amounts of aerosols which dominate the subsequent aerosol behavior in the problem.

The difference between the mass concentrations in the reactor cavity and upper containment after vessel failure is due to the rapid agglomeration and settling of the ex-vessel aerosols, due to the high concentrations in the basement, before they reach the upper containment. Fig. 7 shows that the differences can be almost two orders of magnitude. The results from a single cell calculation are also shown in Fig. 7. The concentrations in the upper containment and the cavity differ by almost an order of magnitude at times from the single cell result. Such differences may be highly significant with respect to the assessment of effects of aerosols on thermohydraulics.

In the QUEST base case, the iodine is released entirely as CsI. The CsI is assumed to volatilize almost completely in vessel, and consequently, almost none is volatilized from the fuel during the core-concrete interaction. The behavior of the airborne iodine is typical of the in-vessel source term. From Fig. 8, it is seen that airborne iodine (present as CsI) in Cell 3 declines more slowly than is implied by the single-cell calculations, with order-of-magnitude differences being present at late times. On the other hand, the amount of tellurium, which is largely released as a continuous source durung the core-concrete interaction, is at least an order of magnitude lower in the upper containment than predicted by the single-cell results. This is demonstrated in Fig. 9.

The tellurium results reflect the relatively low concentrations of ex-vessel aerosols in the upper containment. However, most of the CsI is released from the RCS when the vessel fails and is rapidly carried into the upper containment by the large volumes of gas released at the same time. Since the

ex-vessel aerosols largely agglomerate and settle out before they reach the upper containment, the degree to which they interact with and sweep out the CsI is reduced. In the single cell calculation, the ex-vessel aerosols are assumed to mix with the in-vessel aerosols before they settle out. Hence, the amount of CsI remaining airborne at late times is decreased, relative to the multi-cell calculation. It is evident from this example that multi-cell effects can either increase or decrease the source term by significant factors.

SUMMARY AND CONCLUSIONS

A number of CONTAIN calculations are presented with respect to the implications for integrated analysis. The effects of transport of fission product decay heat, of fission product decay chains, and of condensation on aerosols are discussed in detail. Examples are presented for the transport of fission product decay heat and for fission product decay chains which show that the effects are significant. General arguments are presented which indicate that being able to model condensation and evaporation of water on aerosols simultaneously with the thermohydraulic calculation may be significant. An example is presented which illustrates the effect of this coupling. CONTAIN calculations which address the broader issue of whether condensation on aerosols is important after the initial blowdown are discussed. They seem to indicate that condensing conditions are not prevalent, although they may be present during and after special events. Finally, a multi-cell calculation is presented which demonstrates that significant local variations may be present in the aerosol concentrations in containment. This variation may be highly significant with respect to the assessment of integrated analysis effects which are not modeled in CONTAIN. The multi-cell effects are in addition shown to be able to either increase or decrease the source term by significant factors.

REFERENCES

1. K. D. Bergeron et al, "User's Manual for CONTAIN, A Computer Code for Severe Nuclear Reactor Accident Containment Analysis", NUREG/CR-2224, SAND84-1204, Sandia National Laboratories, to be published.

2. R. J. Lipinski et al, "Uncertainty in Radionuclide Release under Specific LWR Accident Conditions, Volume II: Analysis", (Draft) SAND84-0410/2, Sandia National Laboratories, Albuquerque, 1984.

3. F. M. Gelbard, "MAEROS User's Manual", NUREG/CR-1391, SAND80-0822, (Sandia National Lab., Albuq., NM), Dec. 1982.

4. K. K. Murata et al, "CONTAIN: Recent Highlights in Code Testing and Validation", Proc. Intl. Mtg. on LWR Severe Accident Evaluation, Cambridge, MA (8/28/83 - 9/1/83), p. 5.4-1.

5. K. D. Bergeron et al, "An Overview of the CONTAIN Code for Severe Accident Analysis", NUREG/CP-0048, Proceedings of the Eleventh Water Reactor Safety Research Information Meeting, held in Gaithersburg, MD, Oct. 24-28, 1983.

6. D. A. Powers, Sandia National Laboratories, private communication.

7. C. C. Lin et al., "CONTEMPT4/MOD4: A Multicompartment Containment System Analysis Program", NUREG/CR-3716, (Brookhaven National Lab., Upton, NY), March, 1984.

8. R. O. Wooton et al, "MARCH 2 Code Description and Users' Manual", Draft (December, 1982).

9. R. E. Adams, "Behavior of U_3O_8, Fe_2O_3, and Concrete Aerosols in a Condensing Environment", NUREG/CP-0048, Proceedings of the Eleventh Water Reactor Safety Research Information Meeting, held in Gaithersburg, MD, Oct. 24-28, 1983.

10. J. A. Gieseke et al, "Radionuclide Release Under Specific LWR Accident Conditions -- Volume I: PWR-Large, Dry Containment (Surry Calculations)", BMI-2104 (Draft), Battelle's Columbus Laboratories (1983).

11. J. L. Tills et al.,"CONTAIN Calculations of Severe Accident Sequences at the Surry Nuclear Power Plant", NUREG/CP-0048, Proceedings of the Eleventh Water Reactor Safety Research Information Meeting, held in Gaithersburg, MD, Oct. 24-28, 1983.

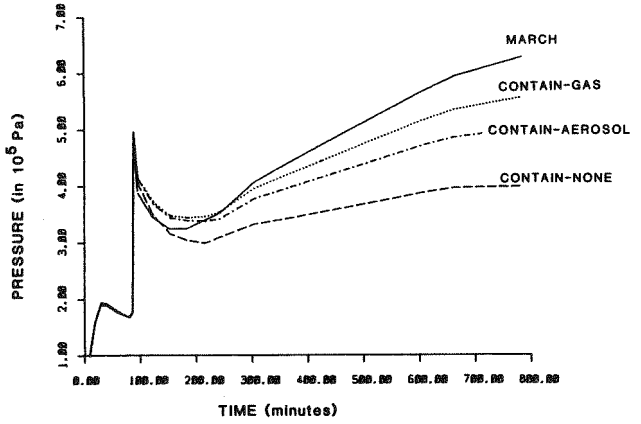

Fig. 1. The containment pressure for Bellefonte TMLB' as calculated by MARCH and by CONTAIN for different heating options.

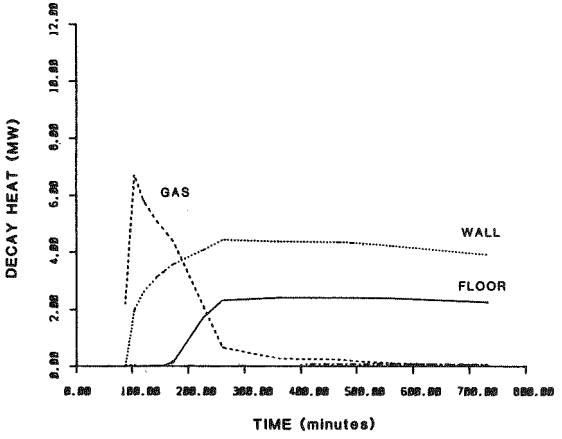

Fig. 2. Distribution of decay heat due to aerosol deposition in the aerosol heating calculation of Fig. 1.

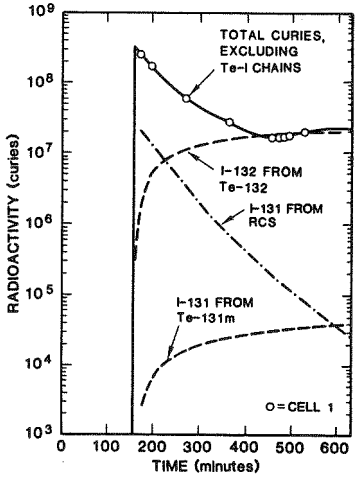

Fig. 3. Comparison of aerosol suspended radioactivity as conventionally calculated with those due to modeling decay chains in the melt.

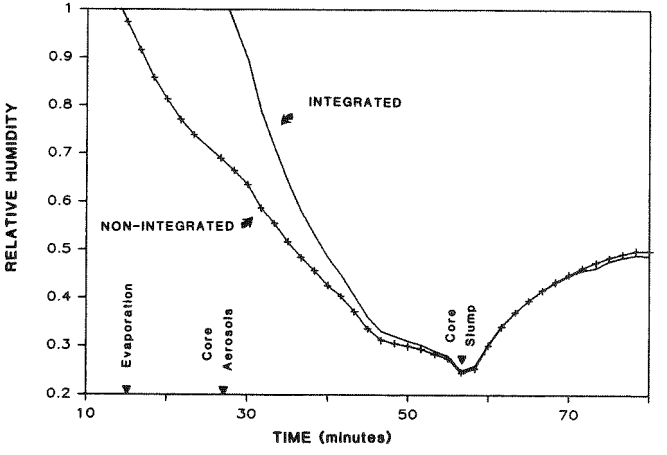

Fig. 4. The relative humidity in the simulated non-integrated analysis of Surry AB compared with that from the integrated analysis.

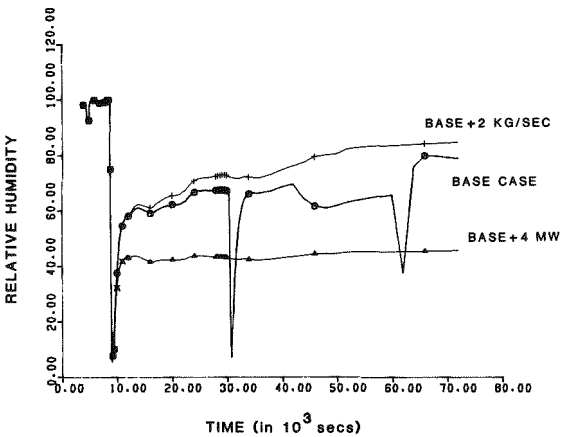

Fig. 5. The relative humidity found in Surry TMLB' and its sensitivity to heat and steam sources.

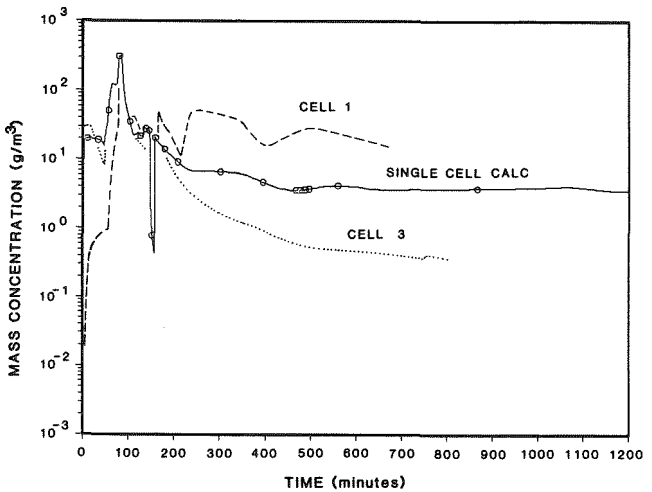

Fig. 7. The aerosol mass concentrations found in the multi-cell and single cell calculations.

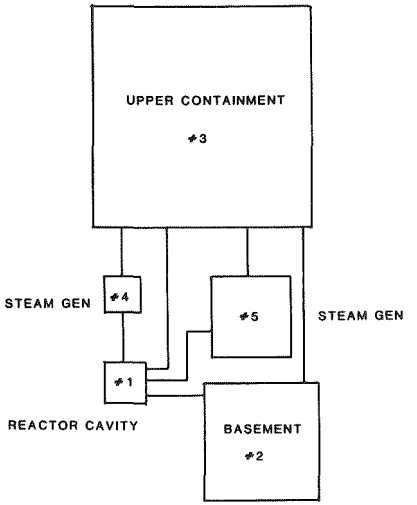

Fig. 6. The five-cell calculation of Surry TMLB'.

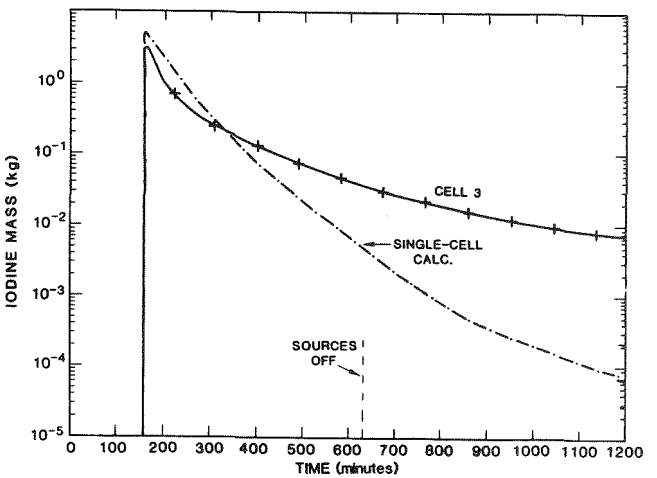

Fig. 8. The suspended iodine in Cell 3 in the multi-cell calculation compared to the amount in the single cell calculation.

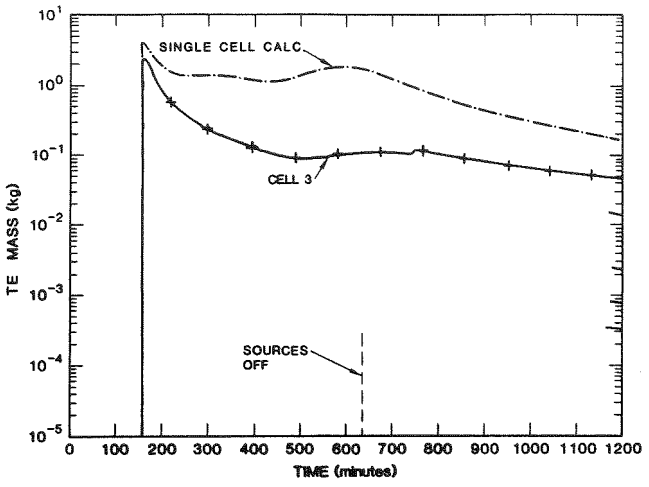

Fig. 9. The suspended tellurium in Cell 3 in the multi-cell calculation compared to the amount in the single cell calculation.

Session IV: Aerosol Measurement and Generation Techniques for Large Scale Experiments

Chair: D. Haschke (EIR Würenlingen, CH)
W. Cherdron (KfK, FRG)

Intercomparison Test of Various Aerosol Measurement Techniques for Sodium Fire Aerosols

S. Jordan, D. Boulaud*, C. Casselman**, W. Cherdron,
J.B. Deworm***, J. P.Mitchell****, V. Prodi*****, G. Tarroni*****

Kernforschungszentrum Karlsruhe GmbH
Laboratorium für Aerosolphysik und Filtertechnik I
Postfach 3640, D-7500 Karlsruhe, W.-Germany

Introduction

During fast reactor accidents aerosols can be formed either by mechanical dispersion of molten fuel and fission products or as a result of combustion of sodium. Sodium fire aerosols will be the major carrier of radioactive species, and will determine the amount of airborne radioactivity available for release via any leaks in the secondary containment during deliberate venting. Therefore, considerable effort has been devoted to study the different sodium fire aerosol phenomena.

The objective of the aerosol measurement workshop was to assess the applicability and reliability of specific aerosol measuring instruments for sodium fire studies. The aerosol experts participating in the exercise agreed to concentrate on the techniques of measuring aerosol particle size distributions. The tests were performed using the aerosol loop at the FAUNA test facility, KfK Laboratory for Aerosol Physics and Filter Techniques. A sodium spray fire was produced under open-loop conditions to give a continuous aerosol source of variable concentration. Measurements performed with equipment from the participating laboratories were evaluated using a standard procedure, enabling an estimate to be made of the accuracy of the experimental data. These results can be used as input data for the mathematical modelling of aerosol behaviour in computer codes, and the work reported here is a contribution to the definition of the radioactive source term for severe accidents in LMFBRs.

Test Loop

The FAUNA facility is shown in Fig. 1. It has a total floor area of about 12 m x 6 m, and consists of a three-storey main building (6 m x 6 m) with a cylindrical test vessel of volume 220 m^3 installed close to the northern wall. The vessel is situated immediately above a room with a floor area of about 6 m x 6 m whose walls form the foundation of the vessel supports. This room can be entered from the main building, and is used to condition and store molten sodium kept under a cover gas.

* CEA Fontenay-aux-Roses, France; ** CEA - Cadarache, France
*** CEN/SCK - Mol, Belgium; **** UKAEA - Winfrith, United Kingdom;
***** ENEA - Bologna, Italy

The facility consists of a fire room, a measuring room, and an aerosol measuring loop. A cylindrical steel vessel of 6 m in diameter and 6 m high with domed ends (volume 220 m^3) serves as the fire room. It can be entered via a circular hatch.

The measuring room is located on the second floor of the FAUNA building. The test vessel is directly accessible from the measuring room via a removable partition. This means that measurements can be undertaken during the tests and that the distances to the measuring instruments are very short. The aerosol mesuring loop is an extension of the original FAUNA facility (Fig. 2). The operating conditions for this loop are as follows: loop length about 80 m; gas flow, up to 20000 m^3 /h; pipe diameter, 700 mm; maximum gas temperature, 75 °C; relative humidity, up to 80 % at 75 °C. The components are accomodated in a separate building adjacent to FAUNA.

The operating conditions within the loop can be set and monitored at a central control panel. The gas flow can be varied between 1000 and 20000 m^3 /h by two speed-controlled axial blowers in series. The two off-gas purification sytems are each equipped with a blower of capacity 4000 m^3 /h. These blowers, which can be operated individually, can be used alone or in combination with the main blower. It is therefore possible to reverse the gas flow in the measuring section by disconnecting the main blower and adjusting the valves. This is of particular advantage because the aerosol can be sampled and analysed before being exposed to the influence of the blower.

A sodium spray fire was chosen as the method of aerosol production in order to keep the mass concentration constant at the sampling points throughout the measurement period. The spray fire offers the following advantages over other methods of sodium fire aerosol generation: a high reaction rate and consequently a low sodium consumption; the ability to change the aerosol yield by appropriate selection of nozzles and spray pressures; ease of clean-up because only small amounts of metallic residue are present; simple design.

Test Conditions

The proposed test conditions were discussed and defined by the participants in the workshop. An important parameter is the aerosol mass concentration which can be varied by changing the gas flow rate in the loop and the aerosol generation rate. Several series of tests were planned in each of which the aerosol generation rate was kept constant. This was achieved by changing the spray nozzle configuration between each series of tests. The aerosol mass concentration was varied within each test series by changing the gas flow rate. The test conditions finally adopted are given in the Table 1.

Exp.	Date	Airborne Na Mass Concentration mg/m³	Gas velocity m/s	Reynolds Number
1	05.10.82	68	6	280 x 10^3
2	05.10.82	230	2	93 x 10^3
3	06.10.82	220	2	93 x 10^3
4	06.10.82	430	1	47 x 10^3
5	07.10.82	1200	1	47 x 10^3

Table 1: Test Conditions

The sodium mass concentration was monitored continuously during all the tests using the sodium aerosol mass monitor (SAMM), developed by KfK/LAF, which was located at the bend of the FAUNA loop. The variation of the sodium mass concentration during the four experiments is shown in Fig. 3. The dotted lines show the original data including fluctuations, the broken lines show the average value for each measurement period, and the solid lines show the smoothed variation of the mass concentration. The SAMM data were checked by either intermittent sampling into a wash bottle followed by the titrimetric determination of the sodium content or intermittent sampling onto an analytical filter followed by dissolution and titrimetric determination of the sodium content.

The temperature and humidity at the sampling points were monitored continuously throughout the tests and are shown in Fig. 4. The residence times of the particles in the test loop were between 40 and a few hundred seconds. Under humid conditions these residence times were sufficiently long for the sodium oxide particles to react with the atmosphere to produce NaOH and Na_2CO_3. The aerosol composition was determined during all tests and most of the particles were found to be solid and to consist of mixtures of NaOH and Na_2CO_3. On the final day droplets were obtained, and it was assumed that only a small fraction of the material was transformed to Na_2CO_3.

Experiments and Results

Six groups from five countries in the European Community participated in the workshop. They used twelve aerosol measuring instruments, of which ten were based on the principle of particle inertia and two provided data evaluated from aerosol photographs. Seven of the instruments were impactors, and the remainder operated under conditions of continuous particle deposition. Details of the instruments are given in Table 2. The various instruments used in the workshop were either calibrated by their user or the manufacturer's calibration was adopted. Fig. 5 gives a schematic representation of the calibration data including the various flow rates used. The effective cut-off size (ECS) which is defined as the aerodynamic diameter of particles which have a 50% probability of penetrating a given stage, was used for data evaluation.

The sodium content of the aerosols was chosen as the basis for the measurement of the mass of aerosol on individual stages. A standard sample of a mixed solution of Na_2CO_3 and NaOH was analysed by each group and

the sodium content was reported. The results are given in Table 3 and can be seen to be in good agreement, indicating that there are very small differences between the sodium analysis data of the participating laboratories.

Country	Sodium (mg Na/l)
Germany	1151
United Kingdom	1130
France	1197 ± 18
Belgium	1140
Italy	1006 ± 32
Mean value	1125
Standard deviation	71.19 (≈ 6.33%)

Table 3: Comparative Sodium Analysis Data

To ensure consistency it was agreed that all groups would use the evaluation program developed by the Italian group. This program enables the experimental data from the different instruments to be compared. The input consists of the cut-off diameters of the impactor stages or equivalent data of the other instruments and the corresponding masses of aerosol sampled. The output gives the mass median diameter and the geometric standard deviation together with graphs of the histogram and the cumulative size distribution by mass plotted against the log normal function on a linear ordinate scale. The log normal function was fitted to the experimental data by means of the least squares method. A subroutine in the data evaluation program enabled the log normality of the measured distribution to be checked using a χ^2 test.

Although the primary objective of the workshop was to determine the particle size distributions of the aerosols, measurements of the sodium mass concentration were also made. Each time an aerosol sample was taken its total sodium content was determined, and the sodium mass concentration was then calculated. The measurements for all the instruments are compared with the SAMM mass concentration data for experiments 3 and 4 (see Table 1) in Fig.6. It should be noted that the SAMM gives mean values of the mass concentration owing to its long time constant, whereas the size-separating instruments which have sampling times as short as 30 s give values which include short-term fluctuations of mass concentration in the pipe. All instruments showed the same trends in the variation of the mass concentration during an experiment, although there was some disagreement among specific values.

The relative standard deviations (S) of the measured AMMDs are given in Table 4. This was only done if at least five out of ten instruments were performing the same measurements under the same conditions. The mean coefficient of variation of the AMMD measurements is 19%, and that for the measured σ_g values is 23%. The χ^2-test for the log normality of the evaluated particle distributions did not fully support or reject assumptions of log normality.

TEM-micrographs were analyzed with a TGZ 3 Zeiss particle counter and an IBAS image analyzer which is an automatic system for the analysis of grey level images. Excellent agreement was found between the data obtained by the two methods.

Discussion

The aerosol mass concentration was monitored using both the SAMM and the light extinction photometer, and the results indicated that many large short-term fluctuations took place. The other instruments sampled the aerosol for discrete periods varying from 30 s to 60 min and provided a single average mass concentration for each period. Comparison of these results with the continuously fluctuating output from the monitors was difficult but it was found that the time-averaged SAMM responses agreed with many of the individual measurements. Occasionally, however, individual results were much higher than the SAMM responses. Some of these discrepancies may have occurred because the time-averaging procedure smoothes out the large concentration increases which in many cases lasted for less than one minute. Unfortunately, the quantity of raw data from the instruments is insufficient to perform a detailed statistical determination of which fluctuations are systematic and which are random. However, it is believed that the time-averaged SAMM data represent all the major long-term aerosol concentration fluctuations since these changes were also detected by the other instruments. The mass concentration results may also have been influenced by a number of systematic factors such as particle losses and instrument handling.

The comparison of the aerodynamic mass size distributions obtained in this workshop is greatly simplified if they can be treated as being log normal since the AMMD and σ_g unambiguously define each distribution. Some of the particle size distributions were log normal but no clear pattern was obtained from any of the instruments used in the workshop. This is not surprising since there is no fundamental reason why these aerosols should have had log normal size distributions.

An important aim of the workshop was to obtain particle size distributions from as many instruments as possible at selected times during each experiment. There were sixteen occasions when most instruments sampled the aerosol at about the same time. The individual AMMD values for each of these occasions were almost always within the 99% confidence limits of the sample mean: the AMMD determined by any one of the instruments was generally within + 20% of the sample mean. Similarily, the individual σ_g values were mostly within the 99% confidence limits of the sample mean: σ_g values varied more widely but were generally within + 50% of the sample mean except for the first experiment when initial experimental difficulties probably accounted for the large spread in the AMMD and σ_g values. In general, the σ_g values for the impactors were greater than those for the spectrometers (spiral duct centrifuge, sedimentation battery and inertial spectrometer). The sample mean AMMDs increased slightly when the aerosol was more concentrated but this was not accompanied by systematic changes in the sample mean σ_g values. The changes in AMMD with increasing aerosol concentration may have been caused by enhanced agglomeration simply because there were more particles present per unit volume. However, it must be

remembered that the air velocity in the loop was reduced at the same time in order to increase aerosol concentration. Under these circumstances an agglomeration mechanism would be expected to produce larger particles simply because the aerosol had more time to age and coagulate before being sampled.

Size distributions obtained by image analysis are not directly comparable with aerodynamic size distributions unless the particles are spherical and their density is 10^3 kg/m^3. There was close agreement between $\overline{d_{vol}}$ and the sample mean AMMD values despite the fact that the particles were non-spherical, presumably because the particle density was greater than 10^3 kg/m^2 and this compensated for the non-sphericity.

Conclusions

The following main conclusions can be drawn from the workshop data:

- There was sixteen occasions when more than five instruments sampled the aerosol at about the same time. The individual AMMDs were almost always within ± 20 % and the σ_gs were generally within ± 50 % of the sample mean values. The occasional large differences in individual results were clearly greater than the random variations and can be attributed to systematic deviations. These differences were particularly evident during the first experiment when participants were developing their sampling procedures.

- All of the instruments used in the workshop produced aerosol data that were consistent and in reasonable agreement. Provided that the AMMDs were within the instrument's range of operation, their magnitude was not influenced by either the width or the resolution of the operating range. However, the σ_gs obtained for the impactors were slightly greater than those obtained for the spectrometers.

- Determinations of the particle size ($\overline{d_{vol}}$) by image analysis of the micrographs agree quite well with the aerodynamic sizes obtained using the other instruments.

- The particles sizes obtained by the two methods of image analysis (Zeiss TGZ 3 particle counter and IBAS image analyser) were in good agreement.

Acknowledgement: The modification and preparation of the FAUNA facility, and the analysis and comparison of the data were sponsored by the Commission of the European Community.

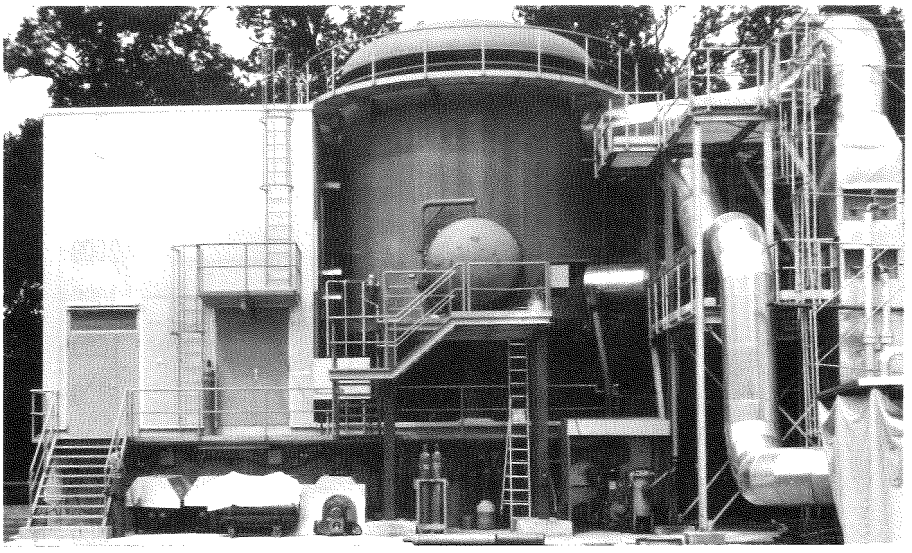

Fig. 1: FAUNA Facility

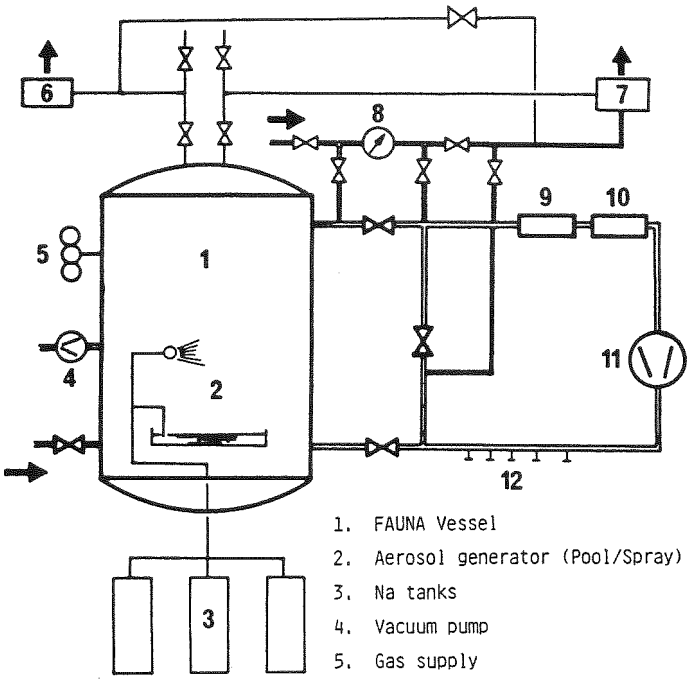

1. FAUNA Vessel
2. Aerosol generator (Pool/Spray)
3. Na tanks
4. Vacuum pump
5. Gas supply
6. Separator (electrostatic filter)
7. Separator (wet cleaning)
8. Gas meter
9. Heater
10. Air humidification chamber
11. Blower
12. Measuring section

Fig. 2: FAUNA Aerosol Loop modified for the EC Workshop

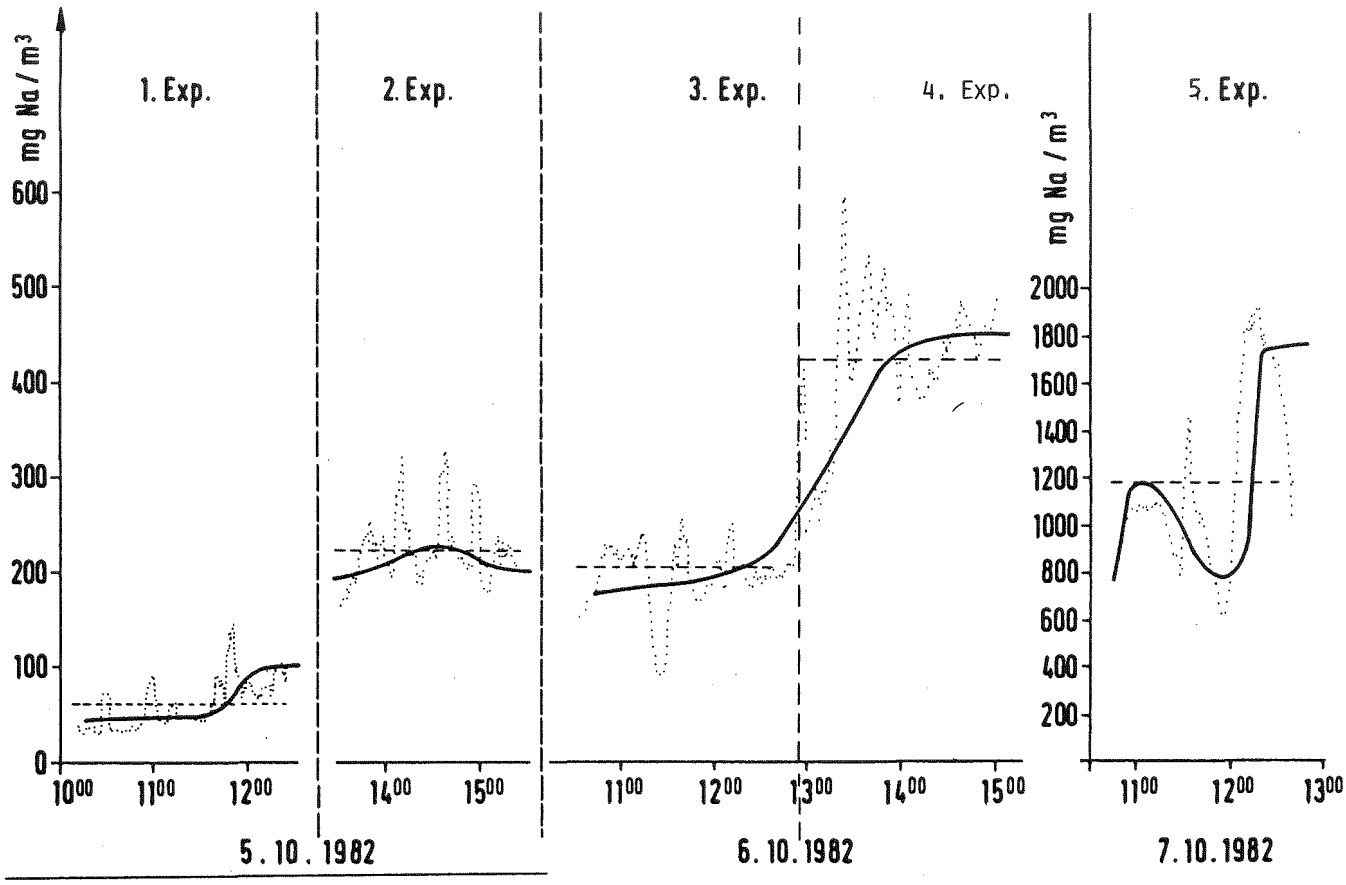

Fig. 3: Sodium Mass Concentration

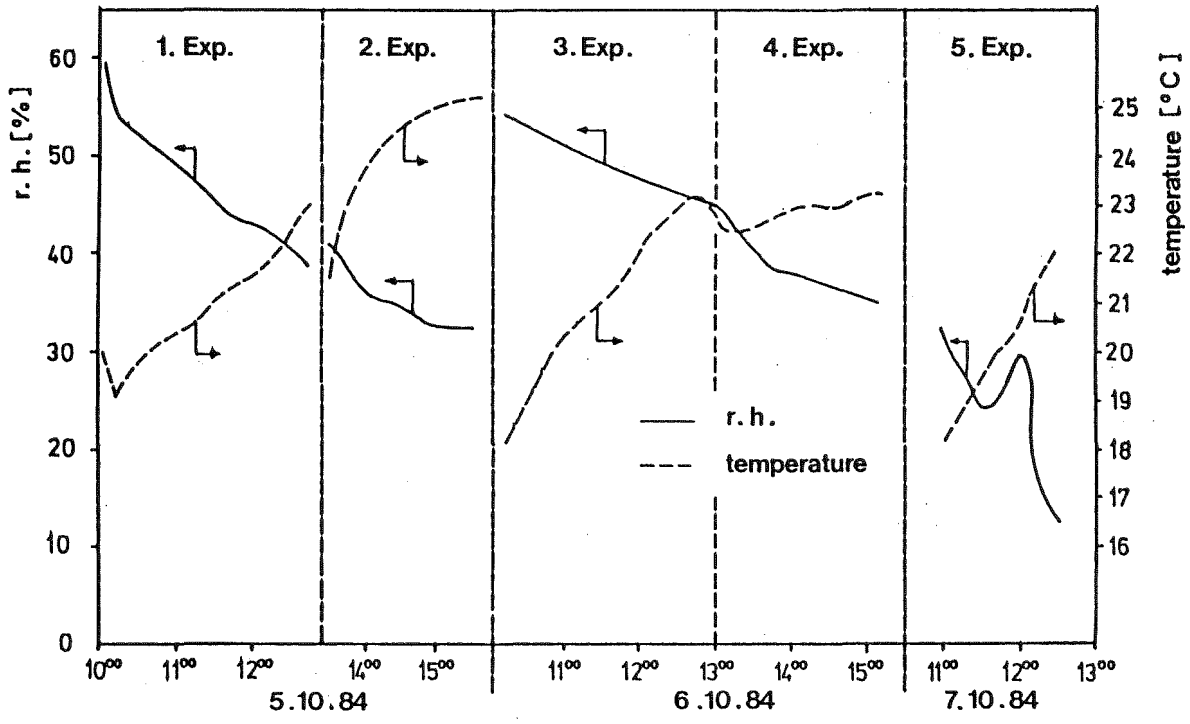

Fig. 4 : **Relative humidity and temperature inside the loop**

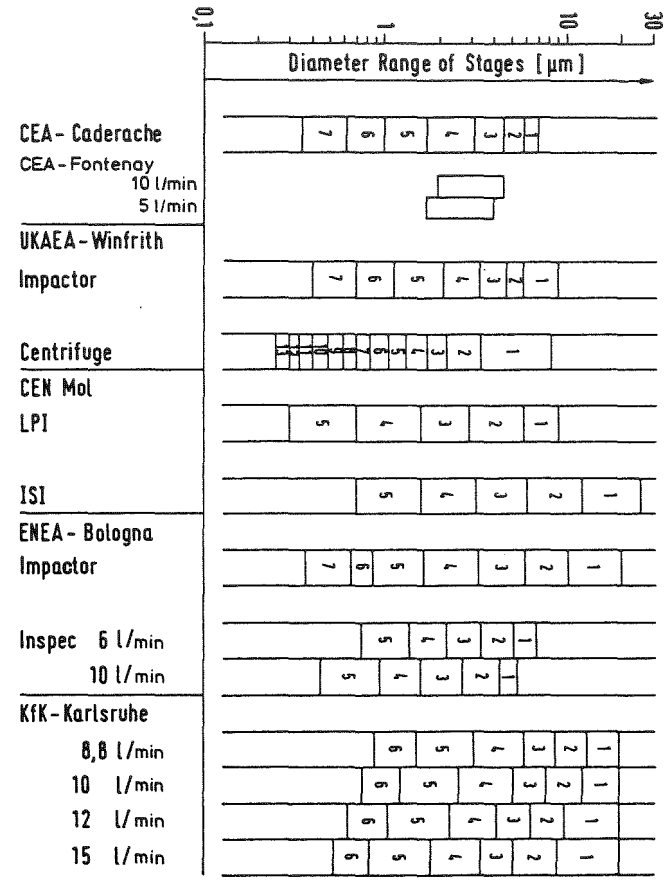

Fig. 5: Calibration Results

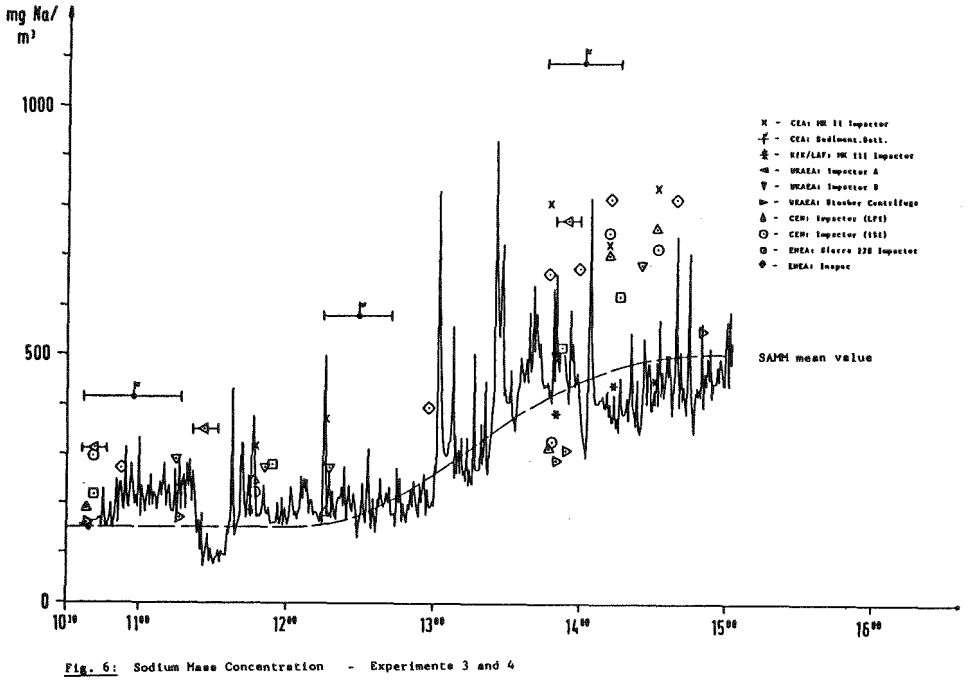

Fig. 6: Sodium Mass Concentration - Experiments 3 and 4

Group	Measuring Instrument	Number of Size Ranges	Collector
CEA-Cadarache	Andersen Mk II impactor	8 + back-up filter	Grease-coated glass plates
CEA-Fontenay-aux-Roses	Sedimentation battery	7 + back-up filter	Stainless steel plates
UKAEA-Winfrith	Andersen Mk II impactor	8 + back-up filter	Stainless steel plates
	Andersen Mk II impactor	8 + back-up filter	Glass fibre
	Stoeber spiral duct centrifuge	15	Stainless steel foil
CEN/SCK-Mol	Low pressure impactor	6 + 3 low pressure	Glass fibre or
	In-stack impactor	6 + back-up filter	cellulose fibre
ENEA-Bologna	Sierra 228 impactor	8 + back-up filter	Glass fibre
	Inertial spectrometer	7	Membrane filter
KfK-Karlsruhe	Andersen Mk III impactor	7 + back-up filter	Glass fibre
	Thermal precipitator and electron micrographs	All	Micrograph evaluation with TGZ 3 counter
UKAEA-Winfrith	Thermal precipitator and electron micrographs	All	Micrograph evaluation with IBAS image analyser

Table 2 : Instruments

Date	Time (h)	Mean AMMD (µm)	$\frac{S}{AMMD}$ %	σ_g	$\frac{S}{\sigma_g}$ %	Number of Instruments
05.10.1982	10.20	1.42	18	1.83	28	5
	11.00	1.75	31	3.27	47	6
	12.00	1.41	28	2.89	56	7
05.10.1982	13.40	1.01	23	1.91	27	7
	14.20	0.96	17	1.91	25	8
	15.00	1.02	21	1.91	27	9
06.10.1982	10.48	1.21	16	1.85	11	10
	11.20	1.20	20	1.84	10	5
	11.50	1.14	16	1.88	19	6
	12.17	1.46	16	1.74	16	5
	13.50	1.40	19	1.83	11	10
	14.15	1.54	14	2.02	19	6
	14.30	1.54	14	2.00	27	6
07.10.1982	10.48	1.50	13	1.76	9	9
	11.20	1.89	16	1.90	18	10
	12.00	1.75	18	1.89	17	9

Table 4: Mean AMMD and mean σ_g values

CALIBRATION OF CASCADE CYCLONE AEROSOL SAMPLER

K. W. Lee, J. A. Gieseke, and W. H. Piispanen

BATTELLE
Columbus Laboratories
505 King Avenue
Columbus, Ohio 43201

ABSTRACT

A four-stage cyclone aerosol sampler has been calibrated. In order to investigate the effects of high temperature and gas viscosity, both air and argon were used as the gaseous medium. The calibration was performed using a series of monodisperse particles. Two different types of particles were used. The first technique involved dioctylphthalate particles produced with a Berglund-Liu aerosol generator combined with fluorometric detection. The second technique was based on the use of commercially available polystyrene latex particles and an optical particle counter.

Particle collection efficiencies of each cyclone stage were measured systematically as a function of particle size and flow rate. Dependency of the 50 percent cut size on the cyclone stage, the flow rate, and the gas viscosity was studied. Comparison of the air with the argon data shows that the cyclone performance depends not only upon the gas viscosity but also on the gas density indicating that the traditional way of correlating cyclone performance using only the Stokes number may not be applicable. A possible correlating parameter which accommodates both air and argon experimental data is discussed.

INTRODUCTION

Small cyclones have recently been introduced as a sampling method for streams which are not suited for inertial impactors or instrumental methods due to high particulate loads or extreme gas conditions. The use of a multi-stage cyclone train allows size determination of relatively large quantities of particulate or aerosols.

Generally cyclone performance is based on theories which include centripetal force equations along with viscous drag and turbulent flow effects. Based on the cyclone dimensions and the gas flow rate a particle size efficiency can be predicted which is proportional to the square root of the ratio μ/Q where μ is gas viscosity and Q is gas flow rate.

In experimental work by Chan and Lippman (1977), an investigation of small sampling cyclone dependence on sample flow rate provided an equation fit of $D_{50} = kQ^n$ where D_{50} is the aerodynamic diameter of particles with a collection efficiency of 50 percent at a given flow rate Q. The parameter k is based on physical dimensions of the cyclone and n represents the exponent which according to theory should be -0.5. In the empirical fitting of 11 cyclones, the value of n varied from -0.636 to -2.13. Consideration of turbulence suggested that from -0.75 to -1.25 indicate a transition point to more turbulent flow regimes.

In the development and calibration of a standard series cyclone sampling train of the same design as used in this study, Smith, Wilson, and Harris (1979) applied the $D_{50} = kQ^n$ relation to develop calibration constants for the various cyclones. Calibrations were conducted at three flow rates of 7.1, 14.2, and 28.3 l/min and with three air temperatures of 25, 93, and 204 C. Tests with particles having densities of 2.04 g/cm^3 and 1.09 g/cm^3 were also included. The collection efficiencies and D_{50} values were reported as equivalent aerodynamic diameters. For cyclones numbered 1, 3, and 5 (in order of decreasing cyclone size), the reported values of n and k were as follows:

Cyclone	1	3	5
n	-0.63	-0.84	-1.11
k	44.6	22.7	14.0

By plotting the D_{50} versus the calculated gas viscosity, the data showed a linear relation between the two parameters with the steepness of the slope of cyclone 1 the largest, and of cyclone 3 the smallest. Viscosities of 183, 214, and 259 micropoise were used and the results were plotted using a linear regression. These results indicated a direct proportionality of gas viscosity to D_{50}.

CALIBRATION PROGRAM

The commercially available Sierra Cyclone Sampling Device was to be applied in a test program for sampling aerosols in a high temperature steam/N_2 environment. Following the redesign of the original sampling train to the configuration

as shown in Figure 1, it was decided to conduct a program of calibration checks using aerosols at ambient temperature. In order to evaluate the effects of gas viscosity for extrapolation of the calibration to high temperatures, the calibration was performed with different gases. Argon and air were chosen such that the gas viscosity could be adjusted between approximately 180 and 210 micropoise.

For the calibration program, two particle generation systems were used. Both systems were able to be connected directly to a 45 x 45 x 60 cm Plexiglas chamber from which samples of the aerosol were extracted through the individual cyclones. A schematic of the calibration setup is shown in Figure 2.

Two different techniques were employed to generate monodisperse particles. The first technique is the vibrating orifice aerosol generation method using the Berglund-Liu generator and the second is based on the use of commercially available monodisperse particles.

The Berglund-Liu aerosol generator was used with 0.98 g/cc density DOP (dioctylphthalate) particles. The size range for particle generation is generally between 1 μm and 20 μm. For these calibrations the DOP was tagged with uranine dye. Following approximately 15 to 20 minutes of sampling, the cyclone and a final filter placed at the cyclone exit were washed with acetone. This solution was analyzed to determine the mass concentration of particles using a Turner fluorometer. The particle collection was calculated for the three volumetric flow rates through the cyclone/filter assembly. The volumetric flow rate was monitored using a hot wire anemometer after the filter. All calibration points were replicated and in cases where replicates were significantly different, additional measurements were performed.

The second used Polystyrene Latex (PSL) solid particles. These particles were generated with a standard nebulizer. As shown in Figure 2, both upstream and downstream sampling points were used to measure the percent particle collection. A Royco 245 optical particle counter was used to monitor the two streams. Care was exercised in assuring that all line losses were either minimized or equalized by using short tubes with equal lengths and equal diameters.

Calibrations were conducted at three flow rates. The nominal or baseline flow rate was specified as that flow rate which would provide a D_{50} cut point of 15 μm in the first (280-10) cyclone. Based on the manufacturer's data, this was calculated to be as shown in Table 1.

The other flow rates would represent 70 percent of the nominal flow and 150 percent of nominal flow. Each cyclone and the probe was to be calibrated individually in the vertical position. Multiple samples were to be included in order to provide a well defined plot of collection efficiency versus particle size. The system also included two mass flow meters. A wet test meter and a gas meter were used to calibrate the mass flow meters. All calibrations were conducted at ambient temperature/pressure using either air or argon. A light bulb in the chamber, as shown in Figure 2, provided a source of low heat to maintain noncondensing conditions.

RESULTS OF CALIBRATIONS

The results of each of the cyclone calibrations for air and for argon were plotted on log normal graphs as efficiency versus D. The results showed that for 13 l/min of argon (viscosity = 2.1 x 10^{-6} kg/ms) the D_{50} of cyclone 280-10 is 15 μm. The D_{50} value for air was slightly less at this flow rate and the manufacturer's data indicated a flow rate of 11 lpm air would provide a D_{50} of 15 μm. While all of the results showed typical responses, the curve for 280-10 cyclone was not as well defined as the other three cyclones.

The other three cyclones showed typical cyclone responses except for occasional outlying data points. In general the agreement between solid and liquid aerosol measurements was very good. It was noted that there was no evidence of particle bounce for solid or liquid particles as shown in the 100 percent collection efficiencies for cyclone 280-5. The results of the D_{50} as calculated from the curves are included in Table 2.

The data as presented in Figures 3 are a composite of flow rate versus D_{50} for all of the cyclones. The two notable points from this figure are (1) the different shape of the 280-10 cyclone curve and (2) the fact that the D_{50} for air is higher than that for argon for the cyclones numbered 1, 3, and 5. This latter effect can be better illustrated by Figure 4 where the data for air and argon are plotted as viscosity for the two cyclones, 280-1 and 280-5. These results imply that for increasing viscosity there was a decrease in the particle cut diameter.

In actual design calibrations by Smith, et al (1979), the D_{50} versus air viscosity was shown as a direct relationship when air viscosity was calculated by $\mu = T^{2/3}/(0.068T + 7.8)$. Therefore with increasing temperatures the D_{50} increased. The data were presented up to only 260 micropoise (204 C) but data by Parker, et al (1981) showed a similar trend at least up to 352 C. In Parker's work however, when effects of increasing pressure were included it was concluded that these cancelled out temperature effects and therefore the observed change in cyclone efficiency may be more dependent on gas density.

DISCUSSION OF RESULTS

In analyzing the results of the cyclone calibrations it is important to consider factors which can have a significant effect on predicted operation. Two important aspects of particle collection are the centripetal and settling velocities. The following values were calculated using results from Smith, et al (1982) for the ratio of particle settling velocity to particle centripetal velocity, Vs/Vc, and for Stokes number, $\sqrt{Stk}$, as listed in Table 3.

Another factor which affects cyclone performance is the gas density. In a sensitivity analysis of cyclone performances by D. W. Cooper (1983), gas density was shown to affect cyclone performance as the fourth ranked factor in absolute (though negative) elasticity (behind diameter, diameter ratio, and gas flow -- also negative). Viscosity was of medium magnitude and equivalent to particle density in the elasticity model.

A final consideration in the analysis of cyclone performance is the Reynolds number, Re. Parker, et al (1981) have shown a correlation of D_{50} versus $Re \cdot Stk^{0.5}$ and included data of Smith, et al (1979). It was concluded that both Reynolds number and the gas flow pattern in the cyclone are important in determining performance.

In a further analysis by Beeckmans (1979), a linear regression analysis of cyclone data resulted in a relationship described as $D = f(Re^b Stk^{0.5})_{50}$ for calibrations performed with constant particle size and varying flow rates. It was therefore concluded that the inclusion of gas density and Reynolds numbers may be important in predicting performance.

ANALYSIS OF RESULTS

The results of the calibrations as reported in Table 2 are somewhat different than the values expected using the manufacturer's relations of $D_{50} = kQ^n$. The deviation from the expected is especially notable in cyclone 280-3 where the difference of calibrated to expected is greater than 1 μm. For cyclone 280-5 the deviation is most pronounced at the low flow rate (1.2 μm expected, 3.4 μm calibrated). Cyclones 280-1 and 280-10 show good agreement between expected and calibrated values at all three flow rates.

In a further analysis of the cyclone performance, the effect of Reynolds numbers on particle collection efficiency was investigated. The Reynolds number (Re) was calculated as $Re = \rho \bar{V} D/\mu$ where,

ρ is gas density (g/cm^3) air = 1.206×10^{-3}, Ar = 1.664×10^{-3}

μ is gas viscosity ($g/cm \cdot s$) air = 1.84×10^{-4}, Ar = 2.15×10^{-4}

$\bar{V}$ is average linear velocity (cm/s) calculated as cyclone flow (Q) divided by inlet $\pi(DIN)^2/4$

D is exit diameter (cm)(DEX).

The values of DIN and DEX are listed in Table 4.

The values of the Reynolds number for each cyclone at the three flow rates of air and argon are reported in Table 5. The results show that based on Reynolds number the flow for cyclone 280-5 is apparently turbulent while cyclone 280-10 is laminar. Cyclones 280-1 and 280-3 are in a transition regime.

A "modified Stokes number" = $\rho D \bar{V}^{1.5}/\mu^{1.5}$ was calculated. These values are listed in Table 6. The results from both Tables 5 and 6 have been plotted as a function of particle D_{50} in Figures 5 and 6.

In Figure 5 the correlation is quite linear with inverse relation of Reynolds numbers to cut diameter, D_{50}. The results of Figure 6 are not as well defined as Figure 5 but a correlation is possible except for an apparent break from a straight line at the low flow rates for cyclone 280-10 and the outlying points for low flow rates in cyclone 280-5.

CONCLUSIONS

The results of these calibrations indicate that parameters other than flow rate and viscosity affect cyclone collection efficiency performance. Gas density possibly through the Reynolds number may be more important in predicting performance. The performance of the cyclones showed a deviation from the expected results at higher Reynolds numbers for both air and argon. The cause of this deviation is unknown. Further work using higher viscosities and other gases will be necessary to provide additional data to develop better correlations of Re to D_{50} values.

REFERENCES

Beeckmans, J. M., "Analysis of the Cyclone as a Size Selective Aerosol Sample", pp 56-65 in Aerosol Measurement, D. A. Lundgren, et al, Editors, University Press of Florida, Gainesville, Florida (1979).

Chan, T. and Lippman, M., Env. Sci. & Tech., 11, 377 (1977).

Cooper, D. W., Atmos. Env., 17, 485 (1983).

Parker, R., Jain, R., Calvert, S., Drehmel, D., and Abbott, J., Env. Sci. & Tech., 15, 451 (1981).

Smith, W. B., Wilson, R. R., Jr., and Harris, D. B., Env. Sci. & Tech., 23, 1307 (1979).

Smith, W. B., Cushing, K. M., Wilson, R. R., and Harris, D. B., J. Aerosol Sci., 15, 259 (1982).

Table 1. Calculated Cyclone Cut Points

T_{gas} (°C)	Viscosity* (poise)	Calculated Cyclone D_{50}'s (μm)				Flow (al/min)
		280-10	280-1	280-3	280-5	
200	174	15	8.8	2.4	1.17	10.3
300	214	15	8.1	2.7	0.76	19.8
350	235	15	8.2	2.9	0.69	23.9
400	255	15	8.4	3.1	0.65	27.7
450	275	15	8.6	3.3	0.63	31.1
500	295	15	8.9	3.4	0.62	34.4

*Viscosity calculated at T_{gas} for 97 percent H_2O + 3 percent N_2.

Table 2. Cut Diameter (D_{50}) for Cyclone Calibrations

Flow Rate	Stage	50% Cut Size, μm	
		Air	Argon
9.1 lpm	280-10	17	16.5
	1	11	9
	3	9.5	2.9
	5	3.3	0.9
13 lpm	280-10	13.0	15
	1	8.0	5.8
	3	3.8	1.6
	5	1.1	0.7
19.5 lpm	280-10	10.0	11.0
	1	6.5	4.7
	3	3.2	1.4
	5	0.74	0.58

Table 3. Operating Parameters of Cyclones

Cyclone	Q (lpm)	Vs/Vc	$\sqrt{Stk}$
280-10	11.4	0.6	0.2
280-1	28.3	1.6×10^{-2}	0.2
280-3	28.3	1.3×10^{-3}	0.1
280-5	28.3	1.6×10^{-5}	0.1

Table 4. Parameters Used to Calculate Reynolds Numbers in Four-Stage Cyclone Train

Parameter	Units	Name	Cyclone Number			
			280-10	280-1	280-3	280-5
Inlet diameter	cm	DIN	1.83	1.27	0.75	0.30
Outlet diameter	cm	DEX	2.17	1.5	0.83	0.36

Table 5. Reynolds Numbers Calculated for Four-Stage Cyclones (x 10^3)

Cyclone Number	280-10		280-1		280-3		280-5	
Gas	Air	Ar	Air	Ar	Air	Ar	Air	Ar
Flow Rate = 9.1 lpm	.820	.968	1.18	1.39	1.87	2.21	5.06	5.98
Flow Rate = 13.0 lpm	1.17	1.38	1.68	1.99	2.67	3.15	7.23	8.54
Flow Rate = 19.5 lpm	1.76	2.08	2.52	2.98	4.00	4.73	10.8	12.8

TABLE 6. Modified Stokes Number Calculated for Four-Stage Cyclone (x 10^6)

Cyclone Number	280-10		280-1		280-3		280-5	
Gas	Air	Ar	Air	Ar	Air	Ar	Air	Ar
Flow Rate = 9.1 lpm	.459	.501	.950	1.04	2.55	2.79	17.3	18.9
Flow Rate = 13.0 lpm	.784	.856	1.62	1.77	4.36	4.76	29.5	32.2
Flow Rate = 19.5 lpm	1.44	1.57	2.98	3.25	8.00	8.74	54.2	59.2

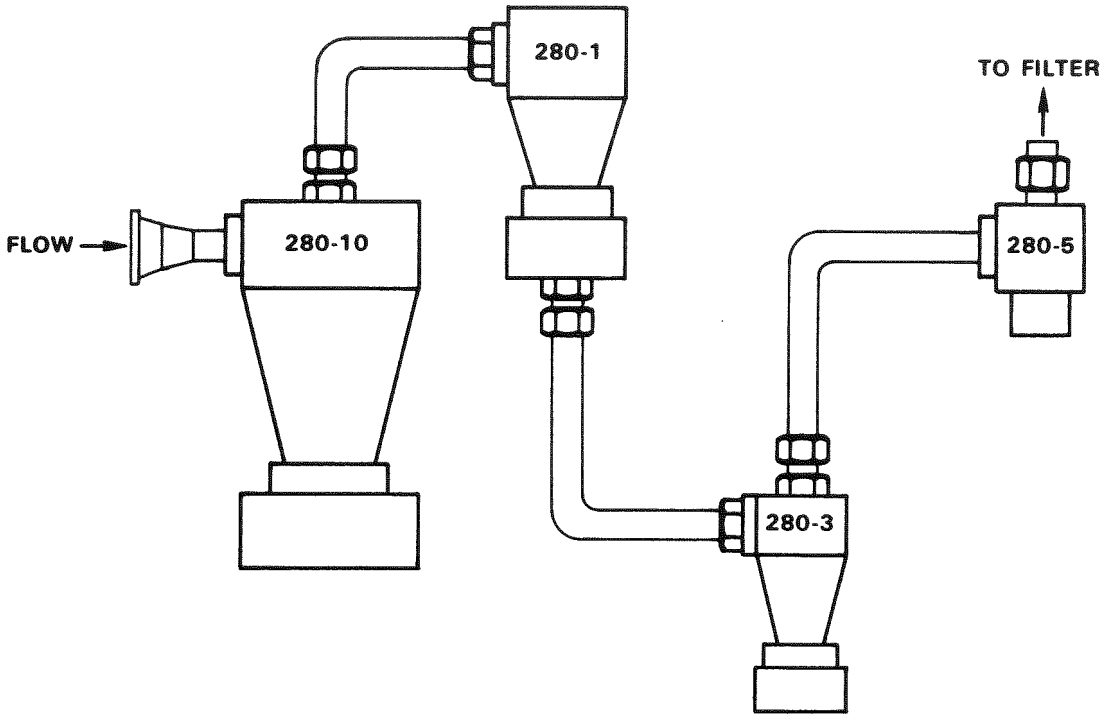

Figure 1. Marviken Aerosol Sampling Cyclone Train

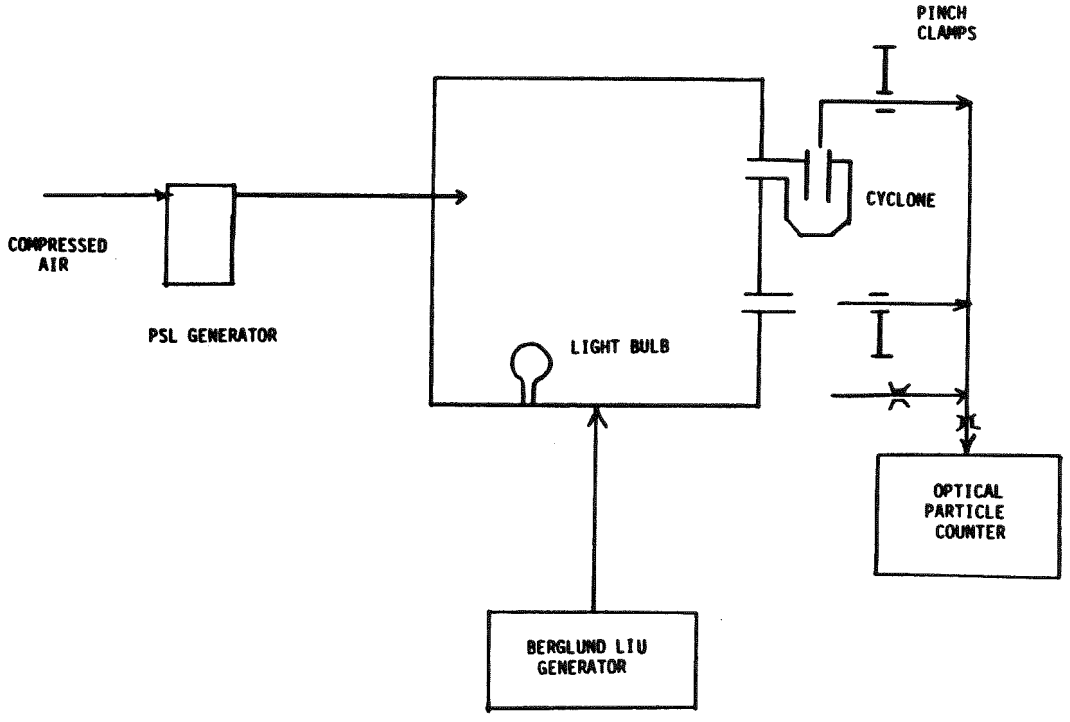

Figure 2. Aerosol Calibration Schematic

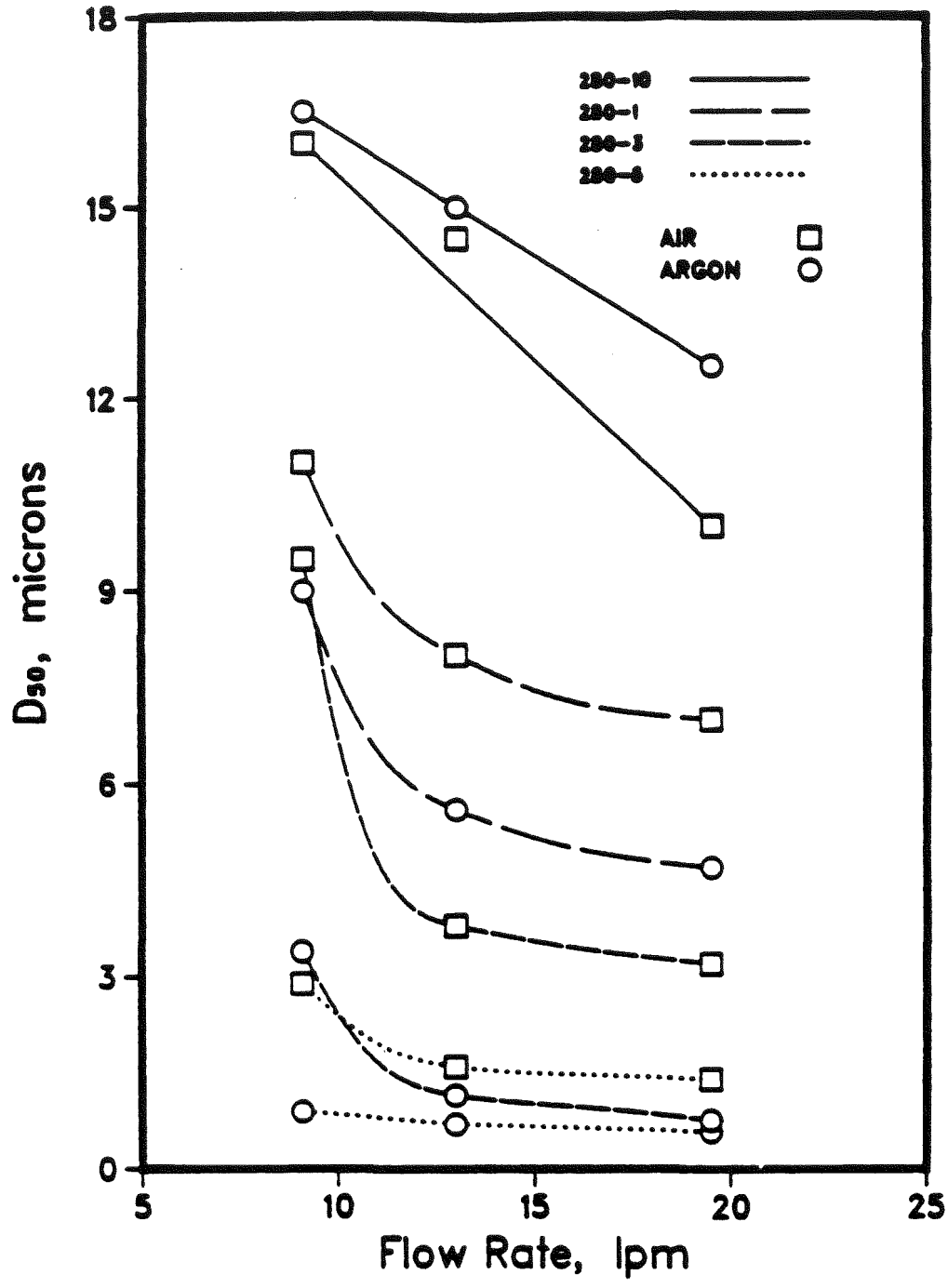

Figure 3. Plot of Flow Rate Versus D_{50}

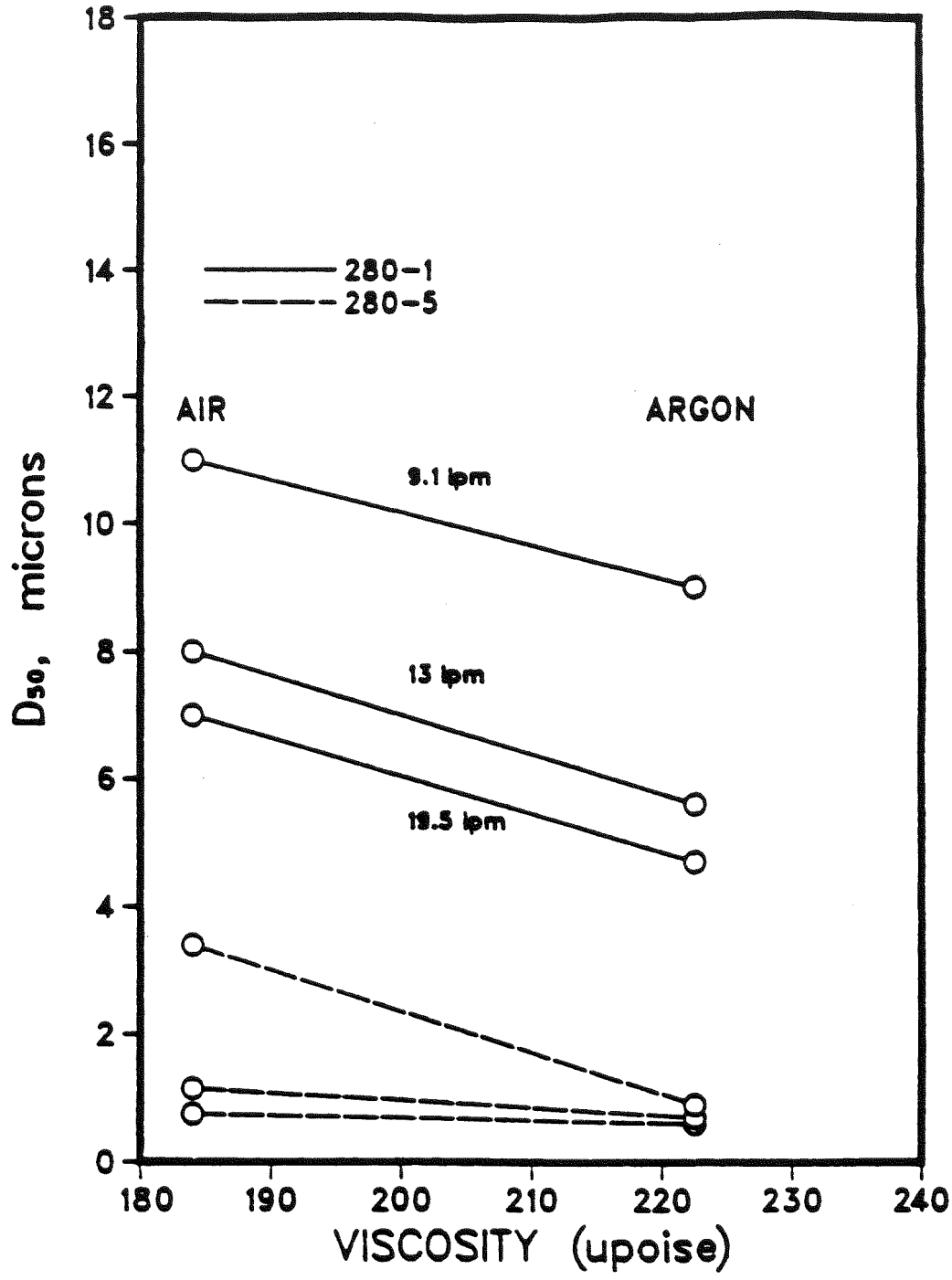

Figure 4. Plot of Gas Viscosity Versus D_{50}

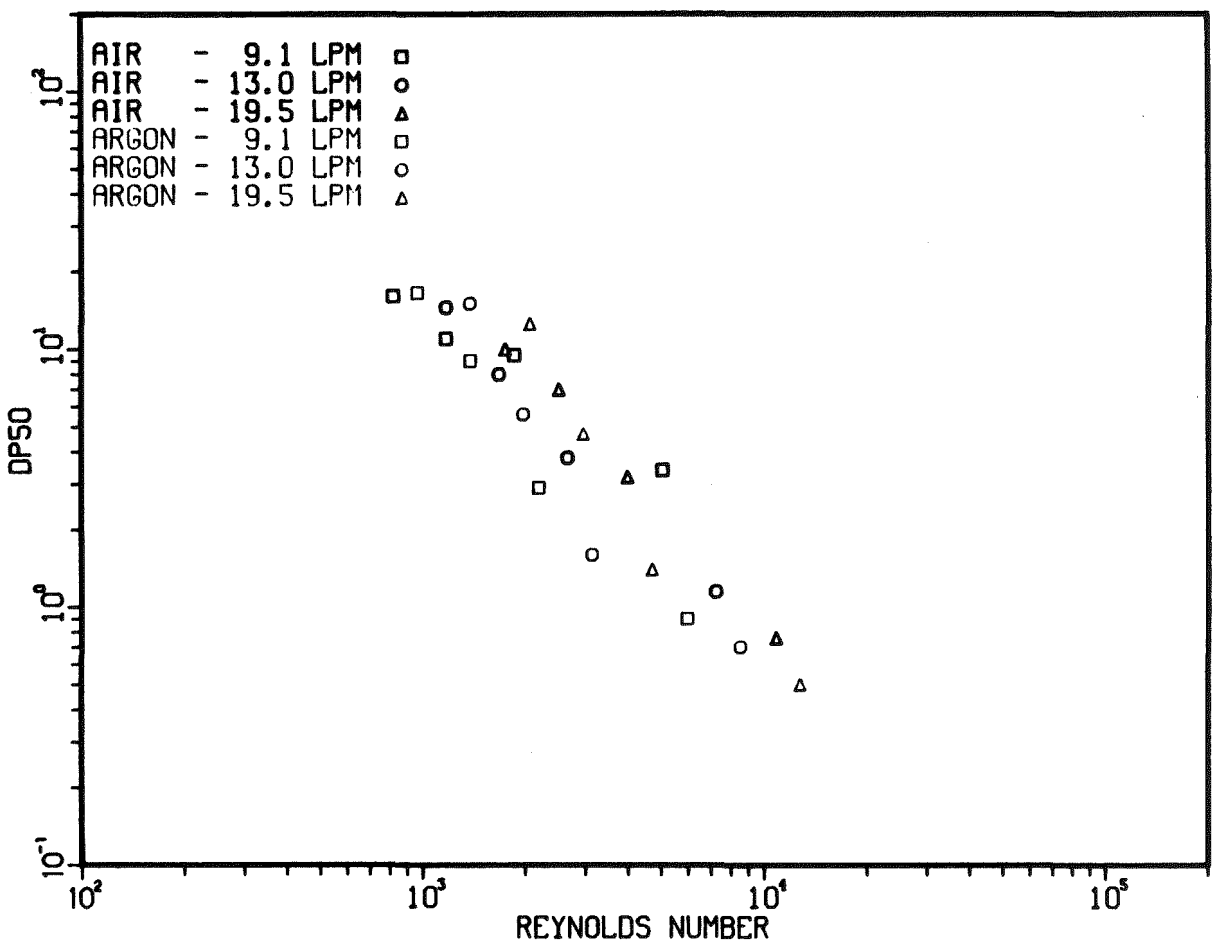

Figure 5. Effect of Reynolds Number on DP_{50}

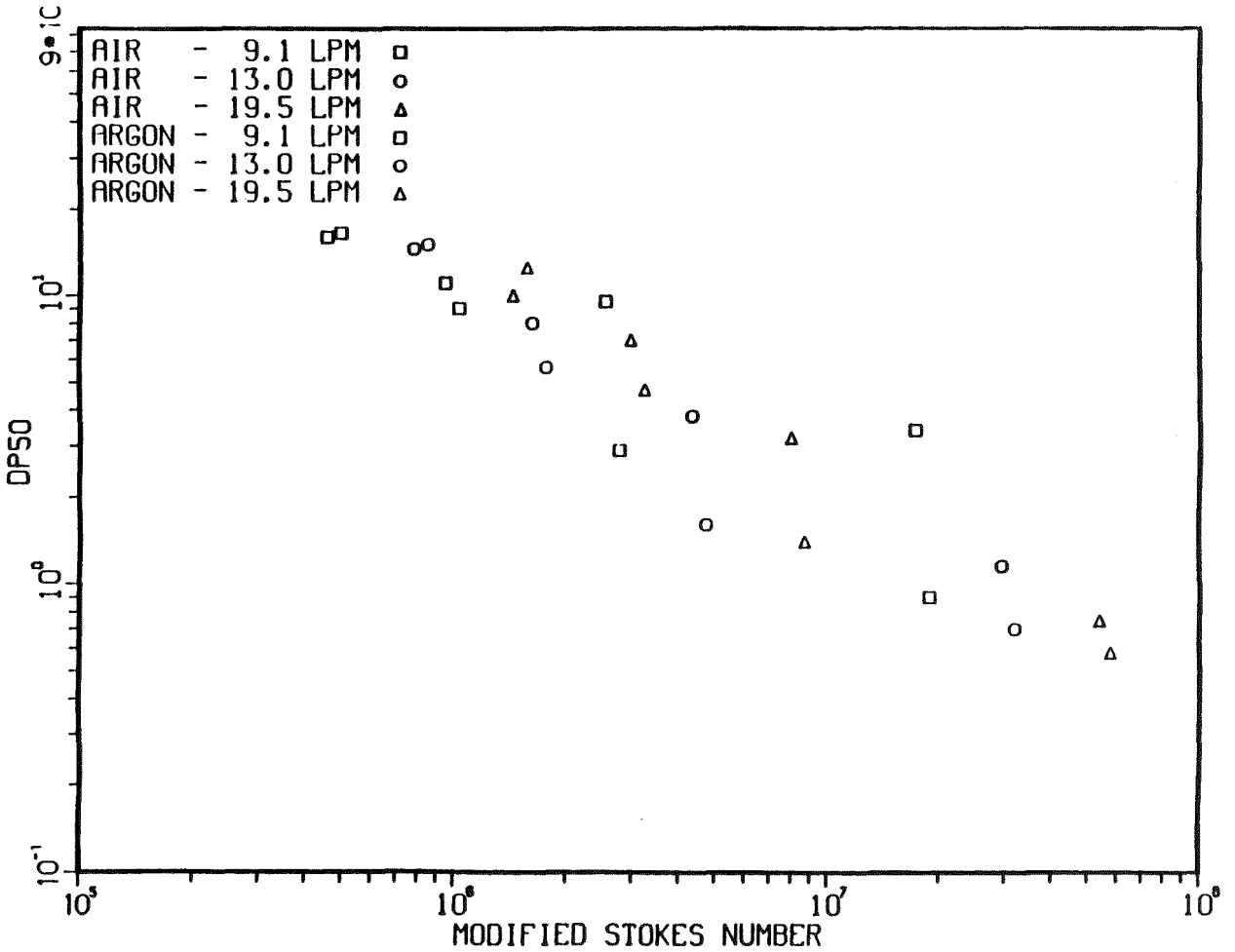

Figure 6. Effect of Modified Stokes Number on DP_{50}

Development and Performance Testing of an Aerosol Generator System for DEMONA

H. Ruhmann and M. Peehs

KRAFTWERK UNION AKTIENGESELLSCHAFT
P.O.Box 3220, D-8520 Erlangen/FRG

ABSTRACT

As part of the DEMONA program an aerosol generator system has been developed. The basis of our development should be the aerosol generating principles proposed by ORNL. Those principles had to be altered considerably. However our improved aerosol generating equipment using iron and tin as feed material provides: C^{max}(iron oxide) = 1,6 g/m³ and C^{max}(tin-oxide) = 5 g/m³ in the 640 m³ volume of the model containment. From on line measurements of the time dependant aerosol mass concentration the generation rates could be evaluated as 20-30 g/min for iron oxide and 160 g/min for tin-oxide.Depending on the aerosol production parameters, the particles show a bimodal size distribution (d_{50} = 2/5 µm) or monomodal size distribution ($d_{50} \stackrel{\sim}{=} 1$ µm).

1. INTRODUCTION

The NAUA code describes the behaviour of aerosols generated during a hypothetical core melt accident. For an experimental demonstration and verification of the aerosol behaviour predictions a test program is going on at the model PWR containment of the Battelle Institute Frankfurt/FRG. Detailed informations about the DEMONA program is given by / 1 / and / 2 /. Our contribution to the program comprises:

- the provision of the aerosol generation system including the necessary development,
- the optimization of the operating parameters,
- the operation of the generators during the different tests.

2.THE AEROSOLGENERATOR

2.1 PRINCIPLE OF AEROSOL GENERATION

To model adequately the aerosols produced during a core melt accident metal oxides are applied as model substances. Particle sizes less than 5 µm are demanded. Aerosols of this kind can be generated by condensation from the oxide gas phase. Vaporization, oxidation of metals and the subsequent recondensation of metal oxides by quenching are the principles proposed by ORNL in the Aerosol Release and Transport Program / 3 /. To realize the as proposed process metal powder is injected into a plasma torch. Here the particles are molten, evaporated and oxidized in a reaction chamber made of magnesiumoxide. Compressed air or steam is used to quench the reaction products at the exit of the reaction chamber and to transport the oxide aerosols into the model containment through a transport tube.

2.2 DESIGN OF THE AEROSOL GENERATOR

Fig. 1 presents a schematic view of the aerosol generator designed to realize the above proposed process. The technical realization is shown in fig. 2.

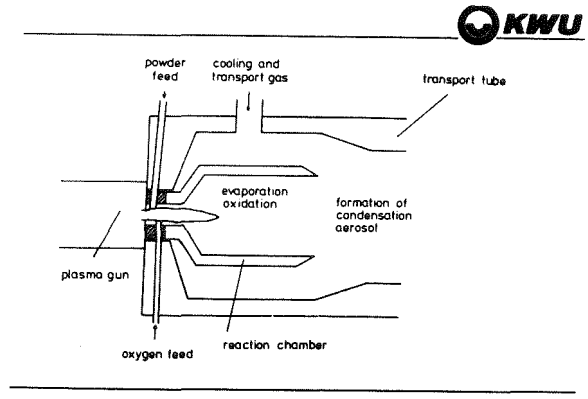

Fig. 1 Schematic cross section through the aerosol generator

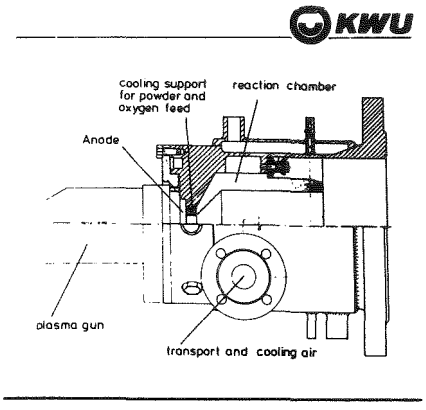

Fig. 2 Design of the aerosol generator

The cylindric reaction chamber - made from MgO base material - is heated by the plasma torch. A powder feed line allows the injection of fine metal powders next to the nozzle of the plasma gun. This position is the necessary precondition to evaporate a main fraction of the injected feed material within the plasma torch. To realize this injection mode the feed nozzle is thermally contacted to the water cooled anode of the plasma gun. Six gas nozzles inject the necessary amount of oxygen to oxidize the feed material. An adequate residence time of the powder particles in the hot plasma is controlled by the flux of the carrier gas transporting the metal powder.

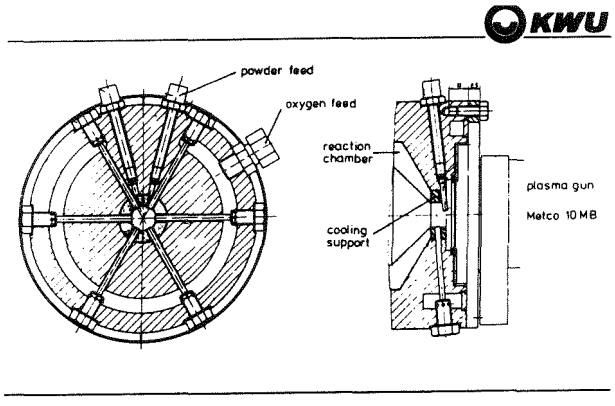

Fig. 3 Feed powder and oxygen injection device

Our concept for the reaction chamber is based on the experimental investigation of particle trajectories and plasma isothermes done by A. Vardelle et al / 4 /. Oxidizing conditions in the reaction chamber are provided by taking two times the stoichiometric quantity of oxygen for complete oxidation of the metal powder feeded into the system. Length and diameter of the reaction chamber determine the surface temperatures.

In a set of pretests those dimensions are determined to stabilize the working temperature at 1800 - 2000 K. Compressed or steam air is used to stabilize simultaneously the structural temperatures of the MgO-structure and to quench the metal oxide leaving the reaction chamber.

Three complete generator systems consisting of a plasma gun, reaction chamber, gas and powder supplying systems are merging in one aerosol feed line (length 6 m, diameter 250 mm) providing the aerosol transport into the model containment. The single system can be separated by a gate valve. A scope of the system is given by figure 4.

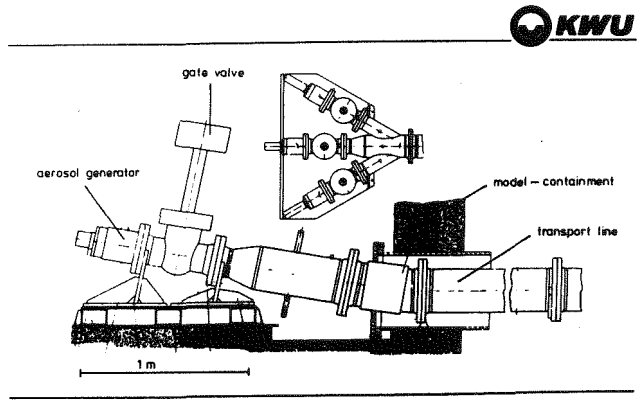

Fig. 4 The threefold aerosol generator System for the DEMONA epxeriments

3. EXPERIMENTAL RESULTS

After completion of the start up tests four fully instrumented tests V 19 - V 23 have been performed so far. The description of the DEMONA test instrumentation is given in / 5 /. To determine on-line the relative amount of air-borne mass photometric extinction measurements are applied. Absolute calibration of those measurements is performed by comparison of the relative measurements with material collected on filters loaded under definite conditions at different times.

3.1 PRODUCTION OF IRON OXIDE AEROSOLS WITH Ar/He AS WORKING GAS

Fig. 5 shows the result for experiment V 20.

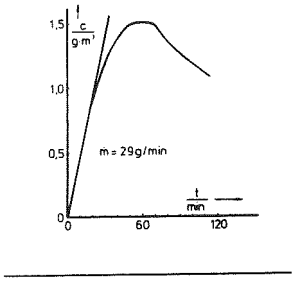

Fig. 5 Time dependant iron oxide aerosol concentration (Experiment V 20)

The increase of iron oxide aerosol concentration in the containment is plotted as a function of time. The slope at the beginning represents a generation rate of 29 g/min. The plasma gas used was a mixture of argon and helium. It is remarkable that saturation of the concentration is reached after 50 min even at continued feed of the aerosols. The saturation concentration is 1 - 2 g/m³. Obviously saturation occurs while generation rate equals the rate of aerosol depletion. The unexpected fact was due to kind of the aerosols generated. Calculations with the code NAUA get into agreement to the experiment assumming an bimodal particle size distribution with mean equivalent diameter of $\bar{d}$ = 5,5 µm (90 %) respectivly $\bar{d}$ = 2,4 µm (10 %). This aerosol characteristic fits well with the experimental determined aerosol particle size distribution.

3.2 PRODUCTION OF IRON OXIDE AEROSOLS WITH N_2 AS WORKING GAS

The test V 22 resulted in an iron oxide aerosol concentration of ≙0,7 g/m³.The working gases had been changed to nitrogen. The commercial plasma gun used however can only be operated with N_2 as working gas for a very short period because of thermal instabilities at the anode. Nevertheless in two runs iron oxide aerosol of very fine particle size could be generated (= 1 µm) with a very good yield (52 %) and satisfying feed rates of air borne iron oxide aerosols (20 g/min).

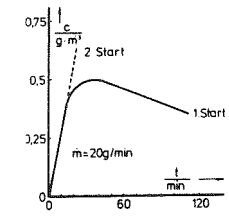

Fig. 6 Time dependant iron oxide aerosol concentration (V 22)

3.3 PRODUCTION OF TIN OXIDE AEROSOL WITH Ar/He AS WORKING GAS

Significant higher aerosol generation rates could be observed injecting tin instead of iron into the plasma torch. In experiment V 23 maximum concentration of 4 - 5 g/m³ could be reached. Fig. 7 shows the time dependant increase of the aerosol concentration in the model containment.

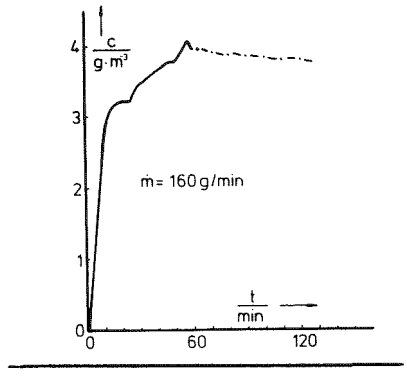

Fig. 7 Time dependant tin oxide aerosol increase (V 23)

The initial generation rate can be calculated from the slope to be 160 g/min. Post test investigations resulted in a particle size distribution with an average particle size less than 1 µm. The yield of the process is about 90 %.

4.SUMMARY OF THE OPERATION EXPERIENCE

Table 1 summarizes the experimental conditions for V 20, V 22 and V 23.

TABLE 1

Test No.	V 20	V 22	V 23
aerosol material	iron oxide	iron oxide	tin oxide
working gas (plasma gas)	Ar/He	N_2	Ar/He
el.energy input	80 kW	55 kW	80 kW
reached max. aerosol concentration	1 - 2 g/m³	0,5 - 0,7 g/m³	4 - 5 g/m³
generation rate	29 g/min	20 g/min	160 g/min
yield	20 %	52 %	90 %

4.1 PHYSICO-CHEMICAL ASSESSMENT OF THE AEROSOL-GENERATION MECHANISM

A common agreed mechanism for aerosol formation using a plasma torch and a high temperature oxidation chamber comprises

- liquifaction and evaporization of a metal powder
- gas phase exothermal oxidation forming a highly volatile oxide at the given temperature in the reaction chamber
- rapid quenching of gaseous oxide vapours to form airborne particles.

This mechanism precludes:

- The existence of a high temperature stable oxide form of the considered metallic feed material in the gaseous phase
- The absence of reactions at given temperatures forming liquid or solid reactants with a considerably high amount.

Assessing the proposed generation mechanism for Fe and Sn as feed material we conclude from the available basic data on high temperature thermodynamics:

Fe/O_2-System

Existing phases at 1800-2000 °C: $(Fe)_l$, $(Fe\text{-}Oxide)_l$, $(Fe, O_2)g$.

Using Gibbs phase rule: If the 3 phases are in equilibrium the system is invariant at given pressure. This means a maximum number of three phases can simultaneously exist: liquid oxide, liquid iron and homogeneous gasphase. There are no literature data of ironoxide vapor pressures available. The gas-phase mainly consists of oxygen over the melt.

Sn/O_2-System

Existing phases at 1800-2000 °C $(Sn)_l$, (Sn , SnO)g.

Two phases are coexistant in the two component system. But in difference to the Fe/O_2-system a stable tin-oxide-form (SnO) exists in the gas phase at 2000 K. Vapor pressure reaches 1 bar at this temperature / 7 /.

$$2(Fe)_g + 3/2\ (O_2)_g \longrightarrow (Fe_2O_3)_l \xrightarrow{\text{quenching}} \text{aerosol}$$

Thus aerosols are formed in the case of iron as reaction aerosol from the elements in the gasphase:

whereas in the case tin:

$$\left.\begin{array}{ll} (Sn)_g + (O_2)_g \longrightarrow (SnO)_g & \xrightarrow{\text{quenching} + (O_2)_g} SnO_2 \\ (Sn)_l + (O_2)_g \longrightarrow (SnO)_g & \xrightarrow{\text{quenching} + (O_2)} SnO_2 \end{array}\right\} \text{aerosols.}$$

This aerosols are formed as condensation aerosols by quenching.
A notable fact is also that oxidation of liquid tin results in formation of a gaseous oxide which increases the yield. In the case of iron this liquid fraction leads to liquid oxide phases which reduce the yield of the process.

This assessment proves that iron aerosol formation process is quite different from tin aerosol formation. The different processes explain the difference in the observed generation rates and yields reported above.

If the assessment of the aerosol production process is correct, much better rates for iron oxide aerosols are to be expected performing the oxidation reaction with feeding a volatile iron compound. In this case all iron reacts in homogeneous gas phase reaction improving the yield of the aerosol formation considerably. This statement could be proved by experiments using $Fe(CO)_5$ introduced into the aerosol generating system instead of iron powder in a pretest. If needed the as demonstrated process can be integrated in our system by additional R+D-effort on a limited extend.

5.CONCLUSIONS

The as-presented work can be summarized as follows:

In the case of iron oxide aerosol formation:

- the maximum concentration reached so far is C_{max} = 1,6 g/m³ in the 640 m³ test volume.
- the corresponding feed rate is $\dot{m}$ = 20 - 30 g-oxide/min.

- using Ar/He as working gas only aerosols with a bimodal particle size distribution can be produced (10 % : $d_{50} \approx 2$ µm; 90 % d_{50} = 5 µm).

- using N_2 as working gas iron oxide aerosols with a monomodal particles size distribution ca be produced (d_{50} = 1 µm).

- the outmost conversion yield was about 52 % for ironoxide aerosol formation.

In this case of tinoxide aerosol formation:

- the maximum concentration reached so far is C_{max} = 5 g/m³ in the 640 m³ test volume.

- the corresponding feed rate is 160 g/min.

- the as produced aerosol show a very fine monomodal particle size distribution.

- the estimated yields are better compared to ironoxide aerosol formation.

The assessment of the aerosol formation processes shows:

- With iron only reaction aerosol can be produced. Thus using iron powder the aerosol production performance of our system is limited. Only the use of gaseous iron compound as feed material may improve the yield of the process.

- Tin produced real condensation aerosol with adequate properties, high feed rate and high yields of the process.

REFERENCES

/ 1 / J.P. Hosemann, D.Haschke,
DEMONA Aerosol Removal Experiments, EIR 505, 1983

/ 2 / W.O.Schikarski et al,
DEMONA Forschungsprogramm zur Demonstration nuklearen Aerosolverhaltens, KfK 3636, EIR 505, 1982

/ 3 / R.E. Adams, M.L. Tobias,
Aerosol Release and Transport Program, Quarterly Progress Report April - June 1983

/ 4 / A.Vardelle, M.Vardelle and P.Fauchais,
Influence of Velocity and Surface Temperature of Aluminium Particles on the Properties of Plasma Sprayed Coatings, Plasma Chemistry and Plasma Processing, Vol. 2, No. 3, 1982, S.255

/ 5 / G.Friedrich et al,
Aerosol measurement system for the DEMONA Experiment, CSNI Specialist Meeting on Nuclear Aerosols in Reactor Safety, Karlsruhe 4-6 September 1984

/ 6 / H.Bunz, W.Schöck,
Comparison of Measured Aerosol Behaviour during DEMONA Experiments to NAUA Code Predictions, CSNI Specialist Meeting on Nuclear Aerosols in Reactor Safety, Karlsruhe 4-6 September 1984.

/ 7 / Gmelin Handbook of Inorganic Chemistry, 8th Edition, Zinn C1, Springer Verlag, Berlin, 1982, S. 46.

AEROSOL MEASUREMENT SYSTEM FOR THE DEMONA EXPERIMENT

G. Friedrich, A. Fromentin, O. Mercier and R. Taubenberger
Swiss Federal Institute for Reactor Research
CH-5303 Würenlingen, Switzerland

W. Schöck
Laboratorium für Aerosolphysik und Filtertechnik I,
Kernforschungszentrum Karlsruhe GmbH, D-7500 Karlsruhe, Germany

ABSTRACT

In the frame of the international large scale DEMONA experiment, highly concentrated metal oxide aerosol particles are produced and measured in a large containment (640 m^3) under unusual conditions (steam saturated atmosphere, temperature of 120-135 ^oC, pressure of 2-3 bar). The initial mass concentration of aerosol particles is between 1 and 10 g/m^3 and the change in aerosol concentration as a function of time is of several orders of magnitude. Additionally, the aerosol is a three components system: besides the gaseous phase (an air-steam mixture), one finds solid aerosol particles, liquid aerosol particles (water droplets) and/or liquid aerosol with a solid core. By using a highly reliable system specially developed for this experiment, mass concentration of solid aerosols and of droplets, particle size distribution of solid and liquid aerosols, density and form of the aerosol particles, the mass of the condensed water on walls and on ground were measured as a function of time and location.

INTRODUCTION

In the frame of the international large scale DEMONA [1,2] experiment, highly concentrated metal oxide aerosol particles are produced and measured in a large containment (640 m^3) under unusual conditions (steam saturated atmosphere, temperature of 120-135 ^oC, pressure 2-3 bar). The initial mass concentration of aerosol particles is between 1 and 10 g/m^3 and the change in aerosol concentration as a function of time is of several orders of magnitude. Therefore, conventional aerosol measurement equipment can not be used without extensive modifications for adapting them to the conditions of these tests. In addition, the aerosol is a three-component system: besides the gaseous phase (an air-steam mixture), one finds solid aerosol particles, liquid aerosol particles (water droplets) and/or liquid aerosol with a solid core. Hence, the aerosol measurement system must be able to measure the following parameters as functions of time and location:

- mass concentration of solid aerosols and of droplets
- particle size distribution of solid and liquid aerosols
- density and form of the aerosol particles
- the mass of the condensed water on the walls and on the ground.

Additionally, a very reliable measuring system is required, due to the length of each test (several days), to the high cost of each test and to the difficulty to repeat a single test.

For all these reasons, the filtration technique was originally chosen. Twenty membrane filters are mounted in boxes, installed in four locations in the Battelle-containment (Fig. 1a). On this figure, the Battelle-Frankfurt containment is shown with a multi-compartment configuration and the location of the instruments are indicated on vertical and horizontal planes. The aerodynamical size of the solid aerosol particles is measured at five times by two Andersen cascade impactors and three Prodi inertial spectrometers. The mass of suspended water in the containment is measured by specially developed calorimeters and the size of the liquid aerosol particles is measured by an optical spectrometer (Polytec). In addition, the condensed water is collected at three locations on the walls and at three locations on the ground. An integral value of the aerosol concentration (liquid and solid) is obtained at 10 different locations (Fig. 1b) by transmissometers. These measurements give the spatial fluctuation in aerosol concentration.

An on-line evaluation of the mass concentration and of the size distribution of the dry aerosol particles is obtained by continuous extraction of the containment atmosphere. On the one hand, after dilution, the aerosol particles are collected by filtration and their mass is obtained on-line by beta-absorption techniques. On the other hand, a well-defined volume of containment atmosphere is diluted in an auxiliary tank, where the aerosol size distribution is measured by an automatic impactor.

Furthermore, three openings are built-through which instruments can be inserted into the containment. This allows the performance of limited measurements as a back-up in case in-containment instrumentation should

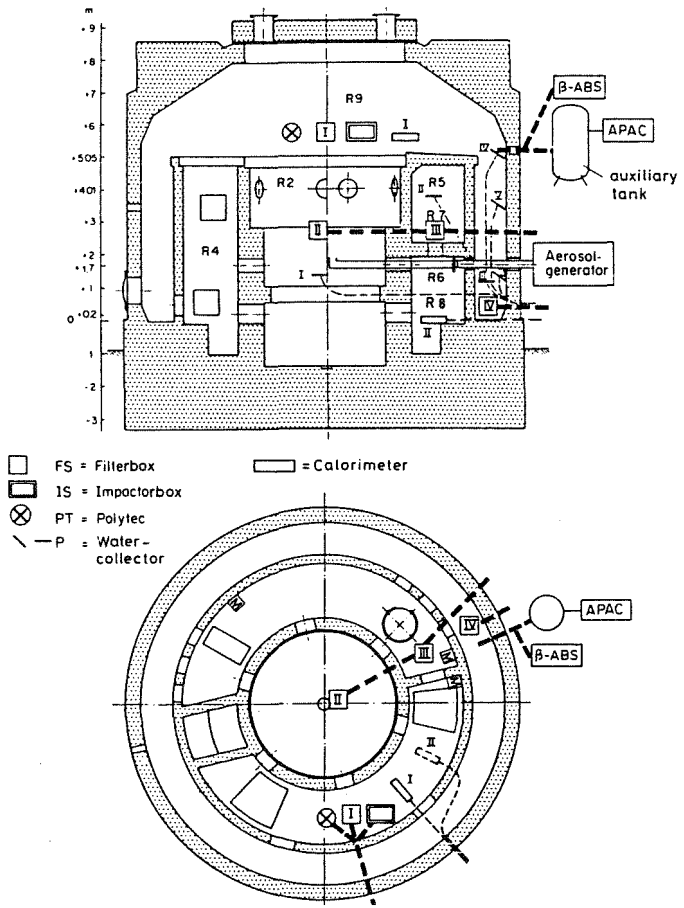

Fig. 1a: Location of the different instruments in containment

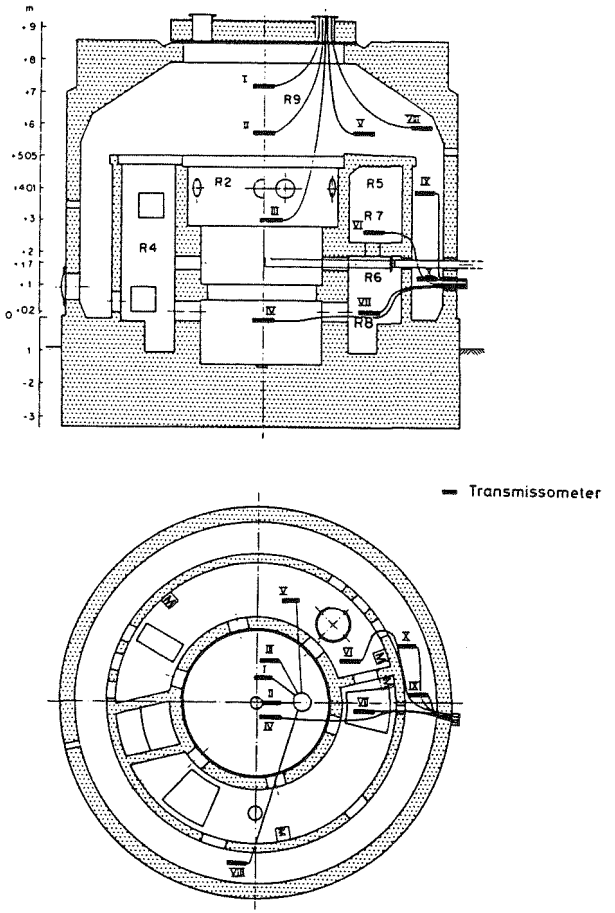

Fig. 1b: Location of transmissometers in containment

fail, this being likely during a 2-3 days experiment with no access to the internals of the containment.

FILTER BOXES

The dry aerosol classification and mass concentration is obtained from samples on membrane filters. Since the aerosol contains a large amount of steam, the filter holder is heated to a temperature slightly higher that the one in the containment in order to avoid steam condensation (Fig. 2).

After filtration the gas mixture passes through a nozzle, which limits the flow: however, depending on pressure, temperature and air to steam ratio, the volumetric flow at the nozzle changes significantly, and has to be continuously recalculated. Outside the containment the gas mixture is cooled down below 20 °C in a condenser where almost all the steam is condensed and separated from the air. The water is then collected and weighted as a function of time. The cold air mass flow is also continuously recorded.

Assuming that the ideal gas law holds for the steam and air components, and that the mixture contains no droplets, the sample volumetric flow can be calculated [3] as follows:

$$\dot{V}_1 = \dot{V}_{2,a} \frac{T_1 \cdot p_2}{T_2 \cdot p_{1,a}}$$

$$p_{1,a} = \frac{p_1 \cdot \dot{V}_2 \cdot \varepsilon \cdot p_{2,a}}{\dot{m}_s + \dot{V}_2(\varepsilon \cdot p_{2,a} + X_2 \cdot p_{2,a})}$$

Index 1 is refer in-containment, index 2 to ex-containment (measurement conditions), index a to air fraction, and index s to steam fraction: p, V, T, ρ are pressure, volume, temperature, and density, respectively. $\varepsilon = 0.62$ is the molar weight ratio of steam to air, $X_2 = \rho_{2,a}/\rho_{2,s}$ is a small correction term describing the residual amount of steam that has not been condensed and is not included in $\dot{m}_s$, the condensed steam mass flow. From the flow $\dot{V}_1$, the sampling time, the sample mass, and the mass concentration can then be evaluated.

The aerosol mass is determined by gravimetry, by wet chemical analysis and by neutron activation technique. The difference in mass between the gravimetry (total mass of the aerosol) and the other techniques (mass of metals) gives an indication of the nature of the aerosol (metal versus metal oxide) [3]. An apparent size distribution is also obtained through the TEM analysis of the filter membranes. Five filter holders are installed in one box and opened at different times of the test. These give the concentration-time function. Four boxes are available, located at different heights and along a diameter, to give the spatial variation in concentration. The filters are installed several days before the start of the aerosol generation and remain in the containment about a week after the end of the test. During these 2 periods, the temperature increases from room temperature to 125-130 °C, the pressure changes from 1-3 bars and large amount of steam

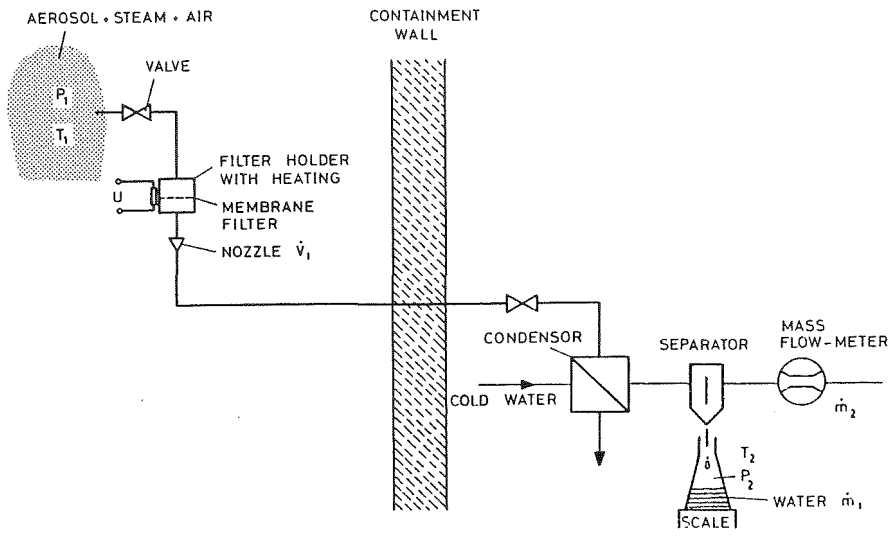

Fig. 2: Schematic diagram of the filtration set-up

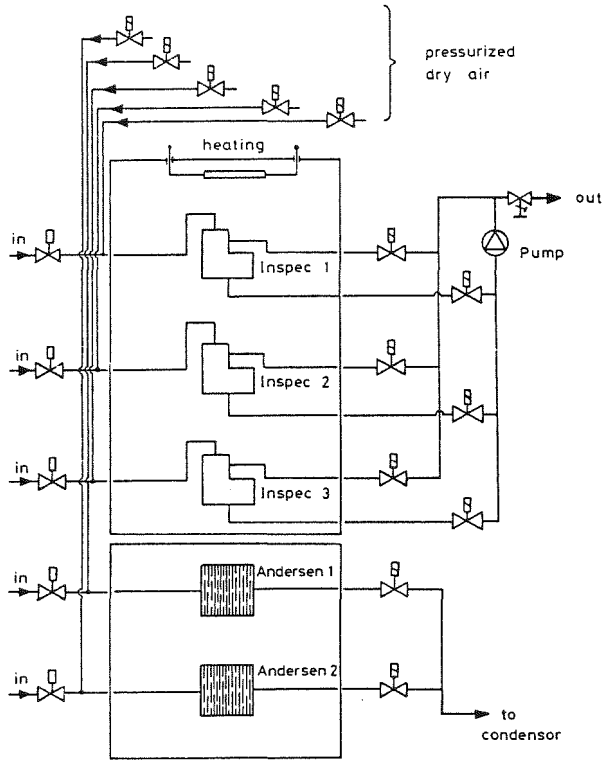

Fig. 3: Impactor box with 3 INSPEC inertial spectrometers and 2 Andersen cascade impactors

condenses everywhere. So in order to protect the filters against moisture, the boxes are filled with dry air under a regulated pressure of 0.1 bar above the one of the containment. The filter holder inlet is also closed by a pneumatic valve acting on a flexible tube. This valve is just open before the measurement, simultaneously to the closing of the dry air valve. The reverse procedure is followed at the end of the measurement. A schematic diagram of a similar box is represented in Fig. 3.

IMPACTOR BOX

The aerodynamical size distribution of the aerosol particles is measured at five times by two Andersen cascade impactors [4] and three Prodi inertial spectrometers (INSPEC) [5]. The INSPEC, specially built in stainless steel, are suitable for the measurement of highly concentrated aerosol, because a dilution system is built in (Fig. 3). They operate in the following way: The pump is turned on, with the entrance and exit valve closed and the pressurized dry air on. After stabilisation, the pressurized dry air valve is closed and the entrance and exit valves are opened. The aerosol enters in the spectrometer where dilution occurs. The aerosol particles are then impacted on a filter, at different distances from the nozzle, according to their aerodynamical diameter. The flow of the containment atmosphere in the INSPEC is obtained from the values, measured at the exit (out). To avoid condensation, the INSPEC is mounted into a heated box. At 120 °C and 3 bars, the INSPEC separate particles with aerodynamical diameters between 0.2 and 7 µm for a flow of 6 l/min.

Two cascade impactors are used when the aerosol is less concentrated. The flow of aerosol goes directly in the heated impactors and then the flow volume is measured by a similar system that the one of filter boxes. At 130 °C and for a flow of 10 l/min, the Andersen separates particles with aerodynamical diameters between 0.6 and 15 µm on 8 filters.

CALORIMETER

The fraction of water content in the suspended water droplets is just a very small fraction of the total water of the containment. Thus a direct measurement of the water partial pressure will not give any indication of the mass of suspended water. Therefore, a special instrument (calorimeter) was developed, based on the fact that the evaporation of 1 g of water needs about 1 000 times more energy than the heating of 1 g of steam 1 by 1 °C. Consequently, small quantities of suspended water influence the heating rate of the containment atmosphere quite significantly. To measure this heating rate, containment atmosphere is pumped in a tube with 2 heating elements and 3 Pt-resistance thermometers. A change of slope indicates that all the water droplets have evaporated and under adiabatic conditions the ratio of the two slopes gives the mass of suspended water. Two calorimeters are installed in the containment.

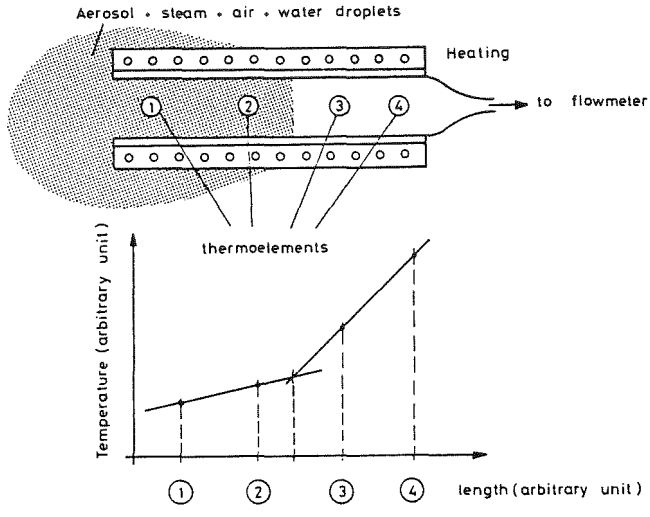

Fig. 4: Principle of the calorimeter measurement

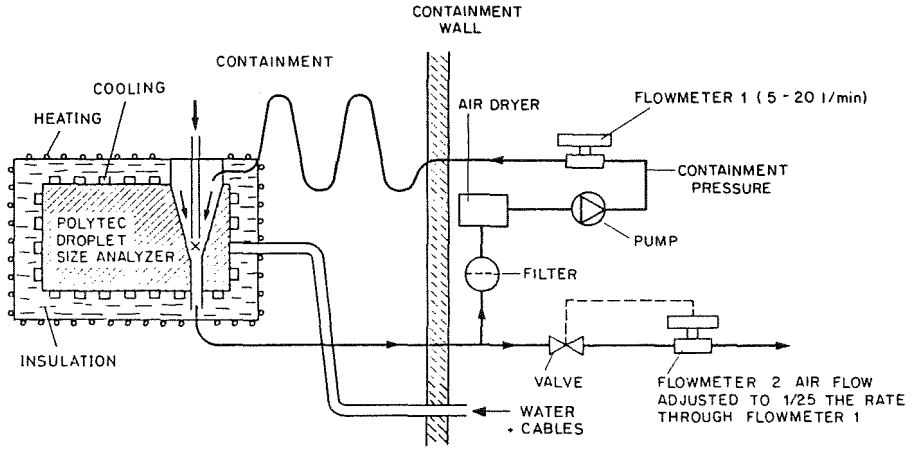

Fig. 5: Air flow for POLYTEC droplet size analyzer

OPTICAL SPECTROMETER

The size distribution of the liquid aerosol particles (water droplets) has to be measured at exactly the same temperature and pressure as the one of the containment to avoid growth or evaporation of the droplets. Hence, to avoid the difficulties in transporting the atmosphere outside the containment without changing its properties, it was decided to bring the optical spectrometer head inside the containment in a pressure vessel, cooled at the inside and heated at the outside (Fig. 5). The aerosol is drawn in the measurement head, protected by a layer of dry air heated at the temperature of the containment and measured in a 200 µm x 200 µm x 200 µm volume by a light beam. The optical spectrometer [6] measures the apparent size of each droplet and records it on a multichannel analyzer. The atmosphere flow-rate is measured by the usual technique.

TRANSMISSOMETERS

An integral value of the concentration of aerosol (liquid and solid) is obtained from the turbidity of the atmosphere. In our case, due to the high concentration of aerosol, the absorption length of light was between 10 cm and 100 cm, which prevents measurements being made outside the containment. For this reason, a transmissometer was developed to sustain the temperature and the pressure of the containment. The light source is an emitting diode with a power of 50mW and a maximum of intensity at 0.88 µm wave length. The light source and light detector (photo-resistance) are installed on the outside of the containment and the light is conducted to the measurement head by optical fibers on a distance of 5 to 10 m (Fig. 6). The optic in the head is protected against moisture by a well regulated flow of heated dry air and the absorption distance is determined by the adjustable distance between 2 blenders. Also the light flux is modulated at 1 kHz to avoid the detection of parasitic light. Ten transmissometers are located at different heights and radial angles as shown on Fig. 1b.

The transmissometers give on-line the volume concentration of aerosol at different locations, which is particularly important during the aerosol generation time and at the end of the test.

OUT-OF-CONTAINMENT AEROSOL MEASUREMENT SYSTEM

An on-line evaluation of the mass concentration and of the size distribution of the dry aerosol particles is obtained by continuous extraction of the containment atmosphere. In the first system, the aerosol is conducted in a dilution chamber through a critical nozzle. From this chamber, a small part of the volume is pumped through a moving filter and the collected mass measured by beta-absorption [7]. This measurement gives an on-line measurement of the mass concentration of dry aerosol in the containment. In the second system, a well-defined volume (1.3 l) of aerosol is extracted through a valve system and diluted in an auxiliary tank of 780 l. There the aerosol particles are analysed by different systems: an automatic cascade impactor, where the weight of each stage is measured by vibrating quartz crystals (APAC [8]), an inertial spectrometer (INSPEC) and filters. These measurements

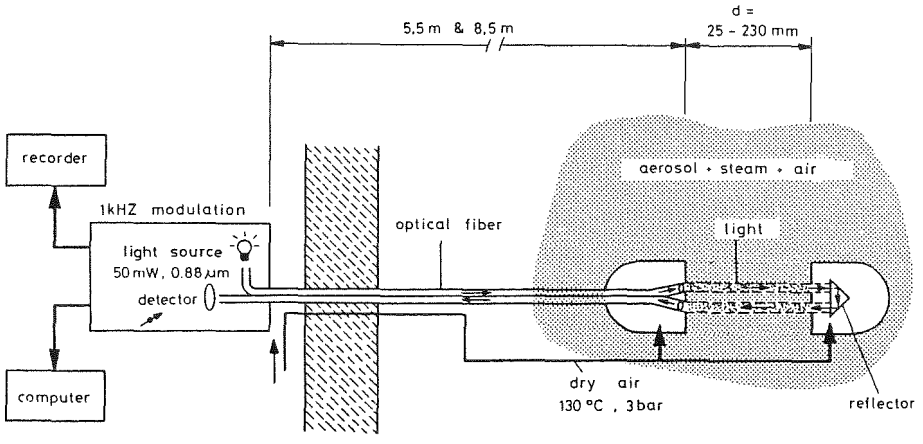

Fig. 6: Schematic diagram of the transmissometer

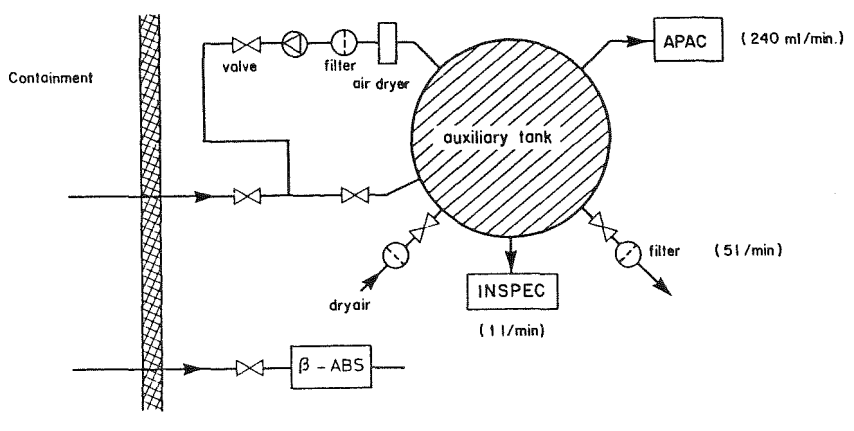

Fig. 7: Out-of-containment aerosol measurement system showing basic circuit arrangement and use of an instrumented auxiliary aerosol tank

give a good on-line indication of the size distribution of the dry aerosol particles.

AUTOMATIC DATA SYSTEM ACQUISITION

All the continuous measurements (temperature, air flow rate, mass of steam (water)) are recorded automatically on a central computer. The discontinuous measurement (size spectra) are also recorded on this computer. In addition the computer records each opening and closing of valves, and so indicates exactly when a measurement has started and during what time the measurement was done. This is specially important for the filtration technique, with the 20 filters, where the accuracy of the mass concentration determination depends on an accurate measurement of the gas flow rate and of the mass of condensed water, and where the measurement times can be shorter than 1 minute. In case of failure of the computer, all the instruments work independently and the data are recorded on separate instruments.

Also, if necessary, the opening can be used to introduce in the containment additional transmissometers and filter holders, and measurements can be conducted completely manually.

ACKNOWLEDGEMENTS

The authors wish to thank Mrs. A. Kuhn, F. Speich and H. Senn for their technical helps during this work.

REFERENCES

1. W.O. Schikarski et al., "DEMONA Forschungsprogramm zur Demonstration nuklearen Aerosolverhaltens, Grundlagen, Ziele, Auslegung", KfK publication, KfK-3636, EIR-502, 1983.
2. J.P. Hosemann, D. Haschke, "DEMONA Aerosol Removal Experiments", EIR-Bericht 505, 1983.
3. W. Schoeck, O. Mercier, A. Fromentin and G. Friedrich, Proceedings of the annual Conference of the GAeV, Munich, 1983.
4. Andersen cascade impactor Mark III, Andersen Samplers Inc., Atlanta.
5. Inertial Spectrometer, Lavoro e Ambiente Soc. Coop. a R.L., Bologna.
6. Partikelgrössen-Analysator HC 70, Polytech GmbH, Waldbronn-Karlsruhe.
7. FAG Staubmessgerätesystem FH 62 IT, FAG Kugelfischer Georg Schäfer Co., Erlangen.
8. Aerosol Particle Analyzer, Model PC-2, California Measurements Inc..

Session V: Aerosol Behavior in the Primary System - Experimental Investigations

Chair: K.O. Johansson (Studsvik Energiteknik, S)
A.L. Nichols (AEE Winfrith, UK)

PHYSICAL AND CHEMICAL FACTORS INFLUENCING FISSION PRODUCT RETENTION IN REACTOR PRIMARY SYSTEMS

J. A. Gieseke

BATTELLE
Columbus Laboratories
505 King Avenue
Columbus, Ohio 43201

To be Presented at

THE CSNI SPECIALIST MEETING ON NUCLEAR AEROSOLS IN REACTOR SAFETY

September 4-6, 1984
Karlsruhe, Federal Republic of Germany

PHYSICAL AND CHEMICAL FACTORS INFLUENCING FISSION PRODUCT RETENTION IN REACTOR PRIMARY SYSTEMS

J. A. Gieseke

BATTELLE
Columbus Laboratories
505 King Avenue
Columbus, Ohio 43201

ABSTRACT

The transport of fission products in vapor and particulate form through a reactor coolant system under accident conditions is accompanied by deposition of the fission products onto system surfaces. Deposition occurs by a number of mechanisms with the predominant mechanisms being vapor condensation and reaction with surfaces, and particle agglomeration and sedimentation. Deposition of more than 90 percent of fission products in the forms CsI, CsOH, and Te have been predicted for some accident conditions.

Several computer codes have been written to perform calculations of transport and deposition and include most physical mechanisms believed to be of importance. However, there are several issues of importance to be resolved. These include processes such as chemical reactions, decay heating of fission product deposits, resuspension of deposits, and natural circulation within the primary system. It is current thinking that decay heating and chemical reactions may be important to retention at long accident times and natural circulation may significantly affect thermal hydraulic conditions. Consideration of these issues are expected to lead to revisions of the transport codes.

Under reactor accident conditions, the core heats to a point where vaporization of various materials occurs. As radionuclides, control rods, and structural materials are vaporized in the core region, they move from the vaporizing surface through a concentration and temperature gradient or "boundary layer" out into the bulk vapor. Much of the initial particle formation occurs by nucleation in this region near the vaporizing surface. The vapors and particles are then moved along through the core region with the gas flow. As this gas flow moves to cooler regions in the core or moves into downstream portions of the primary system along the leak flow path, condensation and sorption of vapors occur on particle and system surfaces, the particles grow by agglomeration and deposit on surfaces, and if the system surfaces are heated either by decay heating or by heat transfer from the gas, the deposited materials may be evaporated from the surfaces. There are other effects such as chemical interactions with the surface which may also influence the transport and deposition process. The overall behavior of the radionuclide transport can be typified as being governed by the physical and chemical processes affecting interactions among particles, vapors, and surfaces.

Fission product deposition in reactor coolant systems under reactor accident conditions is generally expected to be a significant factor affecting the radionuclide source term to the environment. This is in contrast to previous assumptions, such as in the Reactor Safety Study, where no credit was taken for attenuation in the primary system because of expected low deposition rates as well as the possibility for revaporization by decay heating. Recent calculations[1] have estimated that more than 90 percent of the cesium, iodine (as CsI and CsOH), and tellurium inventories may be deposited in the primary system for certain accident sequences. These amounts of deposited materials significantly reduce the amounts available for transport in the containment, and if later revaporization occurs, may lead to conditions where initial primary system deposition is of major concern as a source at later times. The important conclusion is that primary system deposition may be of major importance in either reducing the release to the containment or in changing the release time relative to containment failure time.

Considerable effort has been directed toward developing the complex codes used to predict fission product retention in reactor coolant systems. Nevertheless, there remain issues that must be resolved and code validations to be completed. It is the purpose of this paper to review the general approaches taken for analyzing primary system retention and to identify outstanding issues requiring resolution.

MODELS FOR PRIMARY SYSTEM DEPOSITION

There are basically three computer codes available for predicting the transport and retention of fission products in the reactor coolant system. These are the TRAP-MELT 2, RETAIN, and RAFT codes. Each of these treats fission products in both vapor and aerosol form. Other codes are available for predicting aerosol transport, but since vapor transport is believed to be important, the above three codes will be emphasized. Additional codes are under development (MELCOR and MELPROG) which will be employing more detailed treatments of the entire reactor system under accident conditions. A revision of the

TRAP-MELT 2 code is also in progress which will include predictions of thermal hydraulic conditions in conjunction with fission product transport.

Because it has served as a basis for developing other codes and has been used extensively in accident analyses, the general approach for code development will be discussed in terms of the TRAP-MELT 2 code and then comparisons made with other codes.

TRAP-MELT 2 Code

The TRAP-MELT 2 model is designed to treat radionuclide transport in an arbitrary flow system whose thermal hydraulic conditions are provided as input as functions of time.[2,3] In addition, TRAP-MELT 2 requires the definition of source terms for each radionuclide in terms of mass release rates in the core region. Once the flow system is defined, it is subdivided into a series of control volumes that can, in principle, be arbitrary in number and flow connections and that are chosen on the basis of characteristic geometry, thermal hydraulic conditions, and suspected significant radionuclide behavior such as change of phase, agglomeration, or deposition. Radionuclides in each control volume are assigned, with uniform distribution, to one of two carriers: the wall surfaces and the gas phase. Each radionuclide is allowed to reside on these carriers in either particulate (liquid or solid) or vapor form so that by combining carrier with form in the concept of "state", the condition of a radionuclide in a given control volume is completely determined by its state. TRAP-MELT 2 thus considers five states:

- Radionuclide vapor carried by gas
- Radionuclide particle carried by gas
- Radionuclide vapor carried on wall surface
- Radionuclide particle carried on wall surface
- Radionuclide vapor chemisorbed on wall surface.

This list of states is not exhaustive (for instance, in two-phase flow, the carrier water must be considered) and the logic of the code has been chosen to accept an arbitrary number of states readily.

Radionuclide transport can occur among the five states of an individual control volume or between certain states of different control volumes are connected by fluid flow. The former types of transport are modeled or correlated in the code itself. The latter are assumed to occur in phase with the fluid flow and are imposed on the system. Sources of radionuclides to the system may occur in any volume and any state, and they may be input to the code as mass rate functions of time.

At present, the intravolume transport mechanisms contained in TRAP-MELT are:

- Competitive condensation on, or evaporation from, wall surfaces and particles of cesium iodide, cesium hydroxide, and tellurium

- Irreversible sorption of molecular iodine, cesium hydroxide, and tellurium on stainless steel surfaces
- Particle deposition on surfaces due to
  - -- Settling
  - -- Diffusion from laminar and turbulent flow
  - -- Inertial impaction from turbulent flow
  - -- Thermophoresis.

Particle transport (and evaporation or condensation from or on particles) depends on particle size. TRAP-MELT 2 takes this into account by considering a discretized particle size distribution that is subject to change, in each volume, by the deposition processes themselves, by possible particle sources, by flow of particles from other volumes, by flow of particles out of the volume in question, and by agglomeration. The last can be due to many mechanisms. TRAP-MELT 2 considers the following agglomeration mechanisms:

- Brownian
- Gravitational
- Turbulent (shear and inertial).

Considerations of stiffness and linearity split the system of first order differential equations resulting from the above-listed transport mechanisms into three classes. Most of the deposition mechanisms (transfer from gas to wall surface) are taken as first order in the concentration of radionuclide species on the carrier (gas, particle, or wall) from which the transfer occurs. They constitute the first class, whose transport scheme can be written in the form:

$$\frac{dC}{dt} = S + MC, \qquad (1)$$

where C is the concentration vector of the species in question for each state and volume, S is the source rate vector for each state and volume, and M is the transport matrix between all states and volumes. Because the deposition terms are taken as first order, M is independent of C and depends, with S, on time only. It is thus possible to solve Equation (1) as a set of first order differential equations with constant coefficients by standard techniques. This is done in TRAP-MELT 2 for the class of linear mechanisms. Condensation and evaporation, which have a much shorter time constant than the linear processes, constitute the second class and are treated outside this framework but parallel to it, as is particle agglomeration, which constitutes the third class of mechanisms in the TRAP-MELT 2 code.

The approach to this parallel treatment is as follows: Equation (1) is taken as the master time-translation operation of the radionuclide system. Time steps are adjusted so that S and M change little over a time step and so that the time step does not exceed one-third of the smallest flow residence time for any control volume. The latter assures that the system does not translate excessively between couplings to the other two classes of mechanisms. In addition, the characteristic coagulation time for the aerosol in each volume is evaluated and compared to the master time step. If the former is short compared to the latter, the master time step is appropriately reduced.

At the beginning of each time step, phase transitions of radionuclides are modeled by examining each control volume in turn and solving the molecular mass

transport equations for vapor transport among the gas phase, particles, and wall surfaces. Because of the low heats of vaporization of the radionuclides in question, this transport is assumed to be isothermal. Transfer to the walls assumes the Dittus-Boelter correlation for pipe flow and transfer to the particles occurs by diffusion based on the size distribution at the beginning of the time step. Redistribution of the vapor phase occurs in a time that is small compared to the master time step; therefore, this redistribution is essentially decoupled from the other processes considered which justifies the use of a time parallel solution treatment.

Once redistribution of the vapor phase has been effected, its effect on the existing particle size distribution (in the volume in question) is calculated by assuming that each size class gains (or loses) mass in proportion to the rate of vapor transfer to (or from) that size class. Conservation of number for each size class then dictates redistribution between, in general, two new contiguous size classes, the number in each size class being determined by mass conservation.

At the end of a time step, the particle size distribution in each volume is reevaluated over that time step to account for possible particle agglomeration, sources, and flow terms. The agglomeration algorithm has been excerpted from the QUICK aerosol behavior code[4], which is based on a size discretization scheme.

The approximations inherent in this parallel treatment are minimized by relegating mass redistribution and conservation to Equation (1) except for redistribution due to radionuclide phase change. Agglomeration and particle evaporation/condensation serve only to modify the particle size distribution and therefore affect particle deposition indirectly through mass-distribution-averaged deposition velocities. Thus the aerosol aspect is solved (over a master time step) completely in parallel to Equation (1), using all sources, flow terms, and particle removal terms evaluated for each size class considered. The resultant distribution is used to evaluate average particle deposition terms for use in the master equation only. Similarly, reevaluation of the particle size distribution due to radionuclide phase change affects these average deposition terms only.

In addition to the time-dependent thermal hydraulic conditions and mass input rates by species, the TRAP-MELT 2 code requires input information on the initial particle size distribution of the source, the control volume geometry, and the physical properties of species (including deposition velocities on surface materials). The code provides output in terms of time- and location-dependent mass by species and state, as well as size distribution of suspended particulate material.

TRAP-MELT 2 Comparison with Other Codes

The TRAP-MELT 2 code can be compared with the RETAIN and RAFT codes in terms of differences in methods of analyzing sequences and in the mechanisms included. Table 1 summarizes the various mechanisms in each of the three codes.

Table 1. Phenomena Considered in Codes Predicting Fission Product Transport in Primary Systems

Phenomena/Parameters	CODE		
	TRAP-MELT 2.1	RETAIN	RAFT
Phenomena:			
Aerosol Agglomeration			
- Brownian	yes	yes	yes
- Gravitational	yes	yes	yes
- Turbulent	yes	no	yes
- Discretized Size Representation	yes	no	yes
Aerosol Deposition			
- Sedimentation	yes	yes	yes
- Thermophoresis	yes	yes	yes
- Laminar/diffusion	yes	yes	yes
- Turbulent/diffusion	yes	yes	no
- Turbulent/inertial	yes	yes	no
- Inertial (bends, obstacles)	no	no	no
- Electrostatic	no	no	no
- Diffusiophoresis	no	no	no
Vapor Deposition			
- Condensation/particles	yes	yes	yes
- Condensation/surfaces	yes	yes	yes
- Chemisorption/particles	no	no	no
- Chemisorption/surfaces	yes	no	no
- Nucleation	no	no	yes
Aerosol Resuspension	no	As Input	no
Channel Plugging	no	yes	no
Vapor Reevolution	yes	yes	yes
Combined Thermal Hydraulics	no	yes	no
Equil. Chem. Thermo.	no	no	yes
WASH 1400 f.p. Groups	yes	yes	By Element
Reverse Flow	yes	yes	no
Parameters:			
Input Particle Size (mean)	yes	yes	NA
Input Particle Density	yes	yes	NA
Gas Flow Rate w/time	yes	yes	yes
Gas Temperatures w/time	yes	yes	yes
Pressure	yes	yes	yes
Gas Composition	yes	yes	yes
Surface Temperatures w/time	yes	yes	yes
Multiple Surfaces/Volume	yes	no	no
Fission Product Mass Input w/time	yes	yes	yes
Mass Distribution among species w/time	yes	yes	yes
Predictions (with time and location):			
Particle composition	yes	yes	yes
Airborne vapor cone	yes	yes	yes
Condensed mass by species	yes	yes	yes
Sorbed mass by species	yes	yes	no
Released mass by species	yes	yes	yes
Particle Size Distribution			
Size Intervals	yes	no	yes
Mean Size	yes	yes	yes
Distribution Spread	yes	yes	yes

The RETAIN code[5] predicts vapor and particulate transport in the RCS and was developed from an earlier version of the TRAP-MELT code and therefore is in many ways quite similar. There are, however, several major differences. The first major difference is that the RETAIN code employs the assumption that the size distribution for the aerosols remain log-normal. This assumption is reasonably accurate when low concentrations and low rates of gravitational agglomeration exist. However, for RCS conditions having high aerosol concentrations, the result is to overestimate the deposition rate.

The RETAIN code has the added feature of combining surface heatup from decay heating with the deposition melting. This allows for enhanced revaporization of fission products as a result of the increased deposit temperatures. This effect is expected to be quite important in later stages of an accident and in particular after reactor vessel melt-through.

The RAFT code[6] predicts fission product transport and retention in the RCS and contains many of the same features as the TRAP-MELT and RETAIN codes, but also contains some significant modifications. Although it is limited to flow in one direction only, it tracks chemical changes in the vapor using chemical equilibrium thermodynamics and contains a model for nucleation of fission product vapor to form "new" particles. Theoretical predictions of nucleation rates are likely to be subject to large uncertainties and therefore a strong experimental validation of this portion of the code seems necessary if it is to be acceptable for accident analyses which represent a very complex situation. Conceptually, the inclusion of nucleation rates into the model is an attractive feature but its importance is still to be demonstrated.

IMPORTANT MECHANISMS

Among the mechanisms affecting fission product deposition within the reactor coolant system, the most important as identified from TRAP-MELT 2 calculations are aerosol agglomeration and sedimentation, and vapor condensation and reaction with surfaces. There are short periods of time during some accident sequences where thermophoretic deposition of aerosols is also very important. It should be recognized that materials nominally starting out as vapor, such as CsI or CsOH, are in many cases first condensed onto particles before being removed by aerosol deposition. Therefore a combination of vapor condensation with aerosol behavior becomes critical.

Thermal hydraulic conditions are predicted to have a major effect on deposition. Low gas flow rates lead to higher aerosol concentrations, high agglomeration rates, long residence times and hence, large fractions of the aerosol materials being deposited. The effect of temperature on condensation has been estimated to range from nearly zero to over 50 percent of CsOH deposited in the upper plenum as the upper plenum temperature was varied parametrically from high to low temperatures over a range expected to represent reasonable thermal hydraulic uncertainties.[1]

Even though parametric studies have shown the importance of the various mechanisms included in the codes and the sensitivity to thermal hydraulic conditions is noted, questions still arise concerning mechanisms not currently modeled or modeled in a simplistic manner. Sensitivities to these additional mechanisms

are of possible importance and are often evaluated individually and external to the formalized computer codes. Some of these mechanisms and issues in question will be discussed below.

Revaporization by Decay Heating

A major issue being addressed theoretically at this time is the revaporization of previously deposited fission products by decay heating of the deposits. The conclusions are not yet finalized but some major observations can be made based on current progress. While airborne and after depositing fission products will continue to release decay energy, some of which will be deposited in the gas phase, some in the deposited layer, and some in the primary system structures. This distribution of energy seems to be treated in various ways by several investigators but the major concern has been the increasing temperature of the fission product layer which could lead to revaporization.

The various analyses to date have been consistent in suggesting the revaporization and subsequent redeposition of fission products within the primary system. The impact of this revaporization on release from the primary system is less clear. In some analyses heat loss from external primary system surfaces is sufficient to prevent significant loss from the primary system after a time of vaporization/condensation driven redistribution. Other analyses have not proceeded beyond the time of pressure vessel melt-through and hence long term effects are unknown.

It is the long term revaporization that seems crucial since many accident sequences lead to a predicted containment failure and extending the release from the primary system beyond containment failure could have significant effects on source term to the environment.

It is believed that considerable insight into the long term release will be forthcoming in the near future. There are both experimental and theoretical efforts under way at present.

Chemical Reactions

Chemical reactions have been generally ignored in analytical treatment of transport in primary systems. An exception is the RAFT code which performs chemical thermodynamic equilibrium calculations for the gas phase constituents. There are, however, a number of issues that must be resolved and are the subject of both theoretical and experimental studies.

The usual assumption made in primary system transport calculations is that CsI is the predominant iodine form, and it will transport as a vapor, condensing onto aerosols and surfaces at rates dictated by temperatures and flow conditions. There are several situations where this scheme may be altered. Based on theoretical considerations and supported by experiments, it is becoming evident that CsI may interact with boron compounds in the gas and condensed phases to produce molecular iodine. The kinetics of this process relative to subsequent iodine reactions must still be analyzed to evaluate what impact it may have on source terms to the environment.

Based on preliminary theoretical and experimental results, it appears possible to oxidize CsI at high temperatures such as in burning hydrogen to form molecular iodine. This appears to be most likely to occur in the containment or after melt-through of the primary system.

The chemical interactions of fission product vapors with surfaces has been studied more extensively from experimental approaches and have emphasized CsI, CsOH, and Te reactions with various structural materials. It appears that Te can be expected to react rapidly with structural materials while CsOH will react most effectively with trace components of such materials. The capacity of the sufaces for CsOH reaction seems to need more clarification to permit full utilization of the data.

In general, chemical interactions among fission products and between fission products and surfaces have the potential to alter volatilities. Either higher or lower vapor pressure products can be produced and the impact on condensation or revaporization could be substantial.

Resuspension of Aerosol Deposits

Resuspension of previously deposited aerosols on high pressure failure of the reactor vessel has been identified as a possible mechanism by which the fission product source to the containment could be increased. Reviews of this subject were undertaken as portions of both the QUEST and IDCOR programs. Resuspension can be considered for both liquid or slurry deposits and for dry deposits.

The resuspension of dry deposits could result during blowdown of the reactor pressure vessel if failure occurs at high pressure. The adhesion of particles depends on many factors including particle size, humidity, surface roughness, material characteristics (sticking tendencies), and depth of deposit. There is also a time factor with high gas velocities over the deposit surface being required for some length of time; the fraction resuspended increasing with time. The general conclusion is that for sequences with reactor vessel failure at high pressure, dry deposits would resuspend partially with the resuspended particle size being large enough to be of minor concern for containment transport.

For liquid deposits which appear more likely under primary system conditions (such as noted in the Marviken experiments with CsI, CsOH, and Te), resuspension could occur at flow discontinuities or from liquid surface instabilities. However, it appears unlikely that liquids would be resuspended to a significant extent during the blowdown period. Although some verification seems warranted, resuspension to form a readily transportable aerosol in the containment appears to be a minor effect.

Natural Circulation

Natural circulation flows can lead to exchanges among major portions of the primary system and control the extent of mixing within individual control volumes. The available transport codes are based on the assumption that

individual control volumes are well mixed. The TRAP-MELT 2 transport code maintains the capability for flow exchange in both directions between adjacent control volumes and hence could be matched with a thermal hydraulic prediction involving recycling flows. Efforts supported by both the U.S. Nuclear Regulatory Commission and the Electric Power Research Institute are directed toward more comprehensive descriptions of thermal hydraulic conditions including natural circulation.

The importance ofnatural circulation is expected to be dependent on accident conditions. Preliminary calculations have indicated that for the upper plenum, a hot leg break leads to unmixed conditions while a transient accident gives a well mixed situation. Analyses extended to include more portions of the primary system suggest larger circulation patterns among major components. The implication of these results for primary system transport and deposition is that a finer nodalization of control volumes may be needed and somewhat revised definitions of control volumes and their interchanges would be required.

CONCLUSIONS

The general conclusions regarding fission product transport and deposition in the primary system are:

(1) There appears to be a solid basis for theoretical predictions.

(2) The predictive codes will require improvement to consider additional chemical and physical effects.

(3) Decay heating of deposits and chemical changes and interactions among fission products and with surfaces may have a pronounced effect on release from the primary system, particularly over long time periods.

(4) Resuspension of deposits within the primary system is probably not a major source of transportable aerosol.

(5) Natural circulation is important in some accident sequences, may have a significant effect on thermal conditions, and may lead to revisions in transport codes.

REFERENCES

1. Gieseke, J. A., et al, "Radionuclide Release Under Specific LWR Accident Conditions", BMI-2104, Volume 1 (Draft), July, 1983; Volumes 2-6 (Draft), July, 1984.

2. Jordan, H., Gieseke, J. A., and Baybutt, P., "TRAP-MELT User's Manual", NUREG/CR-0632, BMI-2017 (February, 1979).

3. TRAP-MELT 2.1 User's Manual.

4. Jordan, H., Schumacher, P. M., and Gieseke, J. A., "QUICK Users' Manual", NUREG/CR-2105, BMI-2082 (April, 1981).

5. "RETAIN User's Manual", Impell Corporation, November, 1983.

6. Ahluwalia, "RAFT Computer Model of Aerosol Formation and Transport", presented at the American Nuclear Society Topical Meeting on Fission Product Behavior & Source Term Research, Snowbird, Utah, July 15-19, 1984.

RESULTS FROM SIMULATED UPPER-PLENUM AEROSOL TRANSPORT AND AEROSOL RESUSPENSION EXPERIMENTS*

A. L. Wright** and W. L. Pattison
Chemical Technology Division
Oak Ridge National Laboratory
Oak Ridge, Tennessee 37831

To be presented at

Specialist Meeting
on Nuclear Aerosols in Reactor Safety

Karlsruhe, Federal Republic of Germany

September 4-6, 1984

*Research sponsored by the Office of Nuclear Regulatory Research, U.S. Nuclear Regulatory Commission under Interagency Agreement DOE-40-551-75 with the U.S. Department of Energy under contract DE-AC05-840R21400 with Martin Marietta Energy Systems, Inc.

**Engineering Technology Division.

RESULTS FROM SIMULATED UPPER-PLENUM AEROSOL TRANSPORT AND AEROSOL RESUSPENSION EXPERIMENTS*

A. L. Wright** and W. L. Pattison
Chemical Technology Division
Oak Ridge National Laboratory
Oak Ridge, Tennessee 37831

ABSTRACT

This paper summarizes recent results from the ORNL TRAP-MELT Validation Test Program, which is sponsored by the Fuel Systems Behavior Research Branch of the U.S. Nuclear Regulatory Commission. The objective of the project is to conduct simulated reactor-vessel upper-plenum aerosol deposition and transport tests. The project includes two experimental subtasks: the Aerosol Transport Tests and the Aerosol Resuspension Tests. Results from the first four Aerosol Transport Tests and from the first series of Aerosol Resuspension Tests are presented and discussed.

*Research sponsored by the Office of Nuclear Regulatory Research, U.S. Nuclear Regulatory Commission under Interagency Agreement DOE-40-551-75 with the U.S. Department of Energy under contract DE-AC05-840R21400 with Martin Marietta Energy Systems, Inc.

**Engineering Technology Division.

INTRODUCTION

Recent calculational results published as part of the Battelle-Columbus BMI-2104 source term study [1] indicate that, for some LWR accident sequences, aerosol deposition in the reactor primary coolant system (PCS) can lead to significant reductions in the radionuclide source term. Aerosol transport and deposition in the PCS have been calculated in this study using the TRAP-MELT 2 computer code, which was developed at Battelle-Columbus; the status of validation of the TRAP-MELT 2 code has been described in an Oak Ridge National Laboratory (ORNL) report [2]. The objective of the ORNL TRAP-MELT Validation Project, which is sponsored by the Fuel Systems Behavior Research Branch of the U.S. Nuclear Regulatory Commission, is to conduct simulated reactor-vessel upper-plenum aerosol deposition and transport tests. The results from these tests will be used in the ongoing effort to validate TRAP-MELT 2.

The TRAP-MELT Validation Project includes two experimental subtasks. In the Aerosol Transport Tests, aerosol transport in a vertical pipe is being studied; this geometry was chosen to simulate aerosol deposition and transport in the reactor-vessel upper-plenum. To date, four experiments have been performed; the results from these tests are presented in this paper.

Hydrodynamic aerosol resuspension of deposited aerosols has not been modeled in the TRAP-MELT 2 code and other aerosol behavioral codes. However, the potential exists both in the PCS and in the reactor secondary containment for resuspension of deposited aerosols to occur. The objective of the Aerosol Resuspension Tests is to provide a data base for developing resuspension-rate models that can be included in TRAP-MELT 2 and other aerosol transport codes. The first series of experiments was recently completed; in these tests resuspension rates of deposited aerosols or powders were measured as a function of test section flow velocities. The preliminary results from these experiments are presented in this paper.

AEROSOL TRANSPORT TESTS: DESCRIPTION

The Aerosol Transport Tests are performed in a 2.95-m-long, 0.26-m-diam, segmented vertical pipe; the test configuration is illustrated in Fig. 1. Aerosols are generated by feeding metal powder to a plasma torch aerosol generator. Tests are performed by generating aerosols in the pipe for a period of ~10 min. The generated aerosols can agglomerate, settle on the horizontal floor at the bottom of the pipe, deposit on the pipe sidewalls, or be transported out of the pipe into an aerosol collection bag. During the aerosol generation period, measurements are made of pipe-wall and gas temperatures and airborne aerosol mass concentrations and aerodynamic size distributions in the pipe. At the end of an experiment the slide valve at the bottom of the pipe is closed; based on the mass collected on the slide-valve plate, the amount of aerosol airborne at the end of the aerosol generation period can be estimated. One to two days after the test is completed, the test section is dismantled, and the amounts of aerosol deposited on the three pipe sections, settled on the floor, and transported out of the pipe are determined.

Aerosol transport in the reactor-vessel upper plenum can be influenced by a number of factors; among these are the upper-plenum gas flow rates (residence times) and flow fields, aerosol formation rates and aerosol materials, magnitudes of wall temperature gradients, and moisture conditions in the plenum. Table 1 illustrates the test matrix for the present Aerosol Transport Test series. In the present series, the main variables are the flow residence time and the aerosol material used. The range of residence times spans a factor of six and is reasonably representative of those expected in the upper plenum in core-melt accidents. The choice of aerosol materials was made not to directly simulate core-melt aerosols but to determine if metal and oxide aerosols (both metals and oxide aerosols are expected to be produced in core-melt accidents) behave differently.

AEROSOL TRANSPORT TESTS: TEST RESULTS

A summary of the aerosol deposition results from tests A101 through A104 is presented in Table 2; details for each test can be found in preliminary data record reports [3—6]. The following comments can be made related to the results presented in Table 2:

1. Although results from tests A101 and A102 are presented, it will not be appropriate to model these two tests with TRAP-MELT 2. In test A101, there was an uncertainty as to whether the airborne material was pure aerosol or simply unvaporized particles dispersed by the plasma torch. In tests A101 and A102, a significant fraction of the heat lost to the pipe walls was due to radiation heat loss from the aerosol-generator plasma; because of this, we could not reliably estimate thermal gradients in the first two tests. The test configuration was modified for tests A103 and A104 to eliminate radiation heat loss to the pipe walls.

2. In each test, aerosol plateout was largest in the lower pipe section (nearest to the aerosol generator) and least in the upper section. Variations in averages of measured centerline gas temperatures, wall temperatures, and gas-wall temperature differences are illustrated in Table 3 for tests A103 and A104. We believe that the majority of aerosol plateout on the pipe sidewalls was due to thermophoresis; the variations of radial gas-wall temperature differences and measured aerosol plateout in the test section seem consistent with this assumption.

3. Tests A103 and A104 were performed with the same aerosol material but had different residence times, the A103 residence time using roughly half that for A104. The results that the fractional aerosol transport out of the pipe in A103 was greater than in A104, and that the total aerosol settling in A104 was greater than in A103, were consistent with test A103 having a shorter residence time.

Aerosol agglomerate size measurements were made during the tests using cascade impactors; a summary of data from these measurements is presented in Table 4. The measured size distributions were log-normal, except for that measured for zinc aerosol in test A101 (this is a possible indication that the airborne material in A101 was not pure aerosol).

We are presently in the process of performing TRAP-MELT 2 calculations for tests A103 and A104; however, final results from these calculations are not yet available.

AEROSOL RESUSPENSION TESTS: DESCRIPTION

The Aerosol Resuspension Tests were performed in the test section illustrated in Fig. 2. The main portion of the test section consisted of a 1.83-m-long, 0.076-m-diam pyrex pipe and a 1.83-m-long, 0.051-m-wide deposition surface that could be inserted into the pipe (with the deposition surface in the pipe, the effective pipe hydraulic diameter was 0.072 m). In an experiment, aerosols or powders were artificially deposited by pouring them through a 100-mesh screen and allowing them to settle onto the deposition surface (302 stainless steel). Materials were deposited on a 0.41-m length of the deposition surface such that the gas flow entrance length to the deposit region was 1.22 m. Air flows through the test section of up to 0.094 m^3/s (200 scfm) could be achieved; this meant that maximum plug-flow velocities >20 m/s or flow Reynolds' numbers >100,000 could be achieved.

A typical experiment was performed by first measuring the amount of material deposited on the deposition surface and then inserting the surface into the pyrex pipe. A steady air flow would be produced, measured, and maintained for a time of <300 seconds. After the flow was turned off, the deposition surface was removed from the test section and the amount of material remaining on the surface was removed and measured.

Parameters that can influence the hydrodynamic resuspension of aerosols from surfaces include aerosol material and particle size, the concentration of the aerosol deposits on the surface, system moisture condition, aerosol deposition mechanism, and the aerosol deposition-surface roughness. Table 4 summarizes the test conditions for the test results presented in this paper. In this study, forty-nine experiments were performed for the nine sets of conditions illustrated in Table 4. Parameters varied were the deposited material, particle size and density, and the mass deposited. All tests were performed under essentially dry conditions (relative humidities <~60%). In evaluating the resuspension literature, we found that few experiments have been done using materials with particle sizes representative of aerosols produced in reactor accidents (D<10 μm). In addition, we found that few experiments had been performed at the deposit concentrations that might exist in reactor accidents. Hand calculations indicated that the deposit concentrations in the upper plenum and the secondary containment could range from 0.01 to 0.1 g/cm^2; this range was covered in the experiments.

AEROSOL RESUSPENSION TESTS: TEST RESULTS

Results for the test conditions summarized in Table 5 are presented in Figs. 3 and 4; additional details are found in a preliminary data summary report [7]. Data for measured resuspension rates as a function of the average test flow velocity are presented, where the resuspension rate was determined from:

$$\text{Resuspension Rate} = \Lambda = (M_r/M_i)/(\Delta t) \ ,$$

where

M_r = mass resuspended
M_i = initial mass deposited
Δt = total flow time.

The data in Fig. 3 are for tests where the deposited mass was in the range of 1 to 2 g, while the data in Fig. 4 are for tests where the deposited mass was in the range of 10 to 20 g. The following comments can be made related to these results:

1. The measured resuspension rates and the mechanism for resuspension of the deposited materials varied as the mass loading on the surface was increased. For the low-loading tests summarized in Fig. 3, individual particles seemed to be stripped from the deposition surface in a continuous manner. For the high-loading test results shown in Fig. 4 (except for test group W-3), however, resuspension was characterized by "layer-stripping" or bursts of particle removal from the surface. We believe that in the low-loading tests, particle-surface forces were the major ones resisting resuspension, while in the high-loading tests, particle-particle forces were dominant.

2. Test groups W-2 and W-3 were performed with the same mass loading but with different size tungsten powders. Figure 4 illustrates that powder size had a large influence on the measured tungsten powder resuspension rates. In addition, the larger tungsten powder did not resuspend by "layer-stripping" but by the mechanism exhibited in the low-loading tests.

3. Results in both figures indicate a possible influence of particle density on resuspension rate, but the data for tin-oxide aerosols (SnO_2) and for manganese powder did not follow this trend. It may be, however, that the appropriate density that influences resuspension rates is not the solid particle density but the effective particle-bed density (including voids). We have not yet determined particle-bed densities for the materials used in these tests.

4. The results for the 10-μm manganese and tungsten powders were quite different and illustrate that resuspension rates can be influenced by the material deposited.

The data from this first series of resuspension experiments will be analyzed in more detail in the future. This analysis will form part of the basis for the design of the next series of resuspension experiments, in which resuspension rates of real aerosol deposits will be measured.

SUMMARY AND CONCLUSIONS

The summary and conclusions based on the results presented in this paper are as follows:

1. Four of the eight planned Aerosol Transport Tests have been completed. Measured aerosol plateout in tests decreased with increasing distance from the aerosol source, and seemed to occur largely by thermophoresis. The measured amounts of aerosol deposition in the pipe and transport out of the pipe were influenced by the aerosol residence time produced. TRAP-MELT 2 calculations for the last two experiments (A103 and A104) are now underway.

2. Results from the first series of planned Aerosol Resuspension Tests, in which resuspension rates of various aerosols and powders were measured as a function of test section flow velocities, were presented. These results illustrate that resuspension rates are influenced not only by the flow velocities past the surface, but also by particle material, size, density, and by the amount of material deposited on the surface. These results will be analyzed in more detail in the future, and additional tests will be performed in which resuspension rates of real aerosol deposits will be measured.

REFERENCES

1. J. A. Gieseke, et al., "Radionuclide Release under Specific LWR Accident Conditions — Volumes I—VII (Drafts), BMI-2104, Battelle-Columbus Laboratories, 1983—1984.

2. T. S. Kress and A. L. Wright, "States of Validation of the TRAP-MELT Computer Code for the Accident Source Term Reassessment Study (ASTRS)," part of the report "Status of Validation of Computer Codes Used in the Accident Source Term Reassessment Study (BMI-2104)," ed. T. S. Kress (to be published).

3. A. L. Wright and W. L. Pattison, "Aerosol Transport Test A101 'Quick-Look' Data Report," letter report to the U.S. NRC, September 1983.

4. A. L. Wright and W. L. Pattison, "Aerosol Transport Test A102 Preliminary Data Report," letter report to the U.S. NRC, February 1984.

5. A. L. Wright and W. L. Pattison, "Aerosol Transport Test A103 Preliminary Data Report,"letter report to the U.S. NRC, May 1984.

6. A. L. Wright and W. L. Pattison, "Aerosol Transport Test A104 Preliminary Data Report," letter report to the U.S. NRC, July 1984.

7. A. L. Wright and W. L. Pattison, "Series-1 Aerosol Resuspension Test Preliminary Data Report," letter report to the NRC, August 1984.

Table 1. Aerosol transport test matrix

Test number	Flow residence time (s)*	Aerosol Material
A101	80	Zinc metal
A102	50	Iron oxide
A103	25	Iron oxide
A104	50	Iron oxide
A105	80	Zinc metal
A106	40	Zinc metal
A107	13	Iron oxide
A108	20	Zinc metal

*At estimated average gas temperature.

Table 2. Summary of aerosol deposition results for tests A101—A104

Parameter	A101	A102	A103	A104
1. Aerosol material	Zinc	Iron-oxide	Iron-Oxide	Iron-Oxide
2. Aerosol generation time (min)	11	12.5	9*	11
3. Total aerosol produced (g)	126.9	253.96	92.57	189.14
4. Aerosol plateout, lower section (%)	43.0	59.0	23.8	26.7
5. Aerosol plateout, center section (%)	2.8	9.8	13.5	13.1
6. Aerosol plateout, upper section (%)	1.7	4.2	8.8	11.8
7. Aerosol settling (%)	11.4	19.1	1.6	29.3
8. Aerosol transported out of pipe (%)	41.1	8.0	52.3	19.1

*Total test time was 10 min.: 9 min. with aerosol generation and 1 min. without.

Table 3. Average centerline gas temperatures, wall temperatures, and gas-wall temperature differences for tests A103 and A104

	Centerline gas temperature (°C)	Wall temperature (°C)	Gas-wall temperature difference (°C)
		A103	
Lower section	303	69	234
Center section	168	42	126
Upper section	103	36	67
		A104	
Lower section	312	81	231
Center section	140	35	105
Upper section	83	30	53

Table 4. Summary of aerosol agglomerate size data for tests A101-A104

	Test time when sample taken (min)	Aerodynamic mass-median diameter (μm)	Geometric standard deviation
A101	8.75	6.34	1.72
A102	6.17	1.99	2.95
	11.47	3.03	2.92
A103	5.5	4.01	3.06
A104	5.17	4.95	3.19
	10.25	5.05	3.39

Table 5. Summary of aerosol resuspension test conditions

Test designation	Material type	Average Particle diameter (μm)	Particle density (g/cm^3)	Mass deposited (g)
W-1	Tungsten powder	0.5	19.4	2.4
W-2	Tungsten powder	0.5	19.4	20.3
W-3	Tungsten powder	10	19.4	20.1
Ni-1	Nickel powder	2.5	8.9	1.6
Ni-2	Nickel powder	2.5	8.9	10.1
Mn-1	Manganese powder	10	7.2	19.9
Fe_2O_3-1	Iron-oxide aerosol	<0.2	5.2	1.6
Fe_2O_3-2	Iron-oxide aerosol	<0.2	5.2	9.6
SnO_2-1	Tin-oxide aerosol	<0.2	7.0	1.1

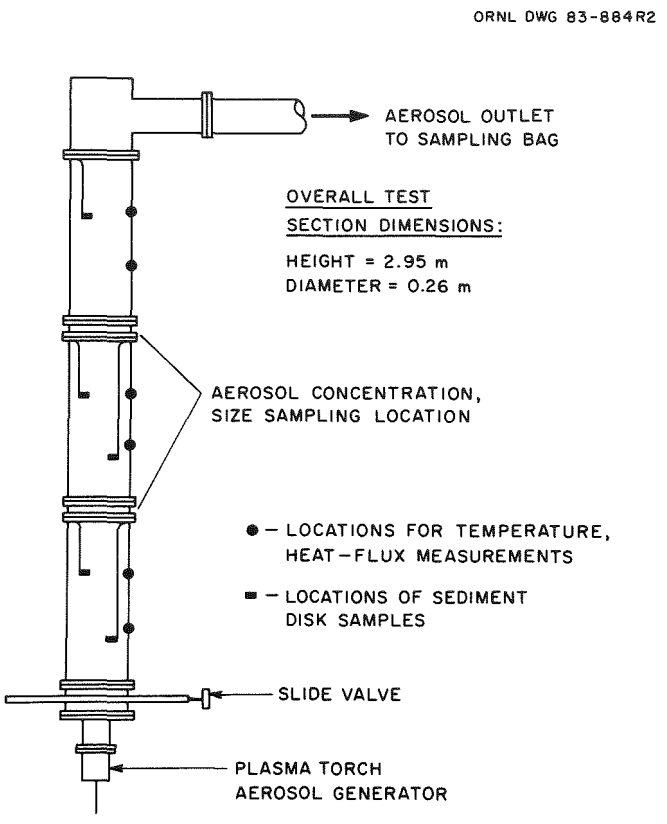

Figure 1. Aerosol Transport Test section schematic.

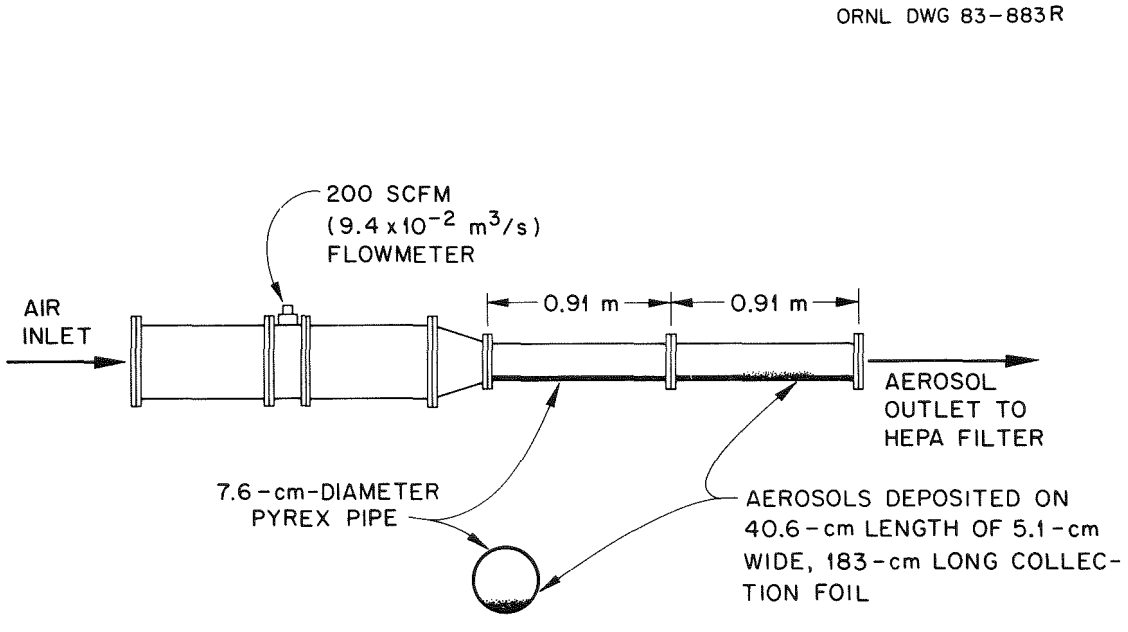

Figure 2. Aerosol Resuspension Test section schematic.

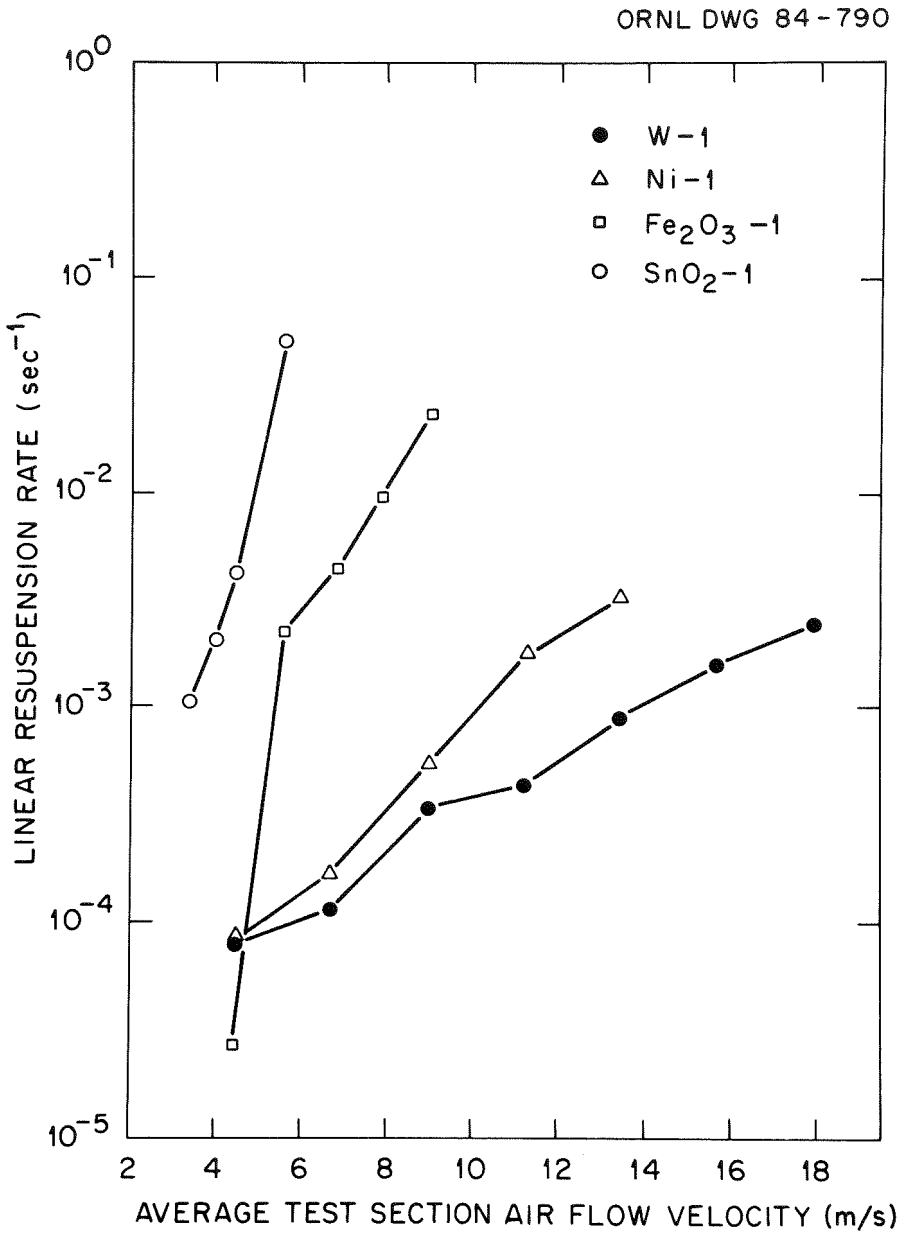

Figure 3. Aerosol Resuspension Test data, test groups W-1, Ni-1, Fe_2O_3-1, and SnO_2-1.

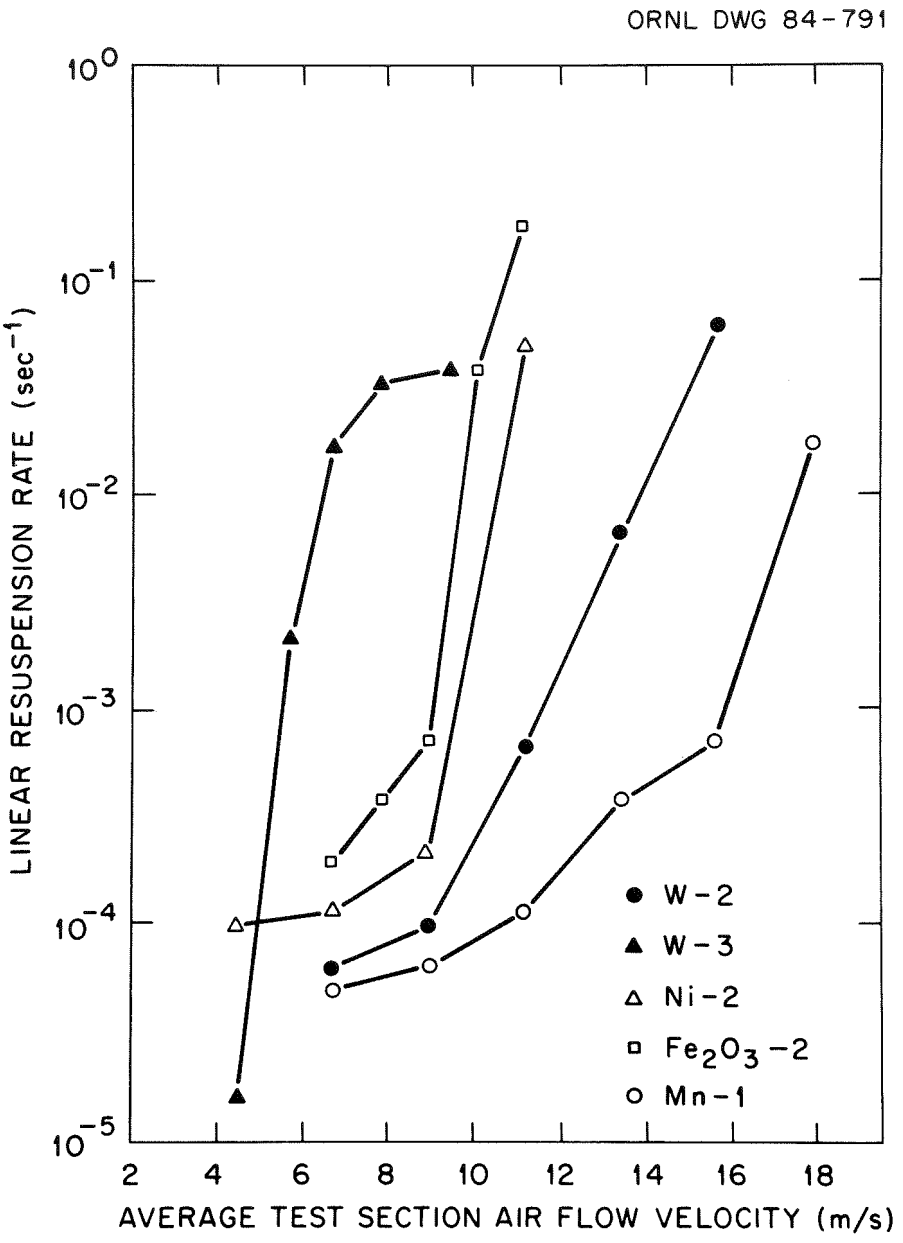

Figure 4. Aerosol Resuspension Test data, test groups W-2, W-3, Ni-2, Fe_2O_3-2, and Mn-1.

TECHNIQUES USED IN THE EXPERIMENTAL STUDY OF THE DEPOSITION OF AEROSOL PARTICLES TO SURFACES IN THE COOLANT OF A COMMERCIAL CARBON DIOXIDE COOLED REACTOR

A C Wells, J A Garland and J B Hedgecock
UKAEA, AERE Harwell, England

ABSTRACT

Deposition of particles in the coolant circuit of a nuclear reactor is a mechanism which reduces the amount of radioactivity that might escape in the event of an accident.

The rate of loss of particles to surfaces was measured with the aid of test aerosols injected into the coolant of a typical commercial advanced gas-cooled reactor (CAGR).

A small pressure vessel containing a specially made nebuliser with a counterflow device was used to produce aerosols rapidly, and ensure their efficient transfer to the reactor. This was used with an iron oxide sol to produce a submicron aerosol and to disperse suspensions of 2 and 5 μm iron oxide particles previously produced by means of a spinning-top aerosol generator. The principle of the air ejector was used to disperse a 17 μm batch of dry alumina particles by means of a jet of helium. Approximately 200 MBq ^{59}Fe were used to label some 10^8 particles of each size injected. The four sizes used were injected with the reactor at power and under full coolant flow. The 17 μm particles were also injected with the reactor shut down with coolant flow at 50% of its normal value. This was followed by measurements of the resuspension of the injected particles when the coolant flow was rapidly increased to normal full flow.

A series of filter samples of the coolant was taken immediately following each injection allowing the change in concentration with time to be determined, for approximately 200 minutes. To ensure adequate particle statistics the experiment was designed so that after an expected decrease in particle concentration by a factor of 1000 not less than 100 particles would be collected on a 20 minute sample.

At full flow, the deposition half-lives were initially about 20 s for the three smaller sizes of particles. For the larger, alumina particles, the initial half-life was $\simeq$ 120 s. The concentration of the sub-micron particles fell very quickly by a factor of about 1000, approaching background. In contrast, when the 17 μm alumina particle concentration had fallen by a factor of 50 a half-life of approximately 2 hours was quickly established. The behaviour of the 2 & 5 μm particles was intermediate but more similar to the sub-micron results. At low flow, the 17 μm particles deposited with an initial half-life of 50 s. On increasing the flow approximately 50% of the particles were resuspended in the gas stream. For 2, 5 & 17 μm, the results suggest that deposition is opposed by bouncing and blow-off.

INTRODUCTION

Certain postulated fault conditions may lead to the release of fission products from the fuel to the coolant of an AGR. Much of this radioactivity may become associated with particulate material suspended in the coolant gas [1]. In such circumstances rapid deposition of particles onto the internal surfaces of the coolant circuit would substantially reduce the amount escaping to the atmosphere with any gas leaking from the circuit.

Previous experience had indicated that deposition would be important. This study was designed to enable the measurement of a one-thousandfold reduction in concentration. The methods employed, and examples of results, are described here. The significance of the results will be discussed elsewhere [2].

METHOD

Experiments have been performed in normal operating conditions using spherical particles of 0.6, 2, 5 and 17 μm diameter. In addition one experiment investigated the behaviour of the 17 μm particles with the reactor shut down and at half normal coolant flow rate. Connections had been made into the coolant circuit of one of the CEGB's advanced gas-cooled reactors, as close as possible to the reactor pressure vessel, for both injection of particles into the coolant and for sampling from the coolant. These connections were in the gas by-pass lines, 300 mm ducts carrying coolant from the reactor to the gas-treatment plant and back (Figure 1).

A 13.8 mm pipe ran from the base of a small pressure vessel via two shut-off valves to the 300 mm duct returning coolant to the reactor. This pipe terminated facing downstream within the duct. Some 4 metres downstream of this injection point, but facing upstream, was a nozzle connected, via two stop-valves, by a 9.4 mm diameter pipe to a filter sampling point used to determine the quantity of material injected. A similar sampling system in the duct coming from the reactor was used to take a series of samples before, during and after the injection. To reduce losses all installed pipe-work was of smooth bore, kept as short and straight as possible. The valves were chosen to have bores the same diameter as the associated pipework.

Before each experiment five or six samples of the ambient reactor aerosol were taken. The previously prepared aerosol material was loaded into the particle pressure vessel from which the air was then flushed. The injection followed during which the particles were dispersed using an aerosol generator inside the pressure vessel and blown into the reactor coolant. A series of samples to monitor the changes in concentration with time due to deposition and mixing, of the injected particles was started at the beginning of the injection.

CHOICE OF PARTICLE AND LABEL

The principal processes influencing deposition (Brownian motion, impaction and sedimentation) depend on particle size, shape and density. Bounce-off and blow-off would also affect net deposition, and are expected

to vary with hardness and surface forces, which depend on composition. Spherical particles were preferred as they are most easily characterised aerodynamically. Diameters of 0.6, 2, 5 and 17 μm were chosen to represent the range of practical importance. Larger particles would be removed rapidly by the Central Inertial Collectors (aerosol collecting devices installed in 50% of the fuel channels), while smaller particles would need to be so numerous to carry a significant amount of activity that agglomeration would quickly cause growth.

Methods for preparing monodisperse iron oxide spheres of 2 μm and 5 μm were available and as iron oxide was thought to be the main constituent of the reactor aerosol these particles were the first to be used. Subsequently heterodisperse iron oxide spheres of MMD 0.6 μm were used to extend the range downwards. As 15–20 μm diameter iron oxide spheres could not be made quickly in sufficient quantity, 17 μm alumina spheres which were readily available [3] were used to extend further the size range.

Because of the expertise and equipment available only radioactive tracers were considered for this investigation. A suitable tracer must satisfy requirements of availability, half-life, radiological safety, chemical and physical properties, and be readily detectable in the presence of contaminants in the coolant gas. To meet the aims of the experiment approximately 10^8 particles would be required for each injection. A high specific activity was needed as 10^8 particles of 2 μm diameter weigh only about 1 mg. To meet logistical requirements, a half-life of several weeks was required; a longer half-life would increase radiological problems. The label must also be insoluble in water and acetone and involatile at reactor temperature.

The coolant background is caused by the presence of many nuclides. Several filter samples were collected to investigate this background. After a few days decay γ-spectrometry revealed significant amounts of ^{82}Br, ^{58}Co, ^{60}Co, ^{51}Cr, ^{131}I, ^{59}Fe and ^{54}Mn. Two nuclides appeared best to satisfy the above mentioned requirements, ^{56}Co and ^{59}Fe. ^{56}Co is not present in the coolant background. Two injections using 2 μm and 5 μm ^{56}Co labelled iron oxide spheres demonstrated that the Compton continuum in the output from the germanium-lithium detector due to ambient radioactivity in the reactor coolant set the amount required for an experiment to 75 MBq, which was beyond the resources of the Harwell variable energy cyclotron at the specific activity required. ^{59}Fe was therefore chosen despite the necessity of using 200–400 MBq amounts for each injection to overcome background ^{59}Fe. Discrimination against the background was improved by sampling prior to the injection and by using other background nuclides to estimate the ^{59}Fe background.

PREPARATION AND INJECTION OF PARTICLES

For the 2 μm and 5 μm iron oxide particles an aqueous sol (prepared by diluting with water/ethanol the dialysed product of the reaction between aqueous ferric chloride and aqueous ammonium carbonate) was fed on to the rotor of a spinning disc aerosol generator [4]. Immediately before use, freshly dried $^{59}FeCl_3$ solution was added to the sol. The $^{59}FeCl_3$ was

obtained at the highest specific activity available, typically 750 MBq $^{59}FeCl_3$ (1 mg Fe^{3+}) in 3 ml 0.1 M HCl. Overnight vacuum desiccation to remove the HCl was found necessary to avoid destabilising the sol which, particularly in the case of the 2 μm particle preparation prevented the formation of spheres.

A typical 2 μm sphere preparation consisted of 3 mg Fe as sol dispersed in 30 ml ethanol/water (1:2) which was then used to dissolve half the dried $^{59}FeCl_3$. The product of two preparations was bulked and used for an injection. The ethanol reduced the surface tension and improved the wetting of the rotor, leading to a more homogeneously sized output. With the disc speed at about 650 Hz the variations in mean particle size were obtained by varying the concentration of the sol used. The amount of sol was increased to 50 mg Fe when 5 μm diameter particles were required. A liquid flow-rate of 0.3 ml/min was found most suitable and resulted in a production run lasting about 100 minutes during which time conditions could be kept sensibly constant. Subsequent analyses indicated coefficients of variation of size of 10% for both 2 μm and 5 μm particles, product density of 2.4 g/ml and composition β FeOOH (by X-ray diffraction).

The generator was positioned in a 200 mm diameter vertical glass tube with dry filtered air drawn downwards past it. The column volume caused a delay during which the droplets evaporated to solid spheres of iron oxide before they were trapped in an impinger at the base of the column. The impinger contained a 50:50 solution of water: ethanol and a surface activating agent (0.2% Shell 'Teepol' 541). The collection efficiency, at least down to 2 μm diameter particles was almost 100%. The overall efficiency of generation, was approximately 60%. The particles were washed and centrifuged several times in water and acetone before being stored in acetone until used. Insignificant leaching of ^{59}Fe occurred during long periods in acetone or water.

The particles were transported to the reactor in suspension in acetone and just before use the acetone volume was adjusted and the suspension ultrasonically agitated to cause complete mixing. The suspension was then added to a reservoir inside the particle pressure vessel (250 mm diameter, 380 mm high). This consisted of a dome which could be raised and lowered onto a base and contained a gas-jet atomiser, a flushing counterflow jet and a suspension mixing device (Figure 2(a)). Two pipes supplied helium at a pressure of 172 kPa above reactor pressure (4 MPa) to operate the atomiser and to flush the aerosol into the reactor circuit through a third pipe, centrally placed and having a shaped exit to reduce losses. Two further pipes enabled the vessel to be depressurised through a filter and provided a pressure relief valve to prevent accidental overpressurisation. Helium, which was supplied from a bank of cylinders was used in preference to carbon dioxide because it could more easily be obtained at a sufficiently high flow rate.

The atomiser was required to disperse a suspension containing approximately 5×10^8 particles within 1 minute. Typically 10 ml of liquid would be required to reduce to acceptable proportions the probability that one droplet would contain more than one particle. A volatile suspending liquid of low viscosity would (a) speed atomisation and (b) facilitate evaporation to reduce particle losses by impaction onto the interior of the

pressure vessel. Acetone was satisfactory in both respects. Many atomisers re-cycle the liquid, an undesirable feature here leading to an increase in concentration. Avoiding this, a compact atomiser of Hounam [5] was chosen and modified to atomise 10 ml in 30 seconds, requiring a supply of helium 172 kPa above the ambient pressure of 4 MPa.

A laboratory test showed that < 5% of the particles were doublets or multiplets and this was confirmed from photomicrographs of the particles filtered from the reactor coolant. This also confirmed that the particles withstood the mechanical and thermal stresses imposed during the experiment. To prevent the particles from sedimenting in the particle reservoir during the few minutes between being loaded into the pressure vessel and being injected into the reactor a bubbling flow, controlled by a fine capillary, was introduced. Without special precautions, the jet from the atomiser would impact most of the aerosol on the base of the pressure vessel. To prevent this the apparatus included a counterflow jet. Laboratory experiments at atmospheric pressure demonstrated that, if the momentum rate (ie the product of efflux velocity and mass flow rate) were the same for the two jets of gas, the sprayed drops lost their forward velocity in a plane mid-way between the nozzles. This resulted in an efficiency of injection of approximately 25%. Before atomisation this counterflow jet was used to purge and pressurise the pressure vessel and after valves connecting the pressure vessel to the reactor were opened a flushing flow was established. Finally helium at pressure was applied to the atomiser to generate the aerosol.

It was not found possible to produce high specific activity ^{59}Fe-labelled monodisperse particles much less than 1 μm diameter by the spinning-disc method, so an aerosol was produced directly by using the pressure vessel atomiser. (MMD 0.6 μm, σg = 2.5). The reservoir contained 2 mg Fe as sol and 0.8 mg Fe^{3+} as dried down $FeCl_3$, in 3.9 ml ethyl alcohol/water (5:1) which was atomised and injected in a period of 30 seconds to 1 minute. An identical mixture was atomised in the laboratory to furnish particle size data by electron micrography.

As it was impracticable to make monodisperse 15 μm iron oxide spheres in sufficient quantity by the method described above, readily available porous alumina spheres ($\rho \sim 1.6$ g cm^{-3}) were used. These were monodisperse (coefficient of variation 10%) and of mean size 17 μm diameter. They were labelled with ^{59}Fe by slowly mixing $^{59}FeCl_3$ in HCl (0.1 M) with 1.5 g alumina spheres already wetted with 0.1 M HCl. The particles were washed several times in water and acetone before being dried, then heated in a furnace in air at 750°C for an hour. The efficiency of labelling was 90%. There was insignificant loss of activity on heating and no disruption of the spheres.

These alumina spheres were dispersed in the dry state inside the particle pressure vessel using the principle of the air-ejector (Fig 2(b)). Helium at a differential pressure of 172 kPa operated the disperser. The rate of suspension and dispersion was controlled by means of a bleed jet in the top of the powder reservoir. Particles were carried to the pressure vessel exit with negligible loss.

SAMPLING

It was required to collect a sequence of filter samples of particles from the coolant circuit with a minimum loss of time between samples. The coolant at the sampling points was at a pressure of about 3.9 MPa and at about 270°C. Considerable thought was given to eliminating unnecessary particle losses due to impaction caused by changes of direction of flow or varying pipe diameters. Thirty stainless-steel filter holders were made, each a small pressure vessel, consisting essentially of two shaped flanges with the filter paper and its pressure backing plate clamped between them. Sealing was effected by two 'o' rings. Each flange was connected to the sampling line by a "Swagelok Quick Connect" coupling.

After testing many combinations, ptfe 'o' rings and glass-fibre filters were chosen. Unprotected, the filters eroded rapidly in the gas-stream, and this was overcome by placing "100-mesh" stainless steel gauzes either side of each filter. This combination had high filtering efficiency, low retention of halides and a low resistance to flow.

The use of interchangeable filter holders in a single sampling position was preferred to a manifold arrangement because of the possible variation in particle losses for various sampling positions in the latter. No claim is made that the samples were strictly quantitative. Losses in the sampling line may have caused significant differences between the estimated concentration and the true concentration in the gas stream. However the main conclusions depend on the ratios between concentrations indicated by samples in a sequence and not on absolute values.

During a sequence of samples one of the two isolating valves was kept open throughout. At the end of each sample the second valve could be closed, the outlet side of the filter holder disconnected, then the inlet side, and a fresh unit inserted. This could be achieved within 10 seconds wearing thick gloves provided the female Swagelok couplings were lubricated every 15 or so changes.

A critical orifice 5.1 mm diameter was used with a pressure gauge and thermocouple thermometer to control and determine the sampled gas mass flow rate, which was approximately 0.115 kg/s.

A sample was taken just downstream of the injection point for the duration of the injection to estimate the amount injected. At the same time a series of short samples of the gas coming from the reactor was started. The sampling duration was increased in steps to ensure satisfactory particle statistics, at least 100 particles being collected per sample after a thousandfold fall in concentration.

The filter holders were taken back to Harwell for unloading. There the complete (mesh/glass-fibre sandwich) filters were placed face down in thin plastic containers for γ-counting in contact with an intrinsic lithium drifted germanium detector coupled to a 2048 channel analyser. The lower limit of detection for injected ^{59}Fe was affected by the presence of reactor ^{59}Fe. The presence of other background nuclides, eg ^{51}Cr, ^{58}Co, ^{60}Co and ^{54}Mn, sometimes enabled a separate estimate to be made of the ^{59}Fe due to the reactor alone. ^{58}Co was a particularly useful aid to the

interpretation of the resuspension experiment carried out in conjunction with the injection at low-flow during the biennial shut-down in April 1984.

RESULTS

Changes in concentration of ^{59}Fe with time for the four sizes, injected at full coolant flow are shown in figures 3(a) and (b) together with the pre-injection background concentrations. A separate injection of a non-depositing tracer, helium, demonstrated that the concentration change in the first few minutes due to mixing did not involve a correction of more than a factor of two. For the 3 smallest sizes a rapid fall in concentration over about 2-3 orders of magnitude (deposition half-life ~ 20 s) was followed by a more gradual one until behaviour was completely masked by ambient background. For the 17 μm particles the initial fall was less rapid ($t_{1/2}$ ~ 120 s) and became markedly more gradual ($t_{1/2}$ ~ 2 h) when the concentration was still ~ 20 times background.

The results for the low-flow injection of 17 μm particles and the subsequent resuspension are shown in figure 3(c). At low flow the 17 μm particles deposited with an initial half-life of 50 s. When full flow was re-established ~ 50% of the particles resuspended. A similar disturbance prior to the injection enabled ^{54}Mn and ^{58}Co ratios to ^{59}Fe to be determined and hence an estimate made of the contribution from resuspended ambient ^{59}Fe.

ACKNOWLEDGEMENTS

The authors are grateful to GNJ Lewis who carried out the γ spectrometry analyses, and to CEGB staff for their generous assistance. This work was funded jointly by the UKAEA and the CEGB.

REFERENCES

1. Collins, D.A. et al. Experiments relating to the control of fission product release from Advanced Gas-cooled Reactors. J. Nuclear Energy, Parts A/B, 20, 97-122.

2. Garland, J.A. et al. Experimental study of the deposition of iodine and other fission products in the coolant circuit of a CAGR. Fifth International Meeting on Thermal Nuclear Reactor Safety, Karlsruhe, 1984.

3. Holdoway, M.J. Physical properties of adsorbents for liquid chromatography. AERE-M 2749.

4. May, K.R. Spinning top homogeneous aerosol generator with shockproof mounting. J. Sci. Instrum. (1966) 43, 841-2.

5. Hounam, R.F. et al. The deposition of aerosol particles in the nasopharyngeal region of the human respiratory tract. Aerosol Sci. (1971) 2, 47-61.

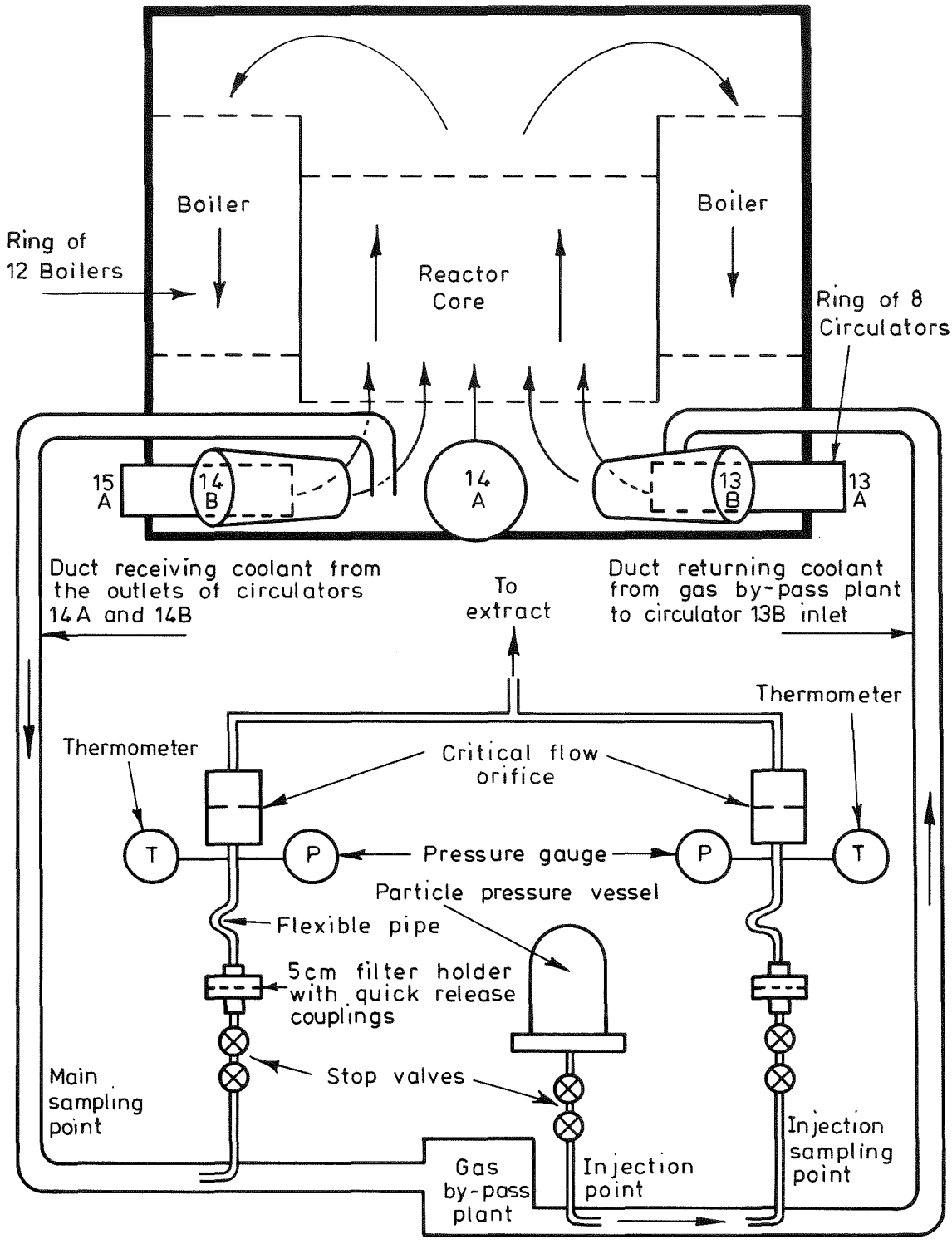

Fig.1. Schematic diagram of coolant flows and sampling and injection positions.

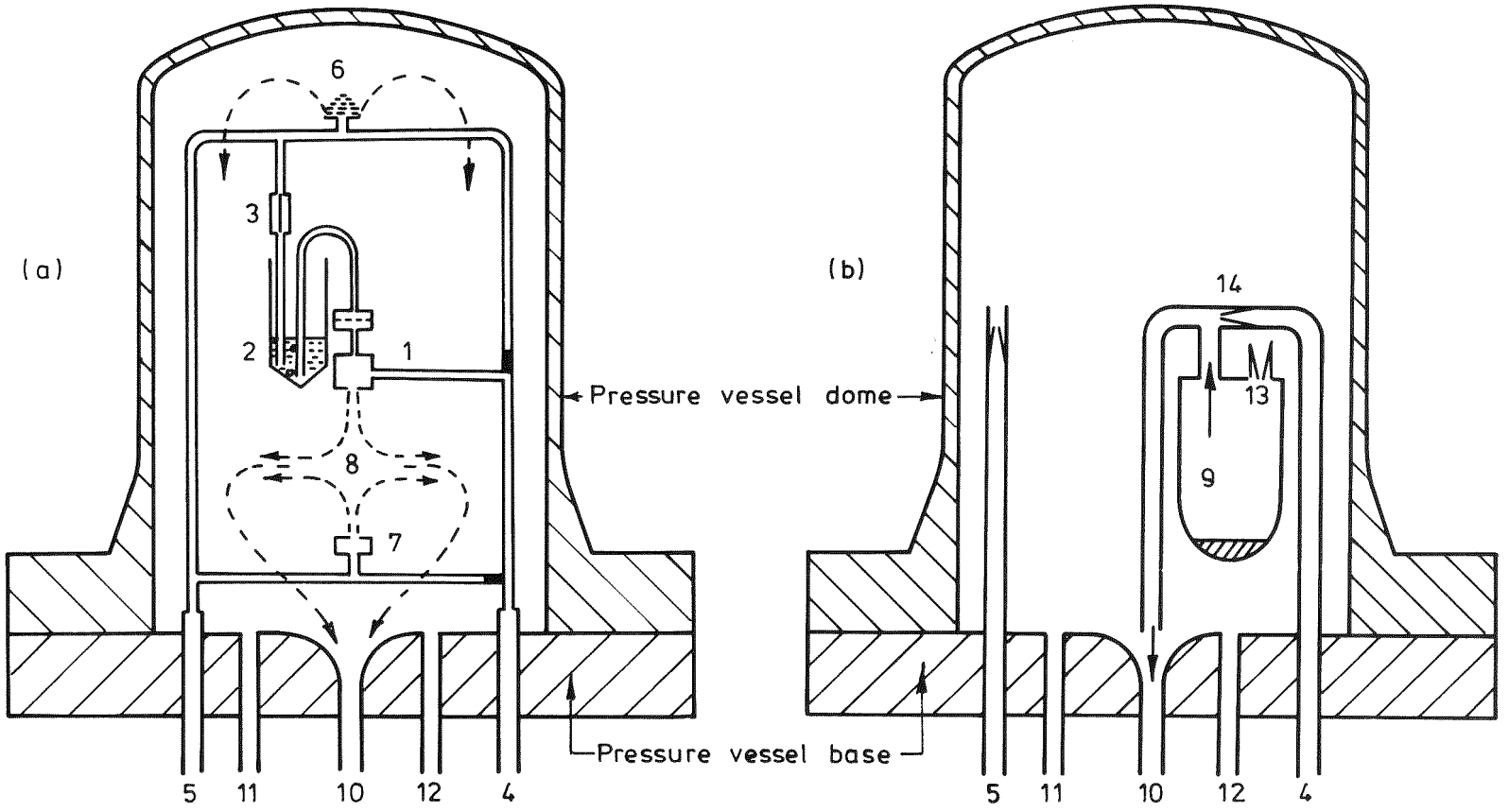

1. Atomiser
2. Suspension reservoir
3. Mixing capillary
4. Helium to Atomiser/Disperser
5. Helium flush input
6. Sinter
7. Counterflow jet.
8. Particle trajectory
9. Disperser
10. Exit to reactor
11. To vent
12. To pressure relief valve
13. Flow control jet
14. Ejector jet

Fig.2 .Particle pressure vessel showing arrangement for injecting (a) iron oxide particles and (b) alumina particles.

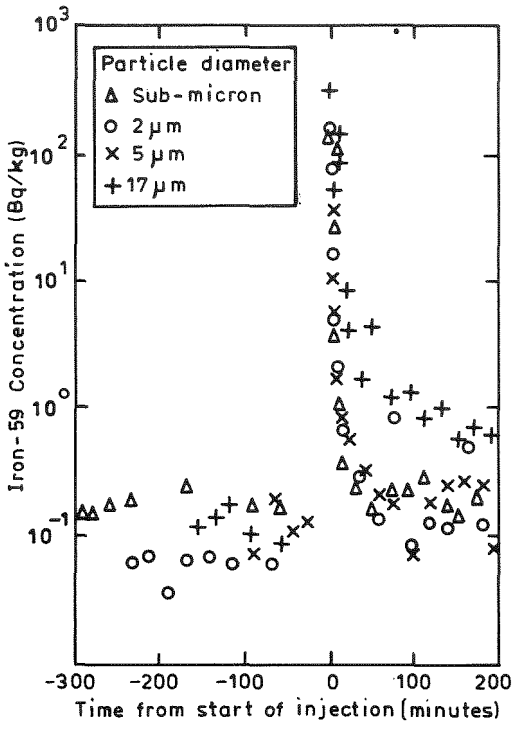

Fig 3(a) Change in concentration with time (full coolant flow)

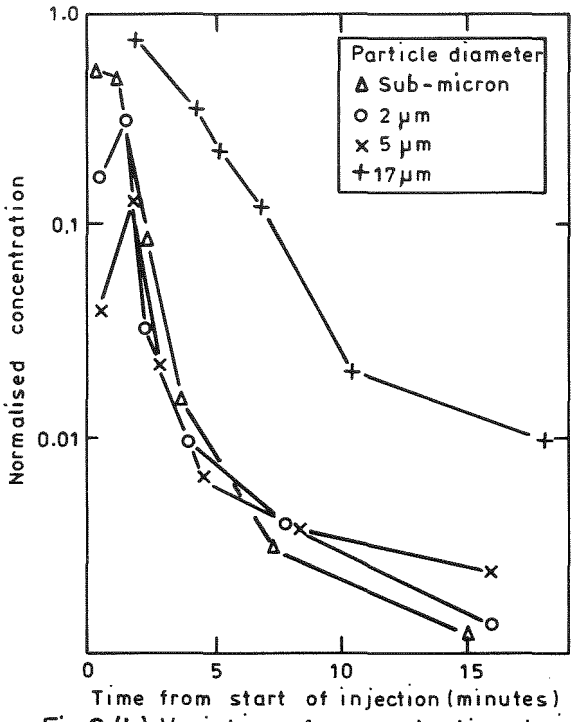

Fig 3 (b) Variation of concentration during the first 18 minutes. Concentration normalised by dividing by $\left(\frac{\text{quantity injected}}{120 \text{ tonne}}\right)$

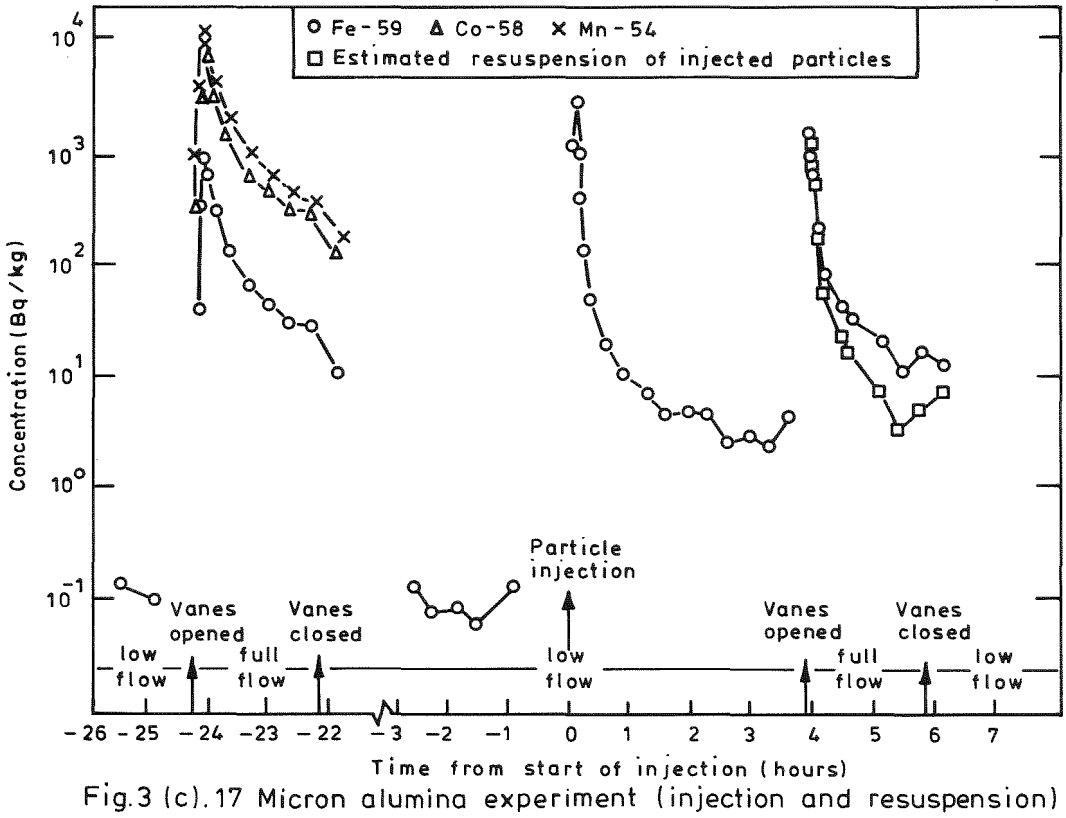

Fig.3 (c). 17 Micron alumina experiment (injection and resuspension)

Session VI: Aerosol Behavior in the Containment Large Scale Experiments and Comparison to Code Calculations

Chair: J. Fermandjian (CEA Fontenay-aux-Roses, F)
S. Jordan (KfK, FRG)

THE ABCOVE PROGRAM:

PRELIMINARY RESULTS OF TESTS AB5 AND AB6

R. K. Hilliard
L. D. Muhlestein

Westinghouse Hanford Company
Hanford Engineering Development Laboratory
Richland, Washington

ABSTRACT

A program for aerosol behavior code validation and evaluation (ABCOVE) is in progress in the United States. The purpose of the ABCOVE program is to provide a basis for judging the adequacy of existing aerosol behavior computer codes to describe inherent aerosol behavior in containment buildings during postulated breeder reactor accidents. The program involves pretest calculations by code developers and users, large-scale confirmatory tests in the 850-m^3 containment vessel of the Containment Systems Test Facility (CSTF), and blind post-test analyses and comparisons with experimental data. Two ABCOVE tests have been performed in the CSTF to date. In the first test, a single-species aerosol was used, with the aerosol generated by spraying sodium at a high rate into an air atmosphere. In the second test, the experimental conditions simulated an accident environment in which a fission product aerosol, NaI, was released in the presence of a sodium fire. Pretest computer code predictions were made by seven organizations using eight computer codes (HAA-3, HAA-4, HAARM-3, SOFIA, QUICK, QUICKM, MAEROS and CONTAIN).

INTRODUCTION

A multi-laboratory program for aerosol behavior code validation and evaluation (ABCOVE) is in progress in the United States. The ABCOVE program is a cooperative effort between the U. S. Department of Energy, the U. S. Nuclear Regulatory Commission, and their contractors currently involved in nuclear aerosol code development, testing or application. The purpose of the ABCOVE program is to provide a sound basis for judging the adequacy of existing aerosol behavior computer codes to describe inherent aerosol behavior in containment buildings during postulated severe breeder reactor accidents. The program involves both analytical calculations by code developers and users and large-scale experiments in the 850-m^3 containment vessel of the Containment Systems Test Facility (CSTF).

Each ABCOVE test is carried out in four stages: (1) planning and pretest computer code predictions based on intended test conditions, (2) test performance and analysis, (3) blind post-test code predictions based on known test conditions, and (4) comparison of code predictions with experimental measurements.

Two ABCOVE tests have been performed to date in the CSTF at the Hanford Engineering Development Laboratory (HEDL). The first test, AB5, was performed in September, 1982. A single-species aerosol was used in test AB5, with the aerosol generated by spraying sodium into an air atmosphere. A maximum suspended aerosol concentration of 170 g/m^3 was measured, providing a condition conducive to very high agglomeration and settling rates. Thus, test AB5 provided an important checkpoint for validating aerosol behavior codes under conditions representative of a severe breeder reactor accident involving a high aerosol source release rate.

A second test in the ABCOVE series (AB6) was performed in July, 1983. AB6 test conditions simulated the release of a fission product aerosol, sodium iodide (NaI), in the presence of a sodium fire which released sodium combustion product aerosol (NaO_x) at approximately 500 times the mass release rate of the NaI aerosol. The NaO_x source was continued well past the NaI source cutoff in order to demonstrate the "washout" effect of NaI by the continuing NaO_x aerosol. The maximum measured suspended concentration of NaO_x was approximately 30 g/m^3 and the maximum NaI concentration was approximately 0.1 g/m^3.

EXPERIMENTAL CONDITIONS

CSTF Containment Vessel

The CSTF containment vessel is 7.62 m in diameter, 20.3 m high, and 852 m^3 in volume. It is a carbon steel vessel with a design pressure of 0.517 MPa gauge. It is installed in a concrete pit with the top half extending above the main floor elevation, as shown in Figure 1. The interior surfaces are

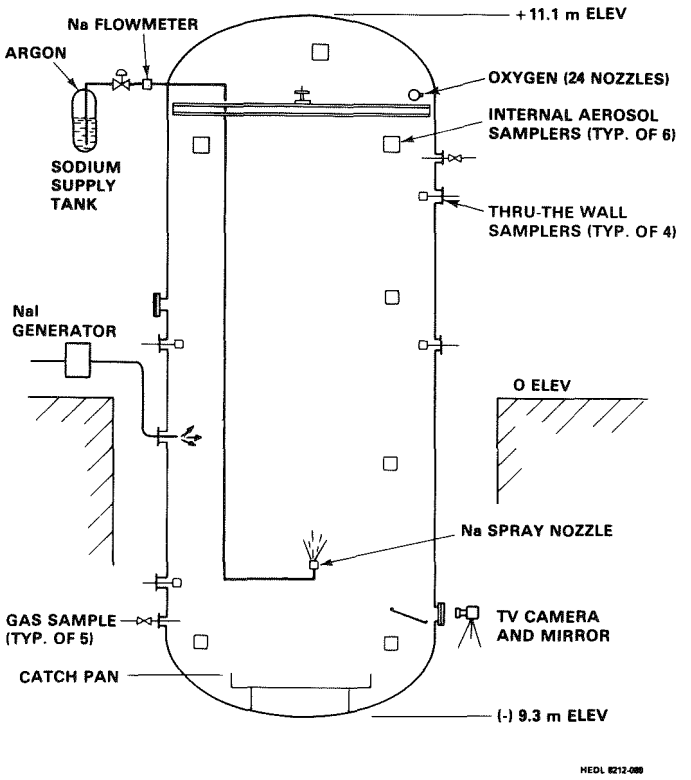

Figure 1. Schematic Diagram of Experimental Arrangement for ABCOVE tests.

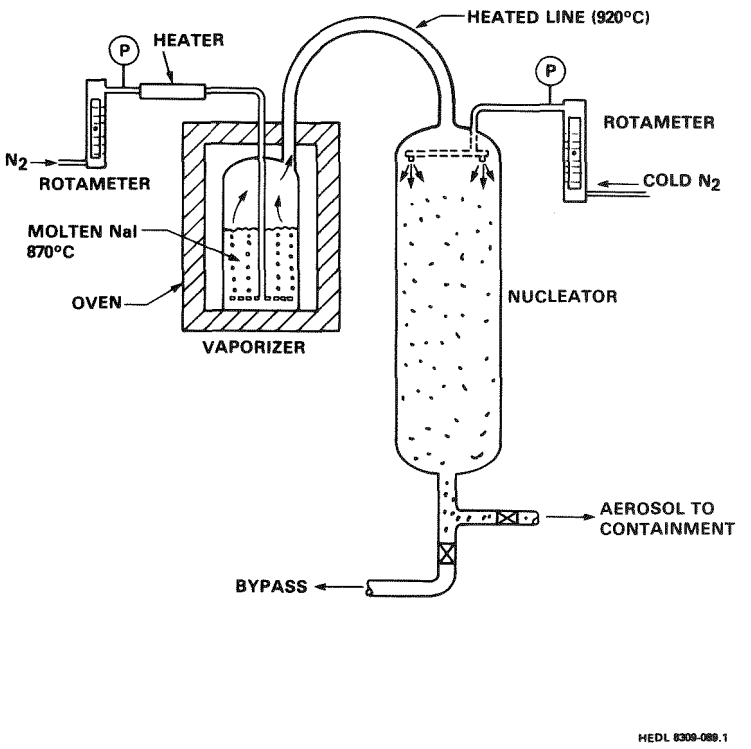

Figure 2. Schematic Diagram of NaI Aerosol Generation System.

coated with a phenolic paint, and the exterior is covered with a 25-mm layer of fiberglass insulation. The nominal leakage rate at 0.1 MPa gauge pressure is 1% per day.

Sodium Oxide Aerosol Generation System

A sodium combustion product aerosol was generated in both tests by spraying elemental sodium into the containment air atmosphere, where it burned to form a mixture of Na_2O_2 and NaOH. For convenience in discussion, this aerosol species is termed NaO_x. The sodium drops were of a size that burned completely before encountering any structural surfaces, so that 100% conversion to aerosol was assumed.

Sodium Iodide Aerosol Generator

NaI aerosol was generated by vaporizing NaI salt in a nitrogen carrier gas and then creating aerosol by a nucleation and condensation process. A sketch of the generation equipment is shown in Figure 2.

The average rate of NaI release to the containment atmosphere in test AB6 was 0.14 g/s. Cascade impactor measurements showed that the NaI source had an aerodynamic mass median diameter (AMMD) of 1.04 ± 0.08 μm and a geometric standard deviation, σ_g, of 1.55 ± 0.10. For spheres of 3.67 g/cm^3 density, this is equivalent to an AMMD of 0.543 um.

Experimental Measurements

The methods and instrumentation for experimental measurements used in these tests have been described previously[1]. The suspended mass concentration was measured by periodically passing a measured quantity of gas through small filters located directly in the containment atmosphere and subsequently analyzing the filter for NaI, Na and total mass. Samples were taken at 10 different locations throughout the containment vessel.

The aerodynamic size distribution was determined by sampling with cascade impactors inserted through the vessel wall. The instantaneous deposition rate was measured by exposing small coupons in a horizontal position in the containment atmosphere for brief periods of time. Total settled mass was measured by collecting aerosol in deposition cans located at 23 locations throughout the vessel. Total plateout on walls and ceiling was measured post-test by wiping representative areas of the vessel wall with a series of damp cloths. Thermal conditions were measured by 90 thermocouples, a pressure transducer, and five oxygen analyzers.

Procedure

After test conditions were defined by joint discussions with ABCOVE program participants, a test plan was prepared and sent to all participants. Pretest computer code predictions, based on the test plan, were completed and distributed before each test was performed. Although the actual test conditions were essentially the same as planned, some deviations did occur. An interim report was therefore sent to all code users which listed actual test conditions, but without information on aerosol behavior. Blind

post-test predictions were then made, based on the actual aerosol source and thermal conditions. No effort was made to improve the agreement of code and test results by post-test adjustment of input parameters, such as particle shape factors and source particle size. Finally, comparisons of code predictions with experimental measurements were made and a summary report issued for each test.

Test Conditions

The pertinent test conditions are summarized in Table I.

TABLE I

CONDITIONS FOR ABCOVE TESTS

Parameter	Test AB5	Test AB6
NaOx Aerosol Source		
Start Time (s)	13	620
Stop Time (s)	885	5400
Release Rate (g/s)	445	77.9
Total NaO_x Released (kg)	388	372
Material Density (g/cm^3)	2.50	2.45
Source Mass Median Radius (μm)	0.25	0.25
Source Geometric Standard Deviation	1.5	2.0
Mass Ratio, Total to Na	1.74	1.82
NaI Aerosol Source		
Start Time (s)	(a)	0
Stop Time (s)	(a)	3000
Release Rate (g/s)	(a)	0.14
Total NaI Released $(g)_3$	(a)	420
Material Density (g/cm^3)	(a)	3.67
Source Mass Median Radius (μm)	(a)	0.272
Source Geometric Standard Deviation	(a)	1.55
Containment Atmosphere		
Initial Temperature (^oC)	29.1	31.0
Initial Pressure (kPa)	122.0	114.2
Mean Temperature at End of Na Spray (^oC)	279	160
Pressure at End of Na Spray (kPa)	213.9	169.5
Maximum Mean Temp. of Vessel Wall (^oC)	93.5	78.9

(a) Not applicable.

COMPUTER CODES USED IN ABCOVE PROGRAM

Codes and Users

The aerosol codes and users participating in the ABCOVE program are identified in Table II. For test AB5, eleven code cases were made, using seven different codes. It should be noted that the MAEROS code is an early stand-alone version of the aerosol behavior model used in the CONTAIN code. For test AB5, three of the codes were used by more than one participant, permitting an assessment to be made of the effect of user-selected input for the same code. For test AB6, seven cases were made using seven different codes.

TABLE II

COMPUTER CODES AND PARTICIPANTS IN ABCOVE PROGRAM

Code	Particle Size Assumption	Particle Composition Assumption	User Organization	
			Test AB5	Test AB6
HAA-3	Log-Normal	Uniform[c]	General Electric, HEDL	HEDL
HAA-4	Log-Normal	Uniform	Rockwell/ESG	Rockwell/ESG
HAARM-3	Log-Normal	Uniform	Battelle-Columbus, HEDL, ORNL	HEDL
SOFIA	Log-Normal	Uniform	(e)	Westinghouse/AESD
QUICK	Discrete Bins	Uniform	Battelle-Columbus, ORNL	(e)
QUICKM[a]	Discrete Bins	Uniform[d] Within Bins	Battelle-Columbus	Battelle-Columbus
MAEROS[b]	Discrete Bins	Uniform Within Bins	HEDL	HEDL
CONTAIN	Discrete Bins	Uniform Within Bins	Sandia National Lab	Sandia National Lab

(a) QUICKM was formerly called MSPEC.
(b) MAEROS is a stand-alone version of aerosol behavior model used in CONTAIN.
(c) Uniform for entire size spectrum.
(d) Uniform within each bin but can vary between bins.
(e) Not used.

Altogether, eight codes were used: HAA-3[2], HAA-4, HAARM-3[3], SOFIA, QUICK[4], QUICKM[5], MAEROS[6], and CONTAIN[7]. The QUICKM code was formerly called MSPEC[5]. Each of the codes has unique differences in its modeling of physical processes, approach used for solution of the integro-differential

aerosol agglomeration equation, method of accounting for multiple aerosol species, and stage of development. Each code has its advantages and limitations. The first four codes listed above are "log-normal" codes, so called because they assume the aerosol size distribution to be log-normal at all times. The last four codes are "discrete," i.e., the aerosol size distribution is divided into a number of groups or bins, with constant physical characteristics assumed for each size group.

Treatment of multiple aerosol species is handled differently by each of the two classes of codes. The log-normal and QUICK codes assume that particle composition is independent of size, i.e., the aerosol is uniformly coagglomerated. The "uniform bin" codes assume only that the particles within each discrete size group have uniform chemical composition.

Code Reporting And Comparison Procedure

Each code user reported the predicted magnitude of eight output parameters which describe aerosol behavior. The reported parameters were: suspended mass concentration, aerodynamic mass median diameter of suspended aerosol, geometric standard deviation of particle size distribution, settling mean diameter, leaked mass, settled mass, plated mass, and instantaneous combined removal rate.

To provide a basis for quantitatively comparing results, the ABCOVE participants were requested to submit their code predictions of the above eight parameters in tabular form at specified points in time. Eleven reporting times were specified for test AB5; sixteen for test AB6.

After blind post-test predictions had been received and experimental measurements analyzed and correlated, the program coordinator (HEDL) prepared a detailed report for each test. Tabular and graphical comparisons of code predictions and experimental results were made for each of the eight aerosol behavior parameters at each of the specified reporting times. No attempt was made to judge the overall merit of any individual code or to rank the codes. However, quantitative comparisons were made and some general observations and conclusions were presented.

COMPARISON OF CODE PREDICTIONS WITH EXPERIMENTAL RESULTS

A large number of experimental measurements and code predictions were made for these tests. Approximately 500 samples were analyzed and 2000 specific code predictions were made for test AB5. Test AB6 had approximately 1000 chemical samples analyzed and over 3000 code predictions completed. Space limitation permits only a few parameters, at selected times, to be discussed in this paper.

Single-Species Aerosol Test (AB5)

Comparisons of blind post-test code predictions with experimental measurements are made in Table III for nine parameter-time combinations. The numbers in the body of Table III are ratios of the value predicted by the

TABLE III

COMPARISON OF CODE PREDICTIONS WITH EXPERIMENTAL RESULTS FOR SINGLE-SPECIES TEST AB5

	Ratio of Code Prediction to Experiment								
	Suspended Conc.								
Code Case	End of Source	10^4s	10^5s	AMMD at End of Source	σ_g at End of Source	Aero. Mean Settling Diam. At End of Source	Total Leaked Mass	Total Settled Mass	Total Plated Mass
HAA-3/GE	1.57	0.039	---	1.89	1.11	0.89	1.05	1.00	0.32
HAA-3/HEDL	1.86	0.017	1E-7	2.18	1.12	1.03	1.17	1.00	0.40
HAA-4/RI	1.35	0.007	---	2.33	1.17	0.84	0.84	1.00	0.71
HAARM-3/HEDL	3.07	1.38	0.047	1.85	0.95	0.61	2.26	0.99	0.51
HAARM-3/BCL	0.58	0.12	0.051	3.09	1.17	1.22	0.43	0.89	1.20
HAARM-3/ORNL	2.20	7E-12	---	1.91	0.95	---	1.07	1.01	0.06
QUICK/BCL	0.58	0.71	1.49	0.60	1.53	1.00	0.51	0.62	8.74
QUICK/ORNL	0.68	0.59	1.67	0.70	1.28	---	0.56	1.04	0.02
MSPEC/BCL	0.49	0.61	1.32	0.44	1.20	1.06	0.45	0.52	10.4
MAEROS/HEDL	1.11	1.66	1.66	0.72	1.31	---	---	1.00	0.25
CONTAIN/SNL	1.05	1.66	3.39	0.69	2.07	0.77	0.98	0.97	0.93
AVERAGE	1.32	0.61	1.20	1.49	1.26	0.93	0.94	0.91	2.14

code to the experimental value. Thus, a ratio of 1.0 would indicate perfect agreement between code prediction and experiment.

The suspended mass concentration was predicted reasonably well during the source release period, as shown by column 2 of Table III. It is interesting to note that the extreme ranges were produced by the same code, HAARM-3, used by different laboratories. An examination of the code input data revealed that a poor choice of values for the shape factors, chi and gamma, was the cause for one case to give high results, and high thermophoretic input values caused the second HAARM-3 case to give low results. The suspended concentration predicted by all eleven code cases are plotted in Figure 3 as functions of time. It should be pointed out that code case six, HAARM-3/ORNL, neglected to correct for non-Stokesian settling, and a post-test calculation using the Klyachko correction gave much better agreement with the other codes and with experimental measurement.

The ratios of code prediction to experimental results for suspended mass concentration are plotted as functions of time in Figure 4. The figure shows that the codes gave better agreement during the source release period than at later times. Figure 4 also shows that the discrete codes (curves 7-11) did much better at long times than the log-normal codes (curves 1-6). The total leaked mass (column 8 in Table III), which is really a form of integral suspended concentration since a constant leak rate was assumed, was predicted much better by all the codes than was the suspended concentration at specific times.

Table III also shows that the log-normal codes tended to overpredict the aerodynamic mass median diameter (AMMD) while the discrete codes underpredicted the AMMD. However, column 7 of Table III shows that all the codes predicted the aerodynamic mean settling diameter much better than the AMMD.

The codes predicted the total settled mass much better than the total plated mass, as shown by columns 9 and 10 in Table III. Most of the variation was due to differences in thermophoretic input data. Some of the codes, notably the discrete codes which handled wall plating correctly, did an excellent job of predicting the overall aerosol behavior in this single-species test.

Two-Species Aerosol Test (AB6)

NaO_x -- In test AB6, NaI aerosol was injected over the time period from 0 to 3000 seconds. Sodium oxide/hydroxide (NaO_x) aerosol was released from 620 to 5400 seconds. Comparisons of blind post-test code predictions with selected experimental measurements are presented in Table IV for each aerosol species.

The suspended mass concentrations of NaO_x predicted by the codes are plotted in Figure 5 as functions of time. The ratios of code predictions to experimental results for suspended concentration are plotted in Figure 6. The discrete codes (curves 5-7) performed better than the log-normal codes for this parameter, but nevertheless overpredicted the concentration by a factor of approximately two during the source release period.

TABLE IV

COMPARISON OF CODE PREDICTIONS WITH EXPERIMENTAL RESULTS FOR TWO-SPECIES TEST AB6

	Ratio of Code to Experiment for NaO_x					Ratio of Code to Experiment for NaI				
	Suspended Conc.		AMMD	Total	Total	Suspended Conc.		AMMD	Total	Total
Code Case	End of Source	$3x10^4$s	at End of Source	Leaked Mass	Plated Mass	End of Source	$3x10^4$s	at End of Source	Leaked Mass	Plated Mass
HAA-3/HEDL	2.89	0.05	1.10	2.41	0.58	1.79	8.7	1.12	1.20	1.39
HAA-4/RI	1.82	0.33	2.95	1.81	0.18	1.18	1.3	2.75	0.92	0.21
HAARM-3/HEDL	2.50	0.07	1.32	2.07	0.22	1.51	17.9	1.36	1.00	0.88
SOFIA/W-AESD	2.66	1.68	1.61	2.21	0.59	1.80	35.9	1.62	(a)	0.69
QUICKM/BCL	1.70	1.03	0.61	1.68	0.21	1.02	2E-8	0.61	0.72	0.19
MAEROS/HEDL	1.75	0.69	0.61	(a)	0.10	1.03	4E-6	0.63	(a)	0.11
CONTAIN/SNL	1.81	1.07	0.67	1.69	0.24	1.06	1E-5	0.65	0.73	0.25
AVERAGE	2.16	0.70	1.27	1.97	0.26	1.34	9.1	1.25	0.91	0.50

(a) Not reported.

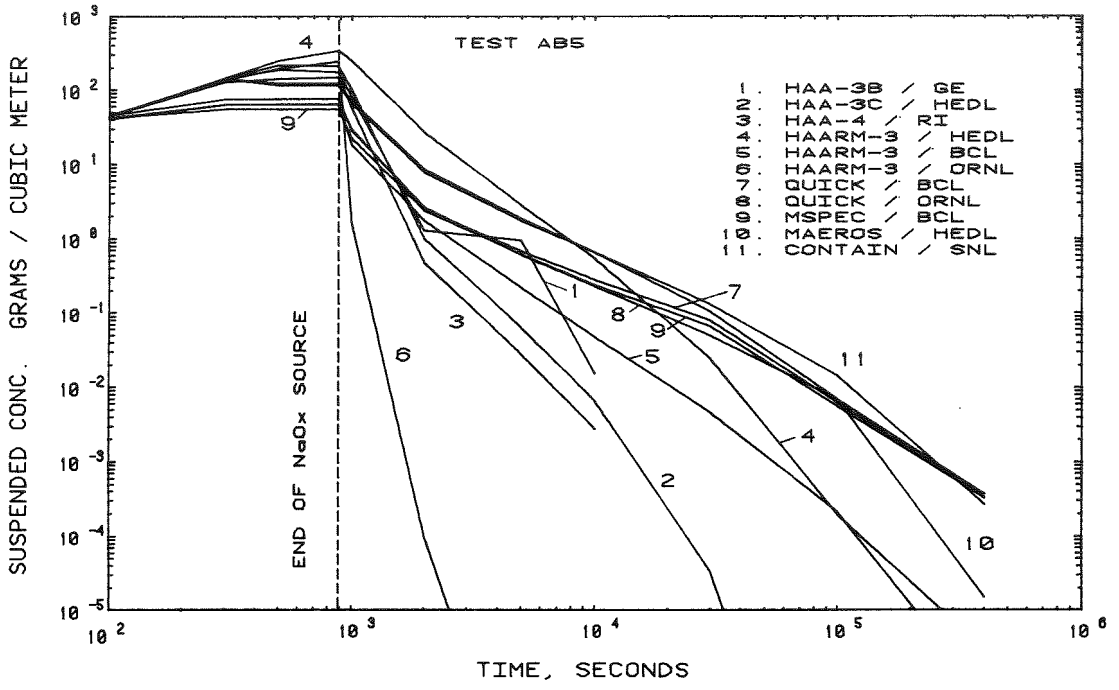

Figure 3. Code Predictions of Suspended Mass Concentration for Test AB5.

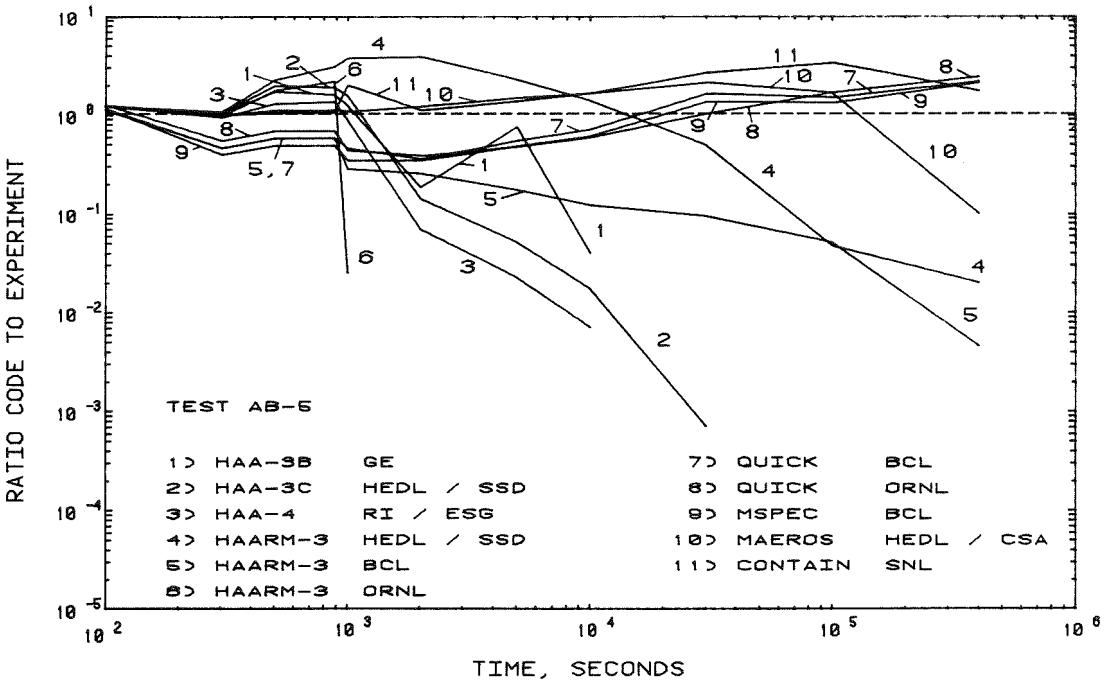

Figure 4. Ratios of Code Prediction to Experiment for Suspended Mass Concentration -- Test AB5.

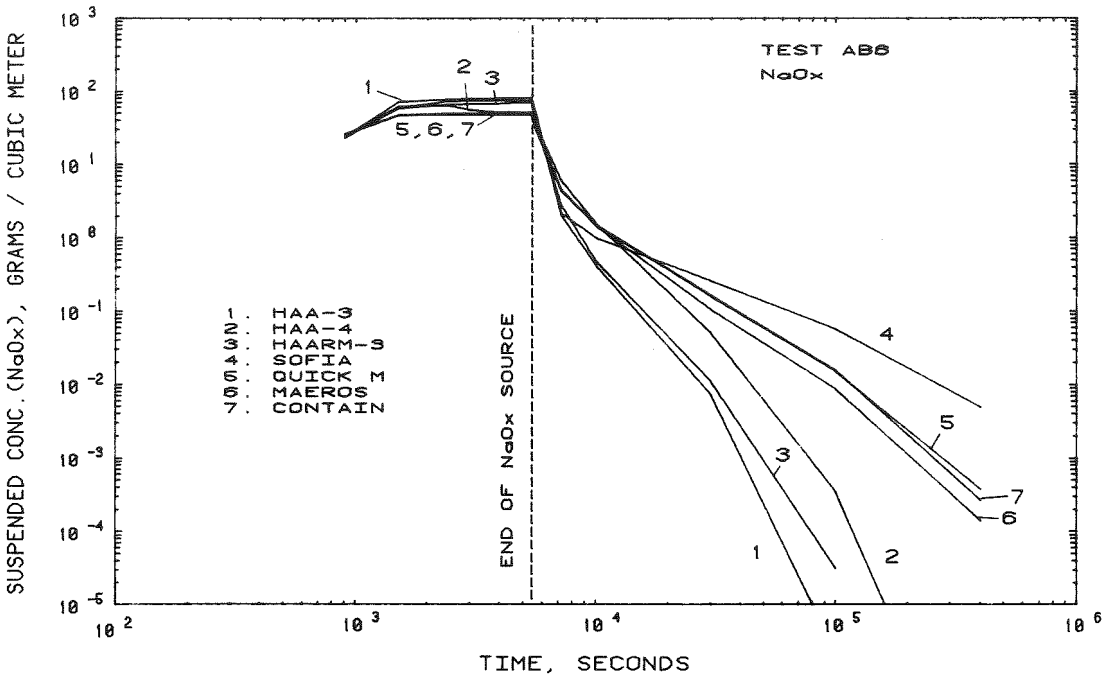

Figure 5. Code Predictions of Suspended NaO_X Mass Concentration for Test AB6.

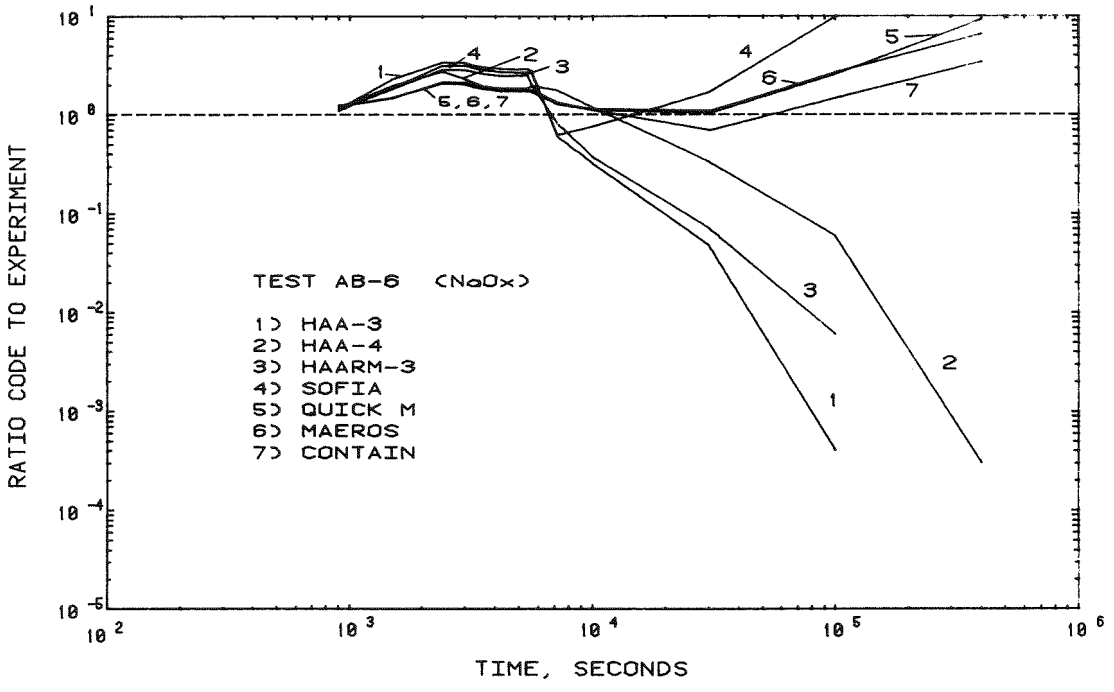

Figure 6. Ratios of Code Prediction to Experiment for Suspended NaO_X Concentration -- Test AB6.

The plated mass of NaO_x was underpredicted significantly by all codes, as shown by column 6 of Table IV. Experimental measurements of deposition on vertical stainless steel panels installed in various locations within the containment atmosphere suggested that thermophoresis was a minor contributor to wall deposition. Turbulent deposition and impaction were postulated to be important processes for vertical wall deposition. None of the codes modeled these processes.

NaI -- The suspended mass concentrations of NaI predicted by the codes are plotted in Figure 7. All of the codes predicted similar concentrations during the source release period. After the end of the NaI source, the discrete codes predicted a very rapid decrease of NaI concentration with time. The log-normal, uniform co-agglomeration codes predicted a much lower rate of decrease. Figure 8 shows that the log-normal, uniform co-agglomeration codes predicted the experimental results better than the discrete codes for NaI. This surprising finding will be investigated further in the next ABCOVE test. One possible explanation is that resuspension of previously deposited NaI acted as a small, unaccounted for source that counteracted the rapid washout effect predicted by the discrete codes.

Table IV shows that all of the codes predicted the total leaked mass of NaI very well (±30%). The plated mass of NaI was also predicted better by all the codes than was the NaO_x mass, though there was still considerable scatter in the results.

The fiberglass paper collection stages used in the cascade impactors were examined for the relative proportion of NaO_x and NaI. The ratio of NaI to NaO_x was not independent of particle diameter, as assumed by the log-normal codes. However, neither did the ratio continuously increase with increasing particle size, as predicted by the discrete codes. This behavior is being investigated further.

CONCLUSIONS

The ABCOVE program is in progress and final evaluation of aerosol codes has not yet been made. However, several preliminary conclusions can be drawn, based on the work completed to date.

1. The ABCOVE program provides an opportunity to assess the true performance of current aerosol behavior codes and their users without the benefit of post-test adjustments to force fit the code with experiment. Undoubtedly, better agreement could be obtained by a post-test effort.

2. All eight codes performed reasonably well in predicting the suspended concentration during source release periods and the total leaked mass for both species (within a factor of 2 for NaO_x, and within a factor of 1.3 for NaI). This is an encouraging finding because of the importance of leaked mass as it relates to radiological consequences for accident cases where containment integrity is maintained.

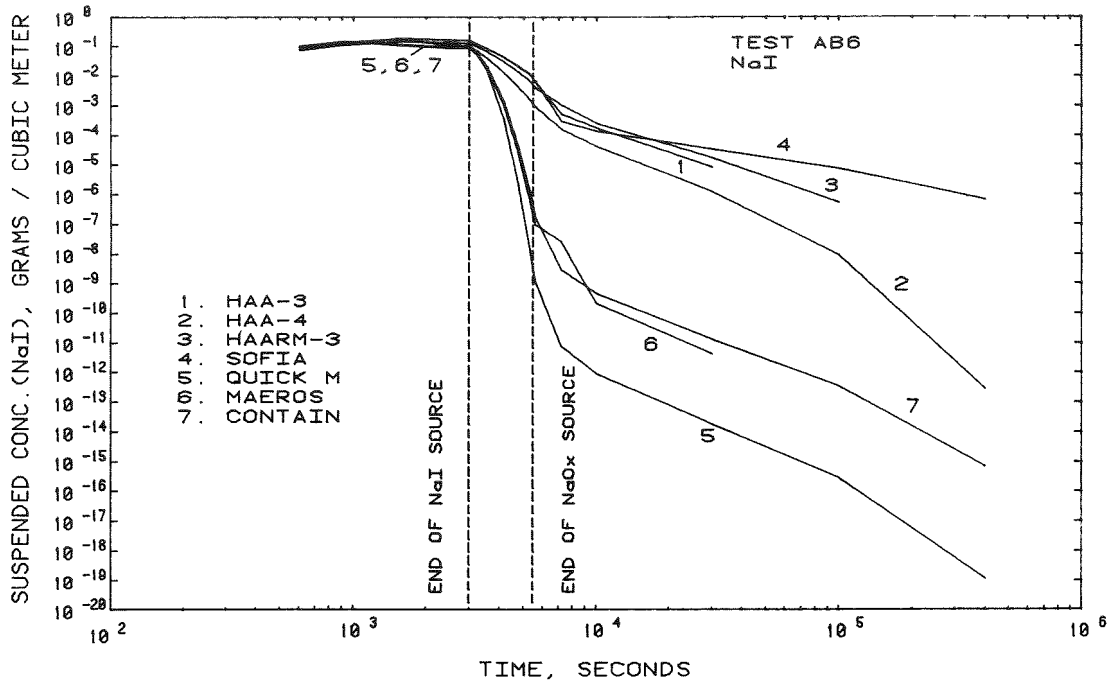

Figure 7. Code Predictions for Suspended NaI Mass Concentration -- Test AB6.

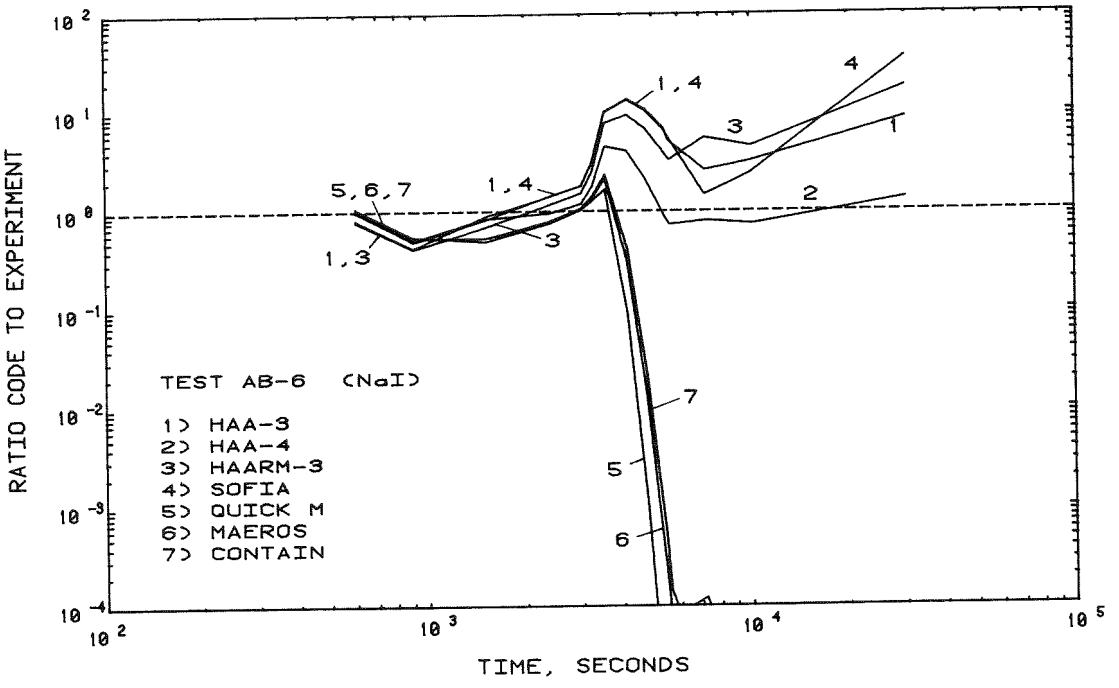

Figure 8. Ratios of Code Prediction to Experiment for Suspended NaI Concentration -- Test AB6.

3. The overall performance of "discrete" codes was somewhat superior to that of log-normal codes. However, the latter group of codes predicted the total leaked mass as well or better than the discrete codes, even for the two-species test. The discrete codes predicted particle sizes and NaO_x concentration better at long times after the end of the source release period.

4. Variations between predictions made by the same codes but by different users can be larger than variations between different codes. Users must use valid input data for user-selected input parameters. When this was done, different users of the same code obtained essentially identical results in the ABCOVE exercise.

5. Sedimentation was by far the dominant aerosol removal process in both tests and for both aerosol species, as predicted by all codes.

6. Predictions of wall plateout were widely scattered among the codes (by a factor of ±10). Experimental measurements suggest that turbulent deposition and impaction are important processes for transport to vertical surfaces. None of the codes included such processes.

7. Resuspension of previously deposited aerosol may have served as a small source term that is unaccounted for in any of the codes. This has negligible effect on aerosol behavior at early times when the concentration is high, but can cause the codes to severely underpredict the concentration at long times.

8. Evaluation and ranking of individual codes has not been done at the present stage of the ABCOVE program. The detailed reports of the experimental results and code predictions for each test will provide a sound basis for such evaluation.

REFERENCES

1. J. D. McCormack and R. K. Hilliard, "Aerosol Measurement Techniques and Accuracy in the CSTF," Proceedings of the CSNI Specialists Meeting on Nuclear Aerosols in Reactor Safety, held in Gatlinburg, TN, April 1980, NUREG/CR-1724, ORNL/NUREG/TM-404, p. 249, Oak Ridge National Laboratory, Oak Ridge, TN, October 1980.

2. R. S. Hubner et al, HAA-3 User Report, AI-AEC-13038, Atomics International Division, Rockwell International, Canoga Park, CA, March 30, 1973.

3. J. A. Gieseke et al, HAARM-3 User's Manual, BMI-NUREG-1991, Battelle Columbus Laboratories, Columbus, OH, January 5, 1978.

4. H. Jordan et al, QUICK User's Manual, NUREG/CR-2105, BMI-2082, Battelle Columbus Laboratories, Columbus, OH, April 1981.

5. H. Jordan, P. M. Schumacher and J. A. Gieseke, MSPEC User's Manual, NUREG/CR-2923, BMI-2100, Battelle Columbus Laboratories, Columbus, OH, June 1982.

6. F. Gelbard, MAEROS User Manual, NUREG/CR-1391, SAND80-0822, Sandia National Laboratories, Albuquerque, NM, December 1982.

7. K. K. Murata, et al, "CONTAIN: Recent Highlights In Code Testing and Validation," Proceedings of the International Meeting on LWR Severe Accident Evaluation, August 28 - September 1, 1983, Cambridge, MA.

Properties of Sodium Fire Aerosols and Recalculation of their Behaviour in Closed Containments

W. Cherdron, H. Bunz, S. Jordan
Kernforschungszentrum Karlsruhe GmbH
Laboratorium für Aerosolphysik und Filtertechnik I
D-7500 Karlsruhe,

Abstract

The characterisation and behaviour of nuclear aerosols is of fundamental importance for the calculation of the radiological consequences of reactor accidents. In LMFBR accidents one of the main sources of nuclear aerosols is burning sodium. The long term behaviour of aerosols depends strongly on the physical and chemical properties of single particles.

Experiments on the chemical transformation have to performed in the aerosol loop of the FAUNA facility. The recalculations of the aerosol behaviour using the codes PARDISEKO IV and KONVEC show a good agreement with the experiments.

Introduction

In LMFBR accidents sodium fires cause the release of large amounts of aerosols consisting of different sodium compounds with different properties. The characterisation of these aerosols is of fundamental importance for the calculation of radiological and chemical consequences, for the lay out of filter systems, reactor components and the environmental impact of reactor accidents. An extensive program was performed in the 60 m long FAUNA aerosol test loop for evaluation of the chemical transformation process of the sodium-fire aerosols.

Using the codes PARDISEKO IV and KONVEC, the aerosol behaviour in closed containments has been calculated and compared with the experimental results.

Chemical behaviour

In normal atmosphere hot sodium burns to sodium oxides. With excess sodium the reaction product is likely to be Na_2O:

$$2\ Na + 1/2\ O_2 \rightarrow Na_2O$$

If there is enough oxygen available, the formation of peroxide Na_2O_2 is likely:

$$2\ Na + O_2 \rightarrow Na_2O_2$$

Only under extreme conditions the reaction to superoxide NaO_2 may happen:

$$Na + O_2 \rightarrow NaO_2$$

This product is not stable and therefore not taken into account for further investigations.

The physical shape of fire particles is strongly influenced by chemical composition of the surrounding atmosphere. Sodium oxide aerosols react very quickly with the water vapor of the atmosphere to become sodium hydroxide.

$$Na_2O_2 + H_2O \rightarrow 2\ NaOH + 1/2\ O_2$$

$$Na_2O + H_2O \rightarrow 2\ NaOH$$

The exposure of sodium oxide aerosols to humid air results in the formation of sodium hydroxide solution droplets. The relative humidity of the atmosphere must exceed the equilibrium relative humidity for the saturated solution before condensation can take place. At higher relative humidities absorption continues until the solution is diluted to the point of equilibrium with the water vapor. The point above which solution droplets will be present, is calculated to be 35 %, but this value was not yet experimentally confirmed.

Sodium hydroxide aerosols react with the carbon dioxide content of the air to form sodium carbonate resp. sodium hydrogen carbonate.

$$2\ NaOH + CO_2 = Na_2CO_3 + H_2O$$

Sodium fire particles are expected to become carbonate within seconds. The persistance of NaOH for longer times may result from the formation of a shell of reacted and solid carbonate. The carbonate particles are under most atmospheric conditions (r. h. not higher than 95 %) dry particles.

Experiments were performed to confirm these calculations of reaction rates. For this purpose, the aerosol loop of the FAUNA facility (Fig. 1) was used as an open loop. Inside the FAUNA-containment sodium fire aerosols were produced by a Na-fire in a circular burning pan of 40 cm diameter. Closely above the burning area a hood was placed sucking aerosols into the open loop. Aerosol samples were taken immediately above the burning pan and in distances from the source where the particles had an age of 160 resp. 260 seconds. At these sample ports mass concentration of the aerosol was determined by filter probes, the size distribution impactor by measurements. Additional filter probes were taken for the wet chemical analysis. The main goal of the experiments was the determination of the reaction time from NaOH to carbonate. (According to Cooper /1/ the transformation from oxides to NaOH is in fractions of seconds) Therefore two kinds of experiments were performed: Experiments under normal atmospheric conditions, mostly at relative humidity > 50 %, and experiments with a closed reaction vessel and artifical gas supply, providing r. h. of 20 % and ≦ 3 %. The results under these conditions are shown in Fig. 2. At relative humidities ≧ 20 % after 60 seconds nearly 50 % of the aerosols are converted to carbonate and after 260 seconds the transformation is nearly completed. The tests showed, that these particles (after 260 sec) contain already 20 % of sodium hydrogen carbonate. At relative humidities of about 3 %, the formation process is much more slower, as can be seen from Fig. 2. After 260 seconds, only about 20 % of the aerosols are converted to carbonate. This is in agreement with the theory that dry particles react much slower than wet particles. Nevertheless the experimental determined reaction rates are slower than the predicted rates by theory. That may be due to the fact, that wet particles are already converted to carbonate on the surface which forms a solid cristal structure. The inside of these particles is still sodium hydroxide. In this case smaller particles should have a higher content of sodium carbonate than larger particles. This assumption have be confirmed by analysing single impactor stages on the sodium carbonate content.

Physical behaviour

During a sodium fire in a closed containment, aerosols of different ages are always mixed. Primary aerosols can only be investigated nearly the flame. Using a high temperature version of the Anderson Impactor operating directly above the burning pan of a pool fire, 10 - 30 seconds old aerosol have been measured. By this method the aerosols were found to have a mass median aerodynamic diameter of about 0.9 µm. 5 minutes after the start of the fire the measurements yielded a mean diameter of 2,35 µm.

In spray fires, larger particles have been measured with up to 4.8 µ mass median aerodynamic diameter. For this behaviour two reasons might be of influence: First the high mass concentrations of spray fires, causing high agglomeration rates. Second the burning process which takes place at

small sodium droplets. As already mentioned chemical transformation processes have no important influence on particle structure if the sodium fire takes place in a completely closed containment. In this case the particles consist of sodium oxides only.

Under this conditions the behaviour and the properties of the aerosols are only influenced by the physical processes of aerosols like coagulation and sedimentation. Therefore the course of the airborne mass concentration can be used for determining the dynamic shape factor χ. The shape of the particles was found to be spheres-like, the aerodynamic shape factor was measured to be 1.1.

Looking at the course of the airborne mass concentration it must be distinguished between pool- and spray fires. In pool fires, there is an aerosol source from the burning pool, the release rate is dependend from the momentaneous burning rate. The duration of the aerosol formation rate is comparable with the burning time. Fig. 4 shows as an example the sodium aerosol mass concentration for a 2 m^2 and a 12 m^2 pool fire in the 220 m^3 containment of the FAUNA facility. After the fire, the mass concentration decreases from approx. 10 g/m^3 to 0.1 mg/m^3 in nearly 100 hours. With spray fires it is possible to produce a high intensive, but short aerosol source. Therefore, the aerosol mass concentration shows, compared with pool fires, a quite different behaviour as shown in Fig. 5. In this spray fire experiment the aerosol source exists only for approximately 10 seconds, but the mass concentration can reach more than 60 g/m^3. In this case the mass concentration decreases in nearly 20 minutes from 60 g/m^3 to 5 g/m^3.

4. The codes PARDISEKO IV and KONVEC

a) PARDISEKO IV

The PARDISEKO IV /2/ computer code describes the behaviour of a polydisperse aerosol system in a closed system. Like other similar codes /3/ it is based on the two assumptions of homogeneous mixing in the volume on the one hand and of the description of the particle properties by one single parameter, the mass equivalent radius, on the other hand. Making these assumptions the general space-dependent aerosol equation can easily be transformed into a set of coupled first-order differential equations which can be solved by standard numerical methods. Except these restrictions any arbitrary situation can be treated by PARDISEKO IV. At the moments the code includes the followong aerosol physical processes:

Brownian and gravitational coagulation
deposition by gravitational settling
deposition by Brownian diffusion
deposition by thermophoresis
time dependent leakage
enhanced deposition by natural turbulent convection /4/.

The last effect was added to the code as discrepancies and inconsistencies were detected between the calculated and the experimental results of the NALA-program being characterized on the one hand by ideal, spherical particles consisting of liquid sodium and on the other side by

strong natural convection due to internal heat sources.

The formulations developed by Sehmel /5/ for wind channel experiments could be generalized and applied to closed vessels. The characteristic parameter, the friction velocity, has to determined by dimensional analysis or can be calculated by the computer code KONVEC being described later.

After introducing these additional removal mechanisms the size dependance of the removal processes was found to reproduce the experimental results much better not only regarding the behaviour of the mass concentration but also regarding the calculated particle size.

b) KONVEC

The experiments on sodium pool fire /6/ showed, that above small burning areas a chinney-like gas convection with velocities up to 8 m/sec exists. This convection causes a mixing of aerosols and influences the temperature distribution inside the containment. For investigating possible influences of the convection movement on the physical processes of aerosols (i.e. turbulent deposition) it is necessary to calculate the friction velocity u*, which is an important input parameter for PARDISEKO IV. For this reason, the code KONVEC had been developed. This code is based on the K-turbulence model /7/ and is designed for axis-symmetric closed cylindrical containments. From this code the kinetic turbulent energy K the friction velocity u* can be derived, as well as the velocity and temperature distribution inside the containment. Fig. 3 shows the FAUNA-containment and the necessary modeling.

5. Recalculations of Experiments and Conclusions

The PARDISEKO IV code is used to recalculate the behaviour of the aeorosol particles observed during the pool fire experiments as well as during spray fires. The most important input data being necessary for the code calculations are:

- release rate of the source particles as a function of the time
- size distribution of the source particles
- fricition velocity u as a function of the time

Unfortunately these parameter cannot be measured directly and have to be determined on the basis of other measurements or calculations of KONVEC for the friction velocity. An upper limit of the release rate is given by the burning rate of the sodium being evaluated using the oxygen consumption rate. The fraction of the sodium oxide being released in the form of aerosol particles can be estimated on the basis of the experience gained in earlier experiments. In these experiment it was determined by balancing the total mass of aerosol depleted in the vessel at the end of the experiment. The size of the source particles are also taken from other experiments performed at a particle concentration being sufficiently low that coagulation can be neglected within the time period necessary for the measurement.

In the case of the spray fire an alternative approach is used to get the initial conditions. Since the actual particle release takes places in a very short time, the calculation is started after the end of the fire at the concentration and with the particle size measured at this time. The

time behaviour of the friction velocity is estimated on the basis of the slope of measured aerosol mass concentration and the measured temperature difference between gas and wall.

The results of the recalculations in comparison to the experiments can be seen in Fig. 4 and Fig. 5. They show that the strong transient effects taking place during and just after the fire are quite well approximated by taking into account the turbulent deposition. To get better agreement on the one hand the experimental data basis should be more strict and complete and on the other hand the modelling of convection and of the behaviour of aerosol particles in transient thermodynamic conditions has to be improved. The today calculations have to be regarded as rough but helpful approximations to the real physical situation being able to evaluate an upper and a lower limit. Therefore, the accuracy seems to be sufficent for any accident scenarios.

Literature

/1/ Cooper, D.W., Predicition of the Rates of chemical Transformation of Sodium Fire Aerosols, Proceedings onf the CSNI Specialist Meeting on Nuclear Aerosols in Reactor Safety, pp 181-195, NUREG/CR-1724, ORNL/NUREG/TM-404, CSNI-45

/2/ H. Bunz, PARDISEKO IV, Ein Computerprogramm zur Berechnung des Aerosolverhaltens in geschlossenen Behältern, KfK 3545, (April 1984)

/3/ Nuclear Aerosols in Reactor Safety, CSNI SOAR # 1, OECD (June 1979)

/4,5/ H. Sauter, H. Bunz, Aerosol Behaviour in a Closed Vessel under the Regime of Natural Turbulent Convection, Part I: Experimental Facts; Part II: Computer Code Calculations, GAeF, München, 14.-16.09.1983

/6/ W. Cherdron, S. Jordan, Die Natriumbrandversuche in der FAUNA-Anlage auf Brandflächen bis 12 m^2, KfK 3041

/7/ A. D. Gosman, W. N. Pun: Heat Transfer, Report No. HTS/74/2, London, 1973

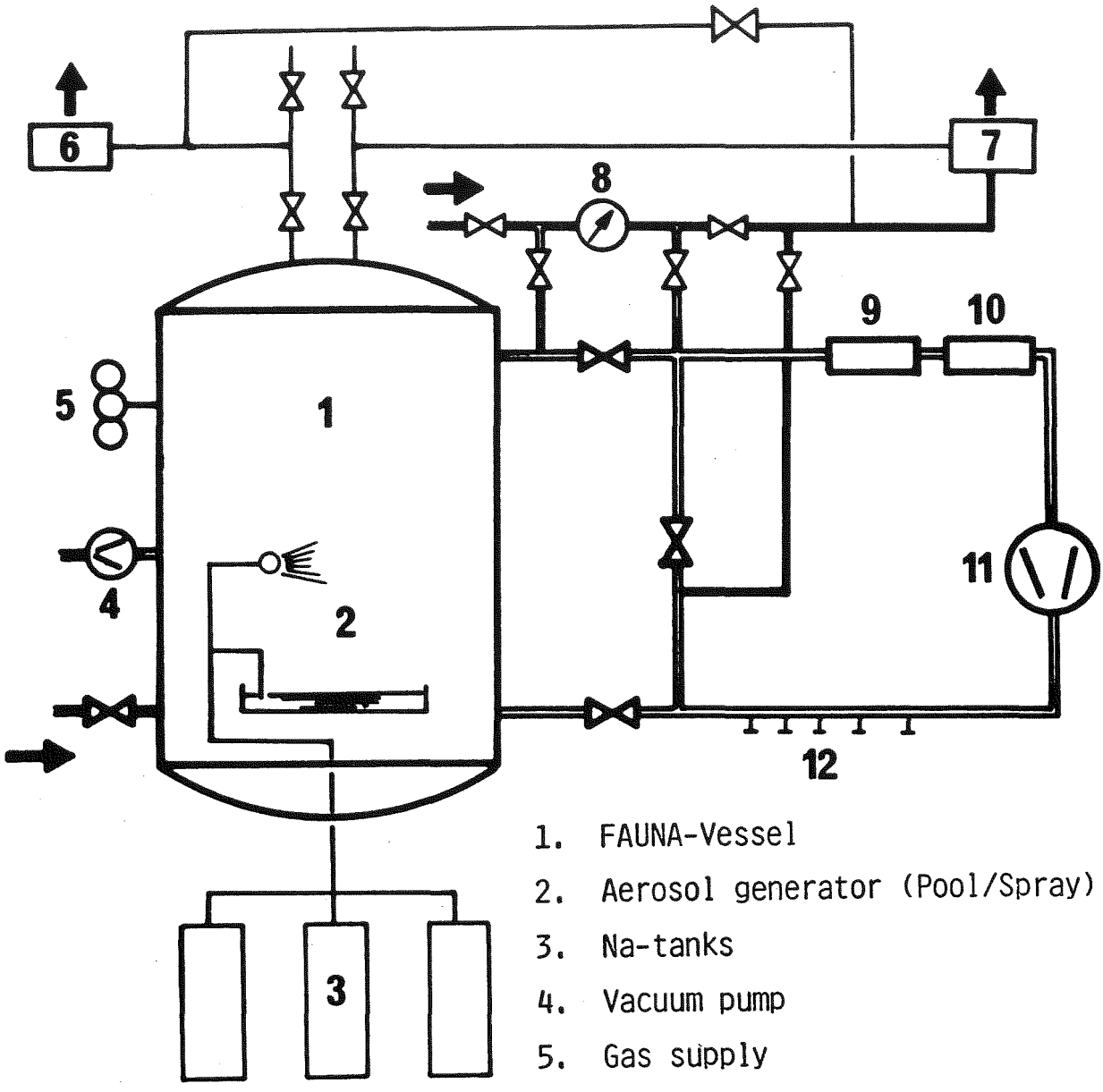

1. FAUNA-Vessel
2. Aerosol generator (Pool/Spray)
3. Na-tanks
4. Vacuum pump
5. Gas supply
6. Separator (electrostatic filter)
7. Separator (wet cleaning)
8. Gas meter
9. Heater
10. Air humidification chamber
11. Blower
12. Measuring section

fig 1: FAUNA aerosol loop

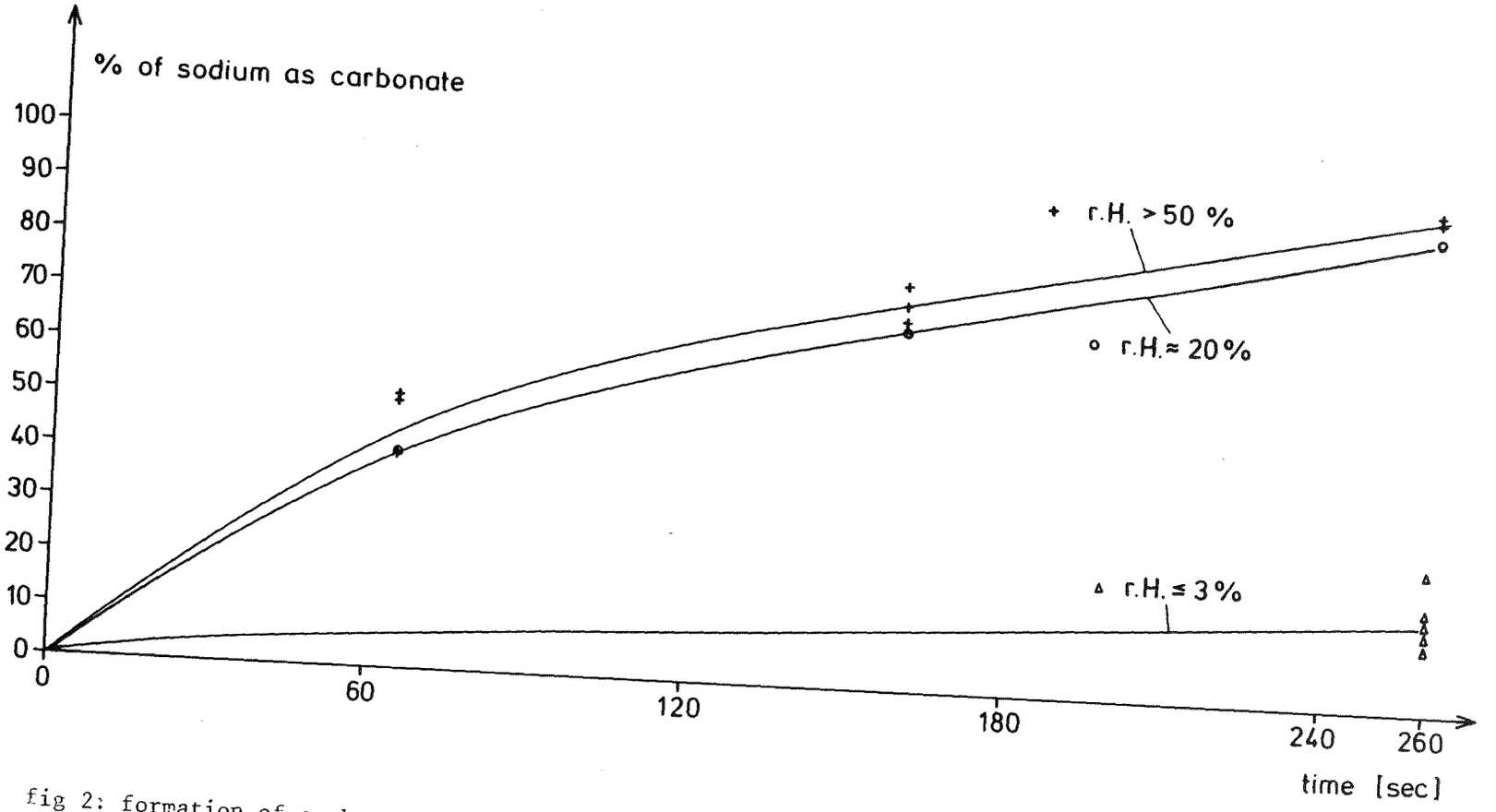

fig 2: formation of carbonate on sodium fire aerosols

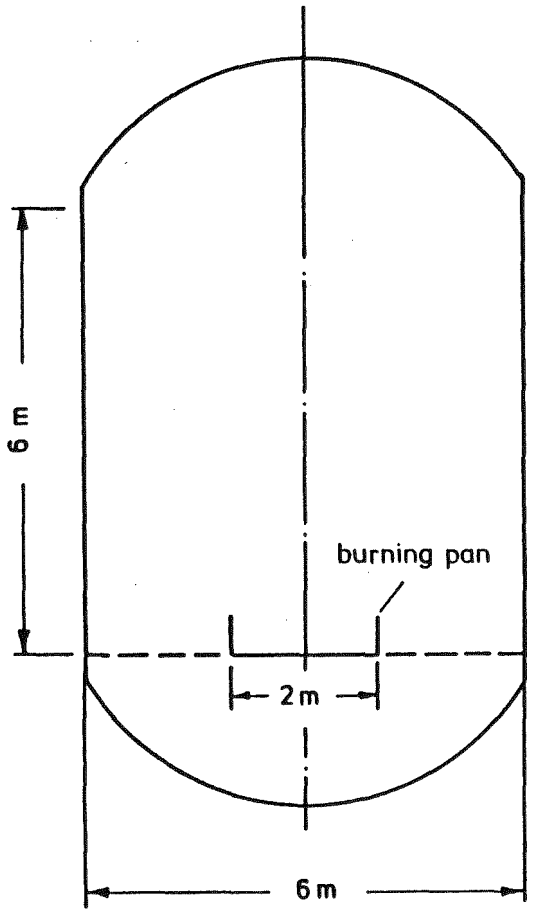

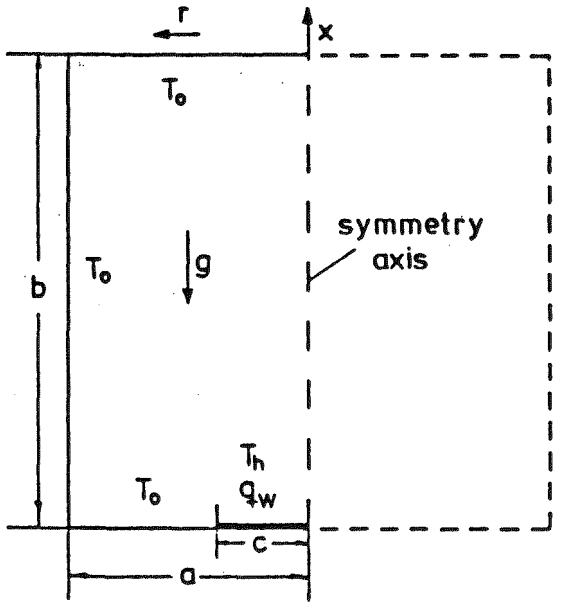

a - radius of the containment
b - height of the containment
c - radius of the heated area
T_h - temperature of the heated area
q_w - heat flux of the heated area
T_o - wall temperature

fig 3 The Fauna - containment and the modeling

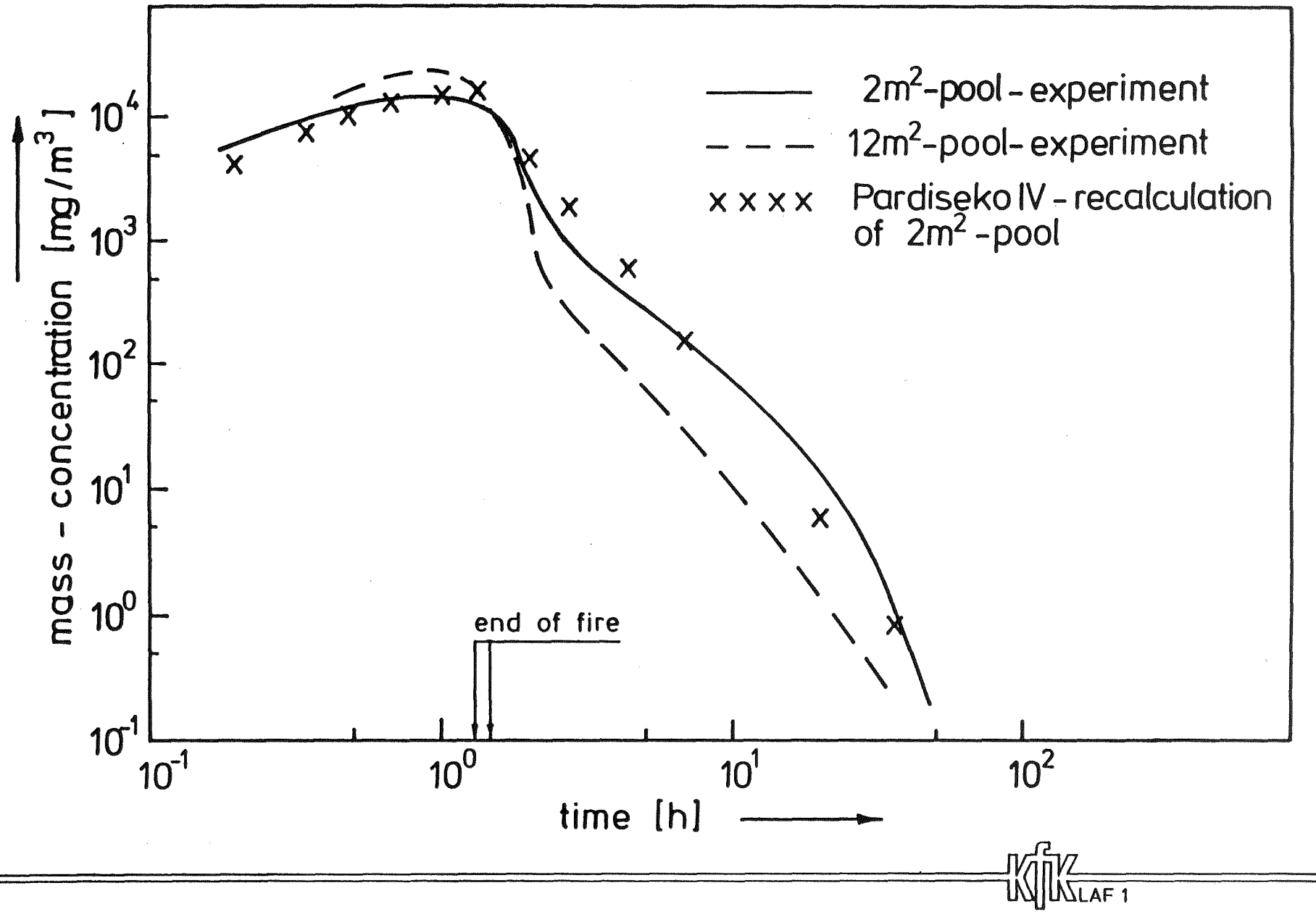

fig 4 Pool fire: measured and calculated course of the aerosol mass concentration

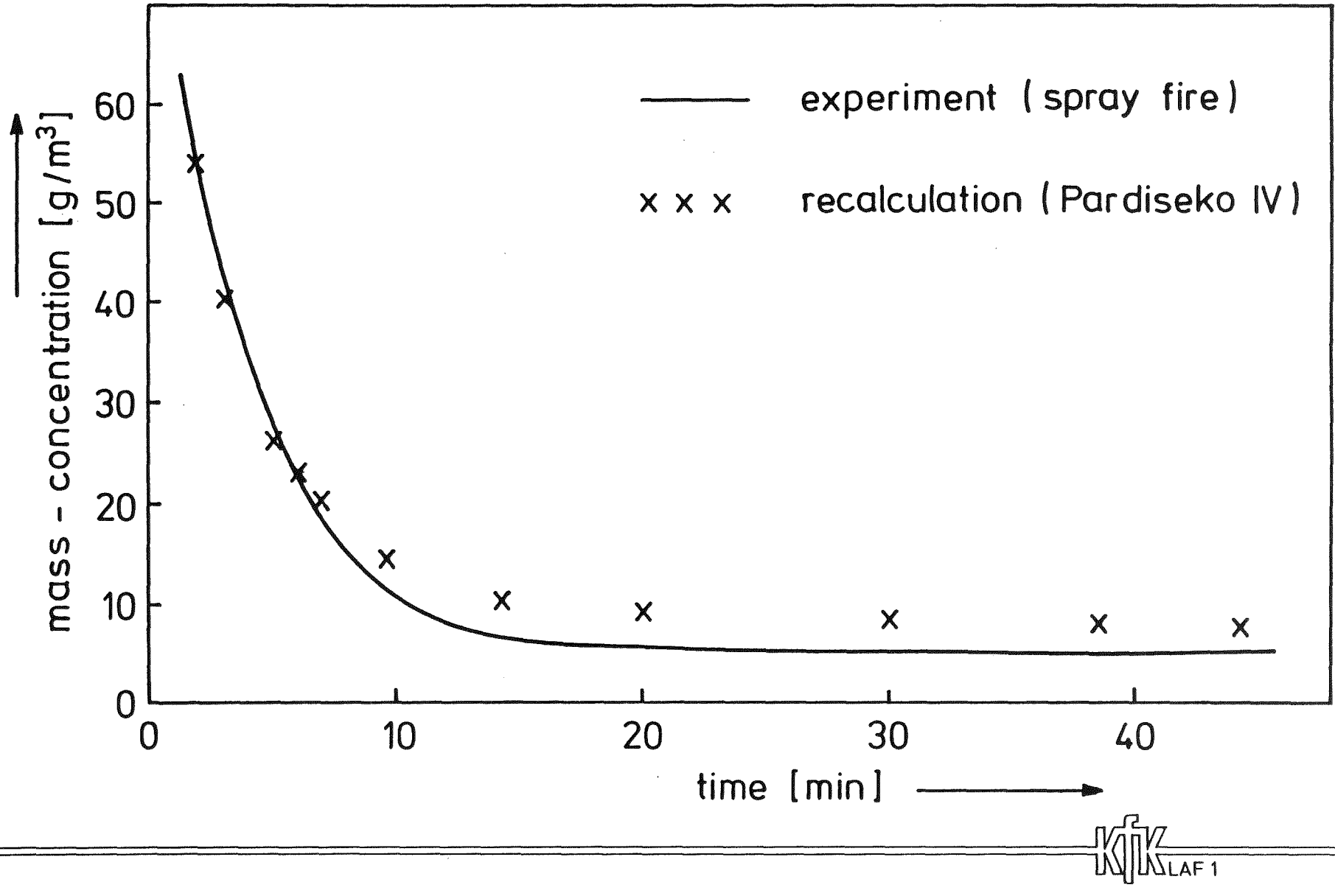

fig 5 Spray fire: measured and calculated course of the aerosol mass concentration

EXPERIMENTAL STUDY OF SODIUM POOL FIRE AEROSOL BEHAVIOUR COMPARISON WITH CALCULATION CODE

C. CASSELMAN, J.C. MALET

CEN CADARACHE

==========

ABSTRACT

Experiments performed in a 4,4 m^3 vessel on the physical behaviour of sodium pool fires are presented. The aim of the experiments is to determine the emission law of the aerosols (source term), as well as the physical behaviour of the aerosols. Experimental results are compared with AEROSOL A_2 code calculation.

The combustion pan of 0,125 m^2 in area, can be covered with a steel lid to insulate the sodium from the ambiant air, thus, experiments with a predetermined time can be performed.

Experimental results deal essentially with :
- pressure of the vessel, gas temperature behaviour,
- aerosol concentration and particle size,
- sedimentation rate,
- wall deposition,
- amount of sodium release.

The aerosols release rate is not constant during the fire.

INTRODUCTION

The aim of this study which involves eight tests, is to determine the release rate of sodium oxide aerosols and to characterize their physical behavior (mass concentration, wall deposition rate and sedimentation rate, particle size) during and after sodium combustion.

The experimental results are used to qualify AEROSOLS A2 computer code.

The purpose of this paper is to present :

- the experimental device and instrumentation,
- the main results of the eight tests,
- the comparison between calculated and experimental values.

EXPERIMENTAL APPARATUS AND INSTRUMENTATION

Experimental apparatus (fig. 1)

The experiments are performed in a 4.4 m^2 cylindrical steel vessel with a removable horizontal floor. The combustion pan is 0.4 m diameter cylinder with a sodium inlet pipe and inlet and outlet nitrogen pipes. A steel lid allows to insulate the sodium from ambiant air on external control at fixed time.

Experimental procedure

To determine the aerosol release rate of a given sodium pool fire, the first step is to perform an experiment of auto-extinguished combustion in the fixed initial conditions. From these first results, the combustion duration is divided in several sequences which correspond at particular points of sodium temperature or gas temperature. Each following experiment represents one of these sequences. In these tests, the combustion is stopped by mean of a steel lid.

Instrumentation

Three class of measurements are carried out :

- thermodynamical ones (pressure, temperature, gas concentration),
- aerosol measurements,
- gas flow rate measurement.

Thermodynamical measurements. Gas temperature inside the vessel is given by 50 thermocouples which are distributed in five horizontal planes : the floor, 0.15 m, 0.5 m, 1.0 m, 1.5 m above this floor. Three thermocouples measure the sodium temperature. Sixteen resistance thermometers are distributed on the external and internal walls.

A membrane pressure probe allows to follow the overpressure in the vessel. An oxygen meter analyses the ambiant gas and commands the injection of oxygen gas to maintain the concentration equal to 21 %.

Aerosol measurements.

Mass concentration is measured by mean of a sample loop (fig. 2). A known vessel volume of gas is sampled and filtered. The filters (glass filters, microporous membranes) are washed and solutions are analysed by atomic absorption spectrophotometer.

For particle size measurement, two apparatus are used :

- the dilution loop with MARK II Andersen impactor (fig. 3),
- the sedimentation battery loop (fig. 4).

The principle of the dilution loop is to sample a gas flow Q_p, to dilute it by an other clean gas flow Q_d to obtain the sum Qp + Qd = QA which is the nominal flow for Andersen impactor. The two flow Q_p and Q_A are measured. This method allows the particle size measurement in high concentration situation.

The sedimentation battery involves 10 parallel channels in which sample gas runs. Particles deposite at a distance which is a function of their size and of their inlet ordinate. Every channel is equiped with removable plates to allow mass deposition analysis.

For sedimentation rate measurement, the system is a rotative plate which involves 30 steel cupels. On external pneumatic control, one cupel is placed in front of the aperture of the covered plate. After the test, cupels are washed and water solutions are analysed by atomic absorption spectrophotometer (fig. 5).

Wall deposition rates are measured by mean of removable pieces of vertical internal walls. These pieces are welded at the extremity of a tube which is perpendicular to the wall. This tube goes through a steel sleeve with a valve (fig. 6).

To know the released aerosol quantity, floor and walls are washed separately ; acidimetric analysis gives the quantity of sodium in the solutions.

Flow rate measurement. Two different technics are used : non linear Pitot tube and double hot wire probe.

EXPERIMENTAL RESULTS

Test duration

The seven sequences are determined from the first test (table 1).

TABLE 1

EXPERIMENTAL PROGRAM

=======

Initial sodium temperature C°	Amount of sodium g	Duration of the test min	Test number	Stopping criterion
272	9400	0-120	E 10	Self extinguishment
270	9600	0-7	E 14	Na temperature : 450°C
273	9600	0-12	E 16	Na temperature : 600°C
272	9600	0-25	E 11	Constant sodium temperature (beginning)
264	9500	0-50	E 15	Plateau on sodium temperature/time curve
275	9600	0-70	E 17	Second increase of temperature on the curve
261	9600	0-80	E 12	Maximum Na temperature
250	9600	0-105	E 13	Last part of the combustion Curve

The combustion pool fire main parameters are :

- sodium initial temperature..... 275 °C
- sodium initial mass..... 9 500 G
- oxygen content..... 0.21 (constant during each test or equal to 0.205 ∓ 0.05)

Thermodynamical results

At low initial sodium temperatures, a double peak appears in gas temperatures and pressure evolution (fig. 7,8). This phenomena takes place in each test of the program.

Aerosol measurements

During the combustion period, the mass concentration value reaches 14 to 25 g Na/m^3 ; 60 minutes after the end of the combustion, it decreases to 0.15 to 0.45 g Na/m^3 (fig. 9).

The Aerodynamic Mass Median Diameter reaches 3 to 5 m during the combustion phase with a standard deviation upper than 2. After this phase, A.M.M.D. increases above 5 m and standard deviation becomes lower than 2.0 (fig. 11).

During the aerosol release, sedimentation mass flow rate settles at a level value included between 1.10^{-5} and 5.10^{-5} g Na/cm^2 s (fig. 10).

Aerosol deposition on the vertical wall seems to be homogeneous on the whole surface area.

The aerosol released masses are listed in table 2 ; sedimentation deposit on the floor represents 75 (± 7) % of the total mass.

TABLE 2

N° TEST	E 10	E 11	E 12	E 13	E 14	E 15	E 16	E 17
TOTAL MASS	1 570.	449.	1 497.	1 667.	118.5	637.	229.	939.

Gas flow rate measurement

The gas velocity measurements above the sodium pool show instabilities and a discontinuity in the velocity evolution. The value during the combustion period reaches 1 m/s.

COMPARISON BETWEEN EXPERIMENTAL AND CACULATED VALUE.

Aerosols A2

AEROSOLS A2 computer code is devoted to the study of sodium aerosol behaviour in a case of sodium fire. This computer code works with the assumption of a log normal granulometric spectrum for the particles.

Phenomena which are taken into account are aerosol source, gravitational settling, wall deposition (brownian diffusion and thermophoresis), leakage, particle coagulation (gravitational settling, brownian diffusion, turbulent gas motion).

The containment volume can be divided into up to 20 zones ; the exchange mass flow rates between them are imput data.

In the case of EMIS test, only one zone is considered. The source is an experimental result. Comparison between experimental and calculated values leads to following remarks :

- calculated mass concentration values are close to experimental ones during combustion phase (fig. 12),

- sedimentation flow rate maximum values are in good agremment but the evolution curves are different between 1 000 secondes and 4 000 secondes (fig. 13),

- calculated Aerodynamic Mass Median Diameter values are higher than experimental ones ; the difference between the two kinds of values is near constant, except the calculated peak which appears just after the end of the source ; calculated standard deviation is higher than experimental one during combustion period and lower after this period (fig. 14).

CONCLUSION

The eight EMIS tests give a lot of results concerning aerosol physical characteristics evolution.

These results confirm that aerosol release rate doesn't stay constant during the combustion. Code calculations give good estimate except for particle size. To know the influence of containment conditions, further experiments will be performed in ventilation conditions.

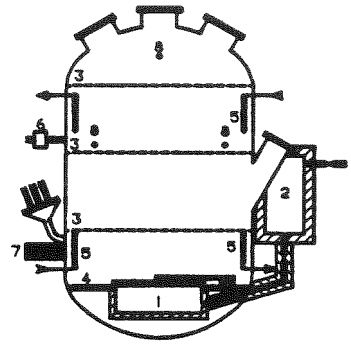

1- COMBUSTION PAN
2- SODIUM TANK
3- THERMOCOUPLE MEASUREMENT LEVELS
4- HORIZONTAL PLANE OF THE VESSEL
5- GAS FLOW INLET AND OUTLET
6- PRESSURE GAUGE
7- THERMOCOUPLE OUTLET
8- AEROSOL MASS CONCENTRATION SAMPLING POINTS

FIGURE 1 - EXAMINATION OF THE 4,4 m³ CYLINDRICAL STEEL CONTAINMENT VESSEL

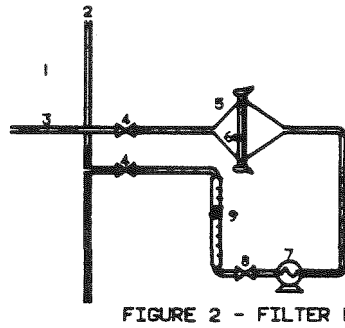

1- TEST VESSEL
2- WALL
3- SAMPLING TUBE
4- STOP VALVE
5- FILTER SYSTEM
6- FILTER
7- PUMP
8- CONTROL VALVE
9- FLOWMETER

FIGURE 2 - FILTER LOOP

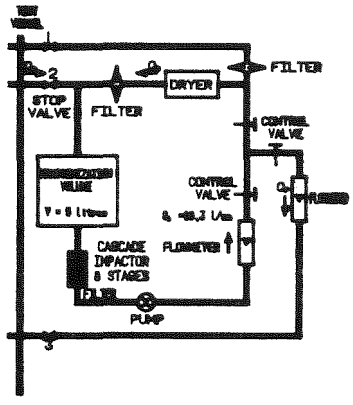

FIGURE 3 - CASCADE IMPACTOR WITH DILUTION SYSTEM

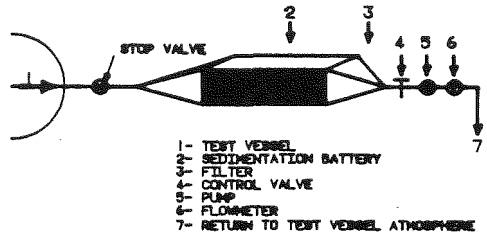

FIGURE 4 - SEDIMENTATION BATTERY

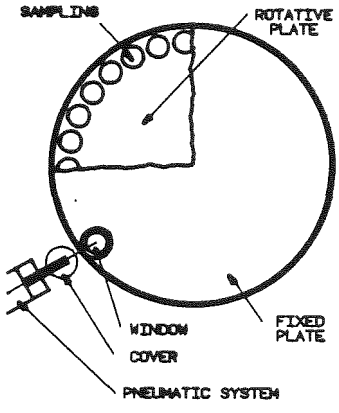

FIGURE 5 - ROTATIVE PLATE TO SEDIMENTATION RATE MEASUREMENT

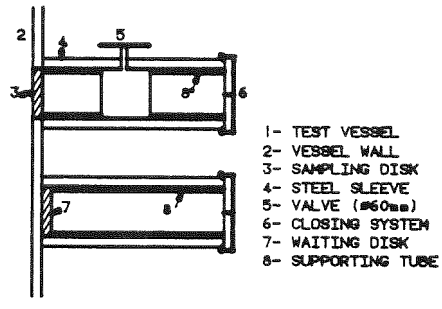

1- TEST VESSEL
2- VESSEL WALL
3- SAMPLING DISK
4- STEEL SLEEVE
5- VALVE (ø60mm)
6- CLOSING SYSTEM
7- WAITING DISK
8- SUPPORTING TUBE

FIGURE 6 - WALL DEPOSIT SAMPLING SYSTEM

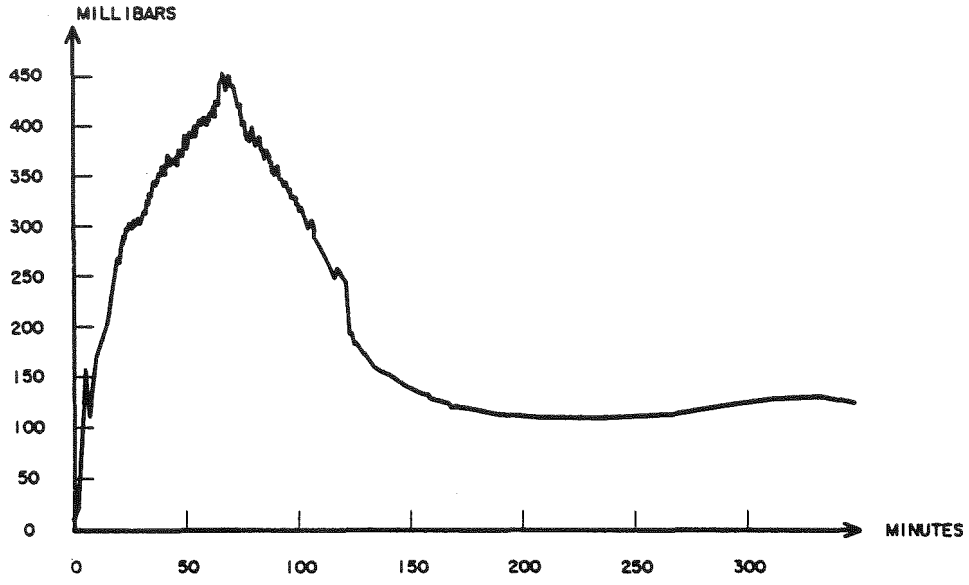

FIGURE 7 . RELATIVE GAS PRESSURE

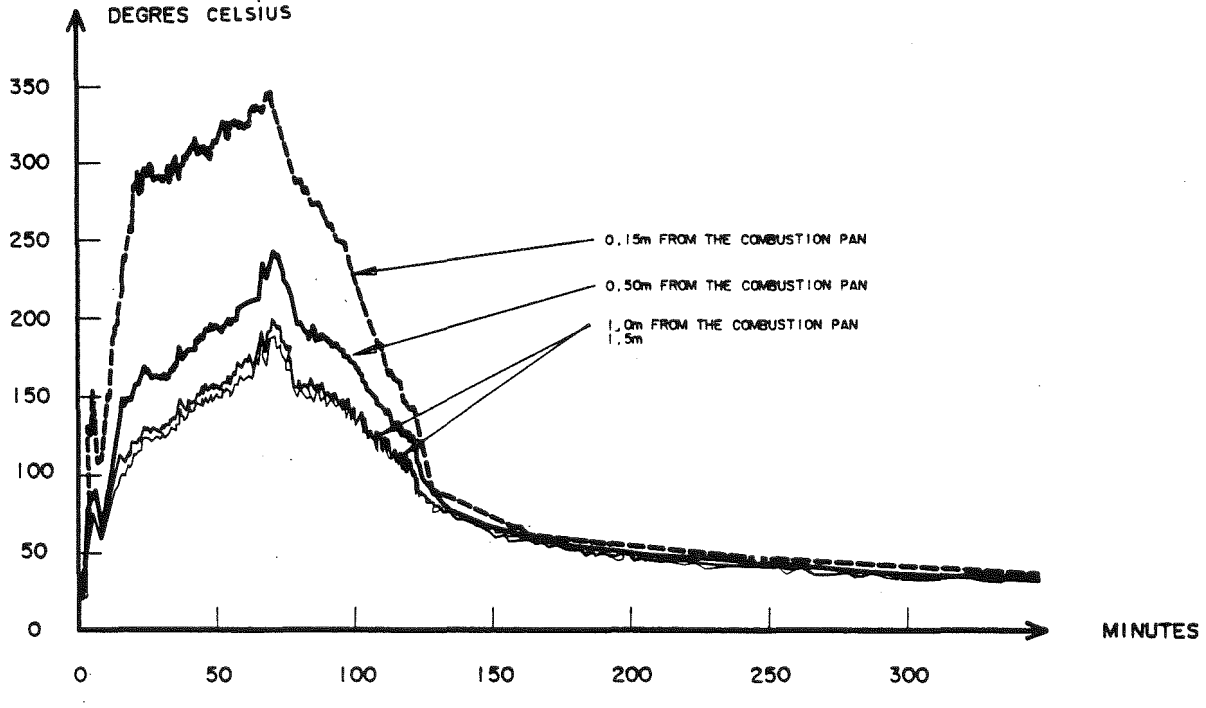

FIGURE 8 . VERTICAL AXIS GAS TEMPERATURE

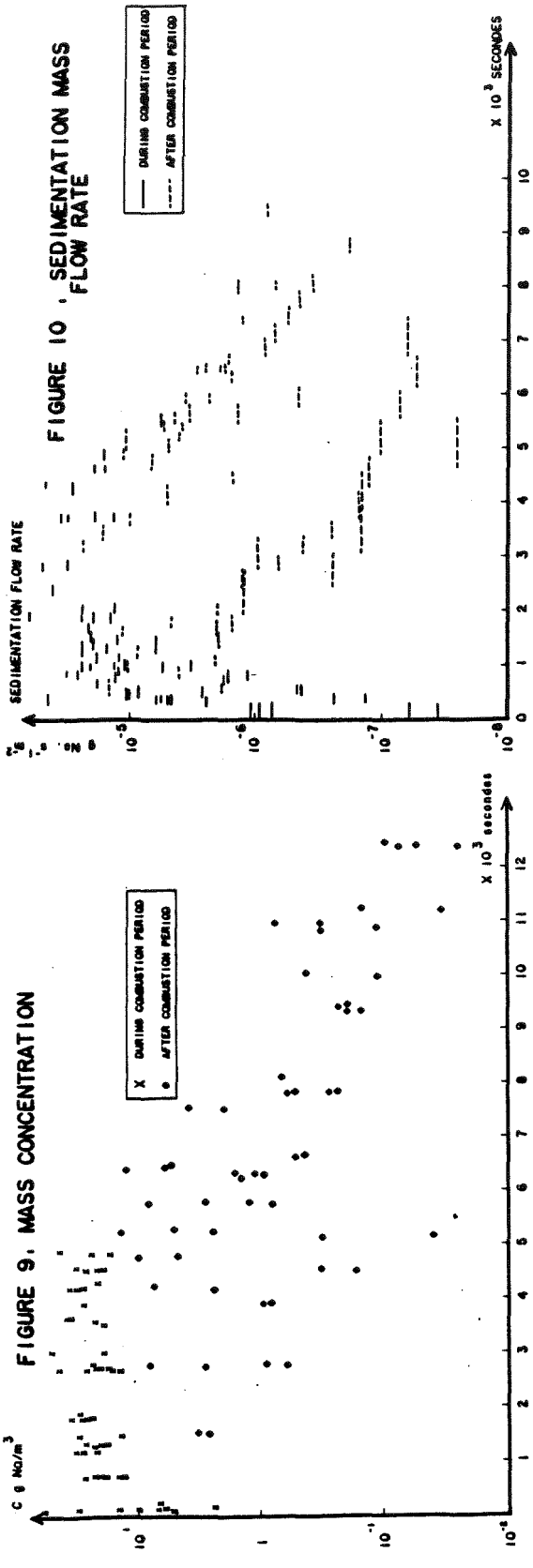

FIGURE 9 . MASS CONCENTRATION

FIGURE 10 . SEDIMENTATION MASS FLOW RATE

FIGURE 11 . PARTICLE SIZE

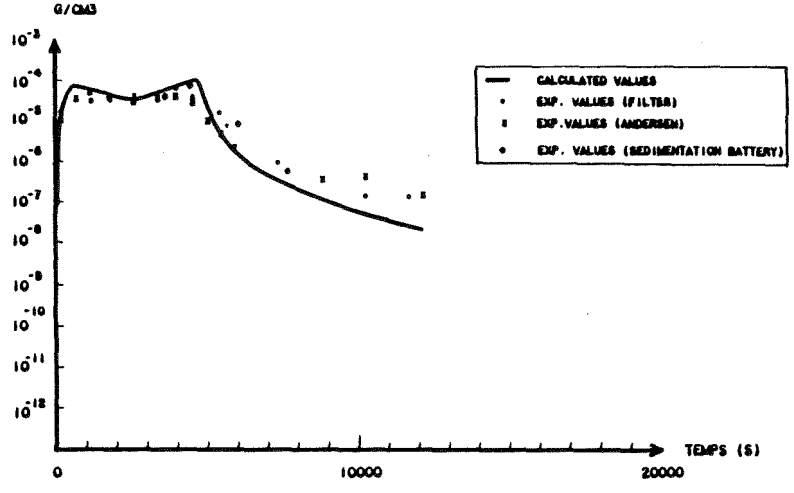

FIGURE 12 . MASS CONCENTRATION

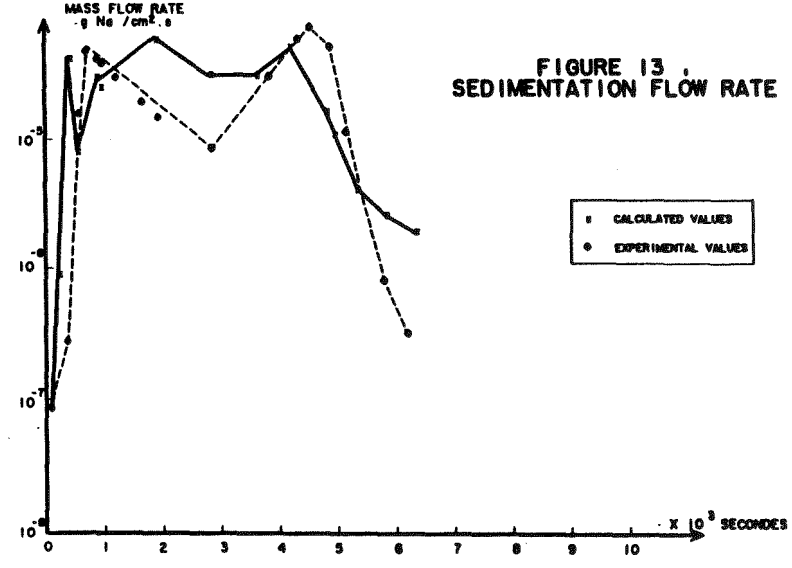

FIGURE 13 .
SEDIMENTATION FLOW RATE

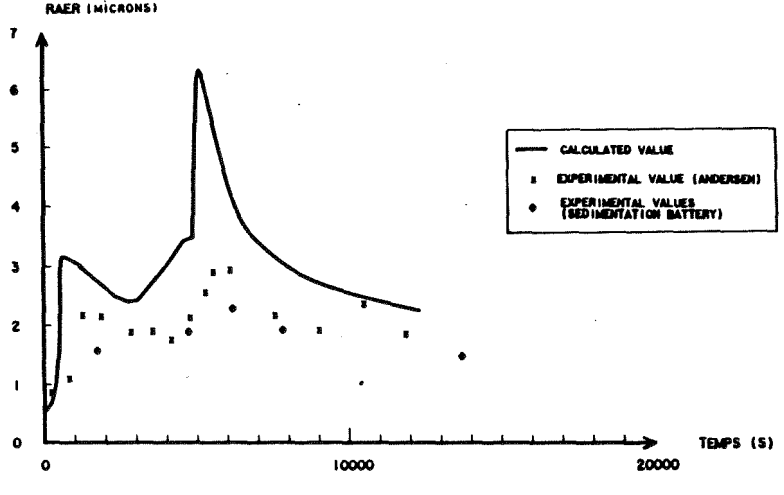

FIGURE 14 a . AERODYNAMIC MASS MEDIAN DIAMETER

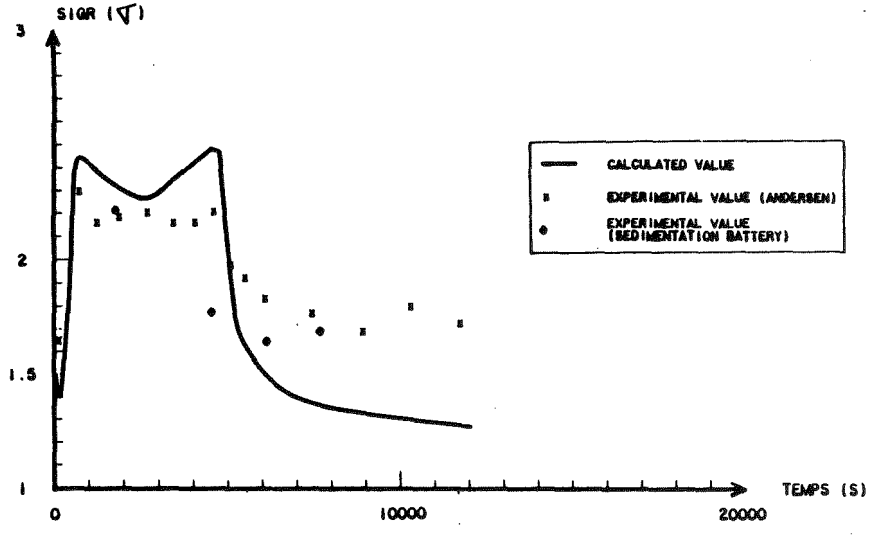

FIGURE 14b . STANDARD DEVIATION

DEVELOPMENT AND VALIDATION OF ABC-INTG CODE

S. Miyahara, N. Mitsutsuka*
Power Reactor and Nuclear Fuel Development Corporation
Tokyo, Japan

H. Obata
Century Research Center Corporation
Tokyo, Japan

ABSTRACT

A computer code, ABC-INTG, has been devloped to analyze the aerosol behavior within a containment following a postulated accident in a liquid metal fast breeder reactor.

ABC-INTG integrates digitally the coagulation probabilities of the particles due to Brownian motion, gravitational settling, and turbulent motion by using the sectional representations proposed by Gelbard, et al. By this method, the code extensively reduces the computing time compared with the former versions of ABC and conserves the aerosol mass almost perfectly.

The numerical validity of ABC-INTG in calculating the coagulation probabilities of the particles has been studied by comparing its numerical predictions with the analytical solutions calculated from the equations by Scott. Good agreement was obtained in this comparison. The code was validated also by comparing its numerical predictions with the test data from the LTV Test by Atomics International and the CSTF Test by Hanford Engineering Development Laboratory. Again, good agreement was obtained with the selected value of the gravitational collision efficiency in the code.

---

* present address: TOSHIBA Corp. Yokohama, Japan.

INTRODUCTION

A postulated accident in a liquid metal fast breeder reactor (LMFBR) is often accompanied by the release of sodium oxide aerosols that contain fission products and nuclear fuels. Although most of these aerosols are confined in a reactor containment system, some leak out to the environment. From the viewpoint of reactor safety, therefore, the analysis of aerosol behavior within a containment is required for evaluating radiological consequence following an LMFBR accident.

To try to meet that requirement, the first version of ABC (Aerosol Behavior in Containment) [1] was developed in 1973. Since that time, the code has been successively improved and the ABC-2 [2], ABC-3B [3], and ABC-3C [4] versions were developed. Although these versions were respectively validated by test data, the experience in these codes showed that they had their own limitations, in particular, in computing time and in aerosol mass conservation.

To eliminate the limitations associated with the former versions, ABC-INTG has been developed by revising the numerical method. In the former verions of the code, the sectional method (the finite difference method) was adopted to discretize the particle size distribution. This method has an advantage in being able to treat an arbitrary distribution of the particle sizes, while the moment method is limited to the log-normal distribution. In ABC-INTG, the same sectional method is used to discretize the particle size distribution. Furthermore, the method to calculate the coagulation probabilities of the particles is revised by using the method of sectional representations proposed by Gelbard, et al [5][6].

In the present paper, the limitations of ABC-3B and ABC-3C that forced the development of ABC-INTG is explained at first. Then, the verification and the validation of the code are presented following the explanations on the numerical features of ABC-INTG.

I. NUMERICAL PROBLEMS WITH THE FORMER VERSIONS OF ABC

(1) Mass Conservation Problem in ABC-3B

The former ABC version, ABC-3B, solved the following integro-differential equation to describe the dynamics of aerosols that have a discrete particle size distribution.

$$\frac{dn_i}{dt} = \sum_{\alpha} K_{j,k} \cdot C^i_{j,k} \cdot n_j \cdot n_k - n_i \sum_{k=1}^{KL} K_{i,k} \cdot n_k + S_i - R_i \cdot n_i \qquad (1)$$

where n_i : number concentration in the i-th class particles,

$K_{i,k}$: coagulation probability between particles in the i-th and the k-th classes,

$C^i_{j,k}$: correction factor, $(= \frac{r_j^3 + r_k^3}{r_i^3})$,

S_i : source rate,
R_i : removal rate,
α : all possible combinations to produce the i-th class particles,
r_i : radius of i-th class particle,
KL : maximum particle size class.

Good agreement was obtained between the ABC-3B code predictions and the JAERI $1m^3$ test data for uranium oxide, sodium oxide, and their mixed aerosols [7]. But, during a run by ABC-3B to check its applicability to an extremely high concentration aerosols ($\simeq 8\times10^{-5}$ g/cm^3) in a large containment, a mass conservation problem was encountered. The calculation of Brownian agglomeration resulted in a gradual increase in the aerosol mass concentration even with no source term or no removal process. Moreover, the addition of gravitational agglomeration to the above calculation resulted in a marked decrease in the concentration. Figure 1 shows the changes in the aerosol mass concentration calculated where neither source term nor removal term was considered. These deviations became smaller at lower concentrations. Further, in a small containment, the deviations became negligibly small compared with the removal rate by gravitational settling.

(2) Numerical Truncation Problem in ABC-3C

To solve the mass conservation problems described with ABC-3B, the numerical scheme to solve the integro-differential equation was rechecked and was revised as follows to strictly conserve the aerosol mass. The code thus revised was named ABC-3C:

$$\frac{d(n_i m_i)}{dt} = \sum_{\alpha} K_{j,k} \cdot n_j \cdot n_k (m_j + m_k) - \sum_{k=1}^{KL} K_{i,k} \cdot n_k \cdot n_i \cdot m_i + S_i - R_i \cdot n_i \cdot m_i \quad (2)$$

where m_i : mass of particles in the i-th class.

With ABC-3C, the aerosol mass was conserved almost perfectly during agglomeration calculations. But its computing time strongly depended on the number of particle classes. The larger the number, the longer the computing time, as shown in Table 2. Although the computing time can be reduced remarkably by reducing the number of particle classes, this results in an increase in the truncation errors. Therefore, the number cannot be reduced below a limited value. The reasonably accurate results were obtained only with the particle size classes larger than 80 as shown in Figure 2, where KL indicates the number of particle size classes. But, such large number is not practicable for most of the cases where calculations are required for long hours, namely several hundred hours.

II. DEVELOPMENT OF ABC-INTG

(1) Numerical Scheme

To further solve the numerical problems associated with ABC-3C and also to make computing time reasonably short, the ABC-INTG code has been developed. In the code, the numerical method has been revised by using the sectional representations by Gelbard and Seinfeld [5][6], which feature as follows:

1) volume concentrations (instead of number concentrations) of particles are calculated as unknown quantities,

2) the coagulation probabilities of particles are numerically integrated.

In the numerical scheme of ABC-INTG, an entire particle size domain is divided into m classes. An integral quantity of volume concentration Q_i in the i-th class is defined by Eq.(3).

$$Q_i(t) = \int_{v_{i-1}}^{v_i} v\, n(v,t)\, dv \qquad (3)$$

where, $i = 1, 2, \ldots, m$,
v is volume of a particle,
$n(v,t)$ is a number concentration.

The integro-differential equation that describes aerosol dynamics is expressed in terms of $Q_i(t)$ ($i=1,2, \ldots m$, where v_{i+1} must be larger than $2v_i$) as follows:

$$\frac{dQ_i}{dt} = \frac{1}{2}\sum_{j=1}^{i-1}\sum_{k=1}^{i-1} {}^1\bar{\beta}_{j,k,i} \cdot Q_j \cdot Q_k - Q_i \sum_{j=1}^{i-1} {}^2\bar{\beta}_{j,i} \cdot Q_j$$
$$- \frac{1}{2}\, {}^3\bar{\beta}_{i,i} \cdot Q_i^2 - Q_i \sum_{k=i+1}^{m} {}^4\bar{\beta}_{k,i} \cdot Q_i$$
$$+ \bar{S}_i(t) - \bar{R}_i(t) \cdot Q_i \qquad (4)$$

where, β : coagulation coefficients.

The coagulation coefficients in Eq.(4) are expressed in Eq.(5) through Eq.(9) as follows:

$${}^1\bar{\beta}_{j,k,i} = \int_{x_{j-1}}^{x_j}\int_{x_{k-1}}^{x_k} \frac{\theta(v_{i-1}<u+v<v_i)(u+v)K(u,v)}{uv(x_j-x_{j-1})(x_k-x_{k-1})}\, dydx \qquad (5)$$

where, $2 \le i \le m$, $1 \le j < i$, $1 \le k < i$, ${}^1\bar{\beta}_{j,k,i} = {}^1\bar{\beta}_{k,j,i}$

$${}^2\bar{\beta}_{j,i} = \int_{x_{j-1}}^{x_j}\int_{x_{i-1}}^{x_i} \frac{[\theta(u+v>v_i)u - \theta(u+v<v_i)v]K(u,v)}{uv(x_j-x_{j-1})(x_i-x_{i-1})}\, dydx \qquad (6)$$

where, $2 \le i \le m$, $j < i$, ${}^2\bar{\beta}_{j,i} \neq {}^2\bar{\beta}_{i,j}$

$$ {}^{3}\overline{\beta}_{i,i} = \int_{x_{i-1}}^{x_i}\int_{x_{i-1}}^{x_i} \frac{\theta(u+v>v_i)(u+v)K(u,v)}{uv(x_i-x_{i-1})^2}\,dydx \qquad (7) $$

where, $1 \leq i \leq m$

$$ {}^{4}\overline{\beta}_{j,i} = \int_{x_{j-1}}^{x_j}\int_{x_{i-1}}^{x_i} \frac{uK(u,v)}{uv(x_j-x_{j-1})(x_i-x_{i-1})}\,dydx \qquad (8) $$

where, $1 < i < m$, $j > i$, ${}^{4}\overline{\beta}_{j,i} \neq {}^{4}\overline{\beta}_{i,j}$

$$ x_i = f(v_i),\ u = f^{-1}(y),\ v = f^{-1}(x) \qquad (9) $$

In Eqs.(5) through (7), the function θ is equal to one if the specified condition is satisfied; and zero, if not.

The source term $\overline{S}_i(t)$ in Eq.(4) for the i-th class is expressed as follows:

$$ \overline{S}_i(t) = \int_{v_{i-1}}^{v_i} v \cdot S(v,\ t)\,dv \qquad (10) $$

The removal rate $\overline{R}_i(t)$ in Eq.(4) for the i-th class is given by Eq.(11).

$$ \overline{R}_i(t) = \int_{x_{i-1}}^{x_i} \frac{R(v)}{(x_i-x_{i-1})}\,dx \qquad (11) $$

Since the size distribution of aerosol particles is usually expressed in terms of logarithms of the particle diameter, Eq.(12) can be used as a variable for the numerical integration of the integro-differential equation.

$$ x = f(v) = \log_{10}(6v/\pi)^{1/3} = \log_{10}(2r) \qquad (12) $$

(2) Addition of Turbulent Coagulation Term

The turbulent coagulation term of particles had not been considered in the former versions of ABC, therefore, this term was added to ABC-INTG. The collision frequency between the particles suspended in a gaseous medium increases with the increase in turbulent motion. Such collision is due to the following two independent processes [8]: one is the collision of particles by random motion of the gaseous medium, and another is the collision of particles by the particle inertia itself. To consider these collision processes, the two coefficients are added to the coagulation coefficients i.e., Brownian and gravitational.

The coagulation rate due to the above first mechanism, K_{T1}, is given as follows:

$$ K_{T1} = \varepsilon\left(\frac{8\pi\rho_g}{15\eta}\varepsilon_T\right)^{1/2}(r_i+r_j)^3\gamma^3 \qquad (13) $$

where, ε_T : the energy dissipation rate in the turbulent fluid,
ε : gravitational collision efficiency,
γ : coagulation shape factor,
ρ_g: density of carrier gas,
η : viscosity of carrier gas.

The coagulation rate due to the second mechanism, K_{T2}, is given as follows:

$$K_{T2} = \varepsilon (r_i + r_j)^2 |v_i - v_j| \frac{\gamma^2}{\chi} \tag{14}$$

where, χ : dynamic shape factor,
v_i is particle velocity and is given by Eq.(15)

$$V_i = \left[\frac{4 \rho \sqrt{2 \pi}}{9 \eta} \right] \left[\frac{1.69 \varepsilon_T^3 \rho_g}{15 \eta} \right]^{1/4} r_i^2 \left(1 + \frac{A_i \lambda}{r_i} \right) \tag{15}$$

where, ρ : density of aerosol,
A_i : Cunningham slip correction factor,
λ : molecular mean free path of carrier gas.

(3) Code Verification

The code verification has been carried out by comparing the ABC-INTG predictions with the analytical solutions that were calculated from the equation proposed by Scott [9]. In this event, changes in the particle number concentration at a constant coagulation probability with no source term or no removal term were calculated.

In case of no source term or no removal term, Scott defined the non-dimensional distribution density that is expressed by Eq.(17). He also derived the total number of particles as expressed by Eq.(16).

$$N(t) = \frac{2 N_0}{\tau + 2} \tag{16}$$

where, N(t) : total number of particles,
N_0 : initial total number of particles,
τ : nondimensional time, = CN_0t,
C : constant coagulation rate,
t : time (sec).

$$\phi(x, \tau) = \frac{8 e^{-2x} \sinh \{ 2x (\frac{\tau}{\tau + 2})^{1/2} \}}{\tau^{1/2} (\tau + 2)^{3/2}} \tag{17}$$

where, $\phi(x,\tau)$: nondimensional number distribution density,
x : nondimensional volume,

$$x = v/v_0$$

v : particle volume,
v_0 : initial averaged volume of particles.

By using Eqs. (16) and (17), the analytical solutions were calculated. On the other hand, the corresponding numerical predictions were calculated by ABC-INTG. Table 1 summarizes the initial conditions for obtaining the analytical solutions and also for the ABC-INTG calculations. The results are given in Figures 3 and 4. The code predictions agree fairly well with the analytical solutions in regard to both the mass concentration and the number concentration.

Table 1 Initial Conditions for Obtaining the Analytical Solutions and the ABC-INTG Calculations

initial number concentration	238.732	(number/cm^3)
initial mass concentration	10^{-6}	(g/cm^3)
geometric count mean radius	10^{-4}	(cm)
minimum radius of particle	10^{-5}	(cm)
maximum radius of particle	3.0×10^{-4}	(cm)
aerosol density	1.0	(g/cm^3)
constant coagulation rate	1.80×10^{-4}	(cm^3/sec)
time step	1.0	(sec)

(4) Code Validation

In the first phase, the code validation was carried out by comparing the ABC-INTG numerical prediction with that by the former version, ABC-3C. Since fairly good mass conservation was obtained by ABC-3C with KL, the number of particle size classes, larger than 80, as explained, the calculation by ABC-3C was carried out with KL equal to 120. On the other hand, the calculation by ABC-INTG was carried out with KL equal to 20. With this KL value, ABC-INTG generated a smaller truncation error than that by ABC-3C with KL equal to 120. Figure 5 shows the ABC-INTG prediction with that by ABC-3C. The ABC-INTG prediction agrees with that by ABC-3C. Table 2 summarizes the relationship between the number of particle classes and the computing times by ABC-INTG and ABC-3C. For ABC-3C, the results at KL equal to 20, 40, and 80 are also presented for the comparison. Table 2 shows that the computing time (CPU time) saving by ABC-INTG is considerable, that is, CPU time by ABC-INTG is 6.66 sec., while that by ABC-3C with KL equal to 120 is 419.12sec.. The mass conservation with ABC-INTG was excellent.

In the second phase, the code validation was carried out by comparing the code predictions with the data from the LTV test by Atomics International [10] and the CSTF test by Hanford Engineering Laboratory [11]. Table 3 summarizes the input data for the ABC-INTG calculation to analyze these tests. The aerosol mass concentration predicted by the code are presented in Figures 6 and 7 with various collision efficiencies, together with the test data. The numerical predictions indicated by "Fuchs" in these figures are those calculated with the Fuchs' definition [12],[13] for the gravitational collision efficiency. These figures indicate that the decay curve of the numerical mass concentra-

tion changes according to the change in gravitational collison efficiency, ε, and the numerical prediction at ε equal to 0.3 agrees well with the test data.

Table 2 Number of Particle Classes and Computing Time (Computer : FACOM M-380)

	number of particle classes	computing time (sec)	simulation time (sec)
ABC-3C	20	2.75	60000
	40	15.63	60000
	80	105.84	60000
	120	419.12	60000
ABC-INTG	20	6.66	60000

Table 3 Input Data for the Analyses of the U.S. Experimental Data

		TEST-3 in LTV/AI	AB-1 in CSTF/HEDL
initial mass conc.	(g/cm^3)	1.505×10^{-7}	2.25×10^{-8}
geometric count mean radius	(cm)	5.0×10^{-4}	5.0×10^{-4}
geometric standard deviation		1.7	1.7
aerosol density	(g/cm^3)	0.3	0.3
vessel height	(cm)	9.00×10^{2}	2.03×10^{3}
vessel volume	(cm^3)	6.00×10^{7}	8.50×10^{8}
inner surface aera	(cm^2)	7.70×10^{5}	5.20×10^{6}
floor area	(cm^2)	6.60×10^{4}	4.23×10^{5}

III. DISCUSSIONS AND CONCLUSIONS

The aerosol codes so far developed and now used in many countries adopt the one of the following methods to represent the particle size distribution: one is the moment method and another is the sectioning method (finite difference method). The former method has an advantage in making computation very short. But this method is restricted only for the log-normal particle size distribution. Therefore, the particle size distribution of a realistic form cannot be treated. In contrast, the latter method has an advantage in treating arbitrary particle size distributions but has a disadvantage of larger truncation errors with a smaller number of particle classes. The former versions of ABC used this sectioning method, therefore, they showed large truncation errors,

unless a longer computing time is spent.

In ABC-INTG, although the method of the discretization is essentially the same as those in the former versions, the numerical method is completely revised by introducing the sectional representations of Gelabrd et al. With the aid of this representations, ABC-INTG can not only perfectly conserve the aerosol mass almost but also greatly reduce the computing time, i.e., almost 1/70 of the former version of ABC. Furthermore, the verification and the validation of ABC-INTG showed good results, indicating that the disadvantage associated with the sectioning method has been eliminated. These advantages of ABC-INTG have also been made clear in the aerosol codes comparison study [14] conducted in the framework of the Commission of European Communities in 1982 and 1983. PARDISEKO-IIIB, AEROSIM, AEROSOLS-A2, and AEROSOLS-B1 joined this comparison study together with ABC-INTG. The essence of the study is that the code predictions by ABC-INTG gave good agreement with those by the other codes whose discretization method is the sectioning. On the other hand, the code with the moment method gave poor results, which indicated the limitation of this method.

In conclusion, the newly developed ABC-INTG code has enough reliability in its application to the analyses of the aerosol behavior within a containment.

REFERENCES

[1] G. Nishio and S. Kitani, "A Hazard Analysis of Plutonium Aerosol Released in an LMFBR Hypothetical Accident (ABC-Code)," PNC J250 74-25 (1974).

[2] K. Akagane, et al., "Analysis of Aerosol Behavior for Fast Reactor Safety," PNC N241 78-06 (1978).

[3] K. Akagane, et al., "Development of a Code for Analysis of Nuclear Aerosol Behavior in Reactor Containment under Fast Reactor Accident Conditions," PNC N241 79-13 (1979) (in Japanese).

[4] H. Obata, "ABC-3C Users Manual," CRC-081-001, March (1981) (in Japanese).

[5] F. Gelbard and J. H. Seinfeld, "Simulation of Multicomponent Aerosol Dynamics," J. of Colloid and Interface Science, Vol.78, No.2 (1980).

[6] F. Gelbard, et al., "Sectional Relationships of Simulating Aerosol Dynamics," J. of Colloid and Interface Science, Vol.76, No.2 (1980).

[7] N. Mitsutsuka and H. Obata, "Analytical Studies on Uranium Oxide, Sodium Oxide and Their Mixed Aerosols by Using ABC-3B," NUREG/CR-1724, ORNL/NUREG/TM-404, CSNI-45, Apr. (1980).

[8] CSNI/SOAR, "Nuclear Aerosols in Reactor Safety," OECD NEA (1979).

[9] W. T. Scott, "Analysis Studies of Cloud Droplet Coalescence I," J. of Atmospheric Science, Jan. (1968).

[10] J. A. Gieseke, et al., "Analytic Studies of Aerosol Behavior Predictions for Fast Reactor Safety," BMI-1932, Mar. (1975).

[11] R. K. Hilliard, et al., "Preliminary Results of CSTF Aerosol Behavior Test, AB-1," HEDL-SA-1381, Jun. (1978).

[12] N. A. Fuchs, "The Mechanics of Aerosols," Pergamon Press,(1964).

[13] G. C. Lindauer and A. W. Castleman Jr., "The Importance of Gravitational Coagulation on the Settling of High-Mass Density Aerosols," Nuclear Science and Engineering, Vol.42 (1970).

[14] J. Fermandjian, et al.,"Comparison of Computer Codes Related to the Sodium Oxide Aerosol Behavior in a Containment Building", to be presented at the OECD/CSNI Specialists' Meeting on Nuclear Aerosols in Reactor Safety, Karlsruhe, 4-6 September (1984).

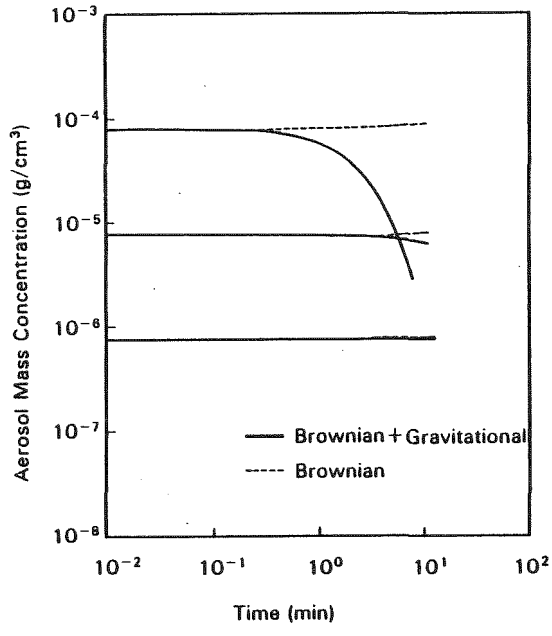

Fig.1 Changes in Mass Concentration in Agglomeration Calculation by ABC-3B

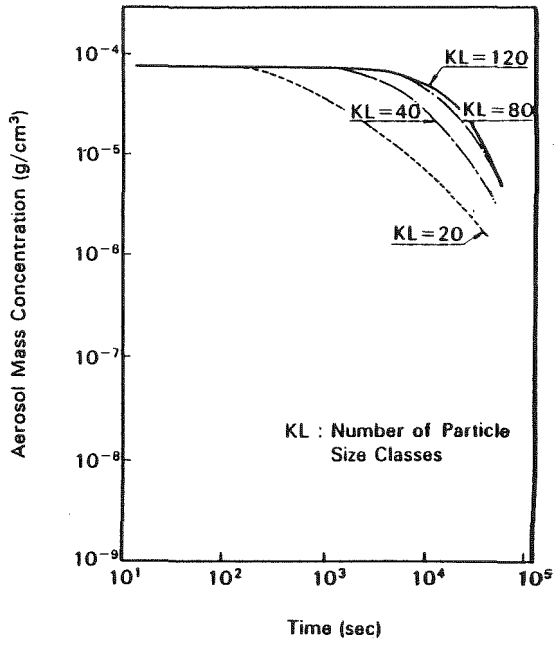

Fig.2 Changes in Mass Concentration by ABC-3C at Different Particle Size Classes

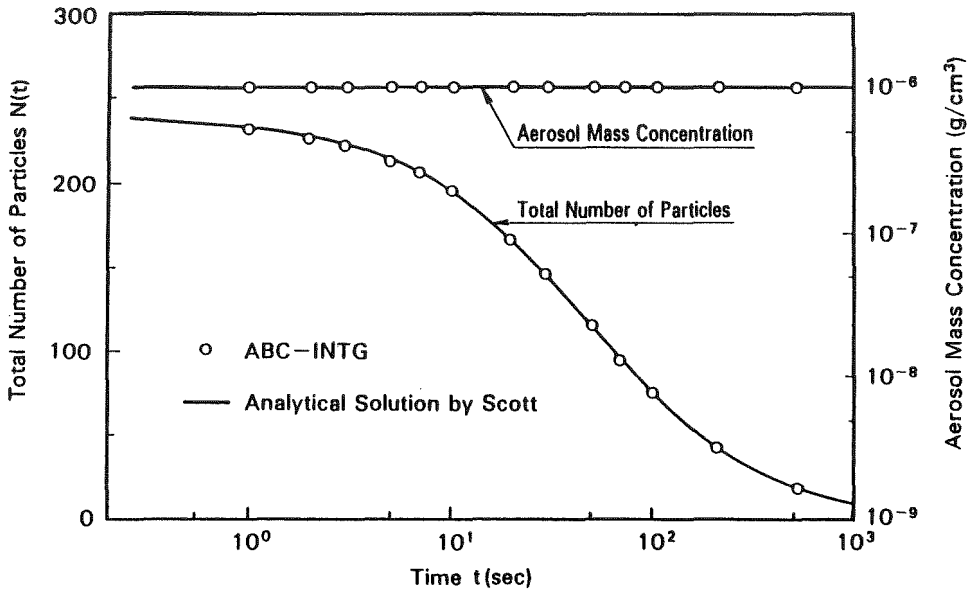

Fig.3 Comparisons of the ABC-INTG Predictions with the Analytical Solutions by Scott

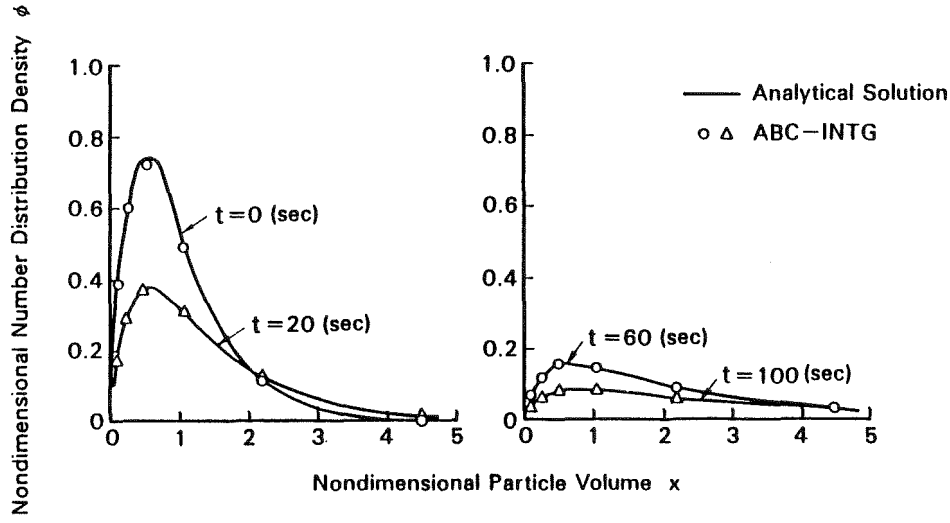

Fig.4 Comparisons of the ABC-INTG Predictions with The Analytical Solutions by Scott (Particle Size Distribution Density)

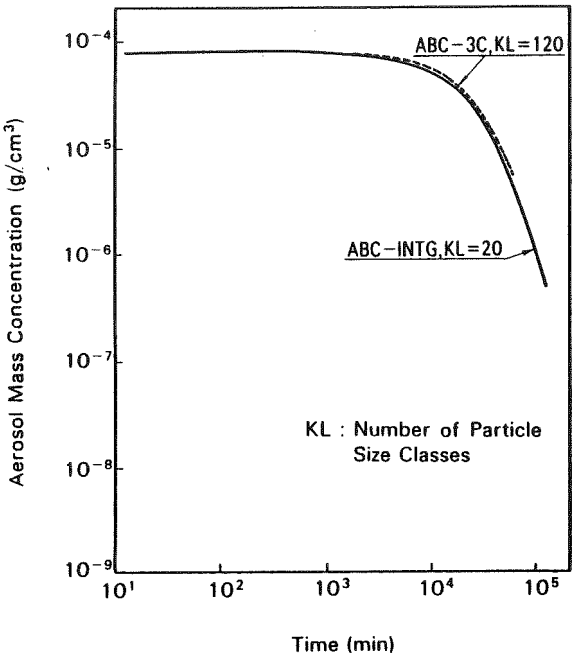

Fig.5 Comparison of the ABC-INTG Prediction with that by ABC-3C

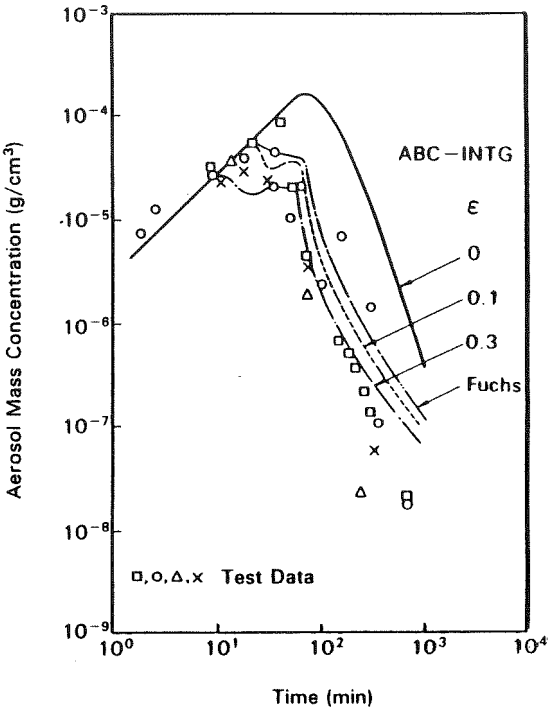

Fig.6 Comparisons of the ABC-INTG Predictions with LTV No.3 Test, Atomics International

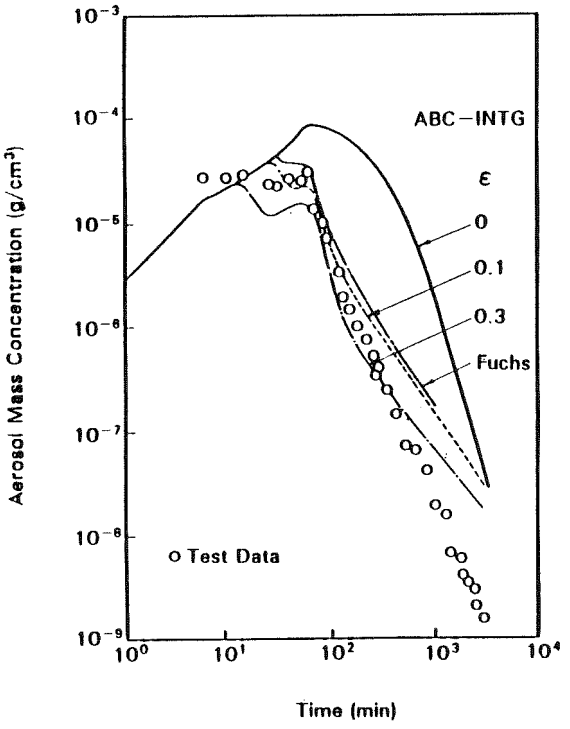

Fig.7 Comparisons of the ABC-INTG Predictions with CSTF AB1 Test by Hanford Engineering Development Laboratory

Test Plan for Aerosol Behavior in the SAPFIRE Facility

Y. Himeno, S. Miyahara, and T. Kinoshita

Fast Reactor Safety Engineering Division
Oarai Engineering Center
Power Reactor and Nuclear Fuel Development Corporation
4002 Narita, Oarai-machi, Ibaraki 311-13, Japan

Abstract

Large scale sodium fire and aerosol behavior tests will start in April 1985 at the new facility, SAPFIRE. The main objectives of this program are to study the structural integrity of some of the plant safety systems and to study the aerosol behavior in the event of a sodium fire accident in an LMFBR. Test rigs for these studies are a $3m^3$ and an $80m^3$ closed vessels and a reactor secondary building simulating a concrete cell.

In regard to the test and the analysis of aerosol behavior, the following studies will be carried out in SAPFIRE Phase-1 during 1985 through 1987.

(1) To study the performance of components under decay heat removal operation and of post-accident monitors in the aerosol containing atmosphere.

(2) To study the aerosol leak and the plugging behavior through the narrow flow channels and small holes (channel model should be considered.)

(3) To improve and validate the ABC-INTG code.

Introduction

In recent years, an accurate evaluation of the response of the plant safety systems in aerosol bearing atmosphere in the event of a sodium fire accident in an LMFBR has become increasingly important. In the past decade, experimental studies have been carried out by many organizations, and these studies have contributed to the understanding of individual phenomena such as pool fire, spray fire, and aerosol behavior in a containment. The computer codes to analyze the above phenomena have also been developed. However, these early studies were insufficient to evaluate the response of the plant safety systems under aerosol conditions. In fact, the spray fire, pool fire, aerosol release, and aerosol transport will proceed almost simultaneously in the event of a real large sodium leak and fire accident. In addition, a large amount of sodium combustion heat and a large mass of sodium aerosols will be generated, if the accident occurs in a secondary building of the reactor. Such complex phenomena cannot be analyzed easily with the knowledge from the early studies alone. Hence, PNC is constructing a large scale sodium leak, fire, aerosol test facility, SAPFIRE, to conduct engineering scale tests.

The whole SAPFIRE program is divided into three phases, namely Phase-1 (from 1985 to 1987), Phase-2 (from 1988 to 1990), and Phase-3 (after 1991). In Phase-1, efforts will be directed to test and analyze the response of the Monju sodium fire and aerosol mitigation systems, particularly, those in the secondary building of the reactor. Phase-2 and Phase-3 are for the source term and the containment response R&D. In the present paper, the test plans for Phase-1 are explained.

1. General Features of Test Facility

Facility construction of SAPFIRE is under way at Oarai Engineering Center, PNC, to be completed at the end of March, 1985. Figure 1 shows the bird's-eye view of the facility in which the following test rigs and utilities will be installed. Table 1 shows the main specifications of the test rigs.

Test Rigs
- *SOLFA-1: Two-story high concrete cell.
- *SOLFA-2: 80m^3 steel vessel.
- *FRAT-1 : 3m^3 steel vessel.

Utilities
- *Aerosol Filtration System: Two units. Each unit consists of HEPA filters and a water scrubber
- *Sodium Supply System: consists of a sodium heater, a 6m^3 sodium recovery tank, and a 20m^3 sodium storage tank equipped with a cold trap.

*Sodium Cleaning and Solution Processing System

In regard to the test rigs listed above, SOLFA-1 is to demonstrate the integrity of the fire mitigation systems. SOLFA-2 is to obtain the test data to validate sodium fire and aerosol behavior codes and also to investigate the durability of components for decay heat removal operation in the aerosol containing atmosphere. Post-accident monitors are also tested in SOLFA-2. FRAT-1 is to make basic tests on sodium fires and aerosol behavior. The interaction between sodium and foreign materials will also be studied with FRAT-1.

2. Test Plan

The test matrix of SAPFIRE ranges from a sodium leak, sodium fire, and aerosol behavior to these interrelated phenomena as described. But, this paper, emphasizes only those test items related to aerosol behavior. Table 2 shows the test items now being planned. The details of each item are as follows.

(1) Test of Reactor Components and Instruments under Sodium Aerosol Containing Atmosphere

In case of a large sodium leak accident in one of the secondary heat transport systems (SHTS) of the reactor, the operation is switched over to the decay heat removal made. In this event, although each SHTS is physically separated from others by the concrete cells and the reactor building walls, sodium aerosols generated in an affected room may leak into neighboring rooms where other SHTS are operating for decay heat removal. This aerosol leak into the neighboring rooms results in the exposure of key components of SHTS to the aerosol containing atmosphere. Furthermore, in the affected room, electrical instruments of the post-accident monitors (PAMs) are also exposed to high temperature atmosphere containing high concentration aerosols.

Taking into account of the above operating conditions of the components and PAMs, the test of their reliabilities and integrities under the simulated accident conditions are essential. In Phase-1 of SAPFIRE, therefore, the tests are to be conducted by exposing the components and the instruments to sodium aerosols in SOLFA-2. The typical components and PAMs to be tested are a pony motor, an air-cooler for decay heat removal, a heat exchanger and a blower for the HVAC (heating, ventilation, and air conditioning) system, a sodium level meter, and a radiation counter. Among them, the tests for the air-cooler and the heat exchanger are most interesting. Early studies were concerned mainly with aerosol deposition under the conditions of natural convection. The deposition studies under forced convection have been very limited. Therefore, by making the tests on the heat exchanger, the deposition behavior under forced convective conditions will be studied in the presence of a very steep temperature gradient at the vicinity of the deposition wall.

(2) Test of Aerosol Leak through Narrow Path

For the realistic evaluation of the radiological consequences of an LMFBR, the modeling of aerosol leak through leak paths in the reactor containment is a key issue [1]. In addition, the environmental protection regulation in Japan is very strict. Therefore, the release of sodium aerosols into the environment should be evaluated accurately and should be limited to a very low level, even though the released aerosol from the secondary building are non-radioactive. But the state of the art is that the modeling is incomplete due to lack of test data.

In the tests, aerosol leaks through narrow gaps and channels will be studied by installing engineering models of a door, hatch or cable penetration in an aerosol duct that connects SOLFA-1 and SOLFA-2. The leak paths in this case are those that appear around the doors and the penetrations in the primary containment cells and the secondary building of the plant. Basic tests with simplified models of leak paths will also be made with FRAT-1.

(3) Aerosol Behavior Test

Following the development of the first versions of aerosol behavior code, ABC-1 and ABC-2 [2] in 1973, the code had been successively improved to ABC-3 [3] in 1974, ABC-3B [4] in 1979, and ABC-3C [5] in 1981. Later in 1983, the new version of the code, ABC-INTG [6], was developed. In the ABC-INTG code, the particle size distribution of the aerosol is discretized by the finite difference method, and the coagulation processes are calculated by using the sectional representation proposed by Gelbard et al [7]. This newly developed ABC-INTG joined the comparison study of aerosol behavior codes from 1982 through 1984, under the auspices of the Commission of European Community, together with the European codes (i.e., PARDISEKO-IIIb, AEROSOLS-B1, AEROSOLS-A2, and AEROSIM). As reported elsewhere [8], the summary and the highlight of the comparison study regarding the ABC-INTG code is that the code predictions showed good agreement with those by the other codes which discretize the particle size distribution.

Despite the efforts, the codes so far developed and now widely used in many countries have their own limitations. One example is on the deposition rate calculation. As is well known, the deposition and the settling are the main sink terms for aerosols. Among them, the thermophoretic deposition is a major deposition process, if the temperature gradient at the vicinity of the wall is very large. However, the thermophoretic deposition rate cannot be accurately calculated by the code unless the temperature gradient data are available as input. This is due to the assumption in the codes that gas natural convection in a closed vessel and the resulting temperature gradient at the vicinity of the wall at different locations are all the same as those calculated from the conventional heat transfer correlation. This assumption makes the realistic evaluation all more difficult.

To improve the above limitation associated with thermophoretic deposition rate calculation, aerosol behavior tests will be made by using SOLFA-2. Thereafter, analyses will be made by combining ABC-INTG with a gas natural convection code that calculates the temperature distribution in the gas phase.

Reference

[1] H. A. Morewitz., "Fission Product and Aerosol Behavior Following Degraded Core Accidents", Nucl. Tech., 53, 120 (1981).
[2] G. Nishio and S.Kitani., "Analysis of Aerosol Behavior in a Containment Following HCDA in LMFBR" (in Japanese), JAERI-memo 5251, April (1973).
[3] G. Nishio and S. Kitani., "A Hazard Analysis of Plutonium Aerosol Released in an LMFBR Hypothetical Accident (ABC-code)", JAERI-memo 5481, August (1974).
[4] N. Mitsutsuka and H. Obata., "Analytical Studies on Uranium Oxide, Sodium Oxide, and Their Mixed Aerosols by Using ABC-3B", NUREG/CR-1724, ORNL/NUREG/TM-404, CSNI-45, April (1980).
[5] H. Obata., "ABC-3C Users Manual" (in Japanese), CRC-081-001, March (1981).
[6] N. Mitsutsuka, Y. Himeno, S. Miyahara, M. Ito, and H. Obata., "Aerosol Behavior Code, ABC-INTG - Features and Validation of the Code - " (in Japanese), PNC Report , under preparation.
[7] F. Gelbard and J. H. Seinfeld., "Simulation of Multicomponent Aerosol Dynamics", Journal of Colloid and Interface Science, 78, No.2, December (1980).
[8] J. Fermandjian. et al., "Comparison of Computer Codes Related to the Sodium Oxide Aerosol Behavior in a Containment Building", to be presented at the OECD/CSNI Specialists' Meeting on Nuclear Aerosols in Reactor Safety, Karlsruhe, 4-6 September (1984).

Table－1 Main Specifications of the Test Rigs

Test Rig	Geometry	Structural Materials	Volume	Maximum Over Pressure	Maximum Temperature
SOLFA-1	Floor : 5m×5m Height : 7m	・Reinforced Concrete ・Steel	175m^3	+0.03bar	・Concrete=150℃ ・Steel=650℃
SOLFA-2	Diameter : 3.6m Height : 9m	Stainless Steel	80m^3	+2bar	450℃
FRAT-1	Diameter : 1.3m Height : 2.1m	Stainless Steel	3m^3	+3bar	550℃

(PSS－PSM－033)

Table－2 Test Items Related to Aerosol Behavior in SAPFIRE, Phase-1

Item	Objective	Test Data To Be Obtained
Component and Instrument Test	to verify reliabilities of DHR* components and PAMs.**	○aerosol mass concentration ○aerosol particle size ○chemical composition of aerosol ○heat transfer coefficient of a heat exchanger ○electrical insulation of PAMs
Aerosol Leak and Plugging Test	to construct aerosol leak and plugging model	○aerosol mass concentration ○aerosol particle size ○chemical composition of aerosol ○pressure drop across a leak path ○leak path geometry
Aerosol Behavior Test	to improve aerosol behavior analysis and to validate the ABC－INTG code	○aerosol mass concentration ○aerosol particle size ○deposition and sedimentation rates ○temperature distribution ○heat trasfer rates

(*) Decay Heat Removal. (**) Post Accident Monitoring.

(PSS－PSM－034)

Fig.1 SAPFIRE Facility

大規模ナトリウム漏洩火災試験施設

サファイア施設

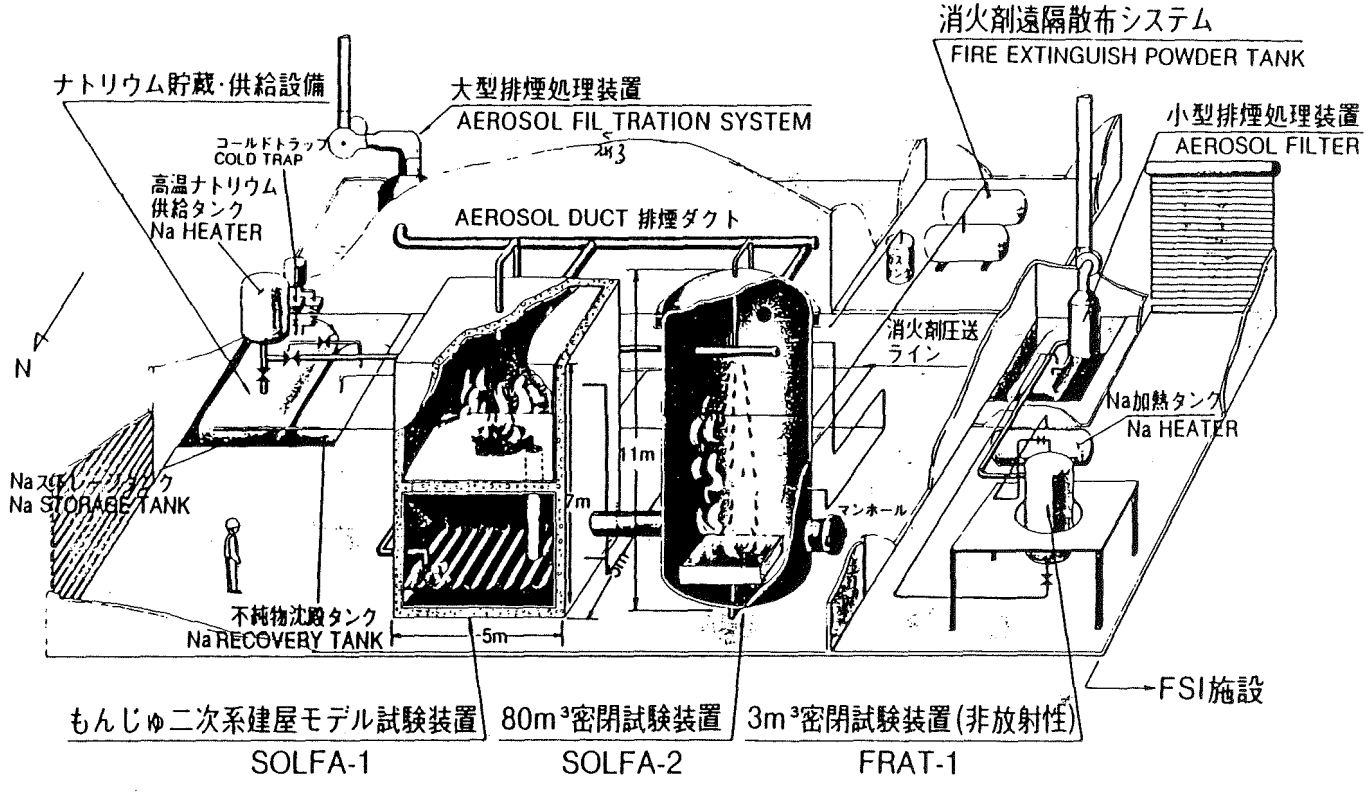

SOLFA (Sodium Leak, Fires, and Aerosols Test Rig)
FRAT (Fission Product and Radioactive Aerosol Release Test Rig)

(PSS−PSM−032)

AEROSOL BEHAVIOR IN A STEAM-AIR ENVIRONMENT*

R. E. Adams
M. L. Tobias
J. C. Petrykowski

Oak Ridge National Laboratory
Oak Ridge, Tennessee 37821
USA

For publication in the Proceedings of the Specialist Meeting on Nuclear Aerosols in Reactor Safety, Karlsruhe, Federal Republic of Germany, September 4—6, 1984

*Research sponsored by the Office of Nuclear Regulatory Research, U.S. Nuclear Regulatory Commission under Interagency Agreements 40-551-75 and 40-552-75 with the U.S. Department of Energy under contract DE-AC05-840R21400 with Martin Marietta Energy Systems, Inc.

AEROSOL BEHAVIOR IN A STEAM-AIR ENVIRONMENT

R. E. Adams,
M. L. Tobias and J. C. Petrykowski
Oak Ridge National Laboratory
Oak Ridge, Tennessee 37831
USA

ABSTRACT

The behavior of aerosols assumed to be characteristic of those generated during light water reactor (LWR) accident sequences and released into containment is being studied in the Nuclear Safety Pilot Plant (NSPP). Observations on the behavior of U_3O_8 aerosol, Fe_2O_3 aerosol, concrete aerosol, and various mixtures of these aerosols in a dry air environment [relative humidity (RH) less than 20%] and in a steam-air environment [relative humidity (RH) approximately 100%] within the NSPP vessel (38.3 m^3 volume) are reported. The primary experimental variables are aerosol mass concentration and aerosol mass ratios.

Under dry conditions the three individual aerosols and mixtures of these aerosols behave differently with regard to rate of removal from the vessel atmosphere. The aerosols are agglomerated in the form of branched chains; the aerodynamic mass median diameter (AMMD) of the U_3O_8, Fe_2O_3 and mixed U_3O_8-Fe_2O_3 aerosols ranged between 1.5 and 3 μm while that of the concrete aerosol was about 1 μm.

Comparison of the behavior of these same aerosols in steam-air with that observed in dry air reveals that a steam-air environment, which would be present in LWR containment during and following an accident, causes the U_3O_8, the Fe_2O_3, and mixed U_3O_8-Fe_2O_3 aerosols to behave in a manner different from that observed in a dry atmosphere; the primary effect is an enhanced rate of removal of the aerosol from the vessel atmosphere. Concrete aerosols were observed to behave differently. Based upon results to date, the presence of steam does not have a significant effect on the removal rate of a concrete aerosol. Electron microscopy showed the agglomerated U_3O_8, Fe_2O_3, and mixed U_3O_8-Fe_2O_3 aerosols to be in the form of spherical clumps of particles differing from the intermingled branched chains observed in the dry air tests; the AMMD was estimated to be in the range of 1 to 2 μm. Steam seemed to have a lesser influence on the physical shape of the concrete aerosol with the shape being intermediate between branched chain and spherical clumps.

The enhanced rate of removal of the U_3O_8, the Fe_2O_3, and the mixed U_3O_8-Fe_2O_3 aerosols from the atmosphere of the NSPP vessel by steam is probably caused by the change in aerosol shape and the condensation of steam on the aerosol surfaces combining to increase the effect of gravitational settling. The apparent lack of an effect by steam on the removal rate of concrete aerosol could result from a differing physical/chemical response of the surfaces of this aerosol to condensing steam.

INTRODUCTION

The behavior of aerosols assumed to be characteristic of those generated during light water reactor (LWR) accident sequences and released into containment is being studied in the Nuclear Safety Pilot Plant (NSPP) which is located at the Oak Ridge National Laboratory (ORNL). This project, which is part of the ORNL Aerosol Release and Transport (ART) Program, is sponsored by the Division of Accident Evaluation, Nuclear Regulatory Commission, and the purpose is to provide experimental qualification for LWR aerosol behavior codes under development.

The program plan for the NSPP aerosol project provides for the study of the behavior, within containment, of simulated LWR accident aerosols emanating from fuel, reactor core structural materials, and from concrete-molten core materials interactions. The aerodynamic behavior of each of these aerosols was studied individually to establish its characteristics; current experiments involve mixtures of these aerosols to establish their interaction and collective behavior within containment. Tests have been conducted with U_3O_8 aerosols, Fe_2O_3 aerosols, and concrete aerosols in an environment of either dry air [relative humidity (RH) less than 20%] or steam-air [relative humidity (RH) approximately 100%] with aerosol mass concentration being the primary experimental variable. Experiments are underway involving mixtures of these aerosols, and, to date, the test aerosol mixtures have been Fe_2O_3 + concrete and Fe_2O_3 + U_3O_8; in these tests the primary experimental variables have been aerosol mass concentration and aerosol mass ratio.

EXPERIMENTAL

The NSPP facility, shown schematically in Fig. 1, includes a test containment vessel, aerosol generating equipment, analytical sampling and system parameter measuring equipment, and an in-vessel liquid spray decontamination system. The NSPP vessel is a stainless steel cylinder with dished ends having a diameter of 3 m, a total height of 5.5 m, and a volume of 38.3 m^3. The floor area is 7.7 m^2 and the internal surface area (including top, bottom, and structural items) is 68.9 m^2. The equipment for the measurement of aerosol parameters includes filter samplers for measuring the aerosol mass concentration, coupon samplers for aerosol fallout and plateout measurement, cascade impactors and a centrifuge sampler for determining the aerodynamic particle size distribution of the aerosol, and devices for collecting samples for electron microscopy. System parameters measured are moisture content of the vessel atmosphere, steam condensation rates on the vessel wall, temperature of vessel atmosphere, temperature gradients near the wall, and vessel pressure.

For the dry aerosol tests the vessel atmosphere was dry air (RH <20%) and the temperature and pressure were slightly above ambient. The slight elevations in temperature and pressure result from the heat produced and gases injected by the plasma torch aerosol generator.

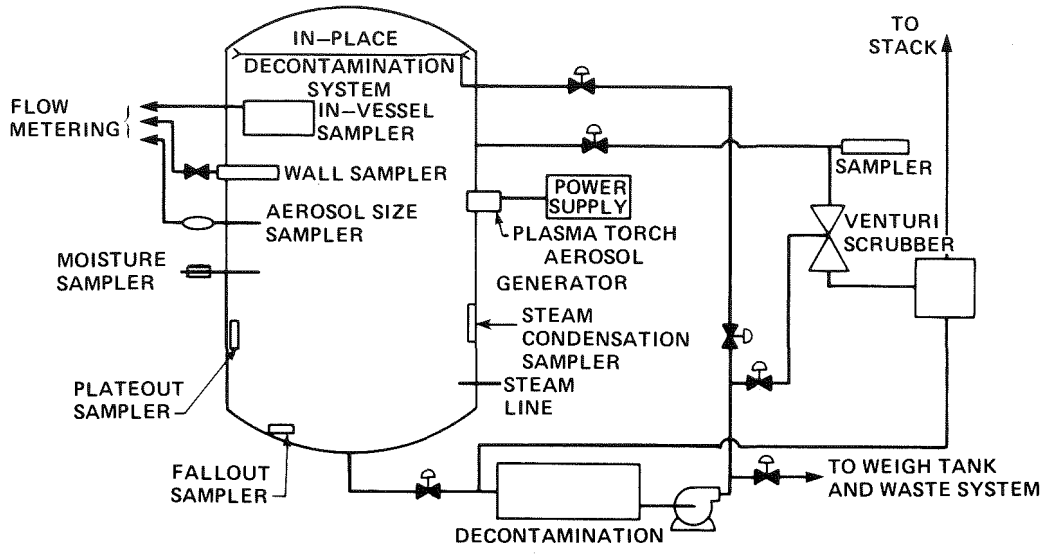

Figure 1. Diagram of the NSPP Facility.

The steam-air aerosol tests were conducted under quasi-steady-state steam conditions. The test atmosphere was prepared by injecting steam into the vessel (initially at subatmospheric pressure) to form a steam-air mixture at elevated temperature and pressure (around 380 K and at an absolute pressure of about 0.2 MPa); upon achieving this condition the rate of steam injection was reduced and the accumulated steam condensate removed from the vessel. The test aerosol was then introduced and steam injection was continued for six hours at a low rate to balance steam losses by wall condensation and assure maintenance of the quasi-steady-state conditions.

Single-Component Aerosol Tests

A number of single-component aerosol tests have been conducted under both dry air and steam-air test environments. Table I lists these tests; results from these tests have been reported [1, 2, 3].

Under dry conditions the three aerosols, U_3O_8, Fe_2O_3, and concrete, behave in a different manner with regard to rate of removal (decrease in aerosol mass concentration) from the vessel atmosphere. Figure 2 compares the behavior of the three aerosols. (Note that the aerosol mass concentration is normalized with respect to maximum concentration and that time is measured from the time of termination of aerosol generation for the purpose of comparison.) Scanning electron microphotography (SEM) shows the aerosols to be agglomerated in the form of branched-chains (Fig. 3). Particle size measurements by cascade impactors and spiral centrifuges indicated that the aerodynamic mass median diameter (AMMD) [4] of the U_3O_8 and Fe_2O_3 aerosols ranged between 1.5 and 3 μm while that of the concrete aerosol was about 1 μm, or less. Based upon

Table I. Details of single-component aerosol tests

Test Nos.	Aerosol	No. of tests	Test environment	Aerosol conc. range ($\mu g/cm^3$)
201-7, 209	U_3O_8	8	Air (dry)	0.05-9.0
208, 210	U_3O_8	2	Air (moist)	7.1, 12.5
401-4, 406-7	U_3O_8	6	Air-steam	5.8-28.0
511	Fe_2O_3	1	Air (dry)	2.4
501-5	Fe_2O_3	5	Air-steam	1.0-8.5
531	Concrete	1	Air (dry)	1.5
521-2	Concrete	2	Air-steam	1.1, 1.5

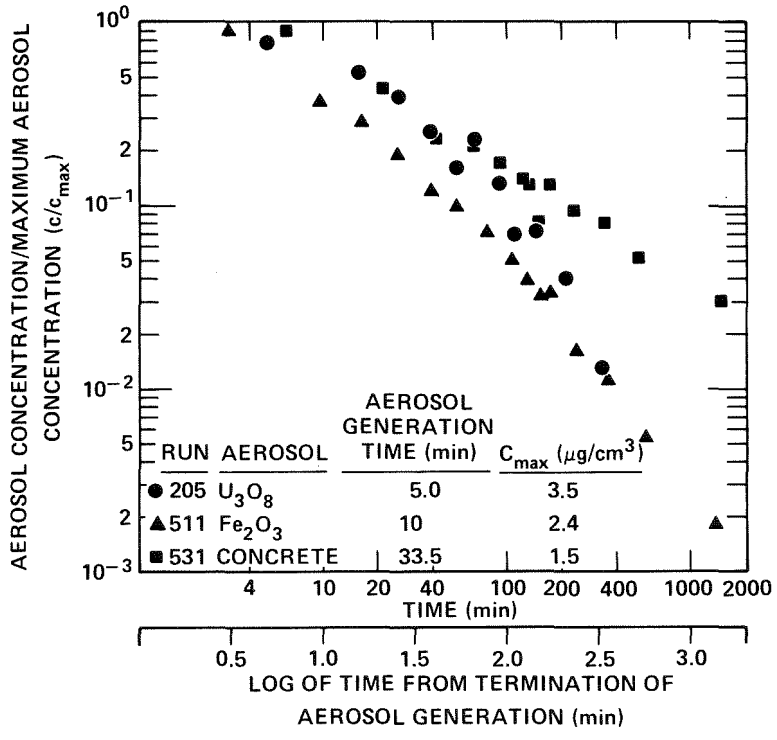

Figure 2. Behavior of Various Single-Component Aerosols in a Dry Air Environment (RH <20%).

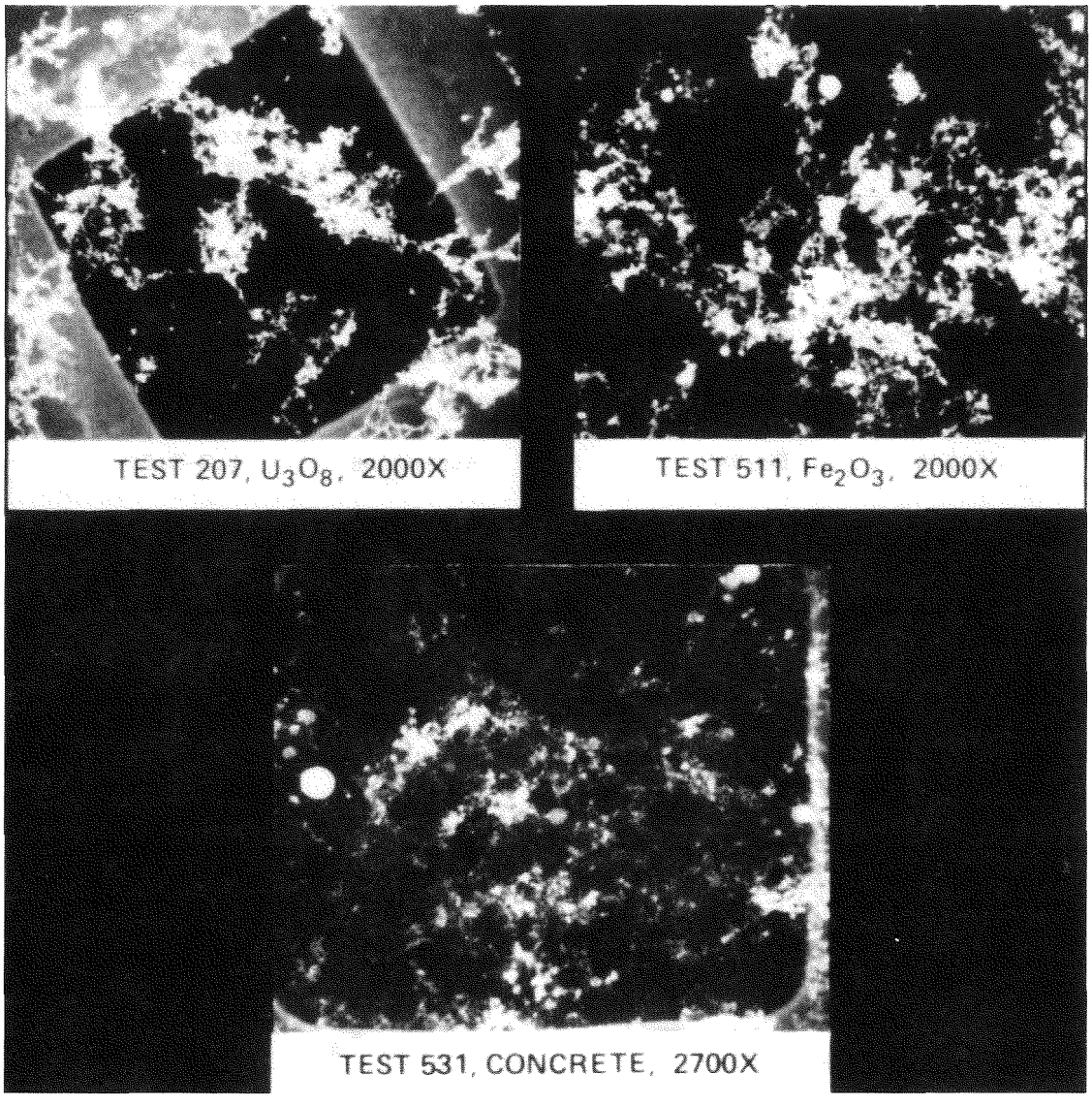

Figure 3. SEM Photographs Illustrating Typical Appearance of Chain-Agglomerate Aerosols in a Dry Air Environment (RH <20%).

the results from these tests under dry conditions, it has been observed that these aerosols have similar sizes and shapes but act aerodynamically in a different fashion.

The presence of steam in the test environment causes a change in both the aerodynamic behavior and the physical shape of these aerosols. The aerodynamic behavior of the aerosols is compared in Fig. 4. The most obvious effect of steam is an enhanced rate of aerosol removal from the vessel atmosphere in the case of U_3O_8 and Fe_2O_3 aerosols. For example, in Fig. 2 under dry conditions, the time required for 99% of

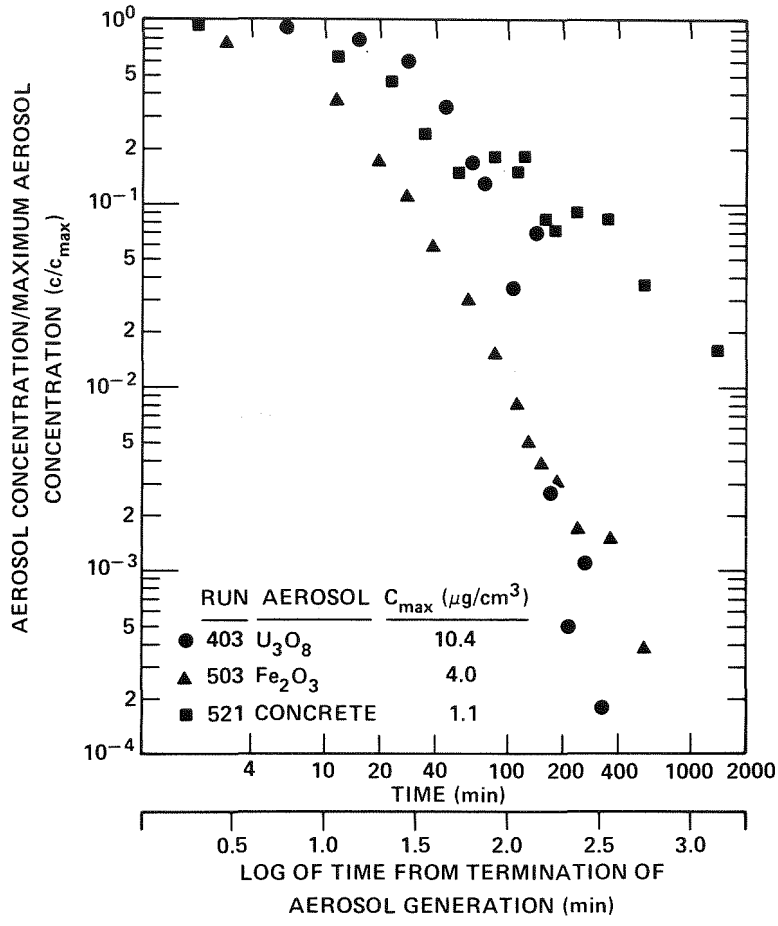

Figure 4. Behavior of Various Single-Component Aerosols in a Steam-Air Environment (RH ~100%).

the Fe_2O_3 aerosol to disappear from the vessel atmosphere is about 350 min.; under steam-air conditions this time is about 100 min. A similar comparison can be made for U_3O_8 aerosol. The shape of these two aerosols is changed from chain-agglomerate to almost spherical by the presence of steam as illustrated in Fig. 5 for U_3O_8. The AMMD for the U_3O_8 or Fe_2O_3 aerosols in steam range from about 1 to 2 μm.

Concrete aerosol does not seem to be affected by the presence of steam in the same manner as U_3O_8 or Fe_2O_3 aerosol. This lack of influence is illustrated in Fig. 6 where the rates of removal of concrete aerosol under dry and under steam-air conditions are compared. This aerosol was generated by passing powdered limestone-aggregate concrete through the plasma torch aerosol generator. The concrete aerosol is not a simple, single-component, aerosol such as U_3O_8 or Fe_2O_3; it is actually a complex mixture of Al_2O_3, SiO_2, CaO, MgO, Fe_2O_3, and various silicates with Al, Ca, Mg, and Fe as the cations. Steam also affects the physical shape of concrete aerosols (possibly to a slightly lesser degree than for U_3O_8 or Fe_2O_3) producing some spherical agglomerates.

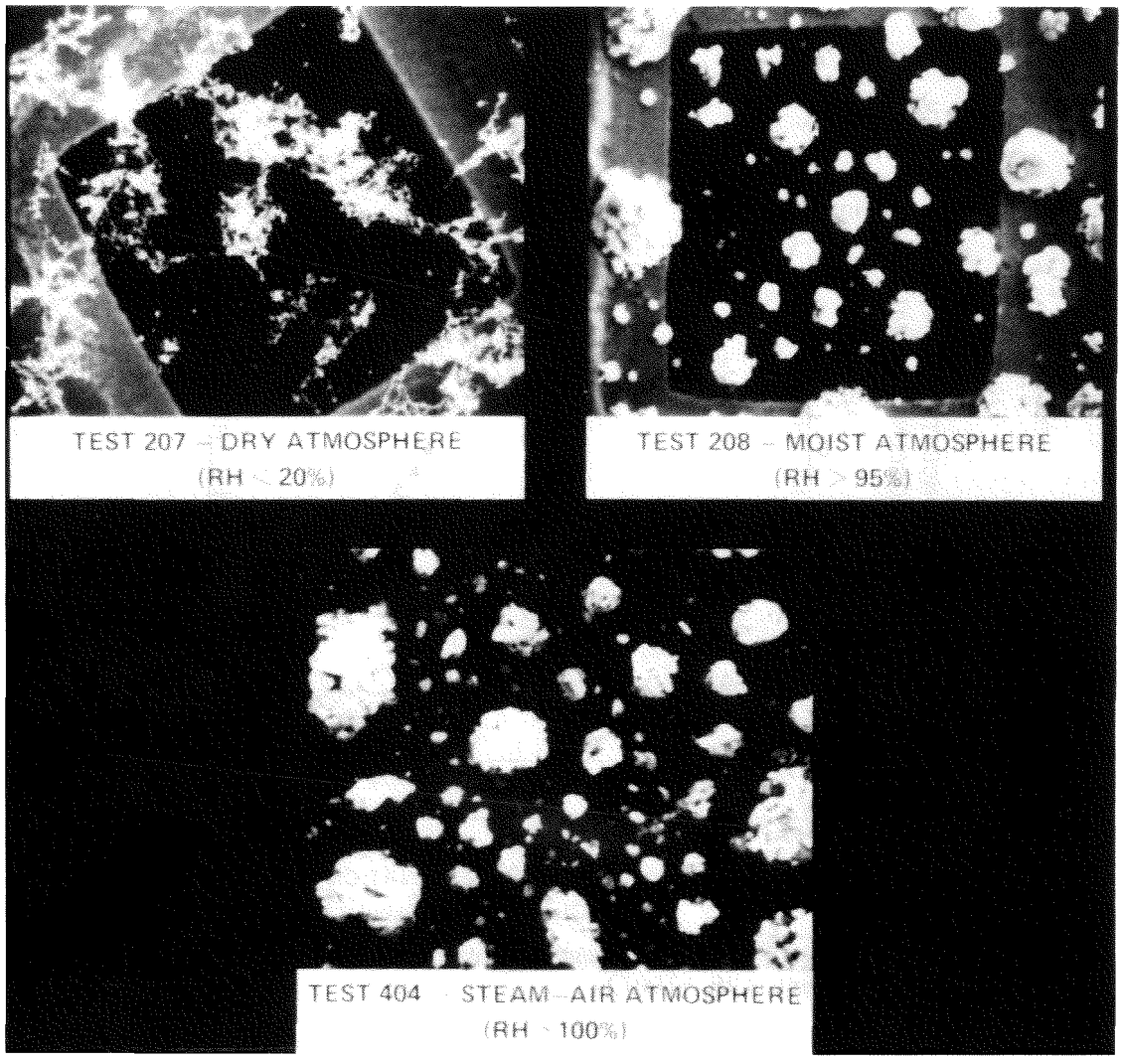

Figure 5. SEM Photographs Illustrating Influence of Moisture/Steam on Physical Shape of U_3O_8 Aerosol.

Figure 7 contains scanning electron microphotographs of a concrete aerosol in a dry air and in a steam-air atmosphere.

Multi-Component Aerosol Tests

Recent activities in the NSPP involve the study of the behavior of multi-component (mixed) aerosols in both dry air and steam-air environments. Details of these tests are contained in Table II. The first mixed aerosol to be studied in detail is U_3O_8 + Fe_2O_3. This mixture simulates those aerosols emanating from molten fuel and molten-core support and structural materials. Experimental procedures are essentially

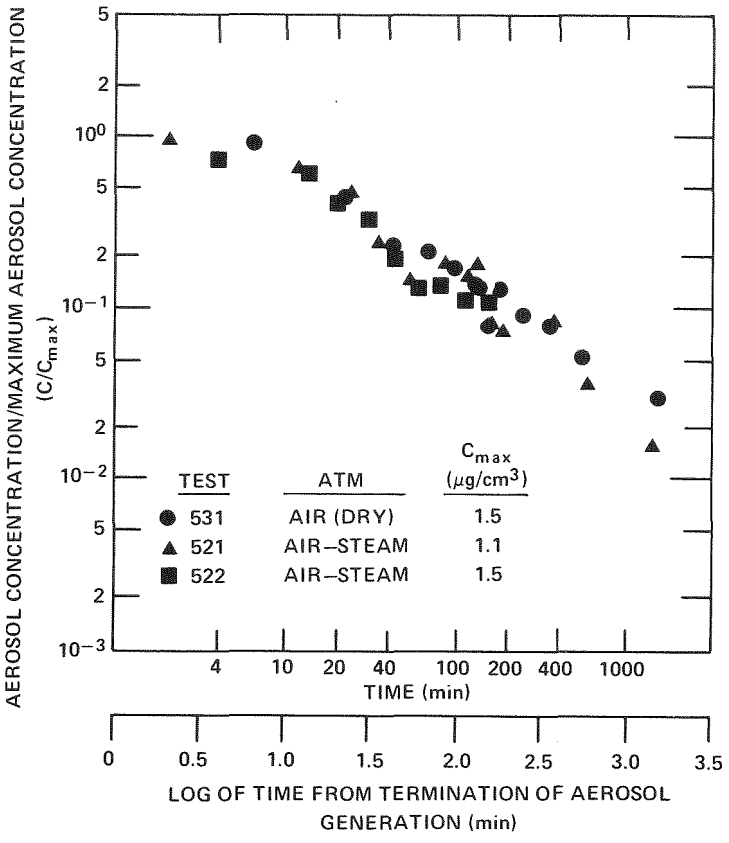

Figure 6. Behavior of Concrete Aerosol in a Dry Air (RH <20%) and a Steam-Air (RH ~100%) Environment.

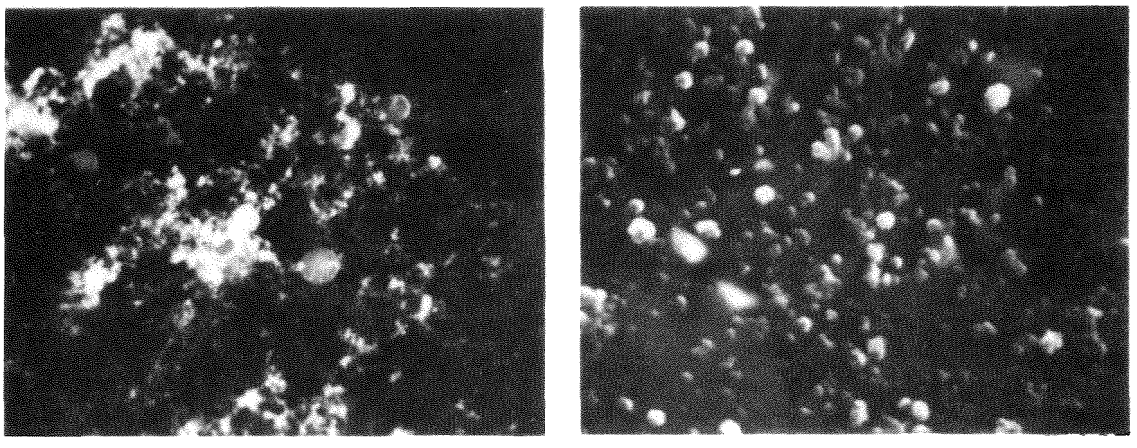

TEST 531 – DRY ATMOSPHERE
(RH < 20%)
6300X MAG.

TEST 052 – STEAM–AIR ATMOSPHERE
(RH ~ 100%)
9000X MAG.

Figure 7. SEM Photographs Illustrating Influence of Steam-Air on Physical Shape of Concrete Aerosol.

Table II. Details of multi-component aerosol tests

Test No.	Mixed aerosol	Test environment	Max. aerosol conc. ($\mu g/cm^3$)	Mass ratio (Fe_2O_3/U_3O_8)
601	Concrete + Fe_2O_3	Air-steam	5.5 2.5	-
611	U_3O_8 + Fe_2O_3	Air-steam	4.0 5.5	1.4/1
612	U_3O_8 + Fe_2O_3	Air-steam	1.8 0.5	0.3/1
613	U_3O_8 + Fe_2O_3	Air-steam	0.7 6.8	9.7/1
631	U_3O_8 + Fe_2O_3	Air (dry)	1.7 1.2	0.7/1

the same as for the single-component aerosol tests. The principal difference is in aerosol generation; the U_3O_8 and Fe_2O_3 aerosols are produced with separate plasma torch generators and allowed to mix within the vessel.

Four mixed aerosol experiments involving various mixtures of Fe_2O_3 and U_3O_8 aerosols have been completed; three were conducted in a steam-air environment and one in a dry air (RH <20%) environment. The behavior of the mixed aerosol (Fe_2O_3 + U_3O_8) in a steam-air environment has been similar in the three experiments conducted, although the mass ratio of F_2O_3 to U_3O_8 has been different in each case. The aerosol mass fraction airborne (C/C_{max}) as a function of time after termination of aerosol generation is illustrated in Fig. 8 for these experiments. Although the rate of aerosol removal during the first 30 min is somewhat larger in Exps. 611 and 613 as compared to Exp. 612, the time required for 99% removal of aerosol mass from the volume of the vessel is about 60 min in all three experiments. SEM photographs of the mixed aerosol showed almost spherical clumps of aerosol in each case. The AMMD of the mixed aerosol in all cases was in the 1 to 1.7-μm range.

To illustrate the effect of steam on the behavior of the mixed aerosol, the results from experiment 631 are compared with those of Nos. 611-613 in Fig. 8. Under dry air conditions, the mixed aerosol tends to remain airborne longer than under steam-air conditions. Note that the time required for 99% of this aerosol to be removed from the vessel is about 400 min as compared with 60 min for the aerosol in the steam-air environment. SEM photographs show the aerosol to be in the form of chain-agglomerates (also observed in previous experiments with Fe_2O_3 or

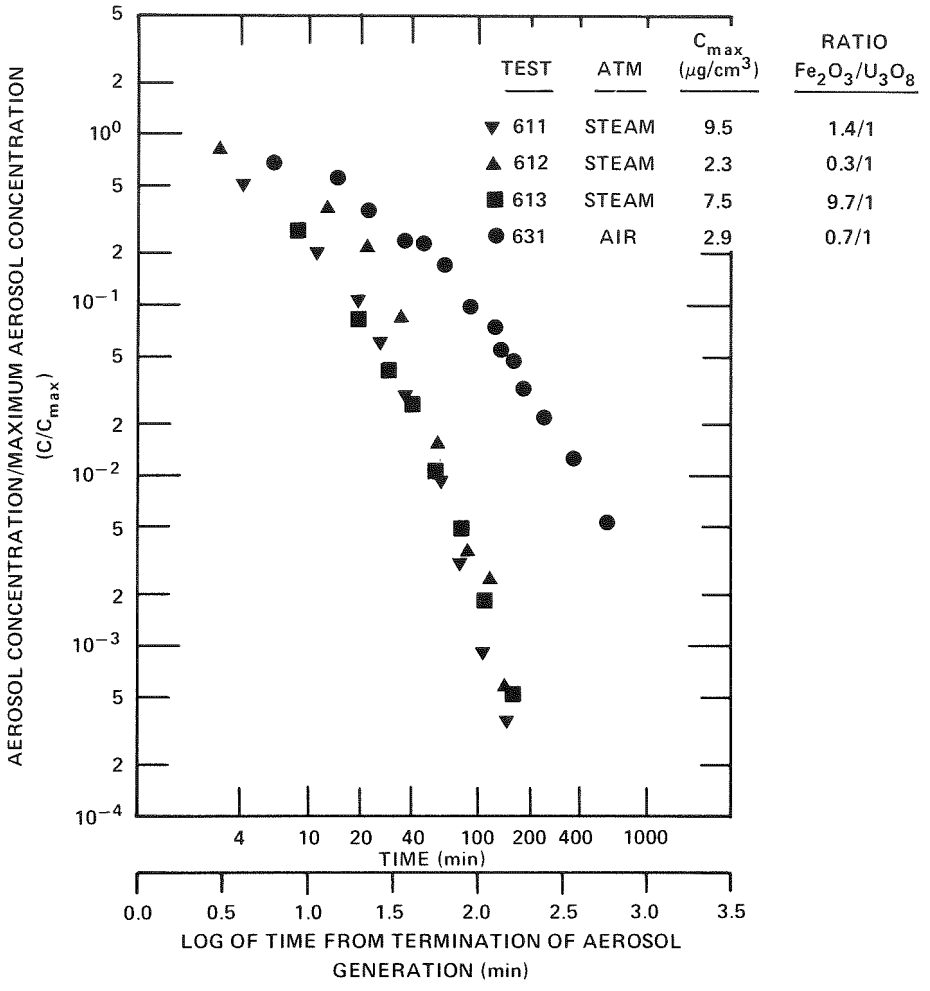

Figure 8. Comparison of Behavior of Multi-Component Aerosol Fe_2O_3 + U_3O_8 in Steam-Air (RH ~100%) and Dry Air (RH <20%) Environments.

U_3O_8 aerosol in dry air) rather than in spherical clumps as in Nos. 611-613. The AMMD for the mixed aerosol is slightly larger in the dry atmosphere with a value as large as 2.7 μm being observed.

It appears, based upon limited data, that the influence of one aerosol component on the other, in a mixed aerosol, can be significant. The behavior of the mixed Fe_2O_3-U_3O_8 aerosol is more like that of Fe_2O_3 aerosol than U_3O_8 aerosol. Data are available which permit a comparison of the influence of concrete aerosol and U_3O_8 aerosol in a mixture with Fe_2O_3 aerosol. Figure 9 compares the behavior of a Fe_2O_3 + concrete aerosol with a Fe_2O_3 + U_3O_8 aerosol in a steam-air environment. Fe_2O_3 + concrete aerosol at a mass ratio of 0.45 to 1 (Fe_2O_3 to concrete) behaves more like a concrete aerosol; Fe_2O_3 + U_3O_8 aerosol at

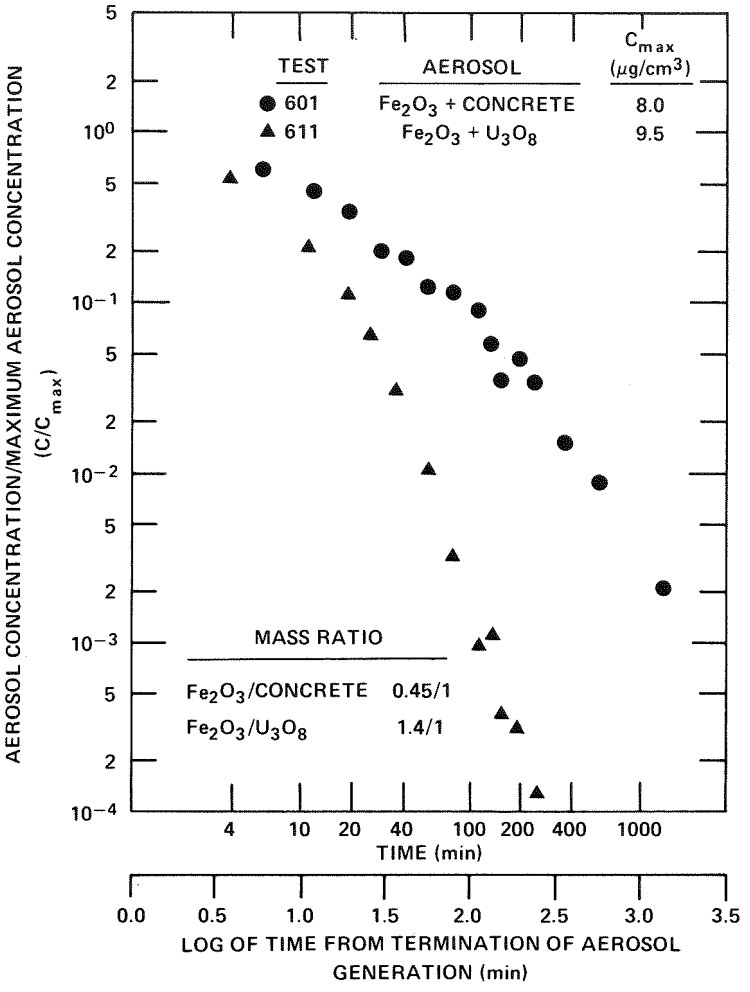

Figure 9. Comparison of Behavior of Multi-Component Aerosols in a Steam-Air Environment (RH ~100%).

a mass ratio of 1.4 to 1 (Fe_2O_3 to U_3O_8) behaves more like a Fe_2O_3 aerosol. Future tests on mixed aerosols will permit a more definitive examination of the influence of one component on another in mixed aerosols.

SUMMARY

General statements may be made on the behavior of single-component and multi-component aerosols in the NSPP vessel. The removal processes for U_3O_8, Fe_2O_3, and U_3O_8 + Fe_2O_3 aerosols are enhanced in a steam-air atmosphere. Steam-air seems to have little effect on removal of concrete aerosol or Fe_2O_3 + concrete aerosol from the vessel atmosphere. A steam-air environment causes a change in aerosol shape from chain-agglomerate to basically spherical for U_3O_8, Fe_2O_3, and U_3O_8 + Fe_2O_3

aerosol; for concrete and Fe_2O_3 + concrete aerosol the change in aerosol shape is from chain-agglomerate to partially spherical. The mass ratio, as well as the identity, of the individual components of a multi-component aerosol seems to have an observable influence on the resultant behavior of these aerosols in steam.

The enhanced rate of removal of the U_3O_8, the Fe_2O_3, and the mixed U_3O_8 + Fe_2O_3 aerosols from the atmosphere of the NSPP vessel by steam-air is probably caused by the change in aerosol shape and the condensation of steam on the aerosol surfaces combining to increase the effect of gravitational settling. The apparent lack of an effect by steam-air on the removal rate of concrete aerosol could result from a differing physical/chemical response of the surfaces of this aerosol to condensing steam.

REFERENCES

1. Adams, R. E., et al., "Influence of Steam on the Behavior of U_3O_8 Aerosols," Proceedings of the USNRC Tenth Water Reactor Safety Research Information Meeting, Gaithersburg, MD, October 12—15, 1982, NUREG/CP-0041, Vol. 2 (January 1983).

2. Adams, R. E., "Behavior of U_3O_8, Fe_2O_3, and Concrete Aerosols in a Condensing Steam Environment," Proceedings of the USNRC Eleventh Water Reactor Safety Research Information Meeting, Gaithersburg, MD, October 24—28, 1983, NUREG/CP-0048, Vol. 3 (January 1984).

3. Quarterly Aerosol Release and Transport Program Progress Reports for the years 1980—1984. R. E. Adams and M. L. Tobias, editors.

4. Mercer, T.T., "Aerosol Technology in Hazard Evaluation,," New York, Academic Press (1973).

Comparison of Aerosol Behaviour Measured during DEMONA Experiments to NAUA Code Predictions

H. Bunz, W. Schöck
Kernforschungszentrum Karlsruhe GmbH
Laboratorium für Aerosolphysik und Filtertechnik I
D-7500 Karlsruhe

Abstract

In order to demonstrate the applicability of the NAUA-code for large volumes the large scale experiment DEMONA is performed. In addition to the pure demonstration aspect, the more scientific questions are of great interest how much the reality differs from some simplifying assumptions in the code as for example the spatial homogeneous mixing in the volume.

The experiments are conducted in the model containment facility at Battelle Frankfurt. The model containment was constructed as a linear 1 : 4 scaled model of the Biblis A PWR (640 m^3) and originally used for blow down investigations. It is subdivided in 9 compartments which are connected with variable openings. Different geometries can easily be established.

The following parameters are measured as function of the time:

- mass concentration separated into the liquid and the solid part
- particle size distribution by optical and inertial devices
- effective density and shape of the particles
- deposition on the walls and the floor at different locations
- chemical composition of the particles in experiments with mixed aerosols

Comparisons of these measured parameters with NAUA-calculations will be presented in this paper. The calculations are performed before and after the experiments to check on the one side the physical model implemented in the code and on the other side how strictly the experimental conditions can be defined in advance.

Introduction

Since an important part of the radioactivity expected to be released during severe nuclear accidents is aerosol-type material, the calculation of the retention of the particles in the containment system and of the fraction available for release into the environment is of great importance. Therefore, a number of computer codes were developed to describe and to calculate the behaviour of aerosol particles in closed systems under the conditions of severe accidents. At KfK/FRG two aerosol codes were developed, the PARDISEKO code /1/, used for hypothetical accidents in LMFBR's and the NAUA code /2/, designed to calculate the aerosol behaviour in LWR containments during severe accidents, especially core melt down sequences. It takes into account the physical effects present only in LWR containments like steam condensation and evaporation on the particles, steam condensation on the walls and the change of hydrodynamic properties of the carrier gas due to varying gas composition. All these aerosol codes are based on simplifying assumptions to enable the mathematical formulation of the

problem and the numerical solution.

The differences between reality and the physical models implemented in the codes have to be evaluated in suitable experiments to obtain the conditions the codes can be applied for. The types of experiments performed can be separated into single effect experiments concentrated mainly on one single physical process implemented in the code and into integral experiments conducted under conditions comparable to the real accident.

The first type of experiments were already performed for a number of processes, e.g. in the case of the NAUA code for the condensation of steam on the particles /3/, whereas integral experiments are only available for accident sequences in LMFBR with large sodium fires. Therefore, the large scale experiment DEMONA was planned in the model containment at Battelle Frankfurt /4/ where quite realistic conditions can be simulated. The first tests of the experimental series have already been performed, compared to the results of pre- and postcalculations and will be presented in this paper. In addition, the problems arising in such large experiments will be discussed.

The NAUA Mod4 Code

The basic physical model in NAUA-Mod 4 is the same as in most of the advanced aerosol behaviour models for closed containers /5/. The following assumptions are used in order to keep computing time at a reasonable level:

- Particles are homogeneously distributed in a control volume except for the boundary layers at the walls.
- Within one particle size class no difference in particle composition is allowed.
- Particle properties are functions of only one independent variable, the particle size, and of the particle density which may change, due to varying particle composition.
- Process coefficient (shape factors, boundary layers etc.) are assumed to be independent of particle size.

For core melt accidents these assumptions are considered to be valid. Internal mixing of species in one size class is quickly achieved by coagulation. The spatial homogeneity in the control volume is accomplished by convection. So, at present no reason is known for not using the physical volumes of the reactor building as control volumes. Within a control volume the code calculates the following processes:

- Removal processes

  . Gravitational settling
  . Diffusional plate out
  . Diffusiophoretic deposition

- Interaction processes

  . Brownian coagulation
  . Gravitational coagulation
  . Steam condensation on particles

- Transport processes

  . Aerosol sources
  . Leakages

If all the mathematical expressions for the different physical processes are combined, the usual and well-known integro-differential equation for the aerosol behaviour under stirred conditions is obtained. Since the direct solution of this equation causes numerical problems it is useful to convert this equation into a set of coupled ordinary differential equations by approximating the particle size distribution n (r, t) by a number N of monodisperse fractions

$$\frac{\partial n(r_k, t)}{\partial t} = S(r_k, t) - (\alpha_D(r_k) + \alpha_S(r_k) + \alpha_{DPh}(r_k) + \alpha_L(r_k)) \cdot n(r_k, t)$$

$$- \sum_{i=1}^{N} (1 - 1/2\, \delta_{ik}) \cdot K(r_i, r_k) \cdot n(r_i, t) \cdot n(r_k, t)$$

$$+ 1/2 \sum_{i=1}^{N} \sum_{j=1}^{N} K(r_i, r_j)\, \beta_{ij}^{k} \cdot n(r_i, t) \cdot n(r_j, t)$$

$$+ (1 - \delta_{1k}) \frac{\dot{V}_{k-1}(t)}{V_k - V_{k-1}} \cdot n(r_{k-1}, t) - \frac{\dot{V}_k(t)}{V_{k+1} - V_k}\, n(r_k, t)$$

for k = 1, ..., N

The coefficients are the removal coefficients due to diffusion, settling, diffusiophoresis and leakage being a removal process for the compartment under consideration, $K(r_i, r_k)$ stands for the total coagulation frequency between particles of size r, and r_k and v_k is the volumetric growth velocity due to steam condensation.

The aerosol source $S(r_k, t)$ has to be specified as input data. Arbitrary time functions, size distribution parameters, particle densities and nuclide composition are acceptable. The leakage is specified as input data, too. No size dependent effects are taken into account by the code but may easily be inserted, if necessary.

The leakage of one compartment can be used as a source function for another compartment to enable multi-compartment calculations.

Additional input values required by the code are the geometry of the compartment and thermodynamic parameters, carrier gas temperature, partial pressure of condensable and non-condensable gas and the source of steam in the compartment.

Applications of the NAUA Code to Accident Sequences

The NAUA code has already been applied to a number of different accident scenarios for German as well as foreign reactor containments.

Two examples will be presented to demonstrate the possible retention of the particles in the containment dependent on the conditions of the accident.

In both cases the accident is initiated by a large break LOCA and the failure of the emergency core cooling system but in the first one (release category: FK6) the containment integrity can be maintained and only the design leakage has to be taken into account up to the time a pressure of 9 bar (1.5 times design pressure) is reached, whereas in the second one (release category: FK2) a large opening of the containment is assumed from the beginning of the accident due to the failure of the ventilation system.

In addition to the depletion of the particles in the containment, in both cases the retention in the annular gap and in the auxiliary building (only for the FK2-case) has to be considered using the multi-compartment option of the NAUA code. The calculated accumulated leaked masses can be seen in Table 1 and 2. These results demonstrate the filtering effect of subsequent compartments reducing the total release even in the FK2-case to less than 1 % of the initial release into the containment. For the FK6-case it can be expected that the filtering system will be working during the accident and will also reduce the release into the environment.

The impact of the aerosol-type activity on the environment is drastically reduced by these results compared to earlier studies treating the aerosol particles similar to gases /6/. But the aerosol codes contain some simplifying assumptions, as already discussed. Therefore, to confirm these results an integral experiment was planned under conditions comparable to the real accident (DEMONA experiments).

Comparisons between NAUA calculations and DEMONA experiments

The DEMONA experiments are conducted in a model (linear scale 1 : 4) of the containment of the Biblis A power station. The experimental matrix is defined in /4/. At the moment the first test is finished and available for comparison. The object of this test is to check the aerosol generator and to serve as a background experiment under dry conditions for the later experiments influenced by steam condensation.

Before the first test was started quite a few precalculations were performed on the one hand to give a basis for the time schedule of the measurements and on the other hand to verify the code by calculations without any backfitting of input data. The quite large number of precalculations /7/ has to be done since many important input data are quite uncertain in advance.

The exact knowledge of thermodynamic data except the leak rate of the containment is not very important for the dry test as long as some convection mixing the atmosphere can be guaranteed. Therefore, the aerosol generation rate and the sizes of the particles produced as a function of the time are the dominating parameters which are difficult to determine

even during and after the experiment as measuring the source particles directly is impossible. The necessary data have to be estimated using results of some preliminary generator tests for the precalculations and to be determined indirectly from the measured aerosol mass concentration for the post-calculations. The exact definition of input data and the boundary conditions is a general problem of such large scale integral experiments since the instrumentation is quite difficult and quite a few side effects may take place. Bearing in mind all these problems of the experiments on the one hand and the simplifications and idealizations of the mode on the other hand, the results of experiments and calculations can be compared. Regarding the precalculations a case has to be selected being based on a generation rate similar to the rate in the later experiment. The result can be seen in Fig. 1. The calculation is performed with a generation rate of 130 g/min within the first 30 min of the experiment, the size of the particles is chosen to be 0.1 µm with a geometric standard deviation of 2 which are typical values for core melt aerosol particles. Luckily, the concentration (6 g/m^3 as maximum value) is so high that the exact particle size does not influence the aerosol behaviour too much. The total released mass in the calculation is 3900 g, in the experiment it is estimated to be 4800 g. But in the experiment the particles are released during two puffs and, therefore the effective maximum concentration is reduced and comparable to the calculation (Fig. 1). Only within the last 18 h of the experiment the difference between the calculated and the measured values is noticeable. The faster decay of the particles calculated by the code at the end may be caused by the leakage being reduced at the end by the skrinking pressure gradient. On the other hand, in the precalculation the leak rate is held constant at 100 %/d.

Therefore, in the calculations performed after the experiment not only the particle source rate is varied to agree with the source rate in the experiment (as far as it is known) but also the leak rate is changed as a function of the time depending on the measured pressure difference (Fig.2). Unfortunately, no measurements of the pressure are available just for the last few hours of the experiments, therefore, the leak rate was held constant at the end at a value of 50 %/d (compared to 100 %/d in the precalculation) even if further reduction can be expected, but it can be seen that the difference to the experimental curve is reduced confirming the influence of the leak rate on the long time behaviour of the particles in the experiment.

Conclusion

Calculations using the NAUA-Mod5 code are compared to the first DEMONA experiment. The principal applicability of the code to the behaviour of aerosol particles in large containers can be shown. As the experimental data are not complete in the sense of a laboratory experiment, it can not be decided at the moment if the differences between the calculations and the experiment are caused by experimental inaccuracies or by the code simplifications.

References:

/1/ H. Bunz: KfK 3545 (Nov. 1983)

/2/ H. Bunz, M. Koyro, W. Schöck: KfK 3554 (Aug. 1983)

/3/ W. Schöck, H. Bunz, M. Koyro: KfK 1353 (Aug. 1981)

/4/ W. O. Schikarski (ed.): KfK 3636 (Dec. 1983)

/5/ Nuclear Aerosols in Reactor Accidents, CSNI/SOAR, OECD (June 1979)

/6/ Deutsche Risikostudie Kernkraftwerke, Verlag TÜV Rheinland (1979)

/7/ W. Schöck: LAF internal note (Febr. 1984), unpublished

	containment	annular gap
Total release into the compartment /g/	3.5×10^6	292
Accumulated leakage out of the compartment without filtering /g/	292	13

Table 1: Basic Results for Release Category FK6

	containment	annular gap	auxiliary building
Total release into the compartment /kg/	3500	657	270
Accumulated leakage out of the compartment without filtering /kg/	657	270	23

Table 2: Basic Results for Release Category FK2

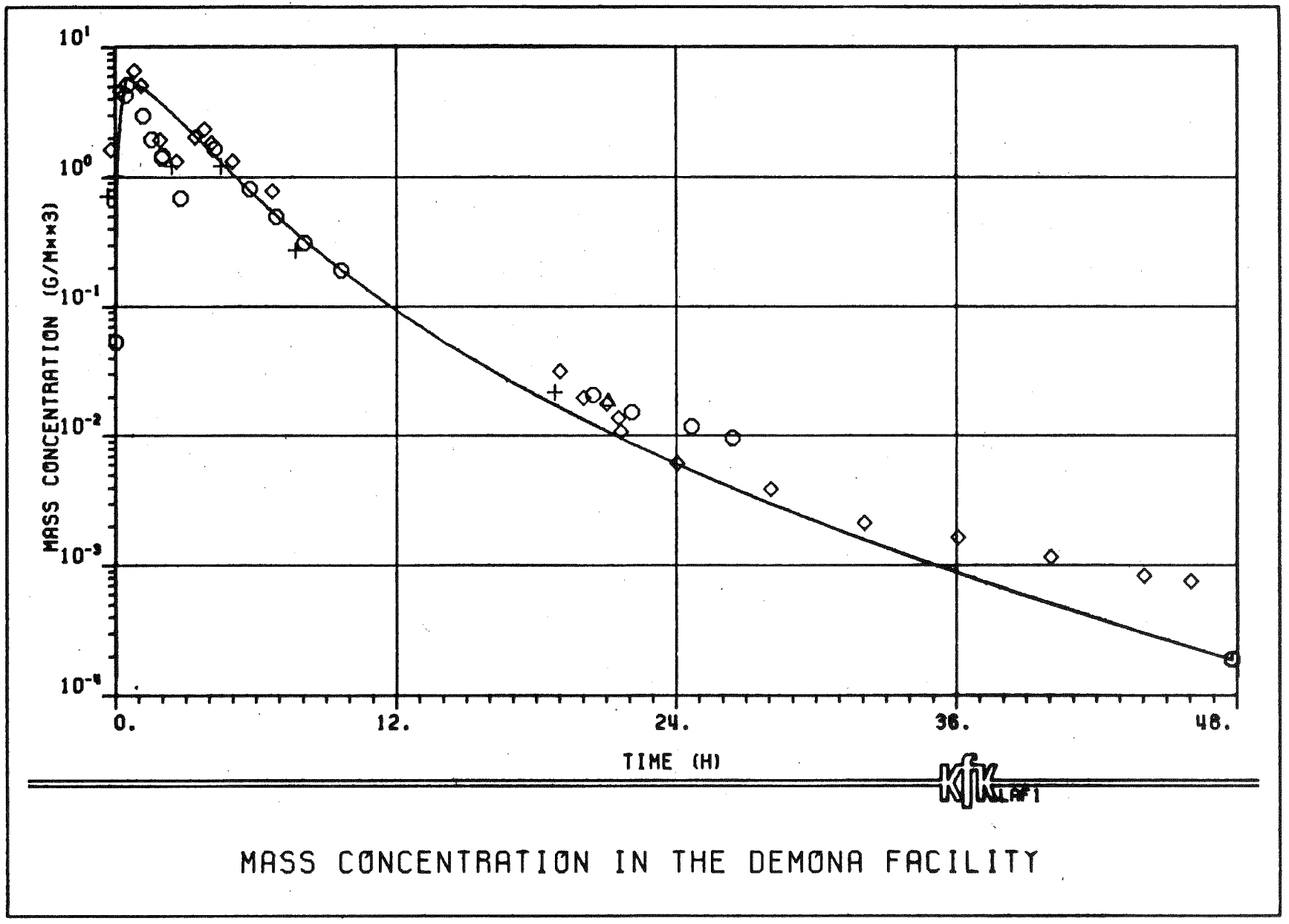

Fig. 1: Comparison of Measured DEMONA Data to the Precalculation Based on Aerosol Generation Rate of 130 g/min during 30 min.

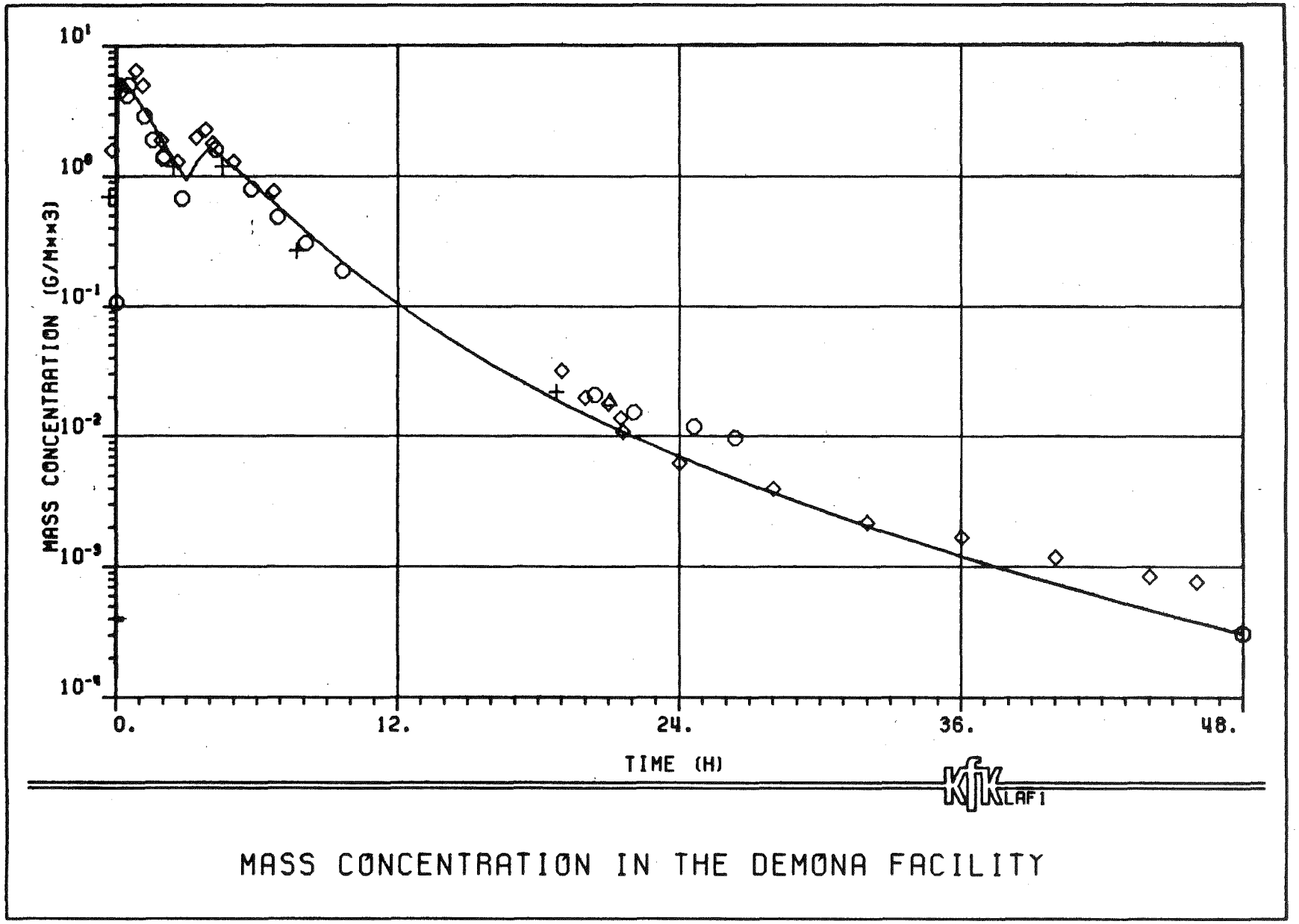

Fig. 2: Comparison of Measured DEMONA Data to the Calculation Performed after the Experiment, Aerosol Generation Rate and Leak Rate fitted according to the Experimental Results

LWR AEROSOL CONTAINMENT EXPERIMENTS (LACE) PROGRAM AND INITIAL TEST RESULTS

L. D. Muhlestein
R. K. Hilliard
G. R. Bloom
J. D. McCormack
Westinghouse Hanford Company
Richland, WA 99352

F. J. Rahn
Electric Power Research Institute
Palo Alto, California 94303

ABSTRACT

The LWR Aerosol Containment Experiments (LACE) program is described. The LACE program is being performed at the Hanford Engineering Development Laboratory (operated by Westinghouse Hanford Company) and the initial tests are sponsored by EPRI. The objectives of the LACE program are: (1) to demonstrate, at large-scale, inherent radioactive aerosol retention behavior for postulated high consequence LWR accident situations; and (2) to provide a data base to be used for aerosol behavior and thermal hydraulic computer code validation. Test results from the first phase of the LACE program are presented and discussed. Three large-scale scoping tests, simulating a containment bypass (event V) accident sequence, demonstrated the extent of agglomeration and deposition of aerosols occurring in the pipe pathway and vented auxiliary building under realistic accident conditions. Parameters varied during the scoping tests were aerosol type and steam condensation.

INTRODUCTION

Extensive research is presently underway around the world to understand the behavior of radioactive materials in both the primary system and containment building of an LWR under postulated severe accident conditions. The objective of this research is to characterize inherent aerosol retention processes which, in the event of a postulated severe accident, will decrease the radioactive source term such that the perceived threat to the public from such an accident would be less than presently calculated.

Early experiments (Containment Systems Experiment(1)) provided valuable information on fission product transport and retention by natural processes and the effect of engineered safety features on fission product removal. Three aspects not realistically accounted for in the CSE tests were: (1) very high aerosol concentrations, (2) transient thermal conditions, and (3) the effect of intercompartmental flows.

The current Marviken program(2) is directed towards demonstrating inherent radioactive aerosol retention in reactor coolant systems. The objectives of the DEMONA project(3,4) are to demonstrate inherent aerosol attenuation in intact single and multi-compartments and to demonstrate the predictive capabilities of the NAUA aerosol code and COCMEL thermal hydraulic code. Pilot-scale, single compartment tests have been performed in the ORNL Nuclear Safety Pilot Plant(5) (NSPP) and in the NAUA facility(6) at KFK to study aerosol behavior for code development and validation.

The LWR Aerosol Containment Experiments (LACE) program will investigate inherent radioactive aerosol retention behavior for postulated high consequence accident situations where the existing data base is inadequate and which are not being addressed by other test programs. Accident situations to be considered are those for which high consequences are presently calculated because either the containment is bypassed altogether (containment bypass sequences), the containment function is impaired early in the accident (early containment leakage or failure to isolate), or delayed containment failure occurs simultaneously with a large fission product release (significant aerosol resuspension or delayed core damage). Significant inherent aerosol retention could reduce the consequences presently calculated for these postulated accident situations. The results of the proposed LACE program should, therefore, considerably improve our ability to realistically assess the consequences of these presently assumed high consequence accidents.

LACE PROGRAM PLAN

Objectives

The objectives of the LACE program are: (1) to provide a data base for validating containment aerosol and related thermal hydraulic computer codes,

and (2) to experimentally investigate, at large-scale, inherent radioactive aerosol retention behavior for postulated high consequence accident situations where the data base is presently inadequate. To meet the above objectives, facilitate program implementation, and encourage international participation, the LACE program has been divided into two parts. Large-scale experiments at the Hanford Engineering Development Laboratory (HEDL) form the Base Program. The base program is complemented by a support program which consists of smaller-scale experiments, calculations, and analytical efforts at other laboratories.

The management of the LACE program will be vested in a project Board of Directors comprised of representatives from each program participant. A Technical Advisory Committee will be established to monitor technical progress of the project, to advise the Board of Directors on program direction, and to coordinate the base and support program efforts.

Support Program

It is intended that the LACE program will be an international program with many countries and organizations involved. The involvement will not only be in providing funds for the base program, but also in participating in various areas of the support program consistent with each organization's expertise and interests. To facilitate implementation, the support program is categorized into three main areas.

The first area is direct support activities which are required to help plan or perform the large-scale experiments and obtain the data. Development and implementation of aerosol generation techniques, thermal hydraulic calculations, chemistry support, and instrumentation are examples of tasks which have been identified in this area.

The second area is separate effects tests needed to clarify individual phenomena difficult to study at large scale. The change in aerosol behavior due to hydrogen burning, aerosol penetration of cracked concrete, aerosol resuspension mechanisms and revaporization effects are part of this effort. While peripheral to the large-scale tests, these phenomena are critical to understanding aerosol behavior in containment structures.

The third area is analytical efforts. An extensive series of pre- and post-test calculations will be required to help design the experiments, analyze data, and participate in code validation efforts. The data analysis and code validation efforts will be organized to achieve many of the aerosol code validation objectives recommended by the aerosol experts group of the Nuclear Energy Agency (NEA) Committee on The Safety of Nuclear Installations (CSNI)(7).

Base Program

The base program consists of large-scale integral tests which will simulate unique postulated accident sequences, yet which are performed to provide

information on specific phenomena required to understand radioactive aerosol behavior. The tests focus on three postulated accident situations: (1) containment bypass sequences, (2) early containment leakage or failure to isolate, and (3) delayed containment failure. A simplified test matrix is shown in Table 1.

TABLE 1

SIMPLIFIED LACE TEST MATRIX

Number Of Tests	Simulated Accident Failure Mode	Phenomena Studied
5	Containment bypass through cold leg interface piping	Aerosol retention in pipe, auxiliary building, and leak path
2	Late containment leakage due to overpressure	Aerosol containment behavior, resuspension
1	Failure to isolate containment	Aerosol containment behavior, leak path retention
1	Early containment leakage due to overpressure	Isentropic expansion effects
1	Failure to isolate containment	Aerosol behavior in inter-compartment flow, leak path retention

The containment bypass test series consist of three scoping tests and two follow-on tests. The scoping tests have been initiated prior to completion of the final LACE program plan in order to obtain early information regarding deposition of aerosols in the interface piping and auxiliary building. The tests used a 63-mm diameter pipe with soluble (NaOH) and insoluble ($Al(OH)_3$) aerosol simulants. The test conditions were chosen so that the tests could be completed quickly without additional development effort and with existing aerosol generation and analysis experience. Parameter changes considered for the follow-on tests are pipe diameter, gas velocity, and more prototypic aerosol materials. Aerosol retention in an auxiliary building and leakage paths from the auxiliary building are being studied. Appropriate thermal hydraulic conditions are being modeled.

The late containment leakage test series consists of two tests which will address conditions associated with late containment leakage by overpressure, and will study aerosol containment behavior with dynamic steam condensation

and heat transfer conditions. The two tests differ in the rate of aerosol injection, with the maximum suspended concentration being approximately 0.1 g/m^3 for the first test and approximately 10 g/m^3 for the second test. Dynamic steam condensation and heat transfer conditions similar to a small pipe break accident will be modeled. Questions regarding aerosol resuspension will also be addressed.

The early containment failure test series consists of three tests. The first test will simulate a failure to isolate containment with leakage through a well-defined pathway to a scrubber. Aerosol behavior and retention in the containment and leakage path will be measured. For the second test, the containment will be isolated initially, but will be rapidly vented from high pressure to simulate early failure by overpressure. Rainout and aerosol modification inside containment caused by isentropic expansion will be studied. The third test will simulate conditions associated with failure to isolate containment, and will study the effect of intercompartment flows on aerosol behavior. Data from this test can be used to evaluate the well mixed volume assumption used in present accident consequence assessment codes.

Aerosols used in the base program tests will be realistic, using materials that may be found in LWR cores or suitable simulants. Both water-soluble and water-insoluble materials will be included. Each test will be designed to provide experimental data for use in validating aerosol and thermal hydraulic computer codes. A formalized procedure of code predictions and data comparisons will be established which includes pretest and "blind" post-test calculations.

CONTAINMENT BYPASS SCOPING TESTS

Introduction And Test Objectives

The objective of the containment bypass scoping tests was to determine the retention of aerosol materials in the interface pipe and auxiliary building during a postulated check valve failure (Event V) accident sequence in a LWR. The specific objectives were to measure the fractional aerosol retention in the pipe, determine changes in aerosol characteristics caused by flow through the pipe, and determine aerosol behavior (deposition, agglomeration, plateout, condensation) in a vented auxiliary building.

Analysis of the event V sequence showed that conditions which would normally be present include high aerosol mass concentrations, high gas velocities in the pipe, a steam/hydrogen carrier gas, long tortuous pipe pathway, and discharge into an auxiliary building. Mechanisms which were considered for particle deposition were fluid turbulence in a straight pipe, gravity settling, inertial impaction in bends, fluid turbulence downstream from elbows, Brownian diffusion, thermophoresis, and diffusiophoresis. Of these mechanisms, fluid turbulence in a straight pipe and inertial and turbulent effects downstream from elbows were expected to dominate. Important auxiliary building conditions considered were volume, wall and gas

temperature, pressure, steam to noncondensible gas ratio, amount of superheat, aerosol residence time and venting conditions.

Test Conditions

The test matrix and test conditions for three completed containment bypass scoping tests are given in Table 2. Sodium hydroxide (NaOH) was used to simulate soluble fission product aerosol materials such as cesium hydroxide (CsOH). Aluminum hydroxide was used to simulate insoluble aerosols formed from structural materials. The amount of steam superheat was varied to determine the effects of condensation and water uptake. Important test pipe parameters kept constant during the tests included pipe geometry, gas flowrate, gas composition and pressure drop along the pipe.

The tests were performed in the HEDL Containment Systems Test Facility (CSTF). A schematic drawing of the equipment and piping systems is shown in Figure 1. The 850-m^3 CSTF vessel was used as the test auxiliary building. The aerosol used for the first test was sodium hydroxide, for the second test a mixture of sodium hydroxide and aluminum hydroxide aerosol was used, and for the third test only aluminum hydroxide aerosol was used.

To generate the sodium hydroxide aerosol, sodium was placed in the burn chamber of the aerosol generator where it reacted with air to form sodium oxide. Steam was added to the reaction chamber to convert sodium peroxide to sodium hydroxide. For the aluminum hydroxide aerosol, preformed particles of hydrated alumina were added to the reaction chamber dispersed in an air stream by a jet pump. Aerosol reactions and mixing were completed in the aerosol generator before the aerosol was discharged through the test pipe.

When pre-established test conditions were met, the inlet valve to the test pipe was opened. The aerosol, air and steam mixture was then swept through the test pipe exiting into the vented test auxiliary building. Following the 60-minute test injection period, the inlet valve to the test pipe was again closed and the aerosol generator operation terminated. Aerosol behavior was monitored at the test pipe inlet and outlet and throughout the test vessel auxiliary building during the aerosol injection period and for an additional 22 hours.

The aerosol airborne mass concentration, particle size, and deposition rate were measured as functions of time by collecting and analyzing filter, cascade impactor, and deposition samples. The pipe and vessel temperatures, the pressure of the aerosol generator and containment vessel, the containment atmosphere composition, and the carrier gas flow rate were measured during the test. Steam fractions in the test pipe outlet and containment vessel atmosphere were determined by withdrawing a known volume of gas sample and measuring the condensible water vapor. The condensation rate on the vessel walls and the total steam condensation in the containment vessel were measured by collecting condensate from a specified vessel surface area and from the vessel sump, respectively. Total sodium and aluminum deposited in the test pipe and containment vessel were determined by post-test cleaning of

separate test pipe sections and vessel regions. An overall sodium and aluminum mass balance were made at the end of each test. In addition, visual observations and photography were used to substantiate aerosol deposition measurements.

TABLE 2

TEST CONDITIONS
CONTAINMENT BYPASS SCOPING TESTS

Parameter	Test CB-1	Test CB-2	Test CB-3
Aerosol			
Species	NaOH	NaOH $Al(OH)_3$	$Al(OH)_3$
Duration (min)	60	60	60
Test Pipe Inlet			
Carrier Gas Thermal Hydraulics			
Steam mass flow rate (kg/s)	0.14	0.14	0.14
Air mass flow rate (kg/s)	0.19	0.23	0.26
Nitrogen mass flow rate (kg/s)	0.08	0	0
Total volumetric flow rate (m^3/s) (at 0^oC, 101 kPa)	0.38	0.35	0.37
Gas velocity (m/s)	100	91	97
Gas temperature (^oC)	186	111	160
Pressure (kPa)	210	179	181
Volumetric fraction steam	0.45	0.48	0.46
Steam superheat (^oC)	88	15	66
N_{RE}	$4X10^5$	$4X10^5$	$5X10^5$
Test Pipe			
Diameter, ID (mm)	63	63	63
Length (m)	27	27	27
No. of elbows	5	5	5
ΔP (Clean) (MPa)	0.1	0.08	0.1
Test Auxiliary Building Conditions			
Volume (m^3)	850	850	850
Initial wall temp. (^oC)	85	81	84
Initial gas temp. (^oC)	85	81	84
Pressure (atm)	1	1	1
Vented	YES	YES	YES

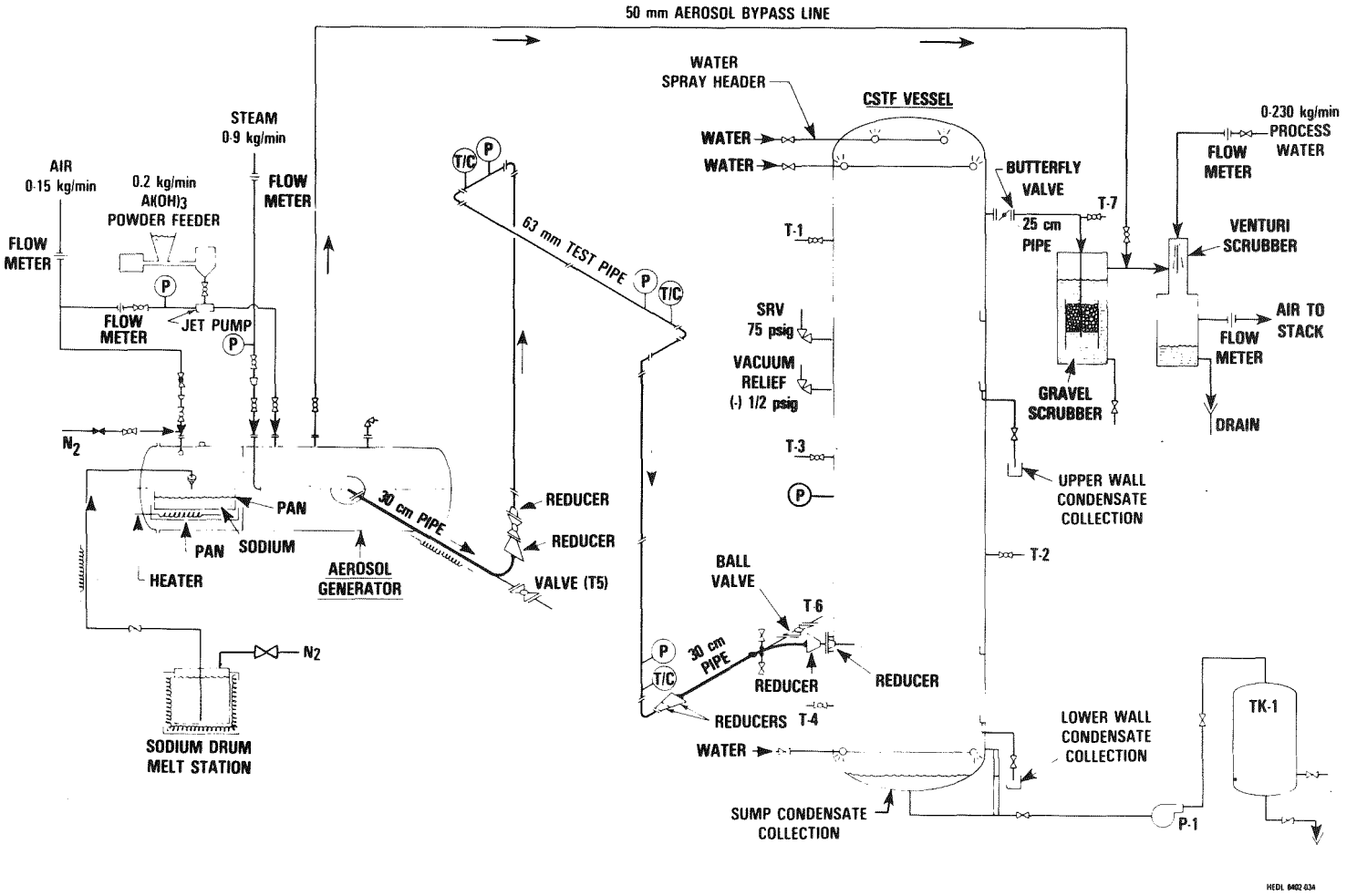

Figure 1. Schematic Diagram of Containment Bypass Tests.

Test Results

A major objective of the LACE program is to provide data for validation of appropriate computer codes, and a major task of the support program is the code validation effort. Aerosol retention code comparison calculations for containment bypass conditions representative of the Surry plant have been completed (sponsored by EPRI). It is intended that these same codes be used for "blind" post-test calculations comparing calculated results to the containment bypass scoping tests. In order to insure that the calculations are truly "blind", only qualitative data regarding aerosol retention factors will be presented. Inlet aerosol properties and characteristics, and test pipe and test vessel hydraulic conditions will be presented.

Atmosphere conditions in the test vessel (simulated auxiliary building) were nearly the same during all three tests. At the start of aerosol source injection, the test vessel was at steady state, with the atmosphere saturated with water vapor and condensation occurring on the slightly cooler walls. During the source injection period, the containment vessel atmosphere became slightly superheated.

Steam superheat in the test pipe varied between tests. During the first and third test, the steam-nitrogen-air carrier gas was superheated in the test pipe. The test pipe wall temperature was also above the local saturation temperature which prevented condensation from occurring anywhere along the test pipe. During the second test, the carrier gas was superheated slightly in the test pipe, but the test pipe wall was below the saturation temperature. Therefore, condensation occurred on the test pipe wall during the second test.

The aerosol entering the test pipe was partially hydrated NaOH in the liquid state for the first test. For the second test, the aerosol was a mixture of co-agglomerated liquid NaOH and solid $Al(OH)_3$. For the third test, the aerosol was dry solid $Al(OH)_3$. It is likely that aerosols in LWR interface piping during V-sequence accidents would be at least partially liquid due to the presence of CsOH, and therefore the aerosol in tests CB-1 and CB-2 may be more typical than the aerosol in test CB-3.

The measured aerosol characteristics at the test pipe inlet are given in Table 3. The average total aerosol source rate and suspended concentration were larger for the first test than for the second test (3.8 g/s and 12 g/m^3 compared to 1 g/s and 3 g/m^3 total, respectively). The aerosol particle size and standard deviation were as expected based on pretest analysis. Measured aerosol characteristics at the test pipe inlet have not yet been determined for the third test.

The major results for the first two tests were very similar even though the aerosol constituents were different. In both tests, deposited aerosol was probably carried along the test pipe as a liquid film by the high velocity carrier gas. As a result, a large fraction of aerosol was collected in either the larger diameter pipe section at the end of the test pipe or in the

containment vessel. For the first two tests, less than 3% of the aerosol was vented from the containment vessel. The third test, with solid aerosol particles, gave significantly different results, with the fraction of aerosol vented from the simulated auxiliary building being approximately six times greater than for the first two tests.

TABLE 3

MEASURED AEROSOL CHARACTERISTICS

Property	CB-1	CB-2	CB-3
NaOH source rate to test pipe (g/s)	3.8	0.6	0
$Al(OH)_3$ source rate to test pipe (g/s)	0	0.3	2.0
Source size, AMMD (microns)	3.9	3.2	4.5
Source geometric standard deviation	2.9	2.5	2.3
Suspended Concentration at Pipe Inlet			
NaOH (g/m^3)	12	2	0
$Al(OH)_3$ (g/m^3)	0	1	6

Conclusions

The results from the containment bypass scoping tests are still preliminary in nature and represent only a limited set of test conditions. However, the results are encouraging. They demonstrate that significant retention of radioactive aerosols could occur in the interface piping and auxiliary building of a LWR following a postulated containment bypass accident situation.

REFERENCES

1. A. K. Postma and B. M. Johnson, Containment Systems Experiment Final Program Summary, BNWL-1592, Battelle Pacific Northwest Laboratories, Richland, WA, July 1971.

2. J. Collen, Overview Of Marviken Procedures, ANS Topical Meeting on Fission Product Behavior and Source Term Research, Snowbird, Utah, July 1984.

3. H. Rininsland, BETA And DEMONA - Key Experimental Programs For Validation And Demonstration Of Source Terms In Hypothetical Accident Situations, Proceedings International Meeting On Light Water Reactor Severe Accident Evaluation, p. 12.3-1, Cambridge, Massachusetts, August, 1983.

4. W. O. Schikarski, DEMONA Forschungsprogramm zur Demonstration Nuklearen Aerosolverhaltens, KfK 3636, December 1983.

5. R. E. Adams and M. L. Tobias, Aerosol Release And Transport Program Quarterly Progress Report For July-September, 1983, NUREG/CR-3422, Oak Ridge National Laboratory, Oak Ridge, TE, April, 1984.

6. H. Bung, M. Koyro and W. Schock, NAUA Mod 4, A Code For Calculating Aerosol Behavior in LWR Core Melt Accident -- Code Description and Users Manual, KFK 3554, Kernforschungszentrum, Karlsruhe, FGR, August 1983.

7. Nuclear Aerosols, State Of The Art Report By NEA/CSNI Experts Group, SINDOC (83) p. 173.

Session VII: Intercomparison and Application of Aerosol Behavior Codes

Chair: T.S. Kress (ORNL, USA)
R.E. Adams (ORNL, USA)

Aerosol Behaviour Codes: Development, Intercomparison and Application

I H Dunbar

UKAEA Safety and Reliability Directorate, Culcheth, UK

Abstract

The results are reported of a recent CEC comparative study of the modelling in sodium fire aerosol codes. This study found that the physical models of the codes were similar apart from important differences in the modelling of gravitational agglomeration. Differences between numerical methods used were identified; the effects were investigated in a parallel study involving benchmark and sensitivity calculations.

Some recent code development highlights are reviewed. These are the development of multi-component codes, the inclusion of turbulent deposition and the modelling of the effects of steam condensation.

Finally the question of how to validate codes is addressed. It is argued that this is best done through an analytic understanding of what controls certain overall features of aerosol behaviour. This then would allow a more meaningful comparison between code prediction and experiment.

1. INTRODUCTION

Since the publication of the first CSNI report on nuclear aerosols in reactor safety [1] work has continued on the development, the inter-comparison and the application of aerosol codes. Many of the developments in aerosol code modelling are catalogued in Chapter IV of the new CSNI report [2]. This review of code developments has three objectives:

- to report on the results of part of a sodium fire aerosol code comparison exercise (section 2.1),
- to review major developments in code modelling since the 1979 CSNI report (sections 2.2 and 3),
- to consider what more needs to be done on modelling and validation before containment aerosol codes can be regarded as reliable tools for accident analysis (section 4).

The scope of the review is restricted to codes modelling aerosol behaviour in the containment. Aerosol transport in PWR primary circuits is modelled only by the TRAP-MELT code [3] and its derivative, RETAIN [4]. These codes model more than simply aerosol processes; viewed as aerosol codes however they are effectively multicompartment codes with, in addition to the usual aerosol processes, models for the deposition of aerosols from a gas stream, the rates depending on the Reynolds number of the flow. Because until recently TRAP-MELT was the only code which looked at primary circuit transport, there have been no code comparisons done, and attempts at experimental validation are still in their early stages.

2. SODIUM FIRE AEROSOL CODES

The Commission of the European Communities (CEC) recently organised a comparative study of these codes. Part of the results of this study are reported on in section 2.1. Section 2.2 looks at the additional questions of multicomponent aerosol modelling and of modelling the turbulent deposition of aerosols on containment surfaces. Since the models in these codes form a subset of those in LWR aerosol codes, most of the discussion in this section is also applicable to the LWR codes. Section 3 considers only the mechanisms peculiar to the LWR containment.

2.1 The CEC Comparative Study of Modelling in Sodium Fire Aerosol Codes

The recent study of sodium fire aerosol codes, co-ordinated and funded by the CEC, has two parts. The first is a modelling comparison, the results of which are reported in this section. The second is a set of comparative calculations, in which each code was used by its owners to make predictions on the basis of an agreed set of input data and an agreed set of variations from this standard case. The results of these calculations were brought together and compared by Fermandjian, who reports on the results in this session [5]. The modelling comparison, carried out by the present author, involved a review of available documentation, and, for the European codes, of the listings as well. The codes which were finally included, here classified by country or origin and discretisation method, are:

AEROSIM	(UK	, finite difference)
AEROSOLS/A2	(France	, method of moments)
AEROSOLS/B1	(France	, finite elements)
HAARM - 3	(USA	, method of moments)
MAEROS	(USA	, finite differences)
PARDISEKO-IIIb	(FRG	, finite differences)

(Note that this list is not exactly the same as that for the comparative calculations.) Information obtained in this study about differences between the models in the codes was used to explain differences found in the comparative calculations. The results of both studies are reported in a document to be published by the European Commission [6].

2.1.1 Review of Physical Models

The modelling comparison considered both the formulae used in the codes for the agglomeration and removal rates and the availability of the input required by these formulae. The task was primarily to discover and comment on differences between the codes; although there was also some critical comment on formulae which were common to the codes there was no attempt made at an exhaustive critical review of aerosol modelling.

All of the codes reviewed used a well-mixed volume approach (either a single volume or several well-mixed compartments coupled by flow terms). The fundamental quantity followed is the number concentration distribution, $C(m,t)$. Its time dependence is given by the familiar integro-differential equation

$$\frac{\partial}{\partial t} C(m,t) = \tfrac{1}{2} \int_0^m d\mu\ \phi(\mu, m-\mu)\ C(\mu,t)\ C(m-\mu,t) - C(m,t) \int_0^\infty d\mu\ \phi(m,\mu)\ C(\mu,t) - R(m)\ C(m,t) + S(m,t) \qquad (1)$$

where $S(m,t)$ = aerosol source term,

$R(m)$ = removal rate of particles, mass m,

$\phi(\mu,\nu)$ = agglomeration rate of particles masses μ and ν.

The MAEROS code used a generalisation of this equation which keeps account of the whereabouts of different species (multi-component modelling) [7]. Because it was the only code to do so in the study, this feature was not examined in detail. This topic is reviewed in section 2.2.1 of the present paper.

The source term, S, has to be supplied from an earlier stage in the accident modelling. The job of the aerosol modeller is to provide formulae

for the removal and agglomeration rates. In each of the codes the removal rate is a sum of terms corresponding to Brownian diffusion, thermophoresis and gravitational sedimentation, and the agglomeration rate is a sum of terms corresponding to Brownian, gravitational and turbulent agglomeration. The only deviation from this pattern is that PARDISEKO IIIb omits the turbulent agglomeration term. It is however simple to change the modelling (at least in finite difference or finite elements codes), so the particular choice of models is not a permanent feature of a code.

Only in the modelling of gravitational agglomeration were significant differences found between the codes. The gravitational agglomeration formulae has the form (here expressed in terms of radii not masses)

$$\phi_G(r_1,r_2) = F(\gamma)\ \varepsilon(r_1,r_2)\ \pi(r_1+r_2)^2\ |v_1 - v_2| \tag{2}$$

$v_{1,2}$ are the terminal velocities of the particles, $\varepsilon(r_1, r_2)$ is the collison efficiency and $F(\gamma)$ is a correction to the collison rate due to departure from spherical shape. γ is the collisional shape factor which occurs in the Brownian agglomeration rate:

$$\phi_B(r_1, r_2) = 4\pi kT\ \gamma[B(r_1) + B(r_2)]\ (r_1 + r_2) \tag{3}$$

T is the gas temperature and B is the particle mobility. All the codes except PARDISEKO IIIb used what might be called, with no implications as to its validity, the standard modelling:

$$\varepsilon(r_1, r_2) = \frac{3}{2}\ \frac{r_2}{r_1 + r_2}^2 \quad (\text{for } r_2 < r_1) \tag{4}$$

$$F(\gamma) = \gamma^2 \tag{5}$$

whereas the PARDISEKO modelling has

$$\varepsilon(r_1, r_2) = \tfrac{1}{2}\ \frac{r_2}{r_1 + r_2}^2 \quad (\text{for } r_2 < r_1) \tag{6}$$

$$F(\gamma) = \gamma \tag{7}$$

(For $r_1 < r_2$ we simply interchange r_1 and r_2 in ε). The standard modelling predicts a gravitational agglomeration rate 3γ times that predicted in PARDISEKO. How this affects the standard case in the code comparison runs is shown by Fermandjian [5].

Equation (4) for the collison efficiency is due to Fuchs [8], whereas equation (7) is due to Pruppacher and Klett [9], following arguments of Friedlander [10]. Both derivations make the following assumptions:

i The particles are small enough for inertial effects to be neglected.

ii The smaller particle is sufficiently small compared to the larger that it does not perturb appreciably the flow pattern around the larger.

iii The Reynolds number of the flow around the larger particle is small enough for Stokes flow to be a good approximation.

The first two assumptions imply that the smaller particle follows the streamlines around the larger; the third says that the streamlines are those of Stokes flow. The difference between the two formulae is that the Fuchs formula is derived for a stationary spherical collector. When going to the aerosol case in which both particles are in motion, care must be taken to add velocities vectorially. When this is done the Pruppacher - Klett formula results. Within the framework of the above assumptions this is the correct formula to use in aerosol physics. The mathematical details are given in appendix 1 of the report on this work [6]. To go beyond these assumptions requires a numerical calculation of the particle motion. Analytic approximations to the results of one such calculation are reported in a paper by Dunbar and Ramsdale given at this conference.

As for the shape factor effect, equation (6) is obtained simply by scaling the $(r_1 + r_2)$ factor by a factor γ. To understand the PARDISEKO alternative one must look more closely at the dependence on $(r_1 + r_2)$ in the Brownian and gravitational agglomeration rates. The $(r_1 + r_2)^2$ in the gravitational rate is a measure of the cross-sectional area. The Brownian dependence comes from a product of two factors : an area factor proportional to $(r_1 + r_2)^2$ and a concentration gradient factor proportional to $(r_1 + r_2)^{-1}$. If the area is scaled as γ^2 and the gradient as γ^{-1} we arrive at the standard result. If on the other hand it is assumed that the shape factor is relevant only to the area, which scales as γ, the concentration factor being unmodified, then we obtained the modelling of PARDISEKO. Which of these assumptions is correct needs to be clarified.

Similar problems arise in turbulent agglomeration modelling. The original Saffman and Turner formulae [11] had neither a collison efficiency factor nor a shape correction. The usage in nuclear aerosol codes has been to use the same collision efficiency as in the gravitational formula and to replace $(r_1 + r_2)$ by $\gamma(r_1 + r_2)$. Neither of these assumptions is self-evidently correct.

Valid models are of little use unless the input they require is available. Some of these data fall within the province of the aerosol modeller; the rest should in principle be supplied by those studying other aspects of the accident. Prominent in the former class are the shape factors. There is some experimental information on the dynamic shape factor, χ, reviewed in the 1979 CSNI report on nuclear aerosols [1]. For branched-chain agglomerates, van de Vate et al [12] have found a correlation between χ and the number, n, of primary particles making up the agglomerate

$$\chi = 0.33\ F_c\ n^{1/3} \qquad (8)$$

where F_c is the Cunningham correction for the mass-equivalent radius of the particle. None of the codes reviewed allowed χ to vary with particle size, although this could easily be changed (except in moments methods codes) if it was felt that an appropriate formula is available.

The situation with the collisional shape factor, γ, is less clear. In the absence of direct measures of agglomeration rates one has to find γ by

fitting the results of integral experiments using the aerosol codes. This would be satisfactory only if one were certain that all the other models in the code were valid. Moreover the interpretation of the results will depend on whether the code uses equation (6) or (8) for the effect of shape on gravitational collisions.

Most aerosol codes require as input the turbulent energy density dissipation rate, E, and the viscous and diffusional boundary layer thicknesses. E is given approximately by u^3/L where L is the length scale of the largest eddies and u is their circulation velocity. If E could be estimated under various accident conditions, then scoping calculations could show whether the formula of Saffman and Turner [11] predicts turbulent agglomeration to be important or not. The adequacy of the formula would still however be an open question.

The viscous boundary layer thickness, δ_L, depends on the velocity of the flow across the surface, and so is not strictly a matter for aerosol modellers to calculate. However once this quantity is given, the subsequent value of the so-called diffusional boundary layer thickness, δ_D, will depend in general on particle size. The model in the codes assumes that turbulence keeps the aerosol well-mixed up to a distance δ_D from the wall, and the remaining transport is by Brownian diffusion. δ_D is therefore defined as that distance from the wall at which the turbulent diffusion coeficient equals the Brownian diffusion coefficient. Fuchs [8] gives a formula due to Landau and Levich in which the dependence of δ_D on particle radius r is as follows

$$\delta_D \sim \begin{cases} r^{-\frac{1}{2}} & \text{for } r \approx \ell \\ r^{-1/4} & \text{for } r \gg \ell \end{cases} \qquad (9)$$

where ℓ is the molecular mean free path of the gas. None of the codes allow δ_D to depend on r.

2.1.2 Discretisation of Equations and Numerical Solution

The integro-differential equation (1) is approximated by restricting the allowed forms of functional dependence of C on m. The three methods and their corresponding functional forms used in nuclear aerosol codes are as follows:

(a) Moments method - lognormal

(b) Finite differences - piecewise constant (histogram)

(c) Finite elements - piecewise linear

Each function is defined by a finite number of parameters whose time dependence is governed by coupled first order differential equations. These equations are solved using standard techniques for ordinary differential equations.

In the moments methods the distribution is required to be lognormal, and there are three parameters, namely the first three moments, which are sufficient to define this distribution. This is much more restrictive than

the other two methods, where at least ten and may be as much as a hundred degrees of freedom are allowed. There is evidence to suggest that the moments method is bad at modelling a continuous source, and particularly the aerosol behaviour when this source is switched off [1,13]. Similar effects were observed in the comparative calculation [5]. The moments methods also makes it cumbersome to change physical models, because of the extra analytic work that has to be done.

Finite difference methods start from the choice of a minimum and a maximum mass : m_o and m_N. This range is divided into N intervals

$$A_i = (m_{i-1}, m_i) \tag{10}$$

In PARDISEKO the N parameters are: i = 1,...,N

$$C_i^p(t) = \int_{A_i} dm \; C(m,t)$$

AEROSIM adopts the slightly different procedure of using a mass-weighted integral

$$C_i(t) = \frac{1}{M_i} \int_{A_i} dm \; m \, C(m,t) \tag{11}$$

where $$M_i = \tfrac{1}{2}(m_{i-1} + m_i) \tag{12}$$

is the mid-point mass of the interval A_i. The error in the subsequent approximations to the equations for the parameters is governed by the widths of the intervals:

$$h_i = (m_i - m_{i-1}) \tag{13}$$

In PARDISEKO the removal and agglomeration rates are approximated by their values $R(M_j)$, $\phi(M_j, M_k)$ at the interval midpoints. The error terms are then $O(h_i^3)$. AEROSIM the approximate rates are integrals over the intervals, and this includes some, but not all of these third order error terms. The PARDISEKO method allows easy computation of the approximate rates, whereas the AEROSIM method allows a reduction in the number of intervals. The discretisation in MAEROS is similar to that of AEROSIM, suitably generalised to deal with equation (2).

The finite elements method of AEROSOLS/B1 is also based on the intervals A_i. The approximating function is however a piecewise linear function interpolating values, $C_i^A(t)$, at the points m_i. Three points can be made about this method.

(1) It treats the source and removal terms exactly as does PARDISEKO.

(2) The finite elements integral in the second agglomeration term is performed exactly.

(3) The finite elements integral in the first agglomeration term is approximated in a mass-conserving manner.

Once the discretised equations are constructed they must be solved. Various standard ODE solvers are used by the different codes. Without

extensive computer experiments it is not possible to say which method is optimal for each code. It is the duty of the code writer to check that the chosen method is both accurate and stable.

2.1.3 Conclusions

This exercise proved the usefulness of the modelling comparison as an adjunct to the comparative calculations. The causes of differences in the results of the calculations were able to be identified, and after a few iterations the codes were able to be run using the same physical models, providing thereby a pure comparison between numerical methods. Without the modelling comparison it would have been difficult to do more than simply record the existence of the differences. On the other hand, because of the complexity of the aerosol problem, it is difficult to draw conclusions without doing comparative calculations. The conclusions summarised below are therefore the joint conclusions of the whole study. They are:

- The codes agreed on the physical modelling except for gravitational agglomeration. The collison efficiency of Pruppacher and Klett should be used instead of that of Fuchs. The question of γ is unresolved.
- It is necessary to model gas flows to determine whether turbulent agglomeration, transport to the walls and deviations from good mixing are important.
- Gravitational sedimentation is the most important removal mechanism.
- The leaked mass is most sensitive to factors affecting the gravitational agglomeration rate.
- The method of moments has severe limitations and the use of the moments code AEROSOLS/A2 should be discontinued.
- The finite difference and finite elements codes are different in detail but give broadly similar predictions when using the same models.
- Separate effects experiments are needed to look at gravitational and turbulent agglomeration.
- Large scale experiments are needed to look at the effect of source mass and rate, the particle size distribution and the possible deviations from good mixing.
- Codes need to be extended to follow more than one chemical species and to handle deviations from good mixing.

2.2 Further Developments

This section deals with two recent developments, beside those associated with steam condensation, not covered in the CEC study: multicomponent aerosol modelling and the inclusion of a model for turbulent deposition.

2.2.1 Multi-Component Modelling

Both the MAEROS [7,14] and QUICKM (formerly MSPEC) [15] codes model multi-component aerosols. For each species, K, we can define a distribution, $q_K(m,t)$, such that at time t the mass of K airborne on particles whose masses are in the interval [m, m + dm) is $q_K(m,t)dm$. Although this is not explicitly mentioned in the code descriptions, the methods used by the two codes are effectively discretisations of the set of equations

$$\frac{\partial}{\partial t} q_K(m,t) = \int_o^m d\mu\ \phi(\mu, m-\mu)\ q_K(\mu,t)\ C(m-\mu,t) - q_K(m,t) \int_o^\infty d\mu\ \phi(m,\mu)\ C(\mu,t) - R(m)\ q_K(m,t) + S_K(m,t) \tag{14}$$

$S_K(m,t)$ is the source distribution of component K. A similar approach has been proposed by Simons [16]. Recognizing that if the radioactivity on the particles were not proportional to their masses, then the radioactivity release predicted by a single-component code would be in error, he proposed using a pair of equations, the first being the usual equation (1) and the second being of the form (14) with q_K being replaced by the radioactivity distribution. The inclusion of this method in the code AEROSIM, is reported to this conference by Stock et al [17].

The method used by Simons [16] to derive his equations can be generalised to derive equations (14). Each particle is described by a vector of masses $\underset{\sim}{m} = (m_1,\ldots,m_L)$, one for each component. Let us write the total mass as

$$||\underset{\sim}{m}|| = \sum_{K=1}^{L} m_K \tag{15}$$

Then we can define the full number distribution over all the component masses as $c(\underset{\sim}{m},t)$. The generalization of (1) is

$$\frac{\partial}{\partial t} c(\underset{\sim}{m},t) = \tfrac{1}{2} \int_o^{m_1} d\mu_1 \ldots \int_o^{m_L} d\mu_L\ \phi(||\underset{\sim}{m}-\underset{\sim}{\mu}||\ ,\ ||\mu||)\ c(\underset{\sim}{m}-\underset{\sim}{\mu},t)c(\underset{\sim}{\mu},t) - c(\underset{\sim}{m},t) \int_o^\infty d\mu_1 \ldots \int_o^\infty d\mu_L\ \phi(||\underset{\sim}{m}||\ ,\ ||\underset{\sim}{\mu}||)\ c(\underset{\sim}{\mu},t) - R(||\underset{\sim}{m}||)\ c(\underset{\sim}{m},t) + s(\underset{\sim}{m}) \tag{16}$$

To recover equation (1), multiply this by the Dirac delta function, $\delta(m-||\underset{\sim}{m}||)$ and integrate over all $\underset{\sim}{m}$. The q_K distribution is given by

$$q_K(m,t) = \int_o^\infty dm_1 \ldots \int_o^\infty dm_L\ m_K\ \delta(m-||\underset{\sim}{m}||)\ c(\underset{\sim}{m},t) \tag{17}$$

To recover equation (14) therefore one multiplies (16) by $m_K\ \delta(m-||\underset{\sim}{m}||)$ and integrates over all $\underset{\sim}{m}$. Note however, that this derivation relies on the assumption in (16) that the agglomeration and removal rates depend only on the total masses.

2.2.2 Turbulent Deposition Modelling

Up till now the codes have assumed that transport of particles to the wall has consisted of turbulent transport up to a distance δ_D from the wall, and then Brownian diffusion the rest of the way. By neglecting the effect of the particle inertia this could underestimate the transport of larger particles to the wall. Models of turbulent transport have been described at this conference by Willers [18]. Such models are included in TRAP-MELT [3] but not until recently in containment codes.

In the latest version (IV) of PARDISEKO however [19], the models of Sehmel [20] have been included, in an attempt to account for experimentally observed deposition. The deposition velocity on vertical walls is

$$v_w = u^*/\mathrm{Int}(r) \tag{18}$$

where u^* is the turbulent friction velocity and Int(r) is the diffusive resistance integral associated with particle radius r. If v is the terminal velocity under gravity then the deposition velocities on floors (f) and ceilings (c) are respectively:

$$v_f = v[1-\exp(-v/v_w)]^{-1} \tag{19}$$

$$v_c = v[\exp(v/v_w) - 1]^{-1} \tag{20}$$

(In these results v_w is not exactly as it is in (18) because Int(r) depends on the orientation of the surface.) Introducing these into a code creates a new item of input, namely u^*. Once again, more detailed knowledge of the thermal-hydraulic conditions is needed if the new aerosol transport model is to be used.

3. THE EFFECTS OF STEAM CONDENSATION

The major development in aerosol codes over the last few years has been the inclusion of the effect of steam condensation both on the walls (giving an additional mechanism for removal) and on the particles themselves (an additional mechanism for growth). From a purely coding point of view the new removal term is simple to handle, involving only a radius-independent removal rate analogous to the leak rate, whereas growth by condensation requires more extensive code modifications because there is a new type of growth term in the basic aerosol equation. We are now approaching the stage when several codes will be able to do both jobs, and therefore a code comparison study will be appropriate. Active consideration is being given to such a study by the CSNI group of experts on the source term, and also by a CEC committee of experts.

3.1 Condensation on the Wall

When steam condenses at a wall from a steam-air mixture there is a net flow of gas (Stephan flow) to the wall, and this takes aerosol particles with it. In the rest frame of this flow the particle sees air diffusing away from and steam towards the wall; the effect of this (diffusiophoresis) is to retard the motion of the particle. (The total effect of condensation is often referred to by the term "diffusiophoresis".)

Waldmann and Schmitt [21] give the particle deposition velocity due to the two effects as

$$v_d = [X_S + X_A (M_A/M_S)^{\frac{1}{2}}]^{-1} [\frac{D}{p_A} |\frac{dp_S}{dx}|] \quad (21)$$

The subscripts S and A refer to steam and air respectively; X is the mole fraction, M is the molecular weight and p the partial pressure. D is the steam-air diffusivity and the derivative refers to distance from the wall. The second factor is the Stephan flow velocity; the first is the diffusiophoresis correction. This formula can be used directly in a code [22], but the evaluation of the gradient requires the introduction of an unknown boundary layer thickness. Equation (21) can be re-expressed in terms of total mass condensation rate, W, and the mass of steam airborne, m_S [23], giving a removal rate:

$$\lambda_d = [X_S + X_A (M_A/M_S)^{\frac{1}{2}}]^{-1} [X_S \frac{W}{m_S}] \quad (22)$$

Note that the second factor is X_S times what would be obtained from modelling the flow velocity simply on the basis of the steam mass flow rate; steam mass is transported to the walls by diffusion as well as Stephan flow. Going from (21) to (22) leaves the responsibility of modelling steam transport to the walls where it belongs with the thermal-hydraulics codes.

3.2 Condensation on the Particles

If steam condenses on aerosol particles of mass m with a mass rate $\xi(m)$ then the basic aerosol equation (1) acquires a new term:

$$\frac{\partial}{\partial t} C(m,t)\Big|_{cond} = - \frac{\partial}{\partial m} [\xi(m) C(m,t)] \quad (23)$$

This formula can also be used for evaporation (negative ξ) but then a two-component treatment is needed so that only the water mass on a particle is evaporated. Given the driving force for condensation, namely steam supersaturation, ξ can be calculated, for example using Mason's equation [24]. However this quantity is not calculated by containment thermal hydraulic codes, because condensation in bulk is so rapid that deviations from saturation are very small. Instead the codes attribute to bulk condensation that mass of water needed to keep the steam partial pressure down to its equilibrium value. (For example see the description of the MARCH code.[25]) Aerosol codes can be designed to take this total condensation rate as input, the only modelling then required being how the water is shared out among the size classes. How this is implemented in the AEROSIM code is described in a paper to this conference [26].

The assumption of equilibrium in bulk still begs an important question, because the equilibrium vapour pressure of water in a drop depends on the size of the drop (its surface curvature) and on the concentration of solutes in the drop. This means that, strictly speaking, the thermal hydraulic calculations cannot be carried out independently of the aerosol calculations. The coupling of thermal-hydraulic and aerosol codes so as to be able accurately to model the transfer of water to and from particles is as yet in its early stages. It is not even clear whether

condensation onto particles will occur at all to any significant extent, or whether decay heating of the containment atmosphere will keep it below saturation.

4. CRITERIA FOR CODE VALIDATION

At what stage will we be able to stop aerosol code development and use existing codes as reliable tools for accident analysis? In this section I give some personal thoughts on this subject. These remarks are confined to the more mature technology of dry, single-component aerosol codes. Experience with these codes suggests that what we need to know in order to predict aerosol source terms are the sedimentation rate of particles between 1 and 10μm in radius, and the rate at which smaller particles grow by agglomeration to reach these sizes. How then are we to reach the stage where we are confident in our ability to model these processes?

In accident modelling we are ultimately interested in a few "target quantities", those which directly influence the radiological consequences. For aerosol codes the main target quantity is the leaked activity, an integral over time of airborne activity weighted by the leak rate. A straightforward route to validation is therefore to perform an experiment simulating as nearly as possible accident conditions, to measure the target quantities and to see how well the codes predict them. The problem with this is the size of the input parameter space for aerosol codes, and the fact that many values are not known independently. The ability to fit the results of an experiment by varying parameters does not validate the code as a predictive tool for situations different from the experimental conditions. The ideal solution would be to measure each input parameter individually in separate effects experiments. This however may not be practicable, nor even possible, and I wish to speculate how progress towards validation could be made using existing experimental data.

What I propose comes in two parts: analytic work on the models, and a re-examination of the existing data from integral, though not full-scale, experiments. An extensive compilation of such results can be found in the first CSNI report [13]. The analytic work would be to derive approximate forms for the rates of change of mass airborne and particle size (the moments method equations could be used here). The aim would be to identify key groups of input parameters, whose values dominate the behaviour of the target quantities. It seems likely that the most important processes are sedimentation and gravitational agglomeration, whose rates can be written in the form:

$$v(r) = \left[\frac{2}{9}\frac{g\rho_1}{\eta} r^2\right] F(r) \qquad (24)$$

$$\phi_G(r_1,r_2) = \left[\frac{2}{9}\frac{g\rho_1}{\eta} \pi(r_1 + r_2)^2 \left|F(r_1)r_1^2 - F(r_2)\, r_2^2\right|\right] G(r_1,r_2) \qquad (25)$$

where ρ_1 and η are gas density and viscosity respectively, F contains density and shape corrections and G is the collision efficiency, corrected if necessary for shape effects. To predict accurately the target quantities it may not be necessary to have a complete knowledge of F and G; certain global features (eg moments) may suffice.

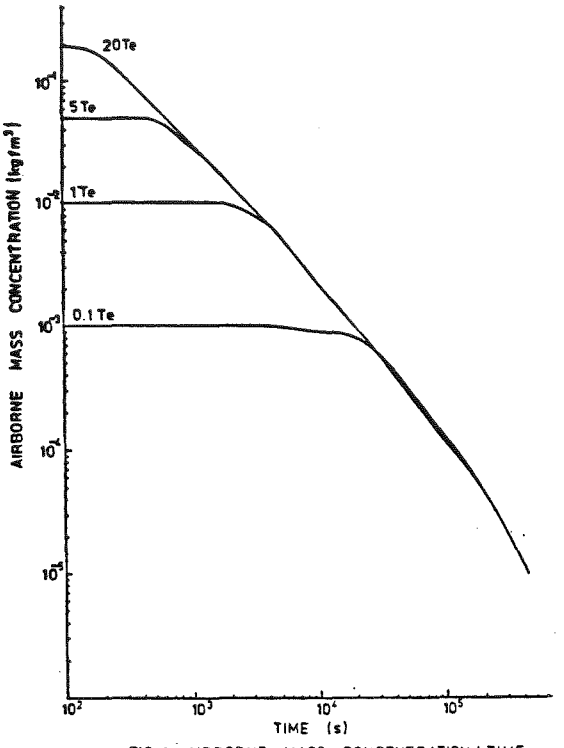

FIG. 1 AIRBORNE MASS CONCENTRATION / TIME - INSTANTANEOUS SOURCE

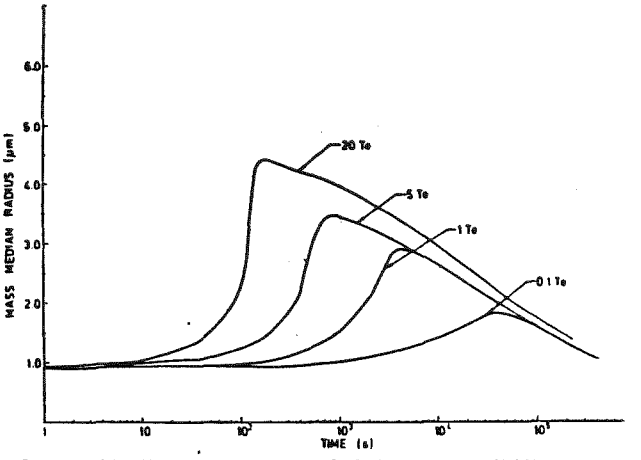

FIG 2 VARIATION OF MASS MEDIAN RADIUS WITH TIME - INSTANTANEOUS SOURCE

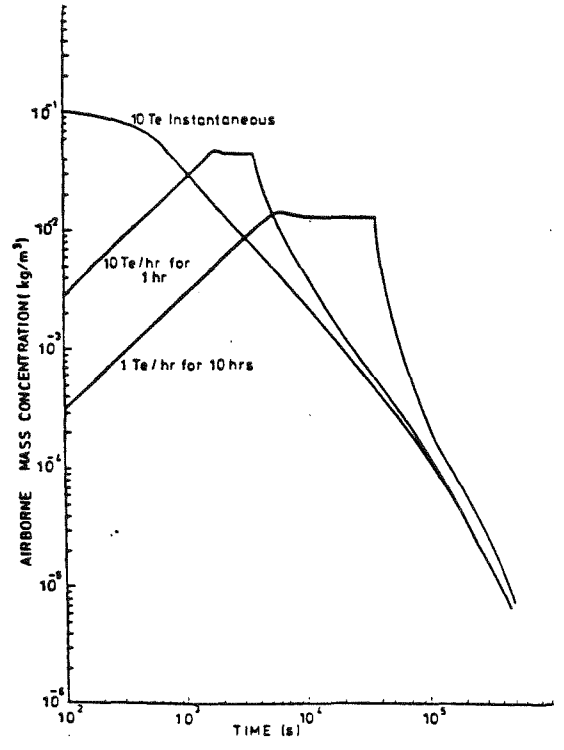

FIG.3 PROLONGED SOURCE AIRBORNE MASS CONCENTRATION/TIME

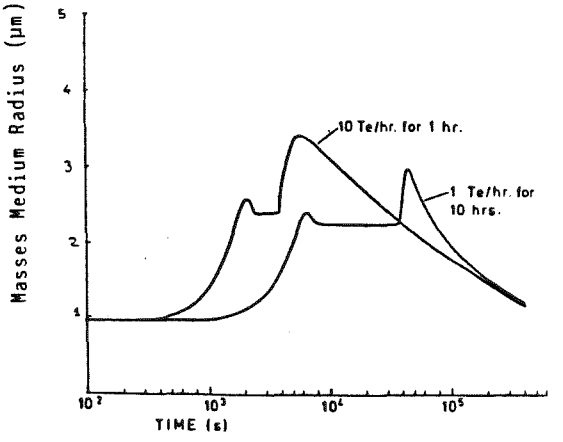

FIG.4 PROLONGED SOURCE - VARIATION OF MASS MEDIAN RADIUS WITH TIME

The next questions to ask would be do the experimental results confirm the approximate picture derived in the analytic study, and if the answer is yes, then what values of the key input parameters are indicated? The results are here being made to play two roles: an overall validation of the models and a measurement of the key parameters. I suggest that for these purposes the results be expressed in terms of certain global features. An idea of what those features might be is given by the figures, taken from an AEROSIM sensitivity study by Underwood, Walker and Williams [27]. Figures 1 and 2 show mass concentrations and mass mean radii following an instantaneous release of different masses of aerosol. What they show is an "induction time", during which there is little fallout, a period of rapid agglomeration, and then a period of rapid fallout during which all the curves come together on an envelope curve independent of the initial mass released. The induction time seems to be a measure of agglomeration rate, and the fallout curve of sedimentation velocity. Figures 3 and 4 look at the effects of 10Te of aerosol being released over various durations. The key features here are the time to reach steady state, the steady state airborne concentration (in accidents with prolonged sources probably the most important determinant of the source term) and distribution, and the decay rate at the end of the source. I am not suggesting that simple correlations for these quantities be used in place of codes, but that these quantities could form a bridge between experiment and modelling.

Underlying these remarks is the belief that to be validated a code must not only make successful predictions, it must make them in a way that is understood, at least approximately. I further conjecture that progress towards such understanding can be achieved by a careful analysis both of the way the models work and of existing experimental data.

REFERENCES

1. Silberberg M (ed), Nuclear Aerosols in Reactor Safety (OECD/CSNI SOAR-1, 1979).
2. Abbey F (ed), Supplementary State-of-the-Art Report on Nuclear Aerosols (OECD/CSNI, to be published).
3. Jordan H, Gieseke J A, Baybutt P, TRAP-MELT Users Manual, BMI-2017 (1979).
4. Burns R D, Rodger W A, Fission Product Transport and Retention in Severe Degraded Core Accidents. Proceedings of the International Meeting on LWR Severe Accident Evaluation (Cambridge, Mass. 1983).
5 Fermandjian J, Comparison of Computer Codes Related to the Sodium Oxide Aerosol Behaviour in a Containment Building. (Paper presented to this conference.)
6. Dunbar I H, Fermandjian J, et al. Comparison of Aerosol Codes, EUR-9172 (1984).
7. Gelbard F and Seinfeld J H, Simulation of Multicomponent Aerosol Dynamics, J Colloid and Interface Science 78, 485 (1980).
8. Fuchs N A, The Mechanics of Aerosols (Pergamon, 1984).
9. Pruppacher H R and Klett J D, Microphysics of Clouds and Precipitation (D. Reidel 1978).
10. Friedlander S K, The similarity theory of the particle size distribution of the atmospheric aerosol, Proc Conf on Aerosols, Liblice (K Spurny ed, Czechoslovak Acad Sci Prague, 1962) p 115.
11. Saffman P G and Turner J S, J Fluid Mech 1, 16 (1956).

12. Van de Vate J F, Van Leeuwen V F, Plomp A, Smit H C D, Aerodynamic Properties of Aerosols and their Leakage through Concrete Containment Structures, Proceedings of the International Meeting on Fast Reactor Safety, Seattle, Washington, Vol II, p804 (1979).
13. Fermandjian J, Etude de le Modelisation du Comportement des Aerosols Sodes dans une Enceinte, CEA R5151 (1982).
14. Gelbard F, MAEROS Users Manual, (NUREG/CR-1391, 1982).
15. Jordan H, Schumacher P M, Gieseke J A, MSPEC Users' Manual (NUREG/CR-2923, 1982).
16. Simons S (1981), The Coagulation and Deposition of Radioactive Aerosols, Annals of Nuclear Energy, 8, 287.
17. Stock J D R, Simons S, Williams M M R, Coagulation and Deposition of Two-Component Aerosols (paper presented to this conference).
18. Willers A, Models of Deposition of Aerosols from Turbulent Flow (paper presented to this conference).
19. Bunz H, PARDISEKO IV, A Computer Code for Calculating Aerosol Behaviour in Closed Vessels (KfK 3545e 1984).
20. Sehmel G A, Particle Diffusivities and Deposition Velocities over a Horizontal Smooth Surface. J Coll Int Sci 37 (1971) p891, and, Particle Eddy Diffusivities and Deposition Velocities for Isothermal Flow and Smooth Surfaces. J Aer Sci 4 (1973), p125.
21. Waldman L, Schmitt K H, Thermophoresis and Diffusiophoresis of Aerosols, In Aerosol Science (C N Davies ed, Academic Press, 1966).
22. Avci H I, Diffusiophoretic and Thermophoretic Deposition of Aerosols on Surfaces in LWR Containments following Severely Degraded Core Accidents. Proceedings of the International Meeting on LWR Severe Accident Evaluation (Cambridge, Mass. 1983).
23. Dunbar I H, The Role of Diffusiophoresis in LWR Accidents, ibid.
24. Mason B J, The Physics of Clouds (OUP, 1971).
25. Wooton R O, Avci H I, MARCH Code Description and Users' Manual (BMI 2061, 1980).
26. Dunbar I H, Vapour Condensation on Particles - AEROSIM Modelling (paper to be presented to this conference).
27. Underwood B Y, Walker B C, Williams R J, Development of Interpolation Formulae for Rapid Evaluation of the Attenuation due to Aerosol Processes of Radioactive Release following Hypothetical Fast Reactor Accidents. Proceedings of the CSNI Specialists Meeting on Nuclear Aerosols in Reactor Safety. (NUREG/CR-1724, CSNI-45, 1980).

COMPARISON OF COMPUTER CODES RELATED TO THE SODIUM OXIDE AEROSOL BEHAVIOR IN A CONTAINMENT BUILDING

J. Fermandjian - CEA/IPSN/DAS/SAER - B.P. 6
F-92260 Fontenay-aux-Roses (France)

I.H. DUNBAR	UKAEA/SRD	Culcheth (United Kingdom)
H. BUNZ	KfK	Karlsruhe (Germany)
A. L'HOMME	CEA	Fontenay-aux-Roses (France)
Y. HIMENO	PNC	Oarai (Japan)
C.R. KIRBY	AERE	Harwell (United Kingdom)
G. LHIAUBET	CEA	Saclay (France)
N. MITSUTSUKA	PNC	Tokyo (Japan)

ABSTRACT

In order to ensure that the problems of describing the physical behavior of sodium aerosols, during hypothetical fast reactor accidents, were adequately understood, a comparison of the computer codes (ABC/INTG, PNC, Japan; AEROSIM, UKAEA/SRD, United Kingdom; PARDISEKO IIIb, KfK, Germany; AEROSOLS/A2 and AEROSOLS/B1, CEA, France) was undertaken in the frame of the CEC: exercise in which code users have run their own codes with a prearranged input.

INTRODUCTION

Although hypothetical fast reactor accidents leading to severe core damage are very low probability events, their consequences are to be assessed. During such accidents, one can envisage the ejection of sodium, mixed with fuel and fission products, from the primary circuit into the secondary containment. Aerosols can be formed either by mechanical dispersion of the molten material or as a result of combustion of the sodium in the mixture.

The priority accorded to the study of sodium aerosols is justified by the fact that they will be the major carrier of radioactive species and hence determine the amount of airborne radioactivity available for release via any leaks in the secondary containment or during deliberate venting.

To ensure that the problems of describing the physical behavior of sodium aerosols were adequately understood, a comparison of the codes being developed to describe their behavior was undertaken. The comparison consists of two parts:

- the first is a comparative study of the computer codes used to predict aerosol behavior during a hypothetical accident. It is a critical review of documentation available.
- the second part is an exercise in which code users have run their own codes with a pre-arranged input.

Both exercises were conducted in the frame of the containment expert group (CONT) of the Fast Reactor Coordinating Committee of the European Communities [1].

BENCHMARK CALCULATIONS

The present paper concerns only the comparative study of the results given by some computer models used in order to assess aerosol behavior inside the reactor containment building (RCB) of a liquid metal fast breeder reactor (LMFBR) during hypothetical accidents.

An exercise in which code users have run their own codes with a pre-arranged set of input has been carried out. The codes included in the present study are the following:

Computer models		Country	Laboratory	Calculation method
ABC/INTG	[2]	Japan	PNC	Finite differences
AEROSIM	[3]	UK	UKAEA	Finite differences
AEROSOLS/A2	[4]	France	CEA	Moments method
AEROSOLS/B1	[5]	France	CEA	Finite elements
PARDISEKO IIIb	[6]	Germany	KfK	Finite differences

The previous computer models are referred to subsequently in this report simply as ABC, AEROSIM and PARDISEKO; for AEROSOLS, the two versions are distinguished.

N.B.: JAPAN has been contacted by the CEC in order to participate in the present exercise.

Definition of the benchmark calculation

The present exercise concerns the behavior of a sodium fire aerosol in the RCB. The hypothetical accident chosen is a sodium pool fire occurring in the RCB of a LMFBR (1200 MWe), the characteristics of which are the following:

Sodium pool mass		50,000 kg
Sodium pool area		100 m^2
Initial sodium temperature		500°C
Fire duration		10 hours
Aerosol release rate		20 kg/h. m^2 (as Na_2O_2)
Reactor containment building		
	Volume	180,000 m^3
	Floor area	2,800 m^2
	Wall area	20,000 m^2

At t=0, there is no airborne material. There is then an injection of aerosol at a constant rate (2,000 kg Na_2O_2/h) for 10 hours. The behavior of the aerosol is investigated for another 24 hours after the end of the source.

The benchmark input data are given in Table 1.

In addition to the reference case, nine cases with parameter variations were studied. In each one, only one parameter was varied, the others taking the values of the reference case. The parameters chosen for variation were those considered most likely to affect the final results appreciably, and the new values chosen attempted to reflect current estimates of uncertainty in those parameters.

Results obtained - Discussion

Mass concentration (figures 1, 7 and 10)

The comments about the results obtained are the following:

- agreement is good between PARDISEKO, AEROSOLS/B1, AEROSIM and ABC,
- discrepancies are large between AEROSOLS/A2 and discrete codes, in particular in the cases where agglomeration rates are high: $\gamma = 5$ (figure 7) and $E = 10^3$ cm^2/s^3 (figure 10). In these cases, the curves show a rapid decline of the mass concentration after source cut-off,
- during the source period (steady-state period), the mass lost by deposition is equal to the mass supplied by source particles; besides, the mass concentration values are about 10-20 g/m^3 for the discrete codes and about 20-40 g/m^3 for AEROSOLS/A2.

There are two distinct features to the mass concentration versus time comparison (figure 1),

a) early in the source period discrete codes show a peak followed by a falling back to the lower, steady state value,

b) after the source period, AEROSOLS/A2 shows a rapid and continuous decline of the mass concentration, while the discrete codes show a much more gradual decline.

We think we can understand these phenomena as follows:

a) the source is so intense and of long enough duration, that a shoulder develops very early in the problem. This shoulder is at a particle diameter of about 50 μm and is fed by coagulation of the source particles faster than it is reduced by sedimentation. The shoulder therefore continues to grow until it reaches a critical size (time $\sim$ 1-2 hours). At this time, a significant fraction of the source particles is immediately captured by the 50 μm particles by means of gravitational agglomeration and then falls out by sedimentation. The mode of the source distribution thus shows a drop in height (figures 13, 14 and 15) and the mass concentration curves their decline. Obviously, AEROSOLS/A2 cannot model such dynamics since it does not permit a shoulder on the distribution. It does however recognize that large particles are being formed by shifting the modal value of the distribution at the time of the mass concentration collapse.

b) The very rapid decline in the mass concentration after source cut-off, predicted by AEROSOLS/A2 but not by the discrete codes, can be understood with the aid of figures 2 and 3. For AEROSOLS/A2, the curves indicate a large modal value ($r_{50} \sim 7$ μm) leading to rapid settling. For the discrete codes, the curves indicate smaller "modal" value ($r_{50} \sim 2$-3 μm) leading to a much more gradual mass concentration decline.

N.B. : Additional runs have been performed using for gravitational collision efficiency (ε) the PRUPPACHER-KLETT formulation instead of the FUCHS relation and a changing from γ^2 to γ (γ: collision shape factor) in the gravitational agglomeration rate. The results obtained show a similar trend, except that the early collapse during the source period is less and the differences between AEROSOLS/A2 and the discrete codes are relatively small. This is because for these variations the rate of gravitation agglomeration is lower, and so the high-mass shoulder is smaller, and those high-mass particle which are formed are less efficient in removing the low-mass particles.

Mass median radius (figures 2, 8 and 11)

At the beginning of the accident (t $\sim$ 1-2 hours) the discrete codes show a peak (formation of large particles by coagulation); then, a steady-state period takes place ($r_{50} \sim 1.5$-2.5 μm) until the end of the source. During the steady-state period, the loss of particles by sedimentation is equal to the supply of particles by coagulation with source particles. At the end of the source, AEROSOLS/A2 and the discrete codes predict large increase of the mass median radius (sudden disappearance of small particles as

the source ceases); in particular, in the case of AEROSOLS/A2, r_{50} reaches values of 16 μm (γ = 5, figure 8) and 11 μm ($E = 10^3$ cm^2/s^3, figure 11). Finally, at long term, r_{50} values are about 2 μm for the discrete codes and 3 μm for AEROSOLS/A2.

Note that the discrepancy between the discrete codes is large (except the values given by PARDISEKO and AEROSOLS/B1); this is perhaps explained from the different ways of calculating r_{50} used in the computer models; in particular, ABC uses definition of geometrical mean radius weighed by the mass distribution.

Standard geometrical deviation (figure 3)

The results obtained show an initial dip ($\sigma_g \sim 1.7$) in the σ_g values; then a steady-state period occurs until the end of the source. At the end of the source, σ_g decreases quickly and at long term, σ_g values are about 1.5.

As previously, the discrepancies between the codes can be perhaps explained by the different ways of calculating σ_g, the standard geometrical deviation; i.e., for example, σ_g used in the computer model ABC uses definition based on mass concentration distribution, while the other codes use those based on number concentration distribution.

Mass balance

Table 2 shows the mass balance, in the reference case, at t = 10 hours, for the different codes.

Note that the released mass are different according to the different codes:

20,000 kg for ABC
19,950 kg for AEROSIM
20,000 kg for AEROSOLS/A2
20,950 kg for AEROSOLS/B1
19,900 kg for PARDISEKO

The discrete codes do not release exactly 20 tons because of approximations in the discretization (Table 3).

Settled mass and diffused mass (figures 4 and 5)

The results obtained indicate that 95 % of the released mass is settled on the floor and 5% is diffused on the walls. Besides, the main part ($\sim$ 90%) of the deposition occurs during the source period.

For settled mass, the values are very small during the two first hours (no large particles formed by coagulation at this time); then, the deposition rate is about 2,000 kg/hour during the source period. Note that for AEROSOLS/B1 the mass settled is higher than for the other codes. This is explained by the fact that the released mass is higher.

The discrepancies between the results can be explained by the different methods used in order to discretize the suspended particle size distribution (Table 3). In particular, concerning the differences between AEROSOLS/A2 and the discrete codes, the explanation is that large particles are missing in the particle size distribution calculated by moments method.

For diffused mass, the aerosol deposition occurs as the source releases, and the deposition rate is about 100 kg/hour during the source period. The differences between ABC and the other discrete codes can be explained by use of different constants in the thermophoresis removal formalism.

Leaked mass (figures 6, 9 and 12)

The major part of the leaked aerosol mass occurs when high aerosol mass concentration exists in the gas phase. In the present case, this corresponds to the source period.

In the reference case, the leaked mass varies from 10.7 kg (AEROSIM) to 21.6 kg (AEROSOLS/A2). The variation between discrete codes is smaller ($\sim$ 10 %).

From the sensitivity analysis (Table 4), the smaller value is given by AEROSIM [3.6 kg (γ = 5)] and the higher value is given by AEROSOLS/A2 [31.8kg (PRUPPACHER-KLETT formulation)].

These values show clearly that the mass leaked is most sensitive to the rate of agglomeration as governed by the collision shape factor, γ, and the collision efficiency, ε.

Mass concentration distribution (figures 13, 14 and 15)

Figures 13, 14 and 15 show the development of the deviation from lognormal behavior in the mass concentration distribution during the source period. The discrete codes give very similar results for the shape of the distributions.

CONCLUSION

This study shows that the lognormal assumption is not justified when agglomeration rates are high. Therefore, the use of the moments method code AEROSOLS/A2 for aerosol calculations should be discontinued.

The discrete codes produce broadly similar predictions. For the reference case the leaked mass predicted by the different codes (ABC, AEROSIM, AEROSOLS/A2, AEROSOLS/B1 and PARDISEKO) varies by a factor of 2. Without the lognormal code AEROSOLS/A2, this variation is reduced to 10 %.

For the sensitivity analysis (in which the parameter variations were chosen in order to reflect current estimates of uncertainty in those parameters), the leaked mass predicted by the different codes varies between approximately 4 kg and 30 kg (between 4 kg and 20 kg without the lognormal code). Besides, this sensitivity analysis shows that the result depends strongly on the values of those factors which affect agglomeration rates

(collision shape factor, gravitational collision efficiency and turbulent energy density dissipation rate).

RECOMMENDATIONS FOR FUTURE WORK

In order to improve the available aerosol computer models and the numerical values of the main parameters, both analytical experiments (small scale experiments to investigate individual processes) and integral experiments (large scale experiments to simulate reactor accident conditions) are necessary:

- The most urgent topics for study in analytical experiments are gravitational collision efficiencies, turbulent agglomeration mechanisms and shape factor effects.

- Integral experiments should address the sensitivity of the aerosol processes to variations in the mass rate of injection due to a pool fire, and to the total mass injected. Such experiments should be adequately instrumented to give information on particle size distribution and on possible deviation from good mixing. A knowledge of the thermal-hydraulic conditions obtaining during the experiment is also important for the interpretation of the results.

Furthermore, in order to make possible a correct assessment of the radiological source term during severe accidents, computer models need to be improved by treating mixed aerosols (in particular, fuel and sodium oxide aerosols) and deviation from good mixing (multi-compartment code).

REFERENCES

[1] Dunbar, I.H., Fermandjian, J., "Comparison of Sodium Aerosol Codes," CEC Report EUR 9172, July 1984.

[2] Mitsutsuka, N., "ABC/INTG Code Features," PNCT N241 84-05, April 1984.

[3] Walker, B.C., Kirby, C.R., Williams, R.J., "Discretization and Integration of the Equation Governing Aerosol Behavior,", SRD R 98, July 1978.

[4] L'Homme, A., Pépin, P., Abbas, A., Carvallo, G., "Présentation du code AEROSOLS/A2,", Private communication, October 1982.

[5] L'Homme, A., Pépin, P., Gauvain, J., Abbas, A., Carvallo, G., Lhiaubet, G., Baptiste, G., "Présentation du code AEROSOLS/B1," Private communication, November 1983.

[6] Bunz, H., "PARDISEKO IIIb, Ein Computerprogram zur Berechnung des Aerosolverhaltens in Geschlossenen Belältern, KfK 2903, April 1980.

TABLE 1 - DATA FOR COMPARATIVE CALCULATIONS

	REFERENCE CASE	PARAMETER VARIATION		DIMENSION
Coagulation shape factor γ	1.5	1	5	-
Source duration	10	-	-	h
Geometrical standard deviation σ_g	2.0	1.5	3.0	
Collision efficiency ε	FUCHS relation	PRUPPACHER-KLETT relation	-	-
Emission rate	2.0	-	-	t/h
Dynamic shape factor X	1.5	3	-	-
Mass median radius r_{50}	0.5	0.25	2	µm
Containment vessel volume	180,000 Ø=60 H=60	-	-	m^3 m m
Gas temperature	100	-	-	°C
Density correction factor	1	-	-	-
Particle density	2.8	-	-	g/cm^3
Gas pressure	1	-	-	bar
Wall area	20,000	-	-	m^2
Floor area	2,800	-	-	m^2
Thermal boundary layer thickness	1	-	-	mm
Thermal gradient	10	-	-	°C
Thermal conductivity ratio	4.10^{-2}	-	-	-
Brownian boundary layer thickness	0.1	-	-	mm
Turbulent energy density dissipation rate E	0	10^3	-	cm^2/s^3
Leak rate	1	-	-	vol%/day

TABLE 2 - MASS BALANCE (IN KG) AT T = 10 HOURS

Reference case

COMPUTER MODEL	ABC	AEROSIM	AEROSOLS / A2	AEROSOLS / B1	PARDISEKO
Settled mass	16,310	16,900	13,018	17,513	16,530
Diffused mass	1,057	703	1,363	770	797
Airborne mass	2,619	2,358	5,601	2,627	2,548
Leaked mass	10.9	9.2	18.9	10.3	9.9
Released mass	19,997	19,970	20,000	20,920	19,885

TABLE 3 - DISCRETISATION OF THE PARTICLE SIZE DISTRIBUTION USED IN VARIOUS COMPUTER MODELS

COMPUTER MODEL	NUMBER OF SIZE CLASSES	R_{min} (µm)	R_{max} (µm)
ABC	20	0.01	158.5
AEROSIM	25	0.05	100
AEROSOLS/B1	50	0.05	100
PARDISEKO	100	0.01	100

TABLE 4 - LEAKED MASS (IN KG) AT T = 34 HOURS

	ABC	AEROSIM	AEROSOLS/A2	AEROSOLS/B1	PARDISEKO	AVERAGE VALUE*	DEVIATION**
Reference case	12.9	10.7	21.6	12.1	11.9	11.9	0
PRUPPACHER - KLETT	21.7	18.1	31.8	21.0	23.2	21.0	+ 76
$\Upsilon = 1$	17.0	14.9	27.8	17.3	17.0	16.5	+ 39
$\Upsilon = 5$	4.1	3.6	10.1	4.1	4.2	4.0	- 66
$\sigma_g = 1.5$	12.5	10.8	19.3	12.4	12.4	12.0	+ 1
$\sigma_g = 3$	11.4	10.1	26.4	11.7	11.4	11.1	- 7
$\chi = 3$	18.4	16.0	31.2	18.2	18.2	17.7	+ 49
$r_{50} = 2\,\mu m$	9.0	7.7	13.9	8.7	8.7	8.5	- 29
$r_{50} = 0.25\,\mu m$	12.6	10.8	24.8	12.6	12.4	12.1	+ 2
$E = 10^3 cm^2/s^3$	11.4	8.8	20.5	9.9	10.8	10.2	- 14

* Average value of the leaked masses given by the discrete codes ABC, AEROSIM, AERESOLS / B1 and PARDISEKO .

** Difference between the average value and that of the reference case (in %) .

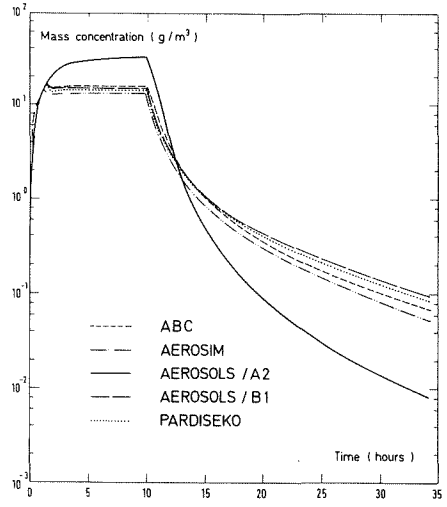

Fig. 1 _ SUSPENDED MASS CONCENTRATION
REFERENCE CASE

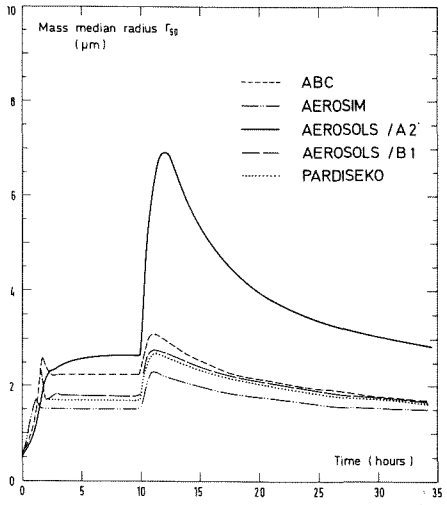

Fig. 2 _ MASS MEDIAN RADIUS
REFERENCE CASE

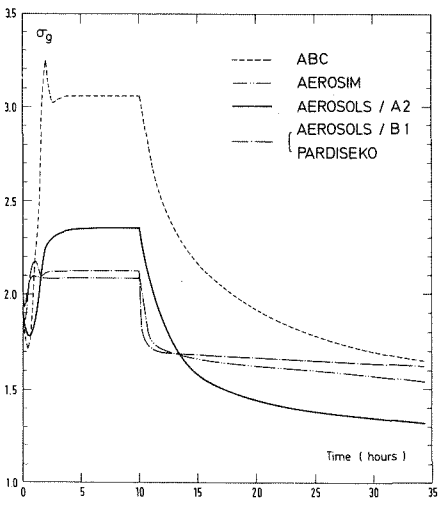

Fig. 3 _ GEOMETRICAL STANDARD DEVIATION
REFERENCE CASE

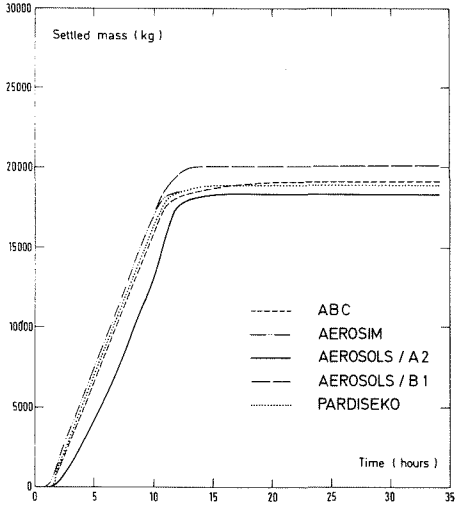

Fig. 4 _ MASS SETTLED ON FLOOR
REFERENCE CASE

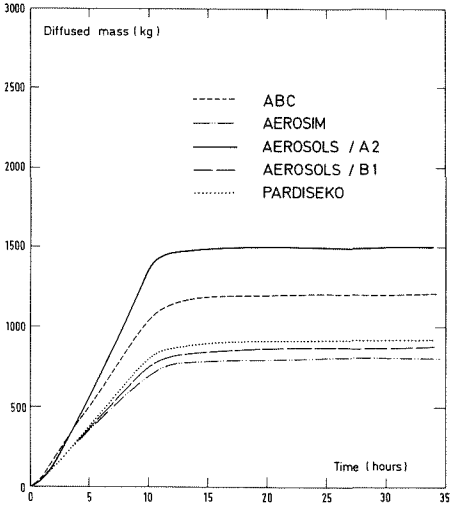

Fig. 5 _ MASS DIFFUSED TO WALLS
REFERENCE CASE

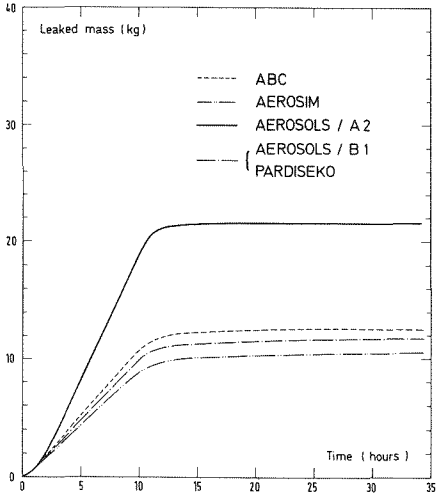

Fig. 6 _ LEAKED MASS
REFERENCE CASE

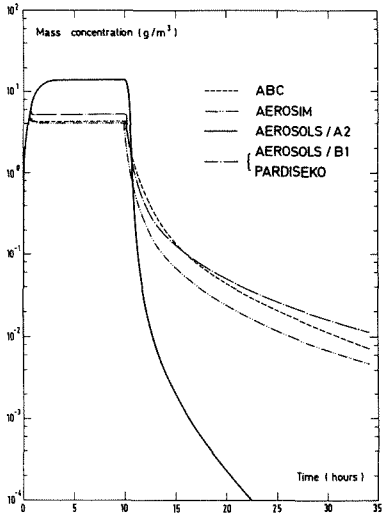

Fig. 7 _ SUSPENDED MASS CONCENTRATION
COAGULATION SHAPE FACTOR $\gamma = 5$

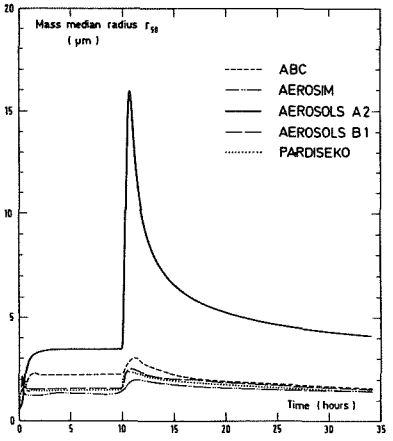

Fig. 8 _ MASS MEDIAN RADIUS
COAGULATION SHAPE FACTOR $\gamma = 5$

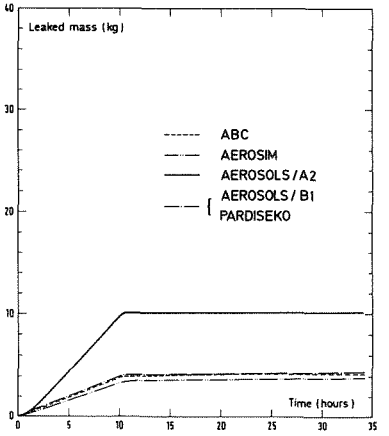

Fig. 9 _ LEAKED MASS
COAGULATION SHAPE FACTOR $\gamma = 5$

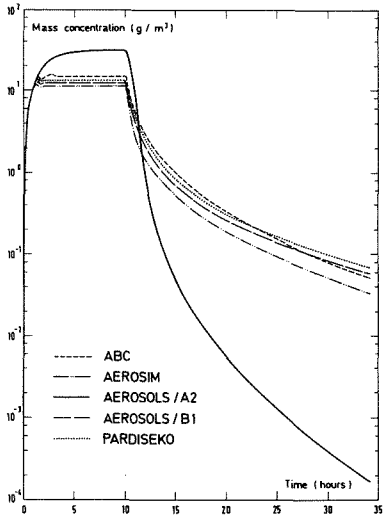

Fig. 10 _ SUSPENDED MASS CONCENTRATION
TURBULENT ENERGY DENSITY DISSIPATION RATE
$E = 10^3\ cm^2/s^3$

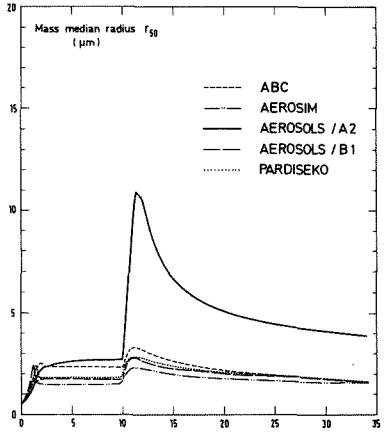

Fig. 11 _ MASS MEDIAN RADIUS
TURBULENT ENERGY DENSITY DISSIPATION RATE
$E = 10^3\ cm^2/s^3$

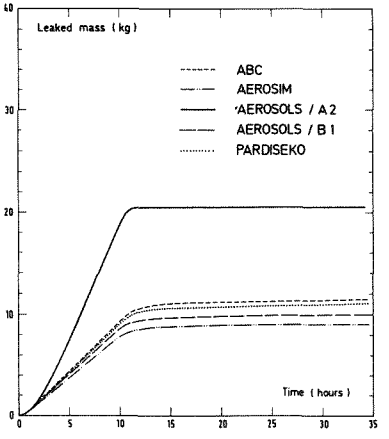

Fig. 12 _ LEAKED MASS
TURBULENT ENERGY DENSITY DISSIPATION RATE
$E = 10^3\ cm^2/s^3$

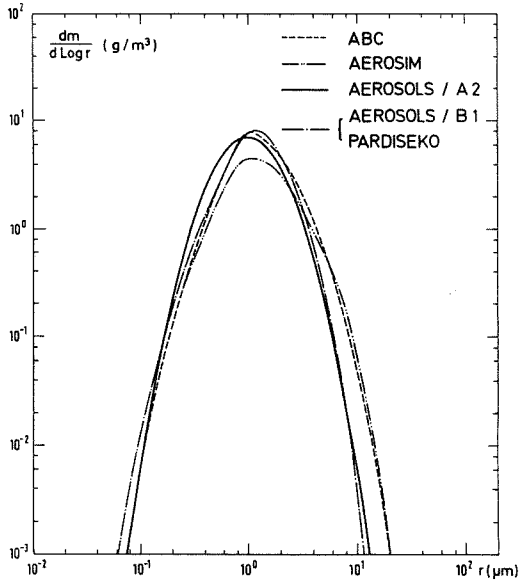

Fig. 13 _ MASS CONCENTRATION DISTRIBUTION AT t = 1 hour
REFERENCE CASE

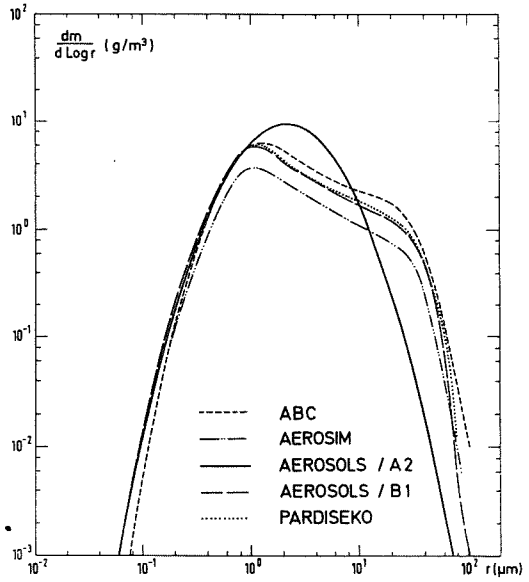

Fig. 14 _ MASS CONCENTRATION DISTRIBUTION AT t = 2 hours
REFERENCE CASE

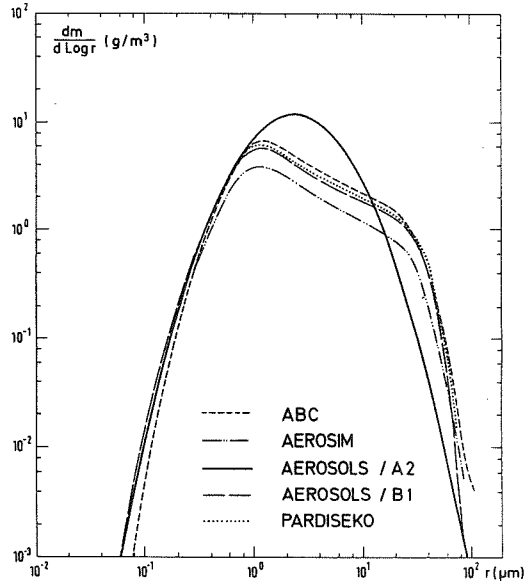

Fig. 15 _ MASS CONCENTRATION DISTRIBUTION AT t = 3 hours
REFERENCE CASE

FISSION PRODUCT TRANSPORT AND RETENTION IN PWR REACTOR COOLANT AND CONTAINMENT SYSTEMS

E.A. Warman, J.E. Metcalf, A. Drozd and M.L. Donahue

Stone & Webster Engineering Corporation
Boston, Massachusetts

ABSTRACT

The quantity and timing of the release of radioactive material to the environment resulting from severe core damage accidents at nuclear power plants are greatly influenced by the transport and retention of fission products in the reactor coolant and containment systems. This paper addresses investigations of such transport and retention in pressurized water reactor (PWR) power plants being conducted by the Stone & Webster Engineering Corporation (SWEC). The various phases of the SWEC investigation of the reactor coolant system (RCS) are discussed along with qualitative observations based on results available to date. Quantitative results of a parametric study of fission product transport and retention in the containment building and contiguous structures are presented. A more complete description of the parametric study is reported in Chapter 6 and Appendix B of the Report of the American Nuclear Society's Special Committee on Source Terms (1). A summary of the study is included in the ENS/ANS Fifth International Meeting on Thermal Nuclear Reactor Safety (2).

The results of the parametric study illustrate that fission product retention in the containment and structures outside the containment during severe core damage accidents is substantial. Retention in the reactor coolant system (RCS) can be combined with these retention factors to result in very large calculated overall retention within the plant.

Fission product transport and retention in the RCS and containment systems are functions of combinations of thermal hydraulics, aerosol and vapor physics, and chemical interactions. In the present paper, physical transport and retention are addressed in some detail and some chemical interactions are briefly discussed.

Thermal hydraulics and fission product behavior are closely coupled in nature. In the RCS, this coupling is even more pronounced than it is in the containment. SWEC studies of the RCS have evolved through three phases. The first employed relatively high temperatures from analyses with a serial representation of the RCS in a small number of linked nodes (principally based on the USNRC sponsored study BMI-2104)(3). The second phase of the investigation centered on a multinode representation of the RCS which combined thermal hydraulic and vapor transport (including recirculation) with decay heating effects. This second phase of the investigation illustrated the participation of the entire RCS. In the third phase of the investigation, aerosol transport throughout the RCS is presently being included in the multinode thermal hydraulic model, which already includes vapor transport and fission product heating.

ACCIDENT SEQUENCES AND ANALYTICAL APPROACH

The investigations of PWR accidents have concentrated on the following three accident sequences: AB (large break LOCA in containment with loss of AC power), TMLB (a transient with loss of AC power followed by the failure of the power conversion system and the loss of the capability of the secondary system to remove heat from the RCS) and V (an interfacing system LOCA in the low pressure emergency core cooling system at a location outside containment). The discussion of the analysis of fission product transport and retention in the RCS in this paper is limited to the TMLB sequence. The discussion relative to retention in the containment addresses both the AB and TMLB sequences. The analyses are based on the Surry plant.

The analyses utilized the following combination of computer programs. The mass and energy release from the RCS and the timing of core uncovery were based on an analysis with the RELAP-4 Mod5 program (4). The timing and rate of release of fission products and other aerosols were based on analyses reported in BMI-2104 Volumes V and I (3,5). The core/concrete interaction mass and energy releases were based on analyses performed by Sandia in support of the ANS source term committee (6). The thermal hydraulic conditions in the containment and contiguous structures were analyzed utilizing the THREED computer program (7). This program combines the thermodynamic modeling of RELAP-4 (4) and the treatment of heat sinks as modeled by the CONTEMPT-LT computer program (8). The program was modified to permit its use in the analysis of the RCS as well as the containment, as discussed later in this paper. The application of THREED to the RCS was accomplished in conjunction with the MATCH computer program (9), which is under development at SWEC. This program includes detailed analyses of aerosol and vapor behavior, as discussed briefly in the next section. In the current phase of the investigation of retention in the RCS, the THREED program is being modified to include several aerosol behavior phenomena included in the TRAP-MELT program (10). The analysis of aerosol behavior in the containment is based on the NAUA-4 computer program (11), as modified by SWEC to include diffusiophoretic removal associated with steam condensation on heat sinks computed by THREED.

TRANSPORT AND RETENTION IN RCS

Description of THREED Representation of RCS

In the context of this investigation, the term RCS includes the reactor vessel and its internals, exclusive of the core. The thermal hydraulic environment into which fission products are introduced is markedly different in the RCS and containment system. A spectrum of conditions exists in the RCS for different accident sequences and different phases within a given sequence. In the TMLB sequence, at the time the volatile fission products escape from the core, the RCS is in a reducing environment with hydrogen-rich super heated steam at $\sim$ 170 atm and ranging in temperature from $\sim$ 370 to $\sim$ 1000°C. By contrast the atmosphere in the containment at the time of injection of fission products is saturated steam with a temperature near 100°C.

The geometry associated with the multinode THREED model of the RCS is depicted in Figure 1. The nodalization is summarized below:

Portion of RCS	No. of Nodes
Upper Plenum	7
RPV Closure Head	1
Downcomer	1
Loop With Pressurizer	
Hot & Cold Legs	5
Steam Generator	6
Pressurizer	1
Other Two Loops (combined)	
Hot & Cold Legs	5
Steam Generator	6
Total	32

The upper plenum, shown in the enlargements in Figure 1, is the first region encountered by fission products exiting the core. In the present model it is divided axially into three sections: from the upper core plate to the bottom of the hot leg nozzles, from the bottom to the top of the hot leg, and from the top of the hot leg to the bottom of the upper support plate. Each of these sections is subdivided into two radial control volumes, one describing the region directly above the fuel assemblies and the other describing an annulus between the first region and the core barrel. The control rod guide tubes are modeled as a single control volume. The downcomer is represented as a single control volume which includes a small leak path to the closure head.

MATCH Analysis of RCS

Because a reducing environment (excess of hydrogen) exists at the time of release of volatile fission products from the core, the representation of the RCS in the MATCH program was developed as follows. The gaseous tellurium is assumed to be in the form of an equilibrium mixture of Te_2, Te, and H_2Te. As shown in Figure 2, these gaseous species also are convected with other gaseous fission products (CsOH and CsI) along with excess quantities of hydrogen and super heated steam. Aerosol of a single particle size is convected with the gas. The aerosol is composed of CsOH, CsI, Fe (from structural components) and $FeTe_2$ (from the gas-phase reaction of Te_2 with Fe). Material that collects on the structures is predominantly CsOH and CsI which is above either the melting point of CsOH (315°C) or the calculated eutectic point of CsOH-CsI ($\sim$ 250°C). Consequently, the film on the structures in the RCS is believed to be in a liquid phase.

The mass balance performed by MATCH includes deposition of aerosols by Brownian or inertial impaction (12) and resuspension as the liquid layer builds up in turbulent flow (13). Gas is allowed to condense or evaporate with either the aerosol or structural surfaces in turbulent (14) or laminar flow (15) regimes. In some instances (as with tellurium) the gas is allowed to react with the surfaces. The driving forces at the

gas-liquid interface are characterized by the use of ideal solution theory. Ideal solution theory (Raoult's Law) is also utilized to address solid-liquid equilibrium.

Some qualitative results are presented in Figure 3 for two domains of interest: temperature and velocity, at transit times of approximately one second. At high temperatures (∿ 700°C), the gas phase has the ability for a high chemical potential driven transfer rate with the wall or aerosol due to the high partial pressures of the fission products. If transport between the gas and wall is dominant, the aerosol is rapidly stripped of (or loaded with, depending on the potential) valatile products. This transport can even occur at isothermal conditions where different liquid mixtures are found between the wall and aerosol. At high velocities (∿ 100's m/s) thin films (∿ 10 μm) are formed with high resuspension rates. At low turbulent velocities, thick films (∿ 100 μm) can form. At low temperatures (∿ 250°C), aerosols will continue to buffer the gas phase, however, because the gaseous vapor pressures are much lower, transport rates between the gas and wall are orders of magnitude lower than at the high temperatures. Consequently, aerosol deposition becomes a more important mechanism for depositing material on the wall. At high velocities the deposition mechanism is one of inertial impaction, whereas at low velocities aerosol deposition occurs by the very slow Brownian diffusion mechanism (which begins to approach the magnitude of transport for gas phase condensation). At lower temperatures, melting point depression of the cesium compounds will help sustain a liquid layer. At high velocities this layer will be thin. Although low velocities may potentially result in the thickest layer, the accumulation rate is so slow as to make the layer build-up beyond the time span of interest in the accident.

Summary of Analysis of RCS

The initial phase of the investigation was predicated on an understanding of the results of the analyses performed with a serial representation of the RCS with a few successive nodes, (e.g., single node upper plenum, hot leg, etc.) as reported in BMI-2104 (3,5). Based on the reported large concentration of aerosols at the base of the upper plenum (i.e., the upper core plate) and the high carrier gas temperature reported by BMI, the initial SWEC analyses resulted in the conclusion that evaporation from this region would result in the volatile fission products being transported predominantly in the vapor phase. In the second phase of the investigation, the results obtained with the multinode RCS model depicted in THREED (with recirculation and decay heating) indicated that the previous models involving serial nodalization of the RCS with a few nodes are unrealistic. Sequential thermal hydraulic and fission product transport analyses with such models do not include the coupling effects, which have been found to be important.

If the volatile species transport was primarily in the vapor phase, the relatively minor modification to the THREED program would adequately treat the transport. However, in performing the analyses it was found that circulation patterns prior to vessel meltthrough result in the participation of the entire RCS in the heating process. Although the high temperatures in the upper core plate region result in rapid evaporation of the volatile

species, the temperature of the carrier gas within the upper plenum in the multinode model is lower than that reported in BMI-2104 by approximately a factor of two. Using the THREED and MATCH programs in combination it was observed that vapor transport appears to be important at the lower portions of the upper plenum and that aerosol transport appears to be dominant for the remainder of the RCS.

In the third stage of the investigation, the multinode THREED model is being modified to include portions of the models of the aerosol dynamics incorporated in the TRAP-MELT program (10). These modifications include the incorporation of gravitational settling and inertial turbulent deposition. In addition, hydrodynamic film thickness is being assessed. This third phase of our investigation is currently in progress at SWEC and quantitative results are not presently available.

FISSION PRODUCT TRANSPORT AND RETENTION IN CONTAINMENT

A parametric study of fission product transport and retention in the containment and adjacent structures was performed, as reported in Chapter 6 and Appendix B of the report of the American Nuclear Society Special Committee on Source Terms (1).

The following parameters and phenomena were included in that study:

- o Containment Opening Size
- o Timing of Opening
- o Diffusiophoresis
- o Suspended Liquid
- o Contiguous Structures
- o Multicompartmentation
- o Release of Non-Volatiles
- o Aerosol Particle Size
- o Aerosol Concentration
- o Timing of Te Release from Core
- o Core Degradation Without Vessel Meltthrough
- o Fission Product Decay Heating
- o Timing of Injection Into Containment

The study illustrated that inclusion of a number of factors, not previously included in accident analysis studies, resulted in a large overall reduction in releases of fission products to the environment. For example, the overall effect of including these factors is a reduction in the leakage fraction from 0.72 to 0.015 for the TMLB sequence. These data assume no retention of iodine and cesium in the core or in the RCS. Quantitative assessments of retention in the RCS would be multiplicative with the retention in the containment and contiguous structures, as a first approximation. (e.g., If a retention factor of 0.9 is calculated for the RCS, the 0.015 release fraction noted above would be reduced to 0.0015).

One of the important findings of this study is the fact that in-leakage into the containment occurs with 1.0 ft^2 ($0.093m^2$) or larger openings. In-leakage was not observed for smaller opening sizes, over the time period of interest in source term determinations. Figure 4 depicts the volumetric leak rate as a function of time for a 0.1 ($0.0093m^2$) and 1.0 ft^2 ($0.093m^2$) pre-existing containment opening for the TMLB sequence.

Another important finding from the parametric study is the effect of timing of containment opening on the leakage fraction of volatile fission products.

Figure 5 shows the effect on iodine and cesium leakage of varying the timing of a 1.0 ft^2 opening in the containment. Data are represented for both the AB and TMLB sequences. It can be observed that an opening coincident with the start of core melt (i.e., at 0.5 hr in the AB sequence) results in an increase in leakage of $\sim$ 30% over that for a pre-existing opening. For the TMLB sequence, the leakage was observed to be essentially the same for a pre-existing opening as for openings during core degradation (i.e., at $\sim$ 3 hr in the TMLB sequence). For both sequences, delay in the timing of the opening beyond the core degradation period results in an exponential decrease in leakage. The dashed and dotted curves in Figure 5 depict the effect of reducing the core/concrete aerosol loading reported in BMI-2104 Volume I by a factor of 0.2 or 0.1 (i.e., repeating the analyses with one-fifth or one-tenth the amount of core/concrete aerosols employed in the baseline calculations).

Analyses of fission product transport and retention were conducted for postulated pre-existing, early, and late breaches of the containment. The results indicate that the release fraction of volatile fission products is essentially the same for pre-existing openings or openings due to postulated early breach of containment. However, the releases associated with postulated late breach of containment are approximately two orders of magnitude lower, as illustrated below for iodine for the TMLB sequence:

	Fraction of Inventory of Iodine Released*	
Timing of Containment Breach	1.0 ft^2 (0.093m^2)	0.1 ft^2 (0.0093m^2)
Pre-existing (Prior to core degradation)	1.5×10^{-2}	2.1×10^{-3}
Early (During or shortly after core degradation)	1.5×10^{-2}	2.1×10^{-3}
Late (Substantially after core degradation - 27 hr)	3.6×10^{-5}**	2.6×10^{-5}**

* Includes retention in RCS from BMI-2104 Volume V.
** Based on 0.2 x nominal aerosol loading, which is close to aerosol loading value reported in BMI-2104 Volume V.

Based on these analyses, the following observations are made (in terms of fractions of the core inventory of volatile species which may be released to the atmosphere).

- Pre-existing openings $\leq$ 0.1 ft^2 (0.009m^2) result in release fractions of the core inventory of volatile fission products of $\sim 1 \times 10^{-2}$ - neglecting retention in the RCS.
- Pre-existing openings $\geq$ 1.0 ft^2 (0.09m^2) result in release fractions $\sim 1 \times 10^{-2}$ - with retention in the RCS as reported in BMI-2104 Vol. V.
- Containment openings $\geq$ 0.1 ft^2 (0.009m^2), whether pre-existing or during early hours of an accident sequence, preclude containment overpressure from occurring.

- With no opening in the containment, slow pressure buildup results in a long time to postulated containment breach, e.g., $\geq$ 1 day (assuming loss of all active engineered safety systems).

- Release fractions for late containment breach (at $\geq$ 1 day) are $< 1 \times 10^{-4}$, even for very large containment openings.

In the above summary, reference is made to the inclusion of retention factors for the RCS as reported in BMI-2104 Volume V. This retention has been included in the present paper as an interim substitute pending the completion of the third phase of the SWEC investigation of retention in the RCS, discussed earlier. It should be noted that the analyses described in this paper assume the loss of function of all active engineered safety features, which is highly improbable.

REFERENCES

1. Report of the American Nuclear Society's Special Committee on Source Terms, (to be published).

2. Warman, E.A., "Parametric Study of Factors Affecting Retention of Fission Products In Severe Reactor Accidents", ENS/ANS Fifth International Meeting on Thermal Nuclear Reactor Safety Safety, Karlsruhe, Federal Republic of Germany, (September 11, 1984).

3. Gieseke, J.A. et al, "Radionuclide Release Under Specific LWR Accident Conditions - Volume V - PWR Large Dry Containment (Surry Recalculations)," Draft Report, BMI-2104, Volume V, Battelle Columbus Laboratories (January 1984).

4. Moore, K.V., and Pettey, W.H., "RELAP4-Mod5: A Computer Program for Transient Thermal Hydraulic Analysis of Nuclear Reactors and Related Systems, Users Manual, Volume I-III, Aerojet Nuclear Company, ANCR-NUREG-1355 (September 1976).

5. Gieseke, J.A. et al, "Radionuclide Release Under Specific LWR Accident Conditions - Volume 1 - PWR Large Dry Containment," Draft Report, BMI-2104, Volume 1, Battelle Columbus Laboratories, (July 1983).

6. Powers, D., Sandia National Laboratories, Personal Communication.

7. Stone & Webster Engineering Corporation, "THREED: A Subcompartment Transient Response Code," (Proprietary Computer Program), NU-092 (March 1975).

8. Wheat, L.L., et al, "CONTEMPT-LT, A Computer Program for Predicting Containment Pressure-Temperature Response to a Loss-of-Coolant-Accident," Aerojet General Corporation, ANCR-1219 (1975).

9. Baron, J. and Doerr, W.W., "MATCH: A Computer Program for Aerosol Transport With Chemistry and Heat Transfer," Stone & Webster Engineering Corporation, (Unpublished).

10. Jordan, H., Gieseke, J.A. and Baybutt, P., "TRAP-MELT Users Manual, NUREG/CR-0632, BMI-2017 (February 1979).

11. Bunz, H., Kayro, M., and Schock, W., "NAUA-Mod4, A Code for Calculating Aerosol Behavior in LWR Core Melt Accidents, Code Description and Users Manual," (March 1982) to be published as KfK-3554 by Kainforschungszentrum Karlsruhe.

12. Gieseke, J.A., Lee, K.W., and Goldenberg, M.A., "Measurement of Aerosol Deposition Rates in Turbulent Flow," NUREG/CR-1264 - BMI-2104, Battelle Columbus Laboratories, Columbus, Ohio (1980).

13. Whalley, P.B., and Hewitt, G.F., "The Correlation of Liquid Entrainment Fraction and Entrainment Rate in Annular Two-phase Flow," AERE-R9187 HTFS-RS237, Harwell, England (1978).

14. Rohsenow, W.M., and Choi, H.Y., "Heat Mass and Momentum Transfer," Prentice Hall, Englewood Cliffs, NJ, P-415 (1961).

15. Bennet, C.O., and Myers, J.E., "Momentum, Heat, and Mass Transfer," McGraw Hill Book Company, New York, P308, 478 (1962).

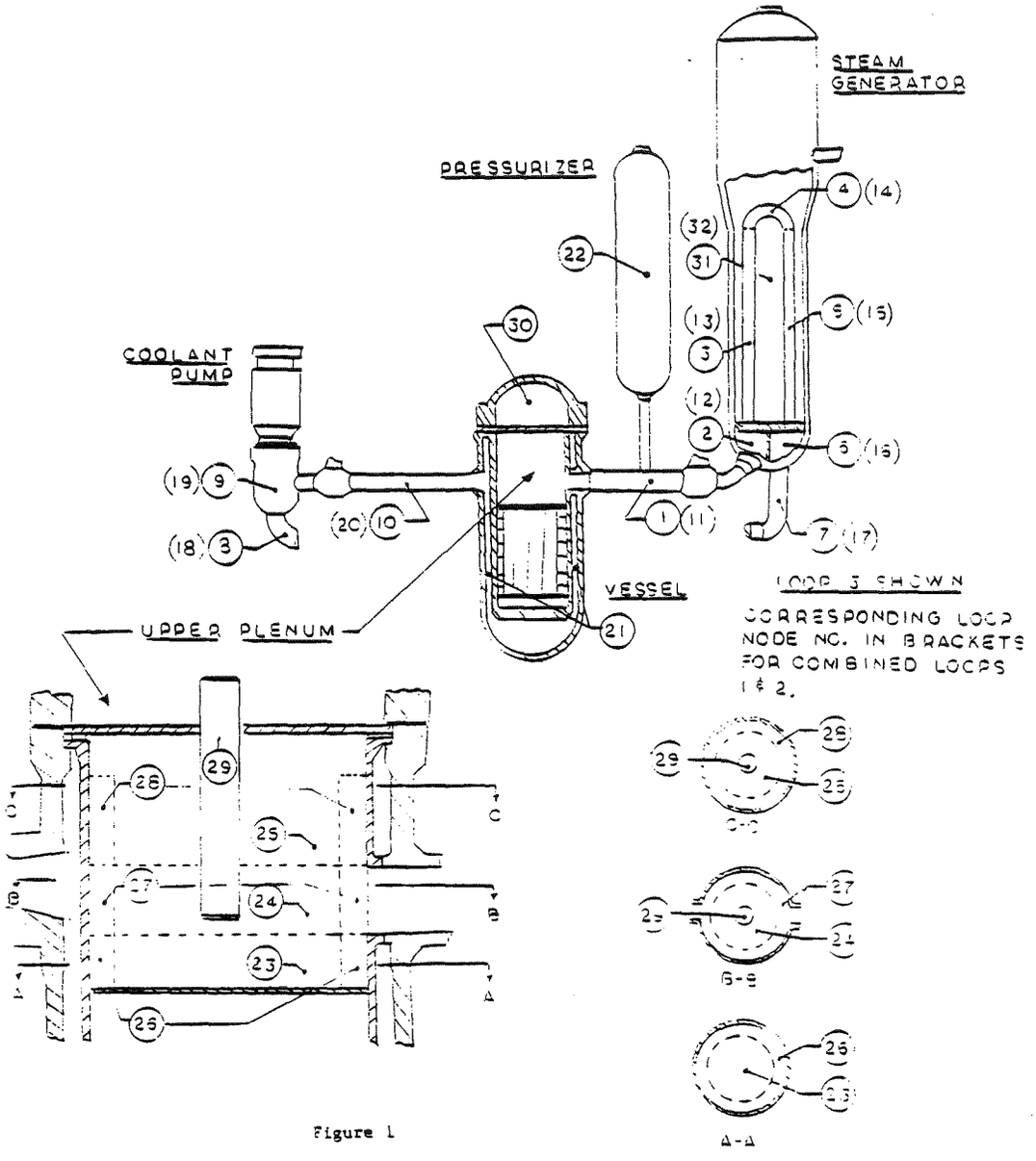

Figure 1

REACTOR COOLANT SYSTEM MODEL

Figure 2

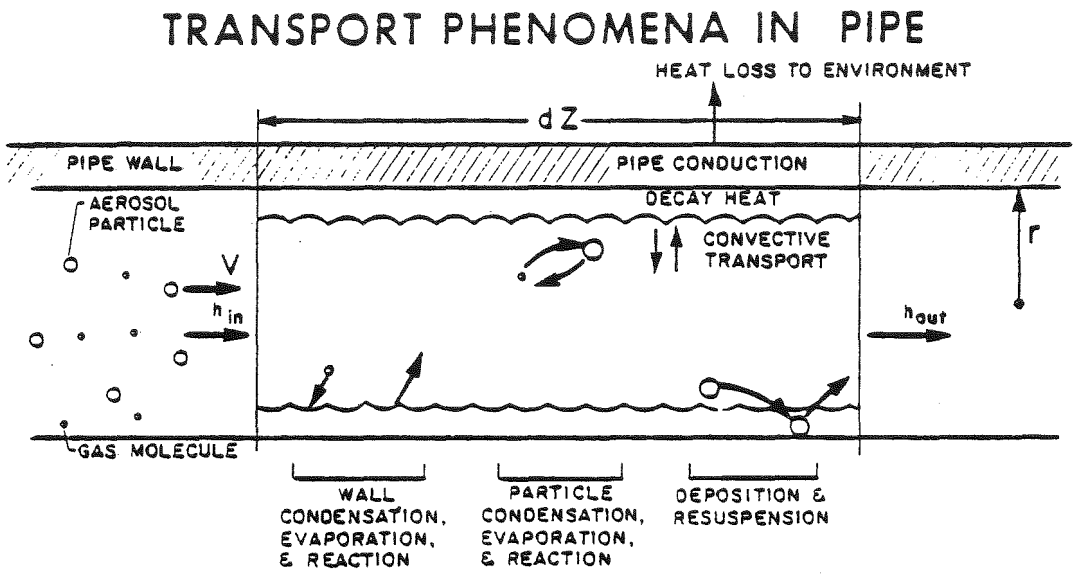

Figure 3

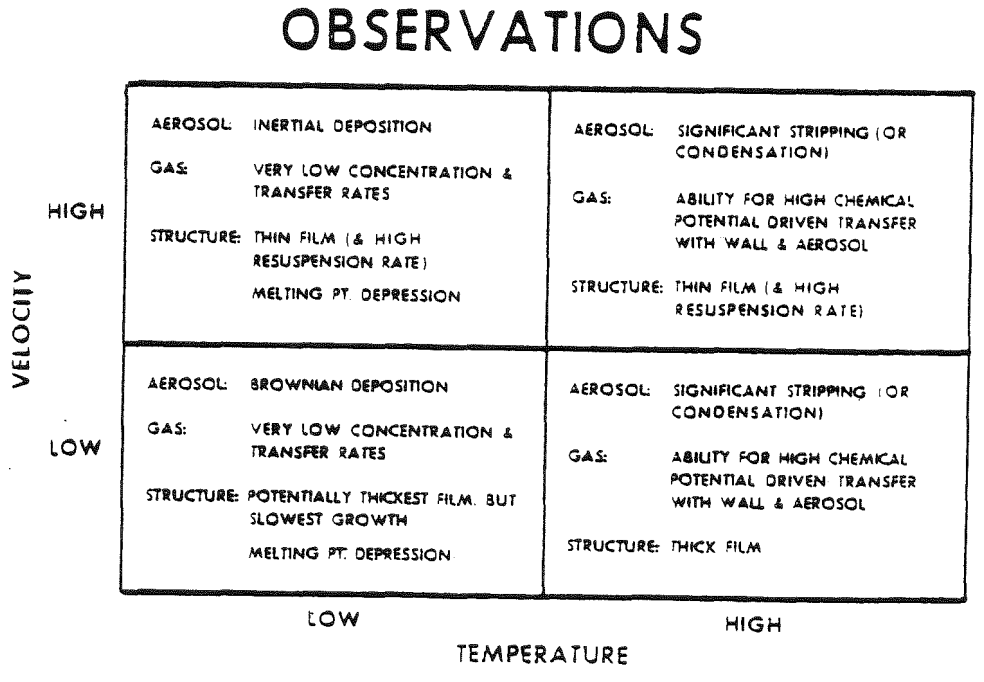

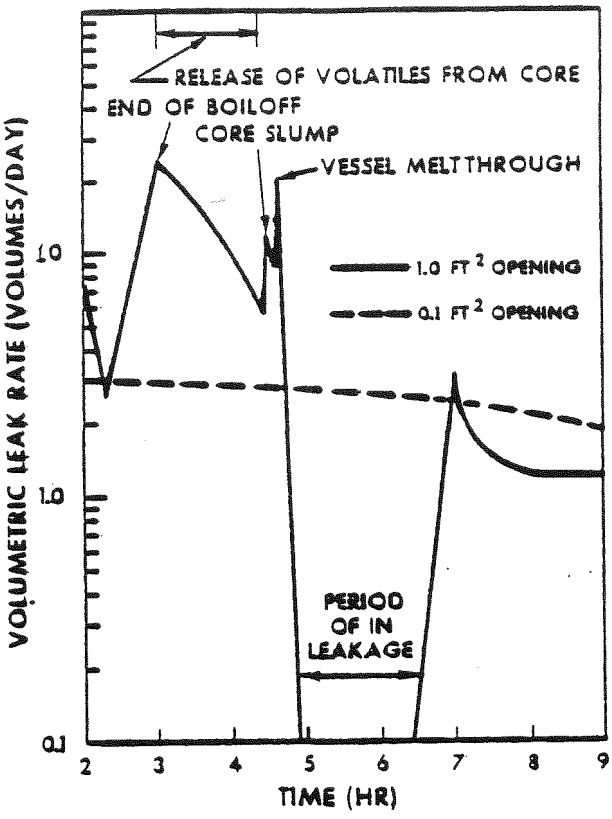

Figure 4

VOLUMETRIC LEAK RATES WITH 1.0 OR 0.1 FT ^{2} PRE-EXISTING OPENING IN CONTAINMENT TMLB SEQUENCE

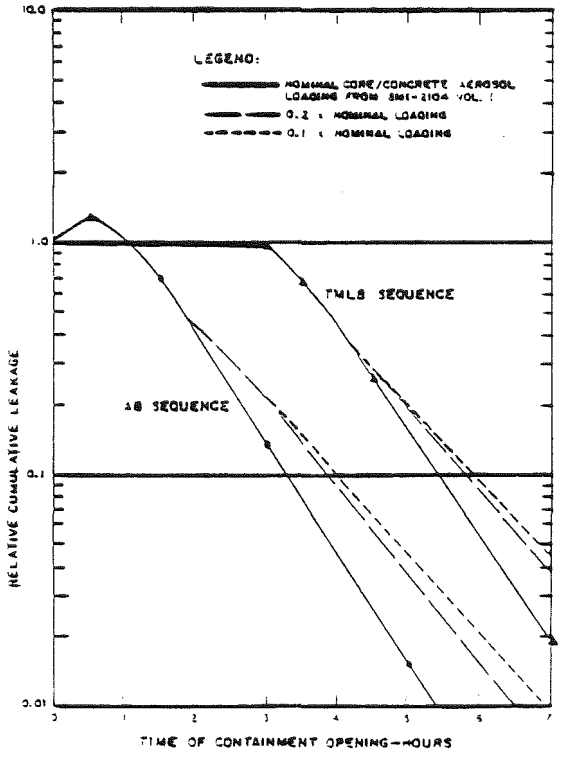

Figure 5

EFFECT OF TIMING OF 1.0 FT ^{2} OPENING IN CONTAINMENT ON LEAKAGE OF IODINE AND CESIUM

NOTE:
NORMALIZED TO A LEAKAGE FRACTION OF 1.0 FOR A PRE-EXISTING OPENING

B3-522023609-593

DOSE CALCULATION PARAMETERS USING REDUCED SOURCE TERMS

P. Karahalios and R. Gardner
Stone & Webster Engineering Corporation
Boston, Massachusetts

ABSTRACT

As convergence on more realistic source terms results from the current international analytical and experimental efforts, there is an increased interest in translation of such source terms into predicted consequences. Two difficulties in comparing source terms by historic methods emerge:

- Increased analytical sophistication allows incorporation of many plant/accident specific details which affect the calculated source terms in detail, if not in general.

- Comparison by calculation of numbers of early fatalities becomes meaningless with reduced source terms because most of these produce no calculated prompt fatalities at all.

A method of comparison based on mean whole body doses, using CRAC2 calculations, is proposed. A simplified calculation method illustrates the effects of the principal parameters and can be used to make very approximate dose calculations.

As source terms are being reduced, consequence models are becoming more important, and conservatisms in such models may prove to be just as important as conservatisms in source terms. Because of the high calculated consequences which result from the very conservative historic source terms, the results of uncertainties in consequence models have been small compared to the overall consequence analyses results. Therefore, simplifications of such models could generally be accepted. However, with the low levels of consequences associated with reduced source terms, such simplifications can lead to erroneous conclusions.

In this work, the uncertainties in two models used in consequence analyses -- plume buoyancy and dry deposition velocity -- were examined parametrically with the following results:

- The dry deposition velocity value of 1 cm/sec, recommended for use in CRAC2, is found to give conservative results for distances of interest for both historic and reduced source terms.

- Incorporation of plume buoyancy in the calculation is found to result in short distance doses markedly below those for nonbuoyant plumes. For reduced source terms, mean doses calculated with plume buoyancy are well below the severe health effects threshold range.

FOREWORD

An important observation made on the basis of data collected at the Three Mile Island accident was that the amount of radioiodine available for release to the environment was much smaller than that which would have been predicted [1]. As a result, a large international research program was initiated to identify and provide understanding of natural processes affecting the retention of radioiodine as well as other fission products. The calculated types, quantities, and timing of releases of all these fission products, taken together, is known as the source term because it establishes the characteristics of the source of radioactivity for use in calculations of accident consequences.

INTRODUCTION

The current international analytic and experimental effort is resulting in reduced uncertainties in the physical and chemical factors affecting source terms. Additionally, the increased sophistication of the release models being developed reflect, to a greater extent than ever before, the details of individual plant design features and of specific accident sequences. The result of this is that while convergence is being approached on the magnitude of more realistic source terms, specific calculations using different computational models, different reference plants, and different accident scenarios result in source terms that differ in detail and are, therefore, difficult to compare.

A series of consequences calculations made by Stone & Webster Engineering Corporation (SWEC), using the CRAC2 computer code [2], offers a way to make comparisons among different source terms. Such comparisons will be useful in consolidating plant/accident specific source terms into categories useful for regulatory and other generalizations. In the process of making these calculations, parametric studies have been made to determine the effect of some uncertainties on the results. While some of these effects are significant for source terms in the higher ranges, they become much less so at the more realistic reduced levels.

BASIS OF COMPARISON

The mean acute whole body dose at distances to 10 miles was selected as the basis of comparison. This was calculated using CRAC2, with the following conditions:

- 2 hours decay prior to release
- 2 hours duration of release
- 10-meter release height
- 24-hour exposure to ground contamination
- Maximum individual dose (no sheltering)
- 3412 MWt PWR end of core life inventory
- 100 percent of the noble gases released
- 1 percent of all other nuclides released
- Miami typical meteorological year weather data
- Four samples per bin in CRAC2
- No heat associated with the release
- 1 cm/sec dry deposition velocity in CRAC2

Acute whole body doses have the following advantages for use in comparisons:

- They are independent of site-specific population distributions.
- They are not affected by the choice of health effect thresholds.
- They are not affected by the interdiction criteria incorporated in CRAC2.
- They allow comparison with the logic of NUREG 0396 [3].

Previous work by the authors [4] shows that the relationships between doses in the 10-mile range calculated for different source terms are not markedly affected by:

- Choice of meteorological area
- Choice of mean or 95th percentile dose
- Time of exposure between 12 and 48 hours
- Duration of release between 2 and 10 hours

Some variability over distance was found with sheltering factors.

Inclusion of the heat associated with the release and variation of the dry deposition velocity are expected to affect offsite doses and are discussed in this paper.

COMPARISON OF SOURCE TERMS

To facilitate comparison of source terms, a base case source term consisting of 100 percent of the noble gases and 1 percent of all other release groups was selected. This and other source terms used in this paper are listed below for convenient reference:

Percent of Core Inventory Released by Groups

Fission Product Group	WASH-1400 PWR2[5]	Sandia SST1[6]	SWEC IST[7]	SWEC RIST	Base Case
Noble Gases	90	100	100	100	100
Volatiles					
Iodine	70	45	1	1	1
Cs-Rb	50	67	1	1	1
Te-Sb	30	64	1	1	1
Nonvolatiles					
Ba-Sr	6	7	1	0.4	1
Ru	2	5	1	0.3	1
La	0.4	0.9	0.4	0.02	1

The "SWEC RIST" is a current revision of the Interim Source Term (IST) proposed by E. A. Warman of SWEC in 1982 [7].

The contributions to the total dose from each group of the base case were calculated individually. These are plotted in Figure 1.

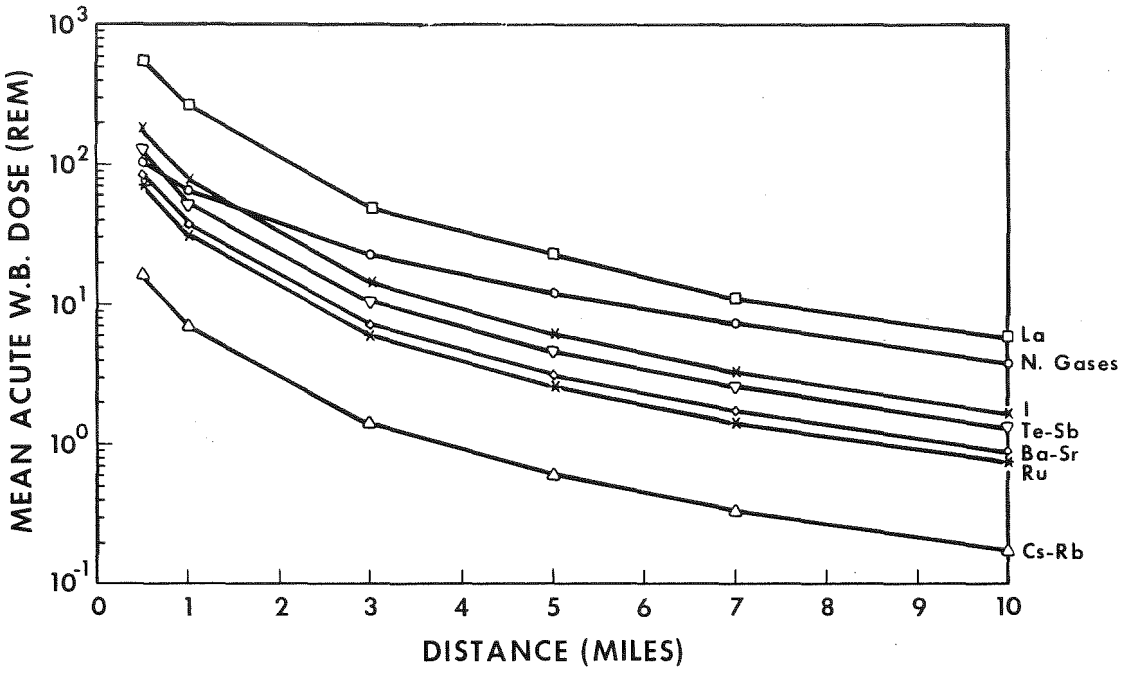

Figure 1. Dose Contribution from Each Release Group (Base Case)

Because these are based on 100 percent or 1 percent releases of each group, the curves can be used conveniently to construct a dose pattern for any source term by multiplying the calculated dose contributions by the postulated release percentages. Thus, for example, the dose contribution at 5 miles of a 2 percent iodine release would be double the (6 REM) contribution shown on the curve.

Figure 2 is a simplified calculation sheet which illustrates the effects of the principal parameters. Part A can be used to obtain approximate total 5-mile mean doses for any source term. These doses are valid for comparison of source terms at the same site and will be good to approximately a factor of 2 for a wide selection of site meteorological patterns [4].

The relatively large contribution from the noble gases (approximately 24 percent of the total 5-mile dose for the base case compared to approximately 2 percent for historical source terms such as PWR2 and SST1) should be noted. As the postulated release fractions of the other source term components shrink, the noble gases play a more prominent part. This qualitative difference will have to be considered in development of appropriate protective actions, with the acceptance of reduced source terms of similar compositions.

The very large contribution to the total from the base case release of 1 percent of the lanthanum group (including Y, La, Zr, Nb, Ce, Pr, Nd, Np, Pu, Am, and Cm) should also be noted. This is an unrealistically high release, but the 0.9 percent of SST1, and even the 0.4 percent of PWR2, will produce dose contributions which are high compared to those from 1 percent of iodine or tellurium. This is not surprising because the lanthanum group contains about 40 to 50 percent of the total curies in the core. Most source term investigators have concentrated on the volatiles, which produced the largest contributions based on the historic source terms. The sensitivity of the whole body dose to the lanthanum group release shown by this data indicates that attention should be focused on the nonvolatiles, as well as the volatiles.

Using the factors developed in a previous study [4], the 5-mile mean doses can be (again, approximately) converted to doses at other distances and for other conditions. These factors are shown in Part B of Figure 2. Figure 3 illustrates the results of a sample calculation for the 95th percentile dose at 2 miles with moderate sheltering from a source term consisting of 100 percent of the noble gases, 1.5 percent of the volatiles, and 0.1 percent of the nonvolatiles.

INVESTIGATION OF UNCERTAINTIES - DRY DEPOSITION VELOCITY

A value of 1 cm/sec for the dry deposition velocity of all the particulate matter released is generally recommended for use with CRAC2 [8]. The concept of using a single value for the dry deposition velocity, of course, is a simplification of the natural process of deposition. In reality there exists a spectrum of deposition velocities corresponding to the instantaneous spectrum of particle size distribution and particle density. Lacking a definitive basis for this value, a parametric investigation was conducted to determine the effect of using values of 0.5, 1.0, 3.0, 5.0, and 10.0 cm/sec. Mean whole body doses to 10 miles were calculated for these values using the SWEC RIST as representative of reduced source terms. The results are shown, with a series of cross curves, in Figure 4. These curves show doses as a function of dry deposition velocity at selected distances. It can be seen, as expected, that high deposition velocities generally produce high doses at short distances and lower doses at greater distances. It can also be seen that, at distances greater than about 2 to 3 miles, the deposition velocity producing the maximum dose quite rapidly approaches the CRAC2 recommended value of 1 cm/sec.

This approach is more clearly shown in Figure 5, which plots the same data in a different way and also shows that the dose profile becomes maximum around the 1 cm/sec value for the distances beyond 3 miles.

Comparable data for the PWR2 source term indicate that doses are maximized at around 1 cm/sec for the historical source terms also. Thus, it appears that in the 3 to 10-mile range, the CRAC2 assumption of a 1 cm/sec dry deposition velocity produces a conservative dose value for either historical or reduced source terms.

A. Calculate 5-mile dose from base case

GROUP	BASE CASE %	BASE CASE 5-mile dose	SPECIFIED CASE %	SPECIFIED CASE 5-mile dose
N.G.	100	12		
I	1	6		
Cs-Rb	1	0.5		
Te-Sb	1	5		
Ba-Sr	1	3		
Ru	1	2.5		
La	1	22		
TOTAL		51		

B. Apply adjustment factors

DISTANCE:	1 mile	x 11
	2 miles	x 4
	3 miles	x 2.2
	10 miles	÷ 3.3
95th PERCENTILE		x 3
12-HOUR GROUND DOSE		÷ 1.6
8-HOUR GROUND DOSE		÷ 2
SHELTERING:		
Normal Activity		÷ 2
Modest Sheltering	<3 mi	÷ 4
	>3 mi	÷ 3
Good Sheltering	<3 mi	÷ 6
	>3 mi	÷ 5
ESTIMATED DOSE (REM)		

Figure 2. Simplified Dose Calculation Sheet

A. Calculate 5-mile dose from base case

GROUP	BASE CASE %	BASE CASE 5-mile dose	SPECIFIED CASE %	SPECIFIED CASE 5-mile dose
N.G.	100	12	100	12
I	1	6	1.5	9
Cs-Rb	1	0.5	1.5	0.75
Te-Sb	1	5	1.5	7.5
Ba-Sr	1	3	0.1	0.3
Ru	1	2.5	0.1	0.25
La	1	22	0.1	2.2
TOTAL		51		32

B. Apply adjustment factors

DISTANCE:	1 mile	x 11	-
	2 miles	x 4	x 4
	3 miles	x 2.2	-
	10 miles	÷ 3.3	-
95th PERCENTILE		x 3	x 3
12-HOUR GROUND DOSE		÷ 1.6	-
8-HOUR GROUND DOSE		÷ 2	-
SHELTERING:			
Normal Activity		÷ 2	-
Modest Sheltering	<3 mi	÷ 4	÷ 4
	>3 mi	÷ 3	-
Good Sheltering	<3 mi	÷ 6	-
	>3 mi	÷ 5	-
ESTIMATED DOSE (REM)			96

Figure 3. Example of Dose Calculation at 2 Miles

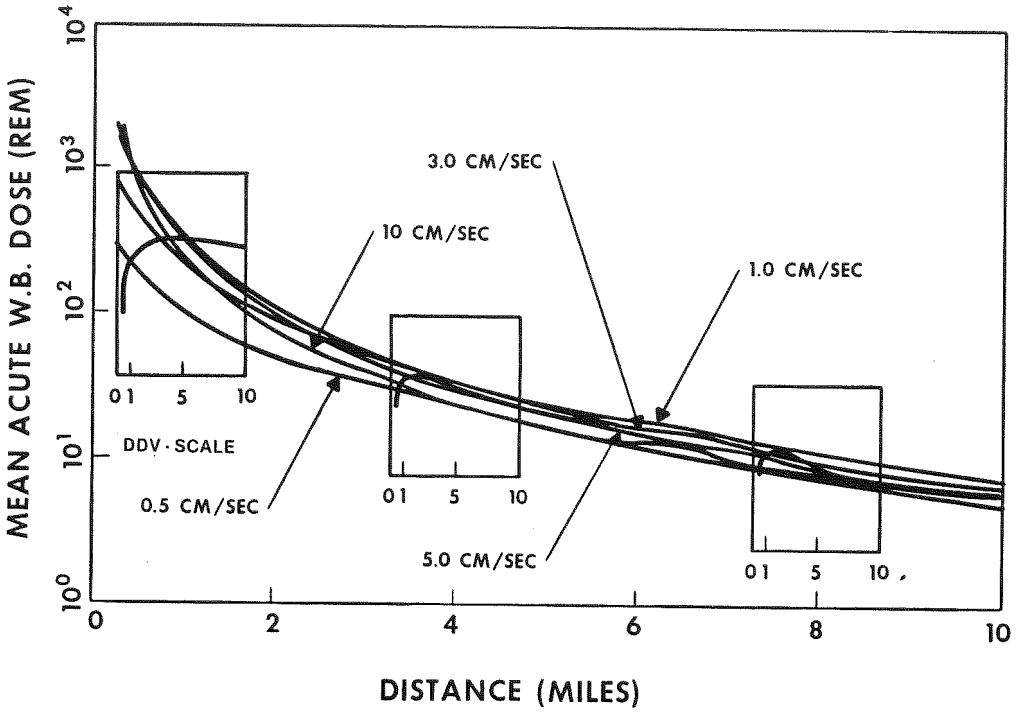

Figure 4. Effects of Assumed Dry Deposition Velocity

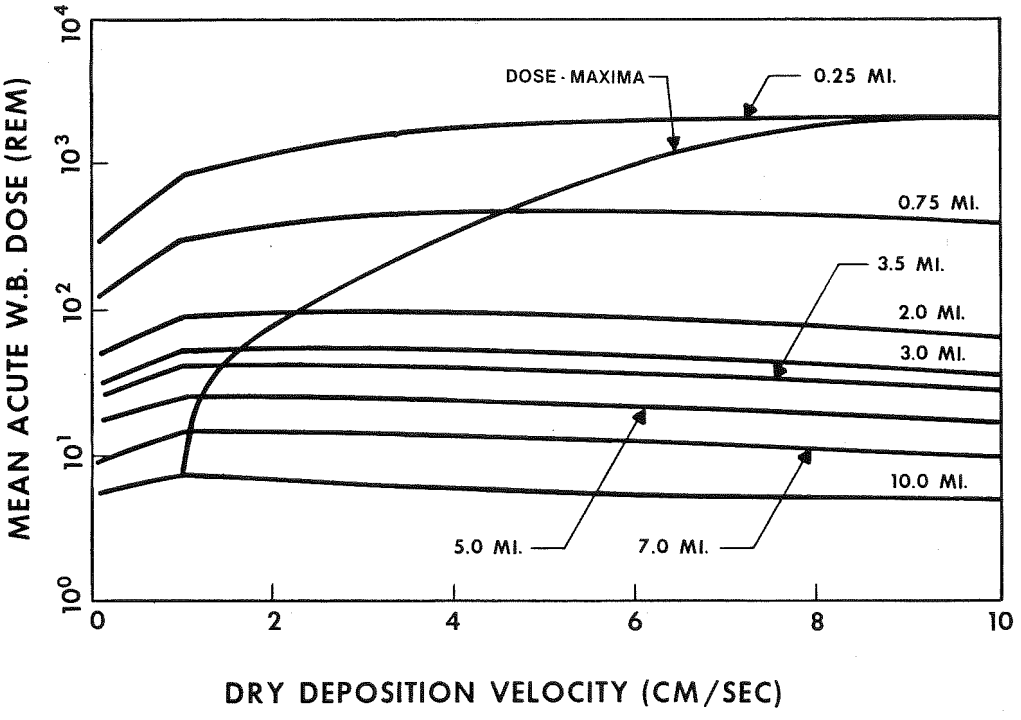

Figure 5. Dose Maxima for Assumed Dry Deposition Velocities

INVESTIGATION OF UNCERTAINTIES - PLUME BUOYANCY

For simplicity, most calculations, including those of the authors as well as such reports as the Sandia Siting Study [6], have assumed a nonbuoyant plume containing no sensible heat. Since considerable heat (on the order of 1.0 E+7 cal/sec) can accompany a release, a parametric study was also conducted to compare the effects of considering the resulting plume buoyancy on doses from historical and reduced source terms. Again, PWR2 and the SWEC RIST were selected as representative, and the effects on the calculated doses of using no energy and 1.2 E+7 cal/sec were compared. This value corresponds to the WASH-1400 value for sensible heat in PWR2 and is large compared to the decay heat energy in either historic or reduced source terms.

The results are shown in Figure 6. It can be seen that, in each case, the effect is a marked reduction in doses at short distances and some increase at larger distances. However, the values are very important. While the reduction factors to 10 miles are essentially the same, even the reduced PWR2 doses are still in the fatality/injury threshold range of 200 to 300 REM. For RIST, however, the effect of plume buoyancy is to reduce the doses, even at short distances, to levels well below the threshold values.

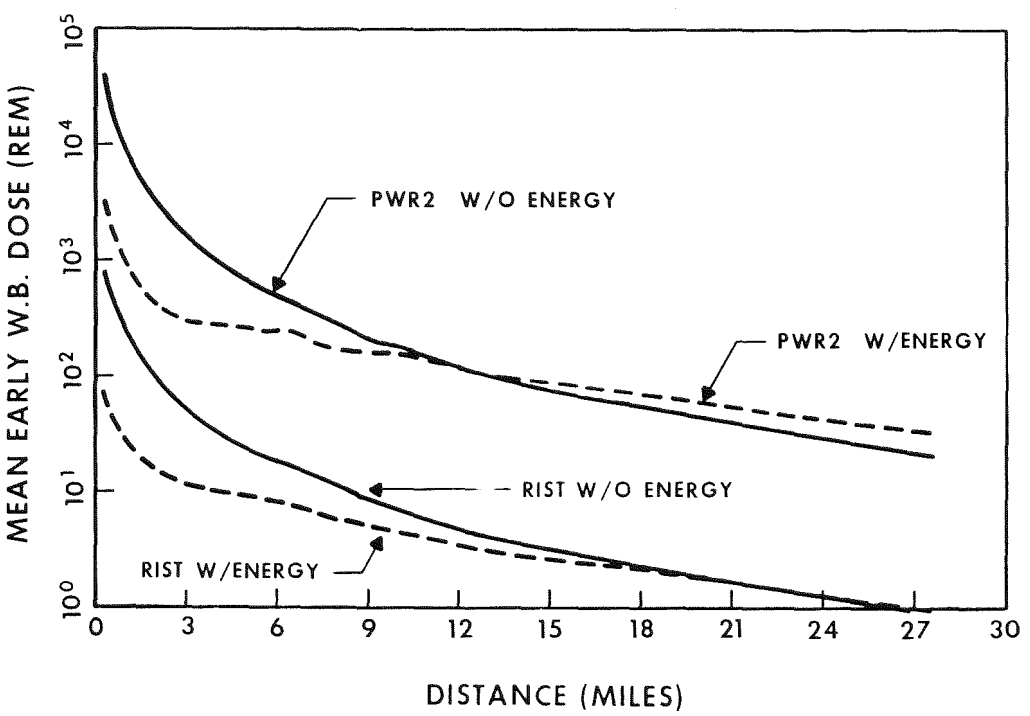

Figure 6. Effect of Plume Buoyancy

Further, it should be noted that with a PWR2 release there is sufficient activity remaining in the buoyant plume at greater distances (15 miles and more) so that dose levels at these distances are significantly (10 to 20 REM) above those calculated for the nonbuoyant plume. This increased level at extended distances may affect relatively large populations, with resultant large increases in calculated latent fatalities. With a RIST release, however, not only are the absolute values of the distant doses more than a decade lower, but the difference between the buoyant and nonbuoyant plumes is very small.

Thus, incorporation of the plume energy in the calculation for reduced source terms results in dose reductions below the threshold range at short distances without compensating increases at greater distances.

CONCLUSIONS

- A simple method has been presented which illustrates the effects of the principal parameters and can be used for comparing source terms by mean acute whole body doses.

- In source term investigations, attention should be focused on the nonvolatile as well as the volatile groups.

- Use of the CRAC2 value of 1 cm/sec for dry deposition velocity of the particulates results in conservative values of doses for both historical and reduced source terms.

- Incorporation of the plume energy in the dose calculations for reduced source terms results in dose reductions below the threshold range at short distances without the compensating increases at greater distances observed with historical source terms.

REFERENCES

1. Kemeny, J.G. (Chairman), "Report of the President's Commission on the Accident at Three Mile Island," Washington, D.C., October 1979.

2. "CRAC2: Calculations of Reactor Accident Consequences," Version 2, NUREG/CR-2326, February 1983.

3. "Planning Basis for the Development of State and Local Government Radiological Emergency Response Plans in Support of Light Water Nuclear Power Plants," NUREG-0396, EPA 520/1-78-016, December 1978.

4. Karahalios, P. and Gardner, R., "Effect of Source Term Composition on Offsite Doses," ANS Topical Meeting on Fission Product Behavior & Source Term Research, Snowbird, Utah, July 1984.

5. "Reactor Safety Study (RSS)," NUREG-75/14, October 1975. (Also referred to as WASH-1400)

6. "Technical Guidance for Siting Criteria Development," NUREG/CR-2339, November 1982. (Also referred to as Sandia Siting Study)

7. Warman, E.A., "Assessment of the Radiological Consequences of Postulated Reactor Accidents," Presented at Second International Conference on Nuclear Technology Transfer, Buenos Aires, Argentina, November 1982.

8. "PRA Procedures Guide," NUREG/CR-2300, January 1983.

Session VIII: Closing Session

Chair: F. Abbey (SRD Culcheth, UK)
W.O. Schikarski (KfK, FRG)

General Discussion

The final general discussion which took place at the end of the meeting contained session summaries presented by the chairmen followed by a short general discussion period. The contributions are reproduced here in full extent. The following is an edited typing of a tape record. In order to preserve the sense of the contributions, only minor alterations have been undertaken to the extent necessary to make the text intelligible.

Abbey: We intend to try to structure the discussion during this general discussion period somewhat. What I propose to do is to ask each of the session chairmen in turn to spend maybe 3 or 4 minutes giving us his view of the highlights of his particular session. Then we will have questions from the floor, and in answering the chairmen might draw in the authors of individual papers if they so wish. But I would suggest that in view of the time limitation that you try and keep the questions you ask of a fairly general nature to illuminate the overall aspect of the meeting, rather than particular points of detail.

So with that general introduction, I suggest we simply go through the sessions of the meeting in chronological order, starting with Dr. Murata.

Murata: Session I was nominally titled 'Aerosol Formation'. There was actually such a diversity of topics covered that the only way to do justice to all the papers will be to summarise them. I have done so in my written summary but what I would like to do is to touch on what I think are the highlights at this point. Dr. Hosemann gave a review paper on the source term research in the KfK Project Nuclear Safety. He noted the following: "Much progress has been made in recent years in understanding the dominant phenomena in the PADHR melt down accidents. We have reached a stage where the source term in core melt accidents may be analysed in a satisfactory way by plausible

and physically justifiable limiting cases. The retention of aerosol particles in containment, calculated within this approach, appears to reduce the source term by several orders of magnitude. The research to develop more detailed codes which may lead to an improvement of a factor of 2 or 3 may not be necessary".

There was in my view a very interesting paper which presented results on the characterization of mixed aerosols from control rod burst or melt through. This was the paper by J. P. Mitchell and A. L. Nichols which describes the vapour aerosol release of control rod alloys. This work is also of interest at Sandia where work has been done on both a vaporization model and a nucleation model which should apply to this situation. Questions which should be addressed, are the shape of the aerosol particles in steam experiments, the actual versus Raoult's law vapour pressure of the constituents above the molten alloy, and the effect of vessel pressure on the precise form of the vapour aerosol release. The possibility of hydrodynamic instability type generation of the aerosol particle should also be kept in mind for sudden burst of the cladding.

Let me comment on a paper by Dr. Heusener. He reviewed the containment systems and main safety features of the SNR 300, Super Pheonix I and II, and the SNR 2 which is presently in the planning stage. He noted that with increasing size breeders have to be built more with

economics in mind. For this reason he noted the containment of an HCDA will probably not be considered in the SNR 2 design. Because of this a realistic source term evaluation is much more important in the case of an SNR 2 than in the case of the SNR 300 which was conservatively designed.

My final comment is that one outstanding problem in aerosol formation is the characterization of aerosols which are formed from physical resuspension of previously deposited aerosols. In the QUEST study of Sandia considerable uncertainty was attributed to aerosols suspended by gas flow over surfaces and by pool flashing on containment depressurisation. This is an area which apparently has some data base but in which more work is needed.

Abbey: Thank you, Dr. Murata. But if I could ask you to keep your powder dry just at the moment, and go straight on to Dr. Gieseke who chaired Session II on 'Aerosol Processes'.

Gieseke: In the review paper, Dr. Schöck discussed various aerosol processes and noted progress made since the 1980 CSNI meeting. In particular, specific data became available on shape factors for agglomeration, on rates of steam condensation on particles, on shape factors and spherification of aerosols as they affect sedimentation, and on diffusio-phoresis and thermophoresis. These processes are generally included in aerosol behaviour codes. New information has also become available for other processes

such as inertial deposition and attenuation during leakage which could be incorporated in the aerosol codes. However, it is believed that the data base is currently insufficient for adding aerosol resuspension mechanisms to the codes. Additional technical information presented during the session emphasized improvements in the various codes and in the mechanisms controlling aerosol behaviour.

The importance of latent heat of vaporization as it affects steam condensation on aerosols was noted as was the importance of large particles on overall aerosol behaviour when it is governed by gravitational agglomeration. This was calculated with new theoretical expressions, and models were presented for deposition from turbulent flows. An improved model for Brownian agglomeration on particles smaller than those in a transition regime was reported and agreement with data was reported. A model for multiple component aerosol behaviour was presented, and in comparison with data the model was shown to have the ability to predict the behaviour of individual components in the mixed aerosol. It seems likely that for certain conditions at least the attenuation of specific aerosol species could be best predicted by using a code that treats multiple species.

Abbey: Thank you Dr. Gieseke.

Dr. P. Clough, Session III, 'The Interrelation of Thermal Hydraulics and Aerosol Behaviour'.

Clough: We heard a lot in this meeting about the importance of taking proper account of interaction of thermal hydraulics and fission product behaviour. I think that an excellent point was made by Dr. Schöck in his introductory lecture to Session II, when he said that it is not the accuracy of the aerosol modelling which is limiting now. It is the input data to the application of the modelling codes and one of the biggest uncertainties undoubtedly is in the thermal hydraulic data. Tom Kress gave us, I thought, an excellent review paper on the interaction of fission product behaviour, specifically aerosols, and thermal hydraulics. If I can just extract what I think he was saying, he was really highlighting three different effects which have to be taken into account. One is the effect of decay heat, the second is the effect of actual aerosol mass on the transport properties in the gas phase, and the third is the effect of phase changes, specifically latent heat, on the thermal properties. Just running quickly through those, I think the mass effects were concluded to be quite significant in the primary circuit. There are certain conditions where the mass flow of fission products actually dominates the total mass flow in the upper plenum of the reactor coolant system. This must be taken into account in the thermal hydraulic modelling. In the containment I think one can estimate that the mass effect will be small, although he did not specifically cover this. Aerosols represent small perturbations since average gas densities will be in the order of 1 kg/m^3 which is very high compared to the aerosol mass densities. The effects of phase changes

are likely to be very small in their interaction with the thermal hydraulic behaviour, and the overall major effect is that of decay heat. This has two aspects, one of which is the effect on the gas phase temperatures, which affects the potential for vapour condensation and the competition of vapour condensation between aerosols and surfaces. On this point I mention the important paper, presented by Dr. Clement on the theoretical treatment of this aspect. The other effect is the deposition on surfaces. In the primary circuit this is clearly a two-way-effect. It affects surface temperatures and possibly leads to revolatilisation of fission products. It also feeds back onto the gas phase temperatures and gas phase flow conditions and can considerably affect the convective flow patterns in the primary circut. In the containment this latter effect brings us to another important theme of the session which was the modelling and treatment of thermal conditions in the containment and we heard two papers concerning the DEMONA experiments of which I think particularly the experimental paper should have had a significant impact. It was a clear demonstration that the well-mixed assumption which is commonly employed in modelling aerosol behaviour in containment is very questionable in large buildings.

Abbey: That was an excellent summary. Thank you.

Dr. Haschke, Session IV 'Aerosol Measurements and Generation'

Haschke: O.K. Thank you. Session IV had four papers presented.

Three dealt with aerosol measurement and one paper with large scale aerosol generation with plasma torches. We started with an intercomparison of aerosol measurement systems involving six groups of five countries which was done at the KfK/LAF I. Results showed the agreement for AMMD and σ_g was in the 20% range. An interesting thing was probably to note that some kind of a learning curve could be observed which could be explained from the expertise acquired during the 3 day exercise in handling instruments. That was quite reassuring but the cold shower followed immediately with the paper telling about difficulties of calibrating cyclone cascade samplers. This is difficult using only a Stokes' number correlation and the result indicated that not only gas viscosity but also density effects are influencing the cyclone performance. A correlation using Reynolds' numbers correlation parameters was hopefully improving the situation. After this paper probably a very important question was raised, and that was that we should maybe look at cascade impactors also to see if there aren't any difficulties in calibrating them the way we do it until now. Then we had a very detailed description of the aerosol measurement system in the DEMONA program which uses a variety of different devices simultaneously in the containment under varied moisture conditions. Some emphasis was given on the upgrading which was done to get those instruments to work in the containment. There was also an interesting question raised during or after this presentation about the particle analyzer which probably has to operate, at

least in the first phase of the experiment, under saturated conditions. In a paper about the generation techniques using plasma burners probably the interesting point was that we got efficiencies in the order of about 50% or slightly higher for iron oxide aerosol generation and about 90% for tin oxide generation. Now a personal remark: this paper should have probably included some indication that the operating time or the reliability of the plasma torches are not yet up to expectations.

Abbey: Thank you, Dr. Haschke.
Mr. Johansson Session V, 'Aerosol Behaviour in the Primary System'.

Johansson: The papers presented in that session, for example the review paper by Gieseke and the experimental papers, and also the subsequent discussion formed the basis for the definition on the needs of further experimental data and validated models. Many of my colleagues here have given such examples and we have compiled those needs into a list of six items. So I will give you that list.
Item No. 1 is that we need continued code development coupled to experimental validation of the processes modelled for the primary coolant and circuit.
Item No. 2 is that we need to assess thermal-hydraulic effects, including natural circulation and the questionable validity of the well-mixed assumption.
Item No. 3 Studies of important chemical reactions that could change the chemical identity and behaviour of fission product species. Such reactions can occur for instance

between vapour and vapour, vapour and structure, vapour and aerosol, vapour and deposit, and deposit and structure.
Item No. 4 Condensation of fission product vapours on aerosols and latent heat effects.
Item No. 5 We need data on aerosol transport and the resuspension of deposits. And last but not least,
Item No. 6 the re-vaporization of vapours by decay heat.
That concludes my list.

Abbey: Thank you again, Mr. Johansson. We get near the end now.

Dr. Fermandjian Session VI, 'Aerosol Behaviour in Containments'

Fermandjian: Yes. Session VI, "Aerosol behaviour in the containment - Large Scale experiments and comparison to code calculation". Since the last meeting in Gatlinburg in 1980 the following additional information has been gained:

1. Modelling and experiments concerning the behaviour of mixed aerosols in the containment vessel have been performed.

2. Some large scale experiments on aerosol behaviour under light water reactor accident conditions have been performed (NSPP test) and other relevant programs are in progress (DEMONA and LACE programs).

3. Experimental measurement in the large containment vessel held in the FAUNA facility showed that sedimentation coupled with turbulent deposition is by far the dominant aerosol removal process.

The matters where additional investigation appear desirable in large scale experiments are the following: effect of atmosphere stratification, i.e. the deviation from good

mixing in the gas phase; for light water reactors; the effect of the suspended water droplets released during the blow-down phase, the role of containment compartmentalisation, resuspension, revaporization of deposited aerosol, and the last item - I think it is very important - is the interaction between liquid droplets, (soluble aerosol) and dry particles (insoluble aerosol).

Abbey: Thank you, Dr. Fermandjian. And finally, Dr. Kress Session VII, 'On Inter-comparison and Application of the Codes'.

Kress: In this session we started out with a very good review of some of the modelling features in the mostly LMFBR applicable codes. And the major difference among these, I think, is whether or not you are using a discretized description of the size distribution or whether it is lognormal. They pointed out that it is wrong to use the lognormal and I believe it should be discarded because it gives big differences and it is basically wrong and hard to change from one model to another with that system. They found remarkable similarities between the discretized codes but there are still some major differences, primarily related to gravitational and turbulent agglomeration and in respect to the collision efficiency. There are two basic forms, the Pruppacher and Klett form and the Fuchs form, and they believed that the Pruppacher and Klett formulation is the correct one and that is what they recommend. There are differences in the functional

dependence of the agglomeration kernels on the collision shape factor and they recommended that additional studies and analyses should be made to actually clarify the form that is most appropriate for that, plus they did recommend additional experimental data in both of these areas. The major recent additions they pointed out in the codes have been the things having to do with steam condensation on the walls and on aerosols, the addition of turbulent deposition models in PARDISEKO IIIb and the multi-component capabilities of some of the codes. They believe each of those are important and good additions. They high-lighted the importance of some of the thermal hydraulics related to the turbulent energy dissipation levels in relation to turbulent agglomeration. And they noted that neither of the shape factors are allowed to be functions of particle size. I believe all of those things are quite important and we are not really at the final stage of modelling where I think we ought to be. The accompanying paper with that, showing the differences between the calculations for a benchmark calculation bore out the differences that these things can cause in the results. For example, they found the leak mass was very sensitive to the collision efficiency, and the dynamic collision shape factors. The last papers by the Stone & Webster people presented, I thought, very interesting alternative source term determinations. Some of the highlights of that are how important it is to have a detailed coupled thermohydraulic analysis with the fission product transport in the primary system. The

tendency when you do that coupled analysis is that it brings the whole upper plenum structure into a more uniform play and lowers the temperatures and enhances the retention capability. And I think they found lower source terms as a result of that. They also found how important it is to have a much more detailed nodalisation rather than 3 or 4 or 5 nodes for those regions, so I think that is an important finding. In the containment studies they varied some parameters that in my mind are not usually varied, things like the containment hole size and its timing, and the quantity of initial liquid water droplets, that are present due to the blow down of the primary system water. What was interesting was that they found an optimum (whatever the word is) hole size for maximum release and it turned out to be about 1 $feet^2$ for the sequence. They also found there is an optimum timing of a failure - it was coincident with the time of start of core melt. This paper to me also highlighted the importance of doing very careful thermohydraulics in your containment because it can have a big influence on the source terms. And finally the implications of possible lower sources to the dose calculation was presented in the last paper, and because some of the lower sources are at such levels as not to predict any early deaths, they proposed using the mean acute whole body dose as a criterion for evaluating source terms and comparing them, and presented to us a very convenient chart based on a postulated set of source terms - i.e. 100% of the noble gases and 1% of anything else. You can use these charts to convert the doses at different

distances, and for alternative source term assumptions and calculations. And they also did some very good minor parametric variations of the dose effects due to the dry deposition velocity assumption in CRAC-2 and the plume buoyancy. They found that the recommended 1 cm/sec deposition velocity gives you a maximum exposure beyond about 2 or 3 miles and is a conservative (I don't like to use the term) number to use, and it is important to include plume buoyancy because it reduces the close-in dose but tends to raise the far-out dose which could be significant, depending on the level of source term he assumed. But at some of the lower levels of source terms the increase at large distances tended to be not so significant.

Abbey: Thank you, Dr. Kress.
Well, you've heard that mixture of summary and comment from one particular subset of experts within the general audience. Are there any supplementary comments or questions from the floor arising from what you heard or from early proceedings during the week? Do you want to say anything in particular, Prof. Schikarski?

Schikarski: If I may, I'd like to throw two points into the audience. I have made during the conference a number of little recommendations or remarks but two of them are sufficiently important in my opinion to justify repeating them. The first one is that I think, we can state that aerosol codes today are much better than their image might be in the

circles of outsiders. The reason I am stressing this is that the ABCOVE data which we heard today are really misleading in that respect because an aerosol code cannot be handled as a black box. It is necessary that an intelligent aerosol physicist is handling it and putting in the right coefficients. We have heard that all those codes depend on large amounts of input data and of course, if you don't use the right ones, you are wrong. The second point I want to make is: there was some discussion about the high mass concentration possible in the primary system above a hot core. I would like to recommend perhaps to the theoretical people that somebody thinks about what could be the maximum mass concentration at all possible under these conditions, because I am sure that we have not realistic aerosol formation rates in the accident scenarios. These aerosol formation rates may be being over-estimated and these are input numbers for all the aerosol code modelling. Thank you.

Abbey: Thank you, Prof. Schikarski. May I have the observations from the floor?

Ms. Longworth: I just want to make a general point. At least some of the calculations and experiments, and I think probably all of them, are now leading in the containment to very high mass depletion rates in the containment mass of aerosol. I think if you look at some of those reduction factors they turn out at about 10^{-5} - 10^{-6} of the original source.

I think one has got to tread very carefully in trying to improve on those numbers when you consider that at least, as far as iodine is concerned, the actual source term at that level is perhaps going to be dominated by the vapour phase including organic iodide and I_2 partition from sump water. I think that has to be taken into account when deciding how much further work needs to be done on the aerosols.

Abbey: Thank you, Ms. Longworth. Perhaps I should have said that if you want to make a comment, really make a comment, if you want to ask a question, perhaps you would indicate to which of these gentlemen your particular question is addressed.

Dr. Clement.

Clement: I would like to make a comment about unsolved problems in the subject because I think in many ways they are always of great interest to me personally, and there still are some areas being mentioned here about which really very little is known, and yet they must obviously be important in some cases. One was mentioned by Dr. Kress and that is the transfer of heat by electromagnetic radiation. This is not really taken into account in most of these codes but it is probably the most important heat transfer mechanism above a very hot core and it can affect such things as condensation and so on in the regions above the core. The second is what Dr. Adams showed in his experiments - that when aerosols were in condensing steam

environments, there was an enormous difference between the way concrete aerosols fell out and iron and uranium oxide aerosols, and this is something I don't think the codes have in them at the moment. I don't know if I could reproduce that difference at all.

Abbey: Dr. Silberberg.

Silberberg: Yes, I have two observations and at the same time, I guess, I would like to turn them into either a clear recommendation or something like that. I guess the first one has to do with the whole question of the dynamic shape factors and collision factors. It seems like every time we have one of these meetings, we always go away concluding that we still have to continue to do something about this. And you know, after hearing that for some years, I wonder what we are going to do. Do we just quit and just recommend some numbers? So it seems to me that there ought to be some kind of a consensus. The other item had to do with the question of the plasma torch, namely some of the observations that have been made like in the case of the concrete aerosols and things like that. Are we sure that we are not again looking at an artefact of the experimental device, and if so, we ought to be concerned about that. Or is there some way one could set up some type of a standard procedure or standard point or characterization of a plasma torch that says: if one runs a plasma torch within this range of conditions or these

types of aerosols or whatever, the community will agree that this is acceptable or not acceptable. It seems like one ought to be able to do some kind of a characterization or at least get some better level of confidence than I think we have today. If, indeed, we are not sure about whether or not that method affects the results. You know, if people say: there's no problem, I think it's O.K. and there is a consensus, and I think that is good. I just throw that out.

Abbey: Thank you, Dr. Silberberg. Just before I continue can I ask if there is anybody who wants specifically to comment on those two points that have just been raised? Dr. Kress?

Kress: Yes, I would like to comment on both of the points, the second one first about the plasma torch. Before we embarked on a systematic, heavy use of it at Oak Ridge, we did attempt to make some comparative studies to see if we were producing our own aerosol Heisenberg principle, that is whether we altered the thing we were looking at by the way we've made it. So we compared the aerosols produced, their behaviour in vessels, compared the plasma torch generated aerosols for a number of materials to alternative ways to produce those aerosols which involve things like ordinary combustion of uranium metal or producing UO_2 aerosols by capacitor discharge and the exploding wire technique. There are a number of ways to produce aerosols - it is a limited number, but there are

a number of ways - and everyway we could produce significant quantities, we did compare them with the plasma and found no significant differences at all in the behaviour, the appearance, the fall-out rates and the U_3O_8 and metal aerosols that we were producing. So, there has been a little bit of that comparative work done.

And I want to comment on Dr. Silberberg's plea about the shape factors and more or less, reinforce that. I agree with him completely on that and I think the only way to put that aside is to make direct measurements of the shape factors, and I think that is what we should do, not backfit the codes but make direct measurements of the shape factors, and the collision efficiency, as well.

Schikarski: I would like to comment only on the shape factor issue. I don't think we have a big problem there. The point is the following, that we have measured for the first time the collision shape factor or the coagulation shape factor for uranium oxide, and these studies which took us 4 years more or less identified a number of problems which have not been discussed or a number of aspects, which have not been discussed during this conference. I will mention a few: first of all the shape factor, the coagulation shape factor and the dynamic shape factor will probably be in many cases more or less the same. This can be supported by theoretical reviews.
Second point: the shape factor is dependent on the production method. If you vaporize uranium oxide just

by vaporization on a hot surface you get a different shape factor than if you put it into an exploding wire. So it is a material dependent factor and it is also dependant on the production method. So, then we are more or less in the jungle because all the materials which are formed in reactor scenarios have too many possibilities and mixtures and so on that I don't think we can handle this in a short way. My approach is therefore to go forward with the assumption that analogy is acceptable and analogy means in the literature, including the non-nuclear literature, that there are hundreds of measurements of the dynamic shape factor of different materials from all types of aerosols. And if you look up all these numbers, they are in a certain band width. Second hypothesis is: The coagulation shape factors probably are in the same band widths and if you have this as a first approach, you can live with it. However, I accept the point that we need some further basic research and I emphasise basic research and not really applied research in this respect.

Silberberg: I made the comment and the request in the context of: if I'm not an analyst and I'm calculating for the XYZ reactor tomorrow, what do I use? What numbers should I use? And then I would put them in the context of whether it is for the LACE tests or the DEMONA tests or NSPP. For now, even putting aside that we might need some basic research, and you know we've rather been waiting for that coming up with the answers, let us consider an exercise with someone again recommending

a set of these shape factors and try them out ahead of time on the experiments, which I guess you have to do when you do the intercomparisons anyway with the tests. That would at least give one some confidence as to whether or not what is available in the literature covers the range of the tests that we are doing.

Nichols: I have three points. They may be discussed with Dr. Gieseke if he is willing, but I'd like to go through all three points first.

Aerosol measurements in the cyclone calibration work that you've been involved in doing, varying the density and the viscosity of the gases; this gives me some cause for concern, because to me it is more inexplicable that you are getting the sort of movements that you have been getting between different cyclones in the train with respect to where Argon is and the air calibrations are.

Do we need to know the aerosol properties in reactor accident conditions, particularly with respect to the primary circuit? The evidence from the Stone & Webster papers are that the temperatures are very high. Is it that important for the codes that you get the right mass median diameter up to those temperatures? I am really concerned about particle size distributions in the aerosol field, I know that sounds like heresy, but I have vague indications that in fact, maybe just concentration really is the key to predicting the aerosol source term from out of the containment. And I throw

that in, maybe as means of somebody savaging me rather than anything else. The second point: we can't avoid the fact that fission product vapours are intimately involved with aerosol behaviour. I mean, we have got to talk about fission products, and I worry about iodine chemistry because I see a lot of work has been done in the past, in fact almost since Einstein suggested we split the atom. And there has been a lot of very good work done with pure systems, and I wonder whether that has really been the right way to go. A reactor is a pretty dirty thing and it seems to me that the role of impurity in the iodine chemistry is very important, but maybe the role of impurity on the aerosol side may also be of some importance. The 3rd point is a comment on the big aerosol experiments. I think in some respects I see the demise of this sort of work; they are very expensive. We all start arguing about whether one experiment has been a success or a failure. I am talking in terms of DEMONA, LACE and MARVIKEN. If these experiments are successful, which I hope they are, is that going to be the end of the story or is there an even bigger and better experiment waiting round the corner?

Abbey: Is there anybody else who wants to respond to those points? Dr. Gieseke?

Gieseke: I respond to the first one: do we need other properties for the particles? I believe we do, for a variety of reasons, because it is not so much that it affects the

transport. You can argue that you should use a shape factor if there are solid agglomerates or agglomerates of solids, or different shape factors if there are molten spheres, but beyond that I think what happens to them after they have come in contact with the surface makes a big difference because if they are dry then under high pressure blow-down in the primary system, you probably get a lot of it moved outside the primary system and at least dispersed enough where it is coolable and you won't revaporize much. On the other hand, if there is liquid which I think is much more likely, you are going to have a material that is perhaps not going to blow away too easily, and then you revaporise materials. So I think the physical properties are important and are a product of chemical properties, of course.

Kress: With respect to your comment about particle size versus concentration, I don't think I'm ready to give up particle size as a prime-independent variable yet.

Abbey: I think we have perhaps time for one more comment of a general nature. Is there anybody wishing to make one?

Johansson: What I intend to say is that my present understanding of the high retention of fission product decay heat in the reactor vessel will heat up the vessel and give a caesium release. Given the hot vessel there will be a vapour pressure of caesium iodide and hydroxide which will constitute a low intensity source of radio-activity on a long time basis. I guess I'm on the

same line as Ms Longworth, that the aerosols cannot decay to a very low level, giving this long term source. That is my general comment.

Abbey: Anything else?

Well, I think at that point I must close this discussion session. I'll try to keep my closing remarks short. I don't propose to try to summarize either this discussion we have just had now or the conference itself. I might feel more inclined to do so tomorrow evening after the extended Program Group meeting, but not now apart from a couple of rather platitudinous comments. Firstly to the effect that it is clear that there have been major advances since the previous specialist's meeting in 1980. And secondly that on the other hand there are still outstanding problems. Clearly the question of needed thermohydraulic data and the back-coupling of that to aerosol behaviour is a major one of those problems and I do wonder whether in fact another meeting in a relatively short space of time, devoted to that particular theme, might be worthwhile. As you know, we had hoped to make that a theme of this meeting but in the event it proved premature. But I think the time might not be far off when we could usefully have a further meeting on that particular topic. The other observation is a pat on the back, I think for the Group of Experts on Nuclear Aerosols in that many of the problems which we have discussed here today were pointed out in the state of the art report that

the aerosols group produced.

I think, that is really all I want to say by way of the summarized technical content of the meeting, which leads me simply to thank everybody who has contributed to making a success of what I think has been a successful meeting. We ought to start by thanking our sponsors, the German Nuclear Society, and the Association for Aerosol Research. We ought, particularly, I think thank our hosts at KfK who have been responsible for the practical arrangements and the fact that everything has gone so smoothly, is very much down to them and, of course, I would particularly mention both, Prof. Schikarski and Werner Schöck, and not forgetting the welcoming address from Dr. Hennies on Tuesday morning. Thirdly, I should say that we thank the authors of the invited review papers and particularly the authoritative introductory papers we had from Dr. Silberberg, which really set the scene for the rest of the meeting in such an able and definitive manner. And lastly, I would like to thank the authors of the contributed papers and people who contributed from the floor to make the whole discussion so interesting. With that, unless there are any comments, I declare the meeting closed, but reminding you that there is a technical visit, of course in the morning and the extended Program Group meeting in the afternoon to which, I hope, all the chairmen of sessions will come as well as the Program Group itself.

Thank you very much for attending and for your contribution.

List of participants

LIST OF PARTICIPANTS

Prof. Dr. Ache, H. J.	Kernforschungszentrum Karlsruhe Institut für Radiochemie Postfach 36 40 D-7500 Karlsruhe
Abbey, F.	Safety & Reliability Directorate UKAEA, Wigshaw Lane Culcheth, Warrington WA3 4NE, UK
Dr. Adams, R.	Oak Ridge National Laboratory P.O. Box Y, Bldg. 9108 MS2 Oak Ridge, TN 37830, USA
Dr. Albrecht, H.	Kernforschungszentrum Karlsruhe Institut für Radiochemie Postfach 36 40 D-7500 Karlsruhe
Dr. Andriesse, C.D.	KEMA Laboratories Utrechtse Weg 310 NL-6812 Arnhem/Netherlands
Aro, M.	Finnish Centre for Radiation and Nuclear Safety P.O. Box 268, SF-00101 Helsinki, Finland
Baggenstos, M.	Swiss Federal Nuclear Safety Inspectorate CH-5303 Würenlingen, Switzerland
Balz, W.	Commission of the European Communities 200, Rue de la Loi, B-1049 Bruxelles, Belgium

Dr. Barilli, L.
ENEA
Via Mazzini 2
I-40138 Bologna, Italy

Basselier, J.
Belgonucleaire S.A.
Rue du Champ de Mars, 25
B-1050 Bruxelles, Belgium

Dr. Belosi, F.
Lavoro E Ambiente SCRL
Via Mazzini 75
I-40138 Bologna, Italy

Bunz, H.
Kernforschungszentrum Karlsruhe
Laboratorium für Aerosolphysik
und Filtertechnik I
Postfach 36 40
D-7500 Karlsruhe

Dr. Casselman, Ch.
Commissariat A L'Energie Atomique
CEN Cadarache, B.P. 1
F-13115 Saint-Paul-Lez-Durance, France

Cazorla Arteaga, F.
TECNATOM, S.A.,
Km 19 C.N.I., Madrid-Irun
San Sebastian de los Reyes
Madrid, Spain

Cherdron, W.
Kernforschungszentrum Karlsruhe
Laboratorium für Aerosolphysik
und Filtertechnik I
Postfach 36 40
D-7500 Karlsruhe

Dr. Clement, Ch.
Theoretical Physics Division 424.4
A.E.R.E. Harwell, Didcot
Oxfordshire OX 11 ORA, UK

Dr. Clough, P. N.	Safety & Reliability Directorate UKAEA, Wigshaw Lane Culcheth, Warrington WA3 4NE, UK
Dr. Cole, R.	Sandia National Laboratory delegate to KfK
Della Loggia, E.	Commission of the European Communities Rue de la Loi 200 B-1049 Bruxelles, Belgium
Deworm, J.-P.	Centre d'Etude de l'Energie Nucléaire CEN/SCK, Boeretang, 200 B-2400 Mol, Belgium
Dr. Dunbar, I.H.	Safety & Reliability Directorate UKAEA, Wigshaw Lane Culcheth, Warrington WA3 4NE, UK
Dr. Eyink, J.	Kraftwerkunion Erlangen Hammerbacherstr. 12-14 D-8520 Erlangen
Dr. Fermandjian, J.	Commissariat à l'Energie Atomique CEN-FAR B.P. 6, F-92260 Fontenay-aux-Roses, France
Dr. Friederichs, H.G.	Gesellschaft für Reaktorsicherheit Glockengasse D-5000 Köln
Fritzke, H.W.	GKSS Postfach 1 60 D-2054 Geesthacht

Dr. Fröhlich, R.
Kernforschungszentrum Karlsruhe
Institut für Neutronenphysik und Reaktortechnik
Postfach 36 40
D-7500 Karlsruhe

Fromentin, A.
Swiss Federal Institute for
Reactor Research (EIR)
CH-5303 Würenlingen, Switzerland

Dr. Fynbo, P.
Riso National Laboratory
P.O. Box 49
DK-4000 Roskilde, Denmark

Gardner, R.
Stone & Webster Engineering Corp.
245 Summer Street
Boston, MA 02107, USA

Gebauer, H.
FAG Kugelfischer
Georg Schäfer KG
Erzeugnisbereich Strahlungsmeßtechnik
Tennenloher Str. 41
D-8520 Erlangen

Dr. Gieseke, J. A.
Battelle Columbus Laboratory
Chemistry Dept.
505 King Avenue
Columbus, Ohio 43201, USA

Haeggblom, H.
Studsvik Energiteknik AB
S-61182 Nyköping, Sweden

Dr. Haschke, D.
Swiss Federal Institute for
Reactor Research (EIR)
CH-5303 Würenlingen, Switzerland

Dr. Hennies, H.
Kernforschungszentrum Karlsruhe
Postfach 36 40
D-7500 Karlsruhe

Dr. Heusener, G.
Kernforschungszentrum Karlsruhe
Projekt Schneller Brüter / PL
Postfach 36 40
D-7500 Karlsruhe

Dr. Hosemann, J. P.
Kernforschungszentrum Karlsruhe
Projekt Nukleare Sicherheitsforschung / PL
Postfach 36 40
D-7500 Karlsruhe

Dr. Hilliard, R.K.
Hanford Engineering Development Laboratory
P.O. Box 1970
Richland, WA 99352, USA

Hocke, K.-D.
Universität Stuttgart, IKE
Pfaffenwaldring 31
D-7000 Stuttgart 80

Johansson, K.
Studsvik Energiteknik AB
S-61182 Nyköping, Sweden

Jokiniemi J.
Technical Research Centre of Finland
Nuclear Engineering Laboratory
P.O. Box 169
SF-00181 Helsinki 18, Finland

Jordan, H.
Battelle Columbus Laboratory
Nuclear Technology and Phys. Sciences Dept.
505 King Avenue
Columbus, Ohio 43201, USA

Dr. Jordan, S.
Kernforschungszentrum Karlsruhe
Laboratorium für Aerosolphysik
und Filtertechnik I
Postfach 36 40
D-7500 Karlsruhe

Kallenbach
Universität Stuttgart
Institut für Kernenergetik und
Energiesysteme
D-7000 Stuttgart 80

Dr. Kanzleiter, T.
Battelle-Institut e.V.
Am Römerhof 35
D-6000 Frankfurt/M 90

Dr. Katscher, W.
Kernforschungsanlage Jülich
Institut für Nukleare Sicherheitsforschung
Postfach 19 13
D-5170 Jülich

Kinsman, P.
Safety and Reliability Directorate
Wigshaw Lane
Culcheth, Warrington WA 3 4NE, UK

Knuth, H.
Kernforschungszentrum Karlsruhe
Projekt Schneller Brüter/PL
Postfach 36 40
D-7500 Karlsruhe

Dr. Kress, T.S.
Oak Ridge National Laboratory
P.O. Box Y, Bldg. 9108
Oak Ridge, TN 37830, USA

Dr. Kuhlman, M.
Battelle Columbus Laboratory
Nuclear Techn. and Physical Sciences Dept.
505 King Avenue
Columbus, Ohio 43201, USA

Prof. Lanza, S.
Instituto di Impianti Nucleari
Facoltà di Ingegneria
Università degli Studi di Pisa
Via Diotisalvi, 2
I-56100 Pisa, Italy

Dr. Lauridsen, K.
Risø National Laboratory
P.O.B. 49
DK-4000 Roskilde, Denmark

Dr. Leuschner, A.
Delegate to
Kernforschungszentrum Karlsruhe
Laboratorium für Aerosolphysik
und Filtertechnik I
Postfach 36 40
D-7500 Karlsruhe

Longworth, J.
Central Electricity Generating Board
Berkeley Nuclear Laboratories
Berkeley, Glos, GL 13 9PB, UK

Prof. Loyalka, S.
University of Missouri-Columbia
College of Engineering
1026 Engineering
Columbia, Missouri 65211, USA

Manilia, E.
Direzione Sicurezza Nucleare e Protezione Sanitaria (DISP) ENEA
Via Vitaliano Brancati, 48
I-00144 Roma, Italy

Matsumoto, M.
Hitachi
1-1, Saiwaicho 3-chome
Hitachi-shi,
Ibaraki-ken, 317 Japan

Dr. Mercier, O.
Swiss Federal Institute
for Reactor Research (EIR),
CH-5303 Würenlingen, Switzerland

Dr. Metzig, G.
Kernforschungszentrum Karlsruhe
Laboratorium für Aerosolphysik
und Filtertechnik I
Postfach 36 40
D-7500 Karlsruhe

Michael, H.
Stone & Webster Engineering Corp.
245 Summer Street
Boston, MA 02107, USA

Miyahara, S.
Power Reactor & Nuclear Fuel Development Corp.
Oarai Engineering Center
4002 Narita, Oarai, Ibaraki, Japan

Moers, H.
Kernforschungszentrum Karlsruhe
Institut für Radiochemie
Postfach 36 40,
D-7500 Karlsruhe 1

Dr. Murata, K.
Sandia National Laboratories
P.O.B. 5800
Albuquerque, NM 87185, USA

Dr. Neri, E.
ENEA; PAS/ISP/AMB
C.R.E. Casaccia
S.P. Anguillarese, 301
I-00100 Roma, Italy

Dr. Nichols, A.
UKAEA
Atomic Energy Establishment, Winfrith,
Dorchester, Dorset, DT2 8DH, UK

Nishio, M.
Nuclear Safety Eng. Section
Reactor Design Eng. Department, Toshiba Co.
8 Shinsugita-Cho, Isogo-ku,
Yokohama-shi, Kanagawa, Japan

Nukatsuka, S.
Mitsubishi Atomic Power Industries, Inc.
4-1, Shibakoen 2-chome, Minato-ku
Tokyo, 105, Japan

Obata, H.
Century Research Center Corporation
2nd Nuclear Energy Department
3-2 Nihonbashihoncho, Chioku,
Tokyo, Japan

Dr. Peehs, M.
Kraftwerkunion Erlangen
Postfach 32 20
D-8520 Erlangen

Poß, G.
Kernforschungszentrum Karlsruhe
Laboratorium für Aerosolphysik
und Filtertechnik I
Postfach 36 40
D-7500 Karlsruhe

Prof. Prodi, V.
Dipartimento di Fisica
University of Bologna
Via Irnerio 46
I-40126 Bologna, Italy

Dr. Quraishi, M.
Atomic Energy of Canada Limited
Sheridan Park Research Community
Mississauga, Ontario, Canada, L5K 1B2

Dr. Ramsdale, S.
UKAEA, Safety & Reliability Directorate
Wigshaw Lane, Culcheth
Warrington WA3 4NE, UK

Prof. Raunemaa, T.
University of Helsinki
Department of Physics
Siltavuorenpenger 20 D
SF-00170 Helsinki 17, Finland

Dr. Rininsland, H.
Kernforschungszentrum Karlsruhe
Projekt Nukleare Sicherheit/PL
Postfach 36 40
D-7500 Karlsruhe

Dr. Röbig, G.
Kraftwerkunion AG
Berliner Str. 295-303
D-6050 Offenbach

Dr. Royen, J.
OECD
Nuclear Energy Agency
38 Boulevard Suchet
F-75016 Paris, France

Sauter, H.
Kernforschungszentrum Karlsruhe
Laboratorium für Aerosolphysik
und Filtertechnik
Postfach 36 40
D-7500 Karlsruhe

Scholle, U.
Interatom
Friedrich-Ebert-Str.
D-5060 Bergisch-Gladbach 1

Dr. Seehars, H.
Fraunhofer-Institut für Toxikologie
und Aerosolforschung
D-5948 Schmallenberg-Grafschaft

Dr. Sehgal, B.R.
Electric Power Research Institute
3412 Hillview Avenue
P. O. Box 10412
Palo Alto, CA 94303, USA

Silberberg, M.	U.S. Nuclear Regulatory Commission Mail Stop 1130-SS Washington, DC. 20555, USA
Dr. Smedley, Ch.	National Nuclear Corporation Limited Cambridge Road, Whetstone Leicester LE8 3LH, UK
Dr. Scheibel, H.	Battelle-Institut e.V. Am Römerhof 35 D-6000 Frankfurt
Prof. Dr. Schikarski, W.	Kernforschungszentrum Karlsruhe Laboratorium für Aerosolphysik und Filtertechnik Postfach 36 40 D-7500 Karlsruhe
Dr. Schikorr, M.	Kernforschungszentrum Karlsruhe Institut für Neutronenphysik und Reaktortechnik Postfach 36 40 D-7500 Karlsruhe
Dr. Schmidt, F.	Universität Stuttgart Institut für Kernenergetik und Energiesysteme D-7000 Stuttgart 80
Schmidt, H.	Europäisches Institut für Transurane D-7514 Eggenstein-Leopoldshafen
Dr. Schöck, W.	Kernforschungszentrum Karlsruhe Laboratorium für Aerosolphysik und Filtertechnik I Postfach 36 40 D-7500 Karlsruhe

Schroeder, T.
Battelle-Institut e.V.
Am Römerhof 35
D-6000 Frankfurt 90

Dr. Schütz, W.
Kernforschungszentrum Karlsuhe
Laboratorium für Aerosolphysik
und Filtertechnik I
Postfach 36 40
D-7500 Karlsruhe

Schückler, M.
Technischer Überwachungs-Verein
Dudenstr. 28
D-6800 Mannheim 1

Dr. Schürenkämper, A.
Commission of the European Communities
Joint Research Centre
I-21020 Ispra, Italy

Dr. Tani, A.
NAIG
Nuclear Research Laboratory
4-1 Ukishima-cho
Kawasaki-ku
Kanagawa, 210, Japan

Dr. Tarroni, G.
ENEA
PAS/FIBI/Aerosol, C.R.E. E. Clementel
Via Mazzini, 2
I-30138 Bologna, Italy

Taylor, F.
H.M. Nuclear Installations Inspectorate
Thames House North, Millbank
London SW1P 4QJ, UK

Dr. ten Brink, H.M.
Netherlands Energy Research Foundation (ECN)
Chemistry Department
P.O. Box 1
NL-1755 ZG Petten/Netherlands

Dr. Torgerson, D.
Atomic Energy of Canada Limited Research Company
Whiteshell Nuclear Research Establishment
Pinawa, Manitoba, Canada ROE 1LO

Warman, E.
Stone & Webster Engineering Corporation
245 Summer Street
Boston, MA 02107, USA

Dr. Weber, G.
Gesellschaft für Reaktorsicherheit
Forschungsgelände
D-8046 Garching

Wells, A.
Environmental and Medical Sciences Division
Building 364, AERE, Harwell,
Didcot
Oxfordshire 0X11 ORA, UK

Willers, A.
Queen Mary College
University of London
Mile End Road
London E1 4NS, UK

Dr. Wright, A.
Oak Ridge National Laboratory
P.O. Box X
Building 4500N
Oak Ridge, Tennessee 37830, USA